



**Investigating the roles of the ubiquitin ligases
Cullin2^{Lrr1} and TRAIP during
DNA replication termination**

**By
Divyasree Poovathumkadavil
Under the guidance of Prof. Aga Gambus**

**A thesis submitted to the University of Birmingham in partial
fulfilment of the requirements for the degree of
Doctor of Philosophy**

**Institute of Cancer and Genomic Sciences
College of Medical and Dental Sciences
University of Birmingham
December 2023**

UNIVERSITY OF
BIRMINGHAM

University of Birmingham Research Archive

e-theses repository

This unpublished thesis/dissertation is copyright of the author and/or third parties. The intellectual property rights of the author or third parties in respect of this work are as defined by The Copyright Designs and Patents Act 1988 or as modified by any successor legislation.

Any use made of information contained in this thesis/dissertation must be in accordance with that legislation and must be properly acknowledged. Further distribution or reproduction in any format is prohibited without the permission of the copyright holder.

Abstract

DNA replication is a well-orchestrated process occurring throughout the S-phase of the cell cycle and unperturbed replication is the basis for genome maintenance. To understand how genome integrity is maintained, it is critical to study the underlying mechanisms and regulation of DNA replication. The defects in the first two stages of DNA replication- initiation and elongation are known to contribute to human diseases and are already targeted by cancer therapies. Recent investigations suggest that disruption of the final stage of replication-termination can also lead to genomic instability. As replication reaches completion and replication forks converge, replisomes are unloaded from chromatin. This unloading mechanism is highly regulated to prevent the unregulated unloading of active replisomes.

Using *Xenopus laevis* egg extracts, the Gambus lab had previously provided the first insights into replisome disassembly mediated by Cul2^{Lrr1}. This PhD project aimed to further understand the mechanism by which Cul2^{Lrr1} identifies its substrate through structural analysis. While the purification of Lrr1 proved technically challenging, we employed in silico methods to gain high confidence structural predictions for Lrr1.

Furthermore, we have also identified the existence of a backup pathway for replisome disassembly in mitosis. This mitotic pathway uses a different E3 ubiquitin ligase - TRAIP. Our findings demonstrate that catalytically active TRAIP plays an essential role in post-termination and stalled replisome disassembly in mitosis. Following this, we also explored TRAIP's involvement in replisome disassembly during S-phase. Intriguingly, the depletion of TRAIP did not affect replisome disassembly in S-phase within *Xenopus laevis* egg extracts. Moreover, this PhD project also indicates that the TRAIP activity in both S-

phase and mitosis is subject to regulation via post-translational modifications, specifically phosphorylation.

Therefore, this thesis expands our understanding of the mechanisms upholding genome stability during termination of DNA replication. It uncovered dual regulation of replisome removal in mitosis versus S-phase through activation of distinct ubiquitin-dependent pathways.

Acknowledgments

First and foremost I would like to thank my Ph.D. advisor Aga Gambus. Aga - your abundant support and guidance have been a beacon throughout my Ph.D. journey. Your belief in my abilities, even during the most challenging moments when my experiments did not yield the expected results, has been a constant source of motivation. You are the person who have shown me the endless possibilities in exploring Science. You have shown me also how to write reports, make presentations, craft manuscripts and teaching students, which are all invaluable for the rest of my career. Also, you had set a shining example, demonstrating that women can pursue their aspirations while maintaining a harmonious work-life balance. I consider myself truly fortunate to have you as my mentor and you will always remain as an inspiration both in my academic and professional journey. I am also very grateful of the opportunity you provided me to pursue a Ph.D alongside my professional commitments. This would not have been possible without your and the backing of our Institute of Cancer and Genomic Sciences, for which I am truly grateful and deserves a special mention.

I also thank all my teammates - Becky, Alicja, Paolo, Angeliki, Cyntia, Georgia, Abi, Chongluan, Chaoyu, as well as past members - Nev, Shaun, Zeynep, Sarmi, Sara, Joaquin- for being such a fun and fabulous teammates. Special acknowledgement goes to Nev and Paolo for their invaluable assistance in my protein purifications and structure predictions. To Becky and Alicja - I extend my appreciation for the collaborative and enjoyable work on TRAIP mitosis and S-phase chapters, which has formed the basis of my thesis work. Angeliki and Cyntia - thank you for always being so helpful in everything. Becky, Abi and Georgia - thank you for dedicating your time and effort to review my final thesis.

I am sincerely grateful to my Postgraduate Research leads, Dr. Clare Davies and Prof. Steve Smerdon, for watching over the scientific progress of my Ph.D. and for their invaluable comments and suggestions throughout the course.

Last but by no means least; I owe a special debt of gratitude to my family for their support. To my husband, Nikhil - your support and encouragement has been my pillar of strength. I could not have accomplished this without you, and your constant reminder to 'Keep going' has been my driving force. Genuinely, I would not have done this Ph.D without your support. Our fun late-night drives to grab my favourite snacks during those late hours will forever remain close to my heart. My deepest gratitude also goes to my dear parents- Asokan and Kanchana - for always standing with me to chase my dreams, and always believing in me, not just during my best moments but more importantly, during the hard times of my life. I have no words to express how important they were to me. Amma, your endless prayers for all of us are our greatest source of strength and our protective shield. I am incredibly blessed to have you both as my parents. My heartfelt appreciation also goes to my two loving sisters - Nilina & Sona and my brothers from a different mother - Sharan & Titto for their continuous motivation and love. A special mention goes to my little nephew, Adi, whose cheerful presence always brought a smile to my face. All of you holds a special place in my heart.

Dedication

To my dear parents and sisters

And

In loving memory of my grandad

P. K. Sankaranarayanan

Contents

List of Figures.....	XI
List of Tables.....	XIII
Abbreviations	XIV
Chapter 1.....	1
1 Introduction.....	1
1.1 Ubiquitin	1
1.1.1 The structure of ubiquitin	2
1.1.2 Ubiquitylation and ubiquitin codes.....	4
1.1.3 Ubiquitin cascade.....	9
1.1.3.1 E1 activating enzymes.....	10
1.1.3.2 E2 conjugating enzymes.....	11
1.1.3.3 E3 ubiquitin ligases	11
1.2 Cullin RING ubiquitin ligases (CRLs)	16
1.3 DNA replication.....	18
1.3.1 Initiation	21
1.3.2 Elongation	26
1.3.3 Termination.....	30
1.3.4 Fork convergence and replisome disassembly.....	31
1.4 Replication stress and its consequences on genome stability.....	33
1.4.1 Replication fork barriers.....	35
1.4.2 Transcription-replication conflicts.....	36
1.4.3 Unbalanced replication conditions.....	37
1.4.4 Replication fragile sites	38
1.4.5 DNA damage repair responses	39
1.5 Regulation of DNA replication by ubiquitylation.....	41
1.5.1 The Role of Ubiquitylation in origin licensing.....	41
1.5.2 The role of ubiquitylation in the initiation of replication.....	42
1.5.3 The role of ubiquitylation in preventing re-replication	43
1.5.4 The role of ubiquitylation in chromatin re-establishment.....	44
1.5.5 The role of ubiquitylation in replication termination	45
1.6 Cullin2 ^{Lrr1}	46

1.7 TRAIP	48
1.8 <i>Xenopus laevis</i> egg extracts model system	51
1.9 Aim of the project	54
2 Materials and Methods	56
2.1 Tables	56
2.2 Working with <i>Xenopus laevis</i> egg extract	64
2.2.1 Preparation of <i>Xenopus laevis</i> egg extracts	64
2.2.2 Preparation of demembranated sperm DNA	66
2.2.3 Using egg extracts and sperm DNA for studying DNA replication	67
2.2.3.1 Activating the <i>X. laevis</i> egg extract	67
2.2.3.2 Measuring replication efficiency of egg extracts	68
2.2.3.3 Isolation of Chromatin to analyse chromatin-associated proteins	69
2.2.3.4 Isolation of nuclear fraction from <i>X. laevis</i> egg extract	70
2.2.3.5 Large-scale immunodepletion of TRAIP from <i>X. laevis</i> egg extracts	71
2.2.3.6 Small-scale immunoprecipitation to test α -TRAIP and α -Lrr1 antibodies	72
2.3 Work involving bacteria	73
2.3.1 Bacterial strains and growth media used in this study	73
2.3.2 Transformation	73
2.3.3 Plasmid purification	74
2.3.4 Testing expression of recombinant proteins	74
2.3.5 Purification of recombinant proteins	75
2.3.5.1 Purification of recombinant <i>X. laevis</i> Lrr1	75
2.3.5.2 Purification of recombinant <i>X. laevis</i> N-Cul2/Lrr1/EloB/C complex	76
2.3.5.3 Purification of recombinant <i>X. laevis</i> Lrr1/EloB/C	77
2.3.5.4 Purification of recombinant <i>X. laevis</i> GST-TRAIPwt and TRAIPmut	78
2.3.5.5 Purification of recombinant <i>X. laevis</i> His/SUMO-TRAIPwt and TRAIPmut	79
2.4 Working with DNA	80
2.4.1 PCR amplification	80
2.4.2 Site-directed mutagenesis	81
2.4.3 Cloning of TRAIP	81

2.4.4 Agarose gel electrophoresis and visualisation	82
2.5 Working with Proteins	83
2.5.1 Dialysis.....	83
2.5.2 SDS PAGE (Sodium Dodecyl Sulphate Poly Acrylamide Gel Electrophoresis)	83
2.5.3 Staining of protein gels.....	84
2.5.4 BSA standard assay	84
2.5.5 Bradford assay.....	85
2.5.6 Immunoblotting.....	85
2.5.7 Antibody purifications	86
2.5.8 <i>In vitro</i> kinase assay	87
2.5.9 Size exclusion chromatography	87
2.6 Softwares.....	88
Chapter – 3	89
3 Optimising conditions for purification of <i>Xenopus laevis</i> Lrr1 and raising antibodies..	89
3.1 Introduction.....	89
3.2 Results.....	90
3.2.1 The ubiquitylation site within Mcm7 is not the only interaction point for Lrr1.....	90
3.2.2 Predicting the structure of <i>Xenopus laevis</i> Lrr1	91
3.2.3 Generation of Lrr1 truncations and patient mutants	97
3.2.4 Purification of <i>Xenopus laevis</i> Lrr1	103
3.2.5 Testing of antibodies raised against <i>Xenopus laevis</i> Lrr1.....	106
3.2.6 Assessing chromatin binding ability of recombinant purified Lrr1	108
3.2.7 Analysis of purified recombinant <i>X. laevis</i> His-SUMO-Lrr1 using size exclusion chromatography	110
3.2.8 Purification of recombinant <i>Xenopus laevis</i> Cul2/Lrr1/EloB/C complex	113
3.2.9 Size exclusion chromatography for recombinant N-Cul2/Lrr1/EloB/C complex.....	114
3.2.10 Expression and purification of recombinant <i>X. laevis</i> Lrr1/EloB/C	117
3.2.11 Mass spectrometry analysis of all purified recombinant <i>X. laevis</i> Lrr1.....	120
3.3 Discussion.....	122

Chapter – 4	131
4 TRAIP drives replisome disassembly in mitosis	131
4.1 Introduction.....	131
4.2 Results.....	132
4.2.1 Cul2 ^{Lrr1} independent mitotic replisome disassembly	132
4.2.2 Purification of Recombinant <i>Xenopus laevis</i> TRAIP.....	134
4.2.3 Raising and testing α -TRAIP antibodies.....	138
4.2.4 Testing α -TRAIP antibodies for immunodepletion and/or immunoprecipitation of TRAIP from egg extracts	139
4.2.5 Effect of immunodepletion of TRAIP from <i>Xenopus laevis</i> egg extract	141
4.2.6 TRAIP can unload post-terminated and stalled replisomes in mitosis	142
4.3 Discussion.....	150
Chapter-5	158
5 Investigating the role of TRAIP in the S-phase.....	158
5.1 Introduction.....	158
5.2 Results.....	159
5.2.1 TRAIP interaction with the S-phase replisome	159
5.2.2 TRAIP depletion in S-phase does not lead to DNA damage	163
5.2.3 TRAIP is dispensable for terminated replisome disassembly in S- phase.....	165
5.2.4 TRAIP can ubiquitylate Mcm7 but cannot prime unloading of terminated CMG in S-phase	167
5.2.5 Post-translational modifications of TRAIP contribute to TRAIP activity.....	171
5.2.6 Recombinant TRAIP can be phosphorylated <i>in vitro</i>	173
5.2.7 <i>In vitro</i> phosphorylation of TRAIP does not support replisome disassembly	177
5.3 Discussion.....	181
Chapter-6	193
6 Discussion	193
6.1 Molecular mechanisms of Cul2 ^{Lrr1} and TRAIP function.....	193
6.2 The significance of Cul2 ^{Lrr1} and TRAIP in cancer biology	199
6.3 Conclusion	202

Appendix	204
Bibliography	205

List of Figures

Figure 1.1:- Structural representation of ubiquitin.....	3
Figure 1.2:- Different types of ubiquitin modifications.....	6
Figure 1.3:- Ubiquitin enzymatic cascade.....	10
Figure 1.4:- Different types of E3 ubiquitin ligases.	12
Figure 1.5:- Schematic representation of Cullin Ring Ligases (CRLs).....	17
Figure 1.6:- Schematic drawing of cell cycle progression of multi-cellular organisms.....	20
Figure 1.7:- Schematic representation of origin licensing.....	23
Figure 1.8:- Schematic representation of origin firing.....	25
Figure 1.9:- Replicating fork with helicase.....	27
Figure 1.10:- Schematic representation of replisome disassembly pathway.	33
Figure 1.11:- Some of the different causes of replication stress.....	34
Figure 1.12:- Domain organisation of Lrr1 protein.....	46
Figure 1.13:- Domain organisation of TRAIP.....	50
Figure 3.1:- Lrr1 likely interacts with Mcm7 and helicase through multiple binding sites.	91
Figure 3.2:- Domain structure of Lrr1.....	92
Figure 3.3:- Predicted structures of <i>X. laevis</i> Lrr1 using Robetta Beta.....	95
Figure 3.4:- Predicted structure of <i>X. laevis</i> Lrr1 from Phyre2.....	96
Figure 3.5 :- Structures of other LRR containing proteins along with their α -helical capping motifs.....	97
Figure 3.6:- Structural model of Lrr1.....	98
Figure 3.7:- Generation of Lrr1 mutants.....	99
Figure 3.8:- Human LRR1 cancer patient mutations.....	101
Figure 3.9:- Alignment of <i>X. laevis</i> Lrr1 and <i>H. sapiens</i> LRR1 protein sequences.....	102
Figure 3.10:- The predicted structure of Human LRR1 patient mutants.....	103
Figure 3.11:- Purification of <i>X. laevis</i> His-SUMO-Lrr1.....	106
Figure 3.13:- Characterisation of <i>Xenopus laevis</i> Lrr1 antibodies.....	108
Figure 3.14:- Chromatin isolation with Recombinant His-SUMO-Lrr1.....	110
Figure 3.15:- Size exclusion chromatography for recombinant His-SUMO-Lrr1.....	112
Figure 3.16:- Purification of recombinant N-Cul2/Lrr1/EloB/C complex.....	114
Figure 3.17:- Size exclusion analysis of N-Cul2/Lrr1/EloB/C complex.....	116
Figure 3.18:- Expression testing for <i>X. laevis</i> His-SUMO-Lrr1/EloB/C.....	118
Figure 3.19:- Purification of His-SUMO-Lrr1/EloB/C 1.....	119
Figure 3.20:- Purification of His-SUMO-Lrr1/EloB/C 2.....	120
Figure 3.21:- Mass spectrometry analysis of recombinant purified Lrr1.....	121
Figure 3.22:- Model of terminated replisomes.....	127
Figure 3.23:- Patient mutations mapped on Cryo-EM model of human replisome and Cul2 ^{Lrr1}	129
Figure 4.1 Replisome disassembly has a backup pathway in mitosis.....	133
Figure 4.2:- <i>Xenopus laevis</i> GST-TRAIP purification.....	135
Figure 4.3:- Effect of the addition of GST-TRAIP to the egg extract.....	136
Figure 4.4:- <i>Xenopus laevis</i> SUMO-TRAIP purification.....	138

Figure 4.5:- Characterisation of TRAIP using in-house purified antibodies.....	139
Figure 4.6:- Immunodepletion using in-house purified α -TRAIP antibodies.....	140
Figure 4.7:- Immunodepletion of TRAIP does not negatively affect DNA replication in S-phase.....	142
Figure 4.8:- TRAIP ubiquitin ligase drives mitotic replisome disassembly in post-termination replisomes.	143
Figure 4.9:- Ubiquitin ligase activity of TRAIP is essential for unloading post-terminated replisomes.	145
Figure 4.10:- Ubiquitin ligase activity of TRAIP is essential for ubiquitylating Mcm7 of post-terminated replisomes in mitosis.....	146
Figure 4.11:- TRAIP ubiquitin ligase drives mitotic replisome disassembly of stalled replisomes.	147
Figure 4.12:- Ubiquitin ligase activity of TRAIP is essential for the unloading of stalled replisomes.	148
Figure 4.13:- Ubiquitin ligase activity of TRAIP is essential for ubiquitylating Mcm7 of stalled replisomes in mitosis.....	149
Figure 4.14:- Predicted model of TRAIP dimer using AlphaFold.....	152
Figure 5.1:- TRAIP interaction with replisome is stimulated when replisomes are retained on chromatin in S-phase.	159
Figure 5.2:- Inhibition of fork convergence stimulates TRAIP interaction with replisomes in S-phase.....	161
Figure 5.3:- TRAIP does not accumulate on chromatin when CMG helicase and polymerases are uncoupled.	163
Figure 5.4:- Immunodepletion of TRAIP does not induce S-phase checkpoint activity.	165
Figure 5.5:- TRAIP is not essential for terminated replisomes disassembly in S-phase.	166
Figure 5.6:- TRAIP does not facilitate the unloading of replisomes in the S-phase.....	168
Figure 5.7:- TRAIP can stimulate Mcm7 ubiquitylation in S-phase.	170
Figure 5.8:- Phosphorylation of TRAIP in mitosis.....	172
Figure 5.9:- TRAIP is only phosphorylated in mitosis.	173
Figure 5.10:- TRAIP can be phosphorylated <i>in vitro</i> by cyclin/CDK complexes.....	175
Figure 5.11:- Effect of addition of cyclin A1 Δ in S-phase.	177
Figure 5.12:- The addition of phosphorylated TRAIP proteins does not affect replication.	178
Figure 5.13:- The addition of <i>in vitro</i> phosphorylated TRAIP proteins does not unload replisomes in S-phase.....	179
Figure 5.14:- The addition of <i>in vitro</i> phosphorylated TRAIP proteins in TRAIP depleted extracts.....	180
Figure 5.15:- In silico predicted model of TRAIP structure and its interactors.	189
Figure 5.16:- Human TRAIP patient mutations.....	192
Figure 6.1:- Current understanding of the regulation of replisome disassembly mediated by Cul2 ^{Lrr1} in S-phase.....	196
Figure 6.2:- Current understanding of TRAIP-mediated replisome disassembly under various conditions.....	197

List of Tables

Table 1:- List of buffers used in this PhD project.....	56
Table 2:- List of plasmids used in this PhD project.....	60
Table 3:- List of primers used in this PhD project.....	60
Table 4:- List of inhibitors added to <i>X. laevis</i> egg extract.....	61
Table 5:- List of recombinant proteins added to <i>X. laevis</i> egg extract.	61
Table 6:- List of antibodies used in this PhD project.....	62
Table 7:- Composition of the PCR reaction mixture.	80
Table 8 :- Thermocycling conditions used for PCR reactions.	81
Table 9 :- Composition of 10% SDS-PAGE gel.....	84

Abbreviations

AAA+: ATPase Associated with diverse cellular Activities

ACS: ARS consensus sequence

AIM: Auto-inducing media

APC: Anaphase-promoting complex

APL: Aprotinin, Pepstatin, Leupeptin

ARS: Autonomously replicating sequence

ATM: Ataxia-telangiectasia mutated

ATP: Adenosine triphosphate

ATR: Ataxia telangiectasia and Rad3-related

BRCA1: Breast and ovarian cancer susceptibility protein 1

BSA: Bovine serum albumin

CDC6: Cell division cycle protein 6

CDK: Cyclin-dependent kinase

Cdt1: Cdc10-dependent transcript 1

CFS: Common fragile site

Chk1: Checkpoint kinase 1

CHROMASS: Chromatin mass spectrometry

CMG: Cdc45/Mcm2-7/GINS complex

CRL: Cullin ring ubiquitin ligase

CSN: Signalosome 205

DDK: Dbf4-dependent kinase

DDR: DNA damage response

DNA: Deoxyribonucleic acid

DNA-PK: DNA dependent protein kinase

DNMT1: DNA (cytosine 5) methyl transferase 1

dNTP: Deoxyribonucleotide

DPC: DNA protein crosslink

DSB: Double strand break

dsDNA: Double-stranded DNA

DUB: Deubiquitylating enzyme

FA: Fanconi anaemia

FANC: Fanconi anemia complementation group protein

FEN1: Flap endonuclease 1

GINs: go-ichi-ni-san

h/Hrs: Hours

HECT: Homologous to E6AP C-terminus

Hif1 α : Hypoxia inducible factor 1 alpha

HR: Homologous recombination

HRP: Horseradish peroxidase

HSS: High speed supernatant

ICL: Interstrand crosslink

IgG: Immunoglobulin G

IP: Immunoprecipitation

IP: Immunoprecipitation

iPOND: Isolation of proteins on nascent DNA

IPTG: Isopropyl β -d-1-thiogalactopyranoside

K: Lysine

l: Litre

LB: Lysogeny broth / Luria-bertani

LRR1: Leucine rich repeat protein 1

LSS: Low speed supernatant

MCM: Mini chromosome maintenance complex

Mw: Molecular weight

NEDD8: Neural precursor cell expressed, developmentally down-regulated protein 8

NF- κ B: nuclear factor kappa-light-chain-enhancer of activated B cells

NHEJ: Non homologous end joining

NPE: Nucleoplasmic extract

Npl4: Nuclear protein localization protein 4

OD: Optical density

ORC: Origin recognition complex

PAGE: Polyacrylamide gel electrophoresis

PBS: Phosphate buffered saline

PCNA: Proliferating cell nuclear antigen

PCR: Polymerase chain reaction

PIP box: PCNA interacting protein box

PMSF: Phenyl methyl sulfonyl fluoride
Pre-RC: Pre-replication complex
PTM: Post-translational modification
PVDF: Poly vinylidene Fluoride
RBR: Ring between ring
RFC: Replication factor C
RING: Really interesting new gene
RNA: Ribonucleic acid
RPA: Replication protein A
SCF: Skp1-cullin-F-box complex
SDS: Dodecyl sulfate sodium
SPRTN: SprT-Like N-Terminal Domain
SSB: Single strand break
ssDNA: Single stranded DNA
SUMO: Small ubiquitin like modifier
TopBP1: DNA topoisomerase 2 binding protein 1
TRAIP: TRAF interacting protein
TSS: Transcription start site
Ubi: Ubiquitin
Ubi-NOK: Ubiquitin no lysine
UBL: Ubiquitin like modifier
UBD: Ubiquitin Binding Domain
UBXN7: UBX Domain Protein 7
Ufd1: Ubiquitin fusion degradation protein 1
Uhrf1: Ubiquitin like with PHD and RING finger domain containing protein 1
V: Volts
VCP: Valosin containing protein
VHL: Von Hippel-Lindau tumour suppressor
wt: Wild type
ZnF: Zinc Finger

Chapter - 1

1 Introduction

1.1 Ubiquitin

Ubiquitin is a highly conserved small protein comprising about 76 amino acid residues. It acts as a post-translational modifier by being attached to the lysine of a target protein via covalent bonds to mark it usually for protein degradation thereby regulating the stability and functionality of a protein. It is ubiquitously expressed in eukaryotic cells and is known to regulate essential events for the cell cycle progression such as cell division, growth, signalling, and apoptosis (Sun and Chen, 2004). Until recently only proteins were considered as substrates for ubiquitylation. Recently, it has been shown that ubiquitylation can occur on non-proteinaceous substrates such as sugars and lipids (Kelsall, 2022). For example; conjugation of ubiquitin to phospholipids has been reported in yeast and mammalian cells (Sakamaki et al., 2022). RNF213 mediated liposaccharide ubiquitylation has been known to target non-proteinaceous biomolecules such as host cell lipids (Otten et al., 2021).

Ubiquitin was first known for tagging proteins for their regulated degradation by 26S proteasomes but is now known as the major post-translational modification regulating diverse forms of physiological processes occurring in eukaryotes (Walczak et al., 2012). Ubiquitin generates functionally distinct signals in proteasomal and lysosomal proteolysis. Non-proteolytic signals are also generated for processes such as sub-nuclear trafficking and maintenance of genome integrity including double-strand breaks and interstrand cross-link repair, or bypass of interference during DNA replication (Hicke and Dunn, 2003; Ulrich and Walden, 2010). Interestingly, prokaryotes do not possess a

ubiquitin-mediated proteasomal degradation system. Instead, they have a unique ATP-dependent substrate tagging mechanism that is functionally analogous to ubiquitin (Kavalchuk et al., 2022).

1.1.1 The structure of ubiquitin

Goldstein first discovered ubiquitin in 1975 from Bovine thymus. This polypeptide was found to have a molecular mass of 8.5 kDa and has been identified in yeast, plants, and animal cells (Goldstein et al., 1975). The ubiquitin fold is made up of five β -stranded sheets, a short helix, and a 3.5 turn α -helix along with a flexible C-terminus, which allows covalent attachment to target proteins (Figure 1.1 a). The Leu 8 residue contained within the β -loop region is known to be important for ubiquitin-binding proteins (Komander and Rape, 2012; Toma-Fukai and Shimizu, 2021).

The amino acid sequence of ubiquitin contains 7 lysine residues (K6, K11, K27, K29, K33, K48, and K63), and the α -amino group of the N-terminal methionine (Met 1) all of which can be ubiquitylated (Figure 1.1 b). Ubiquitin is first synthesised in an immature form with two glycine molecules at the C-terminal end fused to another protein or another ubiquitin unit. Ubiquitin molecules are functionally active only when the C-terminal end is cleaved by ubiquitin proteases, resulting in the exposure of the two glycine residues. This mature ubiquitin is later activated in an ATP-dependent manner and serves as a signal molecule by covalently attaching to its substrate and regulating its function (Pickart and Fushman, 2004).

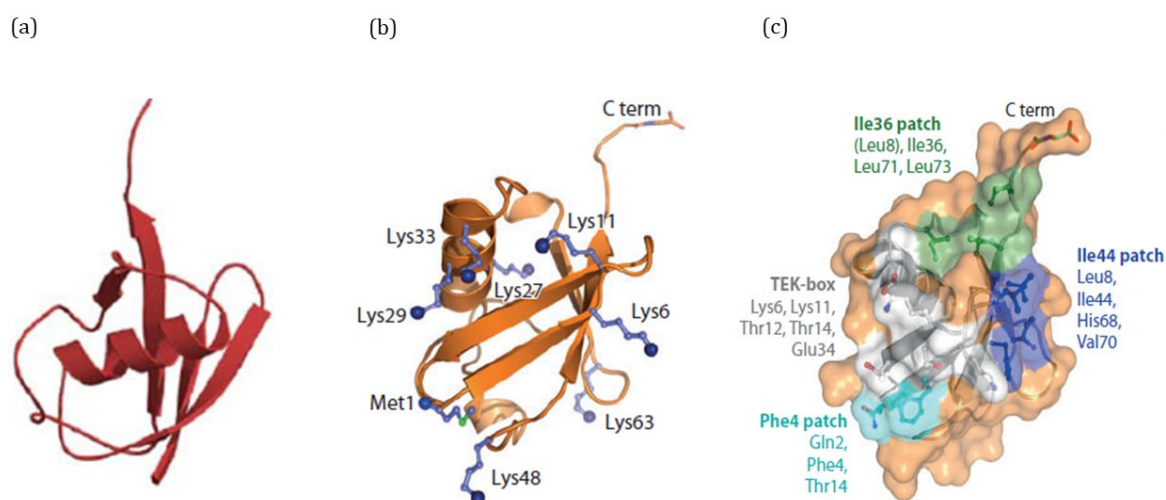


Figure 1.1:- Structural representation of ubiquitin. (a) Ribbon diagram of ubiquitin depicting α -helix (coils) and conserved β -pleated sheets (arrows) fold. (b) Ubiquitin monomer representing the C-terminal tail and 7 lysine residues and methionine residue at the N-terminus responsible for ubiquitylation. (c) The functionally important regions for ubiquitylation such as Ile44, Ile36, Phe4 patches, and TEK-box along with their key residues are represented. Protein Data Bank (pdb) code 1ubq. Figure reproduced from (Pickart and Eddins, 2004; Komander and Rape, 2012)

Distinct surfaces on ubiquitin known as ‘ubiquitin patches’ are recognized by proteins that contain Ubiquitin Binding Domains (UBDs). Ubiquitin binding proteins typically contain a UBD ranging from 20-150 amino acids that has the capability to directly interact with ubiquitin. There are 20 families of UBDs (Dikic et al., 2009). UBDs can differ based on their structure and the type of ubiquitin recognition. Some of the commonly found foldings for UBDs include α -helix, zinc fingers (ZnFs), the UBC (ubiquitin conjugating) domain or plekstrin homology (PH) folds. For example, a vast majority of UBDs including Ubiquitin interacting motif (UIM) and Ubiquitin-associated (UBA) domains uses α -helical structures to bind to the hydrophobic patches within the β -sheet of ubiquitin (Hicke et al., 2005). The zinc finger UBDs contains a zinc finger motif that also interacts with

hydrophobic patches of ubiquitin. The UBC domain, present in ubiquitin conjugating enzymes such as in UBCH5, is important for ubiquitin transfer (Dikic et al., 2009). The PH domain also recognises the hydrophobic patches on ubiquitin such as the Ile44 patch (Hurley et al., 2006; Hicke et al., 2005).

The interaction of the UBDs with specific ubiquitin patches contributes to the various functional roles possessed by ubiquitin. The different patches on ubiquitin along with the residues are depicted in figure 1.1 c. The hydrophobic patches Ile44 and Ile36 are recognized by UBDs and are always positioned relative to each other (Akutsu et al., 2016). Leu8, Ile44, His68, and Val70 together make up the Ile44 patch and are essential for proteasomal degradation and cell division (Sloper-Mould et al., 2001; Komander and Rape, 2012). The Ile36 patch containing Leu8, Ile36, Leu71, and Leu73 mediates interaction with ubiquitin chains made by HECT E3 and can be recognized by deubiquitylating enzymes (DUBs) and UBDs. The Phe4 patch (with Gln2, Phe4, and Thr14) is important for endocytosis and interaction with the USP (Ubiquitin-specific proteases) domain of DUBs. The TEK box is a three-dimensional motif that spans across Lys6, Lys11, Thr12, Thr14, and Glu34 and is important for mitotic degradation in higher eukaryotes (Komander and Rape, 2012).

1.1.2 Ubiquitylation and ubiquitin codes

During substrate modification, an isopeptide bond is formed between the C-terminal glycine-76 of the ubiquitin and amino group of any of the lysine residues from the substrate protein. This is a three-step enzymatic process utilizing the E1 ubiquitin-activating enzyme, E2 conjugating enzyme, and E3 ubiquitin ligases (Swatek and Komander, 2016). In addition to the lysine residues, the amino group at the N-terminus of the methionine can also be ubiquitylated. Very recent studies have also reported the

ubiquitylation of serine; where ubiquitin is added to various proteins in ER and Golgi to regulate its function (Liu et al., 2021; Toma-Fukai and Shimizu, 2021). Ubiquitin can be attached to its substrate protein either as a single moiety or multiple numbers of ubiquitin leading to a chain connected by isopeptide bonds (Komander and Rape, 2012). The attachment of a single ubiquitin results in mono-ubiquitylation (Figure 1.2 a) which plays a crucial role in cellular activity. Similarly, multiple ubiquitins can bind to various lysine residues of the target protein and such a modification is known as multi-monoubiquitylation (Figure 1.2 b). Further extensions of ubiquitin modifications in a form of a chain can lead to a multitude of signal transductions which is referred to as the 'ubiquitin code' (Swatek and Komander, 2016). These polymeric chains can be either short consisting of 2 ubiquitin or long chains with more than 10 ubiquitin known as polyubiquitylation. For example, polyubiquitylation of Mcm7 is a crucial signal that is seen in S-phase and mitotic replisome disassembly (Moreno et al., 2014, 2019a). If the modification occurs on the same lysine residue throughout the ubiquitin chain during elongation, they are called homotypic or homogenous (Figure 1.2 c). If ubiquitylation occurs through the first methionine, it results in linear ubiquitin chains (Figure 1.2 d) and if mixed linkages are involved, then the chains are described as heterotypic or heterogenous (Figure 1.2 e). Sometimes a substrate can be modified by several ubiquitin molecules involving multiple ubiquitin linkages resulting in branched chains (Akutsu et al., 2016)(Figure 1.2 f).

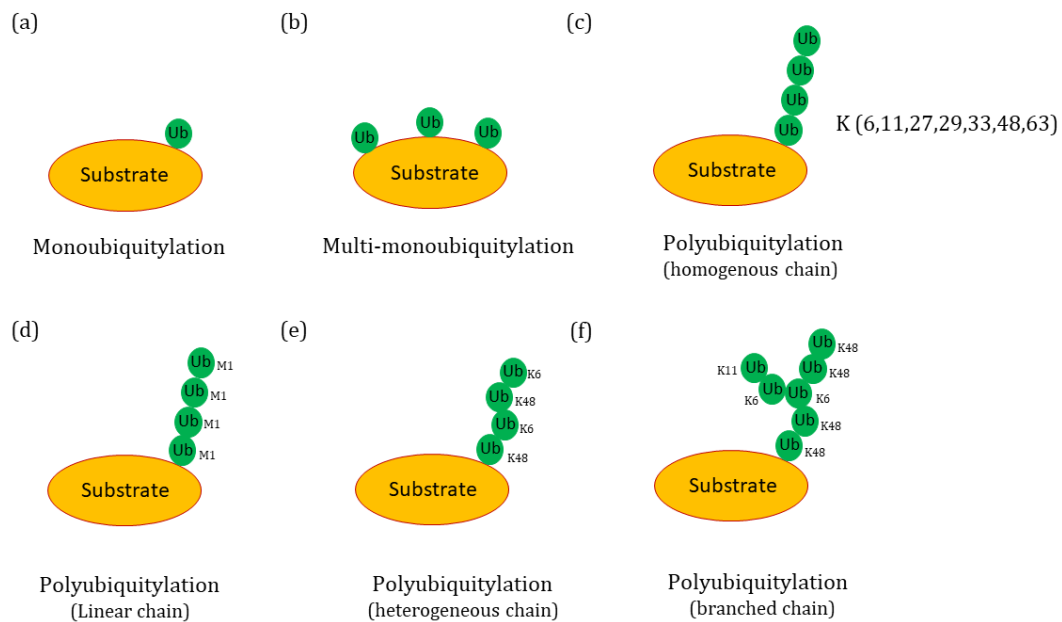


Figure 1.2:- Different types of ubiquitin modifications.(a) Monoubiquitylation. (b) Multi-monoubiquitylation. (c) Polyubiquitylation – Homogenous chain. (d) Linear polyubiquitin chains M1 linked. (e) Heterogenous polyubiquitin chains of K48 and K6-linkages. (f) Branched ubiquitin chains are made of miscellaneous ubiquitin linkages. Yellow represents substrate protein and green represents ubiquitin moiety.

Ubiquitin molecules show a remarkable degree of similarity between yeast and humans differing by only 3 amino acid residues, indicating a conserved role for ubiquitin in its signalling role. Although similar, they generate functionally distinct signals depending on their structure; for example, ubiquitylation can signal for both proteolytic and lysosomal degradation but they differ either in the type of linkages, chain length, ubiquitin conjugate topology or cellular localization of enzymes and substrates to fulfill the function (Pickart and Eddins, 2004; Akutsu et al., 2016). Therefore, the fate of the ubiquitylated protein and its function is influenced by the pattern of ubiquitin chains. These modified ubiquitylated proteins are later recognised by receptors that contain Ubiquitin Binding Domains (UBDs) leading to specific downstream events (Swatek and Komander, 2016). For example, polyubiquitin chains formed via K48-linkages are classically known for proteasomal degradation, monoubiquitylation of PCNA is important during RAD6-

dependent repair of DNA damage (Hoege et al., 2002) and Epidermal Growth Factor Receptors (EGFR) undergo multi-monoubiquitylation as a signal for its movement from the plasma membrane to the lysosome for its degradation (Haglund et al., 2003). Ubiquitin signalling is further regulated by other posttranslational modifications such as acetylation, phosphorylation, and sumoylation (Akutsu et al., 2016; Toma-Fukai and Shimizu, 2021).

Some of the other linkages have been well-established as triggering signals for cross-talk suggesting that ubiquitin can act as a code for signal transmission (Komander and Rape, 2012). The role of K6-linkages in cellular events is still under investigation. K6-linkages are indirectly linked with DNA repair events in association with the BRCA1-BARD1 E3 ubiquitin ligase (Morris and Solomon, 2004; Nishikawa et al., 2004). K6-linkages had been abundantly identified in mitochondrial outer membrane proteins during the depolarisation of these proteins. These linkage types are generated by the E3 ubiquitin ligase Parkin, which is known for its mitochondrial quality control (Ordureau et al., 2014).

K11 ubiquitin chains are generated in Anaphase Promoting Complexes (APC) for proteasomal degradation and mitotic exit (Matsumoto et al., 2010). It has also been reported that only heterotypic K11 chains are targeted readily for proteasomal degradation. K11-linked ubiquitin chains also play a key role in preventing the degradation of Hif1- α , thereby helping to regulate its activity as a transcription factor (Bremm et al., 2014).

K27-linkages are important for DNA damage response. For example, RNF168-mediated damage repair promotes K27-linked ubiquitylation of histone 2A (H2A). K27 chains are also shown to be an important signal in immune responses to microbial DNA (Wang et al., 2014; Gatti et al., 2015).

K29-linkages are generated by HECT E3 ubiquitin ligases and research on human cell lines showed that inhibition of proteasome results in the accumulation of K29-linked ubiquitin chains suggesting its role in proteasomal degradation (Swatek and Komander, 2016). K33-linkages have been shown to have a role in post-Golgi protein trafficking (Yuan et al., 2014).

K48-linked chains, as mentioned above, are the most predominant chain linkage that directs the substrate proteins for proteasomal degradation. Biochemical studies have revealed the minimum requirement for ubiquitin modifications to induce proteasomal degradation. It has been found that a ubiquitin chain containing at least a minimum of 4 ubiquitins is required for degradation and interestingly two di-ubiquitin modifications trigger better degradation than a long chain of 4 ubiquitins (Swatek and Komander, 2016).

K63-linked chains are also extensively studied and responsible for triggering DNA damage response (Komander and Rape, 2012). They have also many non-degradative roles such as regulating the NF- κ B signalling pathway and endocytotic pathway (Swatek and Komander, 2016).

An M1-linkage formed between the N-terminus methionine of ubiquitin and the C-terminus of the next ubiquitin plays a pivotal role in inflammatory and immune responses. It regulates the activation of transcription factor NF- κ B which leads to the activation of cytokine receptors and toll-like receptors, resulting in ubiquitylation and phosphorylation of multiple proteins. It works in combination with K63-linked chains too (Akutsu et al., 2016).

1.1.3 Ubiquitin cascade

The series of biochemical events by which ubiquitin is attached to its target protein is known as the 'ubiquitin cascade'. It involves 3 major steps (Figure 1.3). At first, processed forms of ubiquitin are activated in the presence of ATP and magnesium ions by an E1 ubiquitin-activating enzyme. E1 contains an active-site cysteine to which the glycine at the C-terminus of ubiquitin attaches, resulting in a reactive thioester bond along with the release of AMP. This is known as ubiquitin 'activation'. The E1 then transfers the activated ubiquitin to the catalytic cysteine of an E2 conjugating enzyme to form an E2-ubiquitin thioester complex by the process of 'conjugation'. Finally, an E3 ubiquitin ligase then facilitates the transfer of the ubiquitin from the E2-ubiquitin complex to the target protein. Eventually, an isopeptide bond between a lysine of the target protein and the C-terminal glycine of ubiquitin is generated (Pickart and Eddins, 2004). This cascade controls the ubiquitylation of specific proteins, which leads to post-translational modifications that activate various cellular responses based on the chain type and linkages mentioned earlier. Many enzymes are known to be involved in the ubiquitylation process and it has been reported that the human genome has 2 E1s, ~38 E2s, and about 600-1000 E3s. E3s are the key enzymes that are responsible for the diverse functions of ubiquitin and more understanding of the E3s can help in the development of drugs or inhibitors for clinical use (Ye and Rape, 2009; Akutsu et al., 2016).

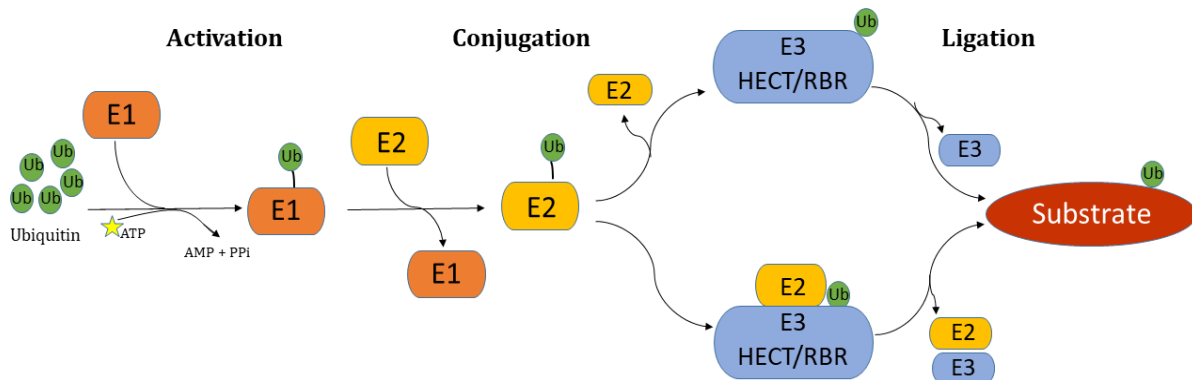


Figure 1.3:- Ubiquitin enzymatic cascade. Initially, ubiquitin (green) undergoes an activation through a mechanism catalysed by the E1 enzyme (orange). This activation involves C-terminal AMPylation of the ubiquitin facilitated by ATP. An intermediate product generated is capable of forming thioester bonds between the catalytic cysteine residues located in the active site of the E1 enzyme and the C-terminus of ubiquitin. This triggers structural changes within the E1 enzyme, enabling the binding of the E2 enzyme (yellow). Ubiquitin is then transferred from the E1 to a catalytic cysteine residue within the active site of the E2 enzyme. Finally, E3 ligase (blue) recognises the E2-Ub complex and facilitates the transfer of ubiquitin from E2 to the target protein (red).

1.1.3.1 E1 activating enzymes

The initial activation step in the attachment of ubiquitin to its substrate is catalysed by E1 activating enzyme and then directs it to downstream pathways. The E1 for ubiquitin is a monomeric protein with a size of 110-120 kDa. In eukaryotes, the ubiquitin-adenylate intermediate interacts with cysteine residue in E1 to form a high-energy ubiquitin-E1 thioester bond along with the release of an AMP. This activated E1 can then interact with several E2s to initiate downstream signalling (Lee and Schindelin, 2008; Schulman and Harper, 2009).

1.1.3.2 E2 conjugating enzymes

After activation of ubiquitin by E1s, the ubiquitin cascade then involves the transfer of ubiquitin from E1 to E2s. The E2s are considered 'ubiquitin carriers' and in yeast and humans, there are 17 and 38 genes, respectively, comprising the E2 family. Active E2s have a ubiquitin-conjugating (UBC) domain consisting of a cysteine residue that is essential for interaction with E1s. The active-site Cys is highly conserved and is located in a shallow groove formed between the α -helices located close to the active site (Ye and Rape, 2009). The binding of E2s to their cognate E1s is highly specific and only happens if the E1 carries its respective modifier. The binding of E1 to ubiquitin triggers a conformational change in E1, which exposes a binding site facilitating E1-E2 interactions (Huang et al., 2007). The ubiquitin from E1 is then transferred to the cysteine residue at the active site of E2 via a thioester bond and such ubiquitin-loaded E2 can cooperate with different classes of E3s downstream. In general, E2s are important as the key determinants of ubiquitin chain formation and chain topology (Ye and Rape, 2009). Several pathological roles of E2s have also been identified in human diseases and some mutations or impairments to E2s can lead to severe disease states, including chromosome instability syndromes, neurodegenerative disorders, cancer, and immunological disorders. The relevance of E2s in human health and disease makes them an appealing class of therapeutic target (Hormaechea-Agulla et al., 2018).

1.1.3.3 E3 ubiquitin ligases

E3 ubiquitin ligases are involved in the final step of the ubiquitin cascade and catalyse the ubiquitylation reaction. There are ~600-1000 E3 ligases present in the human genome. Here, the E3 ligases interact with both E2 and the target substrate enabling the transfer of ubiquitin to the lysine site present on the substrate directly or indirectly. Apart from

lysine, E3s can also interact with serine, threonine, or cysteine residues of the substrate (Zheng and Shabek, 2017). The E3 ligases provide the specificity and regulatory role for the cellular responses to ubiquitylation (Humphreys et al., 2021). Based on the structure, function, and catalytic mode of ubiquitin transfer, E3 ubiquitin ligases have been classified primarily into four different types: HECT (Homologous to the E6-AP Carboxyl Terminus) domain type, RING (Really Interesting New Gene) finger type, U-box type, and RBR (RING-between-RING) type (Yang et al., 2021) (Figure 1.4). Among these, the most abundant E3s are the RING (in humans ~ around 600), followed by HECT (~28), RBRs (~14), and U-box type E3s (in humans ~8) (Metzger et al., 2012; O'Connor and Huibregtse, 2017; Trujillo, 2018).

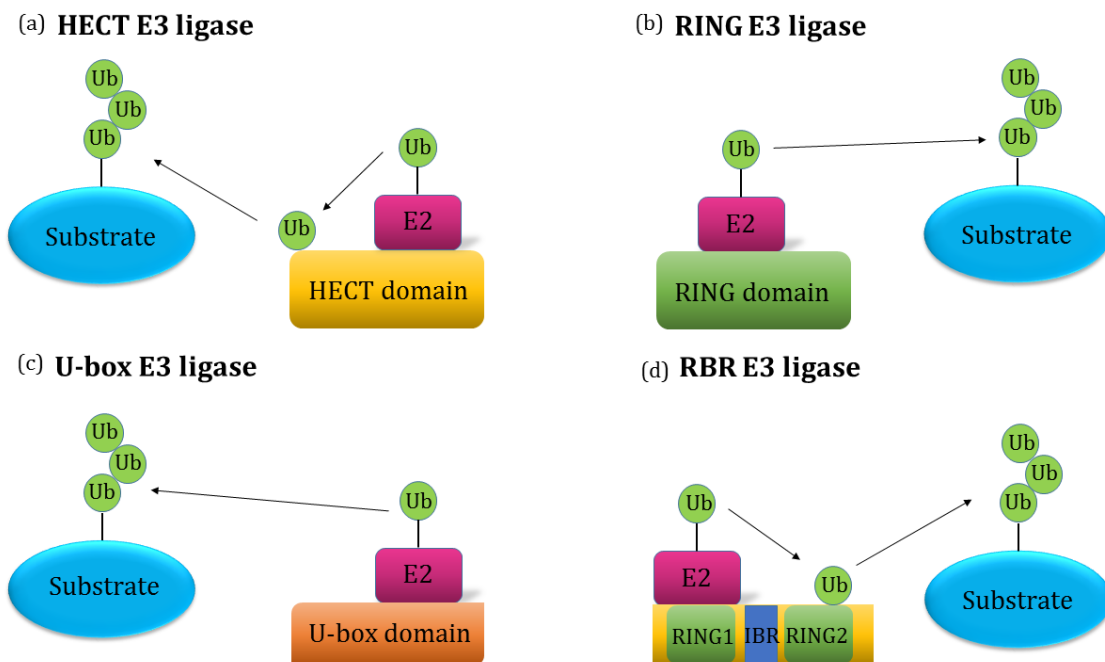


Figure 1.4:- Different types of E3 ubiquitin ligases. (a) HECT E3 ligases exhibit a conserved C-terminus HECT domain and a varying N-terminus. The HECT E3-mediated ubiquitylation is a two-step process where ubiquitin is transferred from E2 to the active cysteine residue on the HECT domain of the E3 ligase. The second step involves the transfer of ubiquitin from the E3 ligase to the target substrate. (b) The RING E3 ligases consist of a zinc-binding domain called the RING finger. RING E3 ligases directly transfer the ubiquitin from an E2 to the target substrate. (c) The U-box E3 ligases possess a U-box domain at the C-terminus where the E2-ubiquitin complex is bound and facilitates the transfer of ubiquitin to the target substrate. (d) The RBR E3 ligases consist of RING1 and RING2 separated by an IBR domain. It utilises the features of both HECT and

RING-type ubiquitin ligases and ubiquitin is transferred in a two-step process where an intermediate is first formed with RING2 and then transferred to the target substrate.

1.1.3.3.1 HECT (Homologous to the E6-Associated Protein Carboxyl Terminus) E3 ligase

HECT E3s consist of a conserved HECT domain (~350 amino acids) located at the C-terminus and have a bi-lobed structure. The C-terminus or 'C-lobe' consists of the active site for cysteine that can form a thioester bond with ubiquitin (Sluimer and Distel, 2018; Qian et al., 2020), whereas the N-terminus or 'N-lobe' is diverse and is involved in interacting with E2. The C and N-lobes are connected using a flexible hinge that allows easy movement for the ubiquitin transfer from E2 to E3 (Figure 1.4 a) (O'Connor and Huibregtse, 2017; Weber et al., 2019). The structural studies propose that these two lobes come closer together during the transfer of ubiquitin (Metzger et al., 2012; Weber et al., 2019). The HECT E3s are subdivided into three groups based on the differences in the N-terminus Nedd4 family (9 members), HERC family (6 members), and HECTs (13 members)(Yang et al., 2021).

The characteristic feature that differentiates HECT from other E3s is the formation of an intermediate thioester bond with ubiquitin before interacting with its substrate (Weber et al., 2019). HECT E3-mediated ubiquitylation is a two-step process whereby ubiquitin carried by the E2 first binds to the HECT domain, which then is transferred to the catalytic cysteine on the E3 ligase. Finally, the ubiquitin from E3 reaches the substrate (Yang et al., 2021).

HECT E3s have been previously shown to play vital roles in cell signalling pathways that regulate growth and proliferation, immune responses, protein trafficking, DNA repair, and immune responses. Their dysfunction or mutations has also been implicated in cancers, neurodegenerative disorders, and diabetes (Weber et al., 2019; Wang et al., 2020).

1.1.3.3.2 RING (Really Interesting New Gene) E3 ligases

RING ubiquitin ligases are the largest family of E3 ligases consisting of ~600 different types in humans. It is conserved from yeast to humans. RING finger consists of a Zn²⁺ finger domain with seven conserved cysteines and one histidine residue (spanning up to 40-60 amino acids) placed in a specific manner. The canonical sequence of this Zinc finger is Cys-X₂-Cys-X₍₉₋₃₉₎-Cys-X₍₁₋₃₎-His-X₍₂₋₃₎-Cys-X₂-Cys-X₍₄₋₄₈₎-Cys-X₂-Cys. This conserved sequence allows stabilising the structure and interaction with the two zinc ions by utilising a 'cross-brace' topology such that the two Zinc ions interact with 4 cysteine residues. The structural analytical studies have shown that all proteins containing a RING finger domain serve as a scaffold in bringing the E2 and substrate together and promoting the direct transfer of ubiquitin to the target protein (Figure 1.4 b) (Garcia-Barcena et al., 2020).

The members of the RING E3s are classified into specific groups based on how their catalytic and substrate recruiting modules are arranged. The different types of RING E3s include monomeric RING finger and multi-subunit RING E3 ligases (Metzger et al., 2012; Yang et al., 2021). Monomeric RING E3s have the domains for both substrate binding and ubiquitylation. Apart from this, they also possess autoubiquitylation properties. TRAF6, Mdm2, and COP1 are examples of monomeric RING E3s. Multi-subunit RING E3s are more complex and diverse but they also possess many common features among themselves (Yang et al., 2021). Examples of multi-subunit E3 complexes include: BRCA1 (breast cancer 1) and BARD1 (BRCA1-associated RING domain 1), Cullin-RING ligases (CRLs) and anaphase-promoting complex (APC) (Zheng and Shabek, 2017). Among these, the Cullin-RING ubiquitin Ligases (CRLs) represent the largest family of multi-subunit RING E3s

(Zimmerman et al., 2010) which can perform distinct functions and are explained in detail in section number 1.2.

The functions of RING E3s can be regulated by different posttranslational modifications such as phosphorylations, neddylation, or ubiquitylation (Yang et al., 2021). Mutations within the key residues that coordinate the Zinc ion interactions or dimerization can lead to protein dysfunction, which can give rise to several human diseases such as cancer or neurological disorders. Therefore, targeting these E3 ligases can be an excellent platform for therapeutic interventions (Garcia-Barcena et al., 2020).

1.1.3.3.3 U-box type E3 ligase

U-box type is a relatively smaller group of ubiquitin ligases and the first example of this family member was isolated from yeast (Wang et al., 2021). U-box ligases consist of a U-box motif located at the C-terminus and have about 70 amino acids that are conserved between yeast and humans. Studies conducted in mammalian cells suggest that the deletion or mutation of the U-box domain leads to the loss of ubiquitylation function proposing that the U-box provides the catalytic activity (Hatakeyama et al., 2004). These ligases possess some similarity in the pattern of amino acid arrangement with RING E3s which potentially contribute to their similarity in protein folding, but they lack the conserved histidine and the RING fingers like in the RING E3s (Ohi et al., 2003). The U-box type ubiquitin ligases function by interacting with the E2 charged with ubiquitin and then facilitate the transfer of ubiquitin onto the lysine site of the substrate (Figure 1.4 c) (Yang et al., 2021).

These ligases are also present in plants, providing signalling pathways in stress response where they act as a central protein modifier for targeting proteins for proteasomal degradation (Sharma and Taganna, 2020). These ubiquitin ligases can also interact with

molecular chaperones and this association helps them to work as ‘quality control E3s’ for the clearance of abnormal proteins (Hatakeyama et al., 2004).

1.1.3.3.4 RBR (RING-between-RING) E3 ligase

RING-between-RING (RBR) E3s are also known as RING-HECT hybrids as they share features of both RING and HECT classes (Zheng and Shabek, 2017). RBR E3s are multi-domain enzymes classed based on the presence of a RING1 domain, a central in-between RING (IBR), and a RING2 domain (Yang et al., 2021). The RING1 domain is where ubiquitin-charged E2s bind, similarly to the RING ubiquitin ligases. The RING2 acts similarly to the C-lobe of HECT E3s where the cysteine residue provides catalytic activity by forming a thioester bond between the catalytic cysteine and C-terminus of ubiquitin. The IBR domain is also heavily populated with cysteine residues but it lacks catalytic and ubiquitylation activity (Spratt et al., 2014) (Figure 1.4 d).

The RBR E3s are known to regulate many biological processes in eukaryotes and there are ~14 different RBRs in the human genome. One example of an RBR E3 is PARKIN that is mutated in Parkinson’s disease. The dysfunction of this gene results in the early onset of the disease. RBRs have also been shown to play a vital role in human diseases such as dementia, inflammation, and cancer making them excellent drug targets (O’Connor and Huibregtse, 2017; Cotton and Lechtenberg, 2020).

1.2 Cullin RING ubiquitin ligases (CRLs)

Cullin-RING ubiquitin Ligases (CRLs) represent the largest family of multi-subunit RING E3. In humans, there are 6 different types of cullins namely: Cul1, Cul2, Cul3, Cul4A, Cul4B, and Cul5 and either of them can form a scaffold within the CRLs (Wang et al., 2016). CRLs contain the catalytic ring subunit Rbx1/Rbx2 (Ring-box protein) which is responsible for

providing ubiquitin ligase activity. These cullin-RING enzymatic cores can take up different architectures by interchanging their substrate receptors, which are responsible for providing substrate specificity towards a diverse range of substrates. Therefore the 6 cullin RING complexes along with their adaptors and substrate receptors in different combinations lead to more than 500 CRL family proteins (Zimmerman et al., 2010). A schematic model of Cullin Ring Ligases is represented in Figure 1.5. Members of the cullin family proteins are known to function in a varied range of cellular activities like signal transduction, transcription, and cell cycle (Wang et al., 2016).

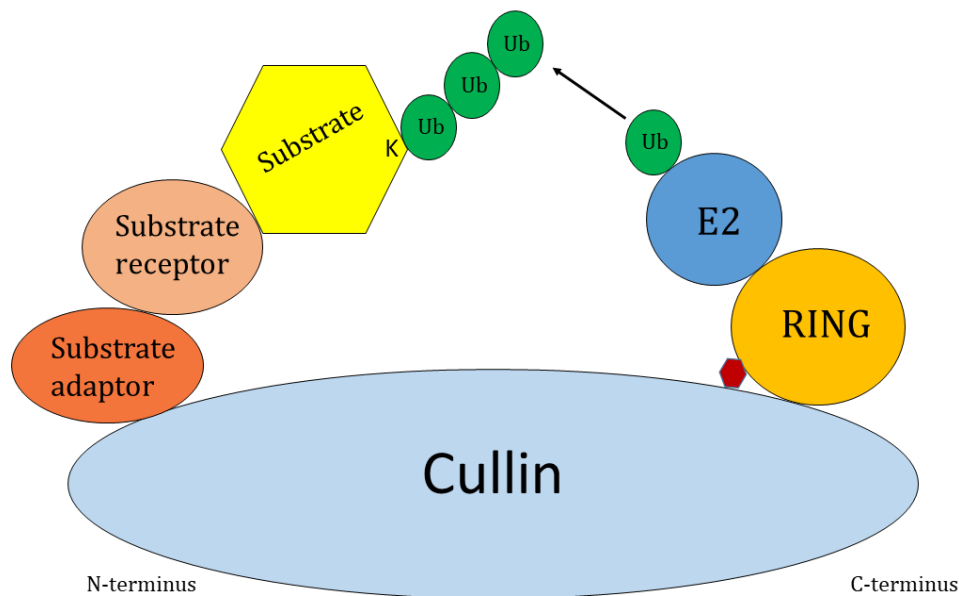


Figure 1.5:- Schematic representation of Cullin Ring Ligases (CRLs). Cullin RING ligases (CRLs) are characterized by a cullin protein scaffold (blue) and a catalytic core comprising the RING domain (deep yellow) at the C-terminus. The N-terminus of cullins interacts with the substrate adaptor (orange) and receptor (brown) to which the substrate binds. The activation of cullins requires neddylation by Nedd8 (red) which is close to the RING domain. This results in ligase activation and ubiquitin transfer from the E2 to the target substrate.

Interestingly, the enzymatic activity of the CRLs is determined by a ubiquitin-like protein, NEDD8. Neddylation of cullins takes place via the activation of a NEDD8-specific E2 by the Rbx RING domain. This neddylation is a reversible process; therefore, the cullins can also

become de-neddylated by the enzyme COP9 signalosome holo-complex (CSN). In this manner, the activity of cullins is regulated. It was suggested that neddylated CRLs interact with a different type of E3 ligase such as RBR E3 ARIH1 which adds the first (priming) ubiquitin moiety to the substrate. Further extension of these monoubiquitylated substrates is facilitated by the traditional CRL mechanism involving E2s (Scott et al., 2016).

Part of this PhD project focuses on the function of Cullin2 based CRL during replisome disassembly. Cullin2 along with its RING-domain subunit forms CRL2/Cullin2-RING ubiquitin ligase. The C-terminus of cullins interacts with the RING domain-containing proteins Rbx1 or Rbx2, which confer the ubiquitin ligase activity. The N-terminus associates with the variant substrate recognition subunits and adaptor/linker proteins responsible for substrate recruitment. The Elongin BC complex acts as an adaptor connecting Cul2 subunit to the substrate receptor (Zimmerman et al., 2010). Some of the variant substrate recognition receptors of Cullin2 include von Hippel-Lindau (VHL), LRR1, FEM1, PRAME, and ZYG-11 (Wang et al., 2016). In this PhD project, I have attempted to study the structure of Cullin2^{Lrr1} ubiquitin ligase.

1.3 DNA replication

Cell division is a fundamental process involved in the existence of life. Each time a cell divides the genetic material from the parent cell is duplicated by DNA replication and passed on to the daughter cells. This forms the basis for genome maintenance. However, this process is highly regulated such that it occurs only once per cell cycle. During replication, there are efficient proofreading and repair mechanisms that facilitate the exact duplication of the genome. Nevertheless, errors can occur and when left unrepaired, they can lead to the accumulation of mutations. These mutations can affect the cell

behaviour and have severe consequences leading to genetic disorders, aging, chromosomal aberrations, or even drive tumorigenesis or other pathological diseases (Blow and Dutta, 2005; Kang et al., 2018).

The eukaryotic cell cycle consists of distinct phases namely G1 (unreplicated DNA), S-phase (DNA synthesis), G2 (replicated DNA) - together known as Interphase, and M (mitotic) phase. The G1 phase prepares the cell for DNA synthesis and the G2 phase prepares for the entry into mitosis. The central factors that control these cell cycle events are CDKs (Cyclin Dependent Kinases) and Cyclins. These are holoenzymes comprising Cyclins as regulators and CDKs as catalytic subunits. CDKs on their own have no enzymatic activity and the binding of CDK to a cyclin is a prerequisite for its activation. During distinct phases of the cell cycle, CDKs associate with specific cyclins and this partnership allows the transition through different phases (Figure 1.6). The activation of these proteins depends on the phosphorylation or dephosphorylation of specific amino acids. The cyclic expression of cyclins is facilitated by the presence of PEST (Proline (P), Glutamate (E), Serine (S), and Threonine (T)) sequence motifs in Cyclins, which target them for degradation or expression at specific times (Schafer, 1998).

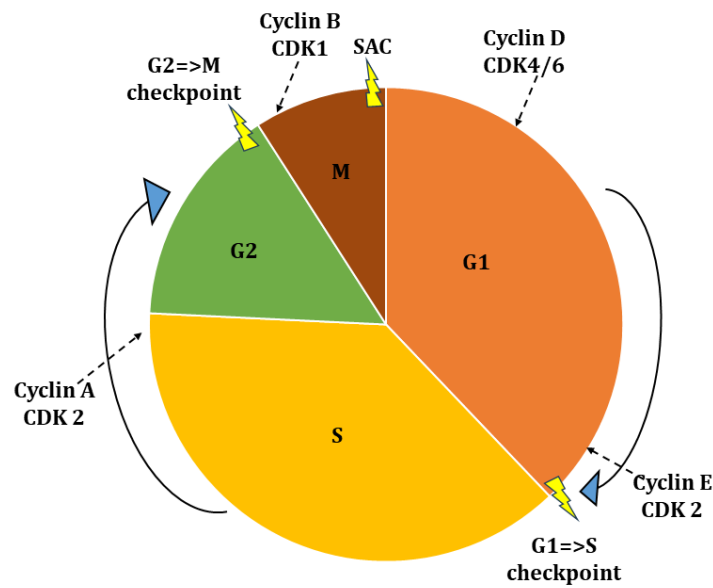


Figure 1.6:- Schematic drawing of cell cycle progression of multi-cellular organisms. Major stages of the cell cycle are represented as G1 (orange), S (yellow), G2 (green), and M (brown) and their progression is regulated through various Cyclin CDK complexes as depicted in the figure. G1=>S, G2=>M, and Spindle Assembly Checkpoint (SAC) represent the major checkpoints. The arrow indicates the direction of progression of the cell cycle.

Cyclin D/CDK4 and Cyclin D/CDK6, functioning during mid-G1, regulate the cell cycle progression from G1/S. The late G1 phase is governed by Cyclin E/CDK2 (Galderisi et al., 2003) and allows entry into S-phase. Cyclin A in combination with Cdk2, synthesised at the onset of the S-phase allows DNA synthesis and progression through the G2 phase (Coverley et al., 2000). Both Cdk2/Cyclin A and Cdk1/Cyclin B regulate progression from the G2 phase to the mitotic phase and Cdk1/Cyclin B participates and completes mitosis and chromosome segregation (Satyanarayana and Kaldis, 2009).

DNA replication involves three major steps: initiation, elongation, and termination. Initiation of replication begins at specific places in the DNA called origins of replication (ORIs). Bacterial genomes are single circular DNA molecules and typically have a single replication initiation region named 'Ori C'. The two replisomes initiating from the Ori C travel in the opposite direction, generating a replication bubble and completing the

genome duplication with the aid of DNA polymerases. The timings for the completion of replication depend on the size of the genome (Costa and Diffley, 2022). While some archaea employ multiple origins of replication to initiate DNA replication, eukaryotic genomes consist of multiple chromosomes. To ensure complete genome duplication in a timely manner, the number of origins ranges from 100s – 50,000s depending on the complexity of the organisms (Fragkos et al., 2015). However, not all origins are activated at the same time. Some remain dormant and are activated only during replication stress or fork stalling to serve as rescuers (Courtot et al., 2018). Once replication is initiated, the core of the replisome, DNA helicase, unwinds the DNA and the formed replication forks move through the chromatin synthesising the new DNA until they meet another converging fork coming from a neighbouring origin in an opposite direction, which is when replication terminates (Moreno and Gambus, 2015).

These different stages of replication utilise numerous multi-protein complexes and are highly regulated at each step.

1.3.1 Initiation

The initiation of DNA replication spans two different stages of the cell cycle. This is a two-step mechanism involving ‘origin licensing’ and ‘origin firing’. Budding yeast has widely been used as a model system for understanding replication initiation and pre-replication complex formation. In yeast, there are multiple replication initiation origins defined by the presence of DNA sequences called Autonomously Replicating Sequences (ARSs). ARSs are made of ARS Consensus Sequences (ACSs) and B elements. ACS forms the binding site for Origin Recognition Complex (ORC) and is essential for the functioning of the origins. The B elements present at the origins help in enhancing the origin functioning. The

origins are occupied by the ORCs and are melted during the initiation of replication (Kang et al., 2018).

There are no well-defined origin recognition sequences for higher eukaryotes. They are generally found to be overlapping with the transcription start sites and CpG islands. ORC binding to origins is followed by binding of Cdc6 forming the ORC-Cdc6 complex, which, with the help of the Cdt1 factor, loads Mini Chromosome Maintenance 2-7 (Mcm2-7) complexes onto the origin. This forms the pre-Replicative complex (pre-RC) and constitutes 'origin licensing'. It happens during late mitosis and G1 phase of the cell cycle when the CDK levels are low (Costa and Diffley, 2022).

The Mcm2-7 core of the helicase complex consists of six subunits, forming a hexameric structure. Each subunit contains an AAA+ ATPase site. The complex is organized into two tiers: one tier is comprised of the N-terminal domains of Mcm2-7, while the other tier consists of the C-terminal AAA+ domains of Mcm2-7. In yeast, the association of Mcm2-7 with Cdt1 results in the formation of a heptameric complex. Cdt1 binds to the flexible N-terminal domains of Mcm2, Mcm4, and Mcm6, leading to the stabilization of the heptameric complex. This Mcm-Cdt1 complex is then recruited to the ORC-Cdc6 which is together represented as the OCCM complex (Kang et al., 2018). The Mcm complexes loaded onto the DNA are in the form of double hexamers and are loaded in a head-to-head orientation such that the N-termini face each other and the C-terminus AAA+ domains are located at the opposite ends. The loading takes place one hexamer at a time. When the Mcm-Cdt1 complex is recruited, the Mcm2-7 contains an open gate in between Mcm2 and Mcm5 to allow clamping onto the DNA. Once the OCCM complex is formed, the Cdc6 is released. This is followed by the release of Cdt1 and closure of the Mcm2-5 gate leaving ORC and Mcm2-7 on the DNA. At this stage, a second Cdc6 binds to the ORC and leads to

recruitment of the second Mcm2-7 complex. Finally, Cdc6 and Cdt1 are released from the intermediate structure leading to the closure of the second Mcm2-5 gate followed by the release of ORC (Figure 1.7). Structural analysis of the Mcm hexamer recruitment also suggests that only one ORC is involved in recruiting both hexamers (Costa and Diffley, 2022).

The energy required for the licensing is provided by ATP binding and hydrolysis facilitated by Mcm2-7, ORC, and Cdc6, which all belong to the AAA+-ATPase family (Coster et al., 2014).

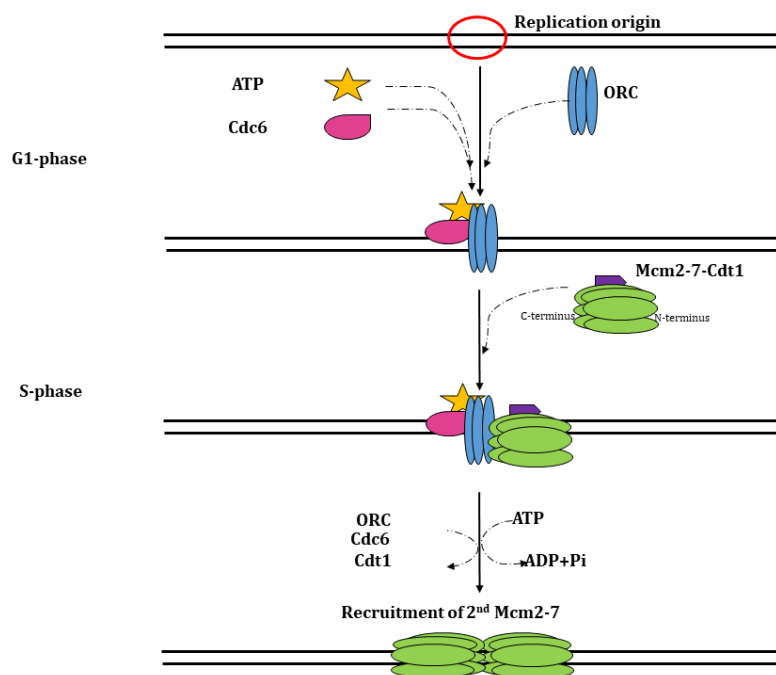


Figure 1.7:- Schematic representation of origin licensing. The Binding of ORC complexes and other proteins such as Cdt1, Cdc6, and Mcm2-7 results in the generation of pre-RC complex during the G1 phase of the cell cycle. The binding of the ORC (Origin Recognition Complex) to replication origins is ATP-dependent, and it binds together with Cdc6. This ORC-Cdc6 complex facilitates the recruitment of MCM2-7-Cdt1. Through ATP hydrolysis, the MCM ring changes from an open to a closed conformation around the DNA, leading to the dissociation of Cdt1 and leaving Mcm2-7 and ORC on DNA. The binding of a second Cdc6 then allows the recruitment of 2nd Mcm2-7.

Studies conducted in *Xenopus laevis* egg extracts and Hela cells suggest that Mcm2-7 are loaded onto chromatin in excess. There are approximately 10-20 Mcm2-7 double

hexamers loaded onto each origin (Laskey and Madine, 2003). Although the Mcm2-7 complexes are loaded in excess, only about 10% of them are initiated for replication, while the majority remains dormant. This is known as the MCM paradox. The excess Mcm2-7 double-hexamers can become activated in the event of replication fork defects such as fork stalling or slower replication rate (Ge et al., 2007; Ibarra et al., 2008).

The second stage of replication initiation is 'origin firing', which is triggered by activation of the helicase. Although Mcm2-7 is regarded as the core of the replisome, it stays enzymatically inactive until additional factors - Cdc45 and GINS complex are attached to it (MacNeill, 2010). As the cell cycle progresses into the S-phase, Cdc45 (Cell division cycle 45) and GINS (Go-Ichi-Nii-San, meaning 5-1-2-3 in Japanese), consisting of 4 subunits Sld5 (Synthetic lethal with Dpb11), Psf1, Psf2, and Psf3 (Partners of Sld5 1, 2 and 3, respectively), associate with the hexameric Mcm2-7 resulting in the formation of CMG (Cdc45-Mcm-GINS)(Costa et al., 2011; Gambus et al., 2006; Yardimci et al., 2010) (Figure 1.8). Nine factors required for activation of helicase have been identified in *S.cerevisiae* namely DDK (Dbf4 dependent kinase), CDK, Sld3/7 (higher eukaryotes Treslin/MTBP), Dpb11 (higher eukaryotes TopBP1), Sld2 (higher eukaryotes RecQL4), Cdc45, DNA polymerase ϵ , GINS and Mcm10 (Yeeles et al., 2015; Heller et al., 2011). DDK phosphorylates Mcm2-7 double hexamers followed by recruitment of Sld3/7 and Cdc45 (Tanaka et al., 2011). CDK phosphorylates Sld2 and Sld3. Dpb11 recognises and binds phosphorylated Sld2 and Sld3, while interacting with GINS and DNA Polymerase ϵ resulting in the active CMG complex formation (Heller et al., 2011; Muramatsu et al., 2010; Zegerman and Diffley, 2007). These molecular events switch on the helicase activity and Mcm10 allows the separation of double hexamers of Mcm2-7 (Quan et al., 2015). The activated helicases move bidirectionally generating two forks and replicating the inter-

origin sequences. This whole process is less well defined in higher eukaryotes. However, recent research has shed light into the orchestration of initiation process in higher eukaryotes. Initiation factors such as Treslin/MTBP and TopBP1 has been shown to be crucial for the assembly of the active CMG helicase. Specifically, these factors play a vital role in the loading of Cdc45 and GINS onto Mcm2-7 helicase (Kumagai et al., 2011; Volpi et al., 2021). Very recent investigations, has identified DONSON as a novel replication initiation factor, essential for loading Cdc45 and GINS onto origins. DONSON achieves this through a direct interaction with TopBP1, and intriguingly, this interaction is dependent on CDK activity (Hashimoto et al., 2023; Kingsley et al., 2023; Lim et al., 2023; Xia et al., 2023).

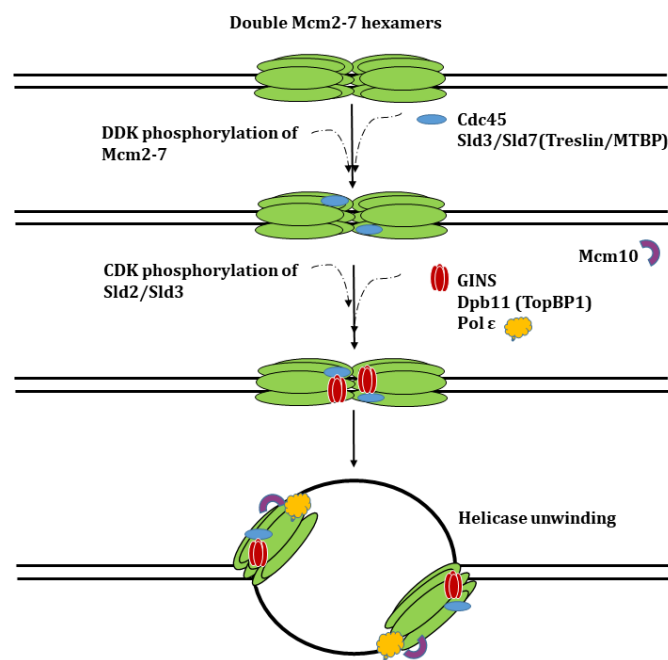


Figure 1.8:- Schematic representation of origin firing. S-phase is marked by the activation of the replicative helicase. Initially, the MCM2-7 complex is phosphorylated by DDK (Dbf4-dependent kinase), which enables the recruitment of Cdc45, Sld3/Sld7. CDKs (Cyclin-dependent kinases) phosphorylate Sld2 and Sld3, leading to the binding of GINS, Dpb11, Mcm10, and Polε to the complex. This result in the activation of the helicase and the MCM double hexamers separate and two CMG helicases move bidirectionally.

To maintain genome integrity and prevent re-replication the loading and activation of helicases are highly regulated. Loading of helicases in the G1 phase requires low CDK activity whereas helicase activation in S-phase needs high CDK activity. The re-replication of DNA in higher eukaryotes is prevented by inhibition of origin licensing in the S-phase (Fragkos et al., 2015). In S and G2 phases, Geminin acts as an inhibitor of DNA replication licensing by forming an inhibitory complex with Cdt1 thus preventing pre-RC formation. In humans, Cdt1 can also be degraded in S-phase by 2 different ubiquitin ligases SCF-Skp2 and DDB1-Cul4 which are activated following Cdt1 phosphorylation by Cdk2 or Cdk4 (Wohlschlegel et al., 2000; Nishitani et al., 2006; Kang et al., 2018). In *Xenopus laevis*, once the first Mcm2-7 hexamers are recruited Cdc6 becomes rate limiting and thereby prevents any reloading of MCMs in the later stages of the cell cycle. Such regulatory mechanisms ensure that replication occurs only once per cell cycle (Kang et al., 2018).

1.3.2 Elongation

Replication elongation begins once the helicase starts unwinding the double-stranded DNA and the forks move bi-directionally, synthesizing new DNA in the 5' to 3' direction. The CMG helicase travels in the 3'-5' direction on the leading strand of the template DNA. Due to the antiparallel nature of the DNA, the helicases travel in the opposite direction generating a replication bubble. It is important to note that while DNA polymerases synthesise new strands in the 5' to 3' direction, the overall direction of DNA replication is depicted as 3' to 5' relative to the parental template strand, reflecting the movement of the replication machinery along the template (Georgescu et al., 2017). The replicative helicase interacts with a group of other proteins that coordinate the progression of DNA synthesis. A schematic of the helicase along with other replication machinery is shown in Figure 1.9. The leading strand DNA is continuously synthesised whereas the lagging

strand is synthesised intermittently in the opposite direction of the fork movement. The leading strand and lagging strand DNA are synthesised by Pol ϵ and Pol δ , respectively (Kang et al., 2018). It has been demonstrated that polymerase δ also plays a role in stimulating leading strand synthesis (Yeeles et al., 2017). Pol ϵ exhibits a remarkable ability to proofread its replication errors, delivering highly accurate DNA synthesis. In fact, Pol ϵ surpasses the accuracy of proofreading-proficient Pol δ and significantly outperforms the proofreading-deficient Pol α in terms of DNA synthesis accuracy. The efficient self-proofreading mechanism employed by Pol ϵ ensures the faithful replication of the leading strand DNA (Burgers and Kunkel, 2017).

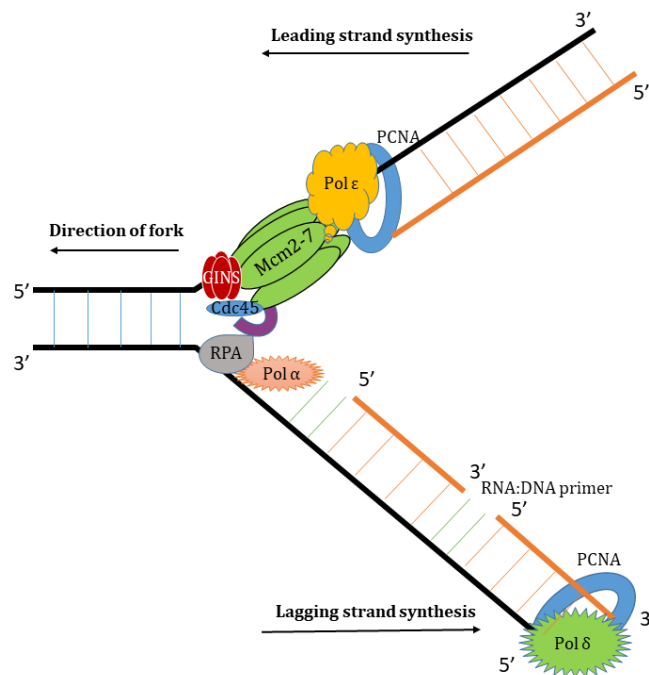


Figure 1.9:- Replicating fork with helicase. The CMG helicase complex is located at the leading strand at the tip of the replication fork and unwinds the dsDNA in a 3' to 5' direction. Leading strand synthesis is continuous and carried out by Pol ϵ in the 5' to 3' direction. The lagging strand synthesis occurs in a discontinuous manner. It begins with the priming activity of Pol α resulting in the formation of an RNA: DNA primer, followed by elongation carried out by Pol δ .

During the process of elongation, single stranded DNA is exposed as a result of unwinding by CMG. This acts as a template for priming by Pol α /primase. DNA Pol α has RNA primase

and DNA polymerase activity. The Pol α initiates DNA synthesis on the lagging strand of the DNA by generating short RNA primers of 7-14 nt using its primase activity. The primer is extended by addition of dNTPs by the Pol α polymerase activity up to 10-20 nt, forming the initial Okazaki fragment (Sheaff and Kuchta, 1993; Nethanel et al., 1988). The recruitment of DNA Pol α to the lagging strand takes place with the aid of Mcm10 and Ctf4. A homo-trimeric Ctf4 interacting peptides present within the Sld5 subunit of GINS and the Pol α facilitate this interaction and bridging with CMG (Simon et al., 2014). Since Pol α lacks the proof reading ability, further primer extension is carried out by two other polymerases, Pol δ and Pol ϵ . These polymerases continues to extend the Okazaki fragments in the opposite direction of the fork movement (Lööke et al., 2017; Kang et al., 2018). The strand displacement capability of Pol δ allows for the displacement of RNA-DNA primers that were generated by Pol α (Zheng and Shen, 2011). The displaced primers are cleaved by FEN1 (5'-flap endonuclease 1) or Dna2 and the nicks generated as a result are completed by DNA Pol δ and finally joined by DNA ligase I to form continuous strands of DNA. To maintain genomic integrity, it is important to remove the segment generated by DNA Pol α as it lacks proof-reading activity (Kang et al., 2018; Attali et al., 2021).

Pol δ , FEN1, and ligase form the core machinery responsible for the maturation of Okazaki fragments. This is facilitated by interaction with PCNA, as the three enzymes contain PCNA interaction motifs. Pol ϵ is not suitable for functioning as the polymerase for lagging strand synthesis because it lacks strand displacement capability (Burgers and Kunkel, 2017). During replication, PCNA forms a ring-shaped sliding clamp for DNA Pol ϵ and Pol δ and enhances its processivity. Once the DNA synthesis is initiated by DNA Pol α , the Replication factor C (RFC) binds to PCNA and this results in the opening of the PCNA ring. This opening triggers the binding of the RFC/PCNA complex to the primer-template junction. Using ATP hydrolysis, RFC is then released, leading to the closure of the PCNA

ring, leaving it securely at the primer junction of Okazaki fragments (Yao and O'Donnell, 2012). Overall, PCNA orchestrates replication events at the fork and during synthesis. It also coordinates other activities such as DNA repair e.g. mismatch repair, nucleotide excision repair, Okazaki fragment maturation, epigenetic inheritance and cell cycle control (Boehm et al., 2016).

Multiple studies in yeast have demonstrated that efficient DNA synthesis relies on the presence of other replisome proteins, namely Mrc1 (Mediator of Replication Checkpoint Protein 1) and Tof1 (Time of Fork 1)/Csm3 (Chromosome Segregation in Mitosis 3). Mrc1 acts as a scaffold protein at replication forks and has been found to interact with polymerase ϵ , indicating its involvement in coordinating the replication process. Tof1 and Csm3 form a complex which also interacts with replication machinery at the replication fork. Similar to Mrc1, Tof1-Csm3 are also involved in the stabilisation of the replication fork and preventing fork collapse during replication stress. Mrc1, Tof1, and Csm3 together form a heterotrimeric complex, Replisome Protection Complex (RPC), that not only contributes to DNA synthesis but also acts as a replication checkpoint-specific mediator and activates the effector kinase Rad53 when replication encounters difficulties. This suggests that these proteins have a dual function in regulating DNA replication and ensuring its fidelity (Bando et al., 2009). Additionally, biochemical studies have identified these three proteins to be part of the replisome progression complex including CMG and other proteins (Gambus et al., 2006).

Apart from these, the unwinding of DNA by the helicases also generates topological stress within DNA in front of the fork called positive supercoiling. This needs to be resolved for the smooth progression of the forks and is accomplished by Topoisomerases I and II. Topoisomerase I acts ahead of the fork and Topoisomerase II is behind the fork. The

coordination of chromosomal replication with the disassembly of parental nucleosomes and the assembly of new nucleosomes also plays a crucial part during DNA synthesis. Histone chaperones such as Asf1 and FACT are important for chromatin remodelling (Kang et al., 2018).

1.3.3 Termination

Termination occurs when two forks from neighbouring origins meet each other and this can happen throughout the S-phase. Genome-wide studies in yeast and human cells have shown that termination occurs around the mid-points between two activated origins (Petryk et al., 2016). The exact location of termination events depends on the relative origin activation timing, as well as efficiency of the progression of each fork (Yardimci et al., 2010; Hawkins et al., 2013). But as replication progresses, the torsional stress generated as a result of the unwinding of parental DNA generates many positive supercoils, which can also cease replication. To avoid this, these supercoils are dealt with type I DNA topoisomerases (Top I) ahead of the fork. When Top I is unable to access the DNA due to space constriction, however, the torsional stress can be released by fork rotation instead. In this way, the torsional stress is translated to the newly synthesised DNA behind the fork, resulting in intertwined sister chromatids that are known as pre-catenanes (Keszthelyi et al., 2016). The entangled pre-catenanes are resolved only by type II topoisomerases (Top II). This process is regarded as one of the first termination-specific events (Dewar and Walter, 2017). In bacteria and viruses, Top II is involved in separating the pre-catenanes to allow for convergence, while in yeast and higher eukaryotes, the depletion of Topo II does not block fork convergence but affects the efficiency of fork convergence (Xia, 2021).

Studies investigating replication events in *Xenopus laevis* egg extracts, utilising plasmid DNA, have shown that during fork convergence the two replicative helicases pass each other on the opposite strands. This is due to the anti-parallel nature of DNA. Polymerases continue replication until they encounter Okazaki fragments from the opposite lagging strand (Dewar et al., 2015). Once the last bit of parental DNA is replicated, the replisomes undergo dissociation to prevent re-replication and avoid interfering with other chromatin-based processes like transcription or subsequent rounds of replication. Interestingly, the disassembly mechanism does not act on replisomes that are actively engaged in replication (Dewar and Walter, 2017).

1.3.4 Fork convergence and replisome disassembly

As the active replisome progresses along the leading strand template, when it encounters a replication fork coming in the opposite direction from the neighbouring origin, the two replisomes will be positioned on the complementary strand, enabling efficient bypass. Once Okazaki fragment maturation and bypass are completed, replisomes are disassembled from chromatin. It is important to note that replication termination mechanisms are highly conserved between species. During termination, in yeast and higher eukaryotes, the replisomes ready for disassembly are marked by K48-linked polyubiquitylation of the Mcm7 subunit by SCF^{Dia2} (yeast) or Cul2^{Lrr1} (higher eukaryotes and mammalian cells), which in turn is recognised by p97 ATPase segregase (Cdc48/VCP) (Maric et al., 2014; Moreno et al., 2014; Dewar et al., 2017a; Sonnevile et al., 2017). Recent investigations have highlighted that p97 collaborates with its cofactors Ufd1, Npl4, and Ubxn7 to effectively unload replisomes from chromatin (Maric et al., 2017; Fujisawa et al., 2022; Tarcan et al., 2022). A schematic representation of the replisome disassembly pathway has been shown in Figure 1.10.

A breakthrough in the replisome disassembly field was made when a new backup pathway for replisome disassembly was reported using *C. elegans* early embryos, *Xenopus laevis* egg extracts, and mammalian cells. The E3 ubiquitin ligase TRAIP ubiquitylates the Mcm7 subunit of any replisomes remaining on chromatin in mitosis with K63-linked chains. Intriguingly, like the S-phase pathway, mitotic disassembly was also dependent on the activity of p97 segregase (Deng et al., 2019; Moreno et al., 2019a; Sonnevile et al., 2019a; Villa et al., 2021).

An outstanding question regarding the regulation of termination factors was the ability to distinguish between active and terminated replisomes. Recent studies suggested that the ubiquitylation of CMG is suppressed during elongation to prevent fork collapse and is only permitted by the presence of Y-shaped fork DNA at termination (Deegan et al., 2020; Low et al., 2020). Cryo-EM analysis of terminating replisomes from yeast and mammalian cells however, shed further light on this conserved mechanism, depicting that both Lrr1 and Dia2, although structurally different, bind to CMG by interacting via Mcm3 and Mcm5 zinc fingers. This interaction is interrupted during elongation by the excluded lagging strand and is only permitted when this excluded strand is lost as a result of the completion of DNA synthesis (Jenkyn-Bedford et al., 2021). On analysis of recombinant *X. laevis* Cul2^{Lrr1}, it has been suggested that a flexible PH domain of Lrr1 facilitates targeting the terminated replisomes. It has also been identified that the RING domain of the Cul2^{Lrr1} complex is placed near the N-terminus of Mcm7 to allow for ubiquitylation and the LRR subunits are located near Mcm3/5 zinc fingers to sense the presence of the lagging strand (Zhou et al., 2021).

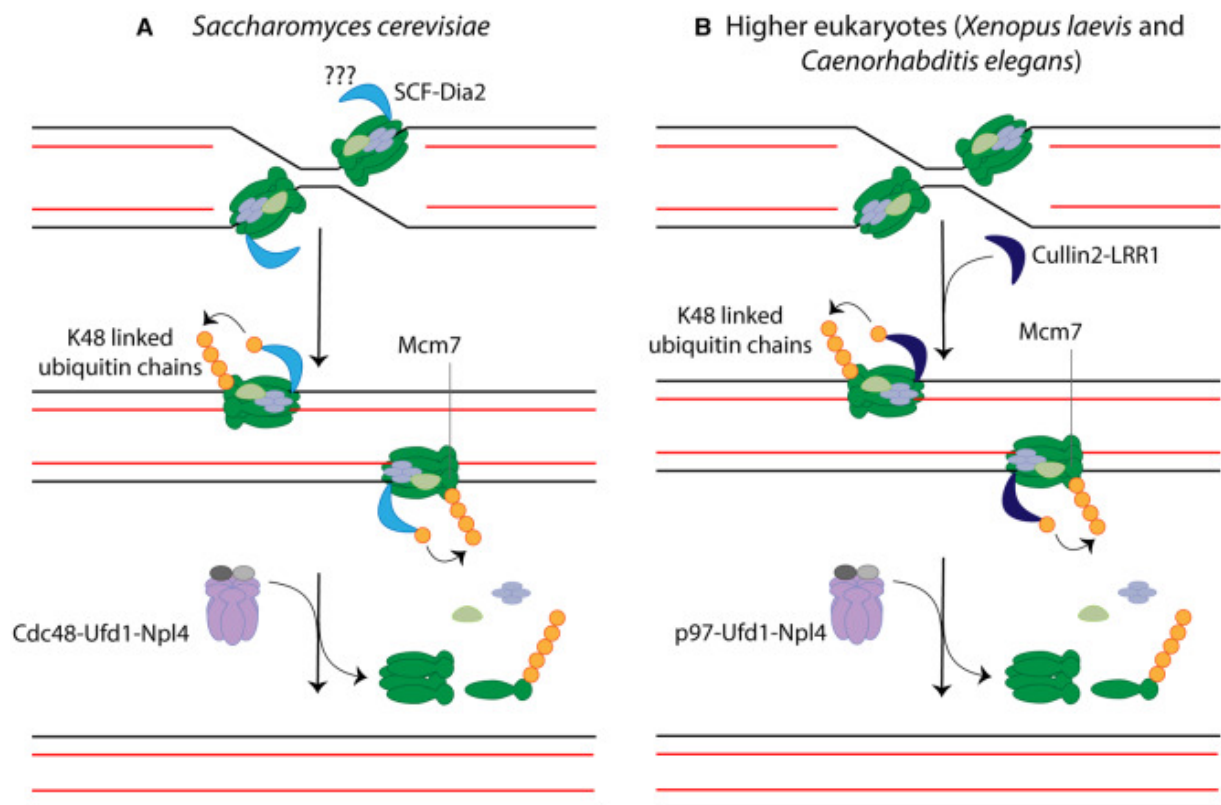


Figure 1.10:- Schematic representation of replisome disassembly pathway. (a) Replisome disassembly in *S. cerevisiae*. SCF^{Dia2} promotes CMG ubiquitylation on its Mcm7 subunit during termination by adding K48-linked ubiquitin chains. CMG ubiquitylation triggers the recruitment of Cdc48-Ufd1-Npl4, leading to replisome disassembly. (b) Replisome disassembly in higher eukaryotes. Cullin2^{Lrr1} promotes CMG ubiquitylation of Mcm7 subunit with K48-linked ubiquitin chains. The ubiquitylated replisome is subsequently disassembled by p97-Ufd1-Npl4. Figure reproduced from (Moreno and Gambus, 2020).

1.4 Replication stress and its consequences on genome stability

DNA replication is a highly accurate process with a remarkably low error rate. Nevertheless, the fidelity of this process is often challenged by many external and internal sources. The impediment of the progression of replication forks can lead to reduced replication fidelity, fork slowing or stalling, and even DNA breaks. Such difficulties confronted by the replication machinery are referred to as replication stress (Saxena and Zou, 2022). Replication stress can arise from different sources. Few examples include DNA lesions caused by ultraviolet (UV) light or oxidative DNA damage, exposure to a wide

range of genotoxic agents used in cancer therapies to target DNA replication, oncogene activation. In addition, unregulated firing of origins, misincorporation of ribonucleotides, transcription- replication conflicts (TRCs), DNA-RNA hybrids, secondary DNA structures, telomeres and even dysregulated repair processes all contribute to replication stress (Mazouzi et al., 2014; Zeman and Cimprich, 2014; Berti and Vindigni, 2016) (Figure 1.11). Cells activate various response pathways depending on the type of stress that interferes with the replication forks. These pathways serve to stabilize, repair, and restart the forks, ultimately ensuring the timely duplication of the genome and thereby maintaining genome stability (Berti and Vindigni, 2016).

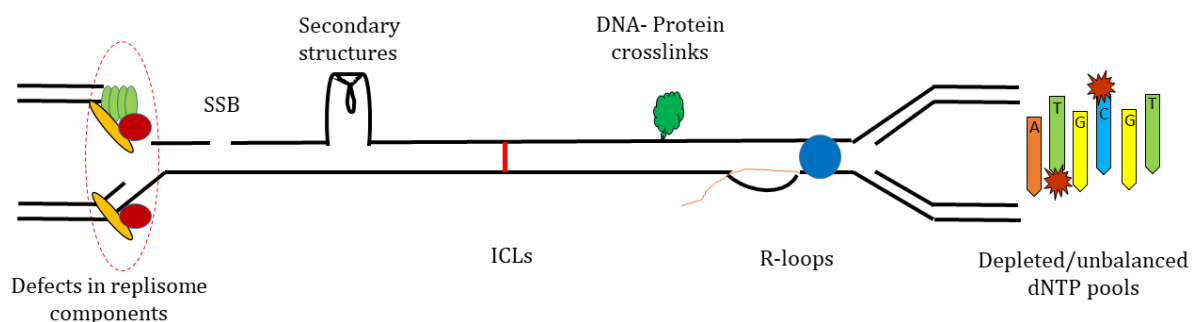


Figure 1.11:- Some of the different causes of replication stress. Endogenous or exogenous sources of replication stress can slow or stall forks. A few examples include faulty replisome components, secondary structures and transcription-replication conflicts or hard to replicate DNA, and unbalanced dNTP pool all can lead to impaired fork progression.

Three major replication stress responses can be observed at the sites of stressed replication forks: ATR (Ataxia Telangiectasia and Rad3 Related) checkpoint activation, fork remodeling, and activation of DNA repair pathways. Replication stress can disrupt

the coordination between the helicases and polymerases resulting in the exposure of ssDNA. Replication protein A (RPA) coats the ssDNA to protect it from nuclease attack. Long stretches of RPA coated ssDNA, highlights the presence of stressed forks in the S-phase and results in the recruitment and activation of ATR checkpoint kinase. The activated ATR stabilises the halted replication forks and activates signalling pathways at these forks (Saxena and Zou, 2022). ATR activation inhibits cell cycle progression and regulates intracellular dNTP levels to allow proper repair and restart. ATR activation also initiates phosphorylation to regulate the activity of replisome components and fork remodeling enzymes (Berti and Vindigni, 2016). In response to stress, forks can also undergo fork remodeling where the stressed forks are converted into four- way junctions thereby regulating the fork speed and enabling repair. In addition to this, there are also various DNA repair pathways or tolerance pathways that are activated at stressed forks and enables them to bypass or recover from stress, for example: translesion synthesis (TLS), PrimPol- mediated repriming, template switching (TS), break-induced replication (BIR) and homologous recombination (HR) (Cortez, 2015; Berti et al., 2020). These coordinated responses collectively tackle the replication stress.

A brief description of some known sources of replication stress are given below.

1.4.1 Replication fork barriers

Any obstacle that comes in the way of fork progression hampers the progression of DNA synthesis and these perturbations can interfere with the forks either directly or indirectly. Most commonly recognised roadblocks include DNA lesions/adducts that arise from UV or DNA alkylating agents (eg: methyl methanesulfonate), reactive oxygen species (ROS), interstrand crosslinks (ICLs) that are caused by cisplatin, mitomycin C, camptothecin etc. In addition, the presence of DNA sequences prone to forming secondary DNA structures

(eg: hairpins, cruciform structures, G-quadruplexes etc) or situations which trap proteins on DNA, known as DNA protein crosslinks (DPCs); all these possess a roadblock for DNA synthesis (Mazouzi et al., 2014; Zeman and Cimprich, 2014; Wu et al., 2019; Saxena and Zou, 2022). Such obstacles are also referred to as 'Replication Fork Barriers' (RFBs).

Replication fork barriers can either block helicases or polymerases and the mechanism of stress response activated is based on this. Formation of ssDNA at the replication forks is a common feature associated with replication fork stalling. The formation of ssDNA results from the physical uncoupling of the polymerases from the helicases. Such scenarios happen when the polymerase stalls in response to base damage or dNTP depletion but the helicase continues to unwind the DNA. On the other hand, obstacles that physically hinder helicase movement, such as interstrand cross-links (ICLs) or torsional stress caused by the DNA topoisomerase I cleavage complex, are not expected to induce this uncoupling (Berti and Vindigni, 2016).

1.4.2 Transcription-replication conflicts

Interferences between transcription and replication programs are another major cause for replication stress. The fact that replication and transcription machineries share the same DNA template makes them prone to collide (Saxena and Zou, 2022). The RNA-DNA hybrids generated during transcription are also a problem leading to replication-transcription conflicts. The newly synthesised RNA anneals to the template DNA strand leaving the non-template DNA unpaired. The resulting three stranded structure along with GC rich regions in the DNA forms an R-loop structure (Allison and Wang, 2019). This structure poses a barrier for fork progression but cells have multiple pathways to resolve these R-loops and to avoid TRCs (Saxena and Zou, 2022). Formation of R-loops are suppressed by RNA processing/splicing factors that are responsible for preventing DNA-

RNA hybrid formation during transcription. However, once R-loops are formed, they can be cleaved by specific nucleases such as RNase H family of enzymes and DNA-RNA helicase Senataxin. Cells have also evolved mechanisms to reduce such conflicts. Helicases and topoisomerases assist in reducing the topological stress that arises between converging replication and transcription complexes. For instance, TOP1 prevents collision of replicating forks with R-loops at transcription termination sites by removing DNA supercoiling (Magdalou et al., 2014; Zeman and Cimprich, 2014; Promonet et al., 2020). Mutations in genes that are involved in these pathways and RNA splicing factors can lead to increased accumulation of R-loops contributing to replication stress that leads to genomic instability (Saxena and Zou, 2022). Recent research has also shown that TRAIP plays a critical role during S-phase by preventing DNA damage at transcription start sites caused by conflicts between replication and transcription (Scaramuzza et al., 2023).

1.4.3 Unbalanced replication conditions

Replication relies on various essential components, and their limitation can have significant impact on replication fork speed and trigger replication stress. Various factors contribute to this. Alterations in origin firing such as firing too many origins at the same time can deplete the available dNTP pool or limit other replication factors and thereby slows down the fork speed. On the other hand, firing of less than the required number of origins can also lead to incomplete replication. The speed of the replication forks plays a significant role in the temporal DNA replication program in both mammals and yeast. When the dNTP pool is below the critical level, then replication forks slow down, and additional origins are activated to ensure complete replication. Insufficient dNTPs can lead to the accumulation of ssDNA and activates the DNA replication checkpoint. Eukaryotic genomes contain excess replication origins to counteract fork stalling, and

compensatory activation of dormant origins helps maintain replication efficiency. Dysregulation of dNTP pools is also associated with genome instability and cancer development. Although origin firing is regulated by replication stress, it is not just a consequence but can also be a source of replication stress (Magdalou et al., 2014; Zeman and Cimprich, 2014).

1.4.4 Replication fragile sites

Some regions within the human genome pose significant challenges and are 'difficult to replicate', making them susceptible to fragility. These are called fragile loci. They can be classified into Common Fragile Sites (CFSs) and Early Replicating Fragile Sites (ERFSs). These regions are sensitive to replication stress and accumulate breaks or gaps in the condensed metaphase chromosome upon partial inhibition of DNA synthesis. Additionally, they tend to replicate later in the cell cycle. On the other hand, ERFSs are characterised by a higher GC content, an open chromatin state, and early replication timing (Magdalou et al., 2014; Mazouzi et al., 2014).

CFSs are enriched with A/T base pairs, which make them prone to forming secondary structures leading to stalling of replication forks. Studies from several cell models suggest that CFSs serve as hotspots for replication stress leading to sister chromatid exchange, translocation and chromosomal deletions and rearrangements in cancers (Glover, 2006). These sites have also been identified as 'initiation poor' regions with reduced numbers of active origins leaving their replication incomplete. Consequently, incomplete DNA replication of CFSs becomes obvious as cells enter mitosis, leading to "expression" of CFSs which is referred to as the breakage of CFSs on metaphase chromosomes (Li and Wu, 2020).

The stability of CFSs is maintained by replication checkpoint. The ATR-mediated replication checkpoint is responsible for monitoring the progression of replication, safeguarding stalled replication forks, fork restart and coordinating replication with cell cycle progression. ATR plays a vital role in protecting CFSs. Loss of ATR and CHK1 leads to their expression, even in the absence of replication stress. Furthermore, inhibiting checkpoint proteins Claspin and HUS1 also induces the expression of CFSs (Li and Wu, 2020).

1.4.5 DNA damage repair responses

As mentioned earlier, replication stress can compromise the fidelity of genome duplication and to cope with the constant challenges, cells activate multiple response and repair pathways, depending on the type of stress. ATM and ATR are the central DNA Damage Response (DDR) kinases that are triggered as a first line of defence during stressed conditions (Mazouzi et al., 2014). ATM (Ataxia Telangiectasia Mutated) protein is a serine-threonine kinase that can phosphorylate relevant proteins during DNA damage involving double stranded breaks (DSBs). ATR (Ataxia Telangiectasia and Rad3 Related) protein is another key kinase prominent at stalled replication forks involving ssDNA (Berti and Vindigni, 2016; Saldivar et al., 2017).

Encounter of replicating forks with DNA lesions often requires the replication machinery to undergo remodelling to overcome these obstacles. DNA lesions present on the lagging strand template are well tolerated due to the discontinuous nature of DNA synthesis of Okazaki fragments, but lesions on the leading strand pose a significant obstacle to the continuous DNA synthesis. In such scenarios, DNA damage tolerance (DDT) mechanisms come into play to allow replication to proceed without stalling the forks. This is enabled by specialised DNA polymerases known as Translesion Synthesis (TLS) polymerases such

as POLH, REV1, POLK, POLI, REV3L/REV7, POLN, and POLQ, which have the ability to replicate through the lesions but with some errors. Sometimes the replisomes can also bypass the lesions leaving the damage to be repaired after completion of DNA synthesis. Such a process termed as fork repriming is carried out by PrimPol in eukaryotes. This allows restart of DNA synthesis, leaving a ssDNA gap behind, which is later fixed by TLS polymerases (Berti and Vindigni, 2016).

Fork reversal is another mechanism used for dealing with stressed forks to enable DNA damage repair. It is considered as an 'emergency brake' where DNA replication can temporarily pause to allow necessary space and time to repair any obstacles or lesions encountered during DNA synthesis. RAD51 has been shown to be important in fork reversal. It has been reported that the binding of RAD51 to ssDNA promotes fork reversal (Zellweger et al., 2015). RECQ1 helicase is known to enable the restart of the reversed forks and this restart is achieved by regulating the activity of RECQ1 by PARP1 (Berti et al., 2013). Although fork reversal is initiated as a mechanism to rescue replication stress, this can also have detrimental effects if forks fail to restart (Neelsen and Lopes, 2015).

The replisome components have also been shown to play a key role in maintaining replication dynamics when forks encounter lesions. During DNA synthesis, the steric exclusion of the lagging strand allows the CMG to translocate on the leading strand in a 5' to 3' direction. This mechanism allows the CMG to efficiently bypass roadblocks present on the lagging strand but not the leading strand (Costa et al., 2011; Fu et al., 2011).

All these mechanisms together ensure timely and error-free completion of DNA synthesis, which allows for maintenance of genome stability. Defects in the ability to deliver these repair pathways lead to several diseases and syndromes in humans. To mention a few, for example, loss of Polymerase η involved in TLS and responsible for the repair of lesions

made from UV exposure can lead to skin cancer, Xeroderma pigmentosum (Mailand et al., 2013). Mutations in proteins such as WRN and RecQL4 cause Werner syndrome and Rothmund-Thomson syndrome, respectively, because of faulty DNA replication fork structure resolution (Follonier et al., 2013). Defects in proteins associated with origin licensing such as ORC1, ORC4, ORC6, CDT1, and CDC6 possess growth retardation and microcephaly leading to Meier-Gorlin syndrome (Bicknell et al., 2011). The Ataxia-Telangiectasia-like disease is a neurodegenerative disease caused because of a defect in Mre11 and disrupts the ATR/ATM activation pathway (Mazouzi et al., 2014; Zeman and Cimprich, 2014).

1.5 Regulation of DNA replication by ubiquitylation

Ubiquitylation is known to regulate every step in DNA replication. One of the functions of ubiquitin in DNA replication is to enable the advancement of the process by directing the proteasomal degradation of crucial cell cycle factors. The regulation of replication at different stages of the cell cycle enables it to prevent under or over-replication of DNA which is critical for maintaining genome stability (Moreno and Gambus, 2015).

1.5.1 The Role of Ubiquitylation in origin licensing

Replication initiation is a tightly controlled cellular process that involves crosstalk between different factors and modifications where ubiquitylation plays a key role. It requires a low CDK activity in G1 which is achieved through the degradation of mitotic CDKs, degradation of a CDK activator Cdc25, and thirdly, by the accumulation of CDK inhibitors (CKi). The degradation of mitotic CDKs and Cdc25 is facilitated through ubiquitylation-mediated proteasomal degradation which is coordinated by the cell cycle

regulator Anaphase Promoting Complex or Cyclosome (APC/C) (Wäsch and Engelbert, 2005).

In yeast, APC/C is a multi-subunit ubiquitin ligase that works together with two adaptor proteins Cdc20 and Cdh1/Hct1 and polyubiquitylates proteins via K48- and K11-linked chains, directing them for proteasomal degradation (Schreiber et al., 2011). Cdc20 specifically binds to APC/C during mitosis to promote the degradation of mitotic cyclins. In addition to maintaining low levels of CDKs, in metazoans APC/C-Cdh1 regulates the activity of Orc1, Cdc6 and allows degradation of geminin (Mailand and Diffley, 2005). In vertebrates, APC/C also targets the Cdt1 inhibitor geminin for degradation (McGarry and Kirschner, 1998). Altogether, the ubiquitin ligase activity of APC/C provides conditions favourable to maintaining origin licensing.

1.5.2 The role of ubiquitylation in the initiation of replication

At the G1/S transition, ubiquitylation plays a crucial role in regulating CDK activity by controlling levels of cyclins and CKIs. As the cell cycle progresses into the S-phase and to initiate replication, it requires increased levels of S-phase kinases, CDK and DDK. The degradation of CKIs and APC/C-Cdh1 via ubiquitylation is a prerequisite to a rise in the level of cyclins. In mammalian cells, the CDK partners involved in early G1 are Cdk4 and Cdk6, and late G1/S transition requires Cdk2 (Bartek and Lukas, 2001). In mammalian cells, ubiquitin ligases such as KPC and Pirh2 targets nuclear p27 generated during G0 to G1 (KPC) and G1 to S-phase and allow for its degradation. A third ubiquitin ligase, SCF^{Skp2} activated in the early S-phase is responsible for the degradation of p21 and p27. F-box substrate receptor of SCF^{Skp2}, 'Skp2' specifically recognizes Thr187-phosphorylated p27 and targets it for degradation. SCF^{Skp2} is also responsible for the proteasomal degradation of CKi, p21 (Kitagawa et al., 2009).

The APC/C-Cdh1 activity is inhibited as the cell cycle enters S-phase, too. Several mechanisms are involved in the blocking of APC/C-Cdh1 activity to allow entry into S-phase. In the first mechanism, Cdh1 is phosphorylated by Cdk2/Cyclin E which results in molecular switch off for Cdh1 making it inactive. In the second mechanism, by the concerted action of, Cdk2/Cyclin A, and Polo-like kinase Plk1 Cdh1 is phosphorylated. This phosphorylation marks Cdh1 for polyubiquitylation by a ubiquitin ligase; SCF^{βTrcp1} resulting in inactivation of Cdh1 and prevents its interaction with APC/C-Cdh1. In the final mechanism, APC/Cdh1 can autoubiquitylate itself using E2 enzyme UbcH10. This results in degradation of APC/Cdh1 rendering it inactive (Fukushima et al., 2013; Lau et al., 2013). This marks the transition of the cell cycle from G1 to S-phase.

1.5.3 The role of ubiquitylation in preventing re-replication

Initiation of replication is regulated such that origin activation is restricted to once per cell cycle. Cdt1 and Cdc6 are prerequisites for origin licensing and their activity is highly regulated. An E3 ubiquitin ligase that plays a vital role in preventing re-replication is Cullin-4 based CRL4^{Cdt2}. It is involved in a PCNA-dependent ubiquitylation pathway (Havens and Walter, 2011). Cdt1 undergoes targeted degradation by CRL4^{Cdt2} in a PCNA dependent manner. It involves binding of the PIP box of PCNA to the degron motif located within the first 28 amino acids of Cdt1. This enables the CRL4^{Cdt2} E3 ligase complex to ubiquitylate Cdt1 and subsequent degradation by the proteasome (Hernández-Carralero et al., 2018). In human cells, phosphorylation of Cdt1 by S-phase CDKs targets it also for degradation by ubiquitin ligase SCF^{Skp2}. Similarly, Cdc6 (or Cdc18 in fission yeast) is another licensing factor regulated for preventing re-replication. Cdc6/Cdc18 is phosphorylated by S-phase CDKs and then ubiquitylated by SCF^{Cdc4}/SCF^{Pop1,2} respectively

(Moreno and Gambus, 2015). This coordinated ubiquitylation of the initiation factors together prevents the re-licensing of already replicated DNA in the S-phase.

1.5.4 The role of ubiquitylation in chromatin re-establishment

Histone proteins can act as signalling molecules by engaging in protein-protein interactions through the addition of ubiquitin and ubiquitin-like (UBL) post-translational modifications (PTMs). Histone ubiquitylation is vital for DNA methylation control, PTM crosstalk, nucleosome structure, etc (Vaughan et al., 2021). During active DNA replication, the chromatin structure is dismantled ahead of the replication fork and subsequently reassembled behind it. The histone chaperones FACT and Asf1 aid in this chromatin re-assembly. The newly formed nucleosomes copy the histone modifications of parental nucleosomes to have the same epigenetic profile (Jasencakova and Groth, 2010). Apart from this, the newly synthesised DNA is not methylated, resulting in hemimethylated sister chromatids. Full methylation is also established behind the fork by DNA methyltransferase 1 (Dnmt1) (Alabert and Groth, 2012). Importantly, these processes are tightly coordinated with DNA replication and ubiquitylation plays a crucial role in various aspects of chromatin reconstitution and epigenetic maintenance during DNA replication.

Synthesis of histones is regulated by ubiquitylation of their transcription factors such that the synthesis is only restricted to the S-phase. In yeast, non-chromatin-bound histones are regulated by ubiquitin-driven proteasomal degradation. This degradation is also dependent on the activity of Rad53 and employs different ubiquitin ligases such as Tom1, Pep5, Snt2, Hel1, and Hel2. Human homologs of these yeast proteins e.g. HUWE1 have also been reported to ubiquitylate histones *in vitro* (Liu et al., 2005).

Ubiquitylation also regulates the deposition of histone H3 onto the newly synthesised DNA. In yeast, ubiquitin ligase Rtt101^{Mms1} is responsible for ubiquitylating histone H3.

This modification leads to the detachment of H3-H4 from other histone chaperones and facilitates its eventual integration into the DNA. A similar mechanism is also seen in humans where the orthologues Rtt101^{Mms1} and Cul4A^{DDb1} incorporate H3 into newly synthesised DNA (Moreno and Gambus, 2015). Apart from this, Histone H3 is found polyubiquitylated at lysine 23 by Uhrf1, an E3 ligase, and a cofactor of Dnmt1. The modified H3 serves as a platform for the binding of Dnmt1 to facilitate the methylation of DNA (Vaughan et al., 2021).

The activation of the intra-S-checkpoint during replication stress is coordinated with chromatin assembly by limiting fork progression during the replication stress (Lin et al., 2014). Impairment of H2B ubiquitylation under stress conditions results in a defect in replication fork progression and replisome stability. Importantly, during normal DNA replication, cells with a mutation in H2B at lysine 123 exhibited a delay in completing DNA replication, highlighting the crucial role of H2B ubiquitylation in normal replication processes (Trujillo and Osley, 2012).

1.5.5 The role of ubiquitylation in replication termination

A conserved mechanism of replisome disassembly again driven by ubiquitylation can be seen across eukaryotes. This has been explained in detail in section 1.3.4.

1.6 Cullin2^{Lrr1}

Cullin2^{Lrr1} (represented as CRL-2^{LRR-1} in worms/Cul2^{Lrr1} in *X. laevis*/CUL2^{LRR1} in humans) belongs to the Cullin-Ring Ligase (CRL) family classically known for modifying substrates for 26S proteasomal degradation. Cullin-type ubiquitin ligases are multi-subunit enzymes where Cullin is the scaffold protein, RING-box protein 1 (Rbx1) is the ring finger protein that catalyses the ubiquitin transfer, Elongin B and C (EloB/C) are adaptor/linker proteins, and Lrr1 is the Substrate Recognition Subunit (SRS). The EloB/C links Lrr1 to the Cullin2 scaffold to form a Cul2^{Lrr1} complex (Wang et al., 2016; Zhou et al., 2021).

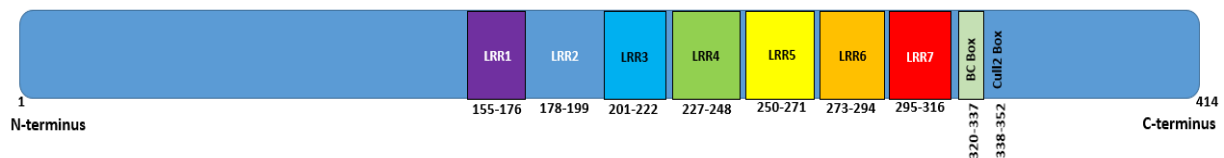


Figure 1.12:- Domain organisation of Lrr1 protein. It includes seven leucine-rich repeats (LRRs), BC box, and Cullin2 box as its primary structural motif. Each LRR consists of a 20-30 amino acid segment that forms a β -strand/ α -helix repeat structure and is responsible for mediating protein-protein interactions.

Lrr1 protein consists of seven Leucine Rich Repeat (LRR) domains, a BC box, and a Cullin2 box (Figure 1.12), which is characteristic of Cullin2-type ubiquitin ligases (Wang et al., 2016). This E3 ubiquitin ligase has been found to play an important role in many aspects of the cell cycle (Merlet and Pintard, 2013). For example, during replication termination in *C. elegans* embryos, *X. laevis* egg extracts, mouse embryonic fibroblasts and human cells, polyubiquitylation of the replisomes by Cul2^{Lrr1} is essential to promote replication termination (Dewar et al., 2017a; Sonnevile et al., 2017; Fan et al., 2021; Villa et al., 2021). In *X. laevis* egg extracts and yeast, the N-terminus of Mcm7 is ubiquitylated by Cul2^{Lrr1} and SCF^{Dia2} at position K27/K28 (Low et al., 2020; Moreno and Gambus, 2020) and K29 (Maric et al., 2017), respectively.

During active replication, CMG translocates on the leading strand template in the 5'-3' direction through its central channel, excluding the lagging strand. Very recent studies using Cryo-Electron Microscopy have shown that Lrr1's recruitment to replisomes is suppressed by the presence of lagging/excluded strands during active DNA replication thereby preventing early ubiquitylation of active helicase. Although the substrate receptors, Dia2 in yeast and Lrr1 in eukaryotes, are structurally distinct, they share a common leucine-rich region that interacts with Mcm3 and Mcm5 zinc finger domains upon termination or when the excluded strand is lost (Jenkyn-Bedford et al., 2021; Zhou et al., 2021). This regulated activity of the ligases helps maintain genome stability by preventing the early recruitment of Lrr1 and polyubiquitylation of Mcm7 at the active DNA replication forks.

In *C. elegans*, the loss of function of Lrr1 affects germ cell proliferation resulting in sterile animals. Both CUL-2 and LRR-1 work cooperatively to regulate the proliferation of germ cells (Merlet and Pintard, 2013). In human cells, loss of LRR1 results in a decreased replication rate in S-phase due to a lack of recycled replisome components. As a result, replisomes accumulate in the G2 phase and activate the G2/M checkpoint dependent on ATR-Chk1-Wee1 thereby preventing mitotic entry (Fan et al., 2021). SiRNA depletion of LRR1 in *C. elegans* also results in activation of the ATL-1/CHK-1 pathway (ATR, Ataxia telangiectasia, and Rad3 related/Checkpoint kinase 1 in humans), preventing the mitotic proliferation of germ cells thus leading to animal sterility (Merlet and Pintard, 2013; Wang et al., 2016).

In *C. elegans* and *Xenopus* egg extracts, there is also a mitotic pathway for CMG disassembly identified to remove any post-termination replisomes that failed to unload

during S-phase, but is catalysed by a different ubiquitin ligase TRAIP (Sonneville et al., 2017, 2019a; Deng et al., 2019; Moreno et al., 2019a).

In addition, to ensure correct G1-phase cell cycle progression in the germline cells of *C. elegans*, CUL-2^{LRR-1} was important for degrading the Cip/Kip CDK-inhibitor, CKI-1 in the nucleus (Burger et al., 2013). Similarly, the orthologs of Cip/Kip CDK-inhibitor in humans (p21^{Cip1}) require the activity of CUL2^{LRR1} for its polyubiquitylation and degradation specifically in the cytoplasm (Starostina et al., 2010). Furthermore, in humans, LRR1 is a negative regulator of cell motility. The depletion of LRR1 resulted in the accumulation of p21 in the cytoplasm, which in turn led to the dephosphorylation of cofilin (a protein responsible for decreasing cell motility). Due to this dephosphorylation, actin proteins necessary for cytoskeletal formation were synthesised, thereby leading to increased cell mobility (Cai and Yang, 2016; Wang et al., 2016).

Additionally, the role of Cullin2^{Lrr1} has been noted to maintain a balance between mitotic proliferation and meiotic entry decisions. It inhibits meiotic prophase by degradation of HORMA domain-containing protein HTP-3, which is important for the assembly of synaptonemal complex components that are essential for meiotic chromosomes. This regulation is enabled by the interaction between HTP-3 and LRR1 (Merlet and Pintard, 2013). These observations suggest that Cul2^{Lrr1} has several independent substrates.

1.7 TRAIP

TRAIP was first discovered as a TNF receptor or TRAF signalling complex and is therefore referred to as the TNF Receptor Associated Factor - Interacting Protein or TRAF-IP or TRIP (Lee et al., 1997; Besse et al., 2007). TRAIP is a RING ubiquitin ligase also referred to as RNF206 (RING Finger protein 206) (Besse et al., 2007). TRAIP was found to regulate the nuclear factor-kappa B signalling pathway but its substrates in this pathway are still

unknown (Lee et al., 1997). The role of TRAIP in DNA damage was first reported when three children with microcephalic primordial dwarfism were found to carry mutations in TRAIP (arginine at codon 18 was mutated to cysteine). This phenotype is a variation of Seckel syndrome, which is a genetic condition, caused because of mutations in genes responsible for DNA damage response (Harley et al., 2016).

The deficiency of TRAIP activity displays phenotypes of a diverse array depicting its broad spectrum of roles in maintaining genome integrity. Homozygous deletion of TRAIP in mouse embryonic studies is lethal shortly after embryo implantation, suggesting its importance during early embryonic development (Park et al., 2007). In human cells, loss of TRAIP activity has also been found to affect cellular proliferation (Harley et al., 2016; Scaramuzza et al., 2023), accumulation of cells in the G2 phase of the cell cycle, and DNA damage with increased levels of γ -H2AX phosphorylation (Yuan et al., 2016; Scaramuzza et al., 2023). Knockdown of TRAIP in Hela cells affected mitotic progression, kinetochore-microtubule attachment, spindle assembly checkpoint control, and resulted in misaligned chromosomes (Chapard et al., 2014; Yuan et al., 2016). Very recently, it is shown that by employing CRISPR/Cas9 mediated gene tagging of TRAIP with a degron tag, auxin-induced depletion of TRAIP in the S-phase leads to cell senescence and generation of DNA damage at transcription start sites (Scaramuzza et al., 2023).

Functionally, the ubiquitin ligase activity of TRAIP had been important for its pleiotropic effects. TRAIP is noted to be an essential ubiquitin ligase for the repair of DNA damage induced by UV, hydroxyurea, mitomycin C- induced interstrand crosslinks etc (Park et al., 2015; Hoffmann et al., 2016).

The domain structure of TRAIP consists of a RING finger at its N-terminus, a coiled-coil motif and a leucine zipper, followed by a PIP box located at its C-terminal end (Harley et

al., 2016) (Figure 1.13). TRAIP is generally found residing in the nucleolus of eukaryotic cells but upon DNA damage it relocates to the site of damage by interacting with PCNA via the PIP-box (PCNA Interacting Protein box) (Feng et al., 2016). The PIP box is found to be essential for TRAIP's recruitment to the sites of damage since upon deletion of the PIP box, TRAIP failed to accumulate at stalled replication forks. Despite this, TRAIP without the PIP box was still proficient in repairing the damage. TRAIP knockdown cells are sensitive to mitomycin C but deletion of the PIP box results in mild sensitivity suggesting that even in the absence of the PIP box, TRAIP can still find its targets (Hoffmann et al., 2016). Another important motif of TRAIP includes the RING finger domain, which confers the catalytic activity of the protein. There is evidence suggesting that the conserved cysteine residues are important for providing the RING-dependent ligase activity for TRAIP. Furthermore, TRAIP mutations observed in patients with primordial dwarfism/Seckel syndrome affects the ubiquitin ligase activity of TRAIP (Besse et al., 2007; Harley et al., 2016).

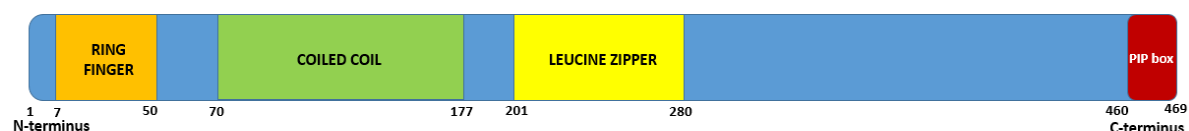


Figure 1.13:- Domain organisation of TRAIP. The E3 ligase TRAIP consists of a RING domain (orange) which provides ubiquitin ligase activity and is located at its N-terminus, a coiled-coil domain (green) which facilitates dimerization, leucine zipper (yellow), and a PIP box (red) which allows interaction with PCNA at the C-terminus.

The ubiquitin ligase activity of TRAIP is also important in replisome unloading in *C. elegans* and *Xenopus* egg extracts (Deng et al., 2019; Moreno et al., 2019a; Sonnevile et al., 2019a; Wu et al., 2019). In S-phase, TRAIP can be involved in replication coupled ICL repair in *Xenopus* egg extracts. Converging replisomes on either side of ICLs can trigger TRAIP to ubiquitylate replisomes leading to NEIL3 glycosylase or Fanconi anaemia (FA)

pathway for ICL repair. A choice between the two repair pathways is made based on short or long ubiquitin chains synthesised by TRAIP on the CMG. Short ubiquitin chains recruit the NEIL3 glycosylase using the ubiquitin-binding domain of NEIL3. NEIL3 then cleaves one of the two glycosyl bonds that form the ICL. Failure of this pathway results in the generation of longer ubiquitin chains by TRAIP, which in turn is recognised by p97 and unloads the replisome to allow for the repair by FA pathway. The removal of replisomes allows the endonucleases to access the DNA to which the FA proteins are recruited and break the phosphodiester backbone surrounding the ICL forming double-stranded breaks which are repaired by homologous recombination (Wu et al., 2019, 2021).

TRAIP-mediated replisome unloading in mitosis has been previously reported in *C. elegans* and *Xenopus* egg extracts (Moreno et al., 2019a; Sonnevile et al., 2019a; Wu et al., 2019). Replisomes remaining on mitotic chromatin regardless of whether terminated or stalled are actively removed by TRAIP (Deng et al., 2019; Moreno et al., 2019a) and lead to fork breakage and DNA repair events driven by DNA polymerase θ (Pol θ), thereby enabling genome integrity (Deng et al., 2019).

1.8 *Xenopus laevis* egg extracts model system

Xenopus laevis egg extracts are powerful tools for investigating biochemical mechanisms *in vitro* to provide fundamental insights into complex activities that occur *in vivo*. These extracts are highly synchronised, cell-free systems with the ability to recapitulate the key nuclear transitions occurring in eukaryotes making it an ideal system in cell cycle research (Almouzni and Méchali, 1988). The cytoplasmic extracts have been a choice for studying cellular events such as DNA replication, S-phase checkpoint activation, fork stalling and inter-strand crosslink repair, DNA repair pathways, mitosis, spindle

microtubule dynamics, nuclear transport, and apoptosis (Knipscheer et al., 2012; Jenness et al., 2018).

Our lab uses *Xenopus laevis* egg extracts for studying DNA replication. The *Xenopus* eggs are rich in enzymes and precursors that are essential for carrying out DNA replication and chromatin assembly. Furthermore, as an embryonic system, egg extract also lacks transcription. All these make egg extract an excellent model system for studying DNA replication (Gillespie et al., 2012; Hoogenboom et al., 2017). Indeed, *X. laevis* egg extract is the only system that enables the study of vertebrate DNA replication outside the cell and supports all aspects of genome maintenance. Importantly, the replication and repair mechanisms in *Xenopus* and mammalian systems are highly conserved, and the discoveries made in the egg extract system are proven to be conserved in human cells (Hoogenboom et al., 2017; Sparks and Walter, 2019).

Unfertilised *Xenopus* eggs (arrested at metaphase of meiosis II) are subjected to different centrifugation protocols to provide three different types of egg extracts namely Low-Speed Supernatant (LSS), High-Speed Supernatant (HSS), and Nucleoplasmic Extract (NPE). The conventional method involves crushing the eggs at a low speed of centrifugation and collecting the cytoplasm. This is called Low-Speed Supernatant or LSS (Knipscheer et al., 2012). I have used LSS throughout my Ph.D. project. The addition of demembranated sperm DNA to egg extract results in the de-condensation of sperm, the formation of a nuclear envelope around the sperm DNA and undergo of semi-conservative DNA replication. We supplement the extracts with cycloheximide to block the cell cycle progression, ensuring just a single round of replication (Gillespie et al., 2012).

We have used LSS in our studies to investigate specifically the mechanisms in replication termination and the factors involved in replisome disassembly during S-phase and

mitosis. Egg extracts can transition into various phases of the cell cycle by altering the levels of cyclins and to study perturbations of DNA replication, we introduce specific proteins or small molecule inhibitors. The functional role of a protein of interest can also be assessed by immunodepleting them from the extract to test their effects on DNA replication. Importantly, supplementing the immunodepleted extract with the recombinant protein of interest should rescue the observed phenotypes.

However, it is important to note that there are certain limitations in using *Xenopus laevis* model system. Working with *Xenopus laevis* model requires preparation of egg extracts that is subject to availability of eggs from induced frogs that can vary in quality and quantity. Each extract requires testing of replication timings as it can vary among batches. In addition, non-specific interactions could also arise as a result of protein additions or depletion or use of antibodies in this system. Another disadvantage of *Xenopus* system is that the proteins need to be identified using antibodies rather than tags as it is not amenable to genetic analysis (Blow and Laskey, 2016). In addition, this is an embryonic system, with very fast replication cycles in which some of the regulation is relaxed. Therefore, the insights obtained from *Xenopus* might not always translate directly into mammalian cells due to evolutionary divergence of some pathways or proteins involved. Hence, verification of findings in *Xenopus* system is required in mammalian cells.

1.9 Aim of the project

Post-translational modifications play a significant role in modulating DNA replication by regulating the stability and function of key proteins involved in this process. Starting from the deposition of the Mcm2-7 double hexamers to replisome disassembly, the entire process is highly regulated. Although the initial stages of eukaryotic replication have been well studied for decades, little was known about the last stage where replication is terminated. Since then, investigations from different research groups worldwide, including the Gambus lab, have made significant discoveries in this area of research.

The tight regulation of once per cell cycle DNA replication is achieved by restricting the loading of Mcm2-7 to only the G1 phase of the cell cycle. This means that if an active helicase is removed from the replication fork, such a fork would collapse as the helicase cannot be re-loaded (Cortez, 2015). Therefore, it is important for genome stability that only terminated replisomes are unloaded. The key regulated step in replisome disassembly is the ubiquitylation of Mcm7 on the post-terminated replisomes. This ubiquitylation process is highly regulated such that only those replisomes that have completed replication are unloaded, and neither Mcm7 ubiquitylation nor the CMG unloading is observed during replication initiation or elongation stages, thereby maintaining genome stability.

Recent investigations from our lab had shown that in higher eukaryotes Cullin2^{Lrr1} is the E3 ubiquitin ligase responsible for ubiquitylating Mcm7 during S-phase at replication termination. This E3 ligase binds specifically to the terminated helicase and not to the active helicase, thereby regulating the replisome disassembly pathway (Sonneville et al., 2017). At the start of this PhD project, we did not know how Cullin2^{Lrr1} could distinguish between the active and terminated replisomes, which then leads to its disassembly.

Therefore, the first aim of this project was to understand this in detail by identifying the domains of Lrr1 that are essential for the recognition of Mcm7 as Cullin2^{Lrr1}'s substrate using *Xenopus laevis* egg extract. We also aimed to deduce the structure of Cullin2^{Lrr1}.

In addition to this, mass spectrometry analysis of terminating replisomes in the presence of p97 inhibitor, performed by a previous lab member, had revealed the interaction of an E3 ubiquitin ligase TRAIP. Therefore, the second aim of this project was to investigate the role of TRAIP in unloading post-terminated and stalled replisomes. Part of this PhD work contributed to the paper published by our lab showing the existence of a mitotic disassembly pathway in higher eukaryotes using *X. laevis* egg extracts (Moreno et al., 2019a). The third aim of my project was to investigate whether TRAIP is involved in replisome unloading in S-phase during unperturbed and perturbed replication conditions, while the final aim was to investigate whether the post-translational modifications of TRAIP can regulate its activity.

Chapter - 2

2 Materials and Methods

2.1 Tables

Table 1:- List of buffers used in this PhD project. All the buffers were prepared in Milli-Q water and filtered using a 0.22 µm membrane filter (Merck) unless otherwise stated.

<i>Buffer</i>	<i>Composition</i>	<i>Storage conditions</i>
Work with <i>X. laevis</i> egg extract		
10X Marc's Modified Ringer's (MMR)	1 M NaCl 20 mM KCl 10 mM MgCl ₂ 20 mM CaCl ₂ 1 mM EDTA 50 mM HEPES Adjust pH to 7.8 with NaOH	Room temperature
Un-activating Extraction Buffer (UEB)	50 mM KCl 50 mM HEPES 5 mM MgCl ₂ 5 mM EGTA Adjust pH to 7.6 with KOH	4°C
Cysteine solution	2.2% Cysteine 5 mM EGTA Adjust pH to 7.6 with KOH, Make up to 1 litre	Freshly prepared
Acetate nuclear isolation buffer- 2X ANIB 100	100 mM HEPES pH 7.6 200 mM KAc 20 mM MgAc 5 mM Mg-ATP (added from a stock of 250 mM ATP; 250 mM MgCl ₂ ; pH 6.7 with NaOH) 1 mM spermidine 0.6 mM spermine 2 µg/ml of each: aprotinin, leupeptin, pepstatin 50 mM β-glycerophosphate 0.2 mM Na ₃ VO ₄	4°C
	Mix 1 volume of 2X ANIB 100 with 1 volume of H ₂ O 0.1% Triton X-100	

1X ANIB	0.1 mM PMSF 10 mM Chloroacetamide	Freshly prepared
Chk1 buffer	50 mM HEPES pH 7.6 100 mM KCl 2.5 mM MgCl ₂ 1.3 M sucrose	Freshly prepared
Energy Regenerator (ER)	1 M phosphocreatine K salt 600 µg/ml creatine phosphokinase Dissolve in 10 mM HEPES-KOH, pH 7.6	-20°C
Cycloheximide	10 mg/ml	-20°C
CaCl ₂	50 mM	-20°C
Cytochalasin D	10 mg/ml in DMSO	-20°C
Licensing Factor Buffer (LFB1/50)	10% sucrose 50 mM KCl 40 mM HEPES pH 8 20 mM K phosphate pH 8 2 mM MgCl ₂ 1 mM EGTA 2 mM DTT 1 µg/ml of each: aprotinin, leupeptin and pepstatin	4°C
LFB1/100	10% sucrose 100 mM KCl 40 mM HEPES pH 8 20 mM K phosphate pH 8 2 mM MgCl ₂ 1 mM EGTA 2 mM DTT 1 µg/ml of each: aprotinin, leupeptin and pepstatin	4°C
MS222	0.2% MS222 0.5% NaHCO ₃ , to pH 7.5	RT
EB	50 mM KCl 5 mM MgCl ₂ 2 mM β-mercaptoethanol 50 mM HEPES-KOH, pH 7.6	Freshly prepared
Lysolecithin	5 mg/ml	4°C

Hoescht	10 mg/ml in H ₂ O; prepare 20 µg/ml dilution on the day of use.	-20 °C
SuNaSp	0.25 M sucrose 75 mM NaCl 0.5 mM spermidine 0.15 mM spermine 15 mM HEPES-KOH, pH 7.6	4°C
Stop C	5 mM EGTA 0.5% SDS 20 mM Tris-HCl, pH7.5	37°C
5% TCA solution	5% TCA 0.5% Sodium pyrophosphate Make up to 10 litres with H ₂ O	4°C
10% TCA solution	10% TCA 2% Sodium pyrophosphate Make up to 10 litres with H ₂ O	4°C
Work with proteins		
10X TBS	121 g of Tris Base 400 g of NaCl Adjust pH to 7.6 and make up to 5 litres with H ₂ O	Room temperature
1X TBST	0.5 litres of 10X TBS 12.5 ml of 20% Tween 20 Make up to 5 litres with H ₂ O	Room temperature
Tris-Glycine running buffer	25 mM Tris-HCl pH 7.4 250 mM Glycine 0.1% SDS	Room temperature
Transfer buffer	25 mM Tris-HCl pH 7.4 190 mM Glycine 20% Methanol	Room temperature
Coomassie Blue Stain	0.1% Brilliant Blue R-250 10% Acetic acid 50% Methanol 40% H ₂ O Mix overnight and filter using 3mm Whatmann paper	Room temperature
Destaining solution	10% Acetic acid 50% Methanol 40% H ₂ O	Room temperature

Coupling buffer	0.1 M NaHCO ₃ , 0.5 M NaCl Dissolve in H ₂ O and adjust pH to 8.3	4°C
Blocking buffer	0.5 M Ethanolamine 0.5 M NaCl; pH 8.3	Room temperature
Washing buffer	0.5 M NaCl 0.1% Triton X-100 in 1X PBS	4°C
3% BSA+ 0.02% Sodium azide solution	3 g BSA 0.02% Sodium azide Dissolve in 100 ml of 1X TBST	4°C
10X PK buffer	0.5 M Tris-HCl 0.1 M MgCl ₂ 1 mM EDTA 20 mM DTT 0.1% Brij-35 Adjust pH to 7.5	Room temperature
10X ATP	Make a solution of 4 mM ATP in 1X PK buffer	-80°C
Aprotinin	10 mg/ml in H ₂ O	-20°C
Pepstatin	10 mg/ml in absolute ethanol	-20°C
Leupeptin	10 mg/ml in H ₂ O	-20°C
Work with Bacteria		
Ampicillin	100 mg/ml in 50% ethanol Use at a final concentration of 100 µg/ml	-20°C
Kanamycin	50 mg/ml in H ₂ O Use at a final concentration of 50 µg/ml	-20°C
Chloramphenicol	30 mg/ml in 100% ethanol Use at a final concentration of 30 µg/ml	-20°C

Table 2:- List of plasmids used in this PhD project.

<i>Gene of interest</i>	<i>Parental vector</i>	<i>Antibiotic resistance</i>
His-SUMO-Lrr1	pET-15b	Ampicillin
His-SUMO-Lrr1-Nterm ^{DEL}	pET-15b	Ampicillin
His-SUMO-Lrr1-LRR ^{DEL}	pET-15b	Ampicillin
His-SUMO-Lrr1-265P>S	pET-15b	Ampicillin
Nterminus-Cul2	pET-24a	Kanamycin
EloB/C	pACYCDuet-1	Chloramphenicol
His-TRAIP	pET-28a	Kanamycin
GST-TRAIPwt	pGS-21a	Ampicillin
GST-TRAIPmut	pGS-21a	Ampicillin
His/SUMO-TRAIPwt	pCA528	Kanamycin
His/SUMO-TRAIPmut	pCA528	Kanamycin
His/SUMO-TRAIPS295	pCA528	Kanamycin
His/SUMO-TRAIP3A	pCA528	Kanamycin
His/SUMO-TRAIP3D	pCA528	Kanamycin

Table 3:- List of primers used in this PhD project.

<i>Mutation</i>	<i>Orientation</i>	<i>Primer sequence</i>
Truncated N-term of Lrr1	Forward	GAAATTGAAAAACCGCGTAG
Truncated N-term of Lrr1	Reverse	CATACCACCGGTCTGTTC
Truncated LRR of Lrr1	Forward	GTTCCGGATATCCAGCTG
Truncated LRR of Lrr1	Reverse	GCTATACGGAAAGCTTTTG
Truncated C-term of Lrr1	Forward	TAAGCGGCCGCATGGGTC
Truncated C-term of Lrr1	Reverse	ACACGGCAGACCGCAATC
BC box mutant of Lrr1	Forward	GCTGCGGCAGAACTTTTGCACGTGCAACCCTGAAATA
BC box mutant of Lrr1	Reverse	CAGCGGAATTTTCAGCTGGATATCCGGAACCAGCGGTG
Cul2 box mutant of Lrr1	Forward	GCTGCCGCCGCGGCAACCCTGTGTCAAAAAGTCT GGCCAAAACCTG
Cul2 box mutant of Lrr1	Reverse	CGGACCATACGGAATACGATATTTTCAGGGTTGCACGTG CTGCGGTTTCCA
GST-TRAIPmut_C25A	Forward	CACGTTCCATCAGGAGTGTGTTTGTACAGTG
GST-TRAIPmut_C25A	Reverse	TGCCCAGCGGTAATCGCGGCCACATC
TRAIP_BamHI	Forward	TTGGATCCACCCATACGCGCCTACTGTACG

TRAIP_HindIII	Reverse	TTAAGCTTTTATTTCAAGAAGTCTTCG
TRAIP_S295A	Forward	GATCTTTGAGgctCCTGCACCCATC
TRAIP_S295A	Reverse	AAACGACTAATTGCTTCATTAG

Table 4:- List of inhibitors added to *X. laevis* egg extract.

<i>Inhibitors</i>	<i>Preparation</i>	<i>Storage conditions</i>
Aphidicolin (A0781, Sigma)	Dissolved in DMSO at 10 mM. Use 40 μ M as final concentration	-20°C
Caffeine (C8960, Sigma)	Dissolved in H ₂ O at 100 mM. Use 5 μ M as the final concentration	Freshly prepared
MLN4924 (A11260-5, Adooq Bioscience)	Dissolved in DMSO at 20 mM. Use 10 μ M as the final concentration	-20°C
NMS-873 (17674, Cayman Chemicals)	Dissolved in DMSO at 10 mM. Use 50 μ M as the final concentration	-20°C
EcoRI (R4014, Promega)	Use 0.05 U/ μ l as the final concentration	-20°C
ICRF-193 (14659, Scientific Lab Supplies)	Dissolved in DMSO at 10 mM and used at 20 μ M as the final concentration	-20°C

Note:- The concentrations of each protein added to the egg extract was made based on ensuring that the replication ability of the extract remains unaffected. With regards to the 'over expression' studies using recombinant TRAIP, we emphasised on utilising the highest concentration of protein possible without affecting replication ability of the extract.

Table 5:- List of recombinant proteins added to *X. laevis* egg extract.

<i>Recombinant Protein</i>	<i>Source</i>	<i>Addition to <i>X. laevis</i> egg extract</i>
His-SUMO-Lrr1_Arctic	This PhD project	Added after sperm DNA from 1 mg/ml stock to 1/50 th volume of the extract (20 μ g/ml)
His-SUMO-Lrr1_BL21	This PhD project	Added after sperm DNA from 1 mg/ml stock to 1/50 th volume of the extract (20 μ g/ml)
Peptide 1 EFYKDDEIGKKHFKYGVQLA (Span Mcm7 ubiquitylation site)	This PhD project	Added after sperm DNA to 1/10 th volume of the extract (40 μ M final concentration)
Peptide 2 IDEGFH DYKFQKL VKGEYAK (Scrambled)	This PhD project	Added after sperm DNA to 1/10 th volume of the extract (40 μ M final concentration)

GST-TRAIPwt	This PhD project	Added after sperm DNA from 0.5 mg/ml stock to 1/10 th volume of the extract (50 µg/ml)
GST-TRAIPmut	This PhD project	Added after sperm DNA from 0.5 mg/ml stock to 1/10 th volume of the extract (50 µg/ml)
His/SUMO -TRAIPwt	This PhD project	Added after sperm DNA from 0.5 mg/ml stock to 1/10 th volume of the extract (50 µg/ml)
His/SUMO -TRAIPmut	This PhD project	Added after sperm DNA from 0.5 mg/ml stock to 1/10 th volume of the extract (50 µg/ml)
His/SUMO -TRAIP3A	In-house, other members of the lab	Added after sperm DNA from 0.5 mg/ml stock to 1/10 th volume of the extract (50 µg/ml)
His/SUMO -TRAIP3D	In-house, other members of the lab	Added after sperm DNA from 0.5 mg/ml stock to 1/10 th volume of the extract (50 µg/ml)
His-Cyclin A1 NΔ56 (from Dr Julian Blow's Lab)	(Moreno et al., 2019a)	Added to extract after completion of DNA synthesis to a final concentration of 826 µM
His-Geminin ^{DEL} (lacking functional destruction box) from Dr Julian Blow's Lab	(Moreno et al., 2019a)	Added to extract 2 minutes before sperm DNA addition at 1.3 µg/ml to allow Cdt1 inhibition
His-UbiNoK	UM-HNOK, R&D System	A stock concentration of 10 mg/ml was prepared in LFB1/50 and added after sperm DNA at 0.5 mg/ml
His-Cyclin B /CDK1	PV3292, Thermo Fisher Scientific	Used in <i>in vitro</i> phosphorylation reactions to a final concentration of 0.3 µg
His-Cyclin A /CDK2	PV3267, Thermo Fisher Scientific	Used in <i>in vitro</i> phosphorylation reactions to a final concentration of 0.3 µg
GST-Cyclin E /CDK2	PV6295, Thermo Fisher Scientific	Used in <i>in vitro</i> phosphorylation reactions to a final concentration of 0.3 µg

Table 6:- List of antibodies used in this PhD project.

Antibody (Species)	Source	Concentration
Primary antibodies		
All primary antibodies were prepared at the indicated concentration in 3% BSA + 0.02% Sodium azide solution and incubated overnight at 4°C.		
α-Mcm7 (Sheep)	In-house, (Moreno et al., 2019a)	1:2000
α-Cdc45 (Sheep)	In-house, (Gambus et al., 2011)	1:500
α-PCNA (Mouse)	P8825-Sigma	1:2000
α-Psf2 (Sheep)	In-house, (Gambus et al., 2011)	1:500
α-His (Mouse)	H1029, Sigma	1:1000

α -Cul2 (Rabbit)	EPR3104 (2), Abcam	1:1000
α -p97 ATPase (Mouse)	65278, Progen Biotechnik	1:1000
α -SUMO1 (Mouse)	21C7, Developmental Studies Hybridoma Bank	1:2
α - γ H2AX (Rabbit)	4418-APC-020, Trevigen	1:1000
α -P-Chk1, S345 (Rabbit)	2348, Cell Signalling	1:1000
α -GST (Rabbit)	G7781, Sigma	1:1000
α -TRAIP (Rabbit)	NBP1-87125, Novus Biologicals	1:500
α -TRAIP #91 (Rabbit)	This PhD project	1:1000
α -TRAIP #52 (Rabbit)	This PhD project	1:500
α -TRAIP #107 (Rabbit)	This PhD project	1:500
α -TRAIP #108 (Rabbit)	This PhD project	1:500
α -TRAIP peptide#73 (Rabbit) Ac-CTSSLANQPRLEDFLK-OH	In-house	1:500
α -TRAIP peptide#74 (Rabbit) Ac-CTSSLANQPRLEDFLK-OH	In-house	1:500
α -Lrr1 (S962D) (Sheep)	S962D, MRC PPU reagents	1:100
α -Lrr1 #27 (Rabbit)	This PhD project	1:500
α -Lrr1 #29 (Rabbit)	This PhD project	1:500
α -Lrr1 #30 (Rabbit)	This PhD project	1:500
α -Lrr1 #32 (Rabbit)	This PhD project	1:500
α -Lrr1 peptide #75 (Rabbit) Ac-CYSQFLDKYLQSTRV-OH	In-house	1:500
α -Lrr1 peptide #76 (Rabbit) Ac-CYSQFLDKYLQSTRV-OH	In-house	1:500
Secondary antibodies <i>All secondary antibodies were prepared at the indicated concentration with 5% milk in 1X TBST and incubated for 1h at room temperature.</i>		
α -Mouse IgG Peroxidase antibody produced in goat (Mouse)	A5278, Sigma	1:5000
α -Sheep IgG Peroxidase antibody produced in donkey (Sheep)	A3415, Sigma	1:10,000

α -Rabbit IgG Peroxidase antibody produced in goat (Rabbit)	A0545, Sigma	1:25,000
α -Rabbit IgG HRP, Rabbit TrueBlot produced in mouse (Rabbit)	18-8816-31, Rockland	1:10,000
α -Sheep IgG HRP, Sheep TrueBlot produced in mice (Sheep)	18-8815-31, Rockland	1:10,000
α -Mouse IgG HRP, Mouse TrueBlot produced in the rat (Mouse)	18-8817-30, Rockland	1:10,000

2.2 Working with *Xenopus laevis* egg extract

All protocols related to egg extracts are based on (Gillespie et al., 2012).

2.2.1 Preparation of *Xenopus laevis* egg extracts

Xenopus laevis egg extracts are used to study DNA replication and chromatin-associated proteins. The extracts are prepared arrested in metaphase of meiosis II, which is suitable for studying different aspects of the cell cycle. To prepare the high-quality extract, the quality of eggs is of utmost importance. To increase the yield of eggs, female frogs are primed with 50 units of Folligon 2-7 days before laying eggs. On the day before egg preparation, 500 units of Chorulon are injected, and female frogs are placed separately in individual laying tanks containing 1X MMR buffer (see table 1) to collect the unfertilised eggs. The high salt concentration in this buffer enables the maintenance of cell cycle arrest. The temperature in the frog room is maintained between 19-23°C throughout the process. The next morning, good quality eggs with clear circumferential differences between larger-sized dark animal poles and smaller and lightly coloured vegetal poles are collected for preparation. The collected eggs are then rinsed in 1X MMR to remove the debris, while activated or apoptosed eggs are removed using a Pasteur pipette. The eggs

are de-jellied using a cysteine solution (see table 1). The dejellying solution can be replaced 2-3 times to enable fast dejellying. The eggs are then washed again with 1X MMR and UEB (see table 1) which is supplemented with 2 mM DTT (A3668.0050, VWR).

The dejellied eggs are packed into 14 ml round bottom polypropylene tubes (187261; Greiner) with 1 ml UEB containing 10 µg/ml protease inhibitors: aprotinin, leupeptin and pepstatin and 50 µg/ml Cytochalasin D (see table 1), and the excess buffer from the settling eggs is removed. The tubes are then spun to pack the eggs in a Beckman JS-13.1 rotor at 900 x *g* for 1 minute (min), at room temperature (RT). The white apoptotic swollen eggs that float to the top are removed using a Pasteur pipette, followed by another centrifugation at high speed at 14,600 x *g* for 10 minute at RT. This results in separating the eggs into a lipid layer at the top, a brown cytoplasmic fraction in the middle, and an insoluble egg yolk pellet at the bottom. The cytoplasmic layer is collected using a 20 G needle and a 1 ml syringe via side puncture, and from this point, the extract is kept on ice.

The extract is supplemented with 10 µg/ml protease inhibitors, 10 µg/ml Cytochalasin D, and 15% of LFB1/50. The extract is gently mixed well using a Pasteur pipette and transferred to SW 55 ultracentrifuge tubes (344058, Beckmann), which are then subjected to a final clarifying spin at 14,600 x *g* for 20 min at 4°C. This spin results in a yellow lipid plug at the top, below this is a white membranous material, followed by golden cytoplasmic fraction, and a black insoluble pellet at the bottom. Using a clean spatula the lipid plug is removed, and the cytoplasmic layer including the wispy membranes floating above is collected into a 50 ml falcon tube without disturbing the dark pellet at the bottom, as this contains the mitochondria, which promotes apoptosis on freeze thawing. The collected extract is supplemented with 2% glycerol solution and mixed thoroughly using a Pasteur pipette. The extracts are then frozen as beads by

dropping them into liquid nitrogen as 20 µl beads and stored at -80°C. Such extracts remain stable for more than 10 years without compromising on quality.

2.2.2 Preparation of demembrated sperm DNA

The *X. laevis* sperm DNA is the physiological substrate used to carry out DNA replication in egg extracts. To increase the yield of sperm nuclei, male frogs are primed with 150 units of Chorulon 5–9 days before the removal of testes to promote sperm maturation. The preparation of the sperm nuclei involved all the lab members. Male frogs are placed in the MS222 solution (Table 1) containing opaque chambers until they stop moving and drop their heads underwater. Frogs are kept in this anaesthetic solution until they lost their swallowing reflex, and death was ensured by cutting through the main arteries around the heart. Testes located in the lower abdominal region are removed carefully without damaging them and immediately placed in EB solution (Table 1) on ice. Testes have a bean or egg shape and ivory colour with a typical length of 0.75-1.5 cm. Generally, a male frog has two testes, which can vary in size.

Testes are washed inside a petri dish containing ~20 ml EB solution, and using clean forceps blood vessels and extraneous tissues are removed without bursting the testes. The cleaned testes are then transferred to a fresh petri dish containing 1ml EB and finely chopped using a razor blade. All chopped material is then pooled together and filtered through a 25 µm nylon filter. The filtered material was collected and stored on ice. At this point, the filtered material looks cloudy. The filtered material is spun down at 2000 x *g* in a swinging bucket rotor for 5 min at 4°C. The pellet fractions are then resuspended with 0.5 ml SuNaSp (Table 1) and supplemented with 25 µl Lysolecithin (Table 1) per each testis and incubated for 5 min at room temperature. Demembration of sperm is confirmed by mixing 1 µl of sperm sample with 1 µl Hoechst 33258 (20 µg/ml) (Table 1)

and viewing it under a UV microscope. Demembranated sperm is stained bright blue with Hoechst, as it can bind to DNA, while non-demembranated sperm does not stain. Once the demembranation reaches > 95%, the sperm is centrifuged at 2000 x *g* in a swinging bucket rotor for 5 min at 4°C, and the pellet is resuspended in 0.5 ml SuNaSp containing 3% BSA per testis to quench the lysolecithin. The samples are centrifuged again, and the pellet was resuspended in 0.5 ml EB per testis. This step is repeated, and the pellet is resuspended in 100 µl EB + 30% glycerol per testis. The final concentration of sperm DNA is estimated using a haemocytometer to count the number of sperm and large somatic-type nuclei. The counting is done twice, and an average number is calculated for statistical accuracy. After estimating the concentration, the stock is diluted to a final concentration of 1000 ng DNA/µl by diluting in EB+ 30% glycerol and the sperm DNA is stored at -80°C in 50 µl aliquots.

2.2.3 Using egg extracts and sperm DNA for studying DNA replication

2.2.3.1 Activating the *X. laevis* egg extract

X. laevis egg extracts prepared in our lab are arrested at the metaphase of meiosis II. Extracts prepared in the presence of EGTA, a Ca²⁺ chelator enable maintenance of arrest. To carry out DNA replication, it is essential to activate this arrested extract so that it can enter the first mitotic interphase. To do this, the extracts are supplemented with 0.3 mM CaCl₂ that mimics the calcium wave generated during fertilisation thereby enabling them to enter into the first mitotic interphase. In addition to this, we also supplement the extract with 1/40th volume of Energy regenerator (ER) (Table 1) to provide sufficient energy to drive the reaction. To further synchronise the extract through the inhibition of cyclin synthesis, we also add 1/40th volume of Cycloheximide (Table 1) at a final concentration of 250 µg/ml. This treatment is left for 15 min at 23°C enabling the release

of extracts from metaphase arrest and activating the replication licensing system, allowing the replication of sperm DNA to commence. Once activated, the extracts are supplemented with ~10 ng/μl of sperm DNA to initiate DNA replication.

2.2.3.2 Measuring replication efficiency of egg extracts

A TCA assay is performed to measure the replication efficiency of newly prepared egg extracts. *X. laevis* egg extracts can incorporate a range of radiolabelled dNTPs into newly replicated DNA, and we used α -³²P labelled dATP (NEG512H250UC, Perkin Elmer) for this purpose. Egg extracts are supplemented with an energy regenerator, cycloheximide and calcium chloride, followed by sperm DNA (as explained in section 2.2.3.1). Along with sperm DNA, radioactive α -³²P-dATP (50 nCi/μl) is added and samples are aliquoted into 3-5 μl and incubated for the duration of the time course at 23°C. During each time point, the replication reactions are terminated with the addition of 160 μl of Stop C solution (Table 1) containing SDS and 0.2 mg/ml proteinase K (740506, Macherey Nagel). Terminated reactions are then incubated at 37°C for 30 min. After the digestion of proteins, the DNA is allowed to precipitate in 4 ml of ice-cold 10% TCA solution at 4°C. The precipitated DNA is then separated from the unincorporated soluble α -³²P-dATP by filtration. A small aliquot of 40 μl was taken from each sample and spotted on a 25 mm Whatman paper (1001-025, GE healthcare life sciences) for measuring the total α -³²P-dATP added to each sample. The remaining sample is poured down a vacuum filter pump (Millipore) containing glass fibre filters (11512083, Fisherbrand) and washed again with fresh 4 ml of 10% TCA to ensure the removal of all DNA from the tubes. This filtration process is repeated for all the samples. This is followed by washing the glass filters with 5 ml of 5% ice-cold TCA and 70% ethanol. The glass fibre filters are removed and dried under an infrared lamp. Each filter was then inserted individually into scintillation vials and filled with 0.5 ml of

scintillant Ultima Gold F (6013179, Perkin Elmer). The amount of DNA and the level of radioactivity were measured using a scintillation counter (Tri-Carb 2900TR).

The percentage of the total ^{32}P incorporated in the newly replicated DNA is normalised by dividing the ^{32}P incorporated in the DNA obtained from glass fibre filters by the total ^{32}P obtained from the paper filter. This gives the total ^{32}P incorporated into the DNA. To calculate the total amount of DNA synthesised in ng/ μl of extract, we multiply this normalised total ^{32}P value by 0.654. This value was estimated on the basis that the extract contains an endogenous dNTP pool of $\sim 50 \mu\text{M}$. Additionally, the average molecular weight of dNMPs is 327 Da and equal quantities of all four dNMPs are incorporated into the newly synthesised DNA. Therefore, the weight of dNMP incorporated in ng/ μl = % total ^{32}P incorporated/100 $\times 50 \times 10^{-6} \times 4 \times 327 \times 10^3$.

2.2.3.3 Isolation of Chromatin to analyse chromatin-associated proteins

This assay is performed either in S-phase or mitotic phase to study the chromatin binding dynamics of various replication-related proteins. It allows us to analyse the effects of adding different proteins (Table 5) or inhibitors (Table 4) in a replication reaction. It is usually performed as a time course experiment, and two important controls, histones, and a 'no DNA' sample, are used here. Histones are used as loading controls as they are abundantly present on chromatin and can be stained by Coomassie as a loading control, but also to detect any contaminating non-histone proteins from the whole extract. A 'no DNA' sample with no sperm added is isolated in parallel to other samples to detect protein precipitation, which otherwise can be misinterpreted as interaction with chromatin. This is done for each treatment tested.

Metaphase II arrested egg extracts are activated as explained in section 2.2.3.1, and 10 ng/ μl of sperm DNA is added to the extract. After the addition of sperm DNA, the extracts

are supplemented with appropriate treatments and corresponding controls for each. For a chromatin sample, we typically use 20 µl of extract per timepoint. All samples are aliquoted appropriately into 1.5 ml Treff tubes (9607811903, TreffLab), and incubated at 23°C for the duration of the time course.

At appropriate time points, the 20 µl samples are resuspended with 0.5 ml of ice-cold 1X ANIB100 buffer (Table 1), followed by underlaying with 100 µl of sucrose cushion (1X ANIB100 with 20% sucrose). The dilution of the extract is essential to reduce the density and viscosity of the extract and allow the disruption of the nuclear envelope with the detergent, to allow the sedimentation of the chromatin through the sucrose cushion. The samples are then spun at 2100 x *g* for 5 min at 4°C in a swinging bucket rotor. After the centrifugation, the buffer above the sucrose cushion is removed and washed twice with 100 µl of 1X ANIB to avoid contamination of the chromatin sample with the diluted extract. The sucrose cushion is carefully removed, leaving ~70 µl in the tube, and then subjected to high-speed centrifugation at >10,000 x *g* at 18°C for 2 min at a fixed angle to focus the pellet. The remaining buffer is carefully removed, and the pellets are resuspended in 30 µl of 2X NuPAGE LDS loading buffer (NP0008, Invitrogen), boiled, separated on a 4-12% NuPAGE acrylamide gel (WG1403BOX, Invitrogen) and analysed by western blotting.

2.2.3.4 Isolation of nuclear fraction from *X. laevis* egg extract

The nuclei isolation assay was performed as described in Moreno et al; 2014 and Davidson et al; 2006. Metaphase II arrested egg extracts (IgG mock and TRAP depleted) were activated as explained in section 2.2.3.1 and 10 ng/µl of sperm DNA was added to the extract. After the addition of sperm DNA, the extracts were supplemented with appropriate treatments and corresponding controls for each. Samples were aliquoted as

20 µl each and incubated at 23°C until the duration of the time course. One sample from the control and the treated was supplemented with aphidicolin (A0781, Sigma) to have a final concentration of 40 µM, and aphidicolin/ 5 mM caffeine (C0750, Sigma) as a positive control.

During each time point, the extract was overlaid onto 300 µl of ice-cold Chk1 buffer (Table 1) and was centrifuged at 3000 x *g* in a swinging bucket rotor for 5 min at 4°C. After centrifugation, 200 µl of the buffer was removed and the remaining was resuspended in 500 µl ice cold Chk1 buffer. This was transferred and overlaid on a fresh set of 500 µl of ice-cold Chk1 buffer and centrifuged again as earlier. The supernatant was removed, leaving ~50 µl in the tube. This was then subjected to centrifugation for 10 seconds (sec) under 5000 x *g* at 4°C. The supernatant was removed carefully, leaving ~20 µl behind. The remaining sample was resuspended with 6.5 µl of 4X loading buffer (NP0008, Invitrogen) and 1X loading buffer to make up to 30 µl. The samples were separated on a 4-12% NuPAGE acrylamide gel (WG1403BOX, Invitrogen) and analysed by western blotting.

2.2.3.5 Large-scale immunodepletion of TRAIP from *X. laevis* egg extracts

To identify the functional role of a protein of interest, it is essential to specifically immunodeplete this protein using specific antibodies that are cross-linked to magnetic beads. The specificity of observed phenotypes can be ensured by adding back recombinant proteins to the immunodepleted extract.

To immunodeplete a protein from extract, we first need to couple the antibodies to Dynabeads. The following protocol describes the coupling of 360 µg of antibodies to 600 µl of magnetic beads. 600 µl of Protein A Dynabeads (10002D, Life Technologies) (for use with antibodies raised in rabbit) are transferred to 1.5 ml Eppendorf tubes and washed with 1 ml 1X PBS. TRAIP immunodepletions are performed using α-TRAIP #91 raised in

rabbit and affinity-purified (Table 6) or nonspecific rabbit IgG (I5006, Sigma). 360 µg of antibodies are added to the prepared beads and topped up to a volume of 600 µl with 1X PBS. The mixture is incubated at 4°C rotating overnight. The next day, the supernatant is removed, and the beads are washed again with PBST, and the beads are subsequently incubated with 17.2 mg of BS3 crosslinker (S5799, Sigma) in BS3 conjugation buffer (20 mM sodium phosphate, 150 mM NaCl, pH7-9) and incubated for 30 min. This is followed by quenching with 1M Tris-HCl, pH 7.5 for another 15 min. The beads are then washed thrice with 100 mM HEPES, pH 7.6 followed by LFB1/50 (twice) resulting in antibody-coupled beads for use in immunodepletions. These crosslinked beads are then incubated with activated egg extracts. Effective immunodepletion requires 2 rounds of 1 h incubation of egg extract with antibody-coupled beads at 50% beads ratio (e.g. 2 rounds of 100 µl of egg extract incubated with 50 µl of coupled beads). After incubation, the beads are separated from the extract using a magnetic rack, and the immunodepleted extracts are collected and dropped as 10 µl beads into liquid nitrogen and stored at -80°C until use.

2.2.3.6 Small-scale immunoprecipitation to test α -TRAIP and α -Lrr1 antibodies

To test if the in-house raised α -Lrr1 and α -TRAIP sera or the purified antibodies can immunoprecipitate Lrr1 and TRAIP from *Xenopus* egg extracts, 20 µl of the extract was used for each IP sample. The extracts were activated as mentioned in section 2.2.3.1. The extracts were then diluted by resuspending in a 4X volume of LFB1/50 and subjected to centrifugation at high speed for 10 min at 4°C. 100 µl of supernatant was collected for each sample and supplemented with 1 µg of antibodies. It was then incubated on ice for 1 h. Each sample was then supplemented with 15 µl of Protein A Dynabeads (10002D, Life Technologies), which were prewashed once with 1 ml 1X PBS and twice with 1 ml of

LFB1/50 using a magnetic rack. After the incubation, the samples with antibodies were transferred to the tubes containing prepared beads and incubated for 1 h at 4°C with rotation. After incubation, the beads were separated using a magnetic rack and washed with 1 ml of LFB1/50 thrice. The beads were supplemented with 30 µl of 2X loading buffer and boiled at 95°C for 5 min. 20 µl of input and depleted samples were taken at the respective stages and boiled with 2X loading buffer for analysis by western blotting.

2.3 Work involving bacteria

2.3.1 Bacterial strains and growth media used in this study

E. coli derivatives such as XL 10-Gold ultra-competent cells (200315, Agilent), BL21 (De3) Competent *E. coli* (C2527, NEB), Arctic Express (De3) (230192, Agilent), C41 (De3) (60442-1, Lucigen) and Rosetta (De3) pLysS Competent Cells (70956, Merck) were different host strains used in this study. All cultures were grown in autoclaved Luria Bertani (LB) broth/agar (L3022, Sigma /L2897, Sigma) or Auto induction media (AIM) (AIMLB0210, Formedium) supplemented with the appropriate amount of antibiotics (Table 1). The bacterial cultures were grown at 37°C in an incubator shaker unless otherwise stated. Cultures grown on LB agar plates were also incubated at 37°C overnight and stored at 4°C.

2.3.2 Transformation

Recombinant plasmids containing the gene of interest were transformed into commercially available competent *E. coli* derivatives mentioned in section 2.3.1 for protein expression. 10 µl of competent cells were taken and 0.4 µl of β-mercaptoethanol was added and incubated for 10 min to increase transformation efficiency (only for XL10-Gold and Arctic cells). For all competent cells, 100 ng of plasmid DNA were added and left

on ice for 30 min, followed by a 45 s heat shock at 42°C. The cells were then transferred to ice for 5 min after which 250 µl of SOC medium (B9020S, NEB) was added and incubated at 37°C for 1 h with constant shaking. 100 µl of bacterial culture was then plated on LB agar plates containing appropriate antibiotics and left overnight at 37°C in an incubator to screen for isolated colonies.

2.3.3 Plasmid purification

The colonies obtained after transformation were inoculated in 5 ml LB broth added with appropriate antibiotics and left overnight in an incubator shaker at 37°C. The plasmids were extracted using the QIAprep Spin Miniprep kit (27104, Qiagen) as per the manufacturer's instructions. The concentration of the plasmids was assessed using a nanophotometer (Implen).

2.3.4 Testing expression of recombinant proteins

The expression of recombinant proteins was tested in different *E. coli* strains. Plasmids were first transformed into different expression strains as described in section 2.3.2. Individual colonies were picked and inoculated into 10 ml LB broth and left in an incubator shaker at 37°C overnight. 100 µl of this overnight culture was inoculated into fresh 10 ml LB broth and grown until the Optical Density (OD) value reached between 0.4-0.6, after which 1 mM IPTG (I6758, Sigma) was added for protein induction. No IPTG was added to cultures grown using auto-induction media. Samples before (500 µl) and after induction (250 µl) were collected and spun down at 10,000 x *g* for 1 min. The pellets were resuspended in 100 µl of 2X loading buffer, boiled at 95°C and analysed on acrylamide gels by Coomassie staining or by western blotting, and the best expression strain for each protein of interest was identified.

2.3.5 Purification of recombinant proteins

The recombinant proteins used in this PhD project were purified using optimised protocols as mentioned below.

2.3.5.1 Purification of recombinant *X. laevis* Lrr1

X. laevis His-SUMO-Lrr1 was expressed (from pET15b; ampicillin resistance) from ArcticExpress cells using auto-induction media (AIMLB0210, Formedium). A 2 litre bacterial culture expressing His-SUMO-Lrr1 was grown at 37°C until the OD value reached ~0.4 and then shifted to 13°C overnight. The cultures were then spun down at 6000 x *g* for 15 min at 4°C in a Beckman Avanti centrifuge and pellets were collected and stored at -80°C until use.

The His-SUMO-Lrr1 containing bacterial pellets were thawed and resuspended in lysis buffer: 50 mM Tris-HCl; pH 8, 0.1 mM EGTA; pH 8, 350 mM NaCl, 0.1% β-mercaptoethanol, 270 mM Sucrose, 0.03% Brij-35, 2 mM MgCl₂, 5 mM Imidazole, 1 µg/ml Aprotinin, 1 µg/ml Pepstatin, 1 µg/ml Leupeptin, 0.1 mM PMSF, containing 1 mg/ml lysozyme with a final pH of 8.4. After resuspension, 5 µl of Basemuncher (25 U/ml) (Expedeon) was added, and the samples were incubated at room temperature (RT) for 20 min followed by sonication for 6 x 30 sec; in a medium setting of 30 kHz. The homogenate was then centrifuged at 16,000 x *g* for 30 min at 4°C, and the supernatant was mixed with Super Nickel NTA Agarose Affinity Resin (SUPER-NINTA100; Genscript) for 1 h at 4°C. The supernatant was separated again by subjecting it to low-speed centrifugation (1000 x *g* for 5 min) and was mixed with a fresh lot of beads. This was incubated for 3 h at 4°C. The two-step incubation was performed to saturate the first batch of beads with His-SUMO, which expresses on its own and preferentially binds to the beads. After incubation, the beads were separated again by centrifuging at 1000 x *g* for 3 min at 4°C. The supernatant was removed, and the beads

were washed 3 times using the same resuspension buffer to remove non-specific proteins. The protein was finally eluted with elution buffer containing 250 mM Imidazole, and those fractions containing the highest amounts were dialysed into LFB1/50. The concentration of proteins was estimated using BSA standards by SDS-PAGE and stored at -80°C until use.

Similarly, for expression of His-SUMO-Lrr1 from BL21 (De3) cells, 2 litres of bacterial cultures were grown at 37°C until the OD value reached ~0.4 and then shifted to 20°C overnight. The same purification procedure as in ArcticExpress cells was used for purifying His-SUMO-Lrr1 from BL21 (De3) cells.

2.3.5.2 Purification of recombinant *X. laevis* N-Cul2/Lrr1/EloB/C complex

To purify *X. laevis* N-Cul2/Lrr1/EloB/C as a complex, they were expressed from three different plasmids. His-SUMO-Lrr1 (from pET15b; Ampicillin resistance), N-Cul2 (from pET24a; Kanamycin resistance) and EloB/C (from pACYCDuet1; Chloramphenicol resistance) were transformed into BL21 (De3) cells. The colonies obtained as a result of transformation were selected on plates containing the three appropriate antibiotics. For large scale expression, transformed BL21 (De3) cells were grown in 2 litres of AIM media. The cultures were grown at 37°C until the OD value reached ~0.4 and then shifted to 20°C overnight. Cultures were then spun down at 6000 x *g* for 15 min at 4°C in a Beckman Avanti centrifuge, and the pellets were collected and stored at -80°C until use.

The bacterial pellets were thawed and resuspended in lysis buffer: 50 mM NaHPO₄; pH 9, 300 mM NaCl, 10% Glycerol, 2 mM DTT, 2 mM MgCl₂, 0.5% Triton, 1 µg/ml Aprotinin, 1 µg/ml Pepstatin, 1 µg/ml Leupeptin, 0.1 mM PMSF, containing 1 mg/ml lysozyme. 5 µl of Basemuncher (25 U/ml) (Expedeon) was added to the lysate and incubated for 20 min. The lysate was then sonicated for 6x10 sec in a medium setting of 30 kHz, while on ice.

The samples were centrifuged at 20,000 x *g* for 30 min at 4°C, and the supernatant was mixed with prewashed Super Nickel NTA Agarose Affinity Resin (SUPER-NINTA100; Generon) for 3 h at 4°C. The beads bound to the proteins were then separated by centrifuging at 1000 x *g* for 3 min at 4°C and washed 3 times using the same resuspension buffer containing protease inhibitors. The protein was eluted with resuspension buffer containing 400 mM Imidazole and protease inhibitors for the first 5 elutions, followed by the same buffer at a lower pH of 4.5 for the remaining elutions. The fractions containing the highest amounts of proteins were dialysed into LFB1/50. The concentration of proteins was estimated using BSA standards by SDS-PAGE and stored at -80°C until use.

2.3.5.3 Purification of recombinant *X. laevis* Lrr1/EloB/C

To purify *X. laevis* Lrr1/EloB/C as a complex, they were expressed from two different plasmids. His-SUMO-Lrr1 (from pET15b; Ampicillin resistance) and EloB/C (from pACYCDuet1; Chloramphenicol resistance) were expressed in 2 litres of Rosetta (De3) pLysS cells in LB media. The cultures were grown at 37°C until the OD value reached ~0.4 and then shifted to 20°C overnight. Cultures were then spun down at 6000 x *g* for 15 min at 4°C in a Beckman Avanti centrifuge and pellets were collected and stored until use in -80°C. Purification of this protein was carried out in two different methods as follows.

Purification of His-SUMO-Lrr1/EloB/C 1- The bacterial cells were resuspended in 50 mM NaHPO₄; pH 9, 300 mM NaCl, 10% Glycerol, 2 mM DTT, 2 mM MgCl₂, 0.5% Triton, 1 µg/ml Aprotinin, 1 µg/ml Pepstatin, 1 µg/ml Leupeptin, 0.1 mM PMSF, containing 1 mg/ml lysozyme. 5 µl of Basemuncher (25 U/ml) (Expedeon) was added. The cells were then clarified using centrifugation and the soluble fraction was further incubated with Ni-NTA beads and incubated for 2 h at 4°C. The proteins bound to the beads were then recovered after washing with 20 mM imidazole containing resuspension buffer followed by final

elutions with buffer containing 250 mM imidazole for elutions 1-5 and 400 mM imidazole from elutions 6-10. The fractions containing the highest amounts of proteins were dialysed into LFB1/50. The concentration of proteins was estimated using BSA standards by SDS-PAGE and stored at -80°C until use.

Purification of His-SUMO-Lrr1/EloB/C 2- The bacterial cells were resuspended in 50 mM Tris-HCl pH 8, 0.1 mM EGTA pH 8, 350 mM NaCl, 0.1% β -mercaptoethanol, 270 mM Sucrose, 0.03% Brij-35, 2 mM MgCl₂, 5 mM Imidazole, 1 μ g/ml Aprotinin, 1 μ g/ml Pepstatin, 1 μ g/ml Leupeptin, 0.1 mM PMSF, containing 1 mg/ml lysozyme, pH 8.4. After resuspension, 5 μ l of Basemuncher (25 U/ml) (Expedeon) was added and incubated for 20 min at RT. The cells were then clarified using centrifugation and the soluble fraction was further incubated with prewashed Ni-NTA beads and incubated for 2 h at 4°C. The depleted supernatant was again subjected to incubation with a fresh lot of beads for 3 hrs at 4°C. The proteins bound to the beads were then recovered after washing with 20 mM imidazole containing resuspension buffer followed by final elutions with buffer containing 250 mM imidazole. The fractions containing the highest amounts of proteins were dialysed into LFB1/50. The concentration of proteins was estimated using BSA standards by SDS-PAGE and stored at -80°C until use.

2.3.5.4 Purification of recombinant *X. laevis* GST-TRAIP^wt and TRAIP^mut

Xenopus TRAIP was cloned into a pGS21 vector and GST-TRAIP was expressed in BL21 (De3) in Auto Induction Media overnight at 18°C. Pellets were lysed in lysis buffer: 50 mM NaH₂PO₄; pH 9, 300 mM NaCl, 10% glycerol, 2 mM DTT, 2 mM MgCl₂, 0.1 mM PMSF, 1 μ g/ml of each aprotinin, leupeptin, and pepstatin and 1 mg/ml lysozyme. After resuspension, 0.03% Brij and 3 μ l of Benzonase (25 U/ml) were added. The samples were sonicated for 8 x 30 sec; in a medium setting of 30 kHz using a wide-diameter probe; while

on ice. The supernatant was separated after centrifugation at 16,000 x *g* for 30 min at 4°C and mixed with Glutathione Sepharose 4B beads (17-0756-01, GE Healthcare) at 4°C overnight. The beads were then separated by centrifuging at 1000 x *g* for 3 min at 4°C, and the beads were washed 3 times using the same resuspension buffer. The protein was eluted with buffer containing 25 mM glutathione (PHR1359, Sigma) and then stored at -80°C until use. The mutant GST-TRAIPmut with a point mutation at C25A was generated by site-directed mutagenesis in the same plasmid and purified analogously.

2.3.5.5 Purification of recombinant *X. laevis* His/SUMO-TRAIPwt and TRAIPmut

Recombinant His/SUMO-tagged *X. laevis* TRAIPwt and mut were expressed in Rosetta (De3) pLysS cells from pCA528 vector in AIM by growing at 37°C for 2 h and when OD value reached 0.4, 50 µM ZnSO₄ was added to the cultures and left for expression at 18°C overnight.

After pelleting of the bacterial cultures, the cells were lysed in 20 mM HEPES-NaOH (pH 7.5), 400 mM sodium acetate, 10% glycerol, 10 µM ZnSO₄, 0.1% NP-40, 1 mM DTT and 1X Roche complete protease inhibitor cocktail) supplemented with 20 mM imidazole. Homogenates were supplemented with 1 mg/ml lysozyme, 12 µl of Benzonase and 2 mM MgCl₂ and then incubated at room temperature for 20 min. The samples were subsequently sonicated (6 × 30 sec; in a medium setting of 30 kHz) on ice and spun down for 20 min at 20,000 x *g* at 4°C. The resulting supernatant was incubated in 2 ml of prewashed Ni-NTA agarose beads (30210, Qiagen) for 1 h with rotation at 4°C. The beads were spun down at 1000 x *g* for 5 min and the supernatant was transferred to a fresh lot of prewashed beads. The samples were incubated again for 1 h at 4°C. After incubation, the beads were separated and washed in low imidazole-containing buffer (20 mM HEPES-NaOH; pH 7.5, 400 mM sodium acetate, 10% glycerol, 20 mM imidazole, 10 µM ZnSO₄,

0.01% NP-40, 1 mM DTT and 1X Roche complete protease inhibitor cocktail) and the protein was eluted with the same buffer containing increased imidazole concentration (250 mM imidazole) and protease inhibitors. Those fractions containing the highest quantity of wt or mutant TRAIP were dialysed into LFB1/100 buffer and stored at -80°C until use.

2.4 Working with DNA

2.4.1 PCR amplification

A high-fidelity Q5 DNA polymerase (M0491S, New England Biolabs) was used for the amplification of DNA from plasmids containing a gene of interest. The PCR reaction mixtures were set up as shown below in Table 7. The annealing temperatures were calculated based on an online tool: NEB TmCalculator. The thermocycling conditions used are described in Table 8.

Table 7:- Composition of the PCR reaction mixture.

Components	Volume for 25 µl reaction (µl)	Final concentration
5X Q5 Reaction Buffer	5 µl	1X
10 mM dNTPs	0.5 µl	200 µM
10 µM Forward Primer	1.25 µl	0.5 µM
10 µM Reverse Primer	1.25 µl	0.5 µM
Template DNA	variable	25 ng
Q5 High-Fidelity DNA Polymerase	0.25 µl	0.02 U/µl
Nuclease-Free Water	Make up to 25 µl	

Table 8 :- Thermocycling conditions used for PCR reactions.

Steps	Temperature	Time	Number of cycles
Initial denaturation	98°C	90 sec	1
Denaturation	98°C	10 sec	25
Annealing	variable	10-30 sec	
Extension	72°C	30 sec/Kb	
Final extension	72°C	2 min	1
Hold	4°C	∞	

2.4.2 Site-directed mutagenesis

Oligonucleotides required for making a mutant for Lrr1 and a mutant for TRAIP were designed using an online tool NEBaseChanger. Table 3 contains the list of primers used for making these mutants. The primers listed were used to set up the PCR reaction using the composition and conditions listed in Table 7 and Table 8 respectively. The PCR product obtained was then subjected to a mix of enzymatic treatment with Kinase/Ligase/DpnI or KLD enzyme (M0554S, NEB) known as the KLD reaction. This enzymatic mix allows for efficient phosphorylation, circularization of the plasmid DNA and removal of template DNA in a 5 min reaction. The remaining product is then transformed (section 2.3.2) into XL10 gold cells. The incorporation of mutation was confirmed by sequencing services by Source Biosciences. The successful mutants were then transformed into the best expression cells.

2.4.3 Cloning of TRAIP

To clone *Xenopus laevis* TRAIP from pET28a into the pGS-21a vector, restriction digestion of both vectors was carried out using NcoI (R3193S; New England Biolabs) and EcoR1

(R3101S; New England Biolabs) enzymes. 25 µl of pET28a-Traip and 25 µl of pGS-21a were digested using 2 µl of NcoI and EcoR1, 5 µl of Cutsmart (B7204; New England Biolabs) and 16 µl of Nuclease free water. The reaction was incubated for 2 h at 37°C. After incubation the samples were run on 0.8% Agarose gel and the appropriate bands were purified using a QIAquick PCR purification kit (28104, Qiagen) according to the manufacturer's instructions.

The ligation reaction was set up with 10 ng of TRAIP, 1 ng of pGS-21a, 1 µl of 10x T4 ligation buffer (B0202S; New England Biolabs) and 1 µl of T4 ligase (M0202S; New England Biolabs). The reaction was left overnight at 16°C and 2 µl of the ligated mixture was transformed into XL10 gold competent cells as mentioned before in section 2.3.2. Single colonies obtained after transformation were picked and plasmids isolated from these were tested for successful cloning both by sequencing and by restriction digestion.

2.4.4 Agarose gel electrophoresis and visualisation

DNA samples from PCR reactions and restriction digestion products were run on 0.8% agarose gels and visualised on a Safe View Mini box (Cleaver Scientific Ltd). The required amount of agarose was weighed out and melted in 1X TBE buffer (A4718, Merck). After the agarose has cooled down to ~55°C 10 µl of SYBR Safe DNA gel stain (S33102, Thermo Scientific) was added so that it intercalates with the DNA and allows for visualization under the UV lamp. Molten agarose was then poured into a casting tray and once set DNA samples were loaded by mixing with 6X purple gel loading dye (B7025, New England Biolabs) in a 1:5 ratio. 1 kb plus DNA ladder (10787018, Invitrogen) was used as a marker for size estimation. Electrophoresis was carried out at 100 V for 1 h and the gel was visualised using a safe view box or gel documentation unit (Syngene). Images were recorded using GeneSnap software.

2.5 Working with Proteins

2.5.1 Dialysis

The elutions obtained from recombinant protein purifications were dialysed to exchange the elution buffer into an egg extract-friendly buffer; LFB1/50 buffer (see Table 1). Pur-A-Lyzer Maxi 25 kDa dialysis columns (PURX25005, Merck) were used for dialysing recombinant Lrr1 and recombinant TRAIP. The columns used were prepared by incubating with distilled water for 5 min during which cellulose membranes are activated. This enables the exchange of buffer and free passage of molecules that are below the size of the membrane. These columns were then filled with protein samples and stirred overnight at 4°C. After dialysis, the proteins were aliquoted as 50 µl and stored at -80°C until use.

2.5.2 SDS PAGE (Sodium Dodecyl Sulphate Poly Acrylamide Gel Electrophoresis)

All protein samples were analysed either on a precast 4-12% NuPAGE Bis-Tris gels (WG1403BOX, Invitrogen) or 10% SDS PAGE gel prepared in-house (see Table 9 below). Protein samples were mixed with 2X NuPAGE LDS sample buffer (NP0008, Invitrogen) and were denatured by boiling at 95°C for 5 min before loading onto the gel. To enable determination of protein sizes 5 µl PageRuler Plus Prestained Protein Ladder (26620, Invitrogen) was used. The apparatus was filled with 1X NuPAGE MOPS SDS running buffer (NP000102, Invitrogen) for precast gels and electrophoresed at 160 V for 1h 15 min, whereas, 1X Tris-glycine buffer (Table 1) was used to run in-house made SDS-PAGE gel at 100 V for 1.5 hrs.

Table 9 :- Composition of 10% SDS-PAGE gel.

	Components	Volume (for 10ml)
10% Resolving gel	Distilled water	4.0 ml
	30% acrylamide solution	3.3 ml
	1.5 M Tris (pH 8.8)	2.5 ml
	10% SDS	0.1 ml
	10% ammonium per sulphate	0.1 ml
	TEMED	0.004 ml
5% Stacking gel	Distilled water	2.7 ml
	30% acrylamide solution	0.67 ml
	1 M Tris (pH 6.8)	0.5 ml
	10% SDS	0.04 ml
	10% ammonium persulphate	0.04 ml
	TEMED	0.004 ml

2.5.3 Staining of protein gels

Proteins resolved on acrylamide gels were visualised by staining with Coomassie stain (Table 1) solution for 1 h on a rocker (SSM4; Stuart) to detect the total protein content. After incubation the stain was discarded and the gel was destained using the destaining solution (Table 1) until the bands were visible.

The loading controls from chromatin isolation experiments (histones) were stained using Simply Blue Safe Stain (LC6060; Invitrogen). The gels containing histones were washed for 3 x 5 min in water and then submerged in the stain for 1 h on a rocker. The gels were destained by washing them in water until the bands were visible.

2.5.4 BSA standard assay

To find the concentration of proteins a BSA standard of known concentration was serially diluted to compare with the target protein. 10 mg/ml of BSA stock solution was prepared

and dilutions of 5, 2.5, 1.25 and 0.625 mg/ml were prepared. Dilutions of purified proteins were also prepared by mixing with LFB1/50 buffer and 2X NuPAGE loading buffer was added. All samples were run on an acrylamide gel and visualised by Coomassie staining.

2.5.5 Bradford assay

Total protein concentration was analysed by using a series of dilutions of BSA stock of 1 mg/ml to use as standards against the target protein. 1 ml of Pierce Coomassie Plus Bradford Assay reagent (23238; Thermo Fisher Scientific) was added to each and mixed well in a cuvette. The absorbance of all samples was measured at 595 nm using a spectrophotometer. The absorbance values from the standard were used to generate a standard curve and the concentration of unknown protein was derived from this.

2.5.6 Immunoblotting

Proteins samples run on acrylamide gels were transferred onto Immobilon-P PVDF membranes (LC6060; Merck) by electroblotting at 100 V for 1 h 30 min. The membranes containing the proteins were then blocked in 5% non-fat dry milk in 1X TBST (see Table 6) to prevent non-specific binding. The membranes were then rinsed in 1X TBST to remove excess milk and then incubated with the appropriate concentration of primary antibodies (Table 6) prepared in 3% BSA + 0.02% Sodium azide solution in 1X TBST and incubated overnight at 4°C. The membranes are then washed in 1X TBST for 3 x 10 min. Washing is an important step as it minimises the background and removes unbound antibodies. The membranes were further incubated for 1 h with the HRP-labelled secondary antibodies (Table 6) specific to the species in which the primary antibody was raised. After the incubation, the membranes were washed again as before, and incubated with chemiluminescent HRP substrate; Western Bright ECL spray (K-12049-D50;

Advansta) which was followed by exposure to X-ray film (MOL7016, Scientific Laboratory Supplies).

2.5.7 Antibody purifications

To purify the antibody against a target protein, the protein was first purified as mentioned in section 2.3.5. The protein samples were then sent to Dundee Cell products to raise antibodies in the selected host species. To purify the antibodies from the animal sera, we made an antigen column specific to the target protein. The protein was first dialysed (section 2.5.1) into a coupling buffer (Table 1) and was coupled to the beads in the HiTrap NHS-activated HP affinity column (17071701, Cytiva), that can be used for any primary amine-containing ligand. A stable amide linkage, formed as a result of covalent bonding between the resin and the amine group of the ligand, enables the column to be used for affinity purification. The column was first activated with 1 mM ice-cold HCl and the antigen solution was loaded onto the column. An antigen concentration of at least 1 mg/ml was found to be the most effective. It was then incubated for 30 min and unreacted NHS groups were blocked using a blocking buffer (Table 1). The column was then washed by alternating with high and low pH twice with 10 mM Tris HCl; pH 8 or 0.1 M glycine; pH 2 and the column was stored with 1X PBS at 4°C.

The antiserum was defrosted and diluted with equal volumes of 1X PBS and filtered through 0.45 µm syringe filters to remove impurities (SLHN033NB; Millipore). The diluted serum was recirculated through the prepared antigen column overnight at 4°C. The column was washed with 50 ml washing buffer (Table 1) to remove excess serum from the column. The antibodies were finally eluted using 0.1 M glycine; pH 2.6 into 1.5 ml Eppendorf tubes containing 100 µl of 2M Tris-HCl; pH 8.5. The concentration of

purified antibodies was assessed by Bradford assay and antibody-containing elutions were stored at -80°C.

2.5.8 *In vitro* kinase assay

In vitro kinase assay was performed based on Cui et al, 2018. Phosphorylation of recombinant TRAIP and its mutant versions were tested with CDK1/Cyclin B (PV3292; Thermo Scientific), CDK2/Cyclin A (PV3267; Thermo Scientific) and CDK2/Cyclin E1 (PV6295; Thermo Scientific). To test phosphorylation, an *in vitro* assay was set up with PK buffer, 1X ATP (Table 1), 0.3 µg of Mitotic/S-phase recombinant CDKs, and 0.125 µg/µl recombinant purified TRAIP in a 20 µl reaction. The samples were incubated at 30°C for 30 min and the reaction was stopped with the addition of 4X SDS loading buffer. The phosphorylated samples were run on a 6% SuperSep Phos-tag gel (192-17401; Fujifilm) for 1 h 15 min at 160 V and analysed by immunoblotting.

2.5.9 Size exclusion chromatography

To analyse purified proteins or any biomolecules in terms of their size and structure, they can be passed through a size exclusion chromatography column known as Superose 6 Increase 10/300GL (GE29-0915-96; Cytiva) using SMART, Amersham Pharmacia Biotech. It has a broad fractionation range of molecules between 5-5000 kDa and the major principle is that the larger molecules cannot enter the pores of the chromatographic medium and come through the column faster while the smaller ones penetrate deeply and come out slowly enabling their separation. The columns were first equilibrated in LFB1/50 buffer (Table 1) and a cocktail of markers; 2.25 mg/ml Thyroglobulin (669 kDa), 1.87 mg/ml Apoferritin (443 kDa), 2.25 mg/ml Albumin (66 kDa), 1.125 mg/ml Carbonic Anhydrase (29 kDa) were mixed and diluted in LFB1/50. Similarly, the recombinant protein samples were prepared by adding 50 µl protein into 150 µl of LFB1/50. The

marker cocktail and protein samples were spun down for 5 min at 4°C, maximum speed. The supernatant was loaded onto the column and processed with a flow rate of 20 µl/min in LFB1/50. 50 µl fractions were collected and 50 µl of 4X NuPAGE loading buffer was added to each of them. From fractions 3-26, 15 µl of each was run on a 4-12% acrylamide gradient NuPAGE gel and analysed by immunoblotting.

2.6 Softwares

Online tools such as Robetta^{Beta} and Phyre² were used for generating the automated structural model of Lrr1. Alphafold 2 was used for predicting the structural model of TRAIP. Predictomes were used for predicting protein-protein interactions of TRAIP. Quantification of western blot signals was performed using ImageJ software. Prism was used for graphical representations. Analysis of sequencing results and multiple sequence alignments were performed using Serial Cloner version 2.6.1 and ClustalW.

Chapter – 3

3 Optimising conditions for purification of *Xenopus laevis* Lrr1 and raising antibodies

3.1 Introduction

Over the last decade, research has brought a rapid development in our understanding of replisome unloading mechanisms and the key ubiquitin ligases involved in this process. Investigations from ours and other labs had shown that in higher eukaryotes Cul2^{Lrr1} is the E3 ubiquitin ligase responsible for ubiquitylating Mcm7 during S-phase at replication termination (Dewar et al., 2017a; Sonnevile et al., 2017). However, further research is needed to fully comprehend the regulation of this pathway. It is important that we understand the mechanisms that lead to replisome disassembly, as unloading of active helicases at the wrong time and/or at the wrong place, or indeed a failure to unload them at the appropriate times, could be detrimental for maintaining genome stability (Moreno and Gambus, 2020).

The first aim of my project was, therefore, to understand how Lrr1 recognises its substrate, Mcm7, for ubiquitylation. At that point of time we did not know that the ubiquitylation of Mcm7 is suppressed throughout DNA replication by the excluded lagging strand. This physically prevents Lrr1 from recognising Mcm7, until the appropriate time, when replication termination takes place (Jenkyn-Bedford et al., 2021; Zhou et al., 2021). Our lab has previously identified K27 and K28 as the ubiquitylation sites within Mcm7 in S-phase in *Xenopus laevis* egg extracts using mass spectrometry

analysis (Moreno and Gambus, 2020). These sites are located within the N-terminus of Mcm7. I therefore wanted to: (i) investigate if the N-terminus of Mcm7 is involved in interaction with Lrr1; (ii) identify which domains of Lrr1 are important for interaction with Mcm7 and CMG, and (iii) characterise the patient mutations found within Lrr1.

3.2 Results

3.2.1 The ubiquitylation site within Mcm7 is not the only interaction point for Lrr1

E3 ligases confer substrate specificity by directly recruiting substrates and catalysing the ubiquitin transfer. Most E3s contain substrate recognition domains or subunits that provide the selectivity by directly binding or interacting with the target proteins (Zheng and Shabek, 2017). Therefore, I first set out to see if the ubiquitylation site within the N-terminus of Mcm7 is the specific point of interaction with Cul2^{Lrr1}. The aim of this experiment was to out-compete the binding of Lrr1 to the ubiquitylation site on Mcm7 with a small peptide that spans the identified ubiquitylation sites. I performed a replication assay over a time course with *Xenopus laevis* egg extract, supplemented with two peptides: peptide 1 spans the Mcm7 ubiquitylation sites and peptide 2 was a scrambled peptide used as a negative control. The peptides were optionally supplemented at a high concentration (40 µM of Peptide 1- EFYKDDEIG**KK**HFKYGVQLA, 40 µM of Peptide 2- IDEGFHDYKFQKLVKGEYAK). Addition of these peptides was found not to interfere with the egg extract's ability to synthesise nascent DNA (Figure 3.1 a). I then isolated the chromatin and studied the status of helicase disassembly and Mcm7 ubiquitylation (Figure 3.1 b). I could observe that the CMG components Cdc45 and Psf2 were disassembled after 60 min in all samples. Ubiquitylation of Mcm7 was also seen at 60 min, coinciding with the disassembly of Cdc45 and Psf2 in all samples. Since there were

no significant differences in the unloading pattern of replisomes, this suggested to us that the addition of peptides could not out-compete Lrr1-replisome interactions. Unfortunately, the use of this short peptide spanning Mcm7 cannot reveal much about the interactions of Cul2^{Lrr1} with the terminated helicase. A most likely reason for this is that Lrr1 interacts with Mcm7 or the helicase through multiple interaction sites, and not just the K27 and K28 ubiquitylation sites identified from our mass spectrometry. I therefore decided to switch and analyse the Lrr1-Mcm7 interaction from the Lrr1 perspective to understand better these interactions.

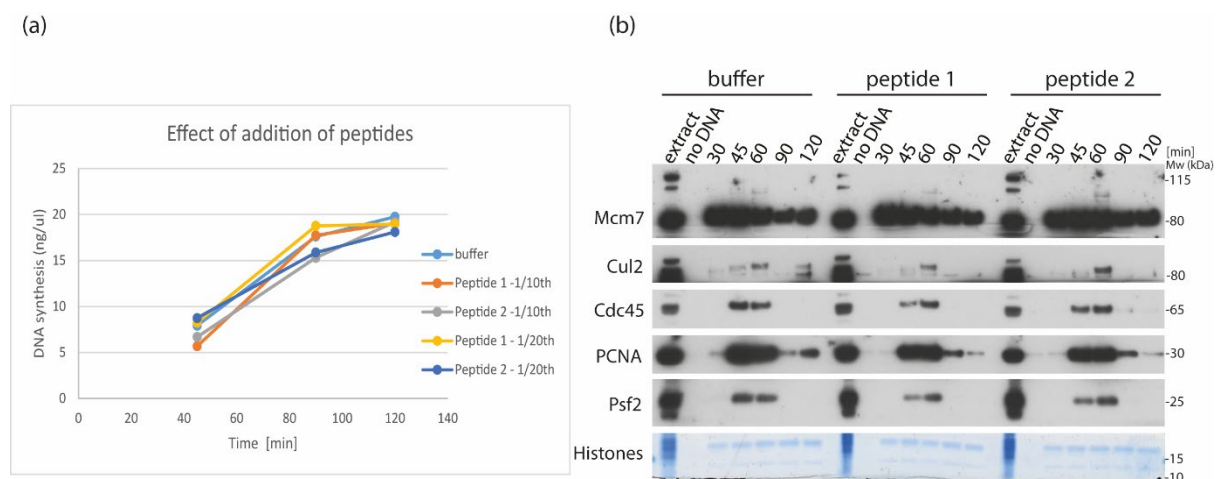


Figure 3.1:- Lrr1 likely interacts with Mcm7 and helicase through multiple binding sites. (a) A replication assay was performed to test the ability of egg extract to synthesise DNA upon addition of peptide 1 and peptide 2 at 40µM and 20µM final concentration by measuring the level of incorporation of radioactive ³²P-dATP into newly synthesised DNA. (b) Interphase egg extract was supplemented with sperm DNA and optionally supplemented with LFB1/50 (buffer control), peptide 1 or peptide 2. Chromatin was isolated at indicated times. The replication factors involved were analysed by immunoblotting with indicated antibodies. 'Extract' sample serves as a control for the western blot to check for the presence of the specific protein in the whole egg extract. 'No DNA' sample is a chromatin specificity control with no sperm DNA and was isolated in parallel. Histones that have been stained with Coomassie, acts as a loading control to visualise total protein. This experiment was performed twice.

3.2.2 Predicting the structure of *Xenopus laevis* Lrr1

To elucidate the molecular mechanism underlying the regulation of CMG ubiquitylation, and to identify which part of Lrr1 recognises the helicase, we needed to learn more about

the structure and functionality of Lrr1. The Lrr1 protein consists of 7 leucine-rich repeat domains and an Elongin BC and Cul2 box (Figure 3.2). It forms the substrate recognition subunit of Cul2 ubiquitin ligase. Generally, leucine-rich repeat proteins are known to fold into a curved solenoid or horseshoe shape, providing a concave region for protein-protein interactions (Bella et al., 2008). In general, LRR (Leucine Rich Repeat) regions are important for protein interactions (Kobe and Kajava, 2001), but we do not know whether the N and C-termini of Lrr1 also have roles in replisome unloading in S-phase.

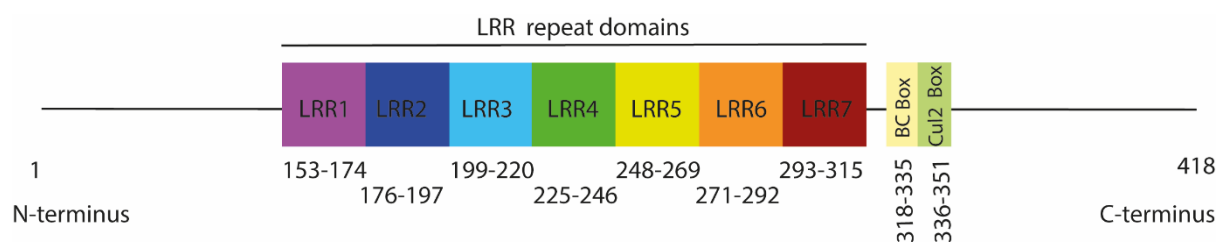


Figure 3.2:- Domain structure of Lrr1. Lrr1 consists of 7 LRR repeats, BC, and Cul2 boxes in addition to its N and C-terminus. The LRR repeat regions can facilitate protein-protein interactions.

Here, I wanted to find out which part of Lrr1 is essential for its substrate recognition. To achieve this, I aimed to make truncation mutants of Lrr1 and then assess their ability to interact with chromatin upon replication termination. To this end, we needed to predict the structure of *X. laevis* Lrr1 which I determined using automated protein structure prediction servers Robetta Beta (Figure 3.3) and PHYRE2 (Figure 3.4). They both work on the principle of comparative modelling. The prediction model from Robetta Beta revealed five different potential structural models for Lrr1. Robetta Beta and Phyre2 software search for confident matches to a protein of known structure found in BLAST, PSI-BLAST, 3D-Jury and use these as a template for predicting the structure of unknown proteins. The predicted structures of *Xenopus laevis* Lrr1 that I obtained also revealed a

concave region where leucine-rich repeats were abundant in the Lrr1 sequence. This was comparable to other LRR containing proteins (Kobe and Kajava, 2001; Bella et al., 2008).

From the literature, we know that proteins containing LRR region tend to stabilise their structure using capping motifs that are present at each end of the LRR region (Matsushima et al., 2005). Interestingly, the computer simulation of Lrr1 shows that, alike other LRR proteins, the seven LRR repeats in Lrr1 tend to arrange themselves in parallel with their β -pleated sheets at their concave ends where the ligands are expected to bind and their convex ends are made of α -helices (Figure 3.3 and 3.4). Each individual LRR repeat consist of one β -strand and α -helix that are interconnected by loops. Apart from this, I also noticed that the protein region just upstream of the LRR domain also arranges itself in the form of an LRR repeat (Glutamic acid 130 to Tyrosine 152). This region could potentially act as an N-terminal cap as it tends to shield the hydrophobic core of the LRR region (Dao et al., 2014). This typical secondary structure arrangement also coincides with the structure prediction results obtained from PHYRE2 (see E130 to Y152 in Figure 3.4). Further upstream to this potential N-terminal cap, I also noticed that the protein folds into an alpha-helical structure around Glycine 96 to Asparagine 108 (see G96 to N108 in Figure 3.4). This alpha-helical secondary structure shows similarity with recognisable capping structures reported in other LRR proteins such as PP32 and Internalin B, see Figure 3.5 (Courtemanche and Barrick, 2008; Dao et al., 2014). But since the capping regions are generally found close to the LRR repeat regions in most proteins, I considered the region closer to the LRR repeat (Glutamic acid 130-Tyrosine 152) as the N-terminal cap for Lrr1.

In an attempt to determine the capping motifs at the C-terminus of Lrr1, I again compared the prediction models from Robetta Beta and PHYRE2 software with other known

proteins containing the LRR regions. In general, the alignment of C-terminal caps of several LRR proteins suggests a consensus sequence for C-terminal caps as YRxxΦxxxΦPxΦxxLD, where x is any amino acid residue and Φ represents hydrophobic residues (Dao et al., 2014). Although I did not observe such a consensus motif present in Lrr1 similar to other LRR containing proteins, the structural models from Robetta Beta and PHYRE2 suggested that this consensus motif might not be present or is located far away from the last leucine-rich repeat, which indicates that this does not take part in shielding the hydrophobic core of the LRR regions (Figure 3.4). Strikingly, in the region downstream of the seven leucine-rich repeats, I observed that Proline 319 to Proline 336 (corresponding to the BC box) folds into an alpha helix (see Figure 3.3 a, an α -helix structure just downstream of the last LRR repeat and in Figure 3.4, see P319 to P336). Earlier reports suggest that in some LRR proteins, the terminal caps are also involved in binding to partner proteins (Dao et al., 2014). Therefore, I presume that either Lrr1 does not possess a C-terminal cap or the BC box itself can act as a capping motif and at the same time interacts with Cul2.

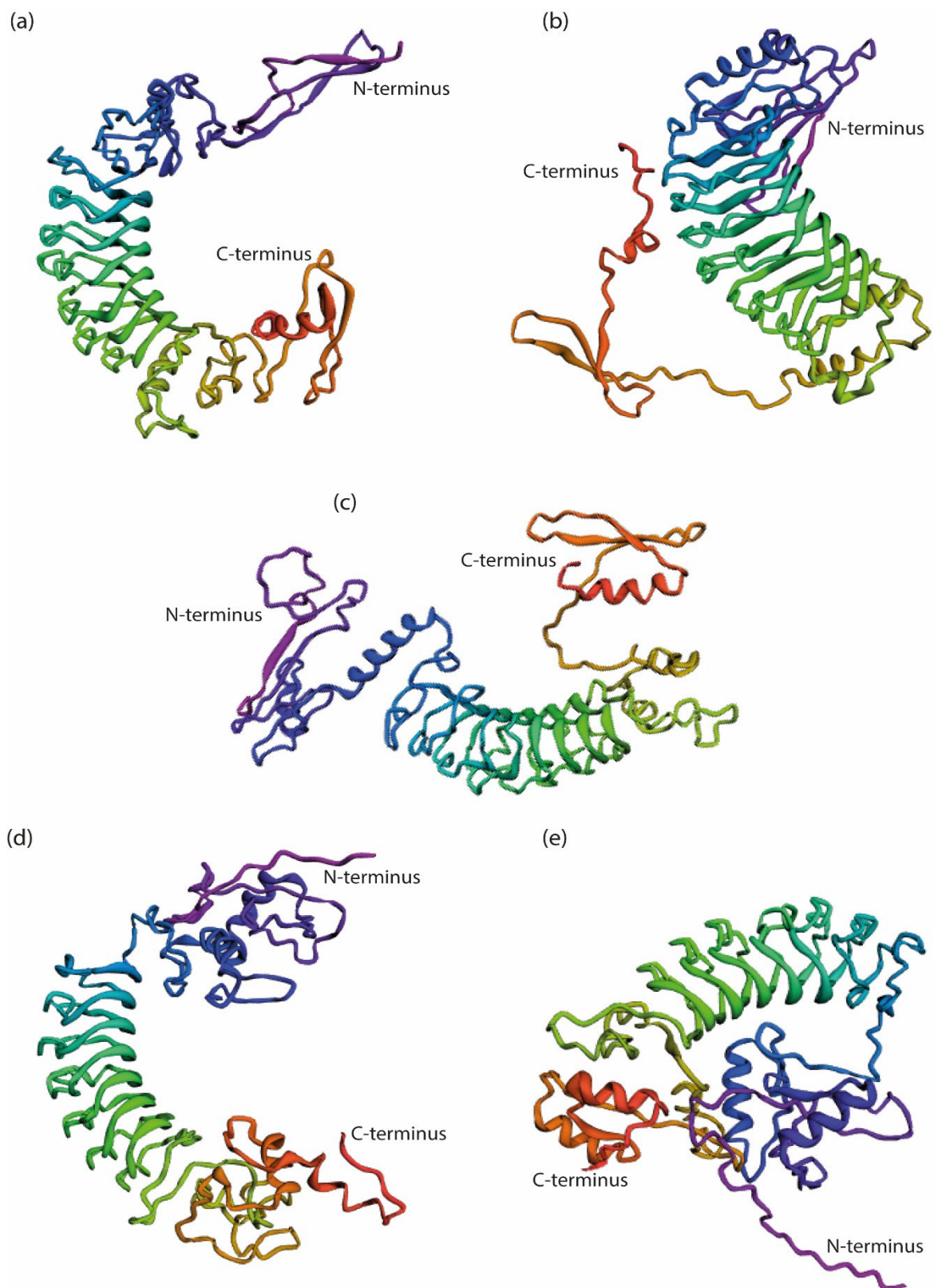


Figure 3.3:- Predicted structures of *X. laevis* Lrr1 using Robetta Beta. The five different models were generated based on the sequence homology to proteins of known structure. The N- and C-termini of predicted Lrr1 are labelled. The seven LRR repeats have been represented in shades of green with each of their β -pleated sheets arranged in parallel at its concave side.

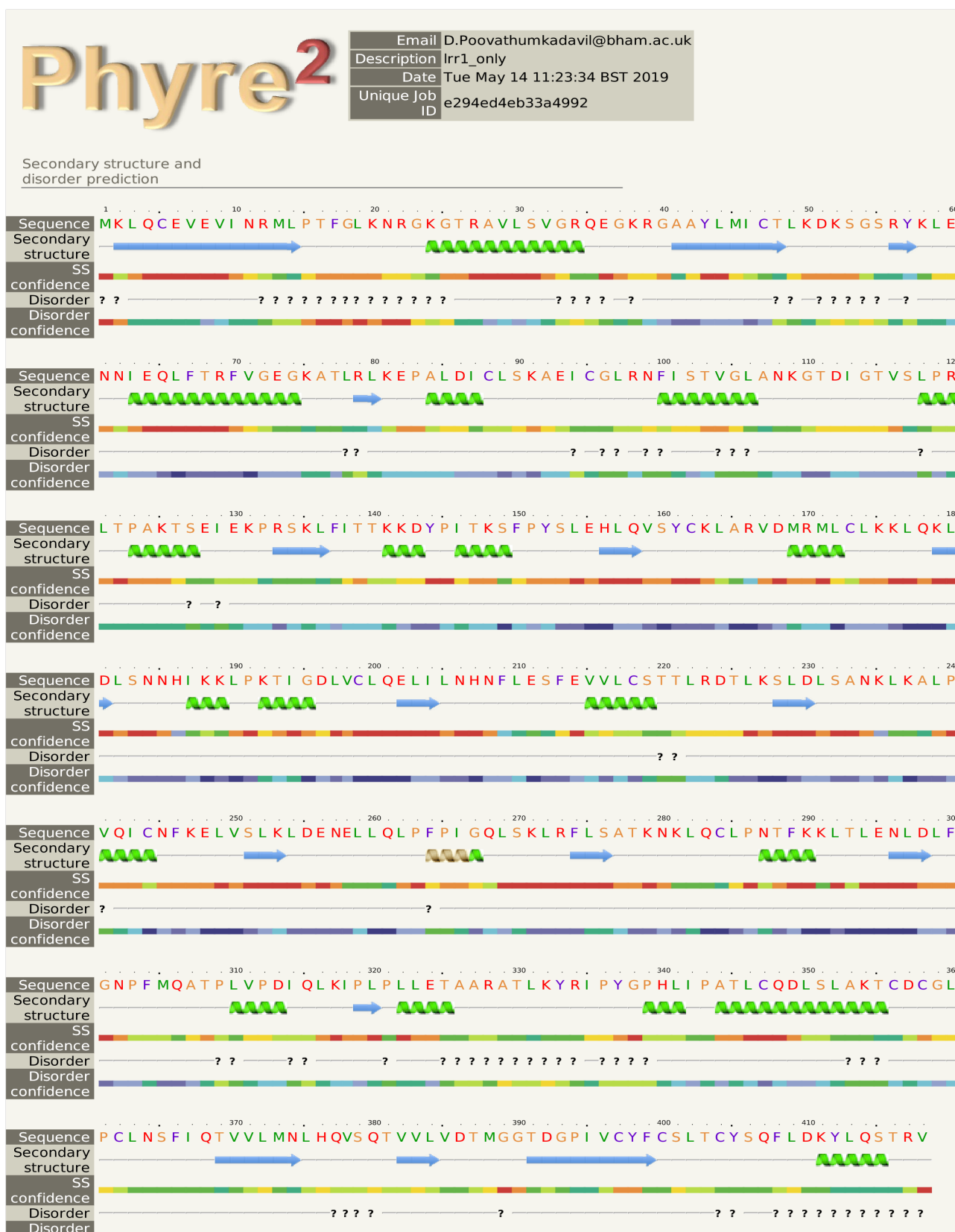
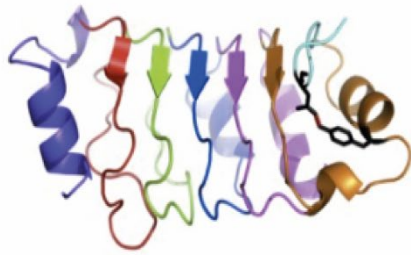


Figure 3.4:- Predicted structure of *X. laevis* Lrr1 from Phyre2. The sequence of *X. laevis* Lrr1 and its respective secondary structure are arranged beneath each other.

(a)



(b)

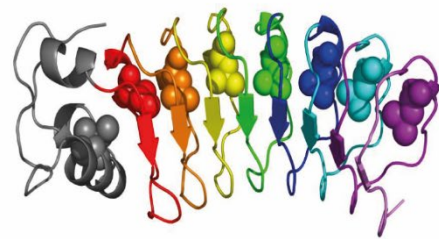


Figure 3.5 :- Structures of other LRR containing proteins along with their α -helical capping motifs. (a) The structure of LRR domain of PP32. The folded N-terminal LRR capping motif is shown in purple and C-terminal capping motif is represented in cyan (b) Structure of 7 LRR repeats of Internalin with their N-terminal capping motifs (represented in black). Figure reproduced from (Courtemanche and Barrick, 2008; Dao et al., 2014).

3.2.3 Generation of Lrr1 truncations and patient mutants

Knowing the structures and the position of the most likely capping elements for the LRR solenoid, we could now generate the Lrr1 domain mutants. I therefore aimed to investigate the functional role of the LRR domain by selectively deleting specific regions within it. The N-terminal truncated mutant was generated by removing the region between Lysine 2 and Serine 127 (Figure 3.6 and Figure 3.7 a) without disturbing the potential capping motif.

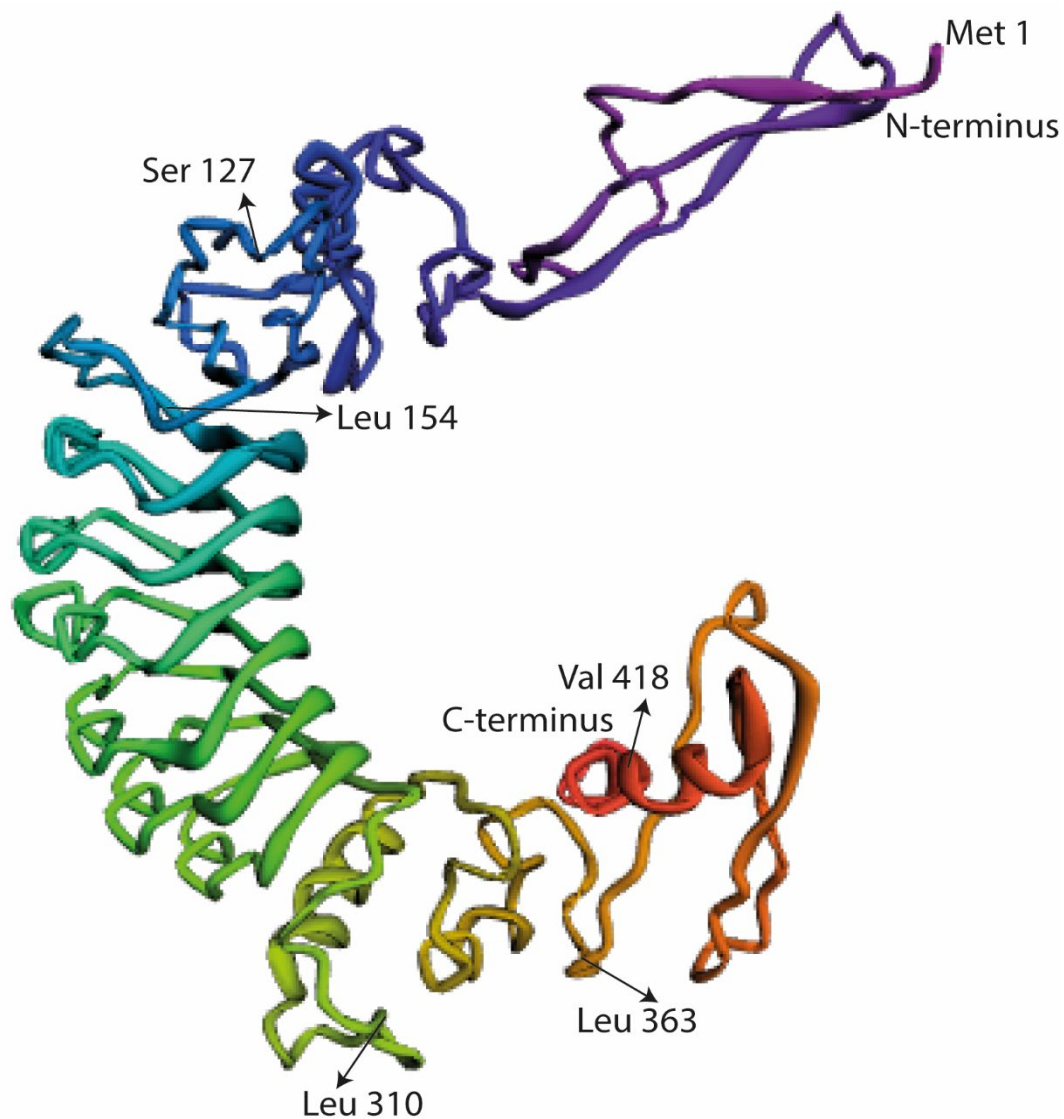


Figure 3.6:- Structural model of Lrr1. This model depicts the various amino acids chosen for making truncated mutants of Lrr1. Lysine 2- Serine 127 was cut off for the N-terminal mutant, Leucine 154-Leucine 310 was cut off for the LRR domain mutant, and Leucine 363- Valine 418 was cut off for making the C-terminal mutant.

I then targeted the deletion of the LRR domain by deleting the regions between Leucine 154 and Leucine 310 (Figure 3.6). This deletion will enable us to understand the phenotype of Lrr1 that lacks the entire LRR region and therefore, I generated LRR deletion mutants lacking each of the seven LRR repeats (Figure 3.7 b).

Finally, I wanted to delete the C-terminal end too. So, I designed the C-terminal truncated mutants without disturbing the VHL box region and deleted the amino acids ranging from Leucine 363 to Valine 418 (Figure 3.6 and Figure 3.7 c).

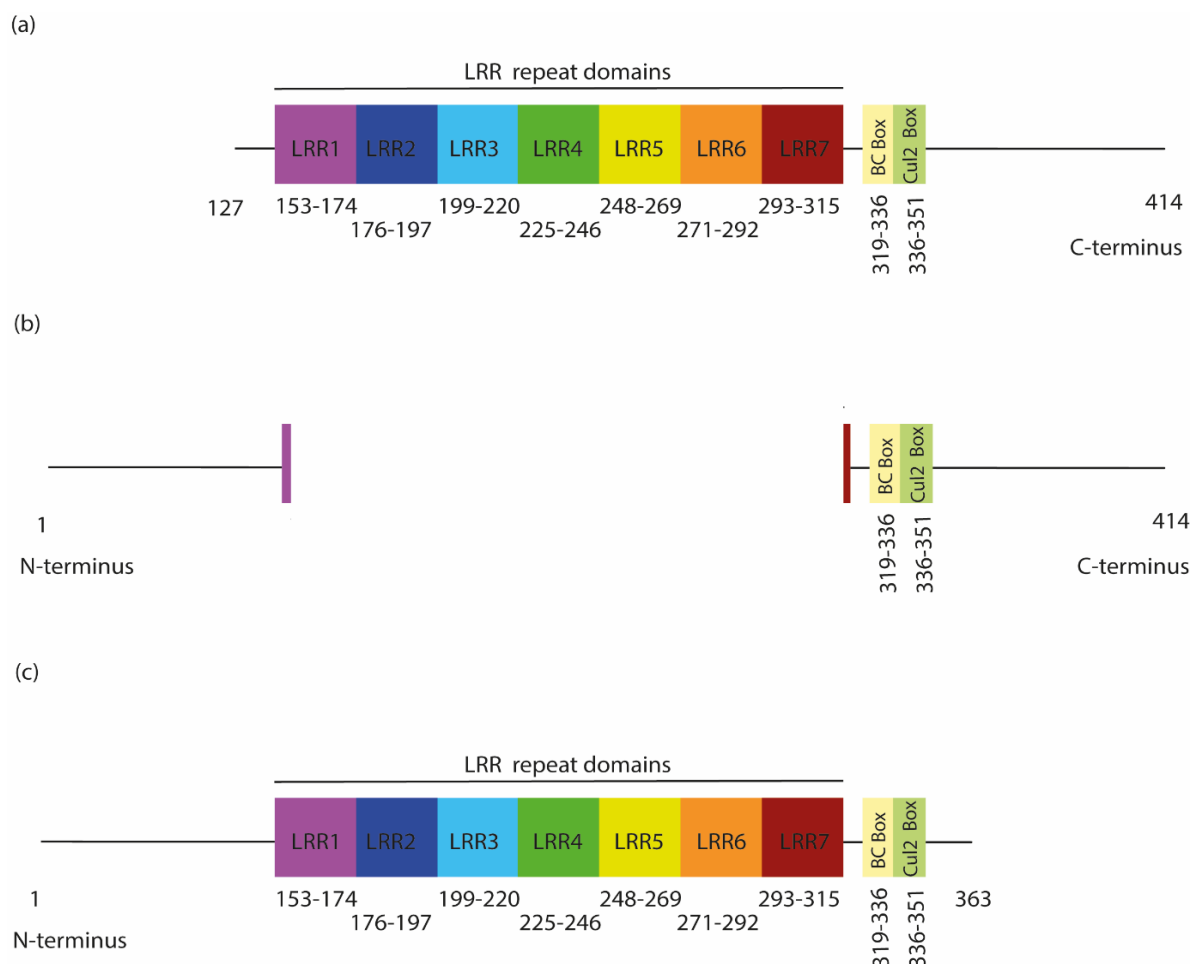


Figure 3.7:- Generation of Lrr1 mutants. Domains of Lrr1 mutants with (a) Truncated N-terminus (b) Deleted LRR domain (c) Truncated C-terminus.

I then designed primers (Table 3) specific for these deletions and used them in site-directed mutagenesis to create the plasmids encoding for the mutants. The plasmids were then transformed into XL-10 Gold competent cells and mutations incorporated were confirmed by sequencing (not shown). With regards to the C-terminal mutant, I was not successful at generating this. It is possible that the primers designed for the C-terminal

region were suboptimal in some way. There may have been problems with specificity, length or melting temperatures that prevented efficient binding and mutant strand synthesis. Therefore, optimisation of PCR conditions or primer re-design could be a way forward. Using the N-terminal truncated mutant and the LRR domain mutant, our next aim was to express, purify and exchange these mutants for the endogenous Lrr1 and study them in the egg extracts.

Replication factors are often found upregulated in cancers and mutations within these factors can contribute to the development of cancer. Mutations correlated with cancer have the potential to disrupt essential functions within the mutated protein. I therefore mapped mutations found within the LRR1 gene in cancer patient samples using the Cosmic and cBioPortal databases (Figure 3.8). These databases revealed the presence of mutated LRR1 in several patients. But we do not know if these specific mutations are disease-inducing or passenger mutations with no functional impact. Strikingly, no mutations were observed in the second and most of the third LRR repeats, suggesting these regions could be essential for the function of Lrr1 such as substrate recognition and that mutations in these regions might be detrimental to cell survival. Notably, I observed that most mutations were clustered within the first LRR repeat. This observation prompted us to focus on these mutations and explore their functional importance. We wanted to assess these mutations to see if they can bring any phenotypical variations to Lrr1 function, which could be interesting to extend our knowledge on Lrr1.

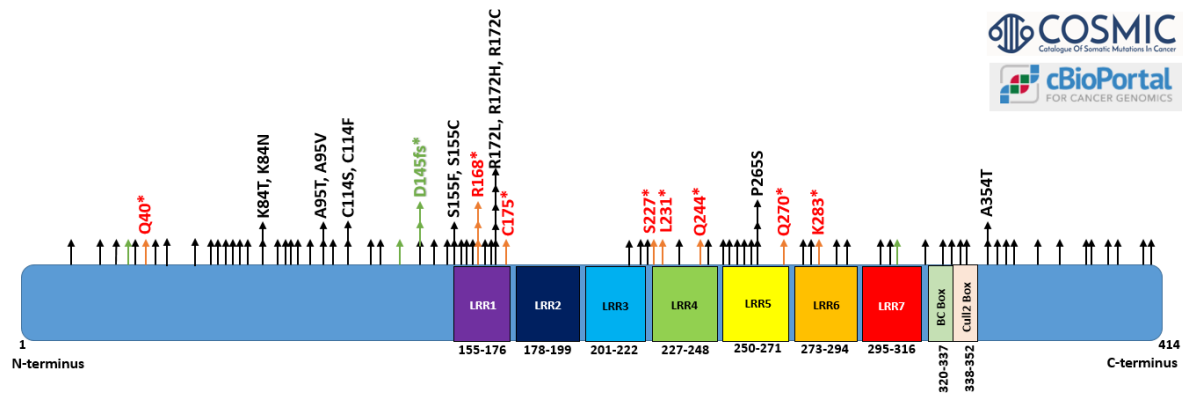


Figure 3.8:- Human LRR1 cancer patient mutations. Mutations found in human LRR1 are indicated on top of each domain. Missense mutations are represented with black arrows, frameshift mutations are represented in green and nonsense mutations are marked in red.

In order to study these patient mutations, I first aligned the protein sequences of *X. laevis* Lrr1 and *H. sapiens* LRR1 (Figure 3.9) to check if these mutated residues were conserved in both. Since I first wanted to focus on the hotspots of mutations that were most repetitive, I chose the three mutations from the databases such as R172>H, R172>C, and P265>S, as they were the most often mutated. Since these positions are conserved both in human and *Xenopus*, I decided to incorporate these mutations into our *X. l.* His-SUMO-Lrr1 expressing plasmid, via site-directed mutagenesis and express, purify and exchange these mutants for the endogenous Lrr1, similarly to the truncation mutants and study their functionality for replisome unloading. The mutagenesis for P265>S was the only successful (not shown) one however and unfortunately the incorporation of the R172 mutation did not work.

X. laevis and *H. sapiens* LRR1 alignment

Species	Position	Sequence	Position
<i>X. laevis</i>	1	MKLQCEVEVINRMLPTFGLNKRGKTRAVLSVGRQEGKRG---AAYILMIC	47
<i>H. sapiens</i>	1	MKLHCEVEVISRHLPAIGLRNRGKGVRAVLSLCQQTSRSQPPVRAFLILIS	50
<i>X. laevis</i>	48	TLKDKSGSRYKLENNIEQLFTRFVGEKATLRLKEPALDICSKAEICGL	97
<i>H. sapiens</i>	51	TLKDKRGTRYELRENIEQFFTKFVDEGKATVRLKEPPVDICSKAISSSL	100
<i>X. laevis</i>	98	RNFISTVGLANKGTDIGTVSLPRLTPAKTSEIEKPRSKLFITTKKDYPIT	147
<i>H. sapiens</i>	101	KGFLSAMRLAHRGCNVDI--PVSTLTPVKTSSEFENFKTKMVIITSKKDYPLS	149
<i>X. laevis</i>	148	KSFYPSLEHLQVSYCKLARVDMRMLCLKLQKLDLSNNHIKKLPKTIGDL	197
<i>H. sapiens</i>	150	KNFPYSLEHLQTSYCGLRVDMRMLCLKSLRKLDLSNNHIKKLPATIGDL	199
<i>X. laevis</i>	198	VCLQELILNHNLFLESFEVVL CSTTLRDTLKS LDLSANKLKALPVQICNFK	247
<i>H. sapiens</i>	200	IHLQELNLNDNHLESFSVALCHSTLQKSLRSLDLSKNNIKALPVQFCQLQ	249
<i>X. laevis</i>	248	ELVSLKLDENELLQLFPPIGQLSKLRFLSATKNKLQCLPNTFFKLTLENL	297
<i>H. sapiens</i>	250	ELKNLKLDDNELIQFPCKIGQLINLRFLSAARNKLFPFLPSEFRNL SLEYL	299
<i>X. laevis</i>	298	DLFGNPFMQATPLVPDIQLKIPLPLETAARATLKYRIPYGPPLIPATLC	347
<i>H. sapiens</i>	300	DLFGNTFEQ--PKVLPVIKLQAPLTLESSARTILHNRIPIYGSHIIPFHLCL	348
<i>X. laevis</i>	348	QDLSLAKTCDLGLPCLNSFIQTIVLMNLHQVSQTIVVLVD TMGGTDGP IVC	397
<i>H. sapiens</i>	349	QDLDTAKICVCGRFCLNSFIQGTITMNLHSAHTVVLVDNLGGTEAPIIS	398
<i>X. laevis</i>	398	YFCSLTCY---SQFLDKYLQSTRV*	419
<i>H. sapiens</i>	399	YFCSLGCYVNSSDMLK-----	414

Figure 3.9:- Alignment of *X. laevis* Lrr1 and *H. sapiens* LRR1 protein sequences. R172 and P265 are marked in red with a star above. All seven Leucine Rich Repeats (LRR) are highlighted in different colours.

Furthermore, I also predicted the structure of these LRR1 patient mutants using PHYRE2 software (Figure 3.10). Interestingly, R172>C was observed to distort the consistently folded structure of LRR1, suggesting a potential impact on the stability of this protein, while R172>H and P265>S were found to possess structures similar to the LRR1 wild type (LRR1wt). Further investigation is necessary however, to determine if these mutations affect the functionality or stability of the protein and to elucidate their potential phenotypic consequences.

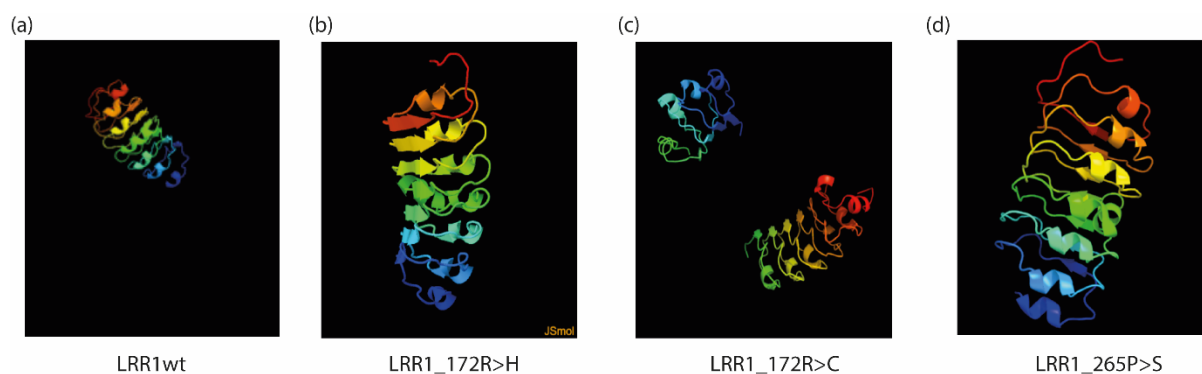


Figure 3.10:- The predicted structure of Human LRR1 patient mutants. Three of the selected mutations found within LRR1 in patients were studied using Phyre2 software. (a) Human LRR1 wild type (wt) (b) LRR1_172R>H (c) LRR1_172R>C possesses a distorted structure. (d) LRR1_265P>S.

3.2.4 Purification of *Xenopus laevis* Lrr1

In order to study the mutants of Lrr1, I first needed to express and purify the recombinant *X. laevis* Lrr1 (*X. l.* Lrr1) from bacteria and exchange it for the endogenous Lrr1 present in the *Xenopus* egg extract and analyse its effect. To this end, I first aimed to purify the wild type Lrr1 to optimise the best conditions for the purification of the protein and to use it to raise antibodies against *X. l.* Lrr1. These will allow us to immunodeplete endogenous Lrr1 from the extract so I can then add back purified mutants and study their effects.

Multiple attempts were made to standardise the best conditions for purifying *X. l.* Lrr1. I first expressed it as recombinant His-SUMO-Lrr1 wild type (wt) from pET15b His-SUMO-Lrr1 vector using Arctic cells, a derivative of *E. coli* BL21 (section 2.3.5.1). Arctic Express competent cells are engineered to overcome the common hurdle of protein insolubility by utilising cold-adapted chaperonins, which allow the expression of protein at low temperatures, potentially increasing the yield of active and soluble recombinant protein. Recombinant His-SUMO-Lrr1 was expressed in Auto Induced Media (AIM) at 13°C overnight. AIM media was used to induce transcription of the gene of interest from an IPTG-inducible promoter and utilises carbon sources in the medium that are metabolized

differentially to promote high-density cell growth and automatically induce protein expression from lac promoters.

The 6xHis-tag located at the N-terminal end was utilised to purify the His-SUMO-Lrr1 fusion protein using the Ni²⁺ beads. The purification involved two batches of Ni²⁺ beads consecutively for binding proteins. The first set of beads targeted leaky expression of His-SUMO protein on its own. The purification results were analysed using Coomassie gel and western blotting (Figure 3.11). The elutions 1-5 (lane 8-12; Figure 3.11 a) from the first batch included His-SUMO-Lrr1 (at ~60 kDa) but it also had the presence of some degradation product at ~26 kDa and a large quantity of His-SUMO protein on its own (~18 kDa). However, the second batch of beads demonstrated good binding to the target protein. The Coomassie gel results showed that elutions 1-5 (lane 20-24; Figure 3.11 a) from the second batch had His-SUMO-Lrr1 (at ~60 kDa) with less contamination from other non-specific proteins. Visualisation of these samples after immunoblotting using anti-His antibodies also confirmed the presence of His-SUMO-Lrr1 at ~60 kDa (Figure 3.11 b). I could also observe a smaller band at ~18 kDa of overexpressed His-SUMO, but in a lower concentration when compared to the first batch.

I also purified Lrr1 from BL21(De3) cells in a similar way to Arctic cells to determine which method would produce a cleaner and a more functional protein for use in the egg extract. BL21 (De3) cells are also *E. coli* derived expression cells that are specialised for protein expression of any gene that is under the control of a T7 promoter. These cells lack lon and ompT proteases, providing more stable protein expression. These cells are specifically engineered to improve yield and tolerance to toxic membrane protein production. Purification of His-SUMO-Lrr1 from BL21 (De3) cells was performed using the same protocol as for Arctic cells. Unfortunately, the yield and quality of purified

protein obtained was poorer when compared to Arctic cells. Elutions 1-5 (lane 18-23; Figure 3.11 c and d) from batch 2 beads included His-SUMO-Lrr1 (at ~60 kDa) but it also had the presence of large amounts of degradation product at ~26-30 kDa (visualised from the western blot) and overexpression of His-SUMO protein on its own (~18 kDa). From both purifications, His-SUMO-Lrr1wt purified from Arctic cells exhibited less degradation compared to that from BL21. Elutions 1 and 2 from batch 2 (lane 20-21; Figure 3.11 a and b) from Arctic and elutions 1 and 2 from BL21 from batch 2 (lane 18-19; Figure 3.11 c and d) were stored at -80°C and also used for raising antibodies against *Xenopus* Lrr1.

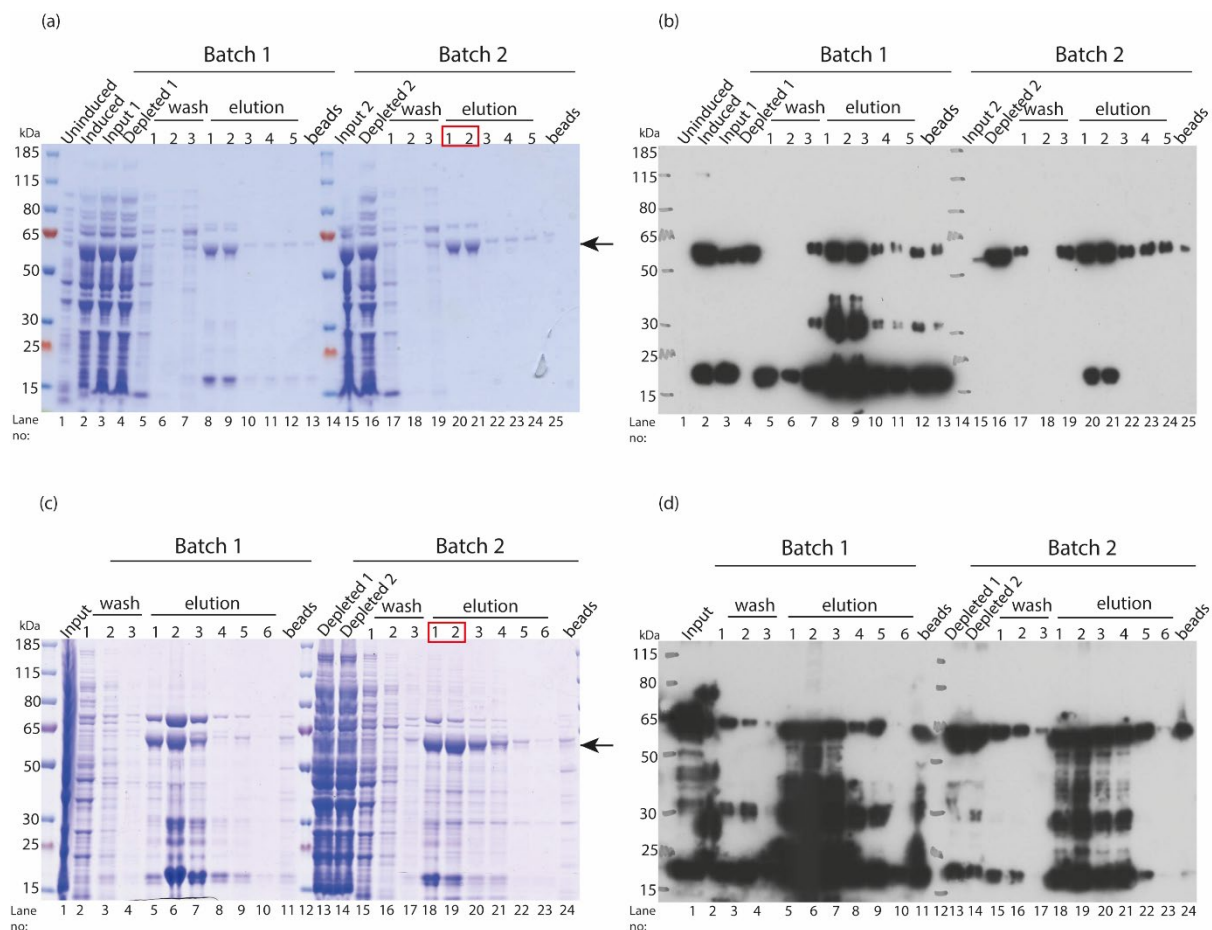


Figure 3.11:- Purification of *X. laevis* His-SUMO-Lrr1. His-SUMO-Lrr1 was expressed in bacteria using AIM media and affinity purified using Ni²⁺ beads. Batch 1 and Batch 2 represent the two sets of beads. The proteins bound to the two batches of beads were eluted with buffer containing 250 mM imidazole (elutions 1-6). Uninduced and induced samples show proteins before and after induction. Input and depleted present the samples before and after incubation with the beads. A small sample of beads taken after elution is also analysed and labelled as beads. Protein samples taken at indicated stages of the purification from Arctic cells (a and b) were analysed on acrylamide gel by (a) coomassie staining and (b) western blotting using anti-His antibodies. Protein samples taken at indicated stages of purification from BL21 (De3) cells (c and d) were also analysed as in (a and b). The arrow on the coomassie gel indicates Lrr1 and the red box in 'elution' indicates the pooled fractions of protein.

3.2.5 Testing of antibodies raised against *Xenopus laevis* Lrr1

To exchange endogenous Lrr1 for mutants, ideally, I needed to immunodeplete endogenous Lrr1 from the egg extract first. Therefore, the raised antibodies against *X. laevis* His-SUMO-Lrr1 purified from Arctic and BL21 (De3) cells in four different rabbits were tested and characterised in *Xenopus* egg extracts. We know from previous experience that detection of Lrr1 in egg extract is very difficult and that to be successful,

we need to accumulate it on chromatin. Hence, I used a small molecule inhibitor, MLN4924 to block the activity of cullins and accumulated Lrr1 on chromatin. A DMSO control was used as a negative control (as we struggle to detect Lrr1 on chromatin during normal replication), and the chromatin was isolated at 90 min time point. In order to test the sera, a small amount of egg extract was run on a 4-12% gradient acrylamide gel alongside isolated chromatin from a control (DMSO) sample and MLN4924 (Cul i) sample. The results obtained from immunoblots showed accumulation of Psf2 and Mcm7 with short ubiquitin chains as expected confirming that the inhibition had worked. I could also see the presence of a band at ~55 kDa corresponding to the size of endogenous Lrr1 (Figure 3.12 a-d) for sera #29. The presence of other non-specific bands could be the result of using crude sera instead of purified antibodies. Sera #27, #30, and #32 could potentially be able to recognise Lrr1 once antibodies are purified and concentrated and when there is less interference from non-specific antibodies.

In addition to this, I also synthesised antibodies against a short peptide of Lrr1. Although they are raised against a short peptide, if the peptide is accessible in the endogenous Lrr1, they should immunoprecipitate (IP) or immunodeplete Lrr1 from the egg extract. To this end, I immunoprecipitated Lrr1 from the egg extract using Lrr1 peptide antibodies raised in two different rabbits - Lrr1 R#75 and Lrr1 R#76. I could observe that both antibodies were able to immunoprecipitate a protein at ~55 kDa (Figure 3.12 e). From these, we established antibodies that could potentially immunodeplete Lrr1 from the egg extract.

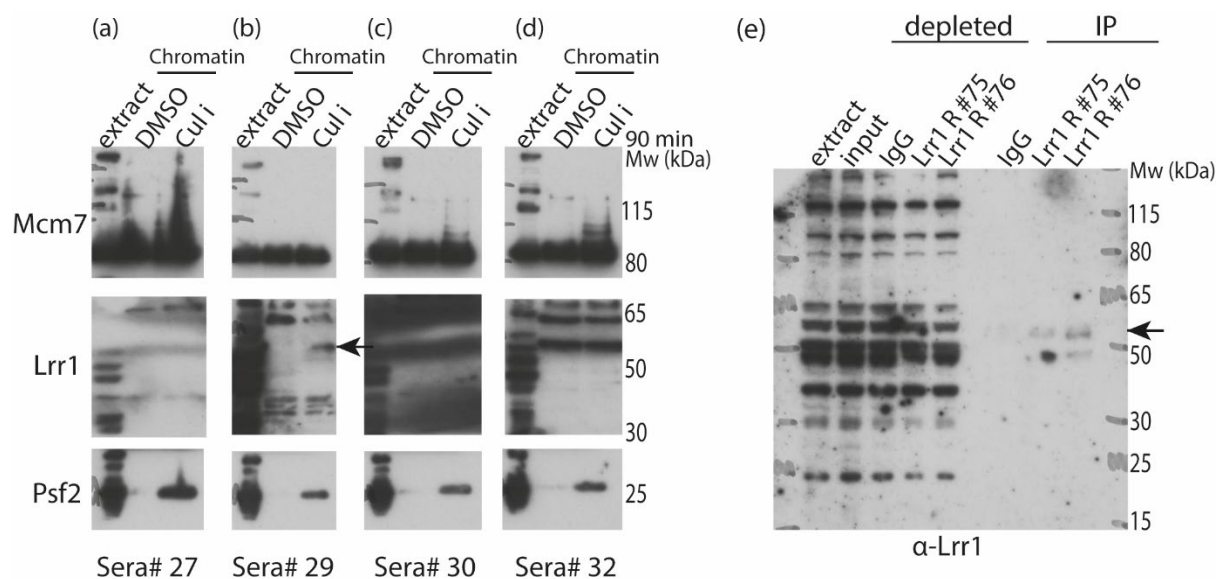


Figure 3.12:- Characterisation of *Xenopus laevis* Lrr1 antibodies. Egg extract was optionally supplemented with DMSO and cullin inhibitor (Cul i) for accumulation of Lrr1 on chromatin. Chromatin was isolated at 90 min and proteins were analysed by western blotting using crude sera from 4 rabbits obtained against *X. l.* Lrr1. (a) Sera # 27 (b) Sera # 29 (c) Sera # 30 (d) Sera # 32 (e) The ability of two Lrr1 peptide antibodies- R#75 and R#76 to immunoprecipitate Lrr1 from egg extract was tested and analysed using western blotting with anti-Lrr1 antibody. The arrow in figure (b) and (e) indicates Lrr1.

3.2.6 Assessing chromatin binding ability of recombinant purified Lrr1

Assuming we will be able to immunodeplete Lrr1 with one of our antibodies after purification, we need the purified recombinant Lrr1 to exchange with endogenous Lrr1 and be able to unload replisomes in S-phase. We decided, therefore, to check whether the addition of recombinant His-SUMO-Lrr1 purified from Arctic or BL21 cells can bind to chromatin during a replication reaction, suggesting that it can act similarly to the endogenous Lrr1 from the egg extract. To this end, I performed chromatin isolation as a time-course experiment to study protein association with chromatin during replication reaction when replisome unloading is blocked. Interphase egg extract was induced and supplemented with sperm DNA and to be able to detect chromatin binding of Lrr1, I blocked replisome disassembly by inhibiting cullin activity with MLN4924. The extract was then optionally supplemented with buffer, purified recombinant His-SUMO-Lrr1

from Arctic or His-SUMO-Lrr1 from BL21 cells. Chromatin from each timepoint was isolated and analysed by immunoblotting and histones were stained with simply blue as a loading control (Figure 3.13). I could visualise the accumulation of CMG components: ubiquitylated Mcm7, Cdc45, and Psf2, while neddylation of Cul2 was inhibited indicating that the MLN4924 treatment had worked. In order to visualise Lrr1, I used both anti-His and anti-Lrr1 antibodies. In the extract samples, I could visualise a band at ~60 kDa for His-SUMO-Lrr1 Arctic and His-SUMO-Lrr1 BL21 in anti-His blots. Regarding the chromatin samples, although I could detect the presence of a band at ~60 kDa that align with the anticipated size, they are considered non-specific (marked with *) since they are not expected to appear in buffer samples and in the 'no DNA' samples. Unfortunately, using anti-His antibodies, I could not detect any clear bands representing Lrr1.

Using anti-Lrr1 antibody, which were a kind gift from the Labib lab, I could detect some faint bands corresponding to Lrr1 in the extract samples possibly from endogenous Lrr1 at ~55 kDa. Regarding the chromatin samples, I could detect some faint bands in all samples at ~55 kDa, which is the expected size for endogenous Lrr1. But the recombinant purified Lrr1 containing His and SUMO tags was expected to run higher at ~60 kDa. I also tried to blot the same using anti-SUMO antibody, but this was unsuccessful too. Unfortunately, despite adding a significant amount of recombinant Lrr1 to the extract (50 µg/ml), I could barely detect it on chromatin.

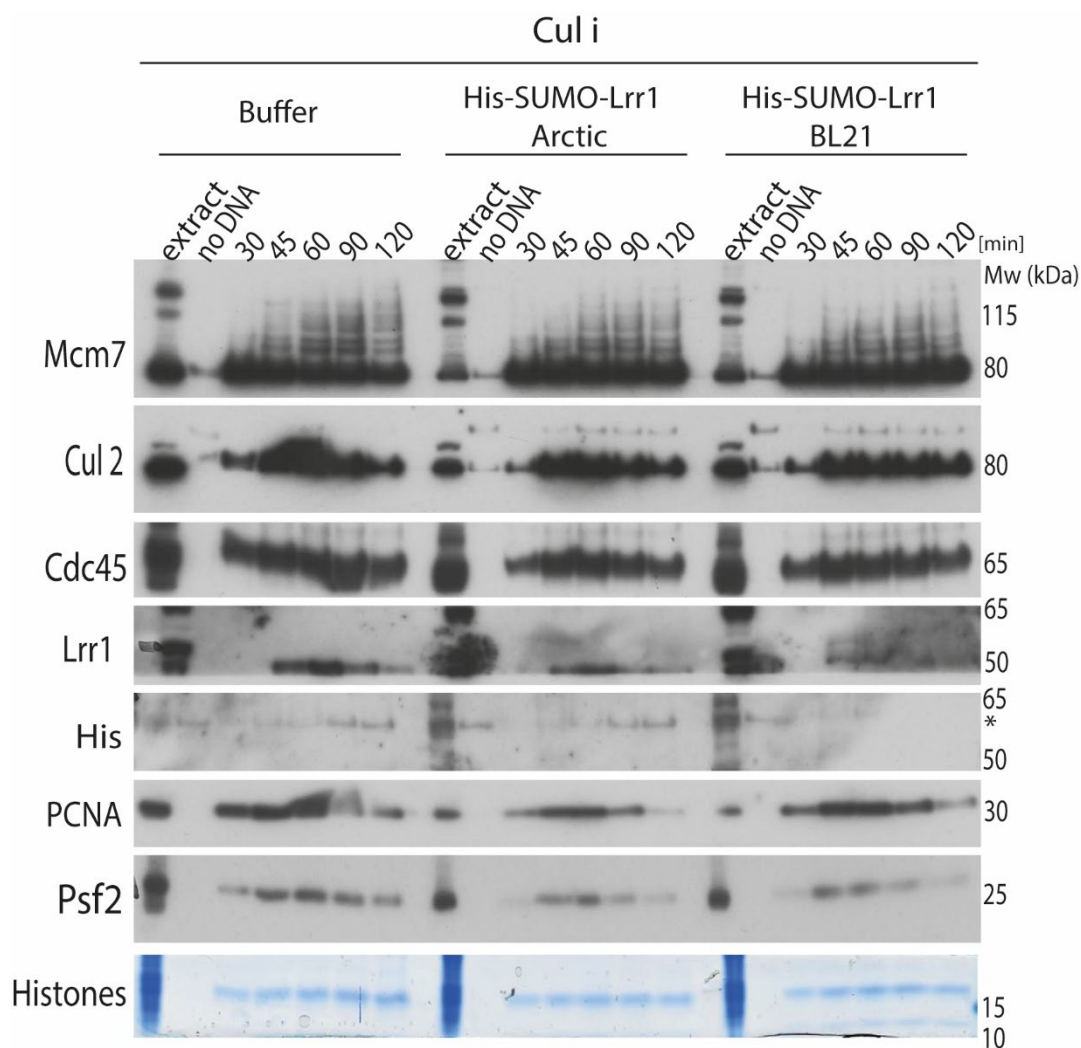


Figure 3.13:- Chromatin isolation with Recombinant His-SUMO-Lrr1. Egg extract was induced into interphase and a replication reaction was initiated by the addition of sperm DNA. The extract was supplemented with Cullin inhibitor (Cul i) and optionally added buffer (control), His-SUMO-Lrr1 purified from Arctic and BL21 cells at a concentration of 50 $\mu\text{g/ml}$. The chromatin was then isolated at indicated time points. The replication factors involved were analysed by immunoblotting using indicated antibodies. Anti-His and anti-Lrr1 antibodies were used to detect Lrr1. *represents a non-specific band. The 'no DNA' sample is a control with no sperm DNA that was isolated in parallel. Histones serve as a loading control stained with coomassie. This experiment was performed twice.

3.2.7 Analysis of purified recombinant *X. laevis* His-SUMO-Lrr1 using size exclusion chromatography

We were surprised by the inability to detect His-SUMO-Lrr1 added to the egg extract. Therefore, our next step was to further analyse our recombinant proteins through gel filtration analysis to check if I have co-purified any non-specific protein along with Lrr1.

Gel filtration enables us to separate different protein complexes based on their size. Size exclusion chromatography was performed using the SMART system for both recombinant *X. l. Lrr1* purified using Arctic and BL21 cells and the fractions obtained from the gel filtration were run on a 4-12% gradient acrylamide gel and analysed by coomassie and western blotting using anti-His and anti-Lrr1 antibodies (Figure 3.14). After analysing the samples, I could observe that His-SUMO-Lrr1 from Arctic *E. coli* cells resolved as one protein peak at ~66 kDa (corresponding to molecular size markers of the column) (Figure 3.14 a), and this peak was also confirmed with anti-Lrr1 (Figure 3.14 b). Unfortunately, anti-His blots had very weak signals and I was only able to detect a small peak representing SUMO at ~18 kDa (corresponding to molecular size markers of the gel) in the late fractions (Figure 3.14 c, Fraction number 25-26).

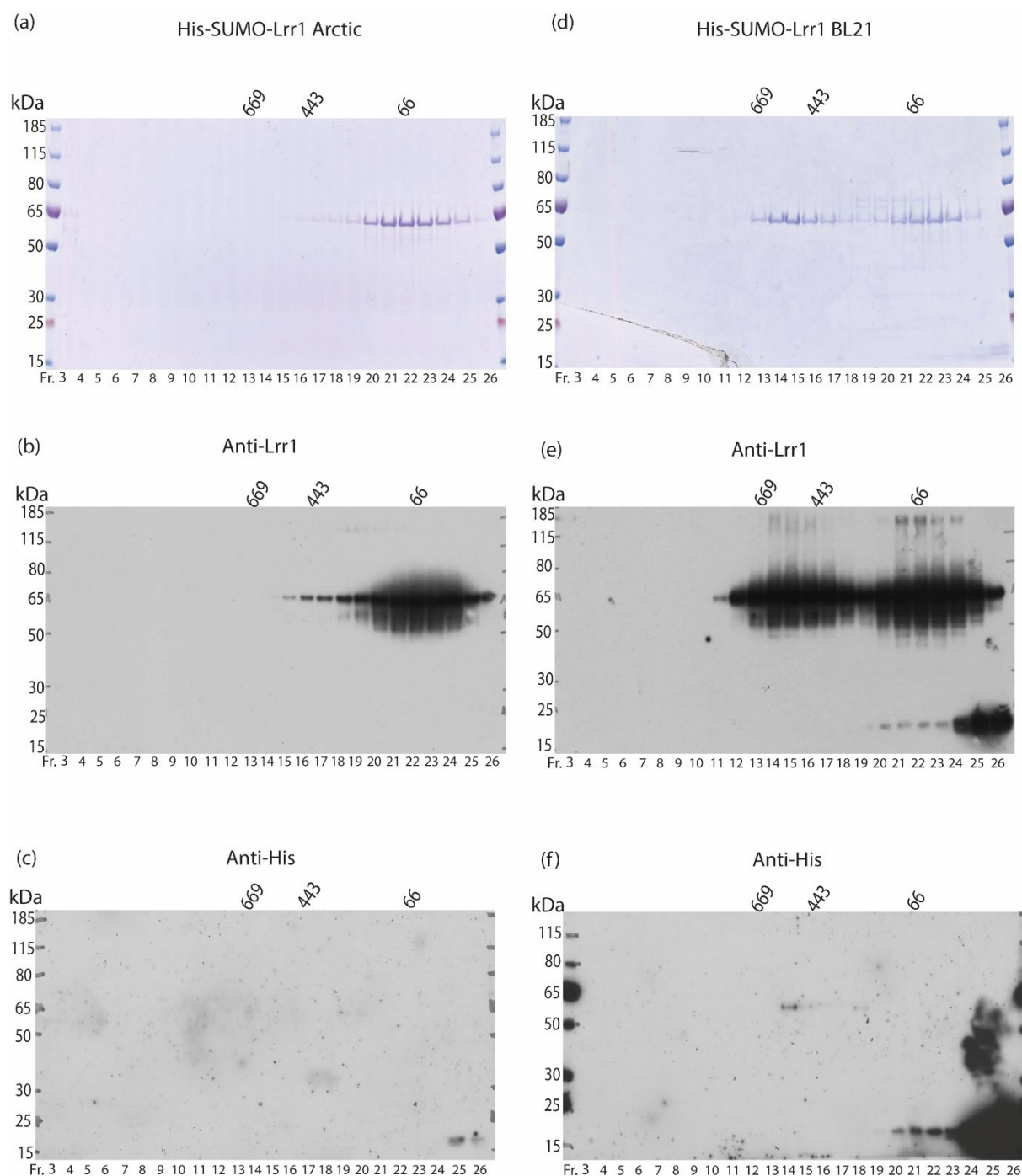


Figure 3.14:- Size exclusion chromatography for recombinant His-SUMO-Lrr1. Recombinant purified His-SUMO-Lrr1 was subjected to gel filtration using a Superose 6 column to check for protein homogeneity. The fractions obtained were run on a gradient acrylamide gel and then analysed by coomassie staining and western blotting. The molecular size markers for the gels are presented on the left hand side of the gel and molecular size markers for the column are presented on the top of each gel. The numbers at the bottom of each gel represents the fraction number. (a) His-SUMO-Lrr1 from Arctic; coomassie stained (b) His-SUMO-Lrr1 from Arctic; anti-Lrr1 blot (c) His-SUMO-Lrr1 from Arctic; anti-His blot (d) His-SUMO-Lrr1 from BL21; coomassie stained (e) His-SUMO-Lrr1 from BL21; anti-Lrr1 blot (f) His-SUMO-Lrr1 from BL21; anti-His blot.

On the other hand, His-SUMO-Lrr1 purified from BL21 (De3) cells when analysed by gel filtration, resolved into two different peaks. The first peak was at a higher molecular weight of ~669 kDa and the second peak was similar to the one observed for His-SUMO-Lrr1 from Arctic cells (~66 kDa) (Figure 3.14 d). I analysed this gel filtration using anti-Lrr1 and anti-His antibodies (Figure 3.14 e and f). Surprisingly, both the peaks (~669 and ~66 kDa) were recognised by anti-Lrr1 suggesting that Lrr1 might have undergone some structural changes enabling self-assembly into larger complexes. In addition to this, I could also observe a small peak potentially representing SUMO in the late fractions (Fraction number 24-26). I did not easily observe any other non-specific protein peaks elsewhere recognised by anti-Lrr1 antibody. Interestingly, the anti-His antibody was able to recognise much better a very small quantity of His-SUMO copurifying as a result of a leaky expression (Figure 3.14 f; Fraction number 21-26), rather than the large quantity of His-SUMO-Lrr1. However, more work is needed to see if Lrr1 can homo- or heterodimerise with itself, or with something else of the same size as His-SUMO-Lrr1.

3.2.8 Purification of recombinant *Xenopus laevis* Cul2/Lrr1/EloB/C complex

To change the tactic in His-SUMO-Lrr1 purification, I wanted to purify Lrr1 as a complex with the N-terminal fragment of Cullin2 (N-Cul2) and Elongins B and C (EloB/C). Such an approach could produce more stable His-SUMO-Lrr1 and we could gain insights into the structural assembly and mode of interactions between these proteins. Therefore, I attempted to express and purify the N-Cul2/Lrr1/EloB/C as a complex by expressing them from 3 different plasmids (described in section 2.3.5.2). N-Cul2 was expressed from the pET24 vector, Lrr1 from pET15b, and EloB/C was expressed from pACYDuet1 in BL21 cells using AIM media. Using Ni²⁺ beads, I attempted to co-purify N-Cul2/Lrr1/EloB/C as a complex utilising the His tag on His-SUMO-Lrr1.

The purification results were analysed using coomassie staining and western blotting (Figures 3.15 a and b). The Coomassie staining of purified fractions showed several bands and it was difficult to assign them to expected proteins. The western blotting analysis of the purification with antibodies against each component suggested that elutions 1-3 contained all three proteins: N-Cul2 (~40 kDa), Lrr1 (~60 kDa) and EloB (~13 kDa) & EloC (~12 kDa).

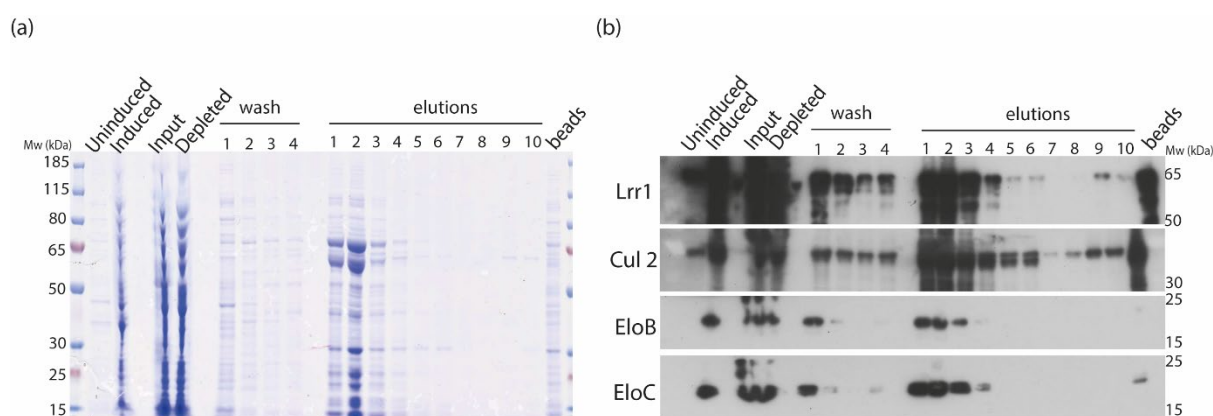


Figure 3.15:- Purification of recombinant N-Cul2/Lrr1/EloB/C complex. Expression of N-Cul2, His-SUMO-Lrr1 and EloB/C was performed in BL21 cells using AIM media and affinity purified using Ni^{2+} beads. The proteins bound to the beads were eluted with buffer containing 250 mM imidazole: elutions 1-10. Uninduced and induced samples show proteins before and after induction. Input and depleted present the samples before and after incubation with the beads. A small sample of beads taken after elution is also analysed and labelled as beads. Protein samples taken at indicated stages of purifications were analysed on acrylamide gel by (a) coomassie staining and (b) western blotting using anti-Lrr1, anti-Cul2, anti-EloB and anti-EloC.

3.2.9 Size exclusion chromatography for recombinant N-Cul2/Lrr1/EloB/C complex

Having potentially co-purified the N-Cul2 with Lrr1 and EloB/C, I wanted to see if they existed as a complex. To this end, I chose elution 1 from our purification (Figure 3.15) and analysed it via gel filtration. Fractions 1-25 from the gel filtration were run on a gradient acrylamide gel and analysed by staining with coomassie (Figure 3.16 a). If the proteins existed as a stable intact complex, we would expect all three proteins to co-migrate as a

single high molecular weight peak fraction following gel filtration. However, the different proteins present in the sample appeared distributed across multiple fractions, suggesting that they did not stably interact under these conditions.

I also confirmed these results by immunoblotting with anti-His, anti-Lrr1, anti-Cul2 and anti-EloB (Figure 3.16 b, c, d and e). In anti-Lrr1 blot (Figure 3.16 c), the main peak for Lrr1 was identified in fractions 10 to 12. However, faint bands potentially corresponding to a low population of Lrr1 interacting with N-Cul2 and EloB/C were observed in fractions 18 and 19. This suggest that the majority of Lrr1, N-Cul2 and EloB/C appeared to elute separately and did not exist as a stable complex. Based on these results, we decided that excluding the large N-Cul2 subunit might facilitate more efficient Lrr1-EloB/C complex formation, possibly by reducing the steric impendence and increasing stability. We therefore decided to perform co-expression and purification of just the Lrr1 and EloB/C components.

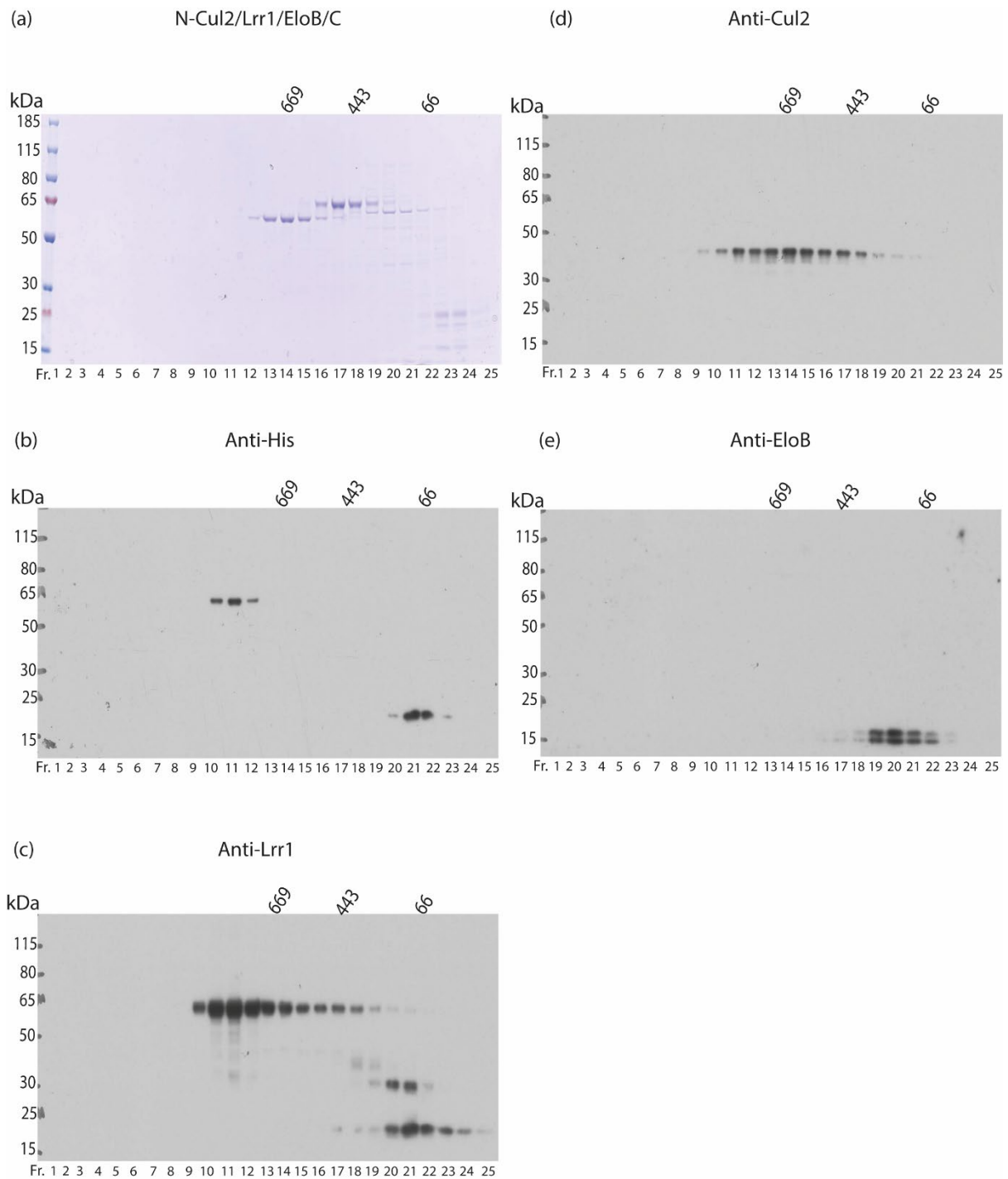


Figure 3.16:- Size exclusion analysis of N-Cul2/Lrr1/EloB/C complex. Recombinant purified N-Cul2/Lrr1/EloB/C was subjected to gel filtration using Superose 6 column to check if they exist as a complex. The fractions obtained were run on a gradient acrylamide gel and then analysed by coomassie staining and western blotting. The molecular size markers for the gels are presented on the left hand side of the gels and molecular size markers for the column are presented on the top of each gel. The numbers at the bottom of each gel represents the fraction number. (a) N-Cul2/Lrr1/EloB/C complex analysed by coomassie staining (b, c, d, e) Immunoblotting of samples with anti-His, anti-Lrr1, anti-Cul2 and anti-EloB respectively.

3.2.10 Expression and purification of recombinant *X. laevis* Lrr1/EloB/C

As the expression of Lrr1 together with its scaffold N-Cul2 and adaptor EloB/C together did not readily form a complex, our next aim was to co-express just the Lrr1 along with EloB/C from the same plasmids as before. Previous work by Low et al; 2020 demonstrated successful reconstitution of the Lrr1-EloB/C complex using the baculovirus system. Encouraged by their findings, I aimed to express Lrr1 and EloB/C components from the same vectors as I used previously, anticipating that this minimized complex may interact and purify more readily. To find the best expressing cells, I tested Rosetta (De3) pLysS and C41 (De3) cells. They are both derivatives of BL21 (De3) cells. Rosetta pLysS has tRNA genes that are rarely used in *E. coli* to enhance the expression of eukaryotic proteins. The pLys enables to suppress the basal expression of T7 RNA polymerase prior to induction. C41 (De3) are used for expressing toxic proteins as it contains a mutation that prevents cell death associated with expression of some recombinant proteins. The expression of *X. laevis* His-SUMO-Lrr1 and *X. laevis* EloB/C was tested in both LB and AIM media and due to the expression of high levels of non-specific bands, it was difficult to distinguish the bands on a coomassie gel (Figure 3.17 a). Upon analysis by anti-Lrr1, I observed expression of Lrr1 (~60 kDa) in Rosetta cells using both LB and AIM media; comparatively with more degradation in AIM. With regards to C41 (De3), despite expressing Lrr1 with less degradation, the amount of protein expressed was also very low (Figure 3.17 b). The anti-His blot could detect Lrr1 better with Rosetta cells in AIM media (Figure 3.17 c) but I could not determine EloB/C expression as the blot was not successful.

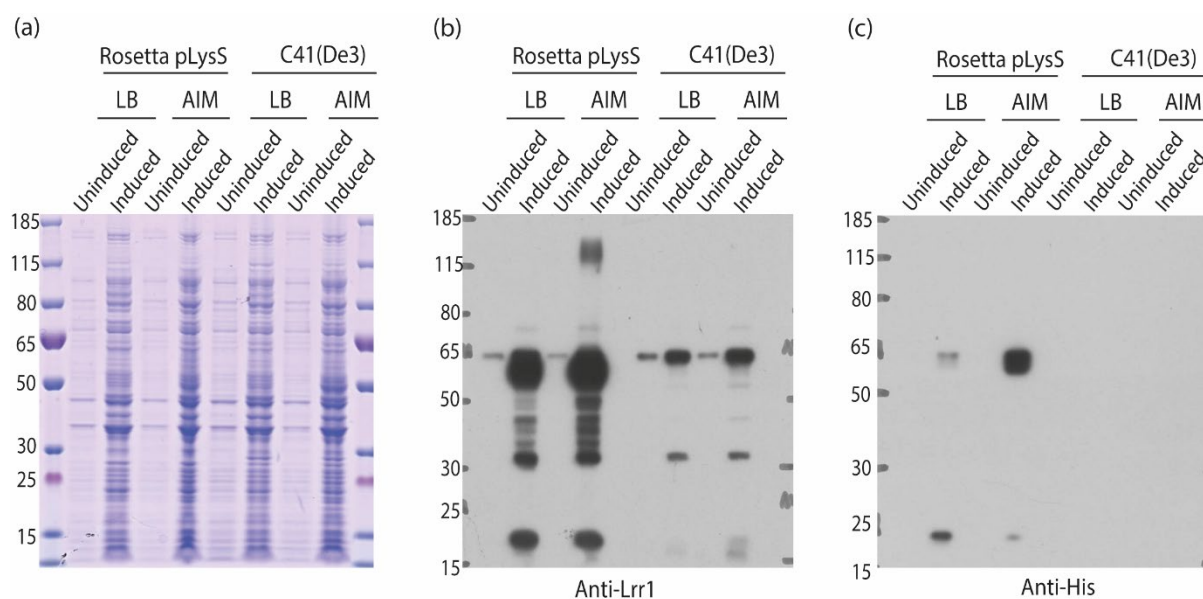


Figure 3.17:- Expression testing for *X. laevis* His-SUMO-Lrr1/EloB/C. Expression of His-SUMO-Lrr1 and EloB/C was tested in Rosetta and C41 (De3) cells using LB and AIM media. Samples before and after induction were collected and analysed by (a) coomassie. Samples were also analysed by immunoblotting with (b) Anti-Lrr1 and (c) Anti-His antibodies.

Subsequently, I chose Rosetta cells for large-scale purification of Lrr1/EloB/C complex in LB media. I used the same optimised protocol (section 2.3.5.3) as previously used for the purification of N-Cul2/Lrr1/EloB/C complex. I could see both Lrr1 and Elongins existing together in elutions 1-8 (Figure 3.18). However, a good amount of protein was found attached to the beads sample and more degradation of Lrr1 was observed in our elutions. The elution containing the highest amount of protein (Figure 3.18, see elution 2) was dialysed into LFB1/50 and stored at -80°C.

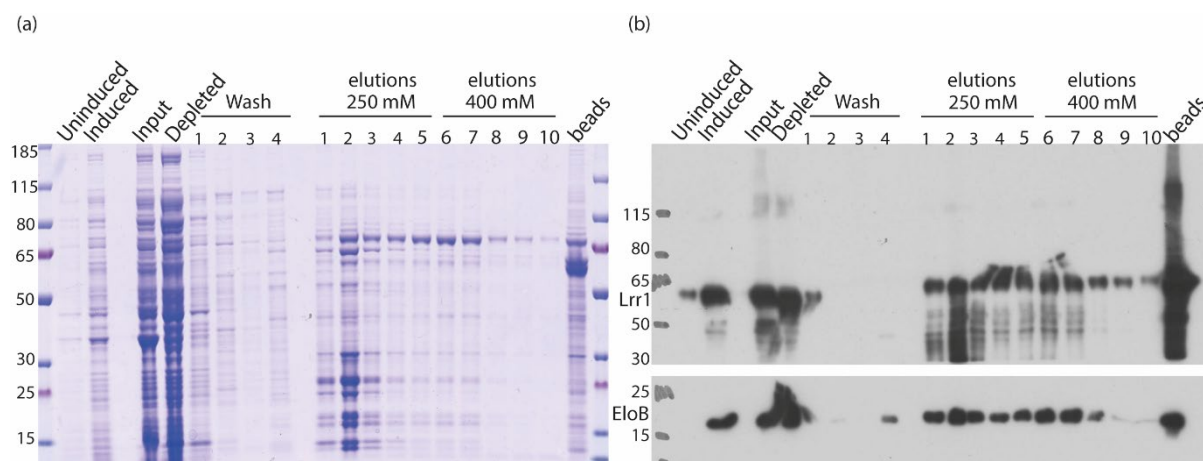


Figure 3.18:- Purification of His-SUMO-Lrr1/EloB/C 1. Expression of His-SUMO-Lrr1 and EloB/C was performed in Rosetta pLysS cells using AIM media and protein was purified using Ni-NTA beads. The proteins bound to the beads were eluted with two different elution buffers containing 250 mM imidazole (elutions 1-5) and 400 mM imidazole (elutions 6-10). Uninduced and induced samples show proteins before and after induction. Input and depleted present the samples before and after incubation with the beads. A small sample of beads taken after elution is also analysed and labelled as beads. Protein samples taken at indicated stages of purification were analysed on acrylamide gel by (a) coomassie staining and (b) western blotting using anti-His.

In order to try and overcome the degradation of Lrr1 and to release more protein from the beads, we decided to repeat the purification but using the buffers I had previously used for purifying His-SUMO-Lrr1 on its own (section 2.3.5.3). Two batches of beads were used here to reduce expression of His-SUMO protein (~18 kDa), which was generated due to leaky expression, or translational defects. This purification reduced the degradation of Lrr1 and I could observe that lesser amount of protein was stuck onto beads after elution (Figure 3.19). Protein samples were analysed by immunoblotting with anti-Lrr1, anti-EloB, and anti-His antibodies (Figure 3.19 b and c) confirming the presence of Lrr1 and Elongins. Both batches of elutions showed the presence of Lrr1 and Elongins; elutions 1-4 (batch 1) and elutions 1-6 (batch 2).

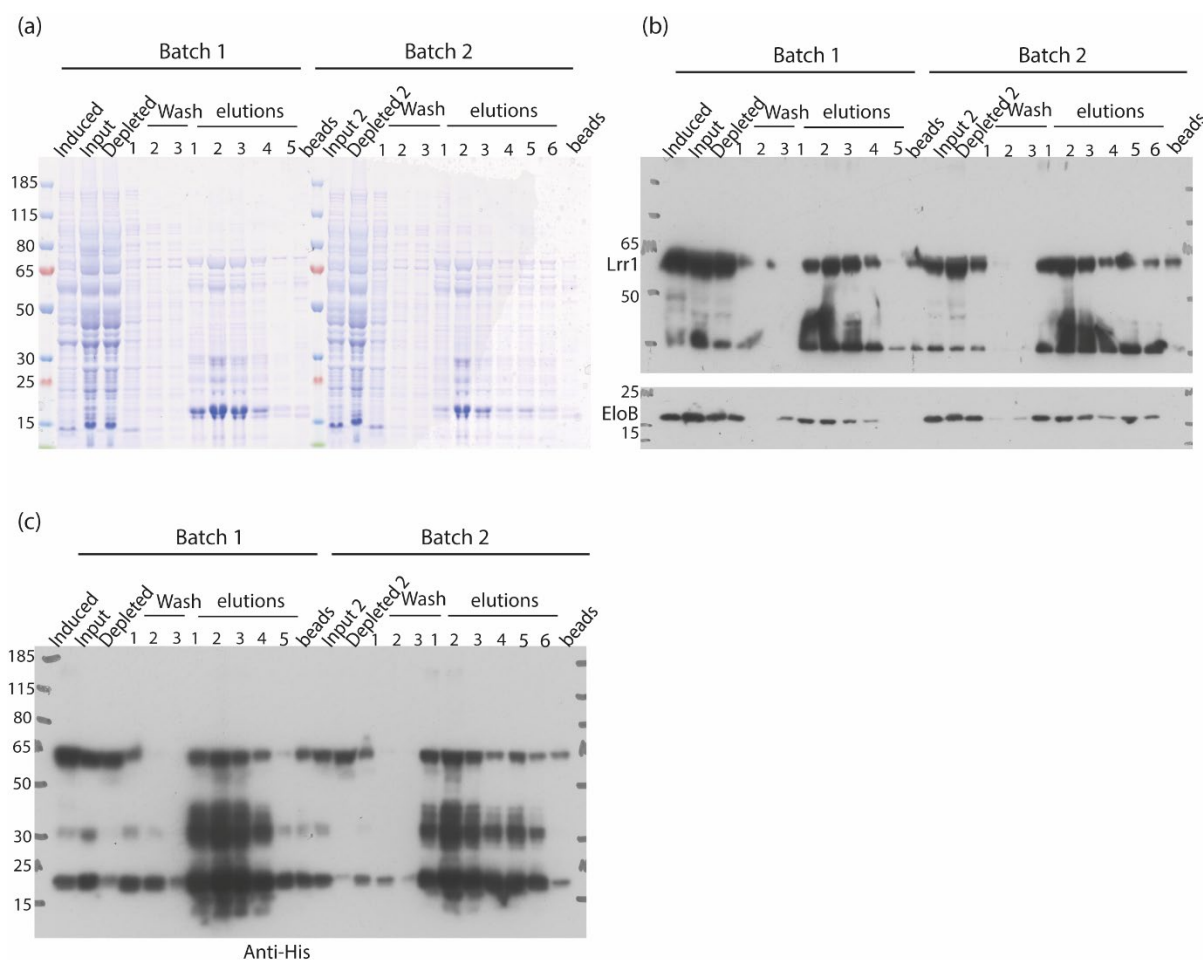


Figure 3.19:- Purification of His-SUMO-Lrr1/EloB/C 2. Expression of His-SUMO-Lrr1 and EloB/C was performed in Rosetta pLysS cells using AIM media and the expressed proteins were purified with Ni-NTA beads. Two sequential batches of Ni²⁺ beads were used (batch 1 and batch 2). The proteins bound to the beads were finally eluted with buffer containing 250 mM imidazole. Uninduced and induced samples show proteins before and after induction. Input and depleted present the samples before and after incubation with the beads. A small sample of beads taken after elution is also analysed and labelled as beads. Protein samples taken at indicated stages of purifications were analysed on acrylamide gel by (a) coomassie staining and western blotting using (b) anti-Lrr1 and anti-EloB (c) and anti-His.

3.2.11 Mass spectrometry analysis of all purified recombinant *X. laevis* Lrr1

Throughout the work presented in this chapter, I purified recombinant Lrr1 in several ways and tried to characterise it as well as use it in functional assays. All the results obtained were challenging and puzzling. In order to verify our different Lrr1 purifications we decided to analyse them via mass spectrometry. A small sample from each purification of Lrr1 was run on a gradient acrylamide gel and stained by SimplyBlue SafeStain. 8

selected bands (Figure 3.20 a) were cut out and analysed by mass spectrometry. It was found that most of the purified protein elutions had a high number of peptides from *E. coli* chaperonin gro EL and few from Lrr1 (Figure 3.20 b). Gro EL is a heat shock protein and plays an essential role in assisting protein folding along with Gro ES. This result suggests that in most of my purifications, I was purifying a lot of protein-folding chaperons that are of the same size as Lrr1 and interact very tightly with Lrr1. The highest number of Lrr1 peptides were found for His-SUMO-Lrr1/EloB/C purification 2.

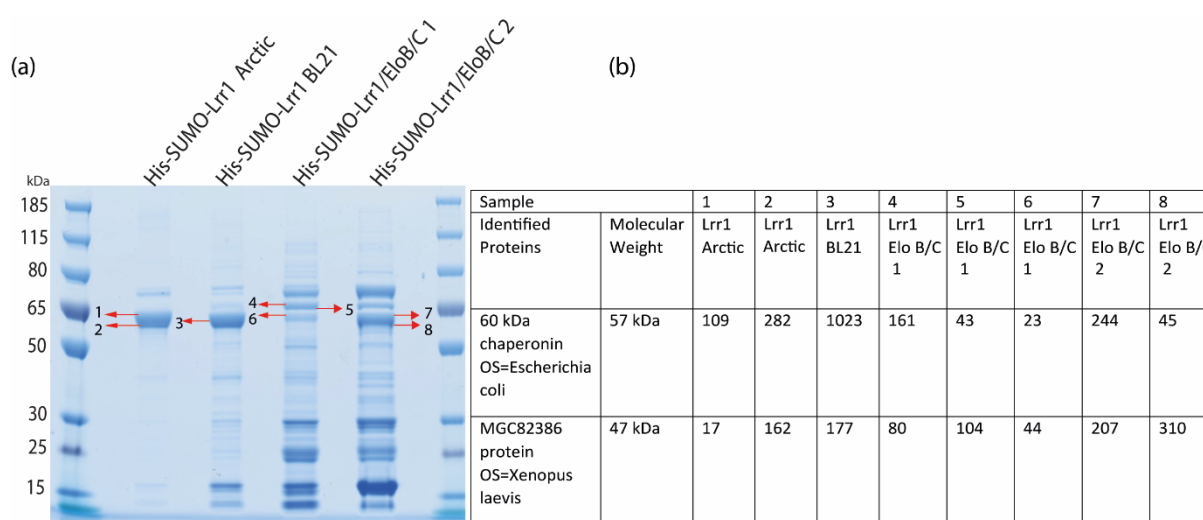


Figure 3.20:- Mass spectrometry analysis of recombinant purified Lrr1. The purified protein samples indicated as His-SUMO-Lrr1 Arctic, His-SUMO-Lrr1 BL21, His-SUMO-Lrr1/EloB/C purification 1, His-SUMO-Lrr1/EloB/C purification 2 samples were run on a gradient acrylamide gel and stained with SimplyBlue SafeStain. 8 bands were cut out from the gel (marked with red arrows) and were sent for mass spectrometry analysis. (a) Gel for analysis. (b) Table indicates the number of Lrr1 (represented as MGC82386) and *E. coli* chaperonin peptides obtained for each sample after mass spectrometry.

By this time, other labs had published the structure of Lrr1. Therefore, there was no point in continuing this project further. Though, I did not achieve my initial goal of solving the structure of Lrr1, I have learned valuable techniques through this initial work that will aid in my future research projects. Specifically, protein purification and gel filtration analysis will provide critical skills that I can apply to many other projects in the future.

Importantly, I learned that it is appropriate to change direction upon receiving new information from the field. Therefore, we decided to focus purely on a different ubiquitin ligase involved in replication termination: TRAIP- discussed in Chapters 4 and 5.

3.3 Discussion

Previous research had established that CMG helicase disassembly at the end of replication in *Xenopus* egg extracts and *C. elegans* requires Lrr1 and neddylation of Cul2 for ubiquitylation of Mcm7 (Dewar et al., 2017a; Sonnevile et al., 2017). However, the specific mechanism by which Cul2^{Lrr1} recognises Mcm7 i.e. the crucial domains of Lrr1 involved in this recognition, the factors that help distinguish the terminated from the active helicase, and the potential direct interaction(s) between Lrr1 and Mcm7 were not previously known.

At the start of this PhD project in September 2016, a crystal structure of Cul2^{Lrr1} was not available. The structure of Cul2^{VHL} was the closest available as it also adopts an elongated cullin scaffold structure, with the Rbx1 subunit on its C-terminus and the substrate adaptors EloB/EloC and the receptor VHL on the N-terminus. Cul2^{VHL} and Cul2^{Lrr1} differ only by their receptors (Cardote et al., 2017). Since the substrate receptor Lrr1 is likely the region of interaction with CMG, it was essential to study the structure of Lrr1 to understand the mechanism of recruitment of Lrr1 to the CMG during replication termination. Throughout this chapter, I have made efforts to optimise purification conditions for recombinant Lrr1, with the aim of studying its structure using *Xenopus laevis* egg extracts.

The recombinant Lrr1 was expressed in bacteria from a hexahistidine SUMO fusion construct. A SUMO fusion recombinant expression system had been shown previously to enhance expressed protein solubility in prokaryotic cells and facilitate purification using

Ni-NTA chromatography, particularly for proteins that are difficult to express or are present in inclusion bodies (Butt et al., 2005). We thus adopted this technique to purify *Xenopus laevis* Lrr1 with a 6x His tag and SUMO tag.

Purifying His-SUMO-Lrr1 wild type protein was essential to first check whether the recombinant protein can be active in the egg extract and substitute the endogenous Lrr1. Additionally, I had raised antibodies against *Xenopus* Lrr1 using the purified proteins so that I could immunodeplete endogenous Lrr1 and add back mutants into our extracts to study the functionality of Lrr1. The assessment of the functional activity of the purified protein was performed in the presence of a small molecule inhibitor MLN4924 to inhibit cullin activity (Soucy et al., 2009) via blocking neddylation of Nedd8. Unfortunately, I could not detect the binding of the recombinant Lrr1 to the chromatin. The four different antibodies raised against Lrr1 were also tested on chromatin samples with inhibited cullin activity, and only one of them was weakly able to detect Lrr1. However, the antibodies raised against the synthetic peptide of Lrr1 (alike in (Dewar et al., 2017a)) was able to immunoprecipitate Lrr1 from the egg extract, which provides a way forward for immunodepleting Lrr1 from the egg extracts.

Regrettably, our results from the analysis of different recombinant Lrr1 proteins revealed the presence of a substantial amount of *E. coli* chaperonins along with the purified Lrr1. These chaperonins have been copurified with Lrr1 to facilitate the native folding and prevent aggregation of Lrr1. But this heterogeneity in our purified protein along with the chaperonins is not ideal for its functionality and may explain why our efforts of analysing the proteins in the egg extract were unsuccessful. Additionally, this observation also aligns well with our antibody characterisation and tells us why our antibodies did not robustly detect Lrr1 in the egg extracts, as they were raised against mainly bacterial

chaperonins. Unfortunately, without a positive control of Lrr1wt, further purifications and experiments with the Lrr1 truncated domain mutants and the cancer mutants that I designed would have not been meaningful. As a result, we made the decision not to proceed with the work involving mutants until the purification conditions were tackled.

GroES is a co-chaperonin of GroEL, and the GroEL-GroES reaction cycle creates a controlled environment for correct folding of the target protein. Once the substrate protein binds to the central cavity of GroEL, GroES binds to this, resulting in encapsulation of the substrate. This encapsulation creates an ambient polar environment for the native protein folding within the GroEL-GroES complex with the physical properties distinct from the bulk of the remaining solution. GroES consists of an ATP binding site and the hydrolysis of ATP results in release of GroES from GroEL allowing the exit of the substrate into the bulk of the solution (Wang et al., 1998). Although I attempted to treat our purified Lrr1 proteins with ATP, this did not facilitate the separation of Lrr1 from the chaperonins (data not shown). To prevent the recombinant Lrr1 from being co-induced and co-purified with the chaperones, I could attempt to express these proteins in SF9 insect cell lines in the future. SF9 cell lines can be used to express recombinant proteins using baculovirus mediated expression systems. They have also the added benefit that as eukaryotic hosts they have the machinery for post-translational modifications of the expressed proteins which can help in its appropriate folding, stability and biological activity (Hong et al., 2022).

Based on our knowledge of known LRR structures and the fact that they generally interact with other proteins via the LRR domain (Bella et al., 2008), we formulated a hypothesis suggesting that Lrr1 and Mcm7 could potentially interact with each other through the LRR domain. This hypothesis is supported by the fact that both substrate receptors-Lrr1

in higher eukaryotes and Dia2 in yeast, despite being non-homologous to each other, possess leucine-rich repeat regions (Maculins et al., 2015). Therefore, we speculated that these regions likely play a crucial role in binding to their substrate Mcm7. Given the availability of the Lrr1 sequence, I used Robetta Beta and Phyre2 softwares to predict the structure of Lrr1. Like other LRR domain containing proteins, the LRR region of Lrr1 exhibited a characteristic folded conformation of a curved solenoid, containing β -sheets and α -helices (Figure 3.3). In 2021, a significant breakthrough occurred when researchers successfully resolved the Cryo-EM structure of Cul2^{Lrr1}. This structural analysis was performed by employing a reconstituted system of CMG ubiquitylation (Jenkyn-Bedford et al., 2021; Zhou et al., 2021). The structure of *Xenopus laevis* Cul2^{Lrr1} in its neddylated and unneddylated forms was studied where purified proteins including CMG, Nedd8 and Cul2^{Lrr1} were expressed and purified utilising the baculovirus expression systems. Reassuringly, our structural predictions of Lrr1, derived through bioinformatic analysis, exhibited consistency with the structures obtained in combination with Cryo-EM and AlphaFold mapping by Zhou et al for *Xenopus laevis* Lrr1.

Prof Walter's structural analysis of Lrr1 revealed four distinct domains - an N-terminal PH (Pleckstrin homology) domain (predicted by AlphaFold), an LRR domain, a VHL box and a Zing finger (ZnF) domain located at its C-terminus (determined from Cryo-EM mapping) (Zhou et al., 2021). Intriguingly, our predicted Lrr1 structure also successfully identified these domains of Lrr1. The PH domain located at the N-terminus and the ZnF located at the C-terminus was most prominently observed in structures depicted in Figure 3.3 c and 3.3 e. These structures exhibited characteristic features, including β -pleated sheets in the PH domain and two anti-parallel β -sheets and an α -helix in the ZnF domain (Zhang et al., 2011; Powis et al., 2023). Zhou et al suggests that the PH domain was connected to the LRR domain through a flexible linker that is essential for targeting

Cul2^{Lrr1} to the terminated CMG complex and mediating its ubiquitylation. This domain however was not clearly observed in the Cryo-EM, possibly due to its flexibility and conformational freedom. Furthermore, the zinc finger domain contained four cysteine residues that are conserved across vertebrates: from *Drosophila* to *X. laevis*, mouse and humans, and was suggested to be important for maintaining overall conformation of the VHL box (Zhou et al., 2021). Our Lrr1 predicted model also displayed an α -helical structure corresponding to the BC box, which was in alignment with the Cryo-EM structural findings. In addition, the Cryo-EM results indicated that this region played a crucial role in the interaction with EloC (Zhou et al., 2021).

Although I had not achieved our aim to determine the important interactions of Lrr1 with the replisome, other studies had indicated that replisome convergence or interaction of CMG complex with dsDNA is not necessary for CMG unloading (Low et al., 2020; Vrtis et al., 2021). Additionally, it was suggested that CMG ubiquitylation during active replication could be suppressed by the typical Y-shaped structure of the replication fork DNA (Deegan et al., 2020; Low et al., 2020). Significantly, the Cryo-EM structures of SCF^{Dia2} and Cul2^{Lrr1} interacting with yeast and human replisomes were resolved and brought essential insights. These structural analyses have revealed that Dia2 in the yeast structure, and Lrr1 in the human structure, bind to a region spanning the Zinc finger domains of Mcm3 and Mcm5. Moreover, the Cryo-EM structure also revealed that during active replication, the presence of an excluded lagging DNA strand between the Zinc finger domains of Mcm3 and Mcm5 generates a steric hindrance that prevents the engagement of LRR domains with Mcms (Figure 3.21). This interaction between Lrr1 and Mcms is crucial for regulating CMG ubiquitylation (Jenkyn-Bedford et al., 2021).

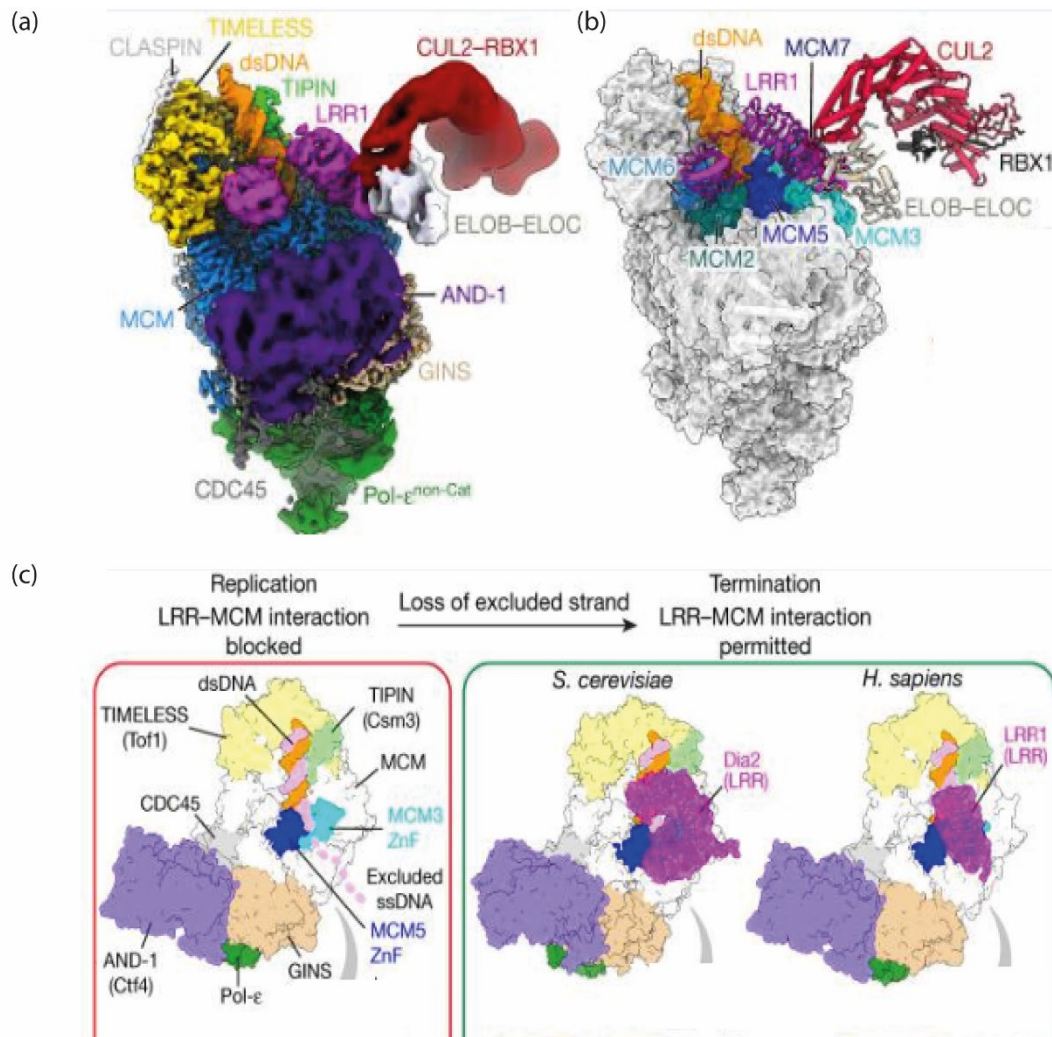


Figure 3.21:- Model of terminated replisomes. (a) Cryo-EM model of human replisome interacting with Cul2^{Lrr1} and other replisome components (b) Atomic model of human replisome engaged with Cul2^{Lrr1} highlighting Cul2^{Lrr1}, ds DNA and Cul2^{Lrr1} interacting regions of Mcms (c) The mechanism of regulating replisome disassembly. The replisome complex with blocked LRR-Mcm interaction is depicted in the red box. The pink dotted line represents the excluded strand or lagging strand that passes through the channel between Mcm3 and Mcm5 ZnF domains and occludes the binding of Lrr1. During termination, the loss of excluded strand allows interaction of LRR domain of Lrr1 with the ZnF domains of Mcm3 and Mcm5, followed by CMG ubiquitylation and replisome disassembly (green box). Figure reproduced from Jenkyn-Bedford et al, 2021.

Another interesting observation from the reported Cul2^{Lrr1} structure is in its open architecture, unlike other Cullin RING ubiquitin ligases, where the LRR domain of Lrr1 has curled away from the catalytic domain of the Cul2^{Lrr1} complex, Rbx1. Notably, it was found that the distance between the LRR domain and the catalytic RING domain of Rbx1

closely matched the distance between the zinc finger interface of Mcm3 and 5 and the ubiquitylated Mcm7 substrate loop (Jenkyn-Bedford et al., 2021; Zhou et al., 2021). This finding further explains why our experiments using a high concentration peptide of Mcm7/scrambled peptide, spanning the ubiquitylation region, did not reveal much about the interaction of Cul2^{Lrr1} with the CMG. The Lrr1 interaction with the zinc finger regions of Mcm3 and Mcm5 is an evident explanation for this and that Lrr1 is docking away from the K27/K28 ubiquitylation residues on Mcm7 (Zhou et al., 2021).

By compiling data from various databases, I was able to map mutations within the human LRR1 gene in several cancer patients (Figure 3.8). I had observed high density of mutations within the first leucine rich repeat, while the second and third repeats exhibited a significantly lower mutation frequency (Figure 3.8). Trying to draw insights from the available structure of '*H. sapiens* replisome-Cul2^{LRR1} complex' from Jenkyn-Bedford et al (2021), we see that, these repeats are in close proximity with Mcm2-Mcm6 and not Mcm3-Mcm5 ZnF domains (represented as light green for Mcm2 and dark green for Mcm6 and dark blue for Mcm 3 and light blue for Mcm5 in Figure 3.22). Consequently, it is unlikely that mutations R172>H and R172>C (located within the first 3 repeats) would disrupt LRR-Mcm3/5 interactions. Interestingly, the mutations located near the C-terminus of LRR1 are more likely to disrupt these interactions. I have mapped other mutations from Figure 3.8- P265>S (located within the fifth repeat) and A354>T (located near the C-terminus) onto the Cryo-EM structure and observed that they are interacting with Mcm3-Mcm5 ZnF domains (Figure 3.22). Hence, mutations within this region might disrupt the LRR-MCM interactions. Moreover, it should be considered that proline residues are known to contribute to the protein folding and unfolding dynamics (Levitt, 1981). Proline can contribute to the beta turns in the amino acid chains and P265 is positioned at the end of a LRR repeat. Therefore, any mutation in proline can highly

destabilise the typical α/β horseshoe fold of Lrr1 and might disrupt the proper folding and functional state of Lrr1, potentially leading to the disengagement of LRR-MCM interactions. Additionally, it should be noted that the mutations resulting in truncated Lrr1 mutants (Figure 3.8) could also have disruptive effects on these interactions.

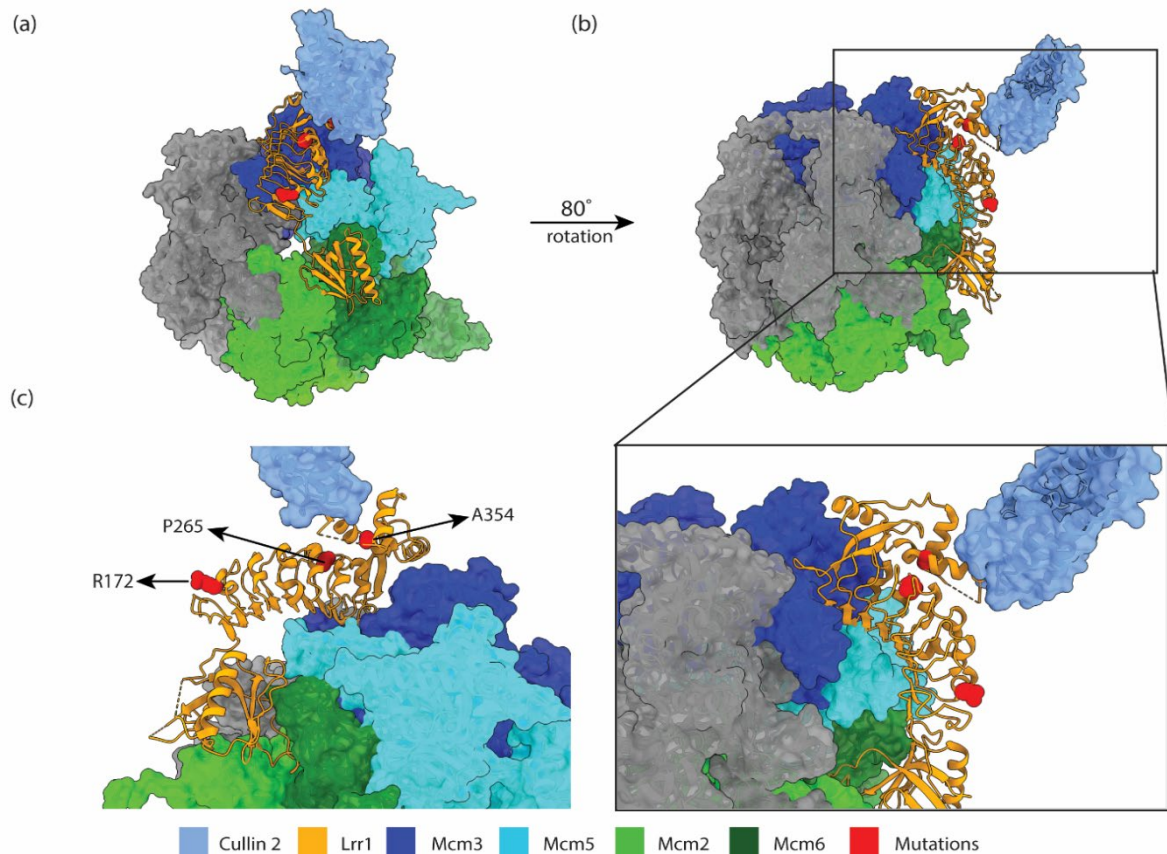


Figure 3.22:- Patient mutations mapped on Cryo-EM model of human replisome and Cul2^{Lrr1} (PDB ID: 7PLO) generated by Jenkyn-Bedford et al; 2021. (a) Shows the front view of Lrr1-McM interactions. Predicted interactions of patient mutations found in human Lrr1 is represented in red. The interacting regions of MCMs are shown in different colours. (b) The structure represented in (a) is rotated by 80° on the vertical axes, for left side perspective. The lower panel represents the magnified view of Lrr1. (c) Three different amino acid mutations R172, P265 and A345 has been depicted and is the left side perspective. A colour panel shown at the bottom of the figure represents the Mcm2/3/5/6, Cullin 2, Lrr1 and mutations. This figure was produced in collaboration with Dr. Paolo Passeratti using ChimeraX.

Further investigation of these mapped mutations can provide insights into their functional importance such as their impact on ligand binding sites or structural alterations resulting in loss of function. It remains unknown whether the mutated Lrr1

contributed towards the diseases observed in these patients and whether there is a subsequent disruption of replisome disassembly leading to genomic instability. Importantly, we do not know what the consequences of these mutations are on human health. The absence of the LRR-1 gene in *C. elegans* was earlier reported to activate DNA damage checkpoint (Merlet et al., 2010). In human cells, blocking replisome disassembly can trigger DNA damage responses (Jones et al., 2022), suggesting that these replication factors involved in replication termination may play a vital role in maintaining genome integrity. It would be interesting to study these mutations and translate these findings into human cells to study their effects and determine if targeting replisome disassembly and the associated factors could be a potential therapeutic strategy in the future.

In summary, our efforts to study the structure of Lrr1 were impeded by impurities in our protein preparation, preventing further progression in this direction. However, the structural predictions I made for the Lrr1 structure exhibited similarities with the Cryo-EM structures solved by others. This also highlights the importance of utilising current in silico methods to gain structural insights rapidly than wet-lab based methods. However, lab based methods remains the gold standard as the resolved Cryo-EM structures from other labs revealed more informative results regarding the regulatory aspects of Lrr1. Such information cannot be obtained just from in silico methods. Moving forwards, integrating the computational methods and experimental data can be a powerful tool. Importantly, the resolved Cryo-EM structures revealed that the regulation of CMG ubiquitylation is maintained by the occlusion of the Lrr1 binding site by the excluded strand. It is interesting to observe that, despite being regulated by different ubiquitin ligases, such as SCF^{Dia2} and Cul2^{Lrr1}, these mechanisms exhibit a high degree of conservation across diverse organisms including yeast and higher eukaryotes like *Xenopus laevis* and humans.

Chapter – 4

4 TRAIP drives replisome disassembly in mitosis

4.1 Introduction

Our lab has previously seen that Mcm7 is polyubiquitylated during termination in S-phase and this is catalysed by Cul2^{Lrr1} (Moreno et al., 2014). Further to this, the Gambus lab investigated the impacts of blocking the replisome disassembly pathway by inhibiting cullin activity, and we have seen that the replisomes were retained on chromatin throughout S-phase. Interestingly, the transition of the extract into mitosis led to rapid replisome disassembly, indicating that a mitosis-specific pathway is active. Notably, the polyubiquitylation of Mcm7, and its subsequent recognition by p97, was observed in the mitotic replisome pathway too. Given these findings, our next aim was to identify the specific ubiquitin ligase responsible for this process. Therefore, a former lab member (Dr. Sara Priego Moreno) of our group performed immunoprecipitation of the helicase, accumulated on mitotic chromatin upon p97 inhibition. Mass spectrometry analysis of the interacting partners revealed a significant number of interacting peptides corresponding to an E3 ubiquitin ligase known as TRAIP. We decided, therefore, to investigate further the role of TRAIP during mitosis. To study this in *X. laevis* egg extracts, we needed to allow our egg extracts to progress into mitosis by supplementing them with cyclin. *Xenopus* eggs synthesise both cyclin A and B (Minshull et al., 1989) that have been shown previously to promote the transition of egg extract into mitosis (Strausfeld et al., 1996). To drive our egg extracts into mitosis, they were supplemented with recombinant cyclin A1ΔN56 (hereafter cyclin A1Δ) after DNA replication was completed. We used a

mutant form of cyclin A1 that lacks the first 56 amino acids responsible for its degradation thereby facilitating the maintenance of mitotic synchronicity throughout the reaction.

4.2 Results

4.2.1 Cul2^{Lrr1} independent mitotic replisome disassembly

Firstly, I confirmed the existence of a backup pathway for replisome disassembly in mitosis using *X. laevis* egg extracts. To achieve this, interphase extracts were used into which demembranated sperm DNA was added to start replication (S-phase). I optionally blocked cullin ubiquitin ligases with MLN4924, an inhibitor of cullin neddylation (Cul i); and replication was allowed to complete (Figure 4.1 a). A part of this reaction was optionally progressed into mitosis by adding cyclin A1Δ. Chromatin was isolated at the indicated time points during the replication reaction and mitosis. The whole reaction setup was also supplemented with Geminin, an inhibitor of origin licensing, 2 min after the addition of sperm DNA into the extract. This was done to limit the level of loaded Mcm2-7 onto chromatin to better visualise Mcm7 disassembly upon termination (see reduced levels of Mcm7 on chromatin). The chromatin-associated replisome components were analysed using a western blot. As seen in Figure 4.1 b, the replisome components (Cdc45 and Psf2) are present on S-phase chromatin only at 45 min in DMSO control samples (lane 4), while inhibition of cullins resulted in the retention of replisomes on chromatin, as expected (lane 9-11) (Sonneville et al., 2017). On the other hand, when the reaction was driven into mitosis with the aid of recombinant cyclin A1Δ, the Cdc45 and Psf2 were disassembled despite the presence of a cullin inhibitor (compare lane 14-16; in late S-phase with lane 20-21; in mitosis). This confirmed the existence of a backup pathway in mitosis which is independent of Cul2^{Lrr1} activity.

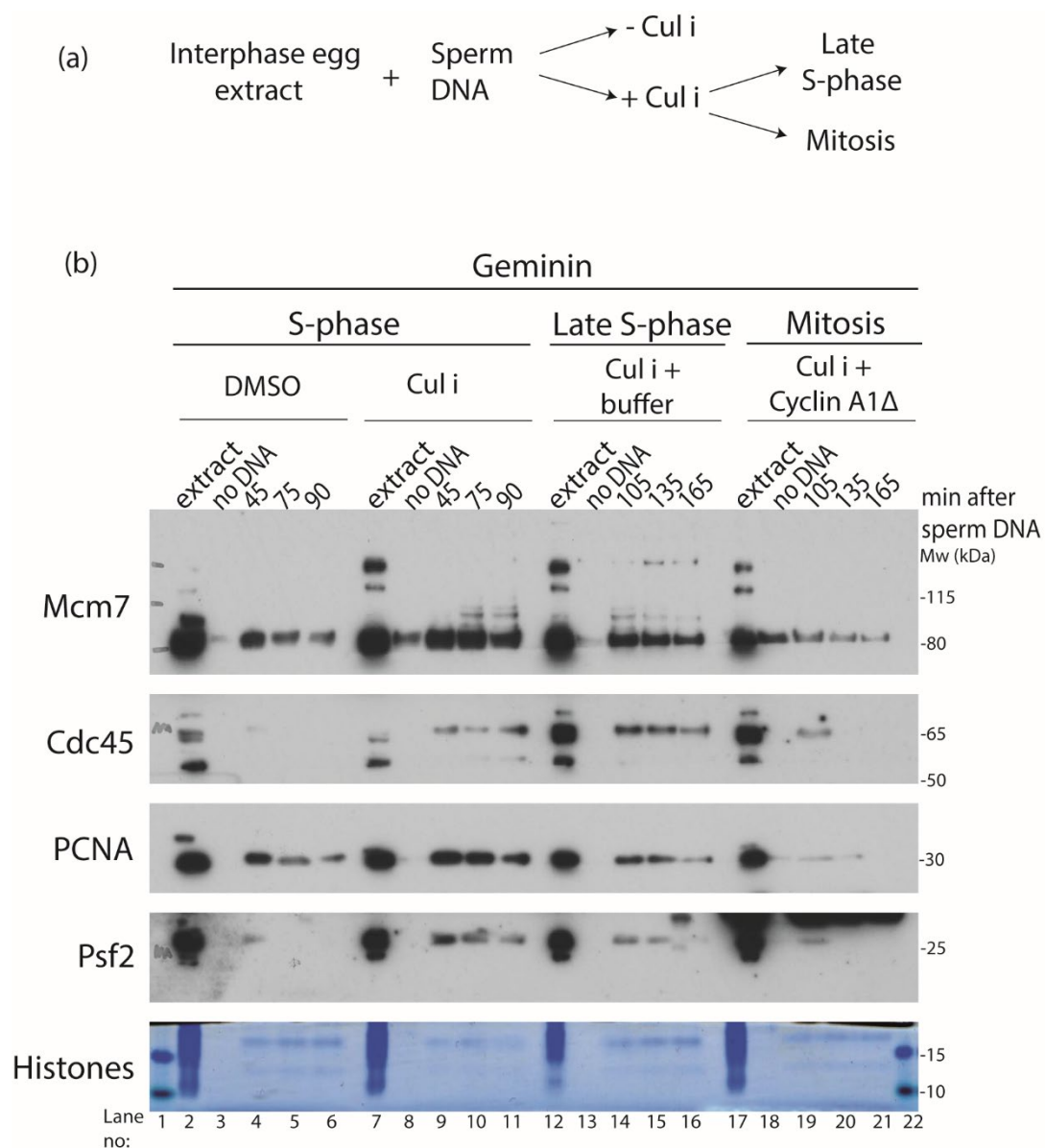


Figure 4.1 Replisome disassembly has a backup pathway in mitosis. (a) Schematic for replisome disassembly assay. Interphase egg extract was supplemented with sperm DNA and optionally with Cullin inhibitor (Cul i). One set of samples were analysed in S-phase, and the second half was analysed in late S-phase and mitosis upon completion of replication. (b) Chromatin-bound proteins from (a) were extracted at indicated time points and analysed by western blotting with indicated antibodies. Histones were stained with coomassie stain and provided loading control. Samples containing no sperm (no DNA) were processed alongside each set of samples to provide chromatin specificity control. This experiment was performed once.

4.2.2 Purification of Recombinant *Xenopus laevis* TRAIP

Our next aim was to check if TRAIP indeed is the ubiquitin ligase responsible for Mcm7 ubiquitylation and replisome unloading in mitosis. To this end, I wanted to immunodeplete endogenous TRAIP from the egg extracts, for which I needed to raise antibodies that are specific against *Xenopus* TRAIP. To do this, I purified recombinant *X. laevis* TRAIP from bacteria. Initially, I tried purification of *X. laevis* TRAIP as 6xHis-tagged protein, but I found it insoluble (data not shown). *X. laevis* TRAIP was, therefore, cloned into a pGS-21a vector using NcoI/EcoR1 restriction enzymes. The vector itself possesses a 6x His and a GST tag. Expression of the GST-TRAIP was tested in different *E. coli* strains (BL21 (De3), C41 (De3), Rosetta (De3) pLys, and ArcticExpress (De3)), at different temperatures (13°C for Arctic, 20°C for BL21 (De3), C41 (De3) & Rosetta (De3) pLys and all four also at 37 °C) and different media (LB broth and auto induced media; AIM) (data not shown). I also tried to solubilise the protein in different buffers and the one providing the most solubility of TRAIP was chosen for purification (see section 2.3.5.4).

Our initial aim was to cut off the 6x His-GST tag using enterokinase and obtain TRAIP containing no GST tag. However, this was challenging as the enterokinase-treated, untagged protein was not soluble and was retained on the beads (see beads lane after enterokinase digestion in Figure 4.2 a). Therefore, I eluted TRAIP as 6x His-GST-6x His-TRAIP using glutathione - represented as GST-TRAIPwt (Figure 4.2 a and b). These elutions were pooled and stored at -80°C and also used for raising antibodies against *Xenopus* TRAIP.

Since the protein I purified contained both His and GST tags, our initial objective was to confirm its functional activity in the egg extract, while waiting for the antibodies to be raised. To achieve this, I wanted to test whether the addition of wt or catalytically dead

TRAIP mutant to the egg extract in mitosis, could affect mitotic replisome disassembly (alike overexpression experiments in human cells). Firstly, I needed an inactive mutant of TRAIP as a control. To address this need, I purified a catalytically dead RING mutant of TRAIP; targeting C25A (Besse et al., 2007; Chapard et al., 2015) (hereafter GST-TRAIPmut) using an analogous purification method (section 2.3.5.4).

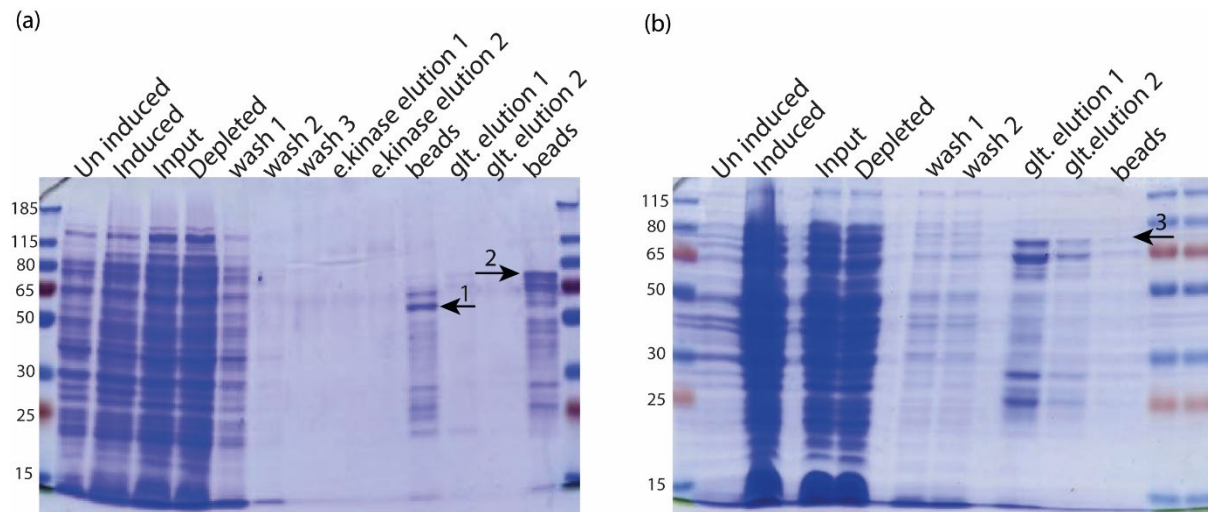


Figure 4.2:- *Xenopus laevis* GST-TRAIP purification. GST-TRAIP was expressed in bacteria and purified using a GST tag. Protein samples were taken from the indicated stages of purification process. (a) The first half of the beads were treated with enterokinase (see lanes with e.kinase elution 1 and 2) to cut off the GST tag from TRAIP and the second half of the beads were treated with glutathione (10 mg/ml) (see lanes with glt. elution 1 and 2). (b) Trial with glutathione (20 mg/ml) containing buffer, GST-TRAIPwt is visible in glutathione elution 1 and 2 at approximately 75 kDa. The gels were stained with Coomassie brilliant blue. The arrow-1 indicating a band in the “beads” lane from enterokinase treatment in (a) points to TRAIP with GST cut off and the arrow-2 and arrow-3 in both (a) and (b) indicate recombinant GST-TRAIP.

The purified recombinant GST-TRAIP was subjected to dialysis into a buffer suitable for compatibility with the egg extract (LFB1/50). We also needed to block the S-phase replisome disassembly pathway using a cullin inhibitor. Once the replication was completed, the extract was induced into mitosis with the addition of cyclin A1Δ, and the purified GST-TRAIP was added to the egg extract, which still contained the endogenous TRAIP. The chromatin was isolated and analysed to determine the effect on replisome disassembly. We found that the addition of both GST-TRAIPwt and GST-TRAIPmut was

blocking the replisome unloading as visualized by Psf2 and Cdc45 retained on chromatin (performed by Dr. Rebecca Jones) (Figure 4.3 a). I also checked the levels of Mcm7 ubiquitylation upon the addition of these recombinant proteins. To visualise the levels of ubiquitylated Mcm7 I needed to retain all ubiquitylated replisomes on chromatin. To this end, all unloading was blocked by inhibiting p97 activity using NMS-873- represented as p97i. I could see that the length of the ubiquitylated Mcm7 after the addition of GST-TRAIPwt was lower than the buffer control and both GST-TRAIPwt and GST-TRAIPmut had similar levels of Mcm7 ubiquitylation (Figure 4.3 b).

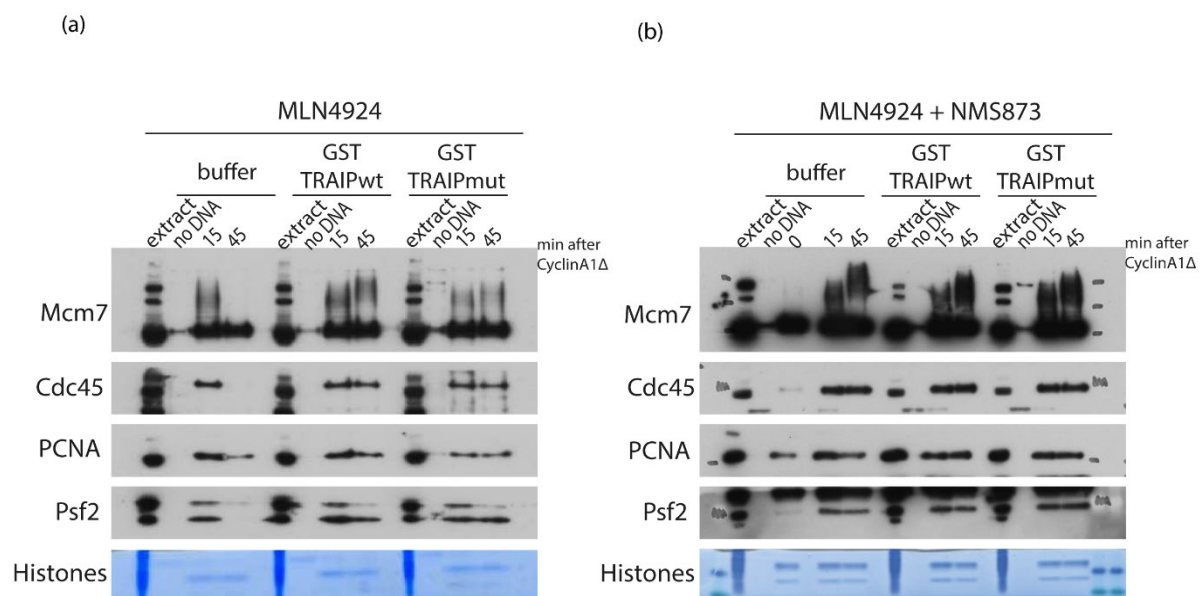


Figure 4.3:- Effect of the addition of GST-TRAIP to the egg extract. (a) Chromatin was replicated in egg extract in the presence of Cul i (MLN4924) and supplemented with cyclinA1Δ to induce mitosis, then optionally supplemented with buffer, GST-TRAIPwt, and GST-TRAIPmut. Chromatin samples were extracted at indicated time points and analysed by western blotting. Figure 4.3a was kindly provided by a lab member; Dr. Rebecca Jones (b) Experiment was set up as in (a) but in addition p97 inhibitor (NMS-873) was also added to be able to visualise Mcm7 ubiquitylation. Chromatin samples were analysed as before. Histones and no DNA samples were processed as before. These experiments were performed twice.

One possible reason for the lack of functionality of our GST-tagged TRAIP could be attributed to the large size of the tag itself. Previous studies conducted in human cells have indicated that bulky tags at the N-terminus of TRAIP can interfere with its

localisation and proper functioning within the cell (Feng et al., 2016). These findings aligned with the disruptions I observed in TRAIP functionality in our experiments.

Our next objective was to express and purify functional recombinant wild-type and mutant versions of TRAIP from bacteria. To achieve this, we opted to purify TRAIP from a SUMO fusion vector (section 2.3.5.5). Therefore, I cloned TRAIP into the pCA528 vector. This vector includes a 6x His and a SUMO tag at the N-terminus of cloned protein of interest. The SUMO tag has a smaller 11 kDa size compared to the bulky GST tag. Like GST, it acts as a chaperone, enhancing solubility, and yield, and facilitating protein folding and functionality. Therefore, using this vector, I expressed recombinant His/SUMO tagged *X. laevis* TRAIP wild type (hereafter TRAIPwt) from Rosetta (De3) pLysS by exploiting the 6x His tag located at its N-terminus and eluting the protein with a high concentration of Imidazole (Figure 4.4 a). To inhibit the ubiquitin ligase activity of TRAIP, I also purified recombinant His/SUMO tagged *X. laevis* TRAIPmut, which lacks catalytic activity by mutating the conserved cysteine at position 25 in its RING domain into alanine; C25A, similar to the GST tagged TRAIPmut (Figure 4.4 b). The presence of purified TRAIPwt/mut proteins was also confirmed by western blotting with commercial α -TRAIP antibodies (data not shown). The purified proteins were then used in our experiments after dialysing with an egg extract friendly buffer; LFB1/100.

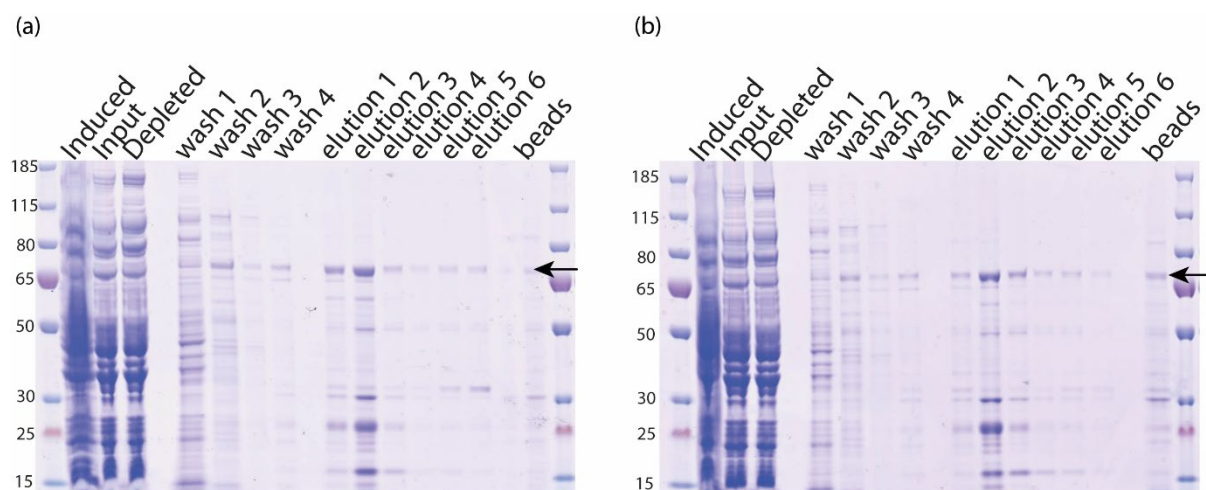


Figure 4.4:- *Xenopus laevis* SUMO-TRAIP purification. His/SUMO tagged (a) TRAIPwt and (b) TRAIPmut was expressed in bacteria and purified using Ni^{2+} beads. Samples were taken from indicated stages of purification. The proteins bound to the beads were eluted with buffer containing 250 mM Imidazole and are represented as elutions 1-6. The protein sample collected after induction is represented as induced. Input and depleted represent the samples before and after incubation with the beads. A small sample of beads taken after elution was also analysed and labelled as beads. The proteins were analysed on gradient acrylamide gels by staining with Coomassie brilliant blue and the arrows indicate where recombinant *Xenopus* His/SUMO-TRAIP are present.

4.2.3 Raising and testing α -TRAIP antibodies

After purifying *Xenopus* TRAIP proteins, our next aim was to raise antibodies against it. The approximate concentration of purified proteins was estimated using acrylamide gel run alongside known BSA concentration titration (data not shown) and ~2 mg of purified TRAIP proteins were sent to Dundee Cell Products to raise antibodies against *Xenopus* TRAIP. I generated antibodies against GST-TRAIPwt and SUMO-TRAIPwt by immunizing four separate rabbits. Subsequently, I purified the TRAIP antibodies from the whole sera of these four animals using SUMO-TRAIPwt as the ligand bound to the HiTrap NHS-Activated affinity column. This purification step was necessary as the whole sera tested showed the presence of numerous non-specific bands in the egg extracts (data not shown).

The characterization of our in-house raised antibodies was performed in egg extract. TRAIP is not very abundant in egg extract and I can detect it best when accumulated on chromatin upon inhibition of replisome disassembly. To test these different purified antibodies, a small amount of extract was run on a 4-12% gradient acrylamide gel alongside isolated chromatin from a control (DMSO) sample and chromatin from extract treated with Cul i, MLN4924 (TRAIP accumulated). The chromatin was isolated at 90 min. The results obtained from immunoblotting confirmed the presence of a band at ~53 kDa corresponding to the size of endogenous TRAIP. This band was detected by all four antibodies - α -TRAIP #91, α -TRAIP #107, α -TRAIP #108, and α -TRAIP #52 (Figure 4.5). α -TRAIP #91, and #52 were raised using His/SUMO-TRAIPwt and α -TRAIP #107, and #108 were produced using GST-TRAIPwt.

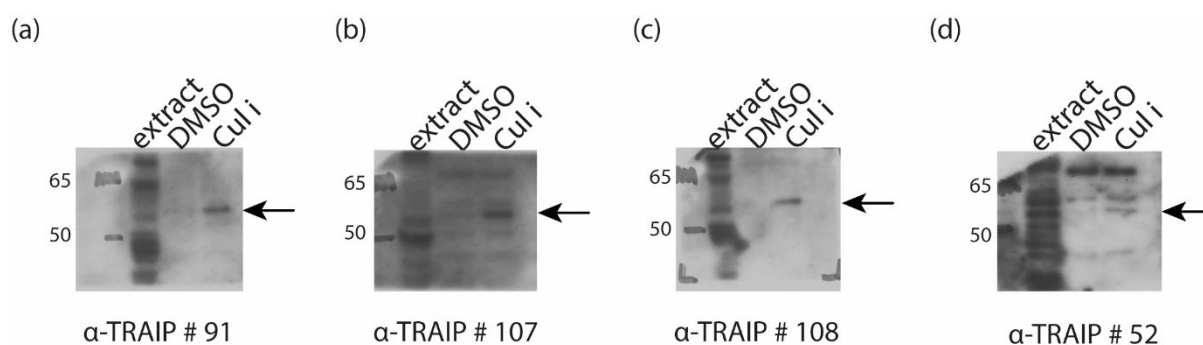


Figure 4.5:- Characterisation of TRAIP using in-house purified antibodies. Egg extract was optionally supplemented with DMSO and Cul i for accumulation of TRAIP. Chromatin was isolated at 90 min and proteins were analysed by western blotting. TRAIP antibodies purified from sera #91, #107, #108 and #52 were able to detect TRAIP at ~53 kDa in cullin-inhibited chromatin samples. The arrow indicates where TRAIP runs on the gel.

4.2.4 Testing α -TRAIP antibodies for immunodepletion and/or immunoprecipitation of TRAIP from egg extracts

Our next aim was to test if the antibodies raised in our lab can immunoprecipitate and immunodeplete TRAIP from the egg extracts. I, therefore, tested all 4 antibodies along with non-specific IgG rabbit sera (IgG mock). I used two rounds of Dynabeads crosslinked

with TRAIP antibodies to immunodeplete TRAIP from the extracts. I found that all antibodies can immunodeplete TRAIP from the extract as observed by the disappearance of TRAIP (Figure 4.6 a). The level of immunodepletion is difficult to judge as the antibody is not very sensitive and does not detect TRAIP beyond 50% of the original concentration in egg extract. However, when the post-immunodepletion beads were analysed I could see the presence of TRAIP only on the beads in the first round of depletion suggesting efficient immunodepletion. The interaction of TRAIP with the beads suggests that all these antibodies can immunoprecipitate and immunodeplete TRAIP from the extracts (Figure 4.6 b).

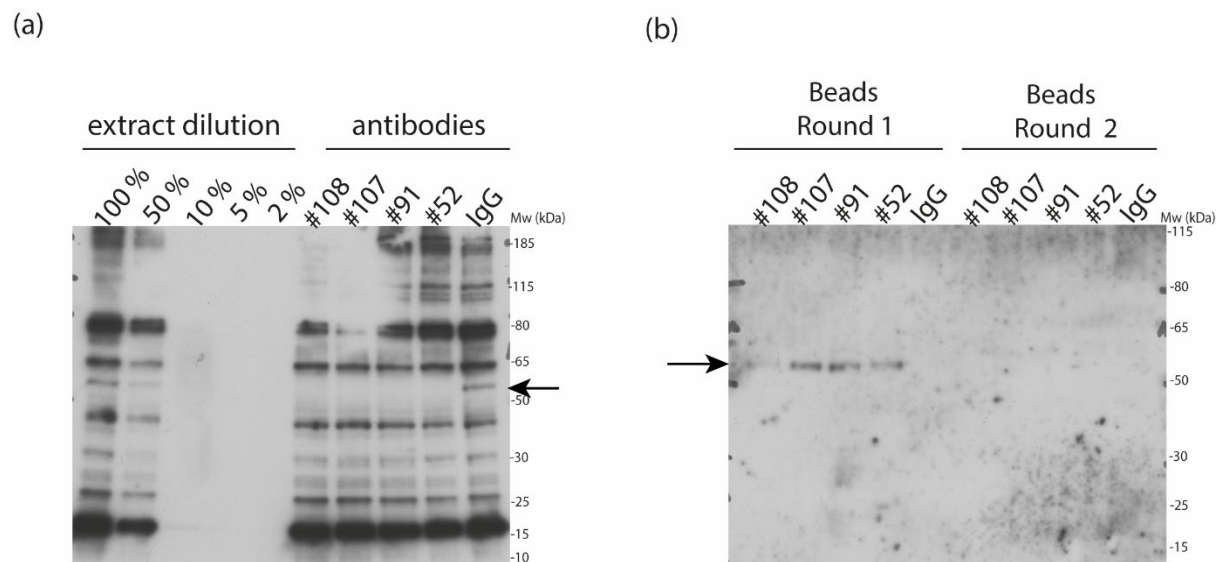


Figure 4.6:- Immunodepletion using in-house purified α -TRAIP antibodies. (a) Immunodepletion of TRAIP from extracts was tested with different TRAIP antibodies #108, #107, #91, and #52 along with non-specific rabbit sera; IgG. The samples were analysed by western blotting with α -TRAIP antibodies. The arrow near the band at ~ 53 kDa represents TRAIP (b) Immunoprecipitated material associated with Dynabeads after each round of depletion was analysed by western blotting using commercial α -TRAIP antibodies. The arrow corresponding to the band at ~ 53 kDa represents TRAIP.

4.2.5 Effect of immunodepletion of TRAIP from *Xenopus laevis* egg extract

Since our purified antibodies were able to efficiently immunodeplete TRAIP from the egg extract, we decided to look further into the consequences of TRAIP depletion. To study further the importance of TRAIP in replication termination, I prepared a large-scale TRAIP-depleted extract using α -TRAIP #91 antibodies. The efficiency of TRAIP depletion was tested by western blotting (Figure 4.7 a) and the replication kinetics of the TRAIP-depleted extract was tested by assessing the rate at which α -³²P labelled dATP, was incorporated into the newly synthesised DNA. The replication rate of the TRAIP-depleted extract was comparable to the IgG mock-depleted extract suggesting that the absence of TRAIP did not interfere with the efficiency of nascent DNA synthesis (Figure 4.7 b).

Interestingly, when I performed chromatin isolation with mock and TRAIP-depleted extracts, I could not see any differences in the replisome unloading patterns in S-phase in the absence of TRAIP. Cdc45 and Psf2 were found to be unloaded after 45 min in both the control and TRAIP depleted extract. The α -TRAIP blot confirms the absence of TRAIP in the depleted extract (Figure 4.7 c).

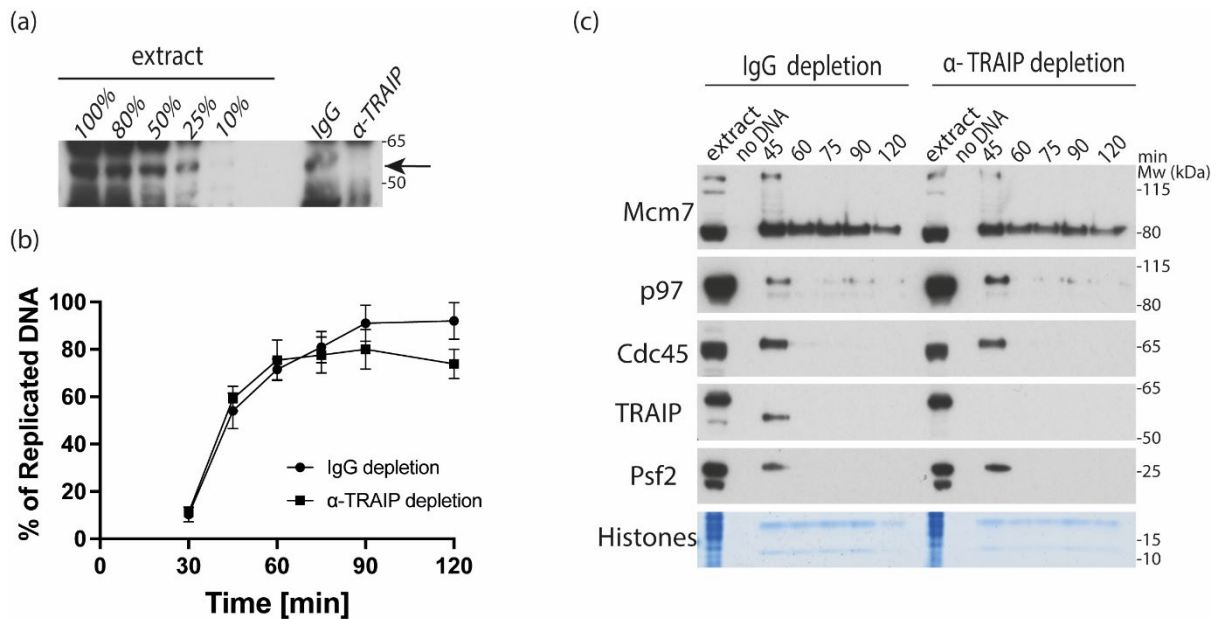


Figure 4.7:- Immunodepletion of TRAIP does not negatively affect DNA replication in S-phase. (a) The remaining levels of TRAIP upon immunodepletion were analysed by western blotting using α -TRAIP antibodies. (b) The ability of TRAIP immunodepleted extract to synthesise nascent DNA was analysed by incorporation of radioactive α - 32 P dATP into newly synthesised DNA. Mean of $n=4$ for TRAIP depletion is presented with SEM. (c) Chromatin was isolated during the replication reaction time course in IgG-depleted and TRAIP-depleted extracts. Chromatin samples were analysed with indicated antibodies. Histones provide loading control for the samples. This experiment was repeated three times.

4.2.6 TRAIP can unload post-terminated and stalled replisomes in mitosis

Having efficiently immunodepleted TRAIP without compromising on the replication ability of the extracts, we decided to use these extracts to determine whether TRAIP is the E3 ubiquitin ligase involved in the mitotic replisome disassembly pathway of higher eukaryotes. Using mock and TRAIP-depleted extracts I set up replication reactions, blocked S-phase replisome disassembly by inhibiting cullin activity, and allowed replication to complete. This interphase extract was further driven into mitosis by adding cyclin A1 Δ and chromatin was isolated (Figure 4.8). Strikingly, I could observe that the Cdc45 and Psf2 disassembled in the IgG-depleted samples just after 15 min whereas the replisomes stayed on chromatin in the TRAIP-depleted extracts. The complete depletion

of TRAIP and its lack of binding to chromatin can be observed from the TRAIP blot. In addition, a sample containing no cyclin A1Δ was processed alongside as a control for absence of mitotic activity. Cdc45 and Psf2 were retained on chromatin in this condition. All these indicated that TRAIP ubiquitin ligase is needed for replisome disassembly in mitosis.

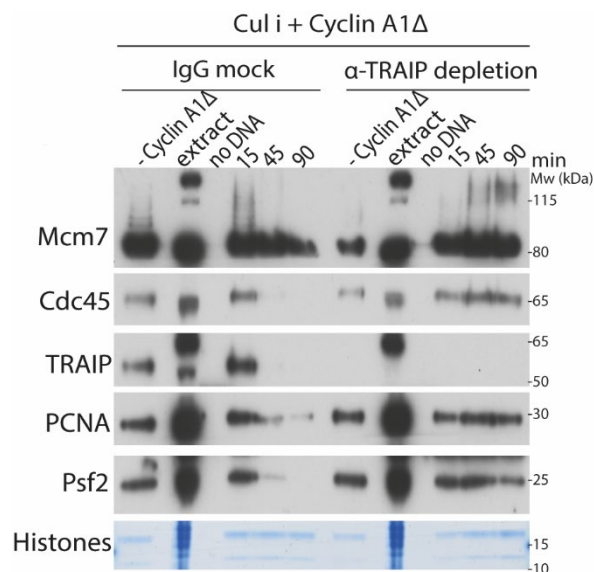


Figure 4.8:- TRAIP ubiquitin ligase drives mitotic replisome disassembly in post-termination replisomes. A replication reaction was set up using mock and TRAIP-depleted extracts in the presence of a Cul i. Extracts were supplemented with cyclin A1Δ after completion of replication and chromatin isolation was performed at indicated timepoints. A sample containing no cyclin A1Δ was also collected as a control for the absence of mitotic activity. Replisome disassembly was analysed by western blotting. A sample containing no sperm (no DNA) was processed alongside each set of samples to provide chromatin specificity control. This experiment was performed once.

I further explored the role of TRAIP in CMG unloading during mitosis by supplementing the extract with a high concentration of recombinant TRAIP (wt or ligase mutant) proteins, similar to overexpression experiments in cell systems. Notably, these extracts have endogenous TRAIP present as well. Addition of these recombinant proteins could also tell us whether the TRAIP mutant I purified could outcompete the endogenous TRAIP present in the extract. To achieve this, I first validated that the addition of the purified

TRAIP proteins does not affect the ability of the extract to synthesise nascent DNA during DNA replication (Figure 4.9 a) and then to look at the replisome unloading pattern, I set up a replication reaction by inhibiting the cullin activity and allowed the replication process to reach completion. Once completed, the extract was driven into mitosis by supplementing cyclin A1 Δ , and appropriate recombinant TRAIP proteins were optionally added to a final concentration of 50 μ g/ml, and chromatin was isolated (Figure 4.9 b). I could observe that buffer control and TRAIPwt samples showed similar replisome disassembly patterns (see Cdc45 and Psf2 blots at 45 min) whereas in TRAIPmut the replisome disassembly was slowed down. This again confirms that the ubiquitin ligase activity of TRAIP is needed for replisome disassembly in mitosis. In addition to this, the levels of Cdc45 remaining on chromatin have been quantified in each condition, with the highest level retained for TRAIPmut samples (Figure 4.9 c). The lack of complete inhibition of disassembly observed with TRAIPmut (as evident from Cdc45 and Psf2 blots at 120 min) is probably due to the presence of endogenous TRAIP in these extracts. This is because we supplemented the recombinant proteins on top of the existing endogenous TRAIP.

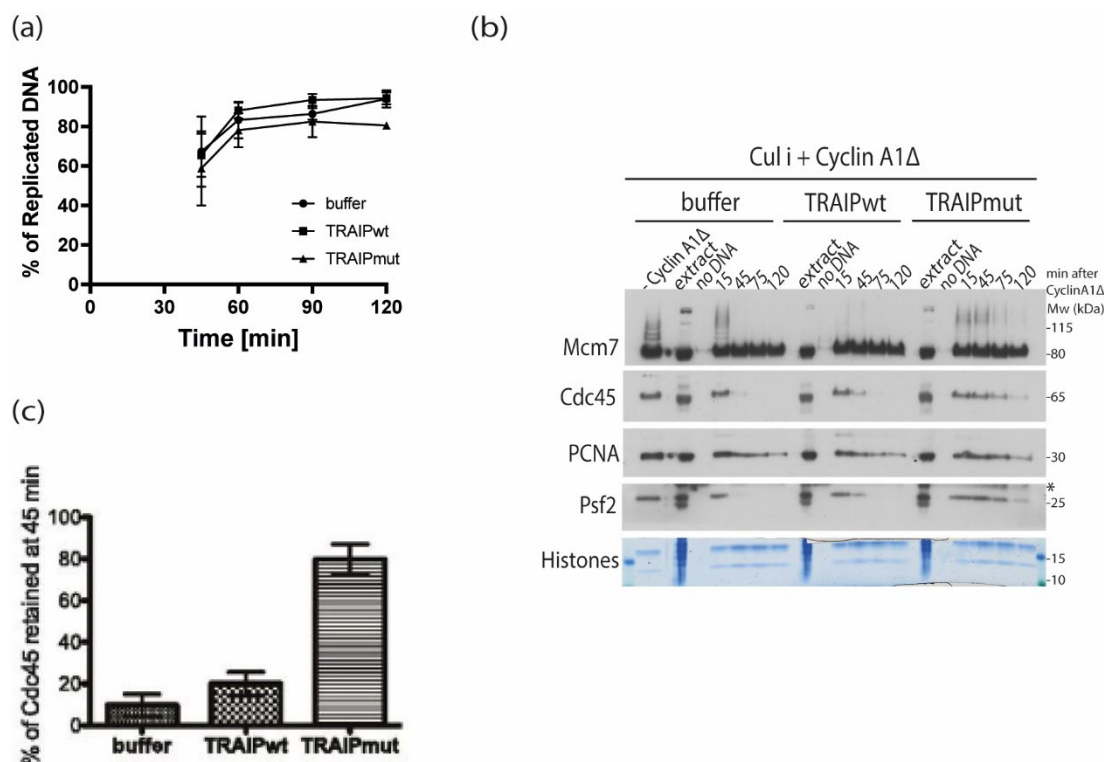


Figure 4.9:- Ubiquitin ligase activity of TRAIP is essential for unloading post-terminated replisomes. (a) Interphase egg extract was supplemented with LFB1/100 (buffer), recombinant wildtype TRAIP (TRAIPwt), RING-domain mutant TRAIP (TRAIPmut). The ability of extracts to synthesise nascent DNA was analysed by incorporation of radioactive α - 32 P dATP into newly synthesised DNA. Mean of $n=4$ for TRAIP addition is presented with SEM. (b) A replication reaction was set up in egg extract containing endogenous TRAIP. The reaction was completed in the presence of Cul i. cyclin A1 Δ was added to drive the extract into mitosis and supplemented with buffer, TRAIPwt, or TRAIPmut to a final concentration of 50 μ g/ml. Chromatin was extracted and analysed by western blotting using indicated antibodies. Sample with -cyclin A1 Δ represents the absence of mitotic activity. A sample containing no sperm (no DNA) was processed alongside each set of samples to provide chromatin specificity control. *indicates band of cyclin A1 Δ which was also recognized by α -Psf2. This experiment was repeated three times. (c) The levels of Cdc45 retained on chromatin were quantified at 15 min and 45 min in each condition and the percentage of the 15 min signal still retained on chromatin at 45 min calculated. The graph represents a mean of three independent experiments with SEM.

To investigate whether TRAIP plays a role in replisome unloading by influencing Mcm7 polyubiquitylation, I repeated the same experiment but in addition, supplemented the mitotic extract with p97 inhibitor; NMS-873. This allowed us to block replisome disassembly and retain all the ubiquitylated Mcm7 on chromatin. As seen in Figure 4.10 a, the addition of the catalytically dead TRAIPmut alters Mcm7 polyubiquitylation levels, evident from the shorter ubiquitin chains in comparison with buffer control and TRAIPwt

(see the level of Mcm7 ubiquitylation above the dotted line on Mcm7 blot for buffer control and TRAIPwt samples in Figure 4.10 a). In addition to this, the levels of Mcm7 polyubiquitylation remaining on chromatin have been quantified in each condition with the lowest levels of Mcm7 ubiquitylation present for TRAIPmut samples (Figure 4.10 b). This provides reassurance that the recombinant TRAIP mutant can effectively outcompete the endogenous TRAIP and that the unloading and ubiquitylation defect that we see in our mitotic experiments is attributable to the recombinant TRAIP proteins. These findings strongly indicate that TRAIP indeed plays a crucial role in the replisome unloading of post-terminated replisomes during mitosis.

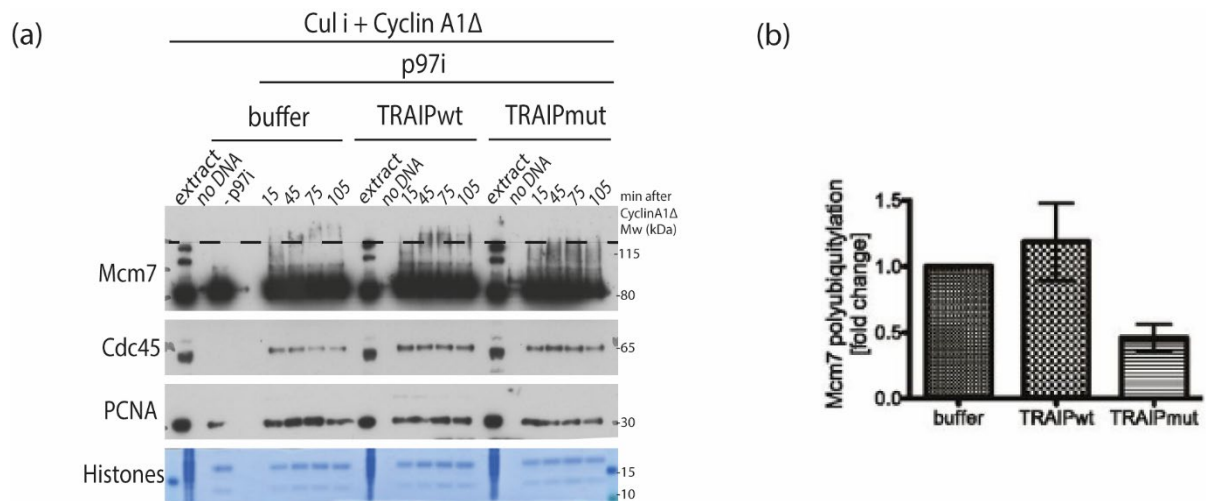


Figure 4.10:- Ubiquitin ligase activity of TRAIP is essential for ubiquitylating Mcm7 of post-terminated replisomes in mitosis. (a) A replication reaction was set up using egg extract containing endogenous TRAIP with Cul i to block S-phase disassembly and p97 inhibitor (p97i) to analyse Mcm7 ubiquitylation on chromatin. Extracts were supplemented with cyclin A1Δ after completion of replication and the reaction was supplemented with buffer, TRAIPwt, or TRAIPmut to a final concentration of 100 μg/ml. Chromatin isolation was performed at indicated time points. Replication factors were analysed by western blotting. The sample represented as -p97i provides a control for p97 activity. A sample containing no sperm (no DNA) was processed alongside each set of samples to provide chromatin specificity control. This experiment was repeated three times. (b) The levels of Mcm7 polyubiquitylation remaining on chromatin have been quantified in each condition. The graph presented here shows the mean fold change of Mcm7 polyubiquitylation signal at 45 min after cyclin A1Δ addition over three independent experiments with SEM.

Having established that TRAIP is needed for the unloading of post-termination replisomes in mitosis, we then wanted to understand whether this backup pathway,

catalysed by TRAIP, could target any replication machinery that failed to complete replication and persisted on chromatin until mitosis. To study this, I used mock and TRAIP-depleted extracts and added aphidicolin – a DNA polymerase inhibitor - to stall forks, and caffeine - a checkpoint inhibitor - to accumulate more of such stalled forks. The extract was then driven into mitosis with cyclin A1 Δ and chromatin samples were isolated (Figure 4.11).

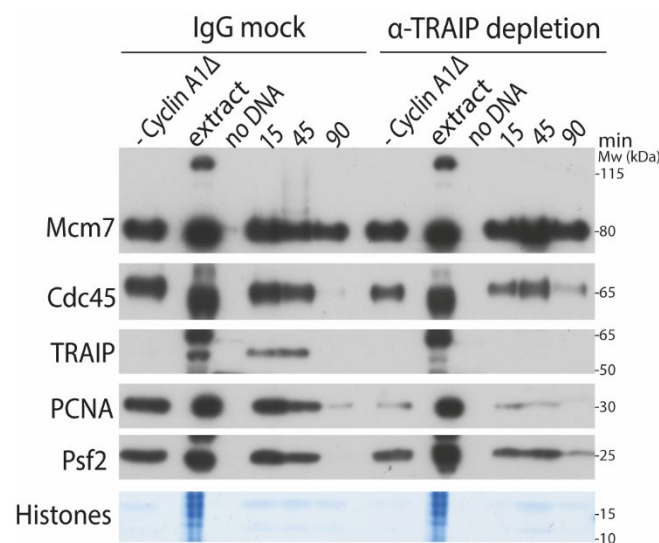


Figure 4.11:- TRAIP ubiquitin ligase drives mitotic replisome disassembly of stalled replisomes. A replication reaction was performed using IgG and TRAIP-depleted extracts in the presence of aphidicolin and caffeine to generate stalled forks. Extracts were supplemented with cyclin A1 Δ and chromatin isolation was performed at indicated time points. A sample containing no cyclin A1 Δ was also collected as a control for assessing the absence of mitotic activity. The replication factors were analysed by western blotting. Histones were stained in Coomassie stain and provided loading control. A sample containing no sperm (no DNA) was also processed alongside each set of samples to provide chromatin specificity control. This experiment was performed once.

I could observe that Cdc45 and Psf2 disassembled after 45 min in mock depleted extracts. Interestingly, Cdc45 and Psf2 failed to disassemble in TRAIP-depleted extracts. The complete depletion of TRAIP and its lack of binding to chromatin can be observed from the TRAIP blot. This indicates that TRAIP is essential for unloading of stalled replisomes too. Please note that at 90 min, there is only a faint band for Cdc45 and Psf2 in the TRAIP-

depleted samples. This is due to a technical error as a small amount of chromatin was lost during isolation which is evident from the low level of histones as well at 90 min.

To confirm that it is the ubiquitin ligase activity of TRAIP that is needed for stalled replisome unloading in mitosis, a replication reaction containing aphidicolin and caffeine was set up, driven to mitosis, and supplemented optionally with purified recombinant TRAIP proteins (Figure 4.12). Interestingly, in the buffer control and TRAIPwt samples, Cdc45 and Psf2 were unloaded, whilst the addition of TRAIPmut blocked replisome unloading - similar to post-terminated replisomes.

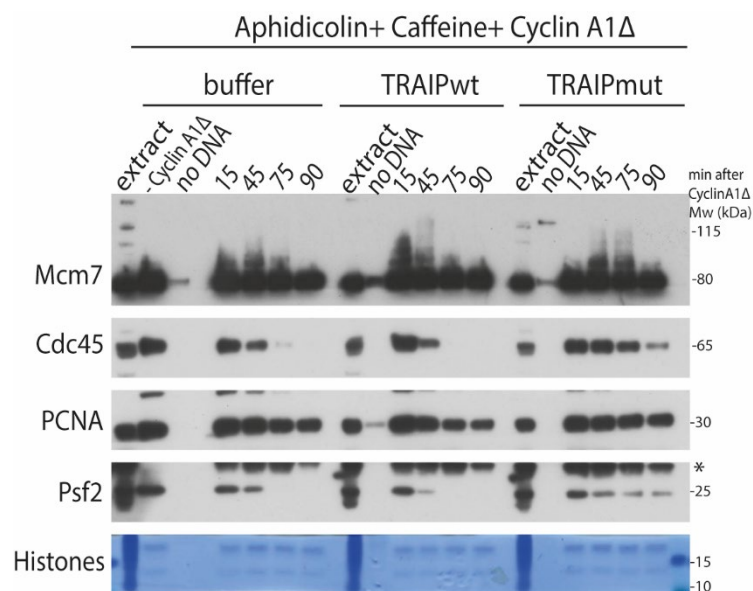


Figure 4.12:- Ubiquitin ligase activity of TRAIP is essential for the unloading of stalled replisomes. A replication reaction was set up in the egg extract in the presence of aphidicolin and caffeine. Cyclin A1Δ was added to drive the extract into mitosis and the extract was supplemented with buffer, TRAIPwt, or TRAIPmut to a final concentration of 50 μg/ml. Chromatin was extracted and analysed by western blotting using indicated antibodies. The sample with -cyclin A1Δ represents the absence of mitotic activity. Histones were stained in Coomassie stain and provided loading control. A sample containing no sperm (no DNA) was processed alongside each set of samples to provide chromatin specificity control. *indicates band of cyclin A1Δ which was also recognized by α-Psf2. This experiment was repeated two times.

This again confirmed that TRAIP is essential for processing replisomes that are retained on chromatin through mitosis and that it requires its ubiquitin ligase activity. A small level

of unloading observed at 90 min in the presence of TRAIPmut is most likely due to the presence of endogenous TRAIP in these extracts.

Consequently, we aimed to determine whether the defective unloading of replisomes caused by the addition of TRAIPmut resulted from defective polyubiquitylation. To explore this, I generated stalled replisomes using aphidicolin and caffeine and in addition, added the p97 inhibitor into the extract during mitosis and followed replisome disassembly. In samples containing TRAIPmut, the ubiquitylation levels of Mcm7 were drastically reduced when compared to the buffer control and TRAIPwt (Figure 4.13). The reduced levels of ubiquitylation observed on Mcm7 in TRAIPmut samples could be due to the presence of endogenous TRAIP present in the extract.

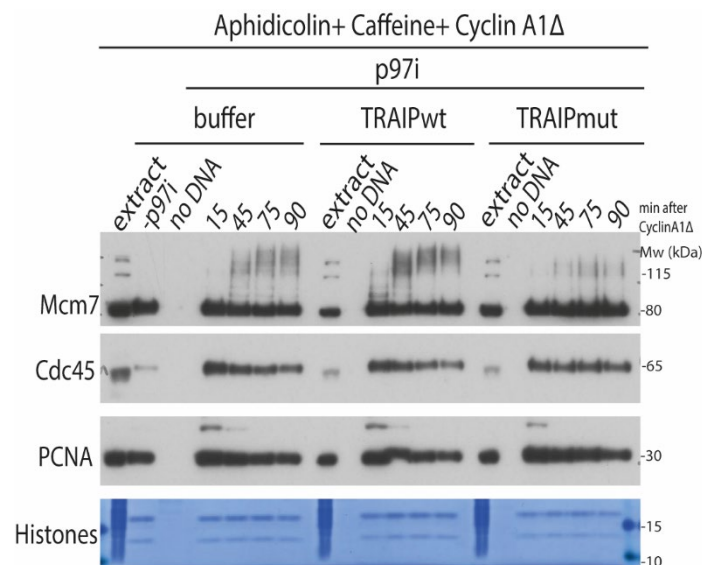


Figure 4.13:- Ubiquitin ligase activity of TRAIP is essential for ubiquitylating Mcm7 of stalled replisomes in mitosis. A replication reaction was set up in the presence of aphidicolin and caffeine and replisome disassembly was blocked with the p97 inhibitor (p97i) to analyse Mcm7 ubiquitylation. After completion of replication, extracts were supplemented with cyclin A1Δ and optionally added with buffer, TRAIPwt, or TRAIPmut to a final concentration of 100 μg/ml. Chromatin isolation was performed at indicated time points and replication factors were analysed by western blotting. The sample represented as -p97i provides a control for p97 activity. Histones and no DNA samples were processed as before. This experiment was repeated two times.

From all these data we can establish that TRAIP E3 ubiquitin ligase plays an important role in unloading CMGs in mitosis.

4.3 Discussion

Ever since the link between TRAIP and microcephalic primordial dwarfism was discovered, much evidence has been accumulated towards the understanding of the mechanisms by which TRAIP facilitates DNA replication and ensures genome integrity. The pleiotropic ubiquitin ligase activity of TRAIP has been found to regulate numerous cellular processes including repair of damage regulation of spindle assembly checkpoint and mitotic progression (Chapard et al., 2014; Park et al., 2015). The absence of TRAIP activity in cells has also been shown to cause chromosomal rearrangements, signs of DNA damage and accumulation of cells in the G2 phase of the cell cycle (Feng et al., 2016; Harley et al., 2016). Additionally, in cells, TRAIP expression has been shown to be regulated by the E2F transcription factor and intriguingly, its expression levels are known to peak during mitosis, providing a strong indication of its involvement in the mitotic phase of the cell cycle (Chapard et al., 2015). Despite these findings, the essential function of TRAIP in mitotic replisome disassembly was not known.

In this chapter, our findings have provided evidence that higher eukaryotes possess a backup pathway during mitosis for the disassembly of the replisomes, similar to what was reported in *C. elegans* (Sonneville et al., 2017). Importantly, I have identified TRAIP as the E3 ubiquitin ligase that is responsible for ubiquitylating Mcm7 and is subsequently recognised by p97 (Moreno et al., 2019a). Similar studies from other labs have also shown the existence of a backup pathway for replisome disassembly mediated by TRAIP in mitosis (Hashimoto and Tanaka, 2018; Deng et al., 2019; Sonneville et al., 2019b). Recent

studies have shown analogous roles of TRAIP using mouse embryonic stem cells, suggesting that it is conserved among diverse species (Villa et al., 2021).

In our experiments, obtaining a significant amount of soluble and functionally active protein posed a major hindrance with GST-tagged TRAIP. Our primary objective was to remove the GST tag from the purified TRAIP using enterokinase and obtain the untagged protein, but this proved to be impossible (Figure 4.2). Interestingly, the N-terminal tagged GST-TRAIP was found to be inactive for mitotic replisome unloading in egg extracts. This functional disruption of TRAIP aligned with a previous study in human cells, where bulky N-terminal tagged TRAIP interfered with its localization and functioning in the cell (Feng et al., 2016). Furthermore, when analysing the TRAIP dimer sequence with GST and SUMO tags using AlphaFold, it revealed a significant disruption in the folding pattern of TRAIP in the presence of the bulky GST tag (Figure 4.14).

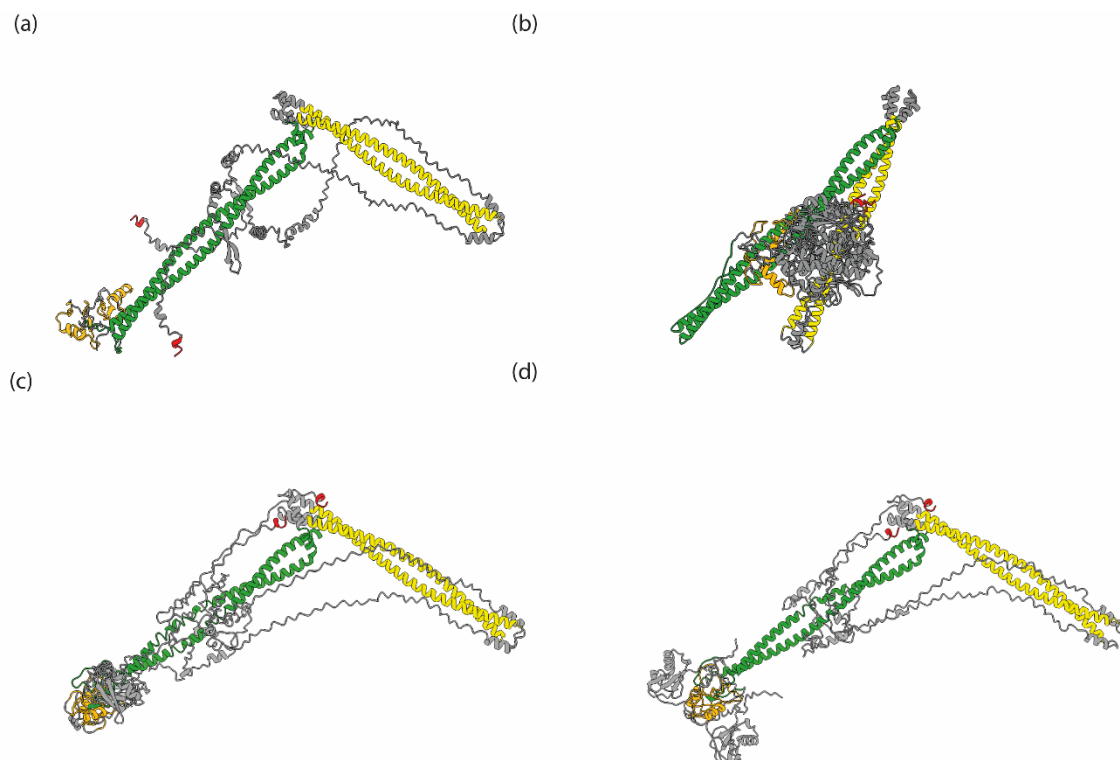


Figure 4.14:- Predicted model of TRAIP dimer using AlphaFold. (a) *X. laevis* TRAIP (b) GST-TRAIP (c) SUMO-TRAIP (d) SUMO-TRAIPmut containing a point mutation at C25A. Each domain of TRAIP has been represented with different colours- RING domain (orange), Coiled coil (green), Leucine zipper (yellow) and PIP box (red). The grey colour represents the linker regions that connects one domain to the next including the bulky GST tag in (b) and the N-terminus SUMO tag in (c and d).

It has previously been demonstrated that TRAIP needs dimerisation to be active during mitosis (Seul Park et al., 2015). The disruption in dimeric structure caused by the attachment of GST tag could have played a significant role in rendering our purified GST-TRAIP inactive in egg extracts. The presence of a large N-terminal tag may have obstructed the protein's active site, preventing its interaction with other molecules, or potentially leading to its misfolding, resulting in the inactivity of GST-tagged TRAIP (Figure 4.3). Additionally, the GST tag itself can result in dimerisation. Although dimerisation is meant to enhance the stability of the fusion protein by promoting proper

folding and protecting it from degradation, it can sometimes influence the function or activity of the fused protein in experimental assays (Harper and Speicher, 2011; Mannervik and Danielson, 1988). This GST dimerization could have potentially added to the further complication in structure of GST-TRAIP, making it biologically inactive in the egg extract. This issue was resolved by replacing the large GST tag with a smaller SUMO tag, through which I could successfully demonstrate the activity of TRAIP.

TRAIP has also been reported to be important for the regulation of cell proliferation, and histone H2B monoubiquitylation (Han et al., 2019; Scaramuzza et al., 2023). Homozygous knockdown of TRAIP in mouse embryos leads to their deaths shortly after implantation, due to defects in proliferation (Park et al., 2007), whilst mutations in human TRAIP can lead to primordial dwarfism (Harley et al., 2016). All these processes rely on the ubiquitin ligase activity of TRAIP. Since the enzymatic activity of TRAIP is attributed to the cysteine residues within its RING domain, I synthesised a TRAIP mutant accordingly. Our findings have conclusively demonstrated that the enzymatic ubiquitin ligase activity of TRAIP is essential for the unloading of replisomes during mitosis. Immunodepletion of TRAIP from the extract directly assessed TRAIP's effect in replisome disassembly during mitosis (Figure 4.8 and 4.11). Furthermore, a complementary 'add-in' experiment, with a high concentration of TRAIPmut also hindered replisome unloading (Figure 4.9 and 4.12). Collectively, our data provides strong evidence that TRAIP acts as an E3 ubiquitin ligase, targeting post-termination and stalled replisomes that escape the normal disassembly process during S-phase and facilitate a secondary unloading pathway in mitosis.

Our data also aligns with the studies conducted using plasmid DNA replication in *X. laevis* egg extracts where mitotic CDK promotes TRAIP-mediated replisome unloading (Deng et al., 2019). Using *C. elegans* early embryos, it has also been shown that TRAIP drives

replisome disassembly in response to incomplete DNA replication and provides access to repair processing factors (Sonneville et al., 2019b). Moreover, it has also been identified that TRAIP ubiquitylates Mcm7 via K6 and K63-linked ubiquitin chains (Moreno et al., 2019a) and the unloading of the CMG requires the activity of p97 segregase (Deng et al., 2019; Moreno et al., 2019a). It is interesting to note that both the S-phase and mitotic replisome disassembly pathways, although they use different E3 ligases (Cul2^{Lrr1} and TRAIP respectively), share the same Mcm7 as their substrate for ubiquitylation and this ubiquitylated Mcm7 is recognised by p97.

One direct benefit of unloading CMG in mitosis is the removal of any terminated CMGs that escaped the Cul2^{Lrr1} mediated ubiquitylation from the preceding S-phase. These leftover CMGs could otherwise interfere with replication, transcription or other cellular events in the next cell cycle. Although TRAIP is present during S-phase, it does not target active CMGs for ubiquitylation when they pass each other during termination (Dewar et al., 2015). This avoidance of *in trans* ubiquitylation (close contact) by TRAIP, observed during ICL or DPC repairs (Larsen et al., 2019; Wu et al., 2019) likely prevents inappropriate disassembly of the active replisome in S-phase. In contrast, during mitosis, TRAIP can freely target any replisome remaining on chromatin. This difference in mode of action could stem from potential structural modifications of TRAIP induced, for example as a result of the increased mitotic kinase activity, or by the displacement of inhibitors that restrain CMG ubiquitylation during S-phase. Alternatively, differences in CMG complexes or conformational changes might also make them more susceptible to TRAIP targeting (Wu et al., 2021). Further structural analysis of TRAIP will help elucidate the mechanism underlying its cell cycle-dependent regulation of CMG ubiquitylation.

Recent investigations have shown that DNA synthesis can take place not only in S-phase but also in mitosis, via a process known as mitotic DNA repair synthesis- MiDAS (Liu et al., 2014). This generally occurs when replication forks encounter any kind of stress and fail to terminate or when late-firing origins fail to complete replication. Additionally, replication forks that stall with no intervening origins to rescue them also contribute to the under-replicated DNA fragments (Liu et al., 2014; Cortez, 2015). The remains of unreplicated DNA from S-phase represent a significant cause of rearrangements found in many cancers leading to a serious threat to genome stability (Bhowmick and Hickson, 2017). This is because unreplicated DNA can result in the formation of ultrafine DNA bridges during anaphase, generation of binucleated cells, aneuploidy or chromosomal rearrangements (Nielsen et al., 2015; Umbreit et al., 2020). Such late replicating regions or under replicated regions contribute to common fragile sites. Consequently, there is a need to address any unfinished replication in early mitosis before cell division, in order to safeguard genome integrity. In such cases, removal of replisomes is essential as it provides access to the DNA by endonucleases - MUS81-EME1, to initiate fork breakage and DNA repair (Sonneville et al., 2019b; Wu et al., 2021). Our findings demonstrate that the induction of incomplete replication forks through aphidicolin treatment (Figure 4.11 and 4.12), leads to the unloading of replisomes during mitosis in the presence of TRAIP. It also suggests that fork convergence is not essential in mitosis for TRAIP-mediated unloading of stalled forks. Furthermore, other studies have demonstrated that this secondary unloading pathway driven by TRAIP during mitosis triggers fork collapse and breakage (Deng et al., 2019; Sonneville et al., 2019b).

Further studies from Prof. Walter's laboratory have revealed that there are two distinct end joining events following fork breakage - SSA (Single-Strand Annealing) and MMEJ (Microhomology-Mediated End Joining). SSA repair mechanisms involve deletion of DNA

segments at the repaired site (Bhargava et al., 2016) and MMEJ or alternative end joining is an error prone mitotic DNA repair mechanism with multiple template switching events mediated by Pol θ (Wyatt et al., 2016; Deng et al., 2019). In *Xenopus* egg extracts, depletion of Pol θ was found to reduce DNA synthesis in mitosis (Deng et al., 2019). Additionally, studies using early embryos in *C. elegans* have demonstrated the importance of TRAIP in mitotic DNA repair synthesis, as the depletion of TRAIP suppressed MiDAS in human cells (Sonneville et al., 2019b). Altogether, this suggests that TRAIP may be important for end joining repair events mediated by Pol θ in mitosis.

TRAIP-mediated fork breakage and repair can be either advantageous or harmful, depending on the level of stressed forks present at the onset of mitosis. It has been shown that TRAIP is essential for performing DNA repair synthesis during mitosis at CFSs where forks cannot complete replication by anaphase (Wu et al., 2021). In such a scenario, where forks stall on either side of CFS, TRAIP can mediate the removal of CMGs, resulting in fork breakage on the leading strand template, as the CMGs travel on the leading strand template. In this context, the leading strand template undergoes cleavage, producing one intact DNA strand and two broken ends. The repair of the intact strand is mediated by gap filling whereas the repair of the two broken ends are accomplished through end joining. Ultimately, these repair processes result in the deletion of a segment that contains unreplicated DNA and the occurrence of sister chromatid exchange, which are distinctive features associated with the expression of CFSs. Although this mechanism leads to a minor deletion, the breakage at CFSs is more advantageous, as it prevents the formation of acentric and dicentric chromosomes which would occur if forks experienced a random breakage (Deng et al., 2019; Wu et al., 2021).

In summary, our data shows that TRAIP protects genome integrity by actively participating in disassembling the replication machinery during mitosis and ensuring that the incomplete replication fork does not persist into the next cell cycle, thus preventing genetic abnormalities.

Chapter-5

5 Investigating the role of TRAIP in the S-phase

5.1 Introduction

I have shown in the previous chapter that TRAIP is important for replisome disassembly in mitosis and that the unloading of the replisomes requires ubiquitylation of Mcm7 with K6/K63-linked ubiquitin chains (Moreno et al., 2019a). Interestingly, using the *Xenopus* egg extract system TRAIP has also been suggested to be a part of the replisome during S-phase and it was shown to ubiquitylate CMG helicase when replication forks converge at Inter-strand cross-links (ICLs) in the S-phase (Deng et al., 2019; Wu et al., 2019). Using the same system, it has also been shown that TRAIP can ubiquitylate protein barriers or DNA Protein Crosslinks (DPCs) ahead of the replisome which otherwise impair fork progression. Moreover, our prior mass spectrometry data of immunoprecipitated S-phase post-termination replisomes retained on chromatin upon inhibition of p97 segregase, revealed the accumulation of TRAIP (Sonneville et al., 2017). In addition to this, very recent studies from our lab have shown that in human cells, TRAIP is important in cell proliferation in S-phase, and the loss of TRAIP can lead to cell cycle arrest in the G2 phase leading to senescence and increased DNA damage at sites of replication transcription collisions (Scaramuzza et al., 2023). Therefore, we wanted to further investigate the role of TRAIP in S-phase.

5.2 Results

5.2.1 TRAIP interaction with the S-phase replisome

To explore whether TRAIP has a role in facilitating the unloading of terminated replisomes during the S-phase, either as part of the primary Cul2^{Lrr1} pathway or as a backup mechanism, I conducted investigations using different methods to inhibit replisome disassembly and analyzed the stimulation of TRAIP's interaction with chromatin. I prevented the formation of polyubiquitin chains using 6xHis-UbiNoK recombinant protein (referred to as UbiNoK) (Figure 5.1 a), inhibited cullin ubiquitin ligase activity with the neddylation inhibitor - MLN4924 (referred to as Cul i), and inhibited the activity of p97 segregase with p97 ATPase inhibitor – NMS-873 (referred to as p97i) or by inhibiting both cullin and p97 activity (Figure 5.1 b).

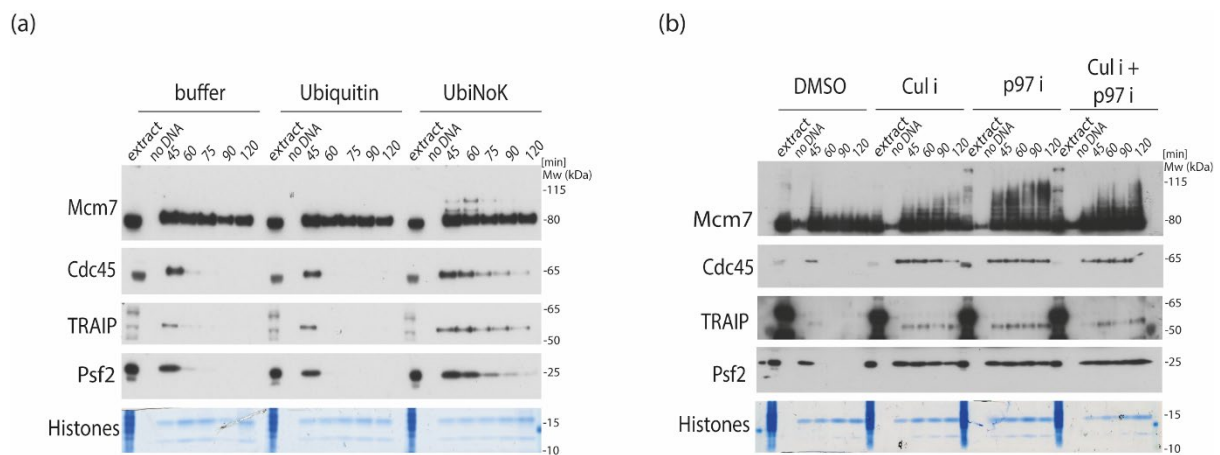


Figure 5.1:- TRAIP interaction with replisome is stimulated when replisomes are retained on chromatin in S-phase. (a) Interphase egg extract was optionally supplemented with buffer (control), Ubiquitin, or UbiNoK, and chromatin was isolated at indicated time points. The binding pattern of TRAIP and other replication factors during unperturbed and perturbed conditions were analysed by immunoblotting using indicated antibodies. Histones were stained with Coomassie stain and provided a loading control. A sample containing no sperm (no DNA) was processed alongside each set of samples to provide chromatin specificity control. **(b)** Egg extract was optionally supplemented with DMSO control, Cul i, p97i, or both, and the experiment was performed as in (a). The binding patterns for TRAIP and other replication factors were analysed. Experiments with the addition of Cul i and p97i were performed more than three times.

Treatment with all these inhibitors resulted in the accumulation of post-terminated replisomes on chromatin. I then analysed TRAIP accumulation on chromatin in these chromatin isolation experiments and I could see that TRAIP associates weakly with the S-phase chromatin in an unperturbed replication reaction (see lanes with buffer and DMSO in Figure 5.1). Notably, TRAIP was found to accumulate on chromatin when replisome disassembly was inhibited with UbiNoK, Cul i, and p97i (see lanes with UbiNoK, Cul i, p97i and Cul i+p97i in Figure 5.1). Additionally, different migrating forms of Mcm7 have been noted as a result of the addition of various inhibitors. Interestingly, the addition of UbiNoK shows distinct mobility shifts suggesting post-translational modifications on Mcm7. These modifications are most likely multi-monoubiquitylation or di-monoubiquitylation. However, these bands could also be a result from other post-translational modifications such as acetylation or SUMOylation etc. To confirm the nature of these modifications, further investigation using *in vitro* biochemical assays is needed.

I then proceeded to assess the chromatin binding ability of TRAIP when fork convergence was blocked (Figure 5.2). To achieve this, I used ICRF-193, a topoisomerase 2 inhibitor that can create a barrier for fork progression by immobilizing Top2 in a closed clamp conformation on DNA (Sun et al., 2020).

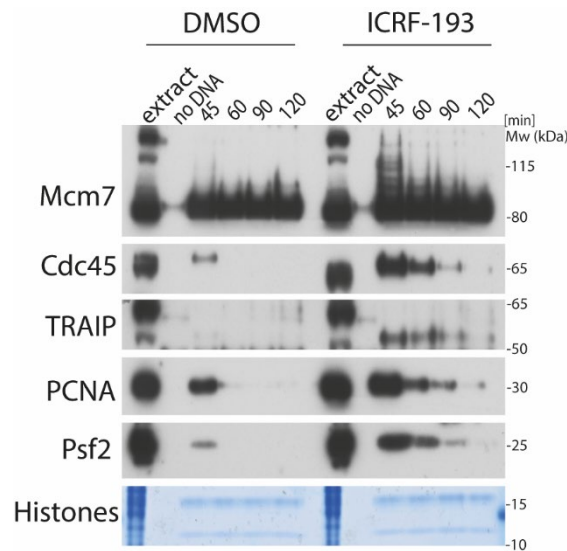


Figure 5.2:- Inhibition of fork convergence stimulates TRAIP interaction with replisomes in S-phase. Interphase egg extract was optionally supplemented with DMSO control or topoisomerase 2 inhibitor; ICRF-193. The binding pattern of TRAIP and other replication factors were analysed by immunoblotting using indicated antibodies. Histones and no DNA samples were processed as before. This experiment was repeated three times.

This resulted in the accumulation of active replication forks and I could observe that the inhibition of fork convergence resulted in the accumulation of replisome components (Cdc45 and Psf2) and increased levels of TRAIP on chromatin. Altogether, these data suggested that TRAIP can interact with replisomes in S-phase too, especially upon their retention on chromatin.

Now that I could see TRAIP accumulation on chromatin together with replisomes in S-phase, we then decided to inhibit replication fork progression through treatment with aphidicolin and caffeine. Aphidicolin is a family B DNA polymerase inhibitor, and caffeine is a checkpoint inhibitor that can override the replication checkpoint caused by ATM/ATR kinases. Upon the addition of aphidicolin, replicative DNA polymerases are hindered, leading to their uncoupling from the helicases. Simultaneously, the inhibition of the checkpoint mechanism by caffeine triggers the activation of numerous replication origins, resulting in a substantial buildup of stalled replisomes on chromatin. Since aphidicolin

prevents new DNA synthesis due to helicase-polymerase uncoupling, the unwinding of DNA by helicases can still proceed resulting in exposure of single stranded DNA. The presence of caffeine in the reaction, disrupt the DNA damage repair by inhibiting the ATM/ATR kinases and allows replication progression despite the presence of incomplete replication. This can potentially lead to the formation of DNA structures such as Double strand breaks or fork reversal or fork collapse that can further lead to genomic instability.

I examined the binding pattern of TRAIP on such stalled chromatin and observed distinct differences in the accumulation of TRAIP compared to its binding during the inhibition of fork convergence and post-terminated replisomes. Notably, I observed a strong accumulation of replisome components, but relatively less TRAIP accumulation in the presence of aphidicolin and caffeine (Figure 5.3 a). I also quantified the levels of TRAIP and Psf2 on chromatin in all different treatments at 45 min (Figure 5.3 b). Interestingly, in the presence of aphidicolin there is a significant reduction in levels of TRAIP, while levels of Psf2 was comparatively higher. Conversely, treatment with caffeine promoted the binding of TRAIP and Psf2 on chromatin to levels similar to that of DMSO (control). Although the addition of both aphidicolin and caffeine increased TRAIP binding more than caffeine treatment alone, the levels were much lower in comparison to Psf2. These observations suggest that TRAIP's interaction with CMG helicase is stimulated in situations when replisomes converge with each other or with protein barriers in front of them, and the replisomes or barriers need to be disassembled, but not when the integrity of replication forks needs to be protected.

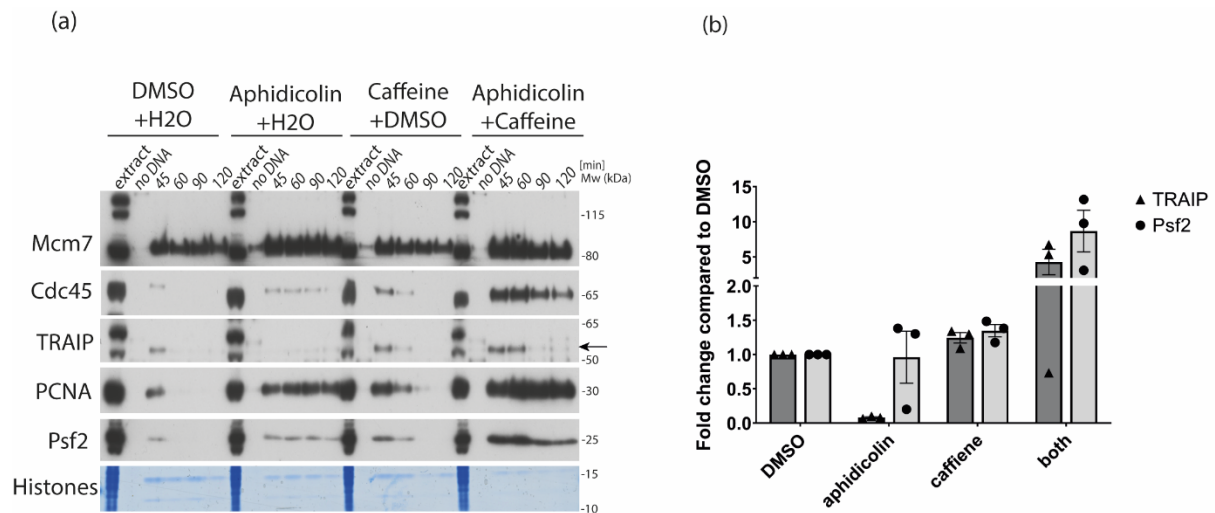


Figure 5.3:- TRAIP does not accumulate on chromatin when CMG helicase and polymerases are uncoupled. Interphase egg extract was supplemented with DMSO (control), polymerases inhibitor - aphidicolin, checkpoint inhibitor - caffeine, or both. Chromatin samples were isolated and the binding pattern of TRAIP and other replication factors was analysed with immunoblotting using indicated antibodies. The arrow beside the TRAIP blot indicates where TRAIP runs on the gel. (b) The fold change of accumulation of Psf2 and TRAIP signal in aphidicolin, caffeine and aphidicolin/caffeine treatment methods at the 45 min time point in comparison to normal replication control (DMSO control) is quantified over n=3 experiments.

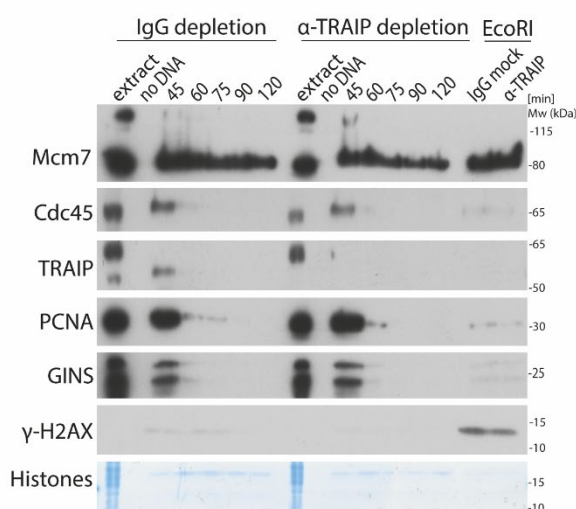
5.2.2 TRAIP depletion in S-phase does not lead to DNA damage

TRAIP tends to accumulate on chromatin particularly when DNA replication forks encounter challenges, and is proposed to help forks to bypass impediments such as ICLs and DPCs (Larsen et al., 2019; Wu et al., 2019). Therefore, it is possible that in the absence of TRAIP, forks will not be able to deal with these impediments, potentially leading to DNA damage. In addition, in human cells, depletion of TRAIP leads to generation of DNA damage at transcription start sites (Scaramuzza et al., 2023). To assess this possibility, I decided to investigate whether the absence of TRAIP results in an increase in DNA damage during replication in egg extract system lacking transcriptional activity. To this end, I immunodepleted TRAIP from the egg extracts and checked its ability to replicate sperm DNA, as previously shown in section 4.2.5. We then examined whether we could observe any signs of DNA damage or checkpoint activation during the S-phase because of

the depletion of TRAIP. However, no increase in γ -H2AX signal on chromatin was observed as a result of the depletion of TRAIP (Figure 5.4 a). I could observe that the DNA damage signalling cascade was still functional in TRAIP-depleted extract as our positive control samples treated with EcoRI, which induces double-stranded breaks, reacted with strong γ -H2AX signals on chromatin in samples from both IgG and TRAIP-depleted extracts.

I also investigated checkpoint activation by monitoring the phosphorylation of Chk1 as a result of the depletion of TRAIP (Figure 5.4 b). ATR and Chk1 are central checkpoint kinases in S-phase. During DNA damage, ATR associates with DNA whereas Chk1 rapidly propagates throughout the nucleus and functions by impeding S-phase progression by phosphorylating target genes within the nucleoplasm (Speroni et al., 2012). Therefore, I isolated nuclei from the egg extracts and as a positive control, a sample from both IgG-depleted and TRAIP-depleted extracts was treated with aphidicolin (induces checkpoint activation) and both aphidicolin and caffeine (checkpoint inhibitor). No induction of phosphorylated Chk1 (P-Chk1) was observed in the nucleoplasm as a result of the depletion of TRAIP, whereas P-Chk1 was readily induced in samples treated with aphidicolin but inhibited in those treated with both aphidicolin and caffeine. These experiments indicate that the depletion of TRAIP in egg extracts does not lead to DNA damage.

(a)



(b)

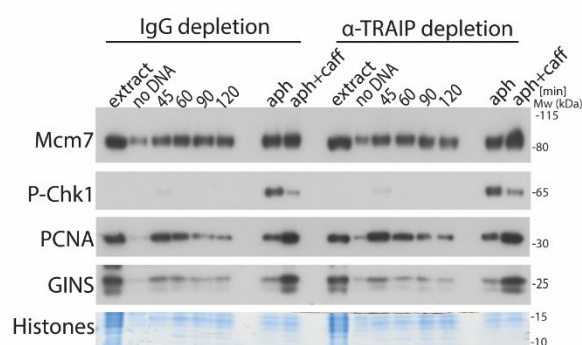


Figure 5.4:- Immunodepletion of TRAIP does not induce S-phase checkpoint activity. (a) A replication reaction was carried out using non-specific IgG-depleted and TRAIP-depleted egg extracts, and chromatin was isolated at indicated times. Chromatin samples were analysed by immunoblotting with indicated antibodies. A sample without sperm (no DNA) was isolated alongside each set of samples to show the chromatin specificity of the signal. Samples from both extracts were treated with EcoRI to induce DNA double-strand breaks (isolated at 60 min of the reaction) and serve as the positive control for the γ -H2AX signal. (b) A replication reaction was set up as in (a) but instead of chromatin, whole nuclei were isolated to measure the levels of active P-Chk1 induction as a result of TRAIP depletion. As a positive control, samples from both non-specific IgG-depleted and TRAIP-depleted extracts were treated with DNA polymerase inhibitor - aphidicolin for Chk1 activation, while samples treated with aphidicolin and caffeine indicate ATM/ATR dependence of these signals (isolated at 75 min of the reaction). Both experiments were repeated twice.

5.2.3 TRAIP is dispensable for terminated replisome disassembly in S-phase

Since the depletion of TRAIP did not affect replication in S-phase, we then turned our attention to determining whether TRAIP in any way facilitates the unloading of terminated or stalled replisomes during the S-phase. Although it has been previously shown that TRAIP is not essential for replisome disassembly on plasmid DNA in a Nucleoplasmic Egg extract system (NPE) (Deng et al., 2019), a fully chromatinised DNA system could potentially show some differences as chromatinisation plays a vital role in regulating the cell's access to the genome (Bellush and Whitehouse, 2017). Such a template may provide more resistance for the fork convergence and passing each other

during the termination and therefore may need more support for completion. To investigate this possibility further, I used TRAIP-depleted egg extracts and followed replisome disassembly. In agreement with the published plasmid DNA data, I also did not observe any defects in the disassembly of terminated replisomes (Figure 5.5 a). In a parallel approach, I also opted to supplement the extract with a high concentration of either wild type (TRAIPwt) or catalytically inactive (TRAIPmut) form of the protein, as previously used for our mitotic experiments, and followed replisome unloading (Figure 5.5 b).

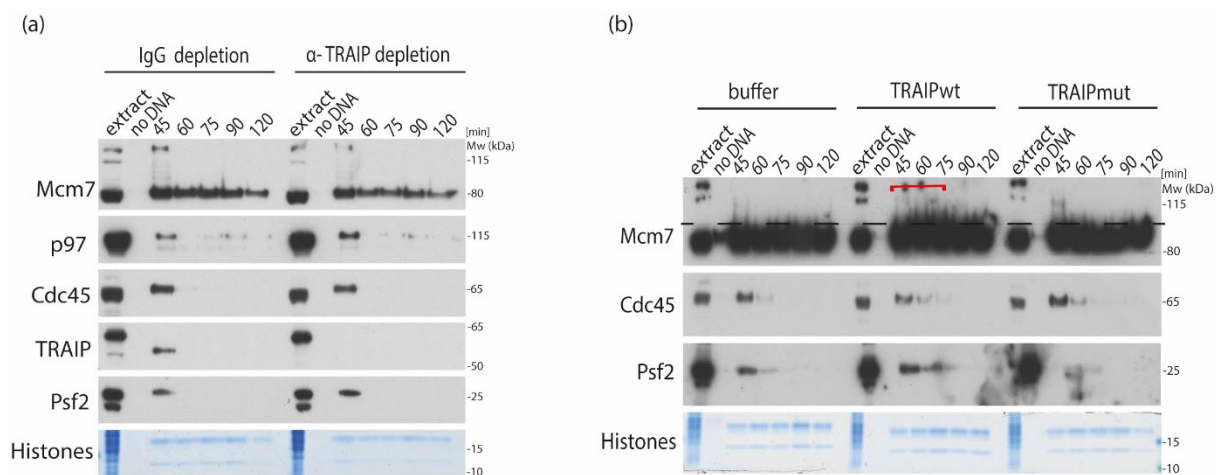


Figure 5.5:- TRAIP is not essential for terminated replisomes disassembly in S-phase. (a) A replication reaction was set up using non-specific IgG-depleted and TRAIP-depleted egg extract, and chromatin was isolated during the time course at indicated time points. Samples were analysed by immunoblotting using indicated antibodies. Histones and no DNA samples were processed as before. (b) Interphase egg extract was supplemented optionally with buffer (LFB1/100), recombinant wildtype TRAIP (TRAIPwt), or RING-domain mutant TRAIP (TRAIPmut). Chromatin samples were isolated and analysed as in (a). The dotted line above Mcm7 indicated ubiquitylation, while the red square bracket in Mcm7 blot of TRAIPwt samples indicates increased Mcm7 ubiquitylation. Both experiments were repeated three times.

I observed that Cdc45 was effectively unloaded in both TRAIPwt and TRAIPmut supplemented samples, indicating that the ubiquitin ligase activity of TRAIP is not essential for replisome disassembly of terminated replisomes in S-phase. Intriguingly, I observed increased levels of Mcm7 ubiquitylation upon the addition of TRAIPwt

compared to the buffer control and TRAIPmut. This suggests that the ubiquitin ligase activity of TRAIP is at least partially functional in the S-phase (Figure 5.5 b, specifically, at the timepoints 45, 60 and 75 mins, indicated by a red bracket in TRAIPwt samples above the dotted line, there is a slight augmentation in Mcm7 ubiquitylation). These experiments indicate that the ubiquitin ligase activity of TRAIP is dispensable for terminated replisome disassembly in S-phase.

5.2.4 TRAIP can ubiquitylate Mcm7 but cannot prime unloading of terminated CMG in S-phase

Until now we have seen that TRAIP's interaction with the CMG helicase is stimulated in S-phase only during situations when replisomes need to be unloaded. In addition to this, we have seen that TRAIP can also ubiquitylate Mcm7 on supplementation of high concentrations of TRAIPwt in S-phase. With this in mind, we next wanted to explore whether TRAIP could actively ubiquitylate Mcm7 and unload replisomes when Cul2^{Lrr1} activity is compromised in S-phase, leaving terminated replisomes on chromatin. To explore the potential role of TRAIP in this process, I used TRAIP-depleted extract with blocked cullin activity and followed replisome disassembly (Figure 5.6 a). A reduced level of Mcm7 ubiquitylation (see Mcm7 blot) was observed in TRAIP-depleted extracts but I could not see any significant differences in the kinetics of replisome unloading (see Cdc45 and Psf2 blots). Although a small level of unloading can be observed at a very late S-phase (see Cdc45 and Psf2 at 150 min) this could be due to incomplete inhibition of neddylation in this experiment.

As a parallel approach, we also opted to supplement TRAIPwt/mut to the egg extracts at the same high concentrations of 50 µg/ml which had worked for our mitosis experiments. Additionally, we also inhibited cullin activity and analysed its effect on Mcm7

ubiquitylation and the kinetics of replisome disassembly. Again, I could observe a stimulation in the lengths of ubiquitin chains built on Mcm7 with TRAI Pwt, suggesting that TRAI P can slightly stimulate Mcm7 ubiquitylation. Nevertheless, the increased chain-building activity as a result of the addition of TRAI Pwt does not enhance the rate of replisome unloading during the late S-phase (Figure 5.6 b, see Cdc45 and Psf2 in lanes with TRAI Pwt at 150 min). Interestingly, I have consistently observed that the addition of TRAI Pmut to Cul i treated extract blocked remaining replisome unloading.

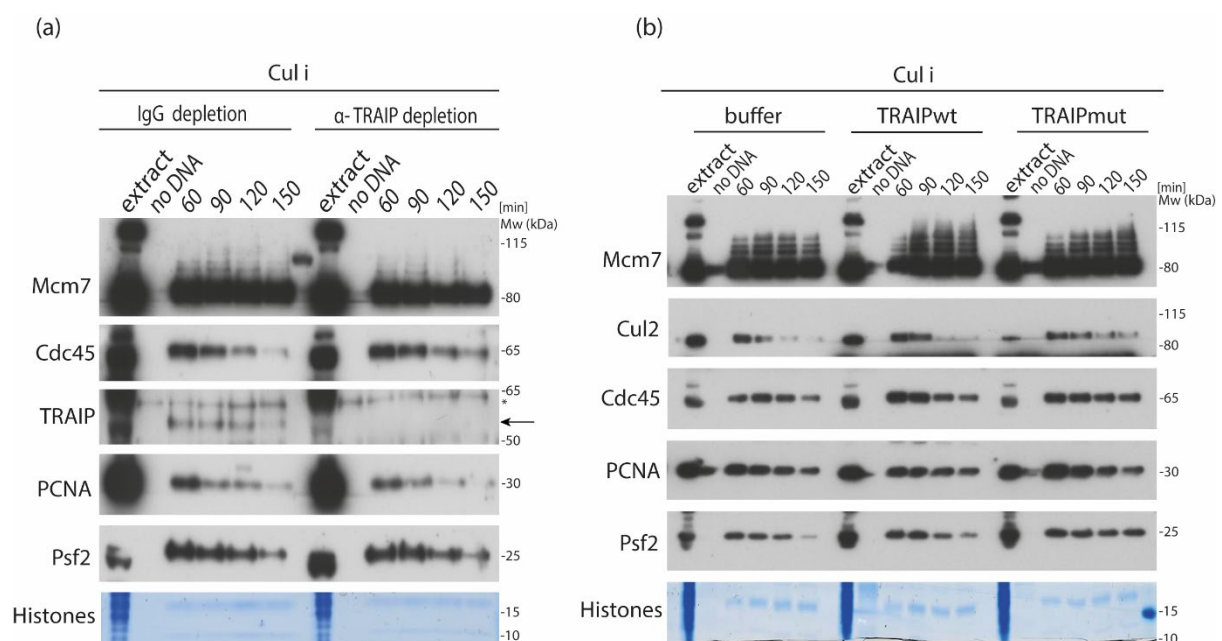


Figure 5.6:- TRAI P does not facilitate the unloading of replisomes in the S-phase. (a) Nonspecific IgG-depleted and TRAI P-depleted extracts were supplemented with Cul i and chromatin samples were isolated. Samples were analysed using western blotting with indicated antibodies to study replisome disassembly and Mcm7 ubiquitylation patterns. The arrow beside TRAI P blot represents TRAI P and a star represents non-specific band. Histones and no DNA samples were processed as before. (b) Interphase egg extracts were treated with Cul i and optionally supplemented with buffer, TRAI Pwt, and TRAI Pmut to a final concentration of 50 µg/ml. Chromatin was extracted at indicated time points and analysed as in (a). These experiments were repeated twice for (a) and thrice for (b).

To exclude the possibility that some Mcm7 is indeed ubiquitylated by TRAI P and unloaded during S-phase, we decided to look further into the ubiquitylation of Mcm7 by TRAI P in the S-phase. I supplemented the extract with high concentrations of TRAI Pwt/mut in the

presence of Cul i and also p97i to completely block unloading which could be facilitated by TRAIP or by incomplete inhibition of cullins (Figure 5.7). As expected, unloading of the replisomes was completely blocked under these conditions. Moreover, looking at the pattern of Mcm7 ubiquitylation, a slight stimulation in Mcm7 ubiquitylation was observed upon the addition of TRAIPwt, in agreement with the previous results.

Notably we detected some levels of Mcm7 ubiquitylation in all the samples even in the presence of Cul i during our experiments. We speculate that this ubiquitylation could be a result of incomplete inhibition of Cullins by the Cul i, apart from the stimulated levels in TRAIPwt. In support to this, the Cul2 blot in Figure 5.7 shows the neddylated form of cullins starting from 90-150 min, suggesting incomplete inhibition of cullins. Therefore it is unlikely that it is the result of a different ubiquitin ligase. However, further investigation will be required to identify whether there is a potential alternative ubiquitin ligase that ubiquitylates Mcm7 and works via the p97 pathway.

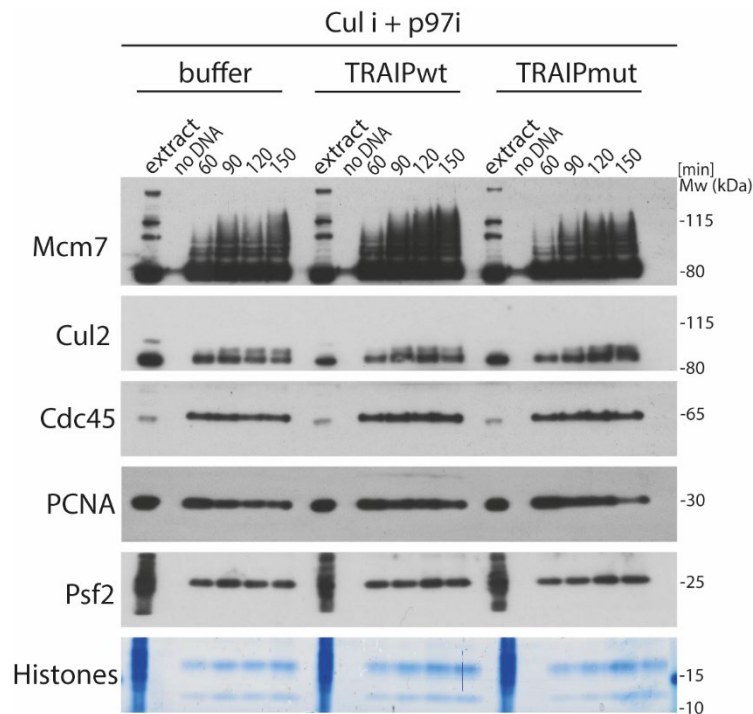


Figure 5.7:- TRAIP can stimulate Mcm7 ubiquitylation in S-phase. A replication reaction was set up with interphase egg extract and supplemented with both cullin and p97 inhibitors. The reaction was also supplemented optionally with buffer, TRAIPwt, and TRAIPmut to a final concentration of 100 µg/ml. Chromatin samples were isolated at indicated time points and analysed by immunoblotting. Histones and no DNA samples were processed as before. This experiment was done once.

Altogether, by investigating the role of TRAIP in terminated replisome disassembly in S-phase, we have determined that TRAIP's interaction with CMG helicase during S-phase is stimulated in situations when replisome unloading is perturbed, and it can slightly ubiquitylate Mcm7 within terminated replisomes. But this TRAIP-driven ubiquitylation of Mcm7 is not effectively recognised and unloaded by p97 in S-phase, despite being effective in unloading replisomes in mitosis (as seen in Chapter -4). This suggests that TRAIP's E3 ligase activity on replisomes is not just regulated through its level of interaction with replisomes, as is the case for Lrr1, but there might be other factors that are involved.

5.2.5 Post-translational modifications of TRAIP contribute to TRAIP activity

The next key question we had was to comprehend the regulatory mechanism governing the activity of TRAIP across different phases of the cell cycle. We observed distinct differences in TRAIP activity in S-phase compared to mitosis. In mitosis, TRAIP efficiently ubiquitylates its substrate Mcm7 and targets it for unloading by p97. However, in S-phase, although TRAIP can interact with Mcm7, the level of ubiquitylation is relatively low. This led us to further investigate the differences between TRAIP in S-phase and mitosis which could contribute to its differential activity. For this purpose, we conducted a mass spectrometry data analysis of immunoprecipitated TRAIP (TRAIP IP) from mitotic chromatin containing post-termination replisomes in the presence of p97i (this experiment was performed by Prof. Aga Gambus). The analysis of this data revealed several peptides of TRAIP interacting with replisome on mitotic chromatin. Importantly, these peptides were found to be phosphorylated at T280, S295, and S352 (Figure 5.8 a). Therefore, our next aim was to confirm whether TRAIP is indeed phosphorylated on mitotic chromatin, and not during S-phase. To this end, I isolated chromatin samples from both S-phase and mitosis in the presence of p97i to block replisome disassembly and confirmed the accumulation of TRAIP in these samples (Figure 5.8 b). Additionally, the S-phase and mitotic chromatin samples were also run on a Phos-tag gel that allows the detection of protein phosphorylation by inducing a band shift and slower electrophoretic mobility of phosphorylated proteins compared to their non-phosphorylated counterparts. Remarkably, I could observe a band shift of TRAIP in mitotic samples when compared to S-phase chromatin samples (Figure 5.8 c).

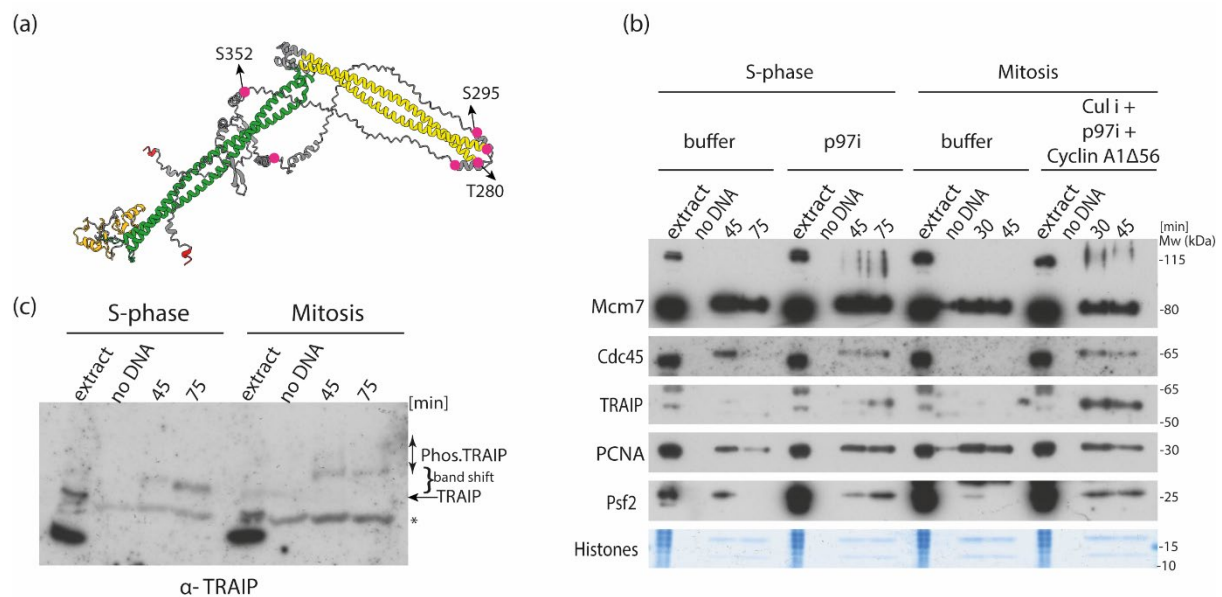


Figure 5.8:- Phosphorylation of TRAIP in mitosis. (a) The phosphorylated sites of TRAIP (represented as pink dots) identified from mass spectrometry have been shown on the dimeric structure of TRAIP generated using AlphaFold. (b) A replication reaction was set up both in S-phase and mitosis. The S-phase reaction was optionally supplemented with p97i to block replisome disassembly thereby accumulating TRAIP. The mitotic extract containing Cul i and high levels of cyclin was also optionally supplemented with p97i to block replisome disassembly and accumulate TRAIP. Chromatin samples were isolated and analysed by western blotting using indicated antibodies. (c) The S-phase and mitotic chromatin samples from (b) were run on a Phos-tag gel and analysed by western blotting using α -TRAIP antibodies. TRAIP and phosphorylated TRAIP have been indicated. The band shift between TRAIP and phosphorylated TRAIP has been indicated using a curly brace. A star represents non-specific band. These experiments were done once.

These findings strongly suggested that TRAIP is phosphorylated in mitosis but not during S-phase, particularly when replisome unloading is blocked due to p97 inhibition. As a result, we wanted to investigate whether TRAIP undergoes phosphorylation under any other conditions during S-phase, especially when TRAIP accumulation on chromatin was observed. To look into this possibility, I isolated chromatin from S-phase in the presence of either Cul i, p97i, UbiNoK, ICRF-193, or aphidicolin and caffeine, and compared this with mitotic chromatin both on an acrylamide (Figure 5.9 a) and a Phos-tag gel (Figure 5.9 b). The chromatin isolated from all the different conditions resulted in the accumulation of replisome components as well as TRAIP. Additionally, I observed a clear

difference in the ubiquitin chain length on Mcm7 between S-phase and mitosis. The longer ubiquitin chains built on Mcm7 during mitosis by TRAIP may be necessary to meet the required threshold of at least 5 ubiquitins for recognition by p97 (Fujisawa et al., 2022).

On analysis of these samples on a Phos-tag gel, I found that TRAIP remained non-phosphorylated in all these situations during S-phase. This confirmed that TRAIP is phosphorylated uniquely in mitosis and we suggest the possibility that the absence of this modification in the S-phase might be contributing to the relatively lower efficiency of Mcm7 ubiquitylation observed previously.

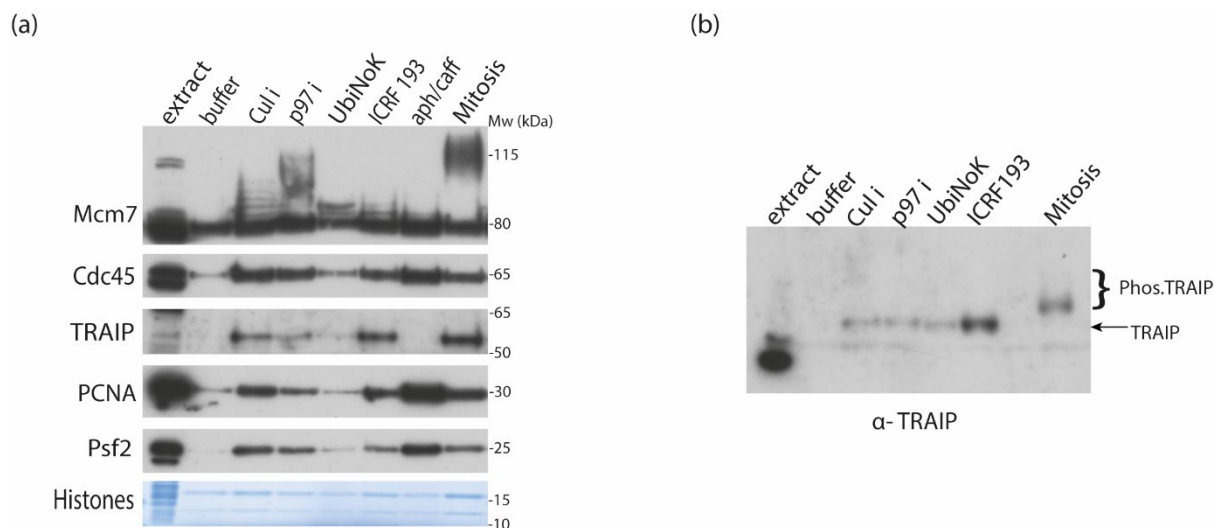


Figure 5.9:- TRAIP is only phosphorylated in mitosis. (a) Egg extract was supplemented with buffer, Cul i, p97i, UbiNoK, ICRF-193, aphidicolin/caffeine in S-phase, and an extract sample with mitotic conditions was set up and chromatin samples were isolated at 60 min and analysed by western blotting. (b) Samples from (a) were run on a Phos-tag gel and analysed using α -TRAIP antibodies. These experiments were done once.

5.2.6 Recombinant TRAIP can be phosphorylated *in vitro*

All three phosphorylated sites identified by mass spectrometry analysis from mitotic chromatin - T280, S295, and S352. Notably, all three sites conform to the characteristic serine/threonine followed by a proline suggesting their potential involvement in

phosphorylation-dependent signaling pathways mediated by the Cyclin-Dependent Kinases (CDKs). CDKs usually are proline-directed serine/threonine-protein kinases with a characteristic S/T-P-X-K/R sequence. In this motif, S/T stands for serine or threonine that can be phosphorylated by kinases, P denotes a proline residue that often follows a phosphorylation site, X is any amino acid residue and K/R represents positively charged lysine or arginine, that are often found in the vicinity of phosphorylation sites and can influence the binding of kinases or other proteins. Our mass spectrometry identified phosphorylation sites adhere to the S/T-P consensus sequence. It is important to note that some CDKs display a less stringent S/T-P-X-K/R consensus, and some can phosphorylate residues even in the absence of a proline residue (Malumbres, 2014). Therefore, the involvement of CDKs in the phosphorylation of these sites cannot be conclusively determined solely based on the motif analysis. Further experimental validation using kinase assays are necessary to establish this. CDKs drive cell cycle progression, and their activity grows slowly during S-phase to peak during mitosis. Different cyclin/CDK complexes are responsible for driving progression at different phases of the cell cycle. cyclin B/CDK1 kinase is a mitotic cyclin and is known to trigger mitosis in eukaryotes (Gavet and Pines, 2010). Since TRAIP is found to be active in mitosis, we analysed the activity of cyclin B/CDK1 with TRAIP. To do this, I set up an *in vitro* phosphorylation reaction with recombinant cyclin B/CDK1 complexes. On analysing these samples using a Phos-tag gel, I observed that TRAIP^wt was efficiently phosphorylated when combined with the mitotic cyclin; cyclin B/CDK1. However, the reaction involving TRAIP^{3A} (a phospho-dead mutant form of TRAIP, where all three identified phosphorylation sites were mutated to alanine; generated by Dr. Alicja Reynolds-Winczura) did not undergo phosphorylation, as anticipated (Figure 5.10 a). In addition to this, I also found that the reactions lacking either cyclin B/CDK1 or ATP consistently failed to phosphorylate TRAIP.

These experiments confirmed that phosphorylation of TRAIP is observed only when TRAIPwt is added, and not TRAIP3A mutant.

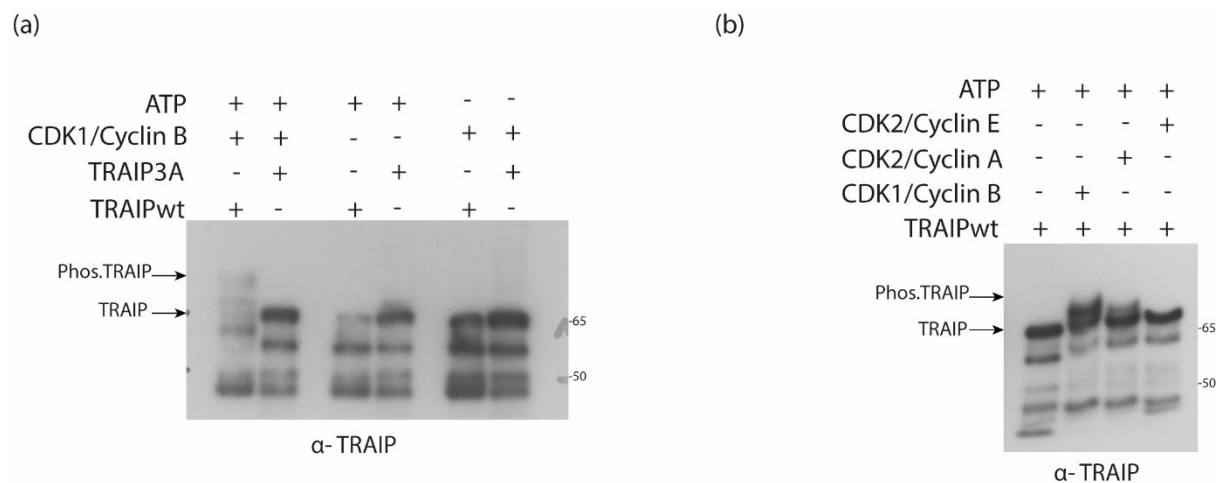


Figure 5.10:- TRAIP can be phosphorylated *in vitro* by cyclin/CDK complexes. (a) *In vitro* phosphorylation reaction was set up with mitotic cyclin B/CDK1 and TRAIPwt and phospho-dead mutant TRAIP3A. The samples were then analysed on a Phos-tag gel by immunoblotting with α-TRAIP antibodies. This experiment was done more than three times. (b) *In vitro* phosphorylation reaction was set up as in (a) but using equimolar concentration of cyclin B/CDK1, cyclin A/CDK2, or cyclin E/CDK2. The samples were processed as in (a). This experiment was done once.

Furthermore, I analysed the phosphorylation of TRAIP using different CDKs. Interestingly, using equimolar concentrations of cyclin/CDK complexes, I observed that TRAIP exhibited higher efficiency in being phosphorylated by the mitotic cyclin B/CDK1 compared to cyclin A/CDK2, which is also active in mitosis (Figure 5.10 b). Conversely, cyclin E/CDK2, which predominantly functions during the S-phase, displayed relatively limited effectiveness in phosphorylating TRAIP. Based on these findings, we hypothesise that the absence of phosphorylation of TRAIP during the S-phase could be due to the S-phase kinases being inefficient in phosphorylating TRAIP.

To further investigate phosphorylation of TRAIP by cyclins, we investigated whether increased levels of cyclins in the S-phase would phosphorylate and activate TRAIP. To this end, I supplemented egg extract with the same cyclin that I used to drive the extract into

mitosis- cyclin A1Δ, and at the same concentration that I previously used in our experiments using mitotic extracts. To determine the optimal timing for increasing cyclin levels in the extract, I conducted a replication assay with the addition of cyclins at different time points (Figure 5.11 a). Interestingly, the addition of cyclin A1Δ at 30 min drastically reduced the levels of replication while the addition at 45 min was found to be the earliest timing for addition without impacting the replication levels. Hence, I added the cyclin A1Δ in the S-phase extract at 45 min and performed chromatin isolation (Figure 5.11 b). I observed that the replisome unloading remained unaffected by the addition of cyclin. However, there was an increase in the binding of TRAIP to the chromatin in the presence of cyclin A1Δ when compared to the control samples (see TRAIP blot; 45 and 60 min). Although the levels of TRAIP were stimulated as a result of the increased cyclins, we speculate that the unloading observed at 45 minutes was primarily due to the presence of cullins, as replication was already established at this stage. The addition of cyclins at an early stage of initiation affected replication (as seen in Figure 5.11 a, at 30 min), possibly by disrupting normal cell cycle progression and leading to nuclear membrane breakdown and chromosome condensation which are hallmarks of mitotic entry. On the other hand, the addition of cyclins at a later stage (45 min) allowed for the establishment and progression of replication forks prior to cyclin addition, eventually leading to replisome unloading (Figure 5.11 a and b). However, this short window between replication establishment and cyclin addition makes it difficult to distinguish whether the unloading was facilitated by Cul2^{Lrr1} or TRAIP. Moreover, inhibiting the cullin activity and increasing the cyclin levels creates a mitotic environment just like our normal mitosis

experiments, but with earlier cyclin addition. In such scenarios, it is challenging to understand the specific role of TRAIP in S-phase.

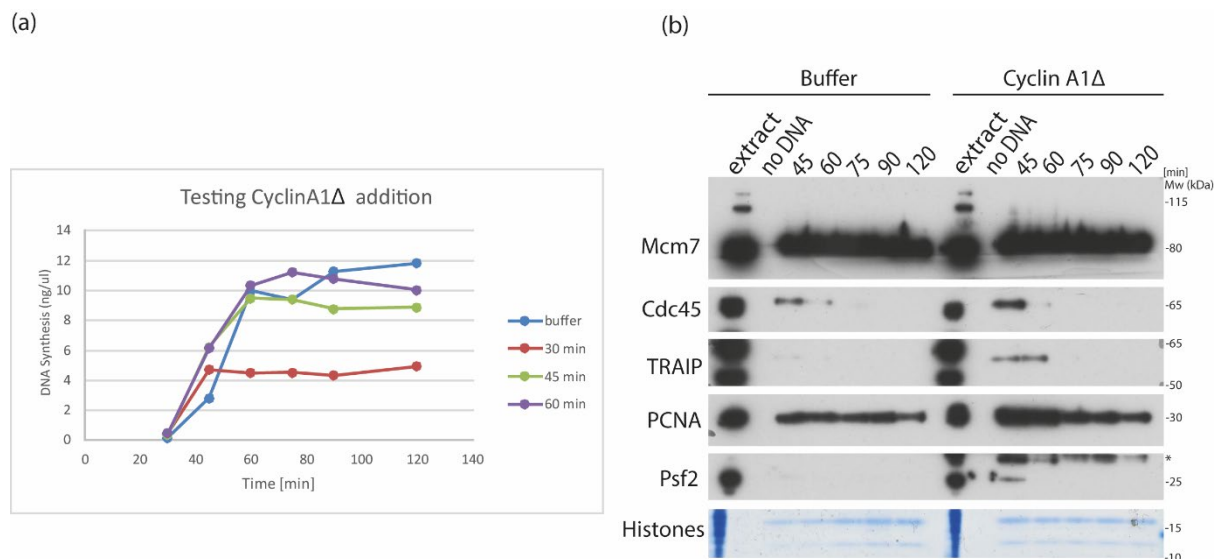


Figure 5.11:- Effect of addition of cyclin A1Δ in S-phase. (a) A replication assay was established with the addition of cyclin A1Δ at different time points and replication levels were analysed. This experiment was done twice. (b) Interphase egg extract was supplemented with high concentrations of cyclin A1Δ buffer at 45 min and followed replisome disassembly. The chromatin binding pattern of replication factors including TRAIP was analysed at indicated time points by immunoblotting with indicated antibodies. Histones and no DNA samples were processed as before. A star beside Psf2 blot indicates cyclin A1Δ recognised by anti-Psf2 antibody. This experiment was done twice.

5.2.7 *In vitro* phosphorylation of TRAIP does not support replisome disassembly

To overcome the difficulty in increasing cyclin levels during the active S-phase, we decided to take a different approach, by supplementing the egg extract with *in vitro* phosphorylated TRAIP. I first tested whether the addition of phosphorylated TRAIP proteins such as Phos.TRAIPwt (wild type), Phos.TRAIP3A (phospho dead mutant) and Phos.TRAIP3D (phospho mimicking mutant TRAIP3D; generated by Dr. Alicja Reynolds-Winczura) affects the egg extract's ability to replicate sperm DNA, measured by the incorporation of radioactive α -³²P dATP (Figure 5.12 a). I could observe that although there was a slight delay in the replication reaction upon addition of the phosphorylation

buffer itself, the addition of the phosphorylated TRAIP does not inhibit replication. I then examined the chromatin binding pattern of the replication factors as a result of the addition of phosphorylated TRAIP (Figure 5.12 b).

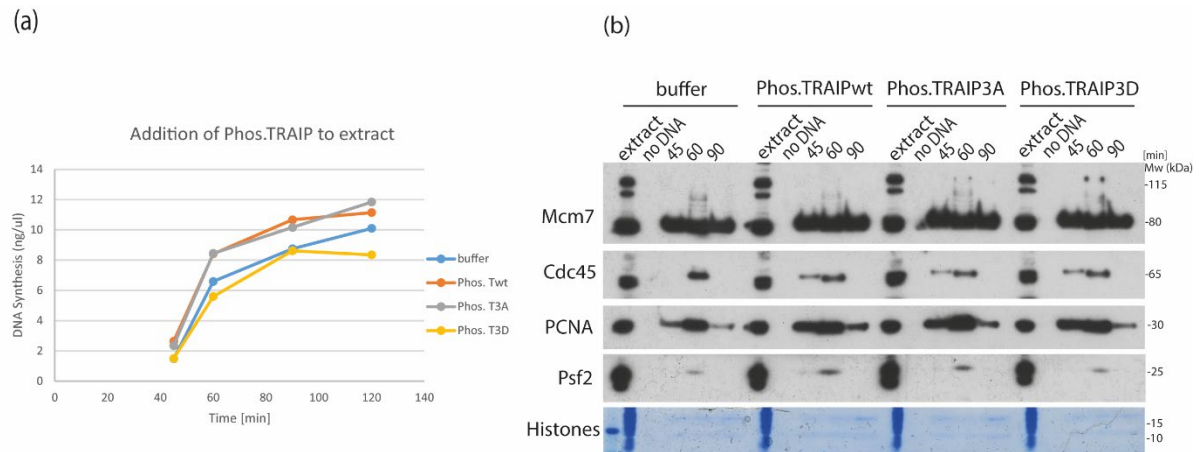


Figure 5.12:- The addition of phosphorylated TRAIP proteins does not affect replication. (a) A replication assay was established with the addition of buffer, phosphorylated wildtype TRAIP (Phos.TRAIPwt), phospho dead mutant TRAIP (Phos.TRAIP3A), and phospho mimicking mutant TRAIP (Phos.TRAIP3D) into the egg extract. The DNA synthesis levels were analysed at different time points. (b) Interphase egg extract was supplemented with phosphorylated TRAIP proteins as in (a) and followed replisome disassembly. The chromatin binding pattern of replication factors including TRAIP was analysed at indicated time points by immunoblotting with indicated antibodies. Histones and no DNA samples were processed as before. This experiment was done once.

We observed that the replisome disassembly remained unaffected, as Cdc45 and Psf2 unloaded in a similar pattern for both buffer control and samples containing phosphorylated TRAIP. Apart from this, in alignment with my TCA results, I observed a delay in the initiation of the replication reaction, as the peak of the reaction was found to be only at 60 min in the buffer control, when the peak for this particular extract was normally at 45 min. We think that this delay in the reaction is contributed by the addition of phosphorylation buffer I used in our experiments.

Since the addition of phosphorylated TRAIP did not affect replication, we next wanted to determine whether supplementing the extract with phosphorylated TRAIP could drive replisome disassembly in the absence of cullin activity during S-phase. To this end, I set

up a replication reaction in the presence of a cullin inhibitor, and supplemented the extract with *in vitro* phosphorylated TRAIP (Figure 5.13). Notably, there were no significant differences in the replisome unloading pattern observed between the samples containing buffer control and phosphorylated TRAIP. Also, there was no obvious differences in the efficiency of replisome unloading as a result of adding Phos.TRAIPwt or Phos.TRAIP3A. This implies that the level of phosphorylated TRAIP supplemented was not enough to drive replisome unloading, or not enough to outcompete the endogenous TRAIP that existed in non-phosphorylated form. In addition to this, I also noted that the samples containing Phos.TRAIP3D exhibited a decreased level of Mcm7 ubiquitylation, and weaker signals for Cdc45 and Psf2 at 120 min. However, this could potentially be attributed to the leaky cullin inhibition as the same phenomenon was observed in the control samples. The lack of signals for Psf2 blot, in Phos.TRAIP3D at 90 and 120 min might be due to a technical error.

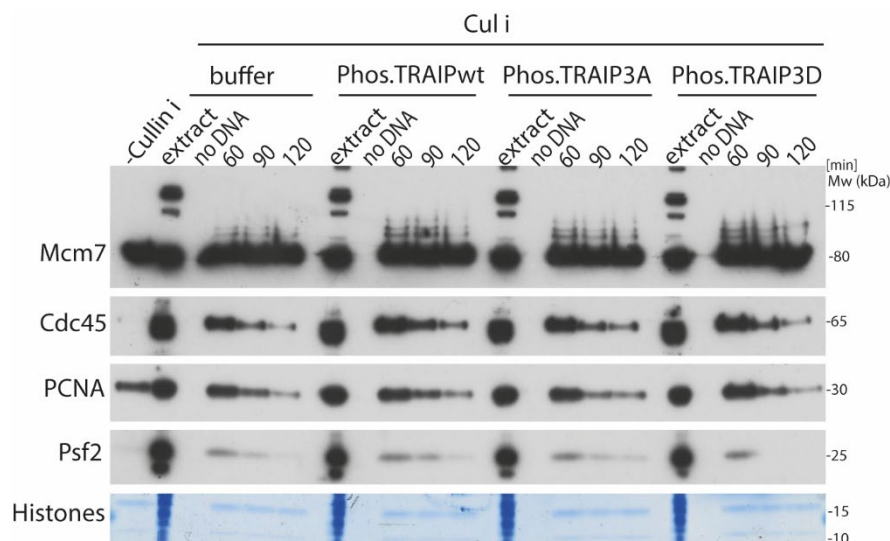


Figure 5.13:- The addition of *in vitro* phosphorylated TRAIP proteins does not unload replisomes in S-phase. A replication reaction was established in the presence of Cul i and supplemented with buffer, phosphorylated wildtype TRAIP (Phos.TRAIPwt), phospho-dead mutant TRAIP (Phos.TRAIP3A), and phospho-mimicking mutant TRAIP (Phos.TRAIP3D) into the egg extract. The chromatin binding pattern of replication factors were analysed at the indicated time points by immunoblotting with indicated antibodies. Histones and no DNA samples were processed as before. This experiment was done once.

To identify whether non-phosphorylated TRAIP in the egg extract prevented TRAIP-mediated unloading, we next decided to experiment using extracts that are devoid of TRAIP. Therefore, I set up a replication reaction using TRAIP depleted extracts, and supplemented the extracts with *in vitro* Phos.TRAIP proteins to determine whether phosphorylation of TRAIP could drive replisome disassembly in the absence of cullin activity in S-phase, without interference from endogenous TRAIP (Figure 5.14).

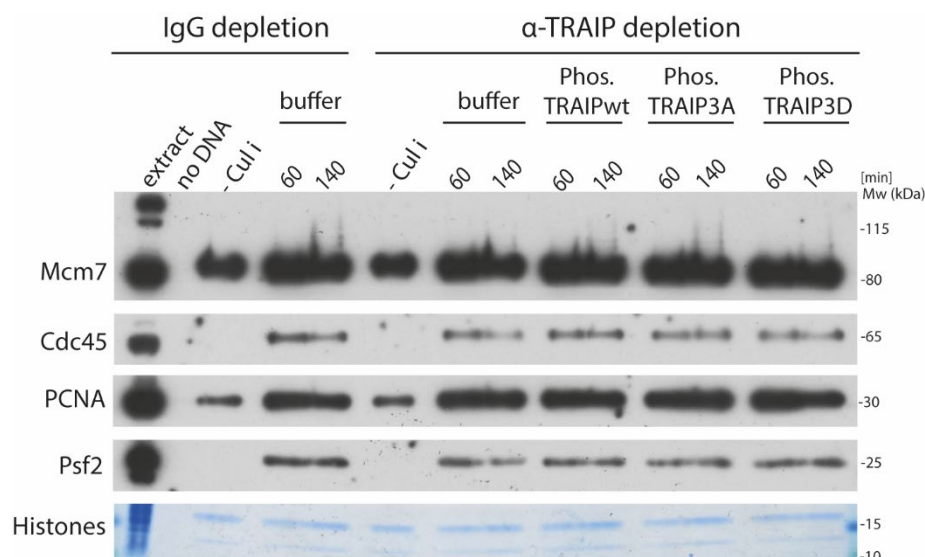


Figure 5.14:- The addition of *in vitro* phosphorylated TRAIP proteins in TRAIP depleted extracts. A replication reaction was established using TRAIP depleted extracts in the presence of Cul i and supplemented with buffer, phosphorylated wildtype TRAIP (Phos.TRAIPwt), phospho-dead mutant TRAIP (Phos.TRAIP3A), and phospho-mimicking mutant TRAIP (Phos.TRAIP3D). The chromatin binding pattern of replication factors were analysed at the indicated time points by immunoblotting with indicated antibodies. A sample each from IgG depleted and TRAIP depleted treated with no Cul i was processed alongside. Histones and no DNA samples were processed as before. This experiment was repeated three times.

I observed that the control samples containing no cullin inhibitor (see IgG depleted/TRAIP depleted - Cul i) unloaded the replisomes. On the other hand, there was no significant differences in the replisome unloading pattern as a result of adding

Phos.TRAIP proteins in the presence of Cul i (see Cdc45 and Psf2). These results indicate that phosphorylation of TRAIP alone was insufficient to drive replisome unloading in S-phase. This raised an intriguing possibility that either additional phosphorylation sites may be present in *Xenopus* and our mass spectrometry analysis may not have captured all the relevant phosphorylation sites present in *Xenopus*. But this is unlikely as the TRAIP3A mutant is not phosphorylated at all in our *in vitro* reactions suggesting that there is no more possible CDK sites. Several databases, such as PhosphoSite Plus and qPTM, report a higher number of phosphorylation sites on TRAIP (12 and 7 sites, for human and mouse orthologs respectively). But this might be due to species-specific differences or the tissue types studies or differences in the cellular context studied. Since databases integrate data from multiple studies, done under different conditions, this might potentially reveal more sites. Another possibility of the Phos. TRAIP protein not leading to replisome unloading in our experiments might be due to the dephosphorylation by endogenous enzymes present within the extract. This might have lead to deactivation of the *in vitro* phosphorylated proteins or may be some additional factors might be required to orchestrate this process effectively.

5.3 Discussion

In this chapter, I have investigated the activity of TRAIP in S-phase. The fact that TRAIP associates weakly with the S-phase replisomes during unperturbed DNA replication led us to investigate further TRAIP's replisome unloading capability in S-phase. Examining proteins isolated from nascent DNA (iPOND) in mammalian cells and from actively replicating forks in *Xenopus* egg extracts, has demonstrated the presence of TRAIP, even in the absence of replication stress. However, when replication stress occurs, more TRAIP

is found interacting with the replisome (Hoffmann et al., 2016; Wu et al., 2019). In human cells, TRAIP is found localised in the nucleolus, and under replication stress TRAIP relocates to the sites of DNA damage by interacting with PCNA via its PIP box. However, mutant TRAIP that lacks this PCNA interacting motif has still been able to localise to its targets during replication stress, suggesting that TRAIP can also act independent of PCNA (Feng et al., 2016; Hoffmann et al., 2016).

The data presented in this chapter provides evidence that TRAIP accumulates at post-terminated replisomes when their disassembly is inhibited (Figures 5.1 and 5.2). Intriguingly, on treatment with aphidicolin (which uncouples DNA polymerases from helicases) and caffeine, there was an increase in the accumulation of replisomes, but the level of TRAIP observed was reduced (Figure 5.3). Notably, the levels of TRAIP and replisome components did not show any correlation. This leads to the question of whether TRAIP's activity is regulated at the level of its interaction with the helicase components or is dependent on other factors. Additionally, the immunoprecipitation of TRAIP from mitotic chromatin (conducted by Dr. Alicja Reynolds-Winczura) and its analysis by mass spectrometry revealed the interaction between DNA Pol ϵ and TRAIP. This raises the question of whether TRAIP's interaction with the replisome is mediated through polymerases, in addition to a direct interaction with the helicase. It is likely that during aphidicolin treatment, TRAIP might lose its interaction platform as helicases and polymerases are uncoupled. We therefore hypothesise that TRAIP interacts with the replisome through a bipartite interaction with both the helicase and polymerase as part of the replisome. However, further research is essential to validate this hypothesis, for example by studying the interaction of TRAIP on chromatin in the context of polymerases. I could do this by blocking primase activity, which is essential for synthesising short RNA primers that serve as starting point for polymerases to initiate replication. This would

give information whether TRAIP interacts specifically through polymerases and/or CMG components.

Unlike Lrr1, which accumulates specifically on terminated forks, TRAIP interacts with chromatin predominantly during challenged replication, indicative of its role at terminating and stalled forks. For instance, Lrr1 is not observed on chromatin during treatments that block fork progression such as addition of both aphidicolin and caffeine or ICRF-193 (Sonneville et al., 2017), whereas TRAIP is found to associate with sites of both DNA damage and stalled forks (Feng et al., 2016; Hoffmann et al., 2016; Moreno et al., 2019a). Overall, these observations raise the possibility that TRAIP's activity may be regulated differently in contrast to Lrr1 whose activity is regulated through core interaction with replisomes (Jenkyn-Bedford et al., 2021; Zhou et al., 2021).

The data presented in this chapter reveals that TRAIP is capable of ubiquitylating replisomes during S-phase. However, this ubiquitylation activity does not translate into efficient replisome disassembly (Figure 5.6). It is possible that the ubiquitin ligase activity of TRAIP in S-phase is not optimal in these particular situations such that it is not able to meet the required threshold of at least 5 ubiquitins to form the ubiquitin chains. This threshold is crucial for the efficient recognition and unfolding of ubiquitylated Mcm7 by the p97 complex, which is necessary for subsequent replisome disassembly (Deegan et al., 2020; Fujisawa et al., 2022). During mitosis, TRAIP could be more efficient at synthesising longer ubiquitin chains, which readily support p97 recognition and unloading.

Furthermore, it is worth highlighting that during S-phase, Cul2^{Lrr1} primarily generates K48-linked ubiquitin chains, while in mitosis, TRAIP produces K6 and K63-linked ubiquitin chains, that are recognised by p97 (Moreno et al., 2014, 2019a). Therefore, it is

also possible that the ubiquitin chains produced by TRAIP during S-phase could be distinct from K6 or K63-linked chains formed in mitosis. The type of ubiquitin chains synthesised can be attributed to the E2s engaged during ubiquitylation. The specific interactions between the E2 and E3 enzymes provide a mechanism for achieving specificity in the type of ubiquitin chains that are attached to a substrate, allowing for precise targeting of different cellular processes and outcomes (Ye and Rape, 2009). More work is needed to determine whether TRAIP indeed synthesises distinct ubiquitin chains during S-phase compared to mitosis. Therefore, the analysis of the different ubiquitin chain types synthesised and different E2s involved in these scenarios will provide more insight into how TRAIP activity is regulated in S-phase. Furthermore, the potential involvement of deubiquitylating enzymes (DUBs) in regulating the ubiquitylation status of the substrates during S-phase is an intriguing possibility. It is possible that a specific DUB might be acting during S-phase, counteracting the ubiquitylation mediated by TRAIP on its substrates as part of its regulatory mechanism. Such regulatory mechanisms are crucial to maintain genome stability, and it is possible that, as the cell cycle transitions from S-phase to mitosis, the specific DUB might undergo deactivation facilitating the rapid ubiquitylation of Mcm7 by TRAIP in mitosis. This rapid ubiquitylation could trigger downstream events such as replisome disassembly by p97 complex.

Additional possibility is a regulatory mechanism mediated by p97, not only towards specific substrate but also towards specific type of ubiquitin chains (Meyer et al., 2012). It has also been shown that p97 displays varying interactions with their substrates modified with different ubiquitin chains based on the cofactors involved (Alexandru et al., 2008). For example, interaction between p97 and the Cul2^{Lrr1} complex, facilitated by Ubxn7 cofactor. Ubxn7 facilitates bridging between the neddylated Cul2^{Lrr1} and p97 complex, enabling the efficient unloading of substrates modified with relatively short

K48-linked ubiquitin chains synthesised by Cul2^{Lrr1}. This increased avidity is attributed to the specific recognition of the ubiquitin chain type by the p97 complex (Tarcn et al., 2022). On that basis, it is possible that a specific p97 cofactor may be required to stimulate its activity towards the K6/K63 ubiquitin chains synthesised by TRAIP in mitosis. In the absence of such a cofactor, p97 may not be able to efficiently recognise or interact with the ubiquitin chains generated by TRAIP during S-phase. While my current data does not provide direct evidence for a p97-dependent adaptor, the existing knowledge about the regulatory mechanism of p97 and its interactions with different ubiquitin chain types support this hypothesis. Additionally, it is known that CDK-dependent phosphorylation can bring about changes in the specificity of the known p97 cofactors (Agrotis et al., 2023; Hänzelmann and Schindelin, 2017). Therefore, it is probable that post-translational modifications such as phosphorylation, can modulate the interaction of p97 complex with its cofactors, which in turn can influence the substrate specificity and functionality of p97 complexes. Alternatively, it may also be that a cofactor is missing in mitosis, which means that there is a need for synthesis of longer ubiquitin chains in mitosis. However, further investigations would be necessary to identify and characterise potential cofactors and their modifications that may facilitate the recognition of TRAIP-mediated ubiquitylation and unloading by p97.

Adding to the complexity of TRAIP functions, TRAIP has been shown to play a crucial role in dealing with replication forks that are stalled at ICLs or DPCs in S-phase (Larsen et al., 2019; Wu et al., 2019). During an encounter with ICLs, where two replication forks converge, TRAIP can target replisome machinery and coordinate two distinct pathways for repair by ubiquitylating CMG and allowing the completion of replication. Shorter ubiquitin chains stimulate the NEIL3 glycosylase pathway to directly unhook the crosslink by cleaving one of the two glycosyl bonds that forms the ICL. On the other hand, longer

ubiquitin chains are needed to facilitate the unloading of CMG by p97, which allows endonucleases to access DNA. This in turn allows for ICL repair by the Fanconi Anaemia pathway to generate a double-strand break, which can be repaired by homologous recombination. In contrast to the conventional replication termination process, TRAIP-mediated ubiquitylation for ICL repair involves ubiquitylation of Mcm2, Mcm3, Mcm4, Mcm6, and Mcm7, and the partial ubiquitylation of Cdc45 (Wu et al., 2019). Notably, it has been shown that TRAIP generates heterotypically linked or branched ubiquitin chains during ICL repair in S-phase, distinguishing this process from the K48-linked chains synthesised by Cul2^{Lrr1} or the K6/K63-linked ubiquitin chains generated by TRAIP in mitosis. This precise way of targeting CMG during fork convergence by Cul2^{Lrr1} and the activation of TRAIP exclusively during ICL repair (in S-phase), prevents the unnecessary unloading of active helicases, and maintains genome integrity (Deng et al., 2019; Wu et al., 2019). On a different note, TRAIP is activated in S-phase even in the absence of fork convergence. For example; during encounters with DPCs. In contrast to ICL repair, TRAIP can ubiquitylate DPC itself when a single replisome collides with a DPC and allows proteasomal degradation of the DPC. In such scenarios, no CMG ubiquitylation can be observed, and this is independent of the SPRTN-mediated degradation and repair (Larsen et al., 2019). It has also been shown that these repair mechanisms orchestrated by TRAIP can occur even with a mutated PIP box, suggesting these repair processes can take place independent of PCNA (Larsen et al., 2019; Wu et al., 2019). Additionally, recent investigations from mammalian cells in S-phase have shown that TRAIP can facilitate resolution of replication-transcription conflicts. In situations where the transcription machinery acts as a barrier to the replicating fork, TRAIP helps to prevent DNA damage at transcription start sites (Scaramuzza et al., 2023).

Based on the numerous interactions of TRAIP observed in S-phase, Prof. Walter had proposed a model stipulating that TRAIP with its RING domain is located at the leading tip of the replisome. This positioning enables TRAIP to facilitate the transfer of ubiquitin to its target proteins located ahead of the replisome in S-phase. This regulated activity of TRAIP protects active single replisomes that are involved in replication from ubiquitylation, thereby preventing untimely replisome disassembly and subsequent fork collapse (Wu et al., 2021). Supporting this model, structural studies reveal that Pol ϵ mediates recruitment of GINS to MCM during CMG assembly, and remains associated with the helicase to enable leading strand synthesis. Pol ϵ is composed of Pol2, Dpb2, Dpb3 and Dpb4. A structural flexibility is observed by the polymerases to facilitate substrate handoff between Pol δ to Pol ϵ . Specifically, the Dpb2 and the C-terminal domains of Pol ϵ (or C-Pol2) anchor it to the Mcm motor, while the N-terminal catalytic domain, Pol2, is flexibly tethered, suggesting a flexible nature of Pol ϵ (Zhou et al., 2017; Goswami et al., 2018). This architecture orients Pol ϵ on the leading strand to be situated at the front of the CMG complex, with its non-catalytic domain positioned at the front of the fork. Furthermore, our AlphaFold structural predictions of dimeric TRAIP revealed that the RING domain of TRAIP is located at the same end of the dimeric TRAIP, near the N-terminus (Figure 5.15 a). Taken together, these data support a model where the RING domain of dimeric TRAIP would be positioned at the tip of the replisome to facilitate the transfer of ubiquitin to substrates encountered ahead of the fork. Additional work focusing on the domain structure of TRAIP has proposed that TRAIP requires homodimerisation, facilitated via its Coiled-Coil (CC) domain, for mitotic progression (Seul Park et al., 2015). Moreover, unpublished findings from Prof Walter's lab indicate that the deletion of the CC domain hindered TRAIP's ability to repair ICLs (CSHL poster; 2021). Furthermore, proteome-wide in silico interaction screens of human proteins using

‘Predictomes,’ generated by Walter’s lab (Lim et al., 2023) have detected numerous contacts between TRAIP and various fork proteins, such as POL ϵ , PCNA, and MCMBP. Notably, Pol ϵ has been found to have 175 contact points with TRAIP, suggesting TRAIP’s bridging between polymerases. Among the other high confidence interactors of TRAIP are the deubiquitinase USP7 and the ubiquitin ligase RFWD3 - important in ICL repair and RPA mediated DNA damage signalling and repair (Mitxitorena et al., 2020; Gallina et al., 2021). A linear domain schematic of TRAIP, with amino acid numbers highlighting the regions predicted to mediate these protein-protein interactions is depicted in Figure 5.15

b. Investigating and characterising such interactions will provide valuable mechanistic insights into TRAIP regulation and its architecture within the replication fork.

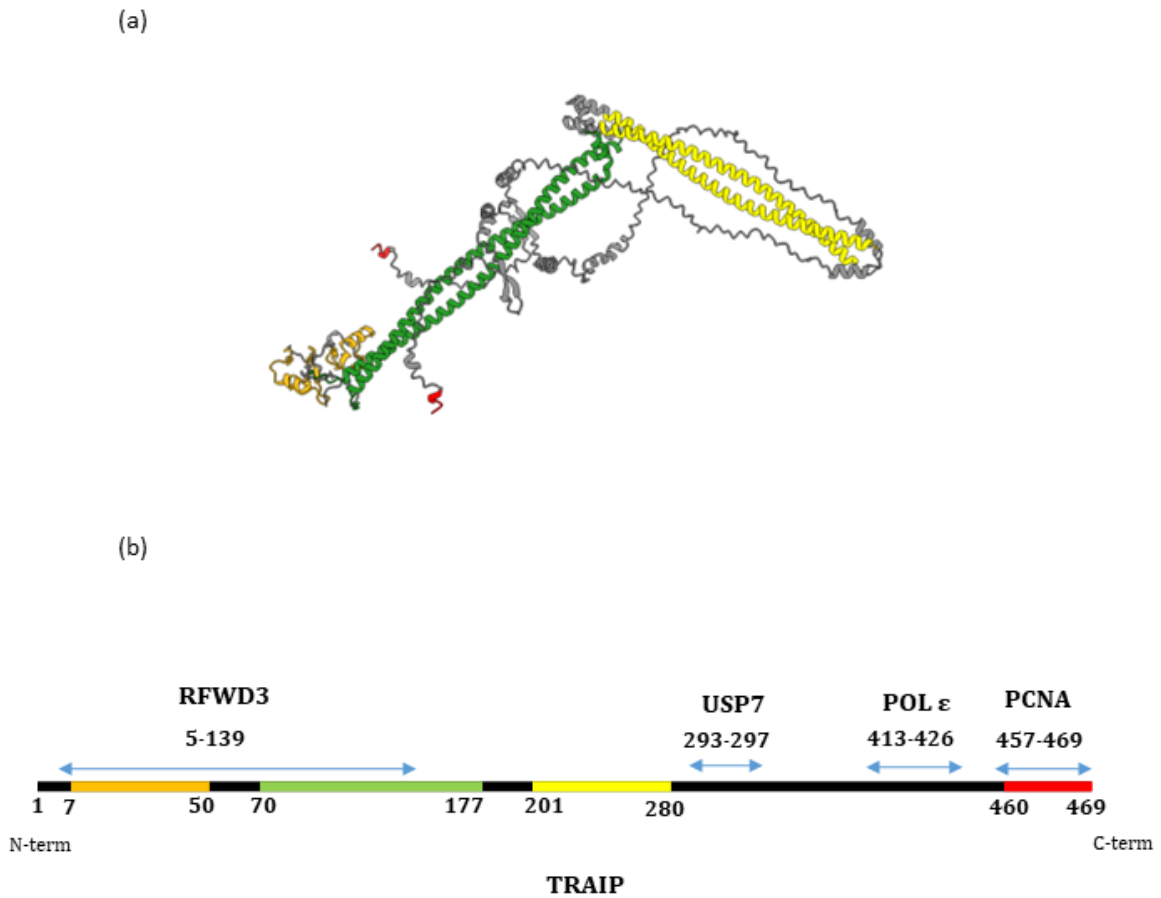


Figure 5.15:- In silico predicted model of TRAIP structure and its interactors. (a) The predicted dimeric structure of TRAIP, generated using AlphaFold is depicted. Different domain regions are marked/coloured as follows- N-terminus, RING domain (orange), Coiled coil (green), Leucine zipper (yellow) and PIP box (red) and C-terminus. Grey colour depicts the linker regions that connects one domain to the next. Notably, the RING domains of dimeric TRAIP localise to the same end as the N-termini. (b) A linear schematic summarising predicted regions of TRAIP interactions with fork associated proteins. The different domains of TRAIP are coloured as in (a). The blue arrow indicates areas of protein-protein interactions, representing regions for RFWD3, USP7, Pol ϵ and PCNA.

Mechanistically, how TRAIP is differentially activated in S-phase and mitosis is still unknown. Our findings suggest that the activation of TRAIP in mitosis is regulated

through post-translational modifications. I analysed TRAIP from S-phase and mitotic chromatin on a Phos-tag gel and observed that TRAIP was phosphorylated specifically in mitosis, and lacks this modification under all other S-phase treatments (Figure 5.8 and 5.9). In addition, our lab has found that the addition of phospho-dead mutant of TRAIP (TRAIP3A) into mitotic extract resulted in a delay in the replisome unloading in mitosis (performed by Dr Alicja Reynolds-Winczura). Protein phosphorylation is a dynamic and reversible process, known for its ability to alter protein functions (Ardito et al., 2017). Consequently, it is plausible that phosphorylation serves as the trigger to enhance TRAIP's activity during mitosis thereby enabling the efficient modification of its target CMGs. During the cell cycle, the levels of cyclins fluctuate cyclically based on the status of the cell division cycle. Cells have very low cyclin levels in G1, which slightly increases during S-phase and elevated levels for transition from G2 to mitosis (Malumbres and Barbacid, 2001; Łukasik et al., 2021). Therefore, we speculate that increased CDK activity during mitosis might initiate the phosphorylation of TRAIP by the mitotic kinases, which in turn could even induce a conformational change in its structure. Our *in vitro* phosphorylation experiments have effectively demonstrated that TRAIP can indeed be phosphorylated using mitotic cyclin B/CDK1 (Figure 5.10). Nevertheless, supplementing this *in vitro* phosphorylated TRAIP into S-phase extract did not support replisome unloading, even when cullin activity was inhibited (Figure 5.13 and 5.14). There are several possibilities for this. Firstly, it is possible that the supplemented protein undergoes rapid dephosphorylation by phosphatases within the S-phase extract. Alternatively, there may exist additional interactors for TRAIP during mitosis that stimulate its functional role in replisome unloading, and might be absent from the S-phase chromatin. Furthermore, there is a possibility that replisomes themselves undergo modification in mitosis which is required in addition to the phosphorylation of TRAIP.

Notably, our lab has also found that the addition of a phosphomimicking mutant of TRAIP (TRAIP3D), into mitotic extract did not support unloading of replisomes in mitosis, indicating that other mechanisms beyond phosphorylation might be involved in TRAIP regulation. These observations raise intriguing questions regarding TRAIP's differential modification of the helicase within S-phase, indicating that a different modification beyond phosphorylation might be involved to activate TRAIP in ICL and DPC repair scenarios. Therefore, further structural analysis of TRAIP is essential to elucidate the precise rationale behind the varying behaviour of TRAIP in S-phase.

At the human organismal level, mutations within the RING domain of TRAIP have been implicated in the failure of TRAIP functioning, leading to microcephalic primordial dwarfism. These mutations are known to cause reduced cellular proliferation observed in Seckel syndrome patients; a form of primordial dwarfism. Two specific homozygous TRAIP mutations identified in such patients are - Cytosine 553 to Thymine and Cytosine 52 to Thymine. These mutations are hypomorphic and impair the ubiquitin ligase activity of TRAIP (Harley et al., 2016). To further expand on these findings, I performed preliminary mapping of patient mutations from COSMIC and cBioPortal, databases that provide cancer genomic datasets and somatic mutation data. Notably, mutations within TRAIP were distributed across its all domains including the RING and CC domains (Figure 5.15). As mentioned previously, we had identified three TRAIP phosphorylation sites as phosphorylated specifically in mitosis - T280, S295, and S352. Notably, the amino acid residue P353, situated adjacent to the phosphorylation site S352, is recurrently found mutated in patients. Since S/P motifs are known CDK phosphorylation targets, mutations of this site could potentially disrupt cell cycle signalling by preventing phosphorylation of TRAIP.

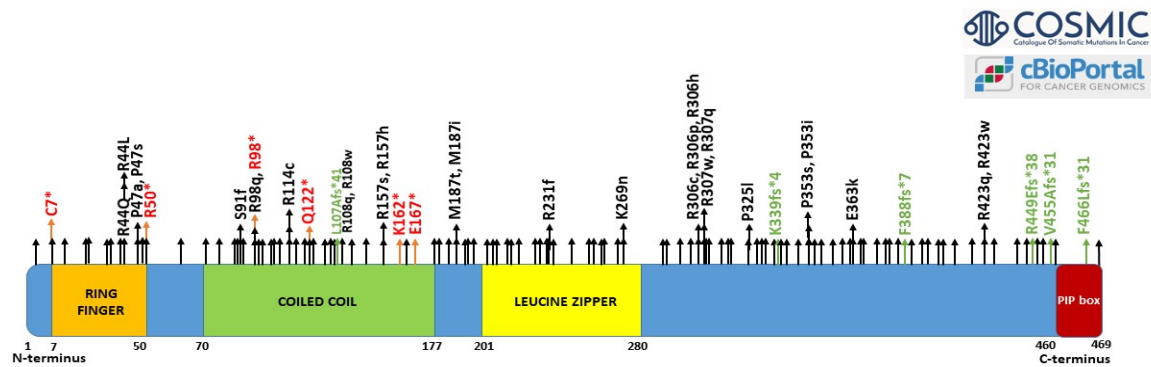


Figure 5.16:- Human TRAIP patient mutations. Mutations found in human TRAIP collected from COSMIC and cBioPortal databases are indicated on top of each domain. Missense mutations are represented with black arrows, frameshift mutations are represented in green, and nonsense mutations are marked in red.

Analysing such patient derived mutations at these key regulatory sites could tell us whether they impact TRAIP's ubiquitin ligase function, disrupt the structure of the protein and affect folding pattern and dimerisation, interaction with binding partners, or affect other cellular activities such as cell proliferation, DNA damage response, ICL repair, mitotic progression etc. Therefore, gaining deeper understanding of the consequences of these mutations in terms of human health would also be of considerable interest.

Chapter-6

6 Discussion

In this PhD project, I have studied two different ubiquitin ligases - Cul2^{Lrr1} and TRAIP, that both ubiquitylate the Mcm7 subunit of the replicative helicase and lead to disassembly of the helicase at the right time. Replisome unloading is carefully regulated by post-translational modifications of proteins, specifically ubiquitylation. Defects in the unloading of the replisomes are problematic for cells as the replisome components can interfere with the DNA templated processes (Maric et al., 2014; Fan et al., 2021). Importantly, premature disengagement of the replisome would result in replication fork collapse and generation of DNA damage (Deng et al., 2019). On the other hand, recent investigations have demonstrated that replisome unloading can also be triggered to facilitate DNA damage repair such as in ICL and DPC repair and during MiDAS (Larsen et al., 2019; Sonnevile et al., 2019b; Wu et al., 2019).

6.1 Molecular mechanisms of Cul2^{Lrr1} and TRAIP function

The role of Cul2^{Lrr1} in polyubiquitylating Mcm7 and unloading the CMG during S-phase is consistent and highly conserved in *C. elegans*, frog egg extracts, mouse embryonic stem cells and human cells (Dewar et al., 2017b; Sonnevile et al., 2017; Fan et al., 2021; Villa et al., 2021). This pathway also functions analogous to SCF^{Dia2} in yeast (Maric et al., 2014). Interestingly, a secondary pathway, mediated by TRAIP, for replisome unloading, was also identified during mitosis and was similarly found to be conserved in *C. elegans*, higher eukaryotes, and in studies using mouse embryonic stem cells (Sonneville et al., 2017, 2019b; Deng et al., 2019; Moreno et al., 2019b). The mechanism of replisome disassembly

clearly displays pathway redundancy and high conservation across different species, highlighting the fundamental role of this process in safeguarding against any errors or disruptions before cell division. It has been demonstrated that the deletion of LRR1 or TRAIP via CRISPR/Cas9 in several human cell lines resulted in cell lethality, indicating their importance for the survival of the cells (Hart et al., 2015). Furthermore, the absence of the human LRR1 gene was shown to reduce the rate of DNA replication by impeding the recycling of a soluble pool of factors crucial for effective DNA replication (Fan et al., 2021). Hence, timely and appropriate unloading of the replisomes is essential and any dysregulation in these mechanisms could lead to detrimental consequences for human health.

The backup pathway, which is dedicated for unloading terminated or stalled replisomes during mitosis, has been proposed to have evolved as an essential step to process any sites of incomplete DNA replication before chromosome segregation. It involves introducing fork breakage and subsequent repair (Deng et al., 2019; Sonnevile et al., 2019b). Although this repair comes with a small deletion of the under-replicated region in one of the sister chromatids, this is still considered more beneficial than the high-frequency sister chromatid exchanges as seen for Common Fragile Sites (CFSs) (Glover et al., 2017). In this way TRAIP mediated unloading contributes to the preservation of genome integrity by repairing any damage prior to cell division.

Importantly both Cul2^{Lrr1} and TRAIP operate independently in separate pathways, and their activation mechanisms for substrate modification are regulated through distinct approaches. The activity of Cul2^{Lrr1} is confined to S-phase and regulated in such a way that the LRR interaction with the zing-finger domains of Mcm3 and Mcm5 is initiated only once the excluded lagging DNA strand is lost. This interaction triggers ubiquitylation of

the substrate, Mcm7 (Jenkyn-Bedford et al., 2021; Zhou et al., 2021). Hence, the direct interaction between the LRR-MCM interfaces, which is exclusively permitted during termination, governs the activity of Cul2^{Lrr1}. On the other hand, TRAIP appears to engage with the replisome at all times (Hoffmann et al., 2016; Dewar et al., 2017b). However, this interaction does not trigger unloading of the replisome during S-phase unless it encounters ICLs (Wu et al., 2019) or transitions into mitosis (Deng et al., 2019; Moreno et al., 2019b; Sonnevile et al., 2019b). These distinct regulatory mechanisms of Cul2^{Lrr1} and TRAIP are needed to enable them to protect active replisomes from premature unloading while efficiently disassembling those that have completed their tasks and terminated in S-phase, or encountered an ICL. How TRAIP is regulated to deliver this differential activity is not yet known. It is likely that TRAIP may have a way to switch between its active and inactive conformation/interaction depending on the type of stress encountered. Additionally, I observed that TRAIP undergoes phosphorylation during mitosis, while this modification was absent during S-phase when replisome disassembly was inhibited. Phosphorylation is a post-translational modification known to influence a protein's function (Ramazi and Zahiri, 2021). Therefore, we propose that unlike Cul2^{Lrr1} that is regulated at the level of substrate interaction, TRAIP is regulated via post-translational modifications influencing its activity and/or interactions. However, the specific consequences of TRAIP phosphorylation remain to be elucidated. It is likely that TRAIP may undergo a conformational change in response to such scenarios where replisomes need to be disassembled or interact with additional factors stimulating its activity (Wu et al., 2021). However, further investigation is essential to confirm this. A schematic representation of Cul2^{Lrr1} and TRAIP mediated replisome disassembly is depicted in Figure 6.1 and Figure 6.2.

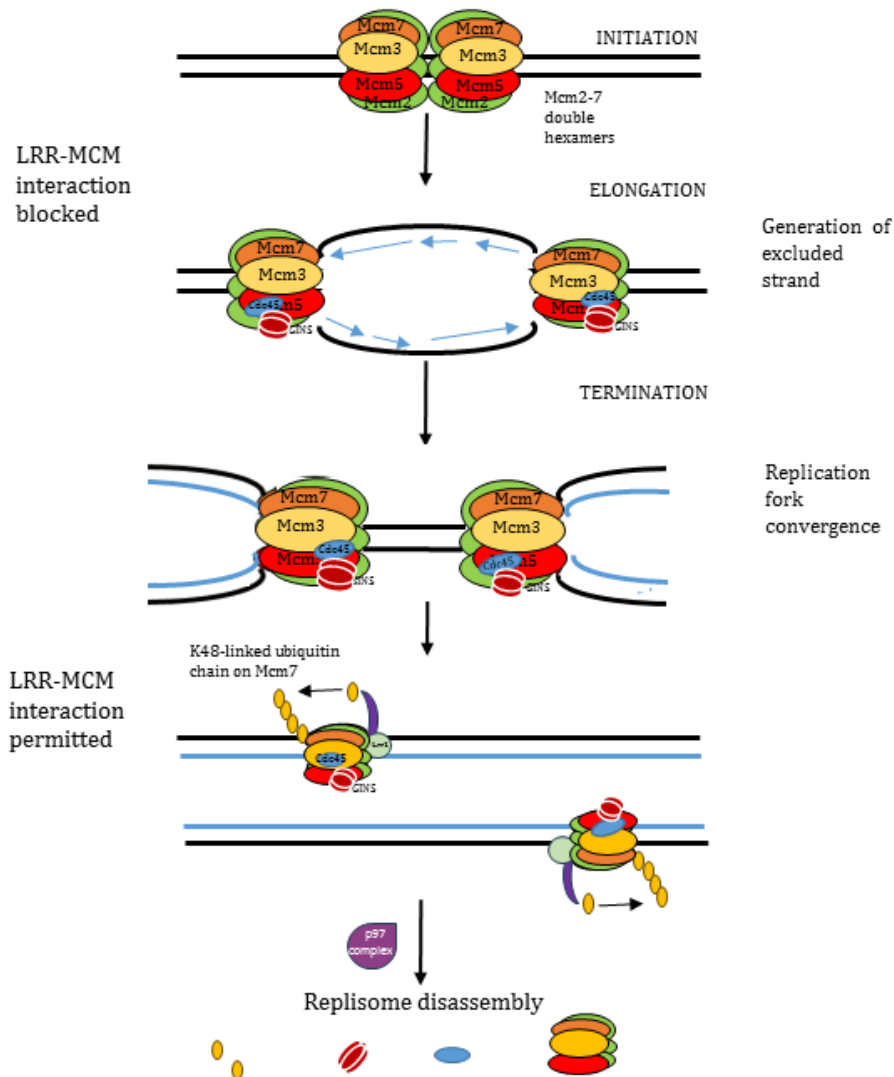
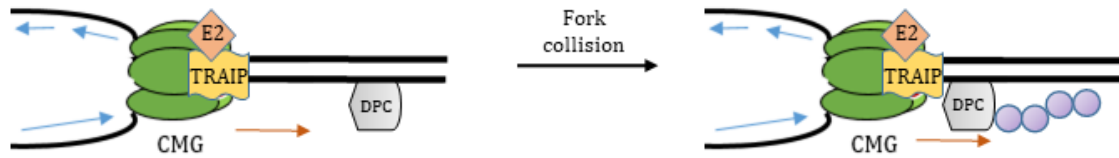


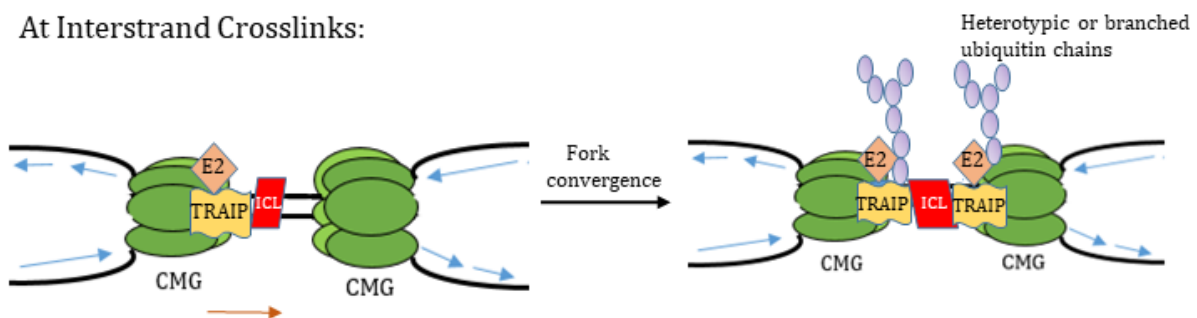
Figure 6.1:- Current understanding of the regulation of replisome disassembly mediated by Cul2^{Lrr1} in S-phase. The LRR-MCM interaction is occluded by the excluded DNA strand during elongation which forms the structural basis for suppressing ubiquitylation before termination. Upon termination, the loss of excluded strand allows LRR-MCM interaction; specifically the Mcm3 and Mcm5 zing finger domains, facilitating Mcm7 ubiquitylation using K48-linked ubiquitin chains and replisome disassembly.

S-phase

At DNA Protein Crosslinks:



At Interstrand Crosslinks:



Mitosis

At all CMGs:

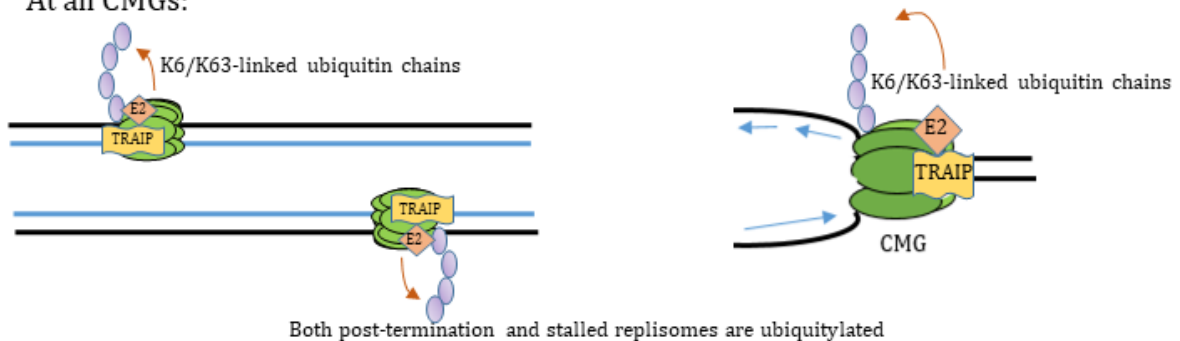


Figure 6.2:- Current understanding of TRAIP-mediated replisome disassembly under various conditions. TRAIP associates with the replisome such that its RING domain is positioned at the tip. During S-phase, TRAIP can directly ubiquitylate DNA-protein crosslinks (DPCs) when they are encountered by the replicating forks. TRAIP also mediates the ubiquitylation of multiple subunits of CMGs that have converged at Interstrand Cross Links (ICLs), leading to their disassembly and repair. DPCs are represented in grey and ICLs are represented in red. In mitosis, TRAIP ubiquitylates any remaining chromatin-bound replisomes using K6 or K63-linked ubiquitin chains, resulting in complete replisome disassembly. The orange arrow indicates the directionality of TRAIP-mediated ubiquitin transfer, with violet beads representing polyubiquitin chains. This model demonstrates how TRAIP promotes replisome disassembly in response to DNA lesions during S-phase while also facilitating global replisome removal during mitosis.

Work from Prof. Walter's lab had shown that TRAIP can ubiquitylate converging forks and protein barriers that are located ahead of forks (Larsen et al., 2019; Wu et al., 2019). Therefore, it would be intriguing to investigate the underlying mechanism for ICL repair in S-phase and how this is distinctly regulated from replisome unloading in mitosis. Distinct types of ubiquitin chains on substrate Mcm7 can lead to replisome disassembly; for example, K48-linked ubiquitin chains during termination in S-phase (Maric et al., 2014; Moreno et al., 2019b), K6/K63-linked ubiquitin chains during mitosis (Moreno et al., 2019b), mixed or branched ubiquitin chains during ICL repair (Wu et al., 2019). It is likely that different E2s might be involved in each of these situations to grant specificity (Ye and Rape, 2009). It is also possible that different p97 cofactors may be involved in these scenarios to confer specificity, similar to the bridging between Ubxn7 with Cul2^{Lrr1} (Fujisawa et al., 2022; Kochenova et al., 2022; Tarcn et al., 2022). Conducting future experiments involving immunoprecipitation of TRAIP along with accumulated replisomes on chromatin, both in mitosis and in presence of ICLs in S-phase may provide insights into the regulatory mechanisms by comparing the replisome components and other interacting partners involved in these different conditions. Additionally, immunoprecipitation of replisomes accumulated with Cul i +/- recombinant TRAIP in S-phase can also provide information about the specific E2s and p97 cofactors involved, or if there are differences in their post-translational modifications under these different scenarios that could influence the functionality of p97 complex. Finally, determining the specific types of ubiquitin chains synthesised by TRAIP in these conditions, which can/cannot be recognised by p97, could shed more light onto this process. The identification of specific type of ubiquitin chains can be achieved by analysing immunoprecipitated samples by western blotting using linkage specific antibodies. Moreover, it is also possible that the activity of a specific DUB might be present in S-phase

and inactivated in mitosis to allow replisome disassembly by TRAIP. We can test the presence of a DUB activity by treating the S-phase reaction with specific DUB inhibitors. By performing these experiments, we should get more understanding of the mechanism regulating TRAIP activity in S-phase and mitosis.

6.2 The significance of Cul2^{Lrr1} and TRAIP in cancer biology

Precise and timely regulation of E3 ligases is crucial, as they play a central role in numerous signalling pathways. It is well documented that the dysregulation of E3s and their substrates is commonly observed in human cancers (Qi and Ronai, 2015). Consequently, any alterations in their regulatory pathways can lead to either activation or inactivation of tumour suppressor genes (Duan and Pagano, 2021). In the context of cancer, there is often a notable upregulation of replication factors that are essential for its growth. Consistent with such a positive role in cell proliferation, high levels of LRR1 expression correlate with poor prognosis in some cancers, such as renal and liver cancer (Uhlen et al., 2017; Hindle et al., 2022). Furthermore, the analysis of CRISPR data screens in human cancer cells has revealed that LRR1 is indispensable for proliferation of normal cells and actively dividing cancer cells (Fan et al., 2021). The inactivation of Cul2^{LRR1} pathway has also been shown to affect the cell motility, as this is important for promoting actin based cell movement which is a key factor in cancer cell migration and metastasis (Starostina et al., 2010; Jang et al., 2020). Overall, LRR1 has been shown to be important in regulating gene expression, proliferation and cell motility. The specificity of E3 ligases, coupled with their implications in cancer hallmarks, has led to the development of compounds that specifically target E3 ligases for cancer therapy (Sampson et al., 2023). Therefore, there is a potential to develop and test a specific inhibitor targeting the activity of Cul2^{LRR1} to effectively inhibit cancer cell proliferation. To enhance the selective

targeting of cancer cells, nanoparticle based drug delivery systems could be explored. Nanoparticles can be engineered to preferentially accumulate in tumour cells, due to enhanced drug half-life, and releasing the drug in a controlled fashion thereby increasing the concentration of the drug in cancer cells while minimizing off-target effects on healthy tissues (Wang et al., 2012; Dang and Guan, 2020). In addition, nanoparticles can also be linked with antibodies or peptides to improve specificity towards cancer cells that overexpress LRR1. Therefore, the use of nanoparticle delivery systems could potentially enhance the efficacy of the Lrr1 inhibitor and reduce toxicity on normal cells by selectively inhibiting cancer cell proliferation. But before stepping into the development of an specific inhibitor, further work is needed but we speculate that LRR1 can be a good candidate for treatment therapies. As a result, understanding the role of LRR1 in cancer biology can provide insights into developing potential therapeutic targets or in the development of prognostic markers for various cancer treatments in the future.

Similarly, TRAIP has been previously reported to exhibit overexpression or under expression in several cancer types (Zhou and Geahlen, 2009; Almeida et al., 2011; Soo Lee et al., 2016). Overexpression of TRAIP is negatively correlated with patient prognosis in liver cancer and its knockdown was found to inhibit malignancy in liver cancer cell lines (Guo et al., 2020). A very recent study carried out in Triple Negative Breast Cancer (TNBC) cell lines have also shown that silencing of TRAIP reduced invasion capabilities of TNBC cells and overexpression of TRAIP increased the invasion (Zheng et al., 2023). This indicates the potential of TRAIP as a therapeutic target.

Additionally, our preliminary mapping data of human Lrr1 (Figure 3.7) and TRAIP (Figure 5.15) genes have also unveiled mutations in these genes of several patient samples. However, it is important to note that TRAIP is involved in numerous other pathways too

(Chapard et al., 2014; Park et al., 2015; Feng et al., 2016; Harley et al., 2016; Hoffmann et al., 2016) and can exhibit various phenotypes. Therefore, the potential of both proteins as targets for therapies should be carefully investigated.

Furthermore, while defects in the initiation and elongation stages of replication have already been extensively studied and linked to cancer and other developmental disorders, it is clear that the precision and efficiency of replisome disassembly also play a vital role in preserving genome stability. Notably, factors that drive replication initiation and assembly of the helicase, such as Cdc7 kinase and TopBP1, have been explored as potential anti-cancer therapies (Montagnoli et al., 2008; Chowdhury et al., 2014). For example, Cdc7 kinase inhibitor - PHA-767491 - blocks DNA synthesis and phosphorylation of the helicase and has been demonstrated to have anti-tumor activity to suppress multiple cancer types. However, it is under clinical studies to use as a combination therapy to reduce the risk of relapse (Montagnoli et al., 2010; Irie and Sawa, 2023). In addition, recent evidences have demonstrated that the ATR inhibitor - AZD6738 - has progressed into phase II clinical trials, as a promising target for cancer therapeutics both as single agent and in combination therapy with chemotherapy, radiotherapy or immunotherapy (Barnieh et al., 2021).

Consequently, it is plausible that termination-specific ligases could also serve as potential drug targets, much like other small molecules designed to target E3 ligases in cancer-related pathways, exemplified by MDM2 with Milademetan (DS-3032b), SKP2 with Curcumin, and CRLs with Pevonedistat (MLN4924), all of which are currently undergoing Phase III clinical trials (Sampson et al., 2023).

Ongoing research in the field of drug development strongly indicates that therapies based on E3 ubiquitin ligases hold significant promise for cancer treatments (Robinson and

Ardley, 2004). Hence, gaining insight into the functions of these mechanisms under healthy conditions and understanding how these fail in human diseases are of paramount importance. Such knowledge can serve as a stepping-stone for future therapeutic strategies and bring significant advancements in medical treatment.

6.3 Conclusion

In conclusion, this thesis has provided important insights into the molecular mechanisms governing timely replisome disassembly by TRAIP in mitosis, which is a key regulator of genomic stability. It highlights the precision of TRAIP's activity, which is coordinated through distinct regulatory mechanisms involving post-translational modifications. However, some key questions remain, particularly concerning the regulation of TRAIP in S-phase and mitosis, specifically its interacting partners in different phases of the cell cycle, the ubiquitin chain types synthesised by TRAIP in each context, and if these ligases have multiple substrates besides Mcm7. Besides, exploring the regulation of additional players in replisome disassembly, such as p97 and its cofactors, provides platforms for further investigation. Moreover, exploring the coordination between Cul2^{Lrr1} and TRAIP pathways and understanding whether any crosstalk exists between these two E3 ligases is of importance. Additionally, further development of the mutational analysis of Lrr1 and TRAIP and correlating their implications in cancer development would also be of interest. Furthermore, performing high-throughput drug screening to identify any small molecule inhibitors that are specific to Cul2^{Lrr1} or TRAIP and testing their efficacy in blocking cancer cell proliferation is crucial. Finally, translating these findings into human cells could establish the evolutionary conservation of the regulation of these ubiquitin ligases. Overall, this thesis contributes some evidence to the current understanding of the termination stage of DNA replication, emphasizing the need to view DNA replication as

an integrated process with initiation, elongation and disassembly, all being critical for preserving genome stability.

Appendix

Publications

1. Moreno, S.P., Jones, R.M., Poovathumkadavil, D., et al. (2019) Mitotic replisome disassembly depends on TRAIP ubiquitin ligase activity. *Life Science Alliance*, 2 (2). doi:10.26508/lsa.201900390.
2. Tarcn, Z., Poovathumkadavil, D., Skagia, A., et al. (2022) The p97 segregase cofactor Ubxn7 facilitates replisome disassembly during S-phase. *The Journal of biological chemistry*, 298 (8). doi:10.1016/j.jbc.2022.102234.
3. Scaramuzza, S., Jones, R.M., Sadurni, M.M., Reynolds-Winczura, A., Poovathumkadavil, D., et al. (2023) TRAIP resolves DNA replication-transcription conflicts during the S-phase of unperturbed cells. *Nature Communications*, 14 (1): 1–20. doi:10.1038/s41467-023-40695-y.

Research Article



Mitotic replisome disassembly depends on TRAIP ubiquitin ligase activity

Sara Priego Moreno*, Rebecca M Jones*, Divyasree Poovathumkadavil, Shaun Scaramuzza, Agnieszka Gambus

We have shown previously that the process of replication machinery (replisome) disassembly at the termination of DNA replication forks in the S-phase is driven through polyubiquitylation of one of the replicative helicase subunits (Mcm7) by Cul2^{LRR1} ubiquitin ligase. Interestingly, upon inhibition of this pathway in *Caenorhabditis elegans* embryos, the replisomes retained on chromatin were unloaded in the subsequent mitosis. Here, we show that this mitotic replisome disassembly pathway exists in *Xenopus laevis* egg extract and we determine the first elements of its regulation. The mitotic disassembly pathway depends on the formation of K6- and K63-linked ubiquitin chains on Mcm7 by TRAIP ubiquitin ligase and the activity of p97/VCP protein segregase. Unlike in lower eukaryotes, however, it does not require SUMO modifications. Importantly, we also show that this process can remove all replisomes from mitotic chromatin, including stalled ones, which indicates a wide application for this pathway over being just a “backup” for terminated replisomes. Finally, we characterise the composition of the replisome retained on chromatin until mitosis.

DOI [10.26508/lsa.201900390](https://doi.org/10.26508/lsa.201900390) | Received 26 March 2019 | Revised 28 March 2019 | Accepted 29 March 2019 | Published online 12 April 2019

Introduction

Faithful cell division is the basis for the propagation of life and requires accurate duplication of all genetic information. DNA replication must be precisely regulated as unrepaired mistakes can change cell behaviour with potentially severe consequences, such as genetic disease, cancer, and premature ageing (Burrell et al, 2013). Fundamental studies have led to a step change in our understanding of the initiation of DNA replication and DNA synthesis, but until discovery of the first elements of the eukaryotic replisome disassembly mechanism in 2014 (Maric et al, 2014; Moreno et al, 2014), the termination stage of eukaryotic replication was mostly unexplored.

DNA replication initiates from thousands of replication origins. They are the positions within the genome where replicative helicases become activated and start unwinding DNA while moving in opposite directions, away from each other, creating two DNA replication forks.

The replicative helicase is composed of Cdc45, Mcm2-7 hexamer, and GINS complex (CMG complex) (Moyer et al, 2006); it is positioned at the tip of replication forks and forms a platform for replisome assembly (Replisome Progression Complex) (Gambus et al, 2006). Once established, the replication forks replicate chromatin until they encounter forks coming in opposite directions from neighbouring origins. At this point, termination of replication forks takes place. As CMG helicases travel on the leading strand templates at the forks, the strand encircled by converging helicases differs because of the antiparallel nature of the DNA molecule (Fu et al, 2011). The two converging helicases can therefore pass each other, allowing for completion of DNA synthesis. Finally, removal of the replisome from fully duplicated DNA is the last stage of termination of forks (Dewar et al, 2015). We have shown that in *Xenopus laevis* egg extract and in *Caenorhabditis elegans* embryos, this replisome removal in S-phase is driven by Cul2^{LRR1} ubiquitin ligase, which ubiquitylates Mcm7 within the terminated CMG complex (Sonneville et al, 2017). Such modified CMG is then recognised by p97/VCP segregase and removed from chromatin allowing for disassembly of the whole replisome built around the helicase (Moreno et al, 2014).

Most notably, we have shown that in *C. elegans* embryos, any helicase complexes that fail to be unloaded in the S-phase are alternatively unloaded in the prophase of mitosis (Sonneville et al, 2017). This potential backup mechanism can be detected when CUL-2^{LRR-1} activity is blocked and, like S-phase pathway, depends on the p97 segregase for unloading. Unlike the S-phase pathway, however, it requires an additional p97 cofactor UBXN-3/FAF1 and the SUMO-protease ULP-4 (Senp6/7 homologue in higher eukaryotes) (Sonneville et al, 2017). Interestingly, budding yeast do not possess this mitotic replisome disassembly pathway; cells lacking SCF^{Dia2} activity, the ubiquitin ligase responsible for Mcm7 ubiquitylation in *Saccharomyces cerevisiae*, accumulate post-termination replisomes on DNA until the next G1 of the next cell cycle (Maric et al, 2014). Our aim, therefore, was to determine if this mitotic replisome disassembly pathway is functioning in higher eukaryotes or if it is a phenomenon specific to *C. elegans* embryos. Here, we show that a mitotic replisome disassembly pathway does exist in *X. laevis* egg extract and determine the first elements of its

Institute for Cancer and Genomic Sciences, College of Medical and Dental Sciences, University of Birmingham, Birmingham, UK

Correspondence: a.gambus@bham.ac.uk

Sara Priego Moreno's present address is Salk Institute for Biological Studies, La Jolla, CA, USA

*Sara Priego Moreno and Rebecca M Jones contributed equally to this work

regulation. We show that only a restricted part of the replisome stays retained on chromatin through into mitosis in *Xenopus* egg extract. The disassembly of this replisome is independent of Cullin-type ubiquitin ligases but requires p97 segregase function. Mitotic replisome disassembly depends on K6- and K63-linked ubiquitin chains but not SUMO modifications. In addition, we show that stalled forms of helicase can also be unloaded using the same mechanism, suggesting that rather than being a backup pathway for the disassembly of terminated replisomes, this process is essential to remove any replisome from chromatin before cell division. Finally, we identify TRAIP ubiquitin ligase as essential for Mcm7 ubiquitylation and replisome disassembly in mitosis.

Results

X. laevis egg extract is a cell-free system, which has proven to be instrumental over the years in studies of DNA replication. *Xenopus* egg extract contains stockpiles of cell cycle factors which support efficient replication of DNA templates in vitro, with the recapitulation of most of the biochemical reactions that take place in living cells. To retain high synchronicity in our system, we restrict the replication reaction in the extract to only one round through blocking protein synthesis with cycloheximide, which blocks cyclins production and progression of extract into mitosis (Gillespie et al, 2012). However, to determine the existence of a mitotic replisome disassembly pathway in *Xenopus* egg extract we needed to allow for this progression. To achieve this, we supplemented the extract with recombinant cyclin after completion of DNA replication. *Xenopus* egg extract synthesises cyclin A1 (embryonic form of cyclin A), B1, and B2 (Minshull et al, 1989). Whereas the B family of cyclins has been shown to drive *Xenopus* meiotic division and oocyte maturation (Hochegger et al, 2001), both cyclin A and B have been shown to promote egg extract transition to mitosis (Strausfeld et al, 1996). We therefore purified His-tagged *X. laevis* cyclin A1 NΔ56 (hereafter: cyclin A1Δ) and added it to the extract upon completion of DNA replication, as described previously, to induce mitotic entry (Strausfeld et al, 1996). The N-terminal deletion to cyclin A1 prevents its degradation and ensures that the extract remains arrested in mitosis, reducing de-synchronisation of our experiments. In all of the experiments described below, we supplemented extract with cyclin A1Δ after completion of DNA replication. As a result, addition of cyclin A1Δ did not stimulate any more DNA synthesis (Fig S1A), but it did lead to progression into mitosis, as evidenced by breakage of the nuclear envelope, condensation of chromatin into chromosomes, and phosphorylation of Serine 10 on histone H3, which coincides with chromosome condensation (Fig S1B and C). Moreover, we could detect chromatin binding of condensin Smc2—another clear sign of the mitosis stage (Fig S1C).

To test if the replisome, which is retained on chromatin in S-phase, can be unloaded as cells enter mitosis, we needed to inhibit S-phase replisome disassembly. To achieve this, a replication reaction was set up in the interphase extract supplemented with Cullin ligase inhibitor MLN4924 to block Cul2^{LRR1} activity (Sonneville et al, 2017). Addition of MLN4924 to egg extract did not affect its ability to synthesise DNA as shown previously (Moreno

et al, 2014) and in Fig S1A. Moreover, the timing of replication completion was very reproducible within a batch of extract (Fig S1A). Throughout this article, we confirmed the timing of replication completion for every extract used. To do this, we determined the time point, after addition of sperm DNA, when no more ³²P-labelled dATP was incorporated into DNA. At this point, the components of the replisome were also seen to be unloaded from chromatin in the control samples, but retained on chromatin in those samples supplemented with Cullin ligase inhibitor MLN4924 (Fig S1D). We then optionally added cyclin A1Δ at the replication completion time (usually 90 min after sperm DNA addition), isolated chromatin at different time points during mitosis progression, and analysed chromatin-bound proteins by Western blotting (Fig 1A and B). The presence of the Cullin ligase inhibitor MLN4924 in the S-phase extract did not affect the DNA synthesis level nor induction of mitosis in our extract (Fig S1A and C). As seen in Fig 1B, in control samples without inhibition of replisome disassembly in S-phase, there were no CMG helicase components (hereafter represented by Cdc45 and Psf2 subunits) associated with chromatin at any times analysed, as replisome disassembly takes place before addition of cyclin A1Δ. Notably, we did detect low levels of PCNA bound to chromatin in late S-phase and mitosis as it remains on DNA after Okazaki fragment maturation and completion of replication, so as to aid post-replicative DNA repair (Gao et al, 2017). When replisome disassembly in S-phase was blocked with MLN4924 treatment, the CMG helicase remained associated with chromatin, as expected, and Mcm7 displayed low levels of ubiquitylation. Similar low levels of Mcm7 ubiquitylation have been shown previously upon both MLN4924 treatment and Cul2 immunodepletion (Moreno et al, 2014; Sonneville et al, 2017) and could indicate residual activity of the Cul2^{LRR1} ligase or activity of yet another unidentified ligase. Importantly, upon addition of cyclin A1Δ, Cdc45, Psf2, and ubiquitylated Mcm7 were efficiently unloaded (Fig 1B). This result indicates that indeed the mitotic replisome disassembly pathway is evolutionarily conserved and that, unlike the S-phase pathway, it does not require the activity of Cullin-type ubiquitin ligases because the Cullin ligase inhibitor MLN4924 was present throughout the reaction. The continuous presence of unmodified Mcm7 in our samples is a result of the high quantity of DNA used in our experiments. This allows us to clearly detect the replication fork components and ubiquitylated Mcm7 by Western blotting. Because of the high quantity of DNA used, some of the nuclei were not able to form completely and failed to initiate replication, resulting in the isolation of unfired Mcm2-7 complexes, as shown previously (Moreno et al, 2014). However, when we added a much lower quantity of DNA and used minimal licensing conditions (addition of recombinant geminin, 2 min after sperm DNA), we could detect unloading of Mcm7 in mitosis together with Cdc45 and Psf2 (Fig S2A).

Next, we tested whether the mitotic replisome disassembly pathway requires the activity of the p97 segregase. We followed the experimental setup as before but now optionally added the inhibitor of p97, NMS873, along with cyclin A1Δ to inhibit p97 activity during mitosis. Addition of NMS873 to the extract together with cyclin A1Δ did not affect extract transition to mitosis (Fig S2B). In these conditions, the retained replisome was unloaded upon cyclin A1Δ addition in the absence but not in the presence of the p97

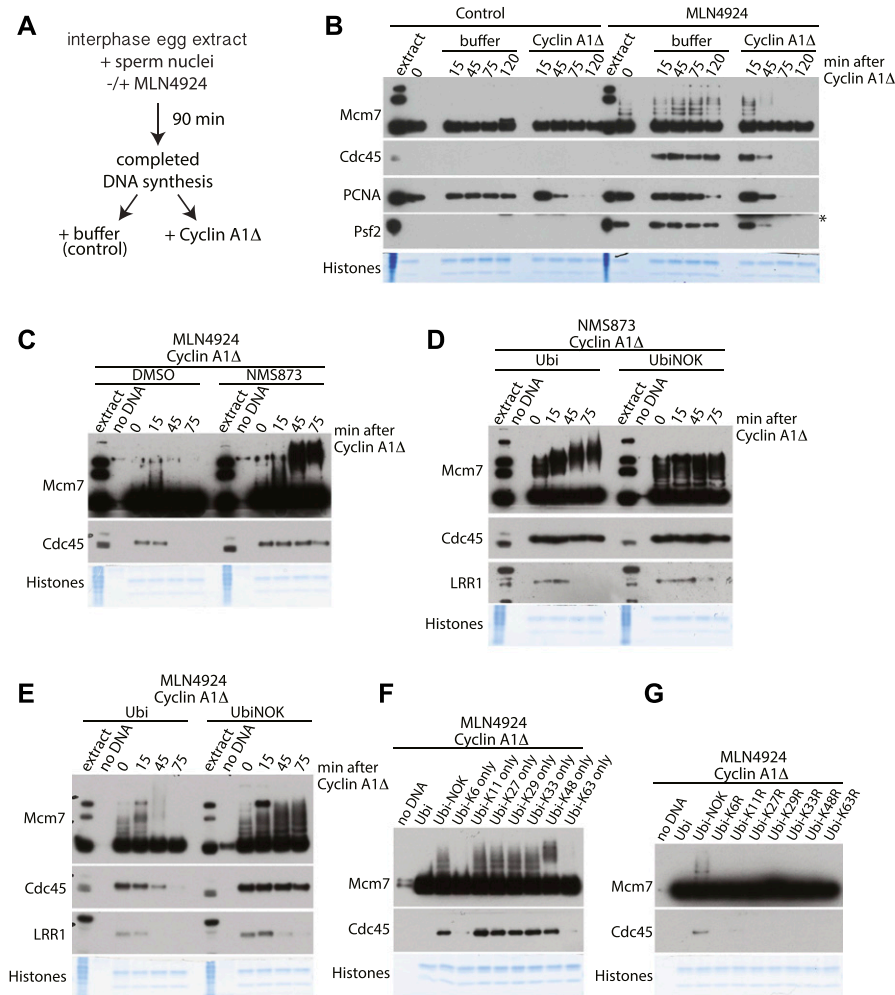


Figure 1. Mcm7 is ubiquitylated with K6 and K63 ubiquitin chains in mitosis and removed from chromatin by p97 segregase.

(A) Experimental design for driving egg extract into mitosis. (B) Experiment following design in (A). DNA was replicated to completion (90 min) in egg extract supplemented optionally with a Cullin ligase inhibitor MLN4924. After completion of the replication reaction, cyclin A1Δ was optionally added to the extract to drive extract into mitosis. Chromatin was isolated at indicated time points after cyclin A1Δ addition and chromatin samples analysed by Western blotting with the indicated antibodies. Time "0" sample was isolated at the replication completion time when cyclin A1Δ was added to the extract. Colloidal Coomassie-stained histones serve as a quality and loading control. An asterisk "*" by the Psf2 blot indicates a band of cyclin A1Δ that is recognised by Psf2 antibody. (C) The replication reaction was completed in the presence of Cullin ligase inhibitor MLN4924 and driven into mitosis by addition of cyclin A1Δ. At the same time as cyclin A1Δ, half of the sample was supplemented additionally with p97 inhibitor NMS873. Chromatin samples were isolated at indicated time points and analysed as in (B). A sample without DNA addition (no DNA) was processed alongside others as a chromatin specificity control. (D) The replication reaction was completed in the presence of p97 inhibitor NMS873 and driven into mitosis by addition of cyclin A1Δ. At the same time as cyclin A1Δ, the samples were supplemented with recombinant wt ubiquitin or UbiNOK. Chromatin samples were analysed as above. (E) Experiment as in (D) but replication reaction was carried out in the presence of Cullin ligase inhibitor MLN4924 instead of p97 inhibitor NMS873. (F, G) Replication reaction was completed in the presence of Cullin ligase inhibitor MLN4924 and driven into mitosis by addition of cyclin A1Δ. At the same time as cyclin A1Δ addition, the extract was supplemented with the indicated mutants of ubiquitin. Chromatin was isolated at 75 min after cyclin A1Δ addition and analysed by Western blotting as above. Source data are available for this figure.

inhibitor, indicating that indeed p97 does play an essential role in promoting mitotic replisome disassembly (Fig 1C). We could also see an analogous result if the p97 inhibitor was present throughout the two stages of the cell cycle as the only way to block replisome disassembly (Fig S2C). Importantly, the presence of p97 inhibitor NMS873 throughout interphase does not impede DNA synthesis (Sonneville et al, 2017) and does not induce additional DNA synthesis when combined with addition of cyclin A1Δ (Fig S2D).

Interestingly, when mitotic unloading of replisome was blocked with p97 inhibitor, we could clearly see accumulation of highly modified forms of Mcm7 on chromatin (Figs 1C and S2C). To examine whether these modifications were due to further ubiquitylation of Mcm7 in mitosis, we blocked S-phase and mitotic replisome disassembly by addition of p97 inhibitor from the beginning of the replication reaction, induced mitosis after completion of DNA synthesis, and optionally supplemented extract with a high concentration of wt ubiquitin (Ubi) or a chain-terminating mutant of ubiquitin with all lysines mutated (UbiNOK). Supplementation of extract with UbiNOK at the same time as cyclin A1Δ addition allowed for normal entry into mitosis as indicated by nuclear envelope breakdown (Fig S2E). Addition of Ubi allowed for accumulation of highly modified Mcm7 on chromatin in mitosis as before (Fig 1D), but

UbiNOK blocked further modifications of Mcm7, leaving only the chains which were built previously in S-phase (Fig 1D). To determine whether this further Mcm7 polyubiquitylation in mitosis is essential for mitotic replisome disassembly, we repeated the experiment with addition of wt Ubi or UbiNOK, but this time only in the presence of the Cullin ligase inhibitor MLN4924 from the start of the reaction (Fig 1E). Indeed, addition of UbiNOK to mitotic extract did block disassembly of the replisome (as shown by permanent Cdc45 chromatin binding), suggesting that further Mcm7 polyubiquitylation is required for mitotic replisome unloading. We also observed that LRR1 (the substrate-specific subunit of Cullin 2, targeting Mcm7 in S-phase) dissociates from chromatin in mitosis irrespectively of replisome disassembly, in agreement with the finding that it does not play an essential role in this pathway (Fig 1D and E). Importantly, these results indicate that a previously unreported ubiquitin ligase is needed for Mcm7 ubiquitylation and replisome disassembly in mitosis.

As the ubiquitin ligase acting in the mitotic pathway differed from that of the S-phase pathway, we decided to test whether the type of ubiquitin chains built on Mcm7 in mitosis also differed. To determine which ubiquitin chains are required for mitotic Mcm7 ubiquitylation and replisome disassembly, we supplemented

extract with Cullin ligase inhibitor MLN4924, allowed for completion of DNA synthesis, and subsequently induced mitosis along with addition of a series of ubiquitin mutants that have only one lysine left in their sequence (Fig 1F). We observed that only wt ubiquitin and ubiquitin containing only lysine 6 (K6 only) or lysine 63 (K63 only) could support mitotic replisome disassembly (as visualised by the absence of Cdc45 on chromatin at 75 min after inducing mitosis) (Fig 1F). Interestingly, chains linked through lysine 48 (K48), which are responsible for S-phase unloading (Moreno et al, 2014), could still be attached to Mcm7 in mitosis (upshift of modified Mcm7 forms), but they could not support unloading of the replisome as Cdc45 remained associated with chromatin. In a reciprocal experiment, we used a series of ubiquitin mutants with only one of the lysines within ubiquitin mutated (Fig 1G). All of the mutants used, apart from the UbiNOK control mutant, supported disassembly of the replisome, suggesting that either K6 or K63 can fulfill the mitotic pathway requirements (Fig 1G).

Having established that the type of ubiquitin chains and the type of ubiquitin ligase used by the mitotic pathway of replisome disassembly were different to those acting in the S-phase pathway, our aim was to identify this ubiquitin ligase. To this end, we decided to immunoprecipitate the replisome retained on mitotic chromatin and analyse all the interacting proteins by mass spectrometry. We set up a replication reaction in the presence of caffeine and the p97 inhibitor NMS873 and induced mitosis upon completion of DNA synthesis (90 min). Neither of the treatments affected the extract's ability to synthesise DNA (Fig S3A). We then immunoprecipitated Mcm3 from mitotic chromatin and analysed the interacting factors by mass spectrometry. First, we determined which components of the replisome are still retained on chromatin in mitosis. For this, we compared the replisome components retained on chromatin in mitosis with S-phase post-termination replisome, reported previously (Sonnevile et al, 2017) (Fig 2A and B). Interestingly, although inhibition of replisome disassembly in the S-phase led to accumulation of the whole replisome on chromatin (Sonnevile et al, 2017), only a selection of replisome components stayed on chromatin in mitosis. All of the lagging strand components of the replisome were lost, as were Mcm10 and Claspin, whereas levels of Ctf4/And-1, Timeless, Tipin, and Pol epsilon were also reduced (Fig 2A and B). This suggests that only components directly interacting with the CMG remained accumulated around it through to mitosis, whereas others, more peripheral to CMG, could dissociate over time.

The level of histone chaperone FACT (Spt16 and SSRP) stayed the same between S-phase and mitosis. This suggests that the retained replisome in mitosis has the potential ability to move through chromatin as FACT is likely to displace nucleosomes in front of such a replisome. We could see also that Cul2^{LRR1}, which strongly accumulated in the S-phase post-termination replisome, is not a major component of the mitotic replisome, as expected from previous data (Fig 1D and E).

Finally, we detected two other ubiquitin ligases interacting with the mitotic helicase: TRAP1 and RNF213. More specifically, we found that TRAP1 interacts with the post-termination replisome in S-phase, but it is enriched in mitosis, whereas RNF213 is a minor interactor of only the mitotic replisome (Fig 2A). The TNF-receptor-associated factor (TRAF)-interacting protein (TRAP1, also

known as TRIP or RNF206) was originally identified through its ability to bind TRAF1 and TRAF2 and shown to inhibit NFκB activation (Lee et al, 1997). It has been since shown that TRAP1 is an E3 ubiquitin ligase, which is essential for cell proliferation (Besse et al, 2007; Park et al, 2007), and which is required for resolution of replication stress (Feng et al, 2016; Harley et al, 2016; Hoffmann et al, 2016) and for regulation of the spindle assembly checkpoint during mitosis (Chapard et al, 2014). TRAP1 is ubiquitously expressed, with its expression regulated by E2F transcription factors and protein stability controlled by the ubiquitin proteasome pathway—as a result, the protein level of TRAP1 peaks in the G2/M stage of the cell cycle (Chapard et al, 2015). On the other hand, RNF213 (mysterin) is a large (591 kD) ATPase/E3 ligase, which is mostly known as being a susceptibility gene for moyamoya disease (cerebrovascular disease) (Kamada et al, 2011; Liu et al, 2011). Of note, RNF213^{-/-} mice do not show any apparent health problems (Kobayashi et al, 2013; Sonobe et al, 2014) and more recently, RNF213 was shown to globally regulate (α-ketoglutarate)-dependent dioxygenases (α-KGDDs) and non-mitochondrial oxygen consumption (Banh et al, 2016). To support our mass spectrometry data, we tested a number of antibodies by Western blotting against RNF213 and TRAP1 to confirm their association with the chromatin-bound replisome in mitosis. Although we were unsuccessful with detection of any signal for RNF213, we were able to show that TRAP1 interacts with the replisome retained on chromatin in mitosis (Figs 2C and S3B).

After confirming that the ubiquitin ligase TRAP1 is the likely candidate responsible for Mcm7 ubiquitylation and replisome disassembly in mitosis, we next characterised TRAP1 chromatin binding dynamics during the two cell cycle stages and the replisome disassembly process. We found that although TRAP1 associated weakly with the S-phase chromatin at times when forks progress through chromatin and replicate DNA, it accumulated strongly on the S-phase chromatin upon inhibition of replisome disassembly with the p97 inhibitor NMS873 (Fig 3A). Importantly, TRAP1 also accumulated on mitotic chromatin when replisome disassembly was inhibited with the p97 inhibitor, following the same pattern as replisome components (Fig 3B). To test whether TRAP1 is indeed the ubiquitin ligase responsible for unloading of replisome in mitosis, we aimed to inhibit TRAP1 enzymatic activity in our extract. As we were unable to efficiently immunodeplete TRAP1 from the egg extract with any of the antibodies tested, we decided to use a dominant-negative, ligase-dead mutant of TRAP1 to out-compete the endogenous TRAP1. To this end, we purified recombinant His/SUMO-tagged *X. laevis* TRAP1, both wt and the C25A RING domain mutant, which has been shown to disrupt TRAP1 ubiquitin ligase activity (Besse et al, 2007; Chapard et al, 2014) and (Fig S3C). We blocked disassembly of the replisome in S-phase by addition of the Cullin ligase inhibitor MLN4924 and drove extract into mitosis by addition of cyclin A1Δ, when we added recombinant wt or mutant TRAP1. Addition of neither wt nor mutant TRAP1 affected the extract's ability to enter mitosis upon cyclin A1Δ addition, as shown through nuclear envelope breakdown (Fig S3D) and Smc2 chromatin loading (Fig 3C and D). As shown in Fig 3C, addition of the enzymatic dead mutant of TRAP1 into mitotic extract inhibits unloading of post-termination replisomes retained on chromatin, whereas addition of wt TRAP1 does not have such an effect. To confirm that enzymatic dead TRAP1 indeed affects replisome

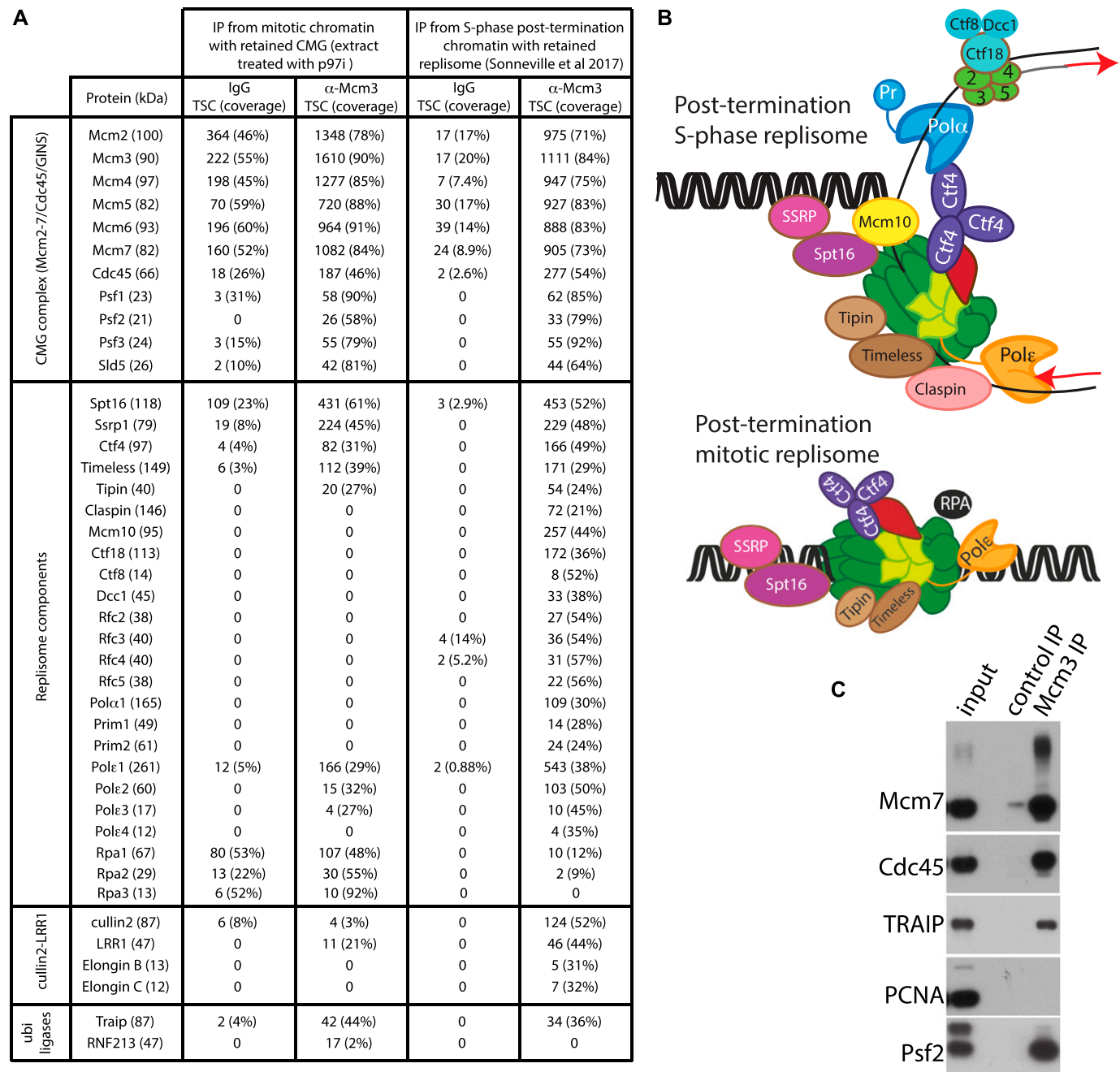


Figure 2. Composition of the replisome retained on mitotic chromatin.

(A) The replication reaction was completed in egg extract supplemented with caffeine and p97 inhibitor NMS873. The extract was then driven into mitosis by addition of cyclin A1 Δ . Chromatin was isolated at 60 min after cyclin A1 Δ addition and chromatin proteins released from DNA. The DNA synthesis kinetics are provided in Fig S3A. Antibodies against Mcm3 (or control IgG) were used to immunoprecipitate replisomes, and the immunoprecipitated samples were analysed by mass spectrometry. The total spectral count for each identified replisome component is presented together with sequence coverage of analysed peptides. The results for this analysis of mitotic retained replisome are compared with the S-phase post-replication replisome reported in Sonnevile et al (2017). (B) Schematic representation of the data presented in (A). (C) A small proportion of the material from the mitotic Mcm3 IP experiment in (A) was analysed by Western blotting with indicated antibodies.

unloading through ubiquitylation of Mcm7 in mitosis, we repeated this experiment but supplemented the mitotic extract also with p97 inhibitor NMS873 to inhibit unloading of ubiquitylated Mcm7. Fig 3D shows that addition of enzymatic dead TRAIP, but not wt TRAIP, perturbs mitotic ubiquitylation of Mcm7 as the ubiquitylated forms

of Mcm7 remain very close in size to the chains built on Mcm7 already in S-phase (15-min time point). The same prevention of ubiquitylation of Mcm7 in mitosis was observed when we used recombinant GST-tagged TRAIP C25A mutant, but not wt GST-TRAIP (Fig S3F). These results suggest that the recombinant mutant of

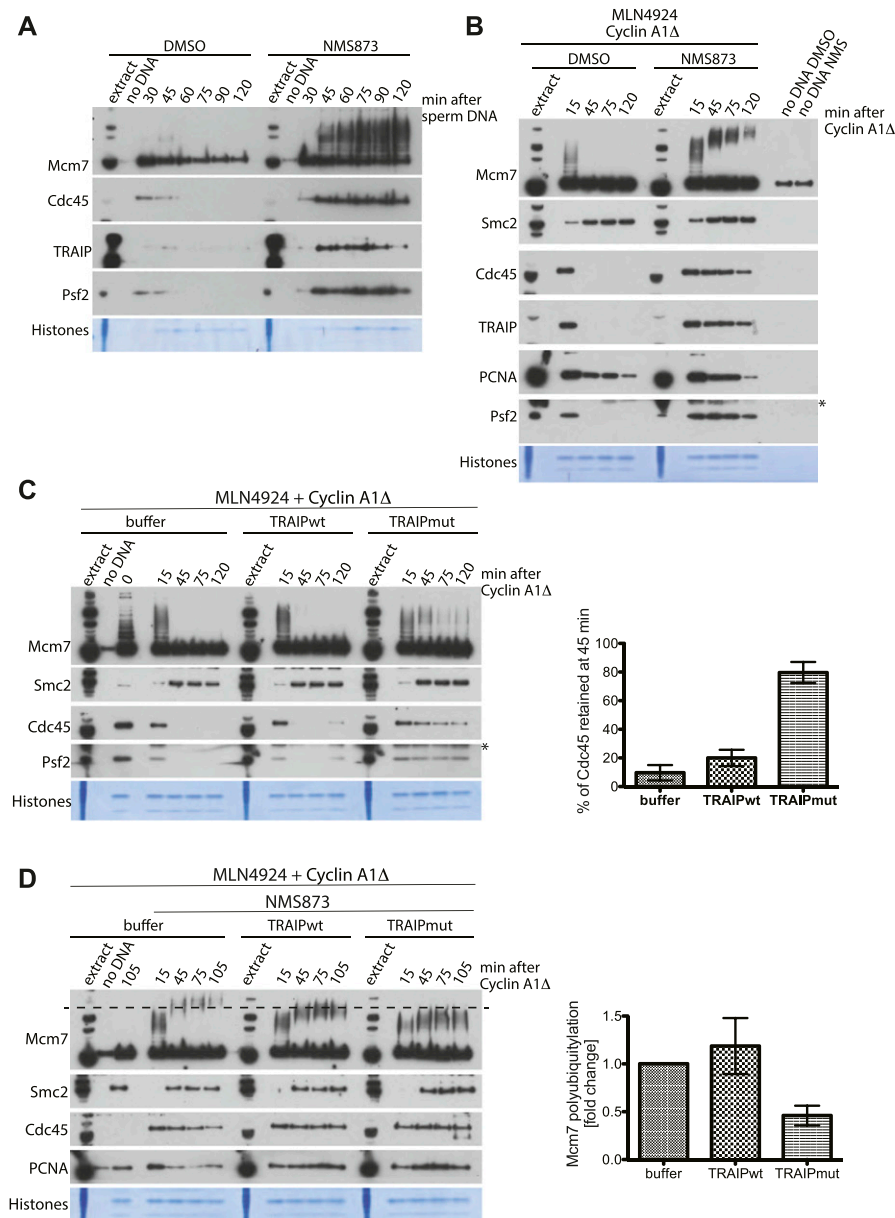


Figure 3. TRAIPI ubiquitin ligase drives replisome disassembly in mitosis.

(A) Sperm DNA was replicated in egg extract optionally supplemented with p97 inhibitor NMS873. Chromatin samples were isolated during the reaction at indicated time points and analysed as in Fig 1. Colloidal Coomassie-stained histones serve as a quality and loading control. A sample without DNA addition (no DNA) was processed alongside others as a chromatin specificity control. **(B)** Experiment analogous to Fig 1C but analysed with indicated antibodies. An asterisk “*” by the Psf2 blot indicates the band of cyclin A1Δ that is recognised by the Psf2 antibody. **(C)** (left) - The replication reaction was completed in the presence of Cullin ligase inhibitor MLN4924 and driven into mitosis by addition of cyclin A1Δ. At the same time as cyclin A1Δ, the samples were supplemented optionally with LFB1/50 buffer, wt His/SUMO-tagged TRAIPI, or RING-mutant (C25A) TRAIPI to a final concentration of 50 μg/ml. Chromatin samples were isolated at indicated time points and analysed with indicated antibodies. Time “0” sample was isolated at the replication completion time when cyclin A1Δ and recombinant TRAIPI were added to the extract. An asterisk “*” by the Psf2 blot indicates the band of cyclin A1Δ that is recognised by the Psf2 antibody. (right) - The level of retained Cdc45 on chromatin was quantified at 15 and 45 min in each condition and the percentage of the 15 min signal still retained on chromatin at 45 min calculated. The graph represents a mean of three independent experiments with SEM. **(D)** (left) - The experiment was performed as in (C) but with addition of p97 inhibitor NMS873 at the same time as cyclin A1Δ to block ubiquitylated Mcm7 on chromatin. His/SUMO-tagged TRAIPIwt and ligase dead mutant were added to a final concentration of 100 μg/ml. The sample isolated at 105 min without NMS873 provides a control for the unloading without p97 inhibition. The dashed line on the Mcm7 blot runs through the middle of the ubiquitylation signal for Mcm7 in mitosis in the control (buffer) sample to aid comparison of chain lengths between samples. (right) - The Mcm7 polyubiquitylation signal was quantified for each condition as explained in materials and methods and an example provided in Fig S3E. The graph presented here shows the mean fold change of Mcm7 polyubiquitylation signal at 45 min after cyclin A1Δ addition over three independent experiments with SEM.

TRAIPI successfully competed with endogenous TRAIPI protein and that ubiquitin ligase activity of TRAIPI is needed for Mcm7 ubiquitylation and disassembly of post-termination replisome in mitosis. The low level of Mcm7 ubiquitylation visible in samples supplemented with TRAIPI mutant is most likely due to the fact that there is still endogenous active TRAIPI in the extract.

To fully understand the requirement for ubiquitin-like modifications during mitotic replisome disassembly in vertebrates, we aimed to establish whether SUMOylation plays any role in this process as ULP-4 is essential for mitotic helicase disassembly in *C. elegans* embryos. To this end, we decided to inhibit or stimulate SUMOylation during mitosis and assess its effect on replisome disassembly. First, we observed that the late S-phase chromatin is full of SUMO2ylated factors and that levels of these proteins go down over time upon

entry into mitosis (Fig 4). To inhibit SUMOylation, we supplemented the mitotic extract with the recombinant active domain of SENP1, which acts as a potent nonspecific deSUMOylating enzyme. Addition of SENP1 indeed wiped out all the SUMO2ylation (Fig 4A) and SUMO1ylation (Fig S5A), but disassembly of the mitotic replisome is not affected (Fig 4A). We also stimulated SUMOylation through addition of a high concentration of recombinant SUMO1 or SUMO2 (Fig S4). In both cases, despite a clear increase of SUMO signal on chromatin, unloading of the mitotic replisome was not affected. Finally, we also blocked de-SUMOylation with SUMO2-VS, a derivative of SUMO2, which binds to the active site of SENPs and blocks their activity. Again, we observed strong accumulation of SUMO2ylated products in the extract and on chromatin without affecting mitotic replisome disassembly (Fig 4B). Interestingly, despite inhibition of

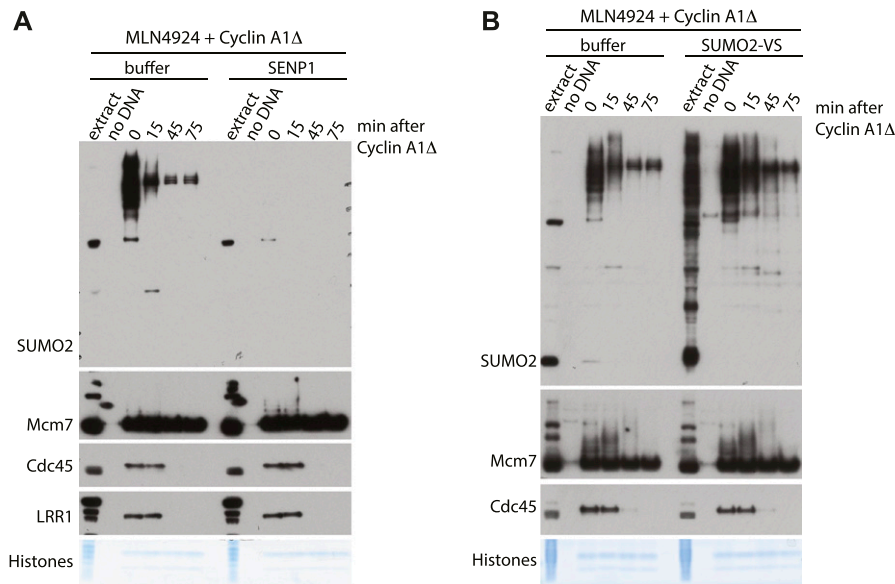


Figure 4. SUMOylation is not required for mitotic replisome disassembly.

(A) The replication reaction was completed in the presence of Cullin ligase inhibitor MLN4924 and driven into mitosis by addition of cyclin A1Δ. At the same time as cyclin A1Δ, half of the sample was supplemented additionally with the active domain of SENP1. Chromatin samples were isolated at indicated time points and analysed as in Fig 1. Colloidal Coomassie-stained histones serve as a quality and loading control. A sample without DNA addition (no DNA) was processed alongside others as a chromatin specificity control. **(B)** As in (A) but instead of supplementing extract with SENP1, it was supplemented with SENPs inhibitor SUMO2-VS.

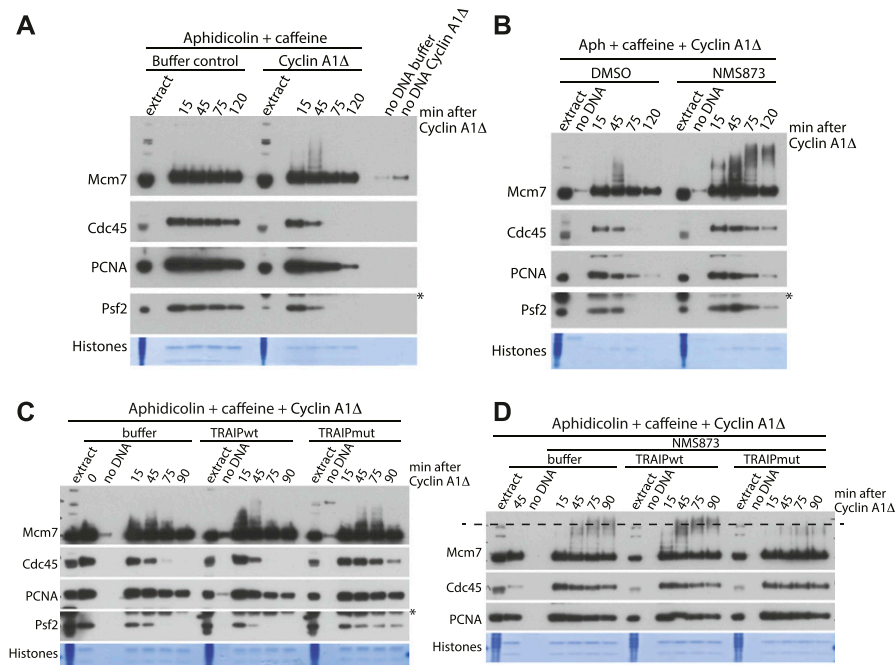
de-SUMOylating enzymes, most of the SUMO signal is still disappearing from chromatin during progression of mitosis, indicating that the SUMOylated proteins are unloaded from chromatin throughout mitosis rather than being de-SUMOylated. In conclusion, we determined that SUMO modifications do not play an essential role in the mitotic replisome disassembly pathway in *Xenopus* egg extract. In an analogous way, we have also shown that they do not play a role during the S-phase replisome disassembly pathway (Fig S5A and B).

Finally, we set out to determine whether this mitotic replisome disassembly pathway was a mere “backup” pathway for replisomes that terminated in S-phase but failed to be unloaded, or if it has a more generic ability to remove any replication machinery still remaining on chromatin in mitosis. To test such a possibility, we stalled replisomes on chromatin by addition of DNA polymerase inhibitor aphidicolin to the egg extract during the DNA replication reaction. To accumulate such replisomes in large numbers, we also supplemented the extract with caffeine so as to block checkpoint activation and fire origins uncontrollably. Upon accumulation of such blocked replisomes, we supplemented the reaction optionally with cyclin A1Δ at 90 min to induce mitotic entry (Fig 5A). Addition of cyclin A1Δ did not stimulate any more DNA synthesis in our samples (Fig S6). Interestingly, active replisomes remained associated with chromatin throughout the experiment in late S-phase (buffer), with no indication of Mcm7 ubiquitylation as expected (Moreno et al, 2014). Upon addition of cyclin A1Δ, however, Mcm7 became ubiquitylated and replisomes were unloaded (Fig 5A, cyclin A1Δ), although we did observe a slight delay in both of these processes compared with terminated replisomes (compare Fig 5A with Fig 1B). Such a delay is likely due to the fact that with no prior ubiquitylation of Mcm7 in S-phase, it takes longer for ubiquitin chains to be built in mitosis. We also determined that unloading of stalled replisomes requires the activity of p97 segregase, as unloading is inhibited in the presence of the p97 inhibitor NMS873 (Fig 5B). Finally, to test whether the activity of TRAIP ubiquitin ligase is needed for the

unloading of stalled replisomes, we added recombinant wt or enzymatic dead TRAIP to mitotic extract and observed its effect on unloading of such stalled replisomes. As with post-termination replisomes (Fig 3C and D), the enzymatic dead mutant of TRAIP inhibited unloading of stalled helicase (Fig 5C), whereas we also observed a clear reduction in the ubiquitylation of stalled Mcm7 (Fig 5D). From these observations, we can thus say that neither prior modification of Mcm7 in S-phase nor the “terminated” conformation of the helicase are essential for mitotic modification of Mcm7 by TRAIP and subsequent replisome disassembly.

Discussion

We have presented here the existence of a mitotic pathway of replisome disassembly in *X. laevis* egg extract. One immediate question is why would the cells need a mitotic pathway of replisome disassembly? Traditionally, it is perceived that all DNA metabolism should be finished before cells enter mitosis. According to this model, the G2 phase of the cell cycle is there to ensure that all DNA replication and damage repair are completed before chromosome condensation and segregation during mitosis. The last decade provided, however, much evidence that this is not the case: unreplicated DNA is detected in many human cells in mitosis; DNA synthesis can proceed during mitosis (mitotic DNA synthesis—MiDAS); under-replicated DNA can lead to the formation of ultrafine bridges in anaphase and structures in the G1 stage of the next cell cycle that are bound by 53BP1 protein (53BP1 bodies) (Liu et al, 2014; Minocherhomji et al, 2015; Moreno et al, 2016). Genome-wide, such unreplicated regions correlate with common fragile sites, which are chromosomal loci responsible for the majority of the rearrangements found in cancer cells (Bhowmick & Hickson, 2017). These unreplicated fragments of DNA result from replication forks not finishing replication and such forks, with their associated replisomes,



His/SUMO-tagged TRAIpwt and mutant were added to a final concentration of 100 $\mu\text{g}/\text{ml}$. The sample isolated at 45 min without NMS873 provides a control for the replisome unloading without p97 inhibition. The dashed line on the Mcm7 blot runs through the middle of the ubiquitylation signal for Mcm7 in mitosis in the control (buffer) sample to aid comparison of chain lengths between samples.

Figure 5. Mitotic unloading of stalled helicases.

(A) The replication reaction was performed in egg extract supplemented with DNA polymerase inhibitor aphidicolin and checkpoint inhibitor caffeine. After 90 min of reaction, cyclin A1Δ was optionally added, and the chromatin samples were isolated during the reaction at indicated time points and analysed as in Fig 1. Colloidal Coomassie-stained histones serve as a quality and loading control. A sample without DNA addition (no DNA) was processed alongside others as a chromatin specificity control. An asterisk “*” by the Psf2 blot indicates the band of cyclin A1Δ that is recognised by the Psf2 antibody. (B) The inhibition of stalled replisomes was achieved as in (A), and the extract was driven into mitosis by addition of cyclin A1Δ and optional supplementation with p97 inhibitor NMS873. The chromatin samples were analysed as in (A). (C) Replication reaction was performed with addition of aphidicolin and caffeine, at 90 min, cyclin A1Δ was added and optionally: buffer, His/SUMO-TRAIpwt, or ligase dead His/SUMO-TRAIpmut (C25A) to a final concentration of 50 $\mu\text{g}/\text{ml}$. The chromatin samples were isolated at indicated time points and analysed with indicated antibodies. Time “0” sample was isolated at the replication completion time when cyclin A1Δ and recombinant TRAIp were added to the extract. (D) The experiment was performed as in (C) but with addition of p97 inhibitor NMS873 at the same time as cyclin A1Δ to accumulate ubiquitylated forms of Mcm7 on chromatin.

are subsequently retained on chromatin into mitosis. It is likely that these unreplicated DNA fragments must be processed in mitosis to ensure correct chromosome segregation, and this processing will involve replisome unloading and fork remodelling—hence the need for a process of replisome disassembly in mitosis.

TRAIp is a pleiotropic ubiquitin ligase involved in numerous cellular processes. It is clear that TRAIp is essential for appropriate repair of DNA damage in many forms: mitomycin C-induced inter-strand crosslinks; damage caused by treatments with camptothecin (Hoffmann et al, 2016), UV (Harley et al, 2016) and hydroxyurea (Feng et al, 2016); as well as for translesion DNA synthesis (Wallace et al, 2014). TRAIp has also been reported to be an important regulator of the spindle assembly checkpoint and regulates mitotic progression (Chapard et al, 2014; Park et al, 2015). For most of these processes, the ubiquitin ligase activity of TRAIp is essential, but the substrate (s) modified by TRAIp is not known.

In support of our observation that TRAIp interacts weakly with the S-phase chromatin when replication forks replicate DNA (Fig 3A), TRAIp has been shown to interact with nascent DNA in unperturbed S-phase in human cells through nascent chromatin capture (Hoffmann et al, 2016), but TRAIp knockdown does not significantly affect replication progression and overall DNA synthesis rates (Harley et al, 2016; Hoffmann et al, 2016). Upon DNA damage, TRAIp relocates from nucleoli to sites of damage in a manner dependent on a PCNA interacting box (PIP-box), present at the C terminus of TRAIp (Feng et al, 2016; Hoffmann et al, 2016). Loss of TRAIp was suggested to interfere with the reconfiguration of stalled replication forks (possibly through unloading of PCNA) (Hoffmann et al, 2016), as further inhibition of proteasomal degradation in the absence of TRAIp did not exacerbate the levels of hydroxyurea-

induced fork stalling. This suggested that degradation of a TRAIp ubiquitylation substrate is not the cause of this phenotype (Feng et al, 2016; Hoffmann et al, 2016). Interestingly, cells expressing the ΔRING mutant of TRAIp as the only TRAIp version, are as sensitive to mitomycin C as TRAIp knockdown cells, while ΔPIP TRAIp cells are only mildly sensitive. This indicates that even without PCNA interaction, TRAIp can still find its targets at the replication forks (Hoffmann et al, 2016). With the data presented here, identifying TRAIp as the ubiquitin ligase needed for Mcm7 ubiquitylation during mitosis, it is interesting to speculate that TRAIp can play an analogous role during DNA damage repair, that is, to stimulate replisome unloading and fork remodeling. Indeed, recently TRAIp has been shown to ubiquitylate CMG during inter-strand crosslink (ICL) repair for replisome unloading (Wu et al, 2019).

Our data are consistent with a model in which TRAIp drives mitotic replisome disassembly by promoting Mcm7 modification with K6- and K63-linked ubiquitin chains. Although there is no previous experimental evidence that TRAIp can support such ubiquitin linkages in vivo, in vitro assays have shown that TRAIp works well with conjugating enzymes (E2s) UbcH5a,b, and c (but not UbcH2, H3, H6, H7, or Ubc13+Uev1A) (Besse et al, 2007) and (Fig S3C). Interestingly, UbcH5a was shown to support formation of ubiquitin chains with no specific topology (Windheim et al, 2008). It is, therefore, plausible that TRAIp/UbcH5 can effectively produce chains of different linkages to support mitotic replisome disassembly.

Replisome disassembly in S-phase is driven by Mcm7 ubiquitylation, specifically with K48-linked ubiquitin chains. In mitosis, however, K48-linked chains are not functional and unloading is driven instead by K6- and K63-linked chains. We know that p97, in complex with Ufd1 and Npl4 cofactors, is responsible for

unloading of the replisome in S-phase (Moreno et al, 2014; Maric et al, 2017; Sonnevile et al, 2017). Although p97 is well known for processing substrates ubiquitinated with K48-linked ubiquitin chains (Meyer et al, 2012), less is known about its contribution in processing other ubiquitin linkages. Interestingly, a recent study shows that upon inhibition of p97 activity, human cells accumulate K6-, K11-, K48- and, to a lesser extent, K63-linked ubiquitin chains (Heidelberger et al, 2018). Moreover, out of five tested p97 cofactors, all were found to associate with K11 chains, four with K48 chains, and three with K63 chains (Alexandru et al, 2008). p97 cofactors are known also to interact with ubiquitin-like modifiers, for example, Nedd8 and Atg8 (reviewed in Meyer (2012)). Finally, p97 was also shown to bind more readily to branched K11-K48 chains than to K11 or K48 chains on their own (Meyer & Rape, 2014). These proteome-wide data imply that the role of p97 does indeed extend beyond recognition of K48-chain-modified substrates, although currently, little is known about its interaction with K6 chains.

Finally, we have shown that in the *Xenopus* system, neither the S-phase (Fig S5) nor the mitotic replisome disassembly requires SUMO modifications (Figs 4 and S4) in contrast to *C. elegans* embryos where ULP-4 is required for mitotic unloading (Sonneville et al, 2017). This requirement may be specific to worm embryos, require ULP-4 protein but not its enzymatic activity, or it may regulate an indirect process that is not well recapitulated in the egg extract cell-free system. Of note, it has been suggested recently that SUMOylation of TRAIP can regulate its stability and ability to move to the nucleus (Park et al, 2016), but this may not be present in the egg extract.

Perturbations in DNA replication initiation and elongation leading to genomic instability are well linked with genetic disorders and can drive cancer development. The disruption of replisome disassembly is, therefore, highly likely to be detrimental to human health too. Although so far we have no solid data to support this claim, previous studies with TRAIP do suggest this to be the case: homozygous *TRAIP* knockout mouse embryos die shortly after implantation because of proliferation defects (Park et al, 2007); mutations in human *TRAIP* lead to primordial dwarfism (Harley et al, 2016); overexpression of human *TRAIP* has been reported in basal cell carcinomas (Almeida et al, 2011) and breast cancer (Yang et al, 2006; Zhou & Geahlen, 2009); and reduced nuclear expression of *TRAIP* was associated with human lung adenocarcinoma (Soo Lee et al, 2016). The fact that cells have evolved multiple pathways to ensure timely replisome disassembly supports the notion of the vital importance of this process for cell biology, and time will tell whether targeting *Mcm7* and replisome disassembly in mitosis is the key mechanism leading to any of these disease phenotypes.

Materials and Methods

Inhibitors

Caffeine (C8960; Sigma-Aldrich) was dissolved in water at 100 mM and added to the extract along with demembranated sperm nuclei at 5 mM. MLN4924 (A01139; Active Biochem) was dissolved in DMSO at 20 mM and added to the extract 15 min after addition of sperm nuclei at 10 μ M. NMS873 (17674; Cayman Chemical Company) was

dissolved in DMSO at 10 mM and added to the extract 15 min after addition of sperm nuclei at 50 μ M. SUMO2-VS (UL-759) was purchased from Boston Biochem and used at 1 μ M in *X. laevis* egg extract. Aphidicolin was dissolved in DMSO at 8 mM and added to the extract along with demembranated sperm nuclei at 40 μ M.

Recombinant proteins

Recombinant His-tagged ubiquitin and ubiquitin mutants were purchased from Boston Biochem, dissolved in LFB1/50 (40 mM Hepes/KOH, pH 8.0, 20 mM potassium phosphate, pH 8.0, 50 mM KCl, 2 mM $MgCl_2$, 1 mM EGTA, 10% sucrose wt/vol, 2 mM DTT, 1 μ g/ml aprotinin, 1 μ g/ml leupeptin, and 1 μ g/ml pepstatin) buffer at 10 mg/ml, and used at 0.5 mg/ml in *X. laevis* egg extract.

pET28a-X.LSUMO1 and pET28a-X.LSUMO2 were purchased from GenScript. Recombinant His-tagged *X. laevis* SUMO1 and SUMO2 were expressed in Rosetta (DE3) pLysS cells over night at 20°C after induction with 1 mM IPTG. The cells were lysed in lysis buffer: 50 mM Tris-HCl, 500 mM NaCl, 10 mM imidazole, 2 mM $MgCl_2$, 0.1 mM PMSF, and 1 μ g/ml of each aprotinin, leupeptin, and pepstatin, pH 7.5. Homogenates were supplemented with 25 U/ml benzonase and incubated at room temperature for 20 min. Homogenates were subsequently spun down at 14,000 *g* for 30 min at 4°C and supernatants incubated with 2 ml of prewashed Super Ni-NTA Affinity Resin (SUPER-NINA100; Genon) for 2 h with rotation at 4°C. Resins were subsequently washed twice with 50 mM Tris-HCl, 500 mM NaCl, 30 mM imidazole, 0.1 mM PMSF, and 1 μ g/ml of each aprotinin, leupeptin, and pepstatin, pH 7.5. Resin-bound proteins were finally eluted in 1 ml fractions with a solution containing 50 mM Tris-HCl, 150 mM NaCl, 200 mM imidazole, 5 mM β -mercaptoethanol, 0.1 mM PMSF, and 1 μ g/ml of each aprotinin, leupeptin, and pepstatin, pH 7.5. Fractions containing the highest levels of recombinant SUMO1 or SUMO2 were dialysed into LFB1/50 buffer. Both SUMO1 and SUMO2 were used at 0.5 mg/ml in *X. laevis* egg extract.

pET28a-pHISTEV30a-SEN1(415-649) was a kind gift from Prof Ron Hay's laboratory. Recombinant active domain of human SEN1 (aa 415-647) was expressed and purified as explained above for recombinant SUMOs.

Recombinant His-tagged *X. laevis* cyclin A1 NΔ56 (pET23a-X.L Cyclin A1 NΔ56) was a kind gift from Prof Julian Blow's laboratory (Strausfeld et al, 1996), was expressed in Rosetta (DE3) pLysS cells over night at 15°C after induction with 1 mM IPTG, and subsequently purified as explained above for recombinant SUMOs but using different solutions. Lysis buffer: 50 mM Tris-HCl, 300 mM NaCl, 2 mM $MgCl_2$, 1 mM DTT, 0.1 mM PMSF, and 1 μ g/ml of each aprotinin, leupeptin, and pepstatin, pH 7.4. Washes: Resin was washed twice with lysis buffer on its own and twice again with lysis buffer supplemented with 0.1% Triton X-100. Elution buffer: Lysis buffer supplemented with 10% glycerol and 250 mM imidazole.

Xenopus TRAIP was cloned into pGS21 vector, expressed in BL21 (DE3) bacterial strain in Auto Induction Media (AIM) media (Formedium) O/N at 18°C. Pellets were lysed in lysis buffer: 50 mM NaH_2PO_4 , pH 9; 300 mM NaCl; 10% glycerol; 2 mM DTT; 2 mM $MgCl_2$; 0.05% Brij; 0.1 mM PMSF; 1 μ g/ml of each aprotinin, leupeptin, and pepstatin; 1 mg/ml lysozyme; and 25 U/ml benzonase. The protein was purified as above but using Glutathione Sepharose 4B (GE

Healthcare) and eluted with 25 mM glutathione. The protein was then dialysed into LFB1/50 buffer (as above) and concentrated up to 0.3 mg/ml of full-length GST-TRAIP. It was used in the egg extract at a final concentration of 30 μ g/ml. pGS21-TRAIP(C25A) was generated by site-directed mutagenesis and purified in an analogous way.

Recombinant His/SUMO-tagged *X. laevis* wt and mutant TRAIP were expressed in Rosetta (DE3) pLysS cells from pCA528 vector O/N at 20°C in AIM media. After pelleting of the bacterial cultures, the cells were lysed in 50 mM NaH₂PO₄, 500 mM NaCl, 0.05% Brij, 10% glycerol, 10 mM imidazole, 2 mM MgCl₂, 0.1 mM PMSF, and 1 μ g/ml of each aprotinin, leupeptin, and pepstatin, pH 9.0. Homogenates were supplemented with 1 mg/ml lysozyme and 25 U/ml BaseMuncher, incubated at room temperature for 20 min and subsequently sonicated (6 × 30 s), and spun (30 min, 31,000 g, 4°C). The resulting supernatant was incubated in 2 ml prewashed Super Ni-NTA Affinity Resin (SUPER-NINA100; Genetion) O/N with rotation at 4°C. Resins were washed five times with lysis buffer, with respect to the following alterations: Wash 1: 100 mM NaCl, no imidazole. Wash 2: 100 mM NaCl, 20 mM imidazole. Wash 3: 250 mM NaCl, no imidazole. Wash 4 and 5: 500 mM NaCl, 20 mM imidazole. Each respective wash was supplemented with 0.1 mM PMSF and 1 μ g/ml of each aprotinin, leupeptin, and pepstatin. Resin-bound TRAIP was eluted in 1-ml fractions using elution buffer (50 mM NaH₂PO₄, 500 mM NaCl, 0.05% Brij, 10% Glycerol, 400 mM imidazole, pH 9.0) supplemented with 0.1 mM PMSF and 1 μ g/ml of each aprotinin, leupeptin, and pepstatin. Those fractions containing the highest quantities of wt or mutant TRAIP were dialysed into LFB1/100 buffer.

In vitro TRAIP autoubiquitylation reaction

The reaction was set up as previously described (Besse et al, 2007). Briefly, GST-TRAIPwt and GST-TRAIPmut were purified as described above but not eluted from Glutathione Sepharose beads. Both beads were then incubated in 100- μ l reaction for 2 h at 37°C with 20 mM Hepes, pH 7.4, 10 mM MgCl₂, 1 mM DTT, 60 μ M His-Ubi (Boston Biotech), 50 nM E1 (UBA1/UBE1; Source BioScience), 850, nM E2 UbCH5a (Source BioScience), 1 mM ATP, 30 μ M creatine phosphate, and 1 U of creatine kinase. After incubation, they were extensively washed, boiled in gel-loading buffer, and run on the gel. The membrane was analysed with α -ubiquitin antibody.

Antibodies

α -PCNA (P8825), α -His (H1029), and α -ubiquitin (P4D1) were purchased from Sigma-Aldrich and α -phospho-histone H3 (ser10) (D2C8) was purchased from Cell Signalling Technology. α -TRAIP (NBP1-87125) and α -RNF213 (NBP1-88466) were purchased from Novus Biologicals. α -SUMO2 and α -SUMO1 were produced in the laboratory by culturing the hybridoma cell lines SUMO2 (8A2), and SUMO1 (21C7), purchased from Developmental Studies Hybridoma Bank (hybridoma cell culture was performed following the manufacturer's instructions and adding 20 mM L-glutamine to the media). Affinity-purified α -Cdc45, α -Psf2, and α -Sld5 (Gambus et al, 2011); α -Mcm3 (Khouidoli et al, 2008); α -SMC2 (Gillespie et al, 2007); and α -LRR1 (S962D) (Sonneville et al, 2017) were previously described. α -Mcm7

was raised in sheep against recombinant *X. laevis* Mcm7, purified from *E. coli*, and affinity-purified in the laboratory.

DNA staining and microscopy

Interphase *X. laevis* egg extract was supplemented with 10 ng/ μ l of demembranated sperm nuclei and incubated at 23°C until completion of DNA replication as described before (Gillespie et al, 2012). Mitosis was optionally driven by addition of 826 nM cyclin A1 NΔ56. At time points -30, 0, 30, and 60 min, after addition of cyclin A1, 10 μ l of the reaction was spotted onto a microscope slide with 10 μ l mix of Hoechst 33258 (5824/50; Tocris Bioscience) and Dil stain (D282; Thermo Fisher Scientific), 1 μ g/ml and 10 μ g/ml final concentration, respectively, and incubated at room temperature for 30 min. Nuclei were viewed as previously described (Strausfeld et al, 1996).

DNA synthesis assay

The replication reactions were started with the addition of demembranated *Xenopus* sperm DNA to 10 ng/ μ l as described before (Gillespie et al, 2012). The synthesis of nascent DNA was measured by quantification of P³² α -dATP incorporation into newly synthesised DNA as described before (Gillespie et al, 2012).

Chromatin isolation time-course

Interphase *X. laevis* egg extract was supplemented with 10 ng/ μ l of demembranated sperm DNA and subjected to indicated treatments. The reaction was incubated at 23°C for 90 min to allow completion of DNA replication as described before (Gillespie et al, 2012), after which mitosis was optionally driven by addition of 826 nM cyclin A1 NΔ56. The extract was then also optionally supplemented with inhibitors or recombinant proteins as indicated. Chromatin was isolated in ANIB100 buffer supplemented with 10 mM 2-chloroacetamide (Millipore) and 5 mM N-ethylmaleimide (Acros Organics) at indicated time points after addition of cyclin A1 NΔ56 as previously described (Gillespie et al, 2012).

For the minimal licensing experiment (Fig S2A), interphase *X. laevis* egg extract was supplemented with 5 ng/ μ l of demembranated sperm DNA. To minimally license chromatin, Cdt1 activity was blocked through addition of geminin^{DEL} (Blow lab) after 2 min of sperm DNA addition. The extract was optionally supplemented with DMSO and Cullin ligase inhibitor (MLN4924 at 10 μ M).

Quantification of Western blots

Western blot films from three independent experiments were scanned to generate high-resolution, 300 dpi, 8-bit JPEG images. The pixel intensity of protein bands was then quantified with Image J (<http://rsbweb.nih.gov/ij/>) and the average intensity (a.u.) calculated for each time point. For quantification of Mcm7 ubiquitylation, a frame was first drawn around the entire ubiquitylation signal to include that which was built in S-phase and that which was extended further in mitosis. This generates a plot for each sample. To then measure only the intensity of ubiquitylation which occurs in mitosis, a line was drawn through the plots to separate the lower region (S-phase) and the upper region (mitosis). The intensity of

this upper region was then measured and a.u. calculated from three independent experiments.

Immunoprecipitation of post-termination CMG associated with mitotic chromatin

3.75 ml of interphase *X. laevis* egg extract was supplemented with 10 ng/ μ l of demembranated sperm nuclei, 5 mM caffeine, and 50 μ M p97 inhibitor NMS873. The reaction was incubated at 23°C for 90 min to allow completion of DNA replication, after which mitosis was driven by addition of recombinant cyclin A1 NΔ56 at 826 nM followed by incubation at 23°C for a further 60 min. At this stage, chromatin was isolated as described above and chromatin-bound protein complexes released into solution by chromosomal DNA digestion with 2 U/ μ l benzonase for 15 min. Solubilisation of chromatin-bound protein complexes was further facilitated by subjecting the sample to 5 min of 30 s ON/OFF sonication cycles using a diagenode bioruptor and increasing the concentration of potassium acetate up to 150 mM. The resulting protein complexes were subsequently subjected to either nonspecific IgG (from sheep serum) or Mcm3 immunoprecipitation and the immunoprecipitated material analysed by mass spectrometry as previously described (Sonneville et al, 2017) in collaboration with Dr Richard Jones from MS Bioworks LLC.

Supplementary Information

Supplementary Information is available at <https://doi.org/10.26508/lsa.201900390>.

Acknowledgements

Dr S Priego Moreno was funded by Wellcome Trust Institutional Strategic Support Fund (ISSF) Award, Dr RM Jones and Dr A Gambus were funded by MRC CDA MR/K007106/1 and Shaun Scaramuzza by Midlands Integrative Biosciences Training Partnership (MIBTP) studentship. We would like to thank Prof Ron Hay for pET28a-pHISTEV30a-SEN1(415-649) and Prof Julian Blow for pET23a-X.L.Cyclin A1 NΔ56 and geminin^{DEL}.

Author Contributions

S Priego Moreno: conceptualization, data curation, investigation, and writing—review and editing.

RM Jones: data curation, investigation, methodology, and writing—review and editing.

D Poovathumkadavil: data curation, investigation, and writing—review and editing.

S Scaramuzza: data curation and writing—review and editing.

A Gambus: conceptualization, formal analysis, supervision, funding acquisition, project administration, and writing—original draft, review, and editing.

Conflict of Interest Statement

The authors declare that they have no conflict of interest.

References

- Alexandru G, Graumann J, Smith GT, Kolawa NJ, Fang R, Deshaies RJ (2008) UBXD7 binds multiple ubiquitin ligases and implicates p97 in HIF1 α turnover. *Cell* 134: 804–816. doi:[10.1016/j.cell.2008.06.048](https://doi.org/10.1016/j.cell.2008.06.048)
- Almeida S, Ryser S, Obarzanek-Fojt M, Hohl D, Huber M (2011) The TRAF-interacting protein (TRIP) is a regulator of keratinocyte proliferation. *J Invest Dermatol* 131: 349–357. doi:[10.1038/jid.2010.329](https://doi.org/10.1038/jid.2010.329)
- Banh RS, Iorio C, Marcotte R, Xu Y, Cojocari D, Rahman AA, Pawling J, Zhang W, Sinha A, Rose CM, et al (2016) PTP1B controls non-mitochondrial oxygen consumption by regulating RNF213 to promote tumour survival during hypoxia. *Nat Cell Biol* 18: 803–813. doi:[10.1038/ncb3376](https://doi.org/10.1038/ncb3376)
- Besse A, Campos AD, Webster WK, Darnay BG (2007) TRAF-interacting protein (TRIP) is a RING-dependent ubiquitin ligase. *Biochem Biophys Res Commun* 359: 660–664. doi:[10.1016/j.bbrc.2007.05.149](https://doi.org/10.1016/j.bbrc.2007.05.149)
- Bhowmick R, Hickson ID (2017) The “enemies within”: Regions of the genome that are inherently difficult to replicate. *F1000Res* 6: 666. doi:[10.12688/f1000research.11024.1](https://doi.org/10.12688/f1000research.11024.1)
- Burrell RA, McClelland SE, Endesfelder D, Groth P, Weller MC, Shaikh N, Domingo E, Kanu N, Dewhurst SM, Gronroos E, et al (2013) Replication stress links structural and numerical cancer chromosomal instability. *Nature* 494: 492–496. doi:[10.1038/nature11935](https://doi.org/10.1038/nature11935)
- Chapard C, Hohl D, Huber M (2015) The TRAF-interacting protein (TRIP) is a novel E2F target with peak expression in mitosis. *Oncotarget* 6: 20933–20945. doi:[10.18632/oncotarget.3055](https://doi.org/10.18632/oncotarget.3055)
- Chapard C, Meraldi P, Gleich T, Bachmann D, Hohl D, Huber M (2014) TRIP is a regulator of the spindle assembly checkpoint. *J Cell Sci* 127: 5149–5156. doi:[10.1242/jcs.152579](https://doi.org/10.1242/jcs.152579)
- Dewar JM, Budzowska M, Walter JC (2015) The mechanism of DNA replication termination in vertebrates. *Nature* 525: 345–350. doi:[10.1038/nature14887](https://doi.org/10.1038/nature14887)
- Feng W, Guo Y, Huang J, Deng Y, Zang J, Huen MS (2016) TRIP regulates replication fork recovery and progression via PCNA. *Cell Discov* 2: 16016. doi:[10.1038/celldisc.2016.16](https://doi.org/10.1038/celldisc.2016.16)
- Fu YV, Yardimci H, Long DT, Ho TV, Guainazzi A, Bermudez VP, Hurwitz J, van Oijen A, Scharer OD, Walter JC (2011) Selective bypass of a lagging strand roadblock by the eukaryotic replicative DNA helicase. *Cell* 146: 931–941. doi:[10.1016/j.cell.2011.07.045](https://doi.org/10.1016/j.cell.2011.07.045)
- Gambus A, Jones RC, Sanchez-Diaz A, Kanemaki M, van Deursen F, Edmondson RD, Labib K (2006) GINS maintains association of Cdc45 with MCM in replisome progression complexes at eukaryotic DNA replication forks. *Nat Cell Biol* 8: 358–366. doi:[10.1038/ncb1382](https://doi.org/10.1038/ncb1382)
- Gambus A, Khoudoli GA, Jones RC, Blow JJ (2011) MCM2-7 form double hexamers at licensed origins in *Xenopus* egg extract. *J Biol Chem* 286: 11855–11864. doi:[10.1074/jbc.m110.199521](https://doi.org/10.1074/jbc.m110.199521)
- Gao Y, Mutter-Rottmayer E, Zlatanou A, Vaziri C, Yang Y (2017) Mechanisms of post-replication DNA repair. *Genes (Basel)* 8: E64. doi:[10.3390/genes8020064](https://doi.org/10.3390/genes8020064)
- Gillespie PJ, Gambus A, Blow JJ (2012) Preparation and use of *Xenopus* egg extracts to study DNA replication and chromatin associated proteins. *Methods* 57: 203–213. doi:[10.1016/j.jymeth.2012.03.029](https://doi.org/10.1016/j.jymeth.2012.03.029)
- Gillespie PJ, Khoudoli GA, Stewart G, Swedlow JR, Blow JJ (2007) ELYS/MEL-28 chromatin association coordinates nuclear pore complex assembly and replication licensing. *Curr Biol* 17: 1657–1662. doi:[10.1016/j.cub.2007.08.041](https://doi.org/10.1016/j.cub.2007.08.041)
- Harley ME, Murina O, Leitch A, Higgs MR, Bicknell LS, Yigit G, Blackford AN, Zlatanou A, Mackenzie KJ, Reddy K, et al (2016) TRIP promotes DNA damage response during genome replication and is mutated in primordial dwarfism. *Nat Genet* 48: 36–43. doi:[10.1038/ng.3451](https://doi.org/10.1038/ng.3451)
- Heidelberger JB, Voigt A, Borisova ME, Petrosino G, Ruf S, Wagner SA, Beli P (2018) Proteomic profiling of VCP substrates links VCP to K6-linked

- ubiquitylation and c-Myc function. *EMBO Rep* 19: e44754. doi:[10.15252/embr.201744754](https://doi.org/10.15252/embr.201744754)
- Hochegger H, Klotzbucher A, Kirk J, Howell M, le Guellec K, Fletcher K, Duncan T, Sohail M, Hunt T (2001) New B-type cyclin synthesis is required between meiosis I and II during *Xenopus* oocyte maturation. *Development* 128: 3795–3807.
- Hoffmann S, Smedegaard S, Nakamura K, Mortuza GB, Raschle M, Ibanez de Opakua A, Oka Y, Feng Y, Blanco FJ, Mann M, et al (2016) TRAP is a PCNA-binding ubiquitin ligase that protects genome stability after replication stress. *J Cell Biol* 212: 63–75. doi:[10.1083/jcb.201506071](https://doi.org/10.1083/jcb.201506071)
- Kamada F, Aoki Y, Narisawa A, Abe Y, Komatsuzaki S, Kikuchi A, Kanno J, Niihori T, Ono M, Ishii N, et al (2011) A genome-wide association study identifies RNF213 as the first Moyamoya disease gene. *J Hum Genet* 56: 34–40. doi:[10.1038/jhg.2010.132](https://doi.org/10.1038/jhg.2010.132)
- Khoudoli GA, Gillespie PJ, Stewart G, Andersen JS, Swedlow JR, Blow JJ (2008) Temporal profiling of the chromatin proteome reveals system-wide responses to replication inhibition. *Curr Biol* 18: 838–843. doi:[10.1016/j.cub.2008.04.075](https://doi.org/10.1016/j.cub.2008.04.075)
- Kobayashi H, Yamazaki S, Takashima S, Liu W, Okuda H, Yan J, Fujii Y, Hitomi T, Harada KH, Habu T, et al (2013) Ablation of Rnf213 retards progression of diabetes in the Akita mouse. *Biochem Biophys Res Commun* 432: 519–525. doi:[10.1016/j.bbrc.2013.02.015](https://doi.org/10.1016/j.bbrc.2013.02.015)
- Lee SY, Lee SY, Choi Y (1997) TRAF-interacting protein (TRIP): A novel component of the tumor necrosis factor receptor (TNFR)- and CD30-TRAF signaling complexes that inhibits TRAF2-mediated NF-kappaB activation. *J Exp Med* 185: 1275–1285. doi:[10.1084/jem.185.7.1275](https://doi.org/10.1084/jem.185.7.1275)
- Liu W, Morito D, Takashima S, Mineharu Y, Kobayashi H, Hitomi T, Hashikata H, Matsuura N, Yamazaki S, Toyoda A, et al (2011) Identification of RNF213 as a susceptibility gene for moyamoya disease and its possible role in vascular development. *PLoS One* 6: e22542. doi:[10.1371/journal.pone.0022542](https://doi.org/10.1371/journal.pone.0022542)
- Liu Y, Nielsen CF, Yao Q, Hickson ID (2014) The origins and processing of ultra fine anaphase DNA bridges. *Curr Opin Genet Dev* 26: 1–5. doi:[10.1016/j.gde.2014.03.003](https://doi.org/10.1016/j.gde.2014.03.003)
- Maric M, Maculins T, De Piccoli G, Labib K (2014) Cdc48 and a ubiquitin ligase drive disassembly of the CMG helicase at the end of DNA replication. *Science* 346: 1253596. doi:[10.1126/science.1253596](https://doi.org/10.1126/science.1253596)
- Maric M, Mukherjee P, Tatham MH, Hay R, Labib K (2017) Ufd1-Npl4 recruit Cdc48 for disassembly of ubiquitylated CMG helicase at the end of chromosome replication. *Cell Rep* 18: 3033–3042. doi:[10.1016/j.celrep.2017.03.020](https://doi.org/10.1016/j.celrep.2017.03.020)
- Meyer H (2012) p97 complexes as signal integration hubs. *BMC Biol* 10: 48. doi:[10.1186/1741-7007-10-48](https://doi.org/10.1186/1741-7007-10-48)
- Meyer H, Bug M, Bremer S (2012) Emerging functions of the VCP/p97 AAA-ATPase in the ubiquitin system. *Nat Cell Biol* 14: 117–123. doi:[10.1038/ncb2407](https://doi.org/10.1038/ncb2407)
- Meyer HJ, Rape M (2014) Enhanced protein degradation by branched ubiquitin chains. *Cell* 157: 910–921. doi:[10.1016/j.cell.2014.03.037](https://doi.org/10.1016/j.cell.2014.03.037)
- Minocherhomji S, Ying S, Bjerregaard VA, Bursomanno S, Aleliunaite A, Wu W, Mankouri HW, Shen H, Liu Y, Hickson ID (2015) Replication stress activates DNA repair synthesis in mitosis. *Nature* 528: 286–290. doi:[10.1038/nature16139](https://doi.org/10.1038/nature16139)
- Minshull J, Blow JJ, Hunt T (1989) Translation of cyclin mRNA is necessary for extracts of activated *xenopus* eggs to enter mitosis. *Cell* 56: 947–956. doi:[10.1016/0092-8674\(89\)90628-4](https://doi.org/10.1016/0092-8674(89)90628-4)
- Moreno A, Carrington JT, Albergante L, Al Mamun M, Haagensen EJ, Komseli ES, Gorgoulis VG, Newman TJ, Blow JJ (2016) Unreplicated DNA remaining from unperturbed S phases passes through mitosis for resolution in daughter cells. *Proc Natl Acad Sci U S A* 113: E5757–E5764. doi:[10.1073/pnas.1603252113](https://doi.org/10.1073/pnas.1603252113)
- Moreno SP, Bailey R, Campion N, Herron S, Gambus A (2014) Polyubiquitylation drives replisome disassembly at the termination of DNA replication. *Science* 346: 477–481. doi:[10.1126/science.1253585](https://doi.org/10.1126/science.1253585)
- Moyer SE, Lewis PW, Botchan MR (2006) Isolation of the Cdc45/Mcm2-7/GINS (CMG) complex, a candidate for the eukaryotic DNA replication fork helicase. *Proc Natl Acad Sci U S A* 103: 10236–10241. doi:[10.1073/pnas.0602400103](https://doi.org/10.1073/pnas.0602400103)
- Park ES, Choi S, Kim JM, Jeong Y, Choe J, Park CS, Choi Y, Rho J (2007) Early embryonic lethality caused by targeted disruption of the TRAF-interacting protein (TRIP) gene. *Biochem Biophys Res Commun* 363: 971–977. doi:[10.1016/j.bbrc.2007.09.103](https://doi.org/10.1016/j.bbrc.2007.09.103)
- Park IS, Han Y, Chung HJ, Jung YW, Kim Y, Kim H (2016) SUMOylation regulates nuclear localization and stability of TRAP/RNF206. *Biochem Biophys Res Commun* 470: 881–887. doi:[10.1016/j.bbrc.2016.01.141](https://doi.org/10.1016/j.bbrc.2016.01.141)
- Park IS, Jo KS, Won HS, Kim H (2015) Dimerization of TRAF-interacting protein (TRAP) regulates the mitotic progression. *Biochem Biophys Res Commun* 463: 864–869. doi:[10.1016/j.bbrc.2015.06.026](https://doi.org/10.1016/j.bbrc.2015.06.026)
- Sonneville R, Moreno SP, Knebel A, Johnson C, Hastie CJ, Gartner A, Gambus A, Labib K (2017) CUL-2LRR-1 and UBXN-3 drive replisome disassembly during DNA replication termination and mitosis. *Nat Cell Biol* 19: 468–479. doi:[10.1038/ncb3500](https://doi.org/10.1038/ncb3500)
- Sonobe S, Fujimura M, Niizuma K, Nishijima Y, Ito A, Shimizu H, Kikuchi A, Arai-ichinoi N, Kure S, Tominaga T (2014) Temporal profile of the vascular anatomy evaluated by 9.4-T magnetic resonance angiography and histopathological analysis in mice lacking RNF213: A susceptibility gene for moyamoya disease. *Brain Res* 1552: 64–71. doi:[10.1016/j.brainres.2014.01.011](https://doi.org/10.1016/j.brainres.2014.01.011)
- Soo Lee N, Jin Chung H, Kim HJ, Yun Lee S, Ji JH, Seo Y, Hun Han S, Choi M, Yun M, Lee SG, et al (2016) TRAP/RNF206 is required for recruitment of RAP80 to sites of DNA damage. *Nat Commun* 7: 10463. doi:[10.1038/ncomms10463](https://doi.org/10.1038/ncomms10463)
- Strausfeld UP, Howell M, Descombes P, Chevalier S, Rempel RE, Adamczewski J, Maller JL, Hunt T, Blow JJ (1996) Both cyclin A and cyclin E have S-phase promoting (SPF) activity in *Xenopus* egg extracts. *J Cell Sci* 109: 1555–1563.
- Wallace HA, Merkle JA, Yu MC, Berg TG, Lee E, Bosco G, Lee LA (2014) TRIP/NOPO E3 ubiquitin ligase promotes ubiquitylation of DNA polymerase eta. *Development* 141: 1332–1341. doi:[10.1242/dev.101196](https://doi.org/10.1242/dev.101196)
- Windheim M, Peggie M, Cohen P (2008) Two different classes of E2 ubiquitin-conjugating enzymes are required for the mono-ubiquitination of proteins and elongation by polyubiquitin chains with a specific topology. *Biochem J* 409: 723–729. doi:[10.1042/bj20071338](https://doi.org/10.1042/bj20071338)
- Wu RA, Semlow DR, Kamimae-Lanning AN, Kochenova OV, Chistol G, Hodskinson MR, Amunugama R, Sparks JL, Wang M, Deng L, et al (2019) TRAP1 is a master regulator of DNA interstrand crosslink repair. *Nature* 567: 267–272. doi:[10.1038/s41586-019-1002-0](https://doi.org/10.1038/s41586-019-1002-0)
- Yang C, Trent S, Ionescu-Tiba V, Lan L, Shioda T, Sgroi D, Schmidt EV (2006) Identification of cyclin D1- and estrogen-regulated genes contributing to breast carcinogenesis and progression. *Cancer Res* 66: 11649–11658. doi:[10.1158/0008-5472.can-06-1645](https://doi.org/10.1158/0008-5472.can-06-1645)
- Zhou Q, Geahlen RL (2009) The protein-tyrosine kinase Syk interacts with TRAF-interacting protein TRIP in breast epithelial cells. *Oncogene* 28: 1348–1356. doi:[10.1038/onc.2008.493](https://doi.org/10.1038/onc.2008.493)



License: This article is available under a Creative Commons License (Attribution 4.0 International, as described at <https://creativecommons.org/licenses/by/4.0/>).

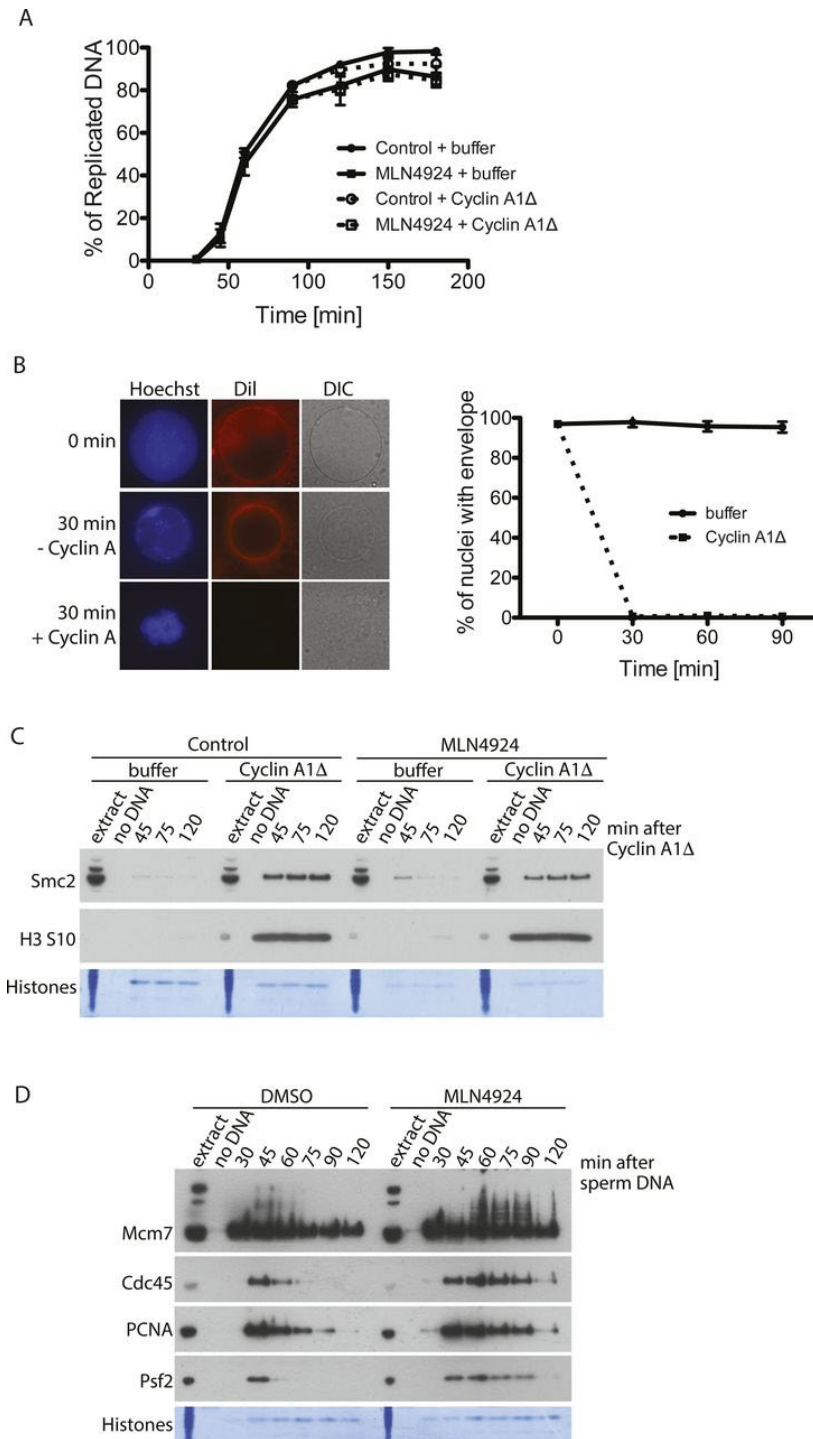


Figure S1. Establishing conditions to analyse mitotic replisome disassembly.

(A) Addition of Cullin inhibitor MLN4924 to the interphase extract does not block extract ability to replicate DNA, and addition of cyclin A1Δ at replication completion point does not stimulate more DNA synthesis. Progression of the replication reaction was measured by incorporation of radioactive dATP into the DNA. $P^{32}\alpha$ -dATP was added to the extract at the beginning of the reaction together with sperm DNA. MLN4924 was added 15 min after sperm DNA addition and cyclin A1Δ was optionally added at 90 min. The graph shows the mean at each time point of three independent experiments with SEM. (B) Nuclear envelope breakdown upon cyclin A1Δ addition. (left) The replication reaction was completed and optionally driven into mitosis by addition of cyclin A1Δ. The nuclei assembled in the extract were visualised by staining DNA with Hoechst

33258, staining nuclear membrane with Dil and visualising the nuclear envelope by differential interference contrast (DIC) microscopy. Examples of nuclei with and without addition of cyclin A1Δ are presented. (right) The percentage of nuclei containing intact envelope stained with Dil was quantified at 0, 30, 60, and 90 min after cyclin A1Δ addition in three independent experiments. The mean for each time point with SEM is presented. (C) Chromatin binding of mitotic factors. DNA was replicated to completion in egg extract supplemented optionally with Cullin ligase inhibitor MLN4924. After completion of the replication reaction, cyclin A1Δ was optionally added to the extract to drive the extract into mitosis. Chromatin was isolated at indicated time points after cyclin A1Δ addition and chromatin samples analysed by Western blotting with indicated antibodies. Colloidal Coomassie-stained histones serve as a quality and loading control. (D) Inhibition of replisome unloading with MLN4924. The replication reaction was carried out with optional addition of MLN4924 at 15 min after sperm DNA addition; chromatin was isolated at indicated time points and analysed by immunoblotting with indicated antibodies.

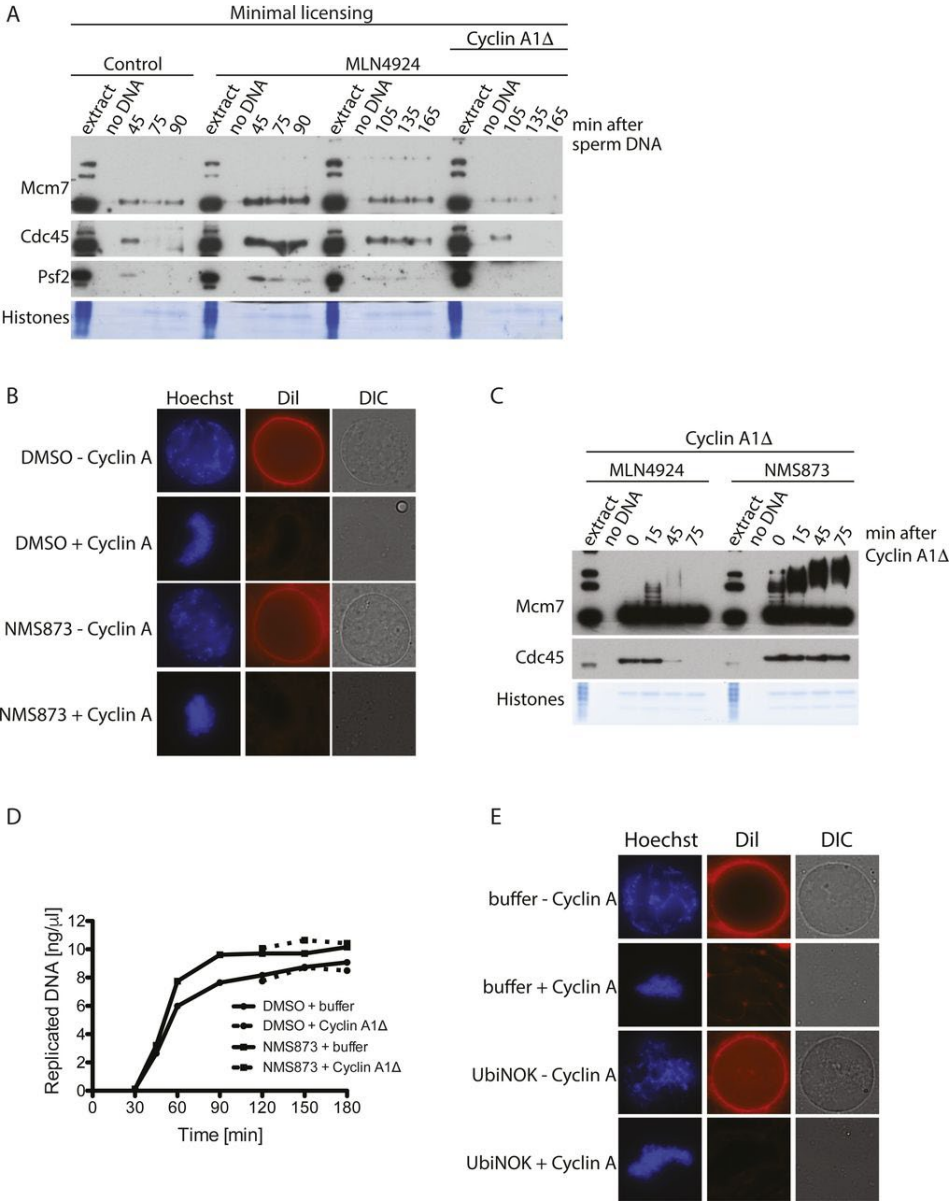


Figure S2. Unloading of replisomes in mitosis.

(A) Mitotic replisome unloading from minimally licensed chromatin. DNA was minimally licensed by addition of geminin at 2 min after DNA sperm addition. The extract was then optionally supplemented with Cullin ligase inhibitor MLN4924 at 15 min after sperm DNA addition and chromatin isolated at time points during the S-phase (45, 75, and 90 min). Upon completion of DNA replication, the extract was optionally driven into mitosis with the addition of cyclin A1 Δ and chromatin isolated at time points during mitosis (105, 135, and 165 min). Note that the time points 105, 135, and 165 min correspond to 15, 45, and 75 min after cyclin A1 Δ addition presented in other figures. Isolated chromatin samples were analysed by immunoblotting with indicated antibodies. (B) Mitotic nuclear envelope breakdown in the presence of NMS873. The replication reaction was completed and optionally driven into mitosis by addition of cyclin A1 Δ . p97 inhibitor NMS873 was optionally added at the same time as cyclin A1 Δ . The nuclei assembled in the extract were visualised at 30 min post cyclin A1 Δ addition by staining DNA with Hoechst 33258, staining nuclear membrane with Dil, and visualising the nuclear envelope by differential interference contrast (DIC) microscopy. (C) p97 is needed for mitotic replisome disassembly. Experiment as in Fig 1C but indicated inhibitors were present in the reaction throughout both stages of the cell cycle. (D) DNA synthesis kinetics in the presence or absence of p97 inhibitor NMS873 and cyclin A1 Δ . Sperm DNA was replicated in extract optionally supplemented with NMS873. At 90 min, cyclin A1 Δ was optionally added. DNA synthesis was analysed as in Fig S1A. (E) Mitotic nuclear envelope breakdown in the presence of UbiNOK. The replication reaction was completed and optionally driven into mitosis by addition of cyclin A1 Δ . The chain-terminating mutant of ubiquitin UbiNOK was optionally added at the same time as cyclin A1 Δ . The nuclei assembled in the extract were visualised as in (B).

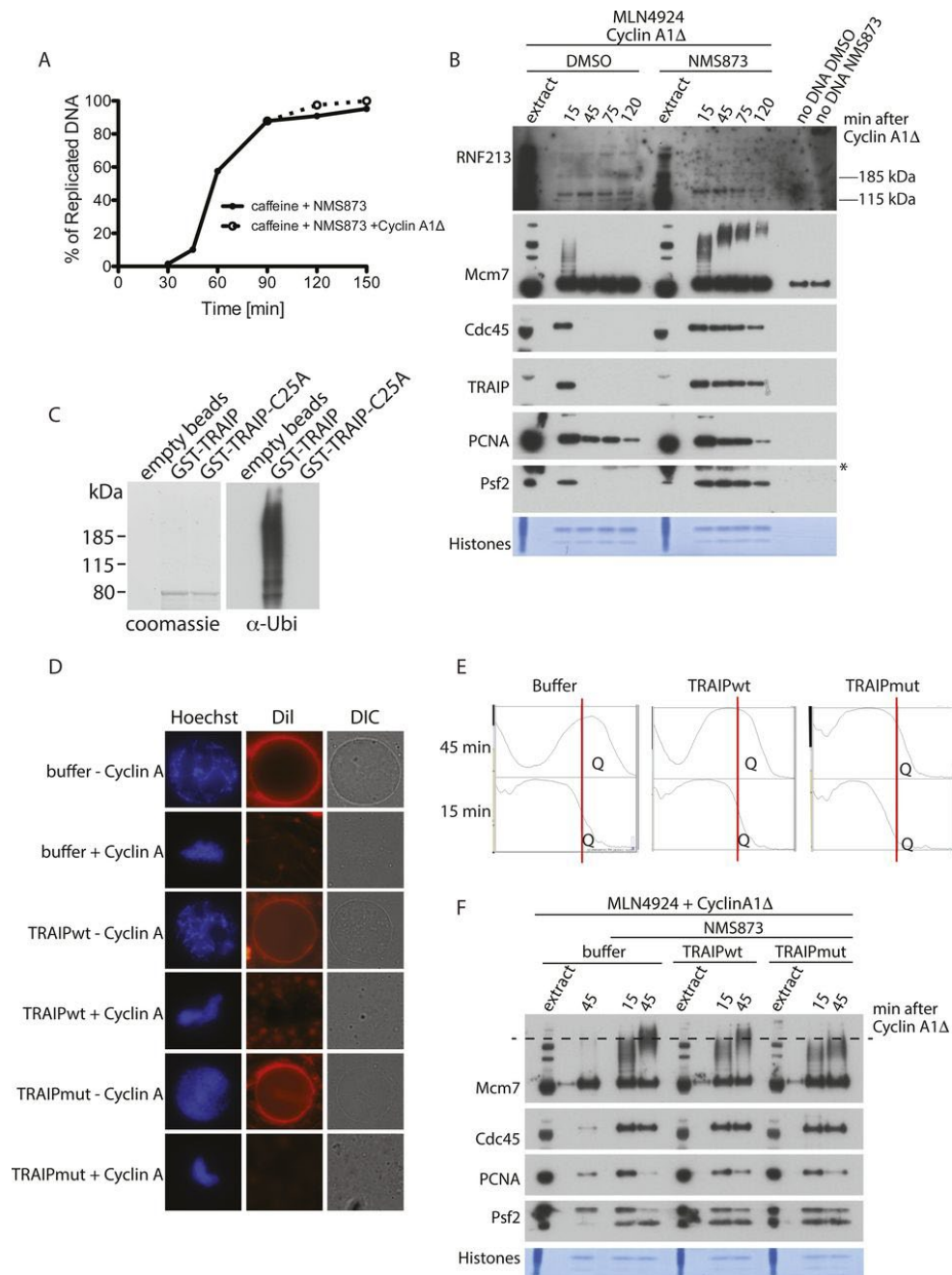


Figure S3. TRAIP activity is required for Mcm7 ubiquitylation in mitosis.

(A) DNA synthesis kinetics for experiment presented in Fig 2. Progression of the replication reaction was measured by incorporation of radioactive dATP into the DNA. $P^{32}\alpha$ -dATP was added to the extract at the beginning of the reaction together with sperm DNA and caffeine. NMS873 was added 15 min after sperm DNA addition and cyclin A1 Δ was optionally added at 90 min. (B) The same experiment from Fig 3B but with addition of the RNF213 blot. (C) TRAIPmut C25A is inactive. A TRAIP autoubiquitylation in vitro reaction was set up with wt GST-tagged TRAIP or RING-mutant (C25A) TRAIP as described in the Materials and Methods section and autoubiquitylation of TRAIP observed through detection of the ubiquitin signal. (D) Mitotic nuclear envelope breakdown in the presence of TRAIPwt and TRAIPmut. The replication reaction was completed and optionally driven into mitosis by addition of cyclin A1 Δ . The extract was then supplemented optionally with LFB1/50 buffer, wt His/SUMO-tagged TRAIP, or RING-mutant

(C25A) TRAIP to a final concentration of 50 $\mu\text{g/ml}$. The nuclei assembled in the extract were visualised at 30 min post cyclin A1 Δ addition by staining DNA with Hoechst 33258, staining nuclear membrane with Dil, and visualising the nuclear envelope by differential interference contrast (DIC) microscopy. (E) An example of the plots gathered during quantification of Mcm7 polyubiquitylation in Fig 3D, as described in the Materials and Methods section, using Image J. The red line represents the cutoff point between the S-phase versus mitotic polyubiquitylated Mcm7. “Q” indicates the region of the plot which was measured. (F) Inhibition of mitotic Mcm7 ubiquitylation by GST-TRAIPmut. The replication reaction was completed in the presence of the Cullin ligase inhibitor MLN4924 and driven into mitosis by addition of cyclin A1 Δ . At the same time as cyclin A1 Δ , the reaction was optionally supplemented with p97 inhibitor NMS873 and LFB1/50 buffer, wt GST-TRAIP, or RING-mutant (C25A) GST-TRAIP at 30 $\mu\text{g/ml}$. Chromatin samples were isolated at indicated time points and analysed by immunoblotting with indicated antibodies. The dashed line on the Mcm7 blot runs through the middle of the ubiquitylation signal for Mcm7 in mitosis in the control (buffer) sample to aid comparison of chain lengths between samples. An asterisk “*” by the Psf2 blot indicates the band of cyclin A1 Δ that is recognised by the Psf2 antibody.

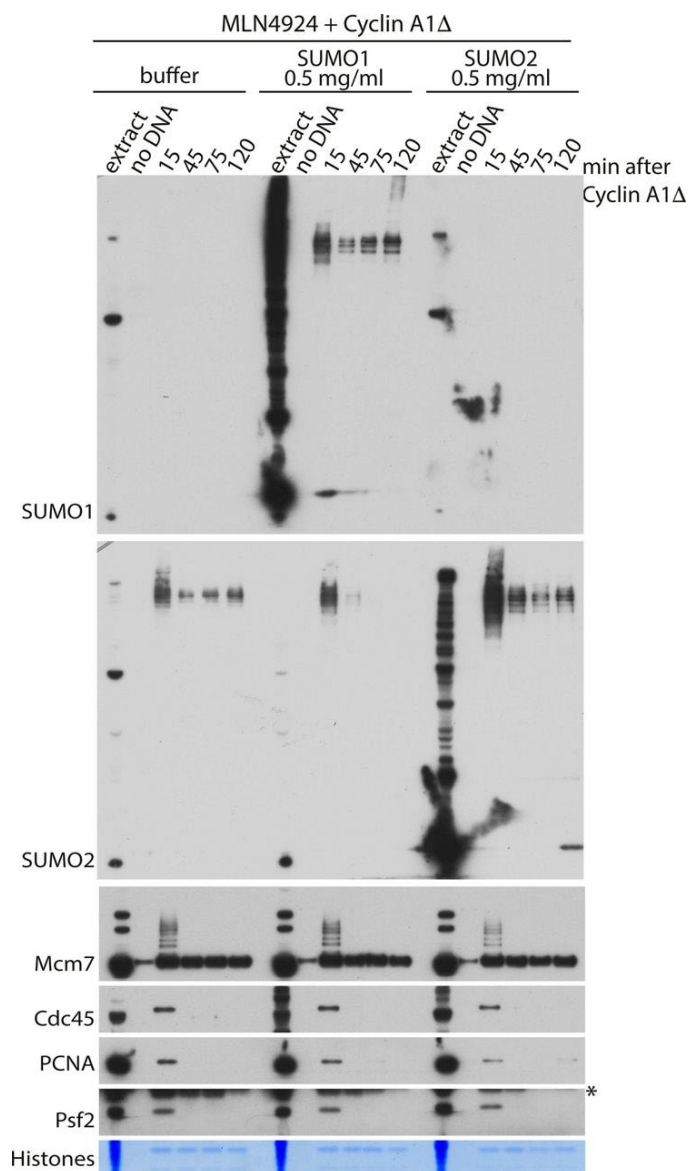


Figure S4. Mitotic replisome disassembly is not affected by stimulation of SUMOylation.

The replication reaction was completed in the presence of the Cullin ligase inhibitor MLN4924 and driven into mitosis by addition of cyclin A1Δ. At the same time as cyclin A1Δ, the extract was optionally supplemented with LFB1/50 buffer, SUMO1, or SUMO2. The chromatin samples were isolated at indicated time points and analysed as in Fig 1.

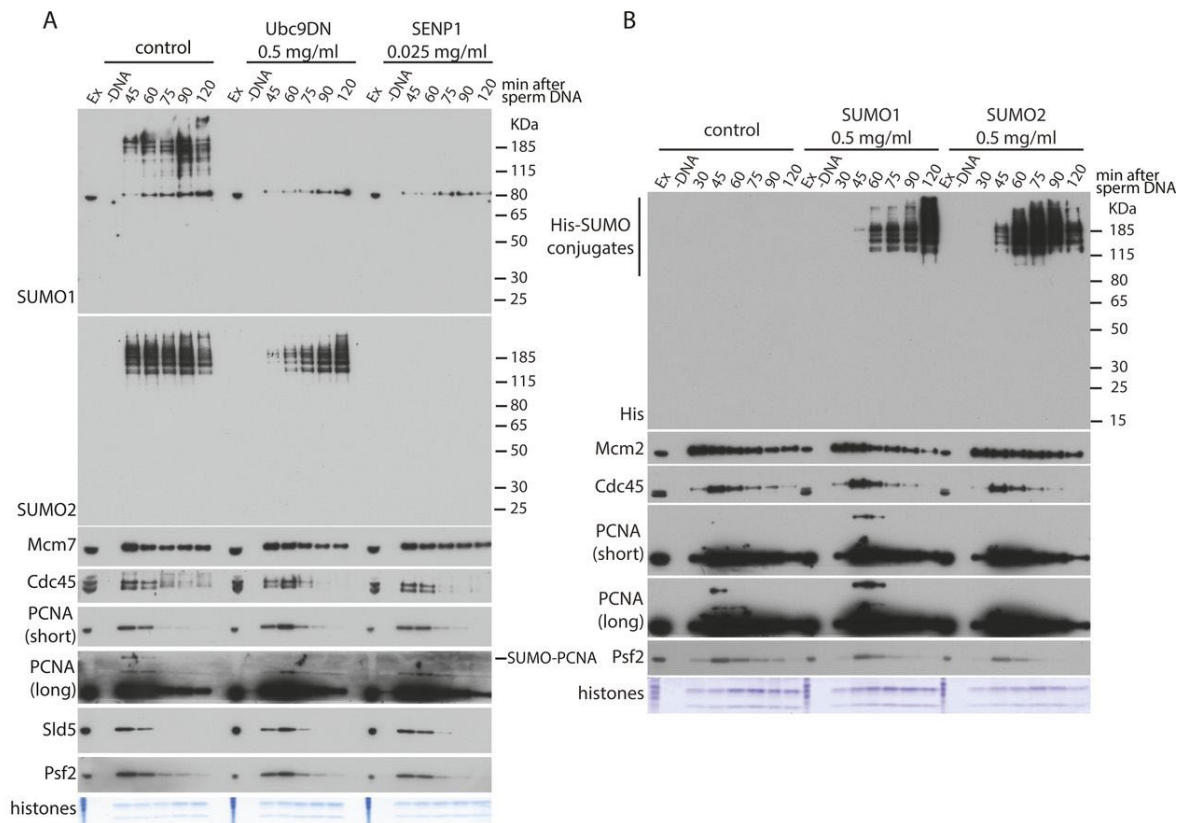


Figure S5. S-phase replisome disassembly is not affected by SUMOylation.

(A) The replication reaction was performed in egg extract supplemented with the dominant negative mutant of Ubc9 (Ubc9DN) or active domain of SENP1. The chromatin samples were isolated at indicated time points and analysed by Western blotting with indicated antibodies as in Fig 1. (B) The replication reaction was performed in egg extract supplemented with 0.5 mg/ml of SUMO1 or SUMO2 (as indicated). The chromatin samples were isolated at indicated time points and analysed by Western blotting with indicated antibodies. Controls as in Fig 1.

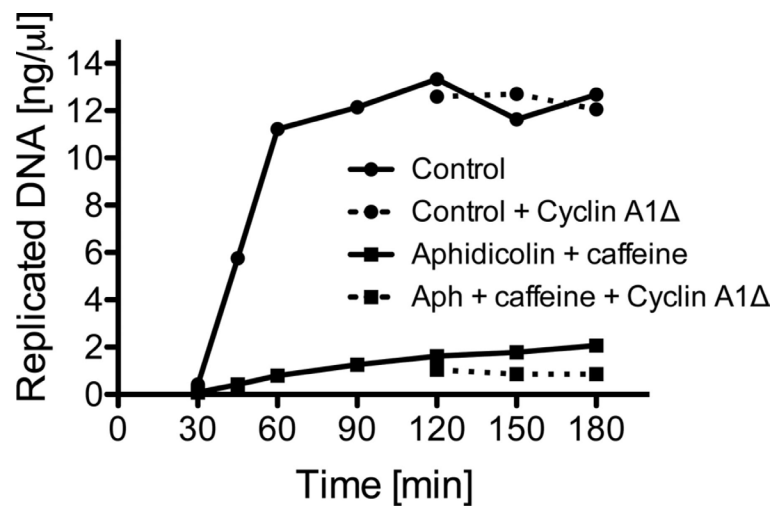


Figure S6. DNA synthesis blocked by addition of aphidicolin and caffeine is not then stimulated by cyclin A1Δ addition.

Sperm DNA was replicated in the extract optionally supplemented with aphidicolin and caffeine. At 90 min, cyclin A1Δ was optionally added. DNA synthesis was analysed as in Fig S1A.

The p97 segregase cofactor Ubxn7 facilitates replisome disassembly during S-phase

Received for publication, December 28, 2021, and in revised form, June 22, 2022 Published, Papers in Press, July 4, 2022
<https://doi.org/10.1016/j.jbc.2022.102234>

Zeynep Tarcan, Divyasree Poovathumkadavil, Aggeliki Skagia, and Agnieszka Gambus*

From the Institute of Cancer and Genomic Sciences, Birmingham Centre for Genome Biology, College of Medical and Dental Sciences, University of Birmingham, Vincent Drive, Birmingham United Kingdom

Edited by Patrick Sung

Complex cellular processes are driven by the regulated assembly and disassembly of large multiprotein complexes. While we are beginning to understand the molecular mechanism for assembly of the eukaryotic DNA replication machinery (replisome), we still know relatively little about the regulation of its disassembly at replication termination. Recently, the first elements of this process have emerged, revealing that the replicative helicase, at the heart of the replisome, is polyubiquitylated prior to unloading and that this unloading requires p97 segregase activity. Two different E3 ubiquitin ligases have now been shown to ubiquitylate the helicase under different conditions: Cul2^{Lrr1} and TRAIP. Here, using *Xenopus laevis* egg extract cell-free system and biochemical approaches, we have found two p97 cofactors, Ubxn7 and Faf1, which can interact with p97 during replisome disassembly during S-phase. We show only Ubxn7, however, facilitates efficient replisome disassembly. Ubxn7 delivers this role through its interaction *via* independent domains with both Cul2^{Lrr1} and p97 to allow coupling between Mcm7 ubiquitylation and its removal from chromatin. Our data therefore characterize Ubxn7 as the first substrate-specific p97 cofactor regulating replisome disassembly in vertebrates and a rationale for the efficacy of the Cul2^{Lrr1} replisome unloading pathway in unperturbed S-phase.

DNA replication is one of the most fundamental processes in life and its faultless execution is essential for normal cell fate. Until recently, the final stage of eukaryotic DNA replication, the termination stage, was mostly unexplored. DNA replication initiates from thousands of replication origins, the positions within the genome where replicative helicases become activated and start unwinding DNA. These then move in opposite directions away from each other, creating two DNA replication forks. The replicative helicase is composed of Cdc45, Mcm2-7 hexamer, and GINS complex (CMG complex) (1) and is positioned at the tip of replication forks forming a platform for replisome assembly (2). Once established, the replication forks replicate chromatin until they encounter forks coming in opposite directions from neighboring origins. At this point the termination of replication forks takes place,

with removal of the replisome from fully duplicated DNA being its final stage (3). In higher eukaryotes (*Xenopus laevis* egg extract, *Caenorhabditis elegans* embryos, mouse embryonic fibroblasts, and human cells), replisome removal in S-phase is driven by the Cul2^{Lrr1} ubiquitin ligase, which ubiquitylates Mcm7 within the terminated CMG helicase complex with lysine 48 (K48)-linked ubiquitin chains (4). The modified CMG is then recognized by the p97 segregase and removed from chromatin allowing for disassembly of the whole replisome built around the helicase (5). Any helicase complexes that fail to be unloaded in S-phase are alternatively unloaded in mitosis. Disassembly of these complexes in mitosis also depends on p97 segregase function, but this time requires the E3 ubiquitin ligase TRAIP (6). Consequently, disassembly in mitosis is driven by alternative species of ubiquitin chains that decorate Mcm7, namely K6- and K63-linked ubiquitin chains. TRAIP ubiquitin ligase can act also during S-phase: it interacts with the replisome and either ubiquitylates CMGs that converge at interstrand crosslinks or ubiquitylates a protein crosslinked to DNA (DPC) that blocks progression of the replication fork (7, 8).

p97 segregase (also referred to as VCP, Cdc48, CDC-48, and Ter94) is a hexameric AAA+ ATPase family member that uses the free energy of ATP binding and hydrolysis to extract ubiquitylated protein targets from stable protein complexes, chromatin, or membranes. As a result, p97 is essential for protein homeostasis in the cell and the dynamic behavior of a multitude of multiprotein assemblies (9). The substrate specificity of p97 recognition is believed to be achieved by a number of regulatory cofactors (reviewed in (10)). In *C. elegans* embryos, the CDC-48 cofactors UFD-1/NPL-4 and UBXN-3 (Faf1 in higher eukaryotes) were shown to be required for replisome removal from chromatin in both S-phase and in mitosis (4, 11). UFD-1/NPL-4 form a heterodimer, essential for most chromatin-related roles of p97, while UBXN-3 provides higher substrate specificity. Interestingly, Ufd1/Npl4 were also shown to interact with p97 and the replisome during replication termination in *Xenopus* egg extract (4). However, while Ufd1/Npl4 are evolutionarily conserved and well characterized, the number and variability of the minor, substrate specific, cofactors of p97 grows through evolution, reflecting the increasing complexity of p97 regulation. So far, roughly three times more cofactors have been identified in mammals

* For correspondence: Agnieszka Gambus, a.gambus@bham.ac.uk.

Role of Ubxn7 in replisome disassembly

than in *C. elegans* (4, 12). Importantly, additional cofactors of p97, which provide substrate specificity towards the terminated replisomes, are as yet to be determined in vertebrates.

Here, we sought to identify p97 cofactors that are facilitating replisome disassembly during S-phase. While we were able to identify two new cofactors for this process, Ubxn7 and Faf1, our findings revealed that the Ubxn7 cofactor specifically is crucial for efficient and fast disassembly of replisomes, as it creates bridges between the essential factors of this process: Cul2^{Lrr1}, ubiquitylated Mcm7, and the p97 complexes.

Results

Identification of p97 cofactors acting during unloading of replicative helicase

Using the *X. laevis* egg extract model system, we have previously shown that the unloading of terminated replicative helicases during S-phase depends on formation of K48-linked ubiquitin chains on the Mcm7 subunit of the CMG helicase by Cul2^{Lrr1} ubiquitin ligase (5). Such modified Mcm7 is in turn recognized and unfolded by p97. We therefore first confirmed that p97 interacts with replicating chromatin in *X. laevis* egg extract with kinetics similar to replication fork components

(Fig. 1A). We found that p97 is a highly abundant protein in *Xenopus* egg extract (13), and only a small proportion of it interacts with chromatin during DNA replication, with the interaction peaking during the exponential stage of replication, when large numbers of replication forks are moving through the chromatin and converging during termination (Fig. 1A). To determine the portfolio of p97 cofactors that interact with p97 during DNA replication termination in egg extract and which may direct p97 to the terminated replisome, we aimed to immunoprecipitate (IP) p97 from a chromatin fraction and analyze its interactors. Firstly, we blocked replisome disassembly by inhibiting p97 activity with NMS-873 (p97i), which is a highly specific allosteric inhibitor of p97 ATPase activity binding to p97 D2 domain (14). We have shown previously that inhibition of p97 ATPase activity stops replisome unloading from chromatin (4). Critically, this treatment does not stop p97 from interacting with substrates or chromatin (Fig. S1A) and should stabilize p97-substrate complexes on chromatin as the substrates cannot be processed. Subsequently, we isolated chromatin with accumulated terminated replisomes, immunoprecipitated p97 and analyzed interacting factors by mass spectrometry (MS). Such analysis revealed numerous components of replication machinery interacting

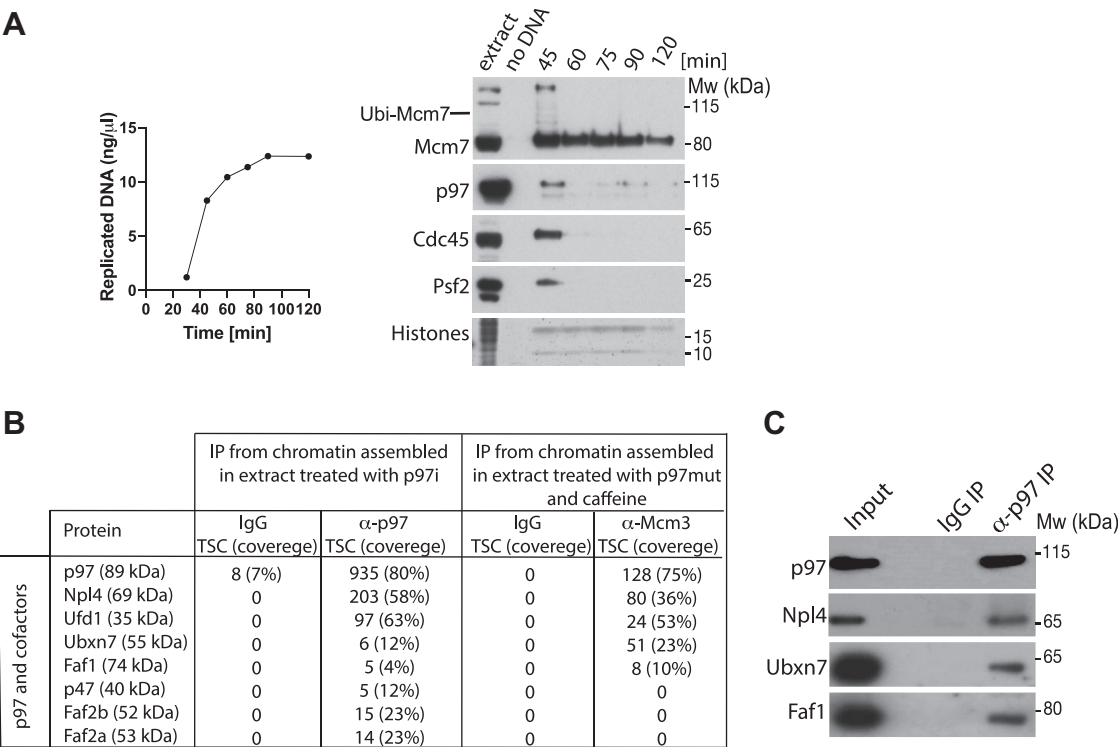


Figure 1. Cofactors interacting with p97 on replicating chromatin in *Xenopus laevis* egg extract. A, chromatin binding of p97 follows replication fork components. A replication reaction was set up in *X. laevis* egg extract and synthesis of nascent DNA was followed by incorporation of radioactive α-³²PdATP into newly synthesized DNA (left). At the same time, chromatin was isolated during the replication reaction at indicated time points after sperm DNA addition. Sample without DNA addition was processed in parallel to provide a chromatin specificity control. Histones at the bottom of the PAGE gel were stained with colloidal Coomassie for loading and sample purity control. Chromatin samples were analyzed by Western blotting with indicated antibodies (right). B, Ubxn7 and Faf1 are identified as cofactors interacting with both p97 and terminated replisome. Interphase egg extract was supplemented with p97i (NMS873) and chromatin was isolated in late S-phase when high levels of terminated replisomes are accumulated on chromatin. Protein complexes were released from chromatin by Benzonase treatment and proteins interacting with p97 segregase were analyzed by mass spectrometry. Identified putative interactors were screened to find known and potential p97 cofactors. Obtained data were compared with the mass spectrometry results of interactors of terminated replisomes published previously (4). Total spectral count is presented with protein coverage in the brackets. Only p97 and its cofactors are presented. Other proteins identified in p97 IP are included in Table S1. C, verification of p97 interaction with Ubxn7 and Faf1 on chromatin. A small proportion of input and immunoprecipitated sample from p97 IP described in (B) was analyzed by Western blotting with indicated antibodies.

with p97, including those which reside in the replisome built around the CMG helicase but also other DNA replication and DNA damage repair factors (Table S1). In order to focus our analysis on potential p97 cofactors, which direct p97 specifically to the terminated replisomes, results from the p97 interactome were compared with those of an Mcm3 IP, which was performed in conditions blocking replisome disassembly. Briefly, the extract was replicated in the presence of a dominant negative ATPase-dead mutant of p97, described previously, and Mcm3 was immunoprecipitated to isolate terminating replisomes (4, 13). This comparison allowed us to determine which of the p97 cofactors identified in the p97 immunoprecipitation are also interacting with the terminated replisomes, as we appreciate that p97 does have other substrates on replicating chromatin (Fig. 1B). In doing this, we identified both major cofactors Ufd1 and Npl4, which are known to facilitate chromatin functions of p97 segregase and were shown previously by us and others to act in replisome disassembly during S-phase (4, 15). Interestingly, only two minor cofactors were identified to interact with both the replisome and p97: Faf1 and Ubxn7 (human UBXD7). Both of these factors have been shown previously to interact preferentially with p97 when in complex with Ufd1/Npl4 (16). To support this finding, we first confirmed by p97 IP and Western blotting that p97 can indeed interact with Ubxn7 and Faf1 on S-phase chromatin when replisome disassembly is blocked (Fig. 1C).

The finding of Faf1 was somewhat unsurprising as it is already known to play a role in maintaining replication fork stability in *C. elegans* and human cell lines (17), and indeed, the *C. elegans* homolog of Faf1 (UBXN-3) is essential for replisome unloading in S-phase and in mitotic prophase (4, 11). In contrast, this is the first time that Ubxn7 has been implicated in the process of replisome unloading. What is already known about Ubxn7, is that inhibition of the human homolog UBXD7 in human cells leads to hyperaccumulation of DNA damage sensors after UV damage (18), although it is best known as a regulator of degradation of the hypoxia inducible factor Hif1 α (19). Like Faf1, Ubxn7 belongs to the ubiquitin-associated (UBA)–ubiquitin regulatory X (UBX) family of p97 cofactors. This means that it interacts with ubiquitylated proteins *via* its UBA domain and with p97 *via* its UBX domain. It also contains a UAS domain of unknown function and an ubiquitin-interacting motif (UIM) (Fig. S2A) (19). Interestingly, while targeting Hif1 α for degradation, UBXD7 simultaneously interacts with active (neddylated) cullin ligase Cul2^{VHL} through its UIM domain and with p97 through its UBX domain (Fig. S2, A and B) (20). Given that the same factors appear to be involved in replisome disassembly, we hypothesized that the association of p97 with its cofactor Ubxn7 could provide a mechanism by which p97 targets Mcm7, ubiquitylated with K48-linked ubiquitin chains, synthesized by Cul2^{Lrr1}.

Ubxn7 stimulates efficient replisome disassembly

To investigate the importance of Faf1 and Ubxn7 for replisome disassembly during S-phase, we decided to

immunodeplete each protein independently from the egg extract and determine the consequences for replisome unloading. To do this, we have raised antibodies against *X. laevis* Ubxn7 and Faf1 (Fig. S7). Both Faf1 and Ubxn7 could be efficiently immunodepleted from egg extracts to less than 5% of total protein (Figs. 2, A and B and S3B). Neither depletion inhibited the synthesis of nascent DNA in a number of independent immunodepletions (Fig. 2, A and B), suggesting that neither are essential for DNA synthesis completion in the egg extract. Importantly, neither Ubxn7 nor Faf1 immunodepletion affected the level of each other (Fig. S3A). We then followed proteins on chromatin during a replication reaction in IgG-depleted and Ubxn7- or Faf1-depleted extracts. Interestingly, while immunodepletion of Faf1 had a very minor effect on replisome unloading during S-phase (Fig. 2, D and E), immunodepletion of Ubxn7 reproducibly delayed unloading of replisomes (Cdc45, Psf2) in independently immunodepleted extracts (Figs. 2, C and E and S3C), suggesting that although Ubxn7 is not essential for replisome disassembly, it does regulate the efficiency of this process.

Importance of Ubxn7 for replisome disassembly

Next, we wanted to understand how the depletion of Ubxn7 delays the unloading of the replisomes in the egg extract. Induction of replication stress, which affects progression of replication forks, can lead to transient accumulation of replisomes on chromatin. However, Ubxn7 depletion did not lead to the accumulation of DNA damage-associated replication stress, as determined by γ H2AX immunoblotting (Fig. 3A), nor the phosphorylation of Chk1 (Fig. S3D). Taken together, this demonstrates that accumulation of replisomes on chromatin in Ubxn7-depleted extract is not due to the effects of replication stress.

We next analyzed how Ubxn7 depletion affects the levels of Mcm7 ubiquitylation and chromatin-bound Cul2 and p97 (Fig. 3A). Interestingly, while the levels of p97 and Faf1 on chromatin were slightly increased by Ubxn7 depletion (Fig. 3A), Cul2 markedly accumulated on chromatin in its active neddylated form (Fig. 3A, neddylated Cul2 runs at a higher molecular size on the gel—compare size of unneddylated Cul2 in egg extract and neddylated on chromatin). Similarly, ubiquitylated Mcm7 also accumulated on chromatin, modified with long ubiquitin chains.

We then decided to ensure that these phenotypes are actually caused by immunodepletion of Ubxn7 rather than an unidentified protein recognized by Ubxn7 antibody, through supplementing immunodepleted extract with recombinant Ubxn7. As shown in Figure 3B, addition of recombinant Ubxn7 could rescue the delayed unloading of CMG components (Cdc45 and Psf2), the accumulation of Cul2 on chromatin, and the accumulation of long-chain modified Mcm7 (Fig. 3B). These results suggest that Ubxn7 may be fine-tuning the process of replisome unloading, acting as a bridge between Cul2^{Lrr1}, p97, and their shared substrate Mcm7. This bridging allows for fast and efficient processing of Mcm7 ubiquitylated with relatively short ubiquitin chains. Without Ubxn7, Cul2^{Lrr1}

Role of Ubxn7 in replisome disassembly

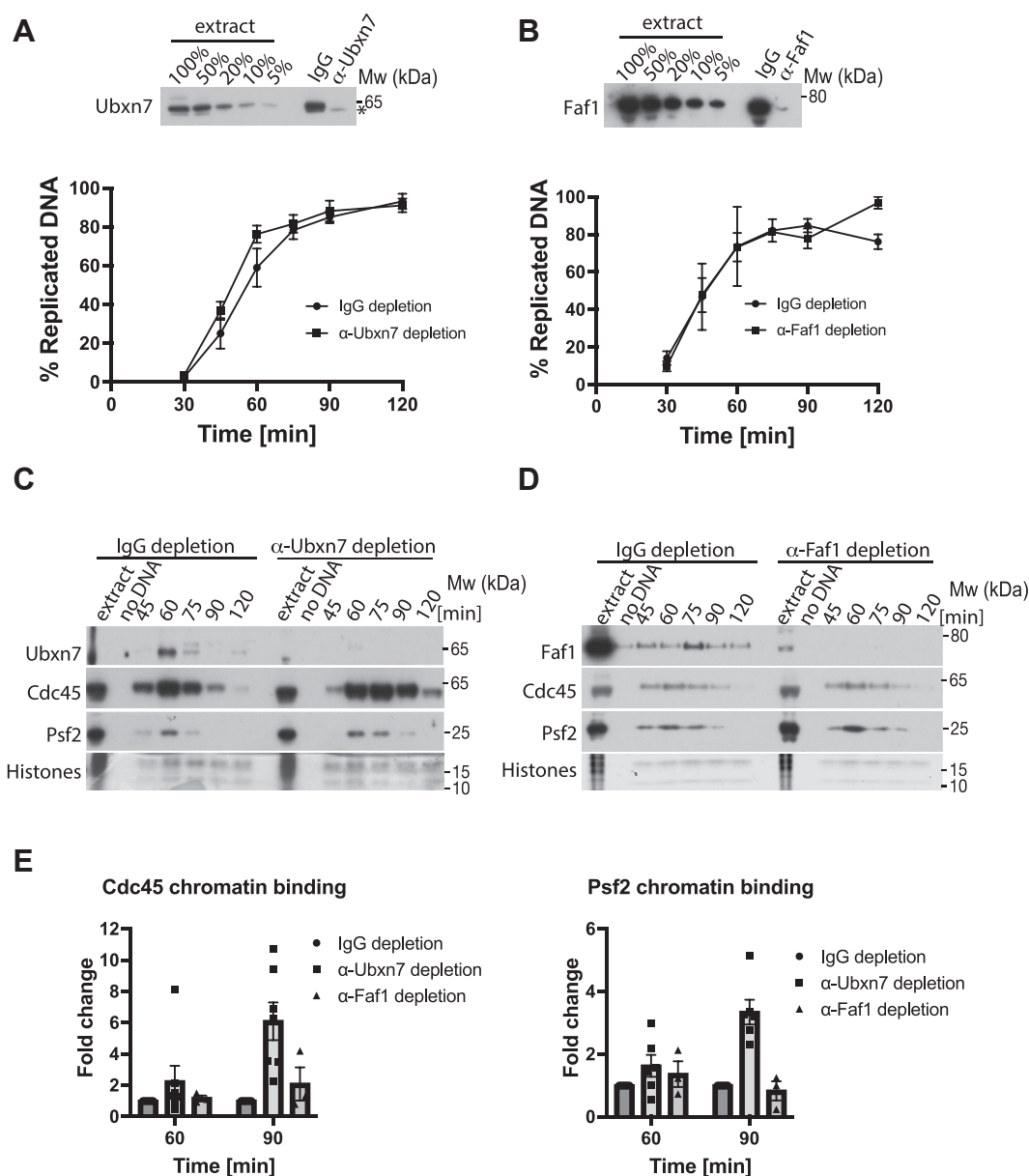


Figure 2. Ubxn7 facilitates terminated replisome unloading. A, Ubxn7 is not required for DNA replication. The remaining level of Ubxn7 upon Ubxn7 immunodepletion was analyzed by Western blotting. The asterisk indicates a nonspecific band (top). The ability of Ubxn7-immunodepleted extract to synthesize nascent DNA was analyzed by incorporation of radioactive α - 32 P-dATP into newly synthesized DNA ($n = 6$) (bottom). B, Faf1 is not required for DNA replication. The remaining level of Faf1 upon Faf1 immunodepletion was analyzed by Western blotting (top). The ability of Faf1-immunodepleted extract to synthesize nascent DNA was analyzed by incorporation of radioactive α - 32 P-dATP into newly synthesized DNA ($n = 3$) (bottom). C, Ubxn7 depletion delays terminated replisomes disassembly. Chromatin was isolated during the replication reaction time course in IgG-depleted and Ubxn7-depleted extract. Chromatin samples were analyzed as in Figure 1A with indicated antibodies. Representative experiment out of $n = 7$. Another repeat of this experiment is presented in Fig. S3C. D, Faf1 depletion does not impact terminated replisomes disassembly. Chromatin was isolated during the replication reaction time course in IgG-depleted and Faf1-depleted extract. Chromatin samples were analyzed as in Figure 1A with indicated antibodies. Representative experiment out of $n = 3$. E, the fold increase of Cdc45 and Psf2 signal on chromatin in Ubxn7- or Faf1-depleted extracts at indicated time points was quantified in comparison to IgG depletion. For Ubxn7-depleted extract $n = 7$ for Faf1-depleted extract $n = 3$. The mean value is presented with all individual points and with SEM as error bars.

recognizes terminated CMG and ubiquitylates Mcm7, but this ubiquitylated Mcm7 is not recognized and processed quickly by p97 due to lack of Ubxn7. Cul2^{Lrr1} stays therefore associated with Mcm7 for a longer time (we can observe this as accumulation of active Cul2 on chromatin), resulting in synthesis of longer ubiquitin chains on Mcm7. Although this most likely enables eventual recruitment of p97, the process is less efficient.

Regulation of Ubxn7 during DNA replication in egg extract

To determine how Ubxn7 is regulated during replication termination and replisome disassembly in the egg extract, we analyzed its pattern of chromatin binding during a replication reaction in egg extract. Throughout normal, unchallenged replication, Ubxn7 transiently interacts with chromatin with timing concomitant to that of replication fork presence and Cul2^{Lrr1} (Figs. 4, B and C and S4, A–C (dimethyl sulfoxide

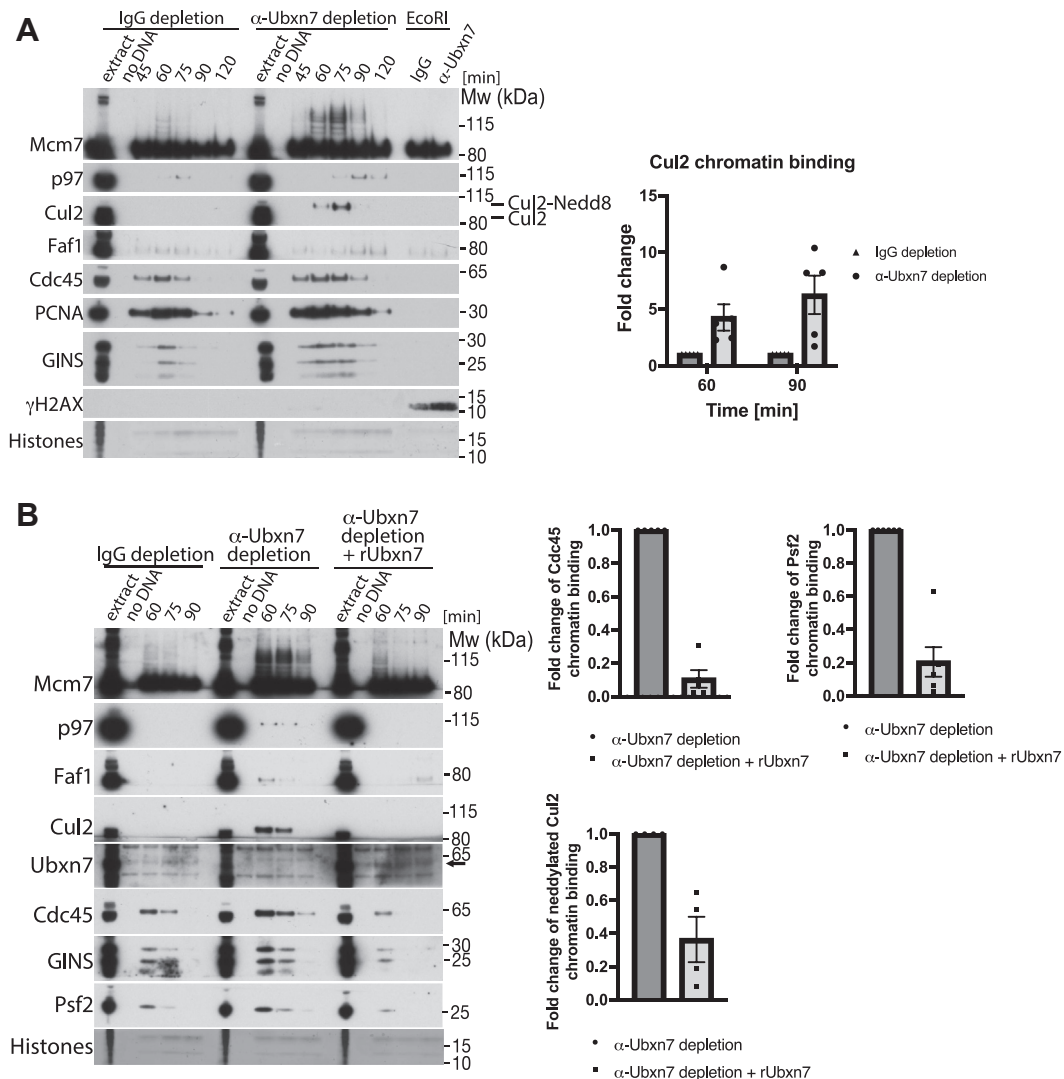


Figure 3. Ubxn7 depletion leads to accumulation of ubiquitylated Mcm7 and active Cul2^{Lrr1} on chromatin. A, chromatin was isolated during the replication reaction time course in IgG-depleted and Ubxn7-depleted extract. Chromatin samples were analyzed as in Figure 1A with indicated antibodies. Representative experiment is presented (left). The fold increase of Cul2 signal on chromatin in Ubxn7-depleted extract at indicated time points was quantified in comparison to IgG depletion (n = 5) (right). The mean value is presented with all individual points and with SEM as error bars. B, chromatin was isolated during the replication reaction time course in IgG-depleted, Ubxn7-depleted, and Ubxn7-depleted extract supplemented with recombinant Ubxn7 at 10 μ g/ml. Samples analyzed as in (A). Representative experiment (left). The rescue of the phenotypes by rUbxn7 was quantified in four experiments and the fold downregulation of Cdc45, Psf2 Cdc45 and Cul2 retention presented as a mean value with SEM (right).

[DMSO] control)). Inhibition of replisome unloading with p97 ATPase inhibitor led to an accumulation of not only CMG and Cul2^{Lrr1} on chromatin as expected (4) but also of Ubxn7 and p97 (Figs. 4A and S4A). We then analyzed the Ubxn7 chromatin-binding pattern upon inhibition of cullin ligases activity. CUL1 MLN4924 acts through inhibition of Nedd8 activating enzyme NAE and therefore inhibiting neddylation of substrates (21). As members of the cullin family of ubiquitin ligases are the main substrate of neddylation in cells, MLN4924 is primarily inhibiting all cullin activity. We have shown previously that, in *X. laevis* egg extract, inhibition of cullin activity during DNA replication inhibits Mcm7 ubiquitylation and replisome unloading from chromatin (5). While inhibition of cullin activity led to accumulation on chromatin of CMG and Cul2^{Lrr1}, as we reported previously (4), levels of chromatin-bound p97 and Ubxn7 were reduced (Figs. 4B and

S4B). This result suggests that the key determinants of p97 chromatin binding during DNA replication in the egg extract are either cullin-driven ubiquitylation of substrates and/or neddylation of cullins.

Finally, we decided to inhibit the polyubiquitylation of all the potential substrates of p97 during DNA replication by supplementing the extract with a chain terminating mutant of ubiquitin: 6xHIS-UbiNoK. Interestingly, despite inhibition of polyubiquitylation by 6xHIS-UbiNoK, as observed through accumulation of di-monoubiquitylated forms of Mcm7 on chromatin, we can reproducibly observe a higher level of p97 and Ubxn7 binding to chromatin (Figs. 4C and S4C). Importantly, neither inhibition of cullins, nor global polyubiquitylation, affects the extracts' ability to replicate DNA (Fig. S4, B and C). Our findings therefore suggest that Ubxn7 behaves like a p97 cofactor and follows the

Role of Ubxn7 in replisome disassembly

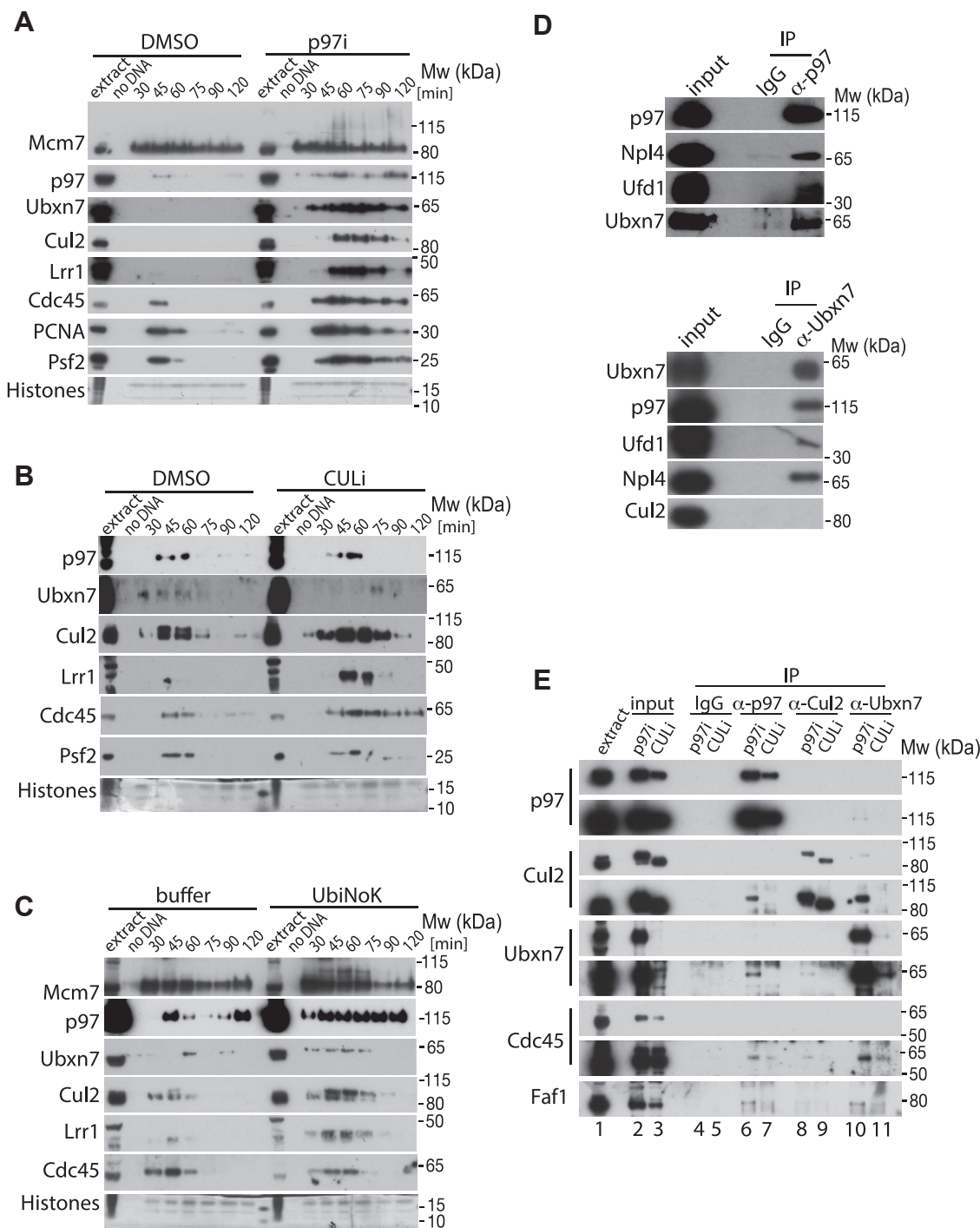


Figure 4. Regulation of Ubxn7 chromatin binding. A, p97 and Ubxn7 accumulate on chromatin upon p97 activity inhibition. Interphase egg extract was supplemented with DMSO or p97i and chromatin was isolated during the replication reaction. Chromatin samples were analyzed as in Figure 1A. Representative experiment is presented here and quantification over $n = 3$ in Fig. S4A. B, p97 and Ubxn7 decrease on chromatin upon cullin activity inhibition. Interphase egg extract was supplemented with DMSO or CULi and chromatin was isolated during the replication reaction. Chromatin samples were analyzed as in (A). Representative experiment is presented here and quantification of $n = 4$ in Fig. S4B. C, p97 and Ubxn7 accumulate on chromatin upon inhibition of polyubiquitylation. Interphase egg extract was supplemented with LFB1/50 buffer or 6HIS-UbiNoK and chromatin was isolated during the replication reaction. Chromatin samples were analyzed as in (A). Representative experiment is presented here and quantification of $n = 3$ in Fig. S4C. D, Ubxn7 interacts with p97 but not with Cul2 in egg extract. Ubxn7 or p97 were immunoprecipitated from egg extract. Interacting partners were analyzed by Western blotting with indicated antibodies. E, interaction between Ubxn7, p97, and Cul2 is disrupted when neddylation of Cul2 is inhibited. Interphase egg extract was supplemented with CULi (MLN4924) or p97i (NMS873). Chromatin was isolated in late S-phase when a high level of post-termination replisomes accumulated on chromatin, protein complexes were released from chromatin by Benzonase treatment and p97, Cul2, or Ubxn7 immunoprecipitated from the chromatin proteome. Immunoprecipitated samples were analyzed by Western blotting with indicated antibodies. Short and long exposures for each of the immunoprecipitated proteins are presented. DMSO, dimethyl sulfoxide.

same patterns of chromatin interaction. Moreover, p97 segregase is not directed to chromatin and terminated replisomes just simply through interaction with polyubiquitylated substrates, as inhibition of polyubiquitylation does not prevent p97 and Ubxn7 from binding to chromatin (Figs. 4C and S4C). It is likely therefore that treatment of replicating extract with the cullin neddylation inhibitor (MLN4924) (Figs. 4B and S4B) downregulates chromatin binding of p97 and Ubxn7 because neddylation of cullins provide a binding platform for Ubxn7.

To support this hypothesis further, we confirmed that Ubxn7 can interact with p97 not only on chromatin (Fig. 1C) but also in the egg extract (cytoplasm) (Fig. 4D). However, we could not detect an interaction between Ubxn7 and Cul2 in the egg extract (Fig. 4D), as Cul2 is present in the cytoplasmic extract in its inactive, unneddylation form. We went on to perform reciprocal immunoprecipitations of p97, Cul2, and Ubxn7 from chromatin where post-termination replisomes were accumulated due to inhibition of cullin neddylation (CULi) or p97 activity (p97i) (Fig. 4E). The level of inhibition achieved in the samples can be judged by the status of Cul2 in the input; while Cul2 is present in the extract mainly in its inactive, unneddylation form (Fig. 4E, lane 1), it accumulates on chromatin during termination upon inhibition of p97 activity mostly in its active, neddylation form (Fig. 4E, lane 2). CULi treatment, however, leads to Cul2 accumulation on chromatin in its inactive unneddylation form (Fig. 4E, lane 3). The dramatic absence of Ubxn7 on chromatin upon neddylation inhibition, despite the presence of p97 and Faf1 in this input (Fig. 4E, lane 3), clearly suggests that Ubxn7 binding to chromatin strongly depends on cullin neddylation. When present in the chromatin input, Ubxn7 could coimmunoprecipitate neddylation Cul2, Faf1, and a little of p97 (Fig. 4E, lane 10). p97 could interact with Ubxn7, Faf1, and neddylation Cul2, but this can only be detected when replisomes have accumulated in their ubiquitylated form due to inhibition of p97 activity (Fig. 4E, compare lane 6–7). Similarly, despite immunoprecipitation of equal quantities of neddylation and unneddylation Cul2 from each sample, Cul2 could only interact with Ubxn7 when in its neddylation form on p97i treated chromatin (Fig. 4E, lane 8 and 9). Reassuringly, all three, p97, Cul2 and Ubxn7, could coimmunoprecipitate a little of the component of the terminated replisome Cdc45. Altogether, these experiments suggest that Ubxn7, although being a p97 cofactor, is recruited to chromatin during the termination reaction through its interaction with neddylation Cul2. Moreover, Faf1 is likely to form a common complex with p97 and Ubxn7 as we can see it interacting with Ubxn7 when present on chromatin (Fig. 4E, lane 10).

Ubxn7 bridges Cul2^{Lrr1} and p97 through its UIM and UB domain

Our results suggest that, analogously to Hif1 α regulation, Ubxn7 acts as a bridge between Cul2^{Lrr1}, its substrate Mcm7, and the p97 segregase complex. To explore this idea in more detail, we decided to make use of separation-of-function

mutants of Ubxn7 that cannot interact with p97 (UB domain mutated, rUbxn7 ^{Δ UBX}) or Cul2 (UIM domain mutated, rUbxn7 ^{Δ UIM}) (Fig. S2, A and C). In human cells, the P459G mutation abolishes interaction with p97, while S297A abolishes interaction with neddylation Cul2, while not affecting p97 interaction (20). Moreover, L290, A293 and S297 were found to be the most conserved amino acids in UIMs of several human proteins (22). We have therefore mutated corresponding P458G in the *X. laevis* Ubxn7 sequence to create rUbxn7 ^{Δ UBX} and the corresponding L286E/A289Q/S293A residues to create rUbxn7 ^{Δ UIM} (Fig. S5A). While we were able to confirm that rUbxn7 ^{Δ UBX} cannot interact with p97 in the egg extract (Fig. S5B), Ubxn7 and Cul2 do not interact in the egg extract (cytoplasm) and so it is not easy to verify whether the rUbxn7 ^{Δ UIM} mutation disrupts this. We did observe, however, that adding a high concentration of recombinant Ubxn7 ^{Δ UIM} mutant to normal egg extract with endogenous Ubxn7 present (mimicking overexpression experiments), caused a substantial increase in active, neddylation Cul2 on chromatin. This was not observed upon addition of wt rUbxn7 or rUbxn7 ^{Δ UBX} mutants (Fig. S5C). This suggests that out-competing endogenous Ubxn7 with a mutant that cannot interact with neddylation Cul2 reproduces the phenotype of Ubxn7 immunodepletion, that is, increased and prolonged association of Cul2 with chromatin (Fig. 3A). Importantly, addition of neither protein affected the synthesis of nascent DNA (Fig. S5D). Altogether, these results suggest that Ubxn7 ^{Δ UIM} is defective in binding to neddylation Cul2.

To further test functionality of these mutants, Ubxn7 immunodepleted extract was supplemented with either WT or mutant Ubxn7. Neither addition to immunodepleted extract affected the synthesis of nascent DNA (Fig. S6A). While addition of WT Ubxn7 could support timely unloading of CMG from chromatin and prevent excessive accumulation of Cul2 on chromatin and long ubiquitin chain formation on Mcm7, neither of the two mutants could fully rescue the Ubxn7 immunodepletion phenotypes (Figs. 5A and S6B). This indicates that both domains are important for Ubxn7 function during replisome disassembly. Altogether, these data suggest that through its UB and UIM domains, Ubxn7 can indeed bridge Cul2^{Lrr1} and the p97 complex and that binding to neddylation Cul2^{Lrr1} through its UIM domain is especially important for restricting Cul2 activity and/or stimulating its dissociation from the terminated replisome during replication termination.

Unrestricted Cul2 activity allows for Mcm7 unloading in Ubxn7 depleted extract

Our aforementioned results show that upon Ubxn7 depletion, we observe accumulation on chromatin of active, neddylation Cul2^{Lrr1} and ubiquitylation forms of Mcm7. It is likely therefore that continuous growth of the length of chains on Mcm7 finally leads to p97 recognition and unloading. To test that it is Cul2^{Lrr1} and not a different ubiquitin ligase (e.g., TRAP1) synthesizing these long chains, we blocked Cul2 activity using CULi in IgG- and Ubxn7-depleted extracts

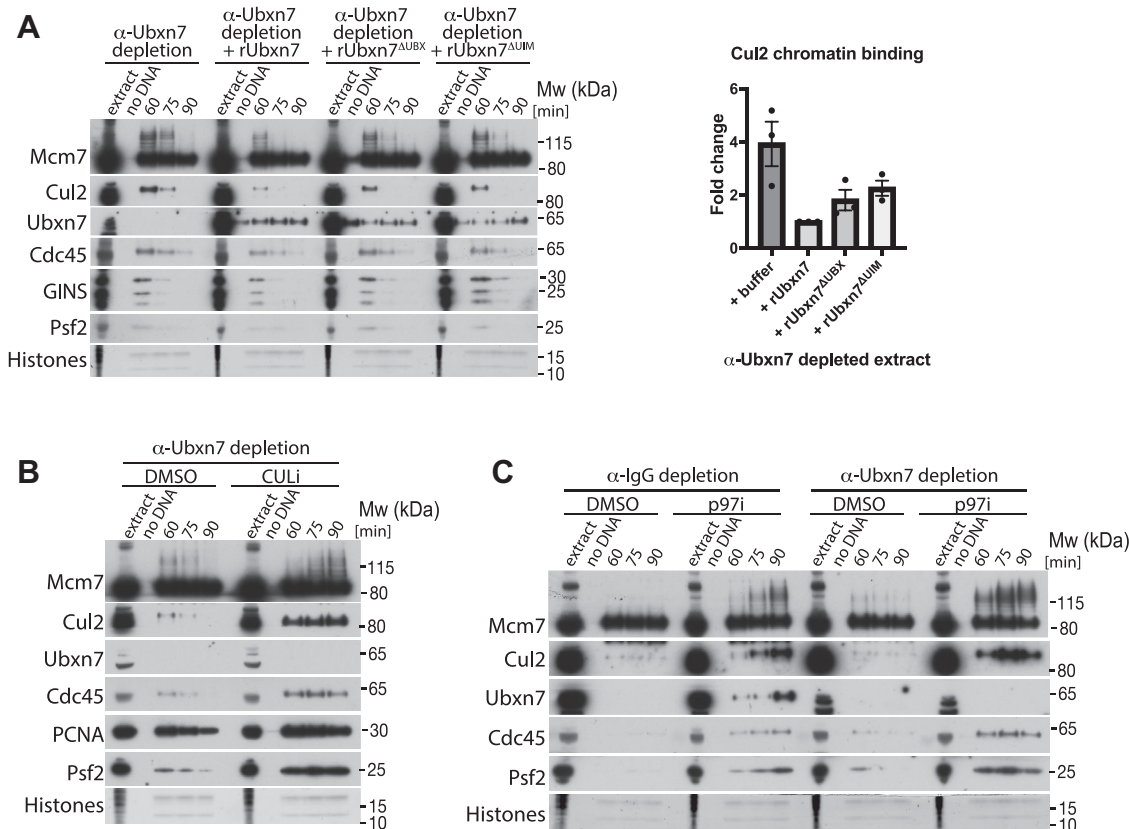


Figure 5. Ubxn7 bridges Cul2^{Lrr1} and p97 complexes leading to efficient unloading of ubiquitylated Mcm7. A, both UIM and UBX domains of Ubxn7 are important for its functions. Ubxn7 depleted extract was supplemented with recombinant Ubxn7 or point mutants that disrupt UBX or UIM domain functions (Ubxn7^{ΔUBX} and Ubxn7^{ΔUIM}, respectively). Chromatin was isolated at indicated time points and analyzed as in Figure 1A. Representative experiment is presented (left). The level of Cul2 chromatin binding at 60 min time point was quantified over three experiments and the fold rescue of the Cul2 accumulation in comparison to Ubxn7 depleted extract is presented (right). Individual values, mean, and SEM are shown. CMG unloading is quantified in Fig. S6B. B, cullin activity is needed for replisome unloading in absence of Ubxn7. Ubxn7-depleted extract was supplemented with DMSO or CULi and chromatin samples isolated during the replication reaction and analyzed as in (A). C, the chains built on Mcm7 in Ubxn7 depleted extract are shorter than those built upon p97 activity inhibition. IgG- or Ubxn7-depleted extracts were optionally supplemented with p97i. Chromatin samples were analyzed at indicated time points as in (A). CMG, Cdc45, Mcm2-7 hexamer, and GINS; DMSO, dimethyl sulfoxide; UIM, ubiquitin-interacting motif.

(Fig. 5B). Indeed, replisome disassembly was blocked in Ubxn7-depleted extract treated with CULi, and the ubiquitylation of Mcm7 observed in Ubxn7-depleted extract at 60 min was strongly inhibited by CULi. Instead, we observed a much more gradual accumulation of ubiquitylated Mcm7, as we always do upon CULi treatment (Fig. 5B, compare also Fig. S6C). This shows that Cul2 activity is still required for replisome disassembly in the absence of Ubxn7.

Finally, we wanted to assess whether the length of chains built on Mcm7 upon Ubxn7 depletion is unusually long, suggesting uncontrolled Cul2^{Lrr1} activity or whether it is comparable to the level of ubiquitylation we observe upon blocking p97 segregase activity and replisome unloading. To this end, we inhibited p97 in Ubxn7 depleted extract (Fig. 5C) and could see that the level of ubiquitylation upon complete inhibition of unloading with p97i is even higher, suggesting that it is just the delay in replisome disassembly that gives Cul2^{Lrr1} more time to ligate longer ubiquitin chains.

Altogether, our data support a model whereby Ubxn7 binds to active, neddylated Cul2^{Lrr1} on chromatin to facilitate fast recruitment of the p97 complex to ubiquitylated replisomes resulting in efficient replisome unloading

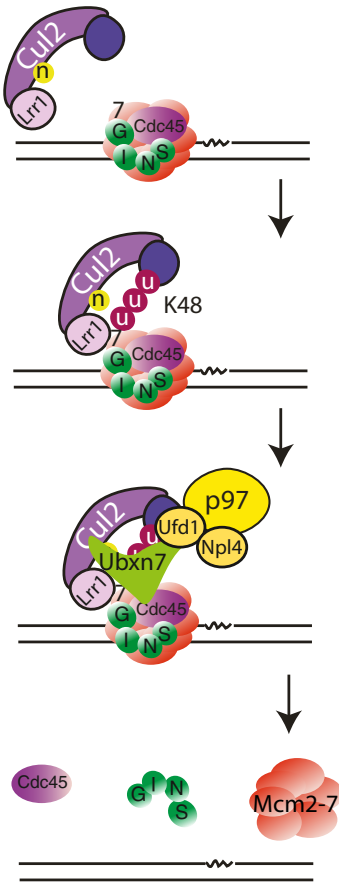
(Fig. 6A). In the absence of Ubxn7, Cul2^{Lrr1} can still bind to terminated replisome but recruitment of p97 is delayed. In the meantime, active, neddylated Cul2^{Lrr1} keeps ubiquitylating Mcm7, forming longer ubiquitin chains, which finally allow for p97 recognition and replisome disassembly (Fig. 6B).

Discussion

Ubxn7 streamlines replisome disassembly during replication termination

Our results suggest that by concomitant interactions with neddylated Cul2^{Lrr1}, ubiquitylated Mcm7, and p97 complex, Ubxn7 facilitates efficient and fast unloading of terminated CMG helicases from chromatin (Fig. 6). The general mode of Ubxn7 operation in replisome disassembly during termination closely resembles the way UBXD7 regulates degradation of Hif1α in collaboration with CUL2^{VHL} and p97/UFN1/NPL4 (19, 20). It is interesting to speculate that Ubxn7 may not only bridge the three factors to facilitate recognition of terminated ubiquitylated replisomes but may also stimulate turnover of Cul2^{Lrr1} and promote its dissociation from terminated

A Normal situation



B No Ubxn7

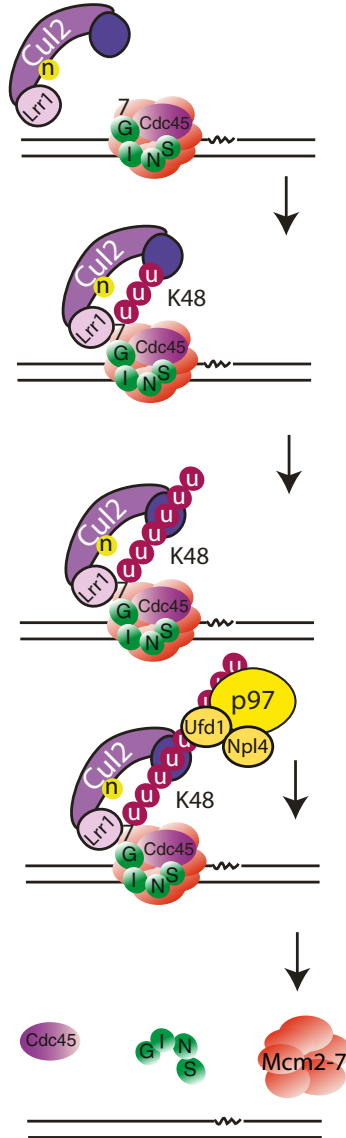


Figure 6. Proposed model of Ubxn7 function. A, Ubxn7 is bridging Cul2^{Lrr1}, ubiquitylated Mcm7, and the p97 complex, leading to efficient CMG helicase unloading. B, delays in replisome unloading upon lack of Ubxn7. p97 can still recognize ubiquitylated Mcm7 but the process is slower and takes longer time. CMG, Cdc45, Mcm2-7 hexamer, and GINS; DMSO, dimethyl sulfoxide.

replisomes. This in turn could facilitate the unfolding of ubiquitylated Mcm7 by the p97 complex.

The ability of Ubxn7 to facilitate unloading of Mcm7 ubiquitylated with short ubiquitin chains synthesized by Cul2^{Lrr1} explains also why we observe such a strong accumulation of Mcm7 modified with short ubiquitin chains after treatment of replication reactions with CULi (Figs. 5B and S6C). CULi inhibits neddylation of cullins, so it not only slows down the activity of Cul2^{Lrr1} but also inhibits the interaction of Ubxn7 with Cul2^{Lrr1}. As a result, the slowly building up chains on Mcm7 have to reach a higher threshold of length to be efficiently extracted by the p97 complex.

CULi (MLN4924) inhibits all cullin activity, and it exerts its main cytotoxic activity by inhibiting degradation of the replication licensing factor Cdt1 by CUL4^{CDT2}, which leads to

re-replication, checkpoint activation, and cell death (21, 23). A possibility exists, therefore, that the effects we observed upon treatment with CULi could arise from inhibition of neddylation of one of the other cullins important for DNA replication, namely Cul4 or Cul1 (24). However, in *Xenopus* egg extract, stabilization of Cdt1 is not enough to induce re-replication due to high activity of the Cdt1 inhibitor geminin (25). Moreover, the progress of nascent DNA synthesis is not affected by inhibition of ubiquitin-driven protein degradation in the *Xenopus* egg extract system (5, 26) and inhibition of Cul1 or Cul4 activity does not affect replisome disassembly process (data not shown). Finally, of all cullins, Ubxn7 binds most preferentially to CUL2 (19). Altogether, the effect exerted by CULi on Ubxn7 and the process of replisome disassembly is most likely directly through inhibition of Cul2 neddylation.

The function of Ubxn7/UBXD7 in streamlining the process of replisome disassembly may not just be through accelerated recognition of ubiquitylated substrate by the p97 segregase complex but also by increasing the rate of substrate unfolding. A recent study has shown that once the substrate is recognized, p97 starts substrate processing by unfolding one of the distal ubiquitins in the ubiquitin chain attached to the substrate. It then pulls both the unfolded ubiquitin chain and the unfolded substrate through the central channel of the hexamer (27), which leads to extraction of the substrate from complex structures. In the absence of Ubxn7, when Mcm7 is modified with long ubiquitin chains, the process of unfolding of such modified Mcm7 is likely to be slower as it is more likely for p97/Ufd1/Npl4 to bind the ubiquitin chain further away from the Mcm7 substrate, which necessitates unfolding of a longer ubiquitin chain before unfolding Mcm7 itself.

Ubxn7 and Faf1 during replication

Immunodepletion of Ubxn7, but not Faf1, from egg extract leads to a delay in replisome disassembly (Figs. 2 and 3). The *C. elegans* homolog of Faf1, UBXN-3, has been shown to be important for CMG helicase unloading by p97 in S-phase and in mitosis (4, 11) but also to regulate other replication factors such as CDT-1 and, recently, to regulate SUMOylated factors at DNA replication forks (17, 28, 29). It is clear, therefore, that UBXN-3 plays a key role in extraction of proteins from chromatin during DNA replication in *C. elegans* embryos. There is, however, no homolog of Ubxn7 in *C. elegans*, and UBXN-3/Faf1 does not contain a UIM domain that could direct it to neddylated cullins, so it is unlikely to directly substitute for the role that Ubxn7 plays in vertebrates.

In our experiments, in the absence of Ubxn7, the unloading of the replisomes is delayed but they are still eventually unloaded (Figs. 2 and 3). At the same time, we observe accumulation of active Cul2^{Lrr1} and higher levels of ubiquitylated Mcm7 on chromatin (Fig. 3). After a delay, p97/Ufd1/Npl4 can, therefore, recognize ubiquitylated Mcm7 and extract it, possibly with help from other cofactors such as Faf1. In other organisms that have no Ubxn7, this process is also likely to be facilitated by other cofactors such as Faf1/UBXN-3. Interestingly, in an *in vitro* reconstitution system of DNA replication with purified budding yeast proteins, where no p97 cofactors were present, Mcm7 needed to be ubiquitylated with a minimum ubiquitin chain length of 5 in order to be recognized and extracted by the CDC48 complex. This process, however, worked much better with longer chains (30). The evolution of Ubxn7 to specifically link neddylated cullins with their substrates and the processing factor p97 is an additional level of regulation that ensures efficiency in p97 substrate targeting.

The role of UBXN-3 in regulating SUMOylated factors at replication forks seems to have been conserved throughout evolution as it is also the case in human immortalized cells (29). It will be very interesting to decipher the contribution of FAF1 and UBXD7 to replisome disassembly in human cells in the future.

Importance of efficient replisome disassembly

Replisome unloading must be carefully regulated to maintain genome stability. Premature replisome unloading would likely lead to a collapse of replication forks and creation of DNA damage (31). However, defects in timely replisome disassembly are also detrimental for cells. For example, *dia2Δ* budding yeast cells, which cannot ubiquitylate Mcm7 during termination, are defective in cell cycle progression, present high levels of genomic instability, are unable to grow at low temperatures, and are sensitive to drugs that compromise replication fork progression (32–35). Genetic loss of *lrr-1* in worms results in mitotically arrested *C. elegans* embryos and germ lines (36, 37). Moreover, while partial disruption of the S-phase or mitotic pathways of replisome disassembly alone had no effect on worm embryo viability, disrupting both pathways led to embryonic lethality (4). Finally, CRISPR/Cas9-mediated deletion of LRR1 or TRAIP in a number of human cell lines is lethal (38). Interestingly, a recent study suggested that efficient LRR1-mediated replisome disassembly is essential for completion of DNA replication, possibly through recycling of replisome components from early activated replication forks to late firing ones (39). With all these in mind, it is clear that timely and efficient replisome disassembly is important for the maintenance of genome stability and that Ubxn7 is pivotal for this.

Experimental procedures

Inhibitors

MLN4924 (A01139, Active Biochem) was dissolved in DMSO at 20 mM and added to the extract 15 min after addition of sperm nuclei at 10 μM. NMS873 (17674, Cayman Chemical Company) was dissolved in DMSO at 10 mM and added to the extract 15 min after addition of sperm nuclei at 50 μM. Caffeine (C8960, Sigma) was dissolved in water at 100 mM and added to the extract along with demembranated sperm nuclei at 5 mM. Aphidicolin was dissolved in DMSO at 8 mM and added to the extract along with demembranated sperm nuclei at 40 μM. EcoR1 (R6011, Promega) was purchased at stock 12 U/μl and added to the extract at 0.05 U/μl.

Recombinant proteins

Recombinant His-tagged ubiquitin and ubiquitin mutants were purchased from Boston Biochem, dissolved in LFB1/50 buffer (10% sucrose, 50 mM KCl, 40 mM Hepes pH 8.0, 20 mM K phosphate pH 8.0, 2 mM MgCl₂, 1 mM EGTA, 2 mM DTT, 1 μg/ml of each: aprotinin, leupeptin, and pepstatin) at 10 mg/ml and used at 0.5 mg/ml in *X. laevis* egg extract.

pET28a-Ubxn7, pET28a-Ubxn7-P458G, and pET28a-Ubxn7-L286E/A289Q/S293A vectors were used for protein expression in 2L of BL21-codon Plus (DE3)-RIPL (1 mM IPTG added at A₆₀₀ = 0.6, followed by incubation overnight at 20 °C). Frozen bacterial pellets were lysed in LFB1/50 buffer (10% sucrose, 50 mM KCl, 40 mM Hepes pH 8.0, 20 mM K phosphate pH 8, 2 mM MgCl₂, 1 mM EGTA, 2 mM DTT,

1 µg/ml of each: aprotinin, leupeptin, and pepstatin) and supplemented with 1 mg/ml lysozyme and BitNuclease. After sonication, the lysate was clarified by centrifugation at 14,000g for 30 min at 4 °C, and supernatants containing soluble proteins were then incubated with 2 ml of prewashed Super N-NTA affinity resin (SUPER-NINTA100, Genexon) for 2 h, rotating at 4 °C. The beads were then washed 2× with 30 ml of LFB1/50 buffer and 2× with LFB1/200 (200 mM KCl), both supplemented with 20 mM imidazole. The beads were transferred to 10 ml columns (Poly-Prep Chromatography Column, Bio-Rad) and eluted with LFB1/50 supplemented with 250 mM imidazole.

To outcompete endogenous Ubxn7, recombinant Ubxn7 was used at 0.3 mg/ml in egg extract, while to rescue Ubxn7 depleted extract, it was added at 10 µg/ml.

Full-length 6xHis-Faf1 was expressed from pET28a-Faf1 in Rosetta (DE3) pLysS competent cells (Novagen, Merck Millipore) bacteria as aforementioned. It was purified as Ubxn7 but using the following buffers: lysis buffer (500 mM NaCl, 50 mM Tris-HCl pH 8.0, 2 mM MgCl₂, 10% glycerol, 0.1% Triton, 1 µg/ml of each: aprotinin, leupeptin, and pepstatin, 1 mg/ml lysozyme). After incubation, beads were washed with lysis buffer supplemented with 20 mM imidazole. Beads were eluted with lysis buffer supplemented with 250 mM imidazole.

X. laevis GINS was expressed in BL21 (DE3) competent *Escherichia coli* cells (C2527H, New England Biolabs) bacteria. The isolated cell pellets were then resuspended into 50 mM Tris pH 7.4, 500 mM NaCl, 0.1 mM PMSF (Sigma), and protease inhibitor tablets (11836170001, Roche). Samples were sonicated for 3X 1 min, 2 s pulses - 50% duty cycle and supplemented with 1 mg/ml lysozyme. The suspension was then incubated on rocker at 4 °C for 1 h and then clarified by centrifugation at 20,000g for 30 min at 4 °C, followed by filtration through 0.22 µm polyethersulfone filters (Millipore). The supernatant was then passed through 5 ml His-Trap HP column (Cytiva) connected to AKTApurifier plus (GE). Gradient elutions were performed with imidazole containing buffer (50 mM Tris pH 7.4, 500 mM NaCl, 500 mM imidazole, and 0.1 mM PMSF). *X. laevis* GINS fractions were eluted with ~79 to 134 mM imidazole. All fractions were pooled and stored in -80 °C.

Antibodies

α-PCNA (P8825) and α-HIS (H1029) were purchased from Sigma; α-Cul2 (EPR3104) was purchased from Abcam; α-p97 (65278) was purchased from Progen Biotechnik, anti-P-Chk1 (S345) from Cell Signaling, γ-H2AX (4418-APC-020, Trevigen).

Affinity purified α-Cdc45, α-Psf2 (40), α-Mcm3 (41), α-LRR1 (S962D) and α-Cul2 (SA206) (4), and α-Mcm7 (6) were previously described. *Xenopus* Ufd1 antibody was a kind gift from Prof Stemmann's lab (13).

Xenopus full-length p97, Ubxn7, Faf1, and GINS proteins were purified as described previously (6, 13) and antibodies raised against such prepared antigens in sheep (p97, GINS,

Ubxn7) or rabbit (Faf1). The resulting antibody sera were purified in-house against the purified antigen. The specificity of each new antibody is presented in Fig S7.

X. laevis egg extract preparation

All of the work with *X. laevis* was approved by Animal Welfare and Ethical Review Body (AWERB) at University of Birmingham and approved by UK Home Office in form of Project License issued for Dr Agnieszka Gambus. *X. laevis* egg extract was prepared as previously described (42).

DNA synthesis assay

Interphase *X. laevis* egg extract was supplemented with 10 ng/µl of demembrated sperm nuclei and incubated at 23 °C for indicated time. Synthesis of nascent DNA was then measured by quantification of α-³²P-dATP incorporation into newly synthesized DNA, as described before (42). The extract contains endogenous deoxynucleoside triphosphate pools of ~50 µM (43). The total amount of DNA synthesized, expressed as nanogram DNA/µl extract, can then be calculated by multiplying percent total ³²P incorporated by a factor of 0.654 (43). This calculation assumes an average molecular weight of 327 Da for deoxynucleoside monophosphate and equal quantities of all four deoxynucleoside triphosphates incorporated into DNA (weight of deoxynucleoside monophosphate incorporated in ng/µl = percent total ³²P incorporated/100 × 50 × 10⁻⁶ × 4 × 327 × 10³) (43).

Chromatin isolation time course

Interphase *X. laevis* egg extract was supplemented with 10 to 15 ng/µl of demembrated sperm DNA and subjected to indicated treatments. The reaction was incubated at 23 °C for indicated length of time when chromatin was isolated in ANIB100 buffer (50 mM Hepes pH 7.6, 100 mM KOAc, 10 mM MgOAc, 2.5 mM Mg-ATP, 0.5 mM spermidine, 0.3 mM spermine, 1 µg/ml of each aprotinin, leupeptin, and pepstatin, 25 mM β-glycerophosphate, 0.1 mM Na₃VO₄, 0.2 µM microcystin-LR, and 10 mM 2-chloroacetamide [Merck]) as described previously (42).

During the chromatin isolation procedure, a sample without addition of sperm DNA (no DNA) is processed in an analogous way, usually at the end of the time course, to serve as a chromatin specificity control. The bottom of the PAGE gel on which the chromatin samples were resolved is cut off and stained with colloidal Coomassie (SimplyBlue, Life Technologies) to stain histones which provide loading controls and indications of sample contamination with egg extract (cytoplasm).

Nuclei isolation for Chk1 phosphorylation

The nuclei isolation was performed as previously described (5).

Immunoprecipitation from egg extract

Twenty microliter of egg extract per IP was induced into interphase, and the extract was then supplemented with 4 vol of LFB1/50 buffer (10% sucrose, 50 mM KCl, 40 mM Hepes

Role of Ubxn7 in replisome disassembly

pH 8, 20 mM K phosphate pH 8, 2 mM MgCl₂, 1 mM EGTA, 2 mM DTT, 1 µg/ml of each: aprotinin, leupeptin, and pepstatin). The diluted extract was cleared of insoluble material by 15 min centrifugation in a microfuge at 4 °C, 16k rcf. About 100 µl of diluted extract was supplemented with 1 µg of affinity purified Ubxn7, p97, or IgG from sheep serum (I5131, Sigma) and incubated on ice for 1 h with sporadic mixing. Twenty microliter of prewashed Protein G Dynabeads (10004D, Life Technologies) were added to each IP sample and incubated for 1 h at 4 °C with rotation. After incubation the beads were washed 3× with LFB1/50 and boiled in NuPAGE LDS loading buffer (Life Technologies).

Immunoprecipitation from chromatin

Hundred microliter of egg extract per IP was induced into interphase and mixed with 10 to 15 ng/µl demembranated sperm nuclei and optionally supplemented with the indicated treatments. The reaction was incubated at 23 °C for the indicated time. Chromatin was isolated in ANIB100 (50 mM Hepes pH 7.6, 100 mM KOAc, 10 mM MgOAc, 2.5 mM Mg-ATP, 0.5 mM spermidine, 0.3 mM spermine, 1 µg/ml of each aprotinin, leupeptin, and pepstatin, 25 mM β-glycerophosphate, 0.1 mM Na₃VO₄, 0.2 µM microcystin-LR, and 10 mM 2-chloroacetamide), and the chromatin pellets were resuspended in the same volume of original extract of ANIB100 containing 20% sucrose. Protein complexes were released from chromatin by digestion with 2 U/µl of Benzonase nuclease (E1014-25KU, Sigma) and sonicated for 5 min using a Diagenode sonicator with following settings: 15s on, 15s off, medium setting. The insoluble fraction was then spun in a microfuge at 4 °C, 10 min, 16k rcf.

Prepared beads,

- (1) 30 µl of Dynabeads M-270 epoxy (14302D, Life Technologies) coupled covalently to 20 µg of affinity purified p97 antibody, affinity purified Ubxn7 antibodies, or IgG from sheep serum (I5131, Sigma) and
- (2) 30 µl of Dynabeads Protein G (10004D, Life Technologies) covalently coupled to 6 µg of affinity purified p97 antibody, affinity purified Ubxn7, affinity purified Cul2, or IgG from sheep serum (I5131, Sigma) using BS3 crosslinker (S5799, Sigma),

were incubated with 100 µl digested chromatin at 4 °C for 1 to 2 h with rotation. Following the incubation time, beads were washed for 5 min rotating at 4 °C twice with ANIB100, once with ANIB100 containing an additional 0.1% Triton X-100, and finally twice with ANIB100 buffer. Each sample was prepared by boiling in 30 µl of 2× NuPAGE LDS loading buffer (Life Technologies) for 5 min.

Immunoprecipitation of p97 and MS

About 3.75 ml of *X. laevis* egg extract was activated and supplemented with 10 ng/µl of demembranated sperm DNA, 50 µM p97 inhibitor NMS873, and incubated at 23 °C for 60 min. Chromatin was isolated in ANIB/100 buffer. Immunoprecipitation of p97 was performed as described previously

(4), and the immunoprecipitated material was analyzed by MS with Dr Richard Jones from MS Bioworks LLC.

Sample preparation

Each sample was run on a 5% to 20% gradient gel (Invitrogen) for 1 cm and cut into 10 bands. Samples were submitted pre-plated for 10 fraction analysis. Gel pieces were processed using a robot (Progest, DigiLab) with the following protocol:

- (1) Washed with 25 mM ammonium bicarbonate followed by acetonitrile.
- (2) Reduced with 10 mM DTT at 60 °C followed by alkylation with 50 mM iodoacetamide at room temperature.
- (3) Digested with trypsin (Promega) at 37 °C for 4 h.
- (4) Quenched with formic acid and the supernatant was analyzed directly without further processing.

MS

The gel digests were analyzed by nano LC/MS/MS with a Waters M-class HPLC system interfaced to a ThermoFisher Fusion Lumos. Peptides were loaded on a trapping column and eluted over a 75 µm analytical column at 350 nl/min; both columns were packed with Luna C18 resin (Phenomenex). A 30 min gradient was employed. The mass spectrometer was operated in data-dependent mode, with MS and MS/MS performed in the Orbitrap at 60,000 FWHM resolution and 15,000 FWHM resolution, respectively. Advanced peak determination was turned on. The instrument was run with a 3 s cycle for MS and MS/MS. Proteome Discoverer v1.4 (ThermoFisher; www.thermofisher.com) was used for peak generation.

Data processing

Data were searched using a local copy of Mascot (Matrix Science; version 2.8.0.1) with the following parameters:

Enzyme: Trypsin Fully Specific

Database: Uniprot *Xenopus* (forward and reverse appended with common contaminants) released on 04/15/2014. 79,274 (including reverse and CON) entries in the database were searched.

Fixed modification: Carbamidomethyl (C)

Variable modifications: Oxidation (M), Acetyl (Protein N-term), Deamidation (NQ), GlyGly (K), Phospho (STY)

Mass values: Monoisotopic

Peptide Mass Tolerance: 10 ppm

Fragment Mass Tolerance: 0.02 Da

Max Missed Cleavages: 2

Mascot DAT files were parsed into the Scaffold (version Scaffold_5.1.0, Proteome Software Inc) software for validation, filtering, and to create a nonredundant list per sample. Data were filtered with 1% protein and peptide false discovery rate (FDR) and requiring at least two unique peptides per protein.

Peptide identifications were accepted if they could be established at greater than 34.0% probability to achieve an FDR less than 1.0% by the Percolator posterior error probability calculation (44). Protein identifications were accepted if they could be established at greater than 99.0% probability to achieve an FDR less than 1.0% and contained at least two

identified peptides. Protein probabilities were assigned by the Protein Prophet algorithm (45). Proteins that contained similar peptides and could not be differentiated based on MS/MS analysis alone were grouped to satisfy the principles of parsimony.

Immunodepletion

Ubxn7 immunodepletions were performed using Dynabeads protein G (10004D, Life Technologies) coupled to antibodies against Ubxn7 or nonspecific sheep IgGs (I5131, Sigma), with two rounds of 1 h incubation at 4 °C. The Ubxn7 antibodies were coupled at 600 µg per 1 ml of beads. Effective immunodepletion required two rounds of 1 h incubation of egg extract with antibody coupled beads at 50% beads ratio.

Faf1 immunodepletions were performed using Dynabeads protein A (10002D, Life Technologies) coupled to *Xenopus* Faf1 antibodies raised in rabbit and affinity purified or nonspecific rabbit IgG (I5006, Sigma). The Faf1 antibodies were coupled at 600 µg per 1 ml of beads. Effective immunodepletion required three rounds of 40 min incubation of egg extract with antibody coupled beads at 50% beads ratio.

HIS-pull down from egg extract

Thirty microliter of interphase egg extract per pull down was supplemented with 10 ng/µl of demembrated sperm nuclei and optionally supplemented with LFB1/50 buffer or 0.3 mg/ml of recombinant Ubxn7^{ΔUBX}, Ubxn7^{ΔUIM}, or Ubxn7^{wt} proteins. The replication reaction was stopped with LFB1/50 buffer supplemented with 0.1% Triton X-100 and chloroacetamide in the middle of the S-phase. The samples were sonicated for 5 min using the Diagenode cold water sonicator with following settings: 15s on, 15s off, medium settings. Insoluble material was clarified for 10 min at 4 °C at 16k rcf and incubated with 60 µl Dynabeads HIS-tag isolation (10104D, Invitrogen) for 2 h with rotation at 4 °C. Beads were subsequently washed two times with LFB1/50 buffer supplemented with 0.1% Triton X-100 and chloroacetamide. Pulled-down HIS-tagged proteins were eluted by boiling the beads in 30 µl of 2× NuPAGE LDS loading buffer for 5 min.

Western blot quantification

The quantification of Western blots is provided to indicate reproducibility of trends in experiments rather than to provide absolute values of increases or decreases in a signal. The quantified experiments were performed in different preparations of extracts and independently immunodepleted extracts to confirm that observed phenotypes are not specific for one extract preparation. As a result, the extracts differ slightly in their kinetics of DNA replication reaction, which can affect the levels of detected proteins on chromatin at the same time points between different experiments. They do, however, all reproducibly show the same trend of change across the experiments.

The density of pixels of each band of the Western blot and scanned stained histones within the gel were quantified using ImageJ software (National Institute of Health; [https://](https://imagej.net/software/imagej/)

imagej.net/software/imagej/). The numeric value in arbitrary units for each band was normalized to loading control (bands of Coomassie stained histones). The analysis of control and treatment samples was always done together and the fold difference between them calculated. Fold change from a number of repeated experiments is plotted on the graphs with mean value and SEM as calculated by GraphPad PRISM.

Data availability

The mass spectrometry proteomics data have been deposited to the ProteomeXchange Consortium *via* the PRIDE repository with the dataset identifier:

Project Name: Immunoprecipitation of p97 from *X. laevis* S-phase chromatin

Project accession: PXD029705

Project DOI: [10.6019/PXD029705](https://doi.org/10.6019/PXD029705)

Supporting information—This article contains supporting information.

Acknowledgments—We would like to thank Dr Rebecca Jones, Dr Neville Gilhooly, Dr Marco Saponaro, Dr Paloma Garcia, and Dr Clare Davies for critical discussions of the manuscript. We would also like to thank our families for the continuous support. Zeynep Tarcan was funded by Islamic Development Bank PhD scholarship and by Wellcome Trust Investigator Award (215510/Z/19/Z) for A. Gambus. Divyasree Poovathumkadavil is funded by College of Medical and Dental Sciences, University of Birmingham. Dr Aggeliki Skagia is funded by BBSRC responsive mode grant BB/T001860/1.

Author contributions—A. G. conceptualization; Z. T. and A. G. methodology; A. G. formal analysis; Z. T., D. P., A. S., and A. G. investigation; A. G. writing—original draft; D. P. writing—review & editing; Z. T., D. P., and A. G. visualization; A. G. supervision; A. G. funding acquisition.

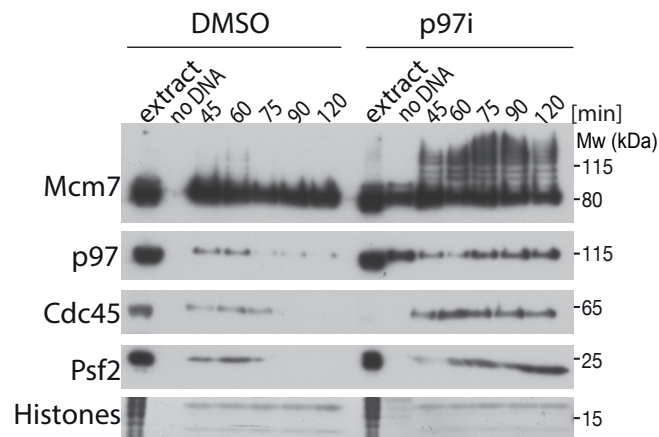
Conflict of interest—The authors declare that they have no conflicts of interest with the contents of this article.

Abbreviations—The abbreviations used are: CMG, Cdc45, Mcm2-7 hexamer, and GINS; DMSO, dimethyl sulfoxide; FDR, false discovery rate; IP, immunoprecipitate; MS, mass spectrometry; UIM, ubiquitin-interacting motif.

References

1. Moyer, S. E., Lewis, P. W., and Botchan, M. R. (2006) Isolation of the Cdc45/Mcm2-7/GINS (CMG) complex, a candidate for the eukaryotic DNA replication fork helicase. *Proc. Natl. Acad. Sci. U. S. A.* **103**, 10236–10241.
2. Gambus, A., Jones, R. C., Sanchez-Diaz, A., Kanemaki, M., van Deursen, F., Edmondson, R. D., *et al.* (2006) GINS maintains association of Cdc45 with MCM in replisome progression complexes at eukaryotic DNA replication forks. *Nat. Cell Biol.* **8**, 358–366.
3. Dewar, J. M., Budzowska, M., and Walter, J. C. (2015) The mechanism of DNA replication termination in vertebrates. *Nature* **525**, 345–350.
4. Sonnevile, R., Moreno, S. P., Knebel, A., Johnson, C., Hastie, C. J., Gartner, A., *et al.* (2017) CUL-2LRR-1 and UBXN-3 drive replisome disassembly during DNA replication termination and mitosis. *Nat. Cell Biol.* **19**, 468–479.

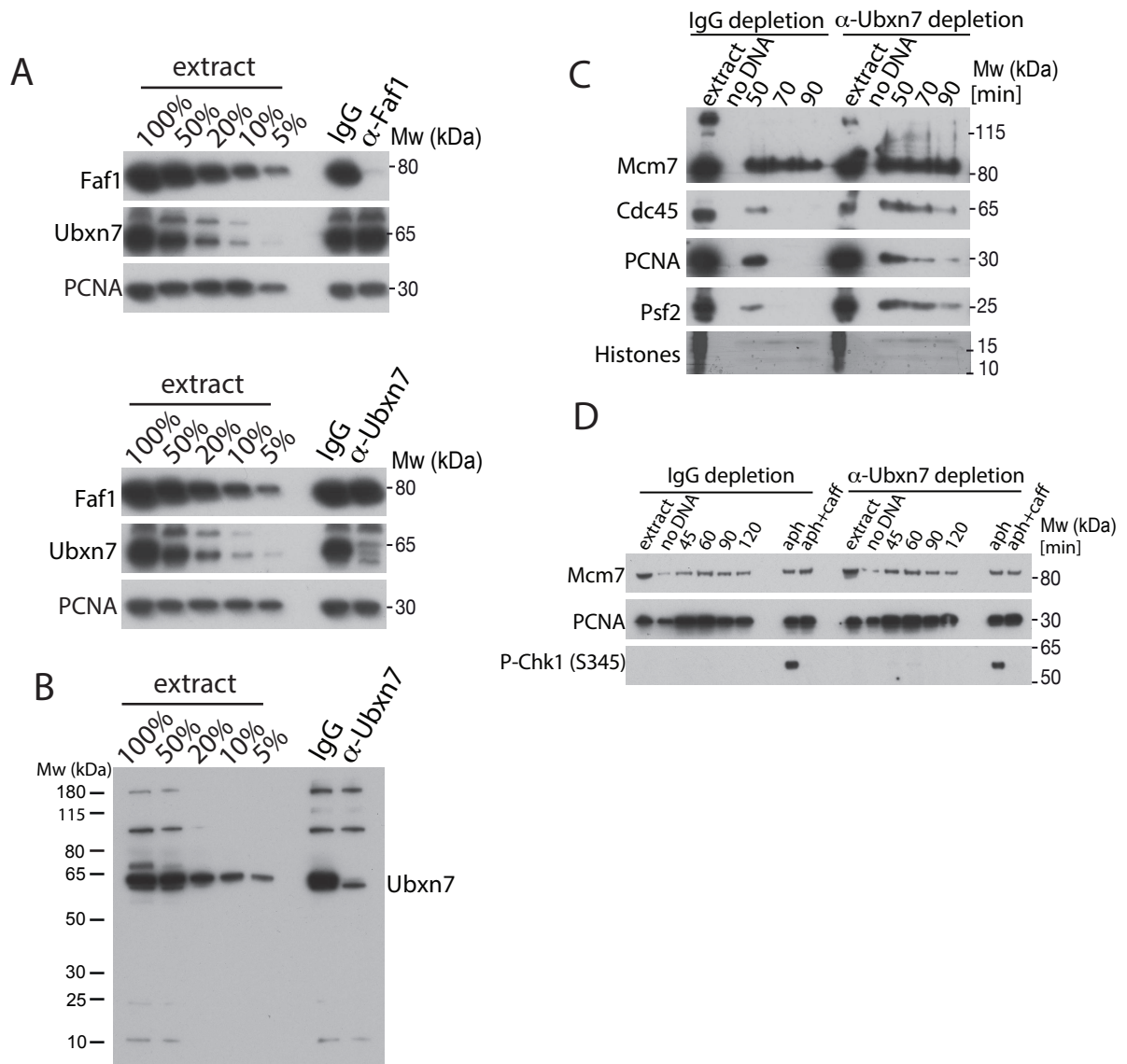
5. Moreno, S. P., Bailey, R., Campion, N., Herron, S., and Gambus, A. (2014) Polyubiquitylation drives replisome disassembly at the termination of DNA replication. *Science* **346**, 477–481
6. Priego Moreno, S., Jones, R. M., Poovathumkadavil, D., Scaramuzza, S., and Gambus, A. (2019) Mitotic replisome disassembly depends on TRAP1 ubiquitin ligase activity. *Life Sci. Alli.* **2**, e201900390
7. Wu, R. A., Semlow, D. R., Kamimae-Lanning, A. N., Kochenova, O. V., Chistol, G., Hodskinson, M. R., et al. (2019) TRAP1 is a master regulator of DNA interstrand crosslink repair. *Nature* **567**, 267–272
8. Larsen, N. B., Gao, A. O., Sparks, J. L., Gallina, I., Wu, R. A., Mann, M., et al. (2019) Replication-coupled DNA-protein crosslink repair by SPRTN and the proteasome in *Xenopus* egg extracts. *Mol. Cell* **73**, 574–588.e577
9. Meyer, H., Bug, M., and Bremer, S. (2012) Emerging functions of the VCP/p97 AAA-ATPase in the ubiquitin system. *Nat. Cell Biol.* **14**, 117–123
10. Hanzelmann, P., and Schindelin, H. (2017) The interplay of cofactor interactions and post-translational modifications in the regulation of the AAA+ ATPase p97. *Front. Mol. Biosci.* **4**, 21
11. Xia, Y., Fujisawa, R., Deegan, T. D., Sonnevile, R., and Labib, K. P. M. (2021) TIMELESS-TIPIN and UBXN-3 promote replisome disassembly during DNA replication termination in *Caenorhabditis elegans*. *EMBO J.* **40**, e108053
12. Buchberger, A., Schindelin, H., and Hanzelmann, P. (2015) Control of p97 function by cofactor binding. *FEBS Lett.* **589**, 2578–2589
13. Heubes, S., and Stemmann, O. (2007) The AAA-ATPase p97-Ufd1-Npl4 is required for ERAD but not for spindle disassembly in *Xenopus* egg extracts. *J. Cell Sci.* **120**, 1325–1329
14. Her, N. G., Toth, J. I., Ma, C. T., Wei, Y., Motamedchaboki, K., Sergienko, E., et al. (2016) p97 composition changes caused by allosteric inhibition are suppressed by an on-target mechanism that increases the enzyme's ATPase activity. *Cell Chem. Biol.* **23**, 517–528
15. Dewar, J. M., Low, E., Mann, M., Raschle, M., and Walter, J. C. (2017) CRL2Lrr1 promotes unloading of the vertebrate replisome from chromatin during replication termination. *Genes Dev.* **31**, 275–290
16. Hanzelmann, P., Buchberger, A., and Schindelin, H. (2011) Hierarchical binding of cofactors to the AAA ATPase p97. *Structure* **19**, 833–843
17. Franz, A., Pirson, P. A., Pilger, D., Halder, S., Achuthankutty, D., Kashkar, H., et al. (2016) Chromatin-associated degradation is defined by UBXN-3/FAF1 to safeguard DNA replication fork progression. *Nat. Commun.* **7**, 10612
18. Puimalainen, M. R., Lessel, D., Ruthemann, P., Kaczmarek, N., Bachmann, K., Ramadan, K., et al. (2014) Chromatin retention of DNA damage sensors DDB2 and XPC through loss of p97 segregase causes genotoxicity. *Nat. Commun.* **5**, 3695
19. Alexandru, G., Graumann, J., Smith, G. T., Kolawa, N. J., Fang, R., and Deshaies, R. J. (2008) UBXN7 binds multiple ubiquitin ligases and implicates p97 in HIF1alpha turnover. *Cell* **134**, 804–816
20. Bandau, S., Knebel, A., Gage, Z. O., Wood, N. T., and Alexandru, G. (2012) UBXN7 docks on neddylated cullin complexes using its UIM motif and causes HIF1alpha accumulation. *BMC Biol.* **10**, 36
21. Soucy, T. A., Smith, P. G., Milhollen, M. A., Berger, A. J., Gavin, J. M., Adhikari, S., et al. (2009) An inhibitor of NEDD8-activating enzyme as a new approach to treat cancer. *Nature* **458**, 732–736
22. den Besten, W., Verma, R., Kleiger, G., Oania, R. S., and Deshaies, R. J. (2012) NEDD8 links cullin-RING ubiquitin ligase function to the p97 pathway. *Nat. Struct. Mol. Biol.* **19**. <https://doi.org/10.1038/nsmb.2269>
23. Lin, J. J., Milhollen, M. A., Smith, P. G., Narayanan, U., and Dutta, A. (2010) NEDD8-targeting drug MLN4924 elicits DNA rereplication by stabilizing Cdt1 in S phase, triggering checkpoint activation, apoptosis, and senescence in cancer cells. *Cancer Res.* **70**, 10310–10320
24. Jang, S. M., Redon, C. E., and Aladjem, M. I. (2018) Chromatin-bound cullin-ring ligases: regulatory roles in DNA replication and potential targeting for cancer therapy. *Front. Mol. Biosci.* **5**, 19
25. Li, A., and Blow, J. J. (2005) Cdt1 downregulation by proteolysis and geminin inhibition prevents DNA re-replication in *Xenopus*. *EMBO J.* **24**, 395–404
26. Mahaffey, D. T., Gorbea, C., and Rechsteiner, M. (2003) Evidence that DNA replication is not regulated by ubiquitin-dependent proteolysis in *Xenopus* egg extract. *Exp. Cell Res.* **288**, 225–234
27. Twomey, E. C., Ji, Z., Wales, T. E., Bodnar, N. O., Ficarro, S. B., Marto, J. A., et al. (2019) Substrate processing by the Cdc48 ATPase complex is initiated by ubiquitin unfolding. *Science* **365**, eaax1033
28. Franz, A., Orth, M., Pirson, P. A., Sonnevile, R., Blow, J. J., Gartner, A., et al. (2011) CDC-48/p97 coordinates CDT-1 degradation with GINS chromatin dissociation to ensure faithful DNA replication. *Mol. Cell* **44**, 85–96
29. Franz, A., Valledor, P., Ubieto-Capella, P., Pilger, D., Galarreta, A., Lafarga, V., et al. (2021) USP7 and VCP(FAF1) define the SUMO/Ubiquitin landscape at the DNA replication fork. *Cell Rep.* **37**, 109819
30. Mukherjee, P. P., and Labib, K. P. M. (2019) *In vitro* reconstitution defines the minimal requirements for cdc48-dependent disassembly of the CMG helicase in budding yeast. *Cell Rep.* **28**, 2777–2783.e2774
31. Deng, L., Wu, R. A., Sonnevile, R., Kochenova, O. V., Labib, K., Pellman, D., et al. (2019) Mitotic CDK promotes replisome disassembly, fork breakage, and complex DNA rearrangements. *Mol. Cell* **73**, 915–929.e916
32. Pan, X., Ye, P., Yuan, D. S., Wang, X., Bader, J. S., and Boeke, J. D. (2006) A DNA integrity network in the yeast *Saccharomyces cerevisiae*. *Cell* **124**, 1069–1081
33. Koepp, D. M., Kile, A. C., Swaminathan, S., and Rodriguez-Rivera, V. (2006) The F-box protein Dia2 regulates DNA replication. *Mol. Biol. Cell* **17**, 1540–1548
34. Blake, D., Luke, B., Kanellis, P., Jorgensen, P., Goh, T., Penfold, S., et al. (2006) The F-box protein Dia2 overcomes replication impedance to promote genome stability in *Saccharomyces cerevisiae*. *Genetics* **174**, 1709–1727
35. Morohashi, H., Maculins, T., and Labib, K. (2009) The amino-terminal TPR domain of Dia2 tethers SCF(Dia2) to the replisome progression complex. *Curr. Biol.* **19**, 1943–1949
36. Burger, J., Merlet, J., Tavernier, N., Richaudeau, B., Arnold, A., Ciosk, R., et al. (2013) CRL2(LRR-1) E3-ligase regulates proliferation and progression through meiosis in the *Caenorhabditis elegans* germline. *PLoS Genet.* **9**, e1003375
37. Merlet, J., Burger, J., Tavernier, N., Richaudeau, B., Gomes, J. E., and Pintard, L. (2010) The CRL2LRR-1 ubiquitin ligase regulates cell cycle progression during *C. elegans* development. *Development* **137**, 3857–3866
38. Hart, T., Chandrashekar, M., Aregger, M., Steinhart, Z., Brown, K. R., MacLeod, G., et al. (2015) High-resolution CRISPR screens reveal fitness genes and genotype-specific cancer liabilities. *Cell* **163**, 1515–1526
39. Fan, Y., Koberlin, M. S., Ratnayeke, N., Liu, C., Deshpande, M., Gerhardt, J., et al. (2021) LRR1-mediated replisome disassembly promotes DNA replication by recycling replisome components. *J. Cell Biol.* **220**, e202009147
40. Gambus, A., Khoudoli, G. A., Jones, R. C., and Blow, J. J. (2011) MCM2-7 form double hexamers at licensed origins in *Xenopus* egg extract. *J. Biol. Chem.* **286**, 11855–11864
41. Khoudoli, G. A., Gillespie, P. J., Stewart, G., Andersen, J. S., Swedlow, J. R., and Blow, J. J. (2008) Temporal profiling of the chromatin proteome reveals system-wide responses to replication inhibition. *Curr. Biol.* **18**, 838–843
42. Gillespie, P. J., Gambus, A., and Blow, J. J. (2012) Preparation and use of *Xenopus* egg extracts to study DNA replication and chromatin associated proteins. *Methods* **57**, 203–213
43. Blow, J. J., and Laskey, R. A. (1986) Initiation of DNA replication in nuclei and purified DNA by a cell-free extract of *Xenopus* eggs. *Cell* **47**, 577–587
44. Kall, L., Storey, J. D., and Noble, W. S. (2008) Non-parametric estimation of posterior error probabilities associated with peptides identified by tandem mass spectrometry. *Bioinformatics* **24**, i42–48
45. Nesvizhskii, A. I., Keller, A., Kolker, E., and Aebersold, R. (2003) A statistical model for identifying proteins by tandem mass spectrometry. *Anal. Chem.* **75**, 4646–4658



Supplementary Figure 1

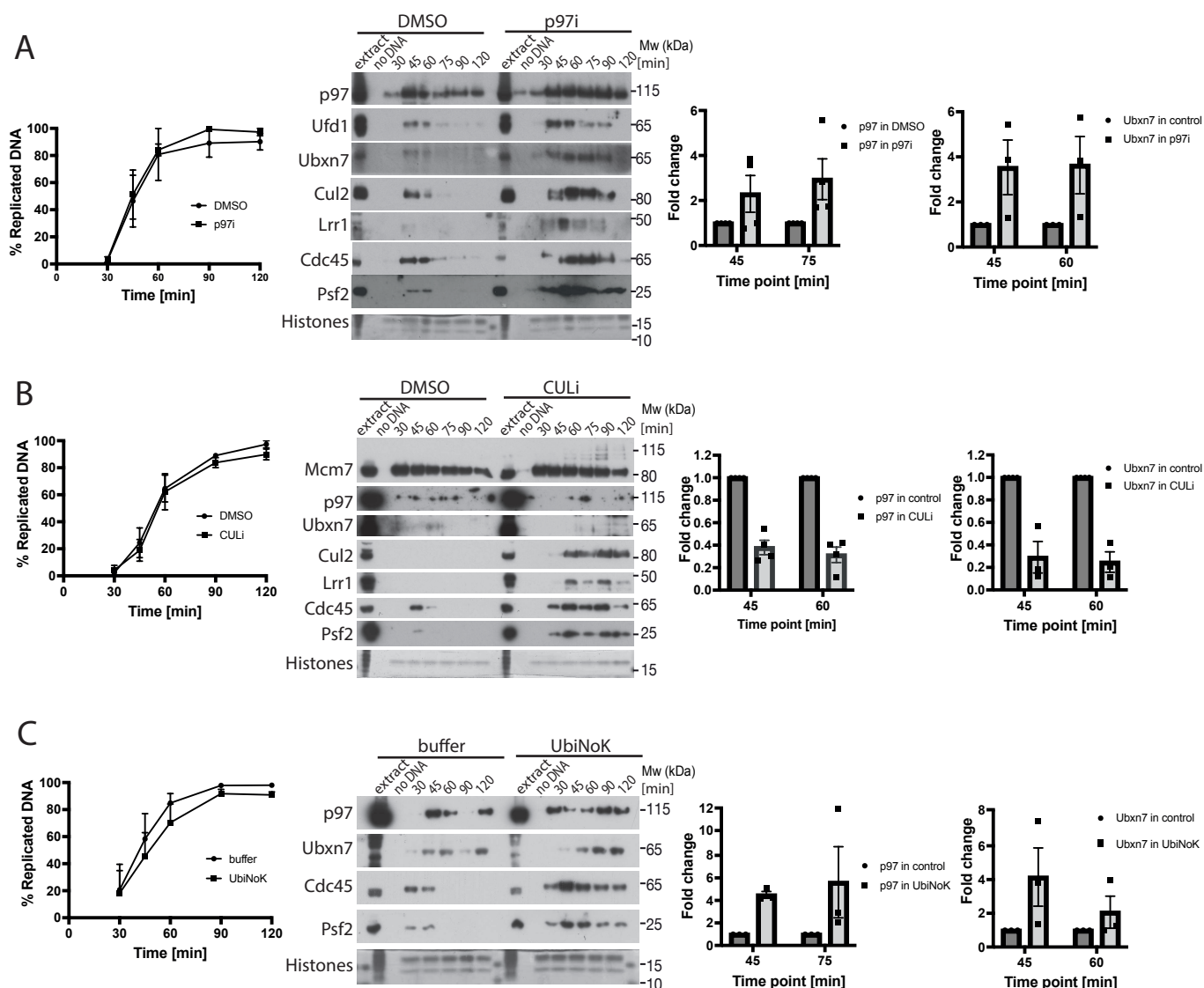
p97 accumulates on chromatin upon inhibition of its ATPase activity. Interphase egg extract was supplemented with DMSO or p97i and chromatin samples isolated at indicated timepoints during replication reaction. Chromatin samples were analysed by western blotting with indicated antibodies as in Figure 1A. Presence of a ladder of bands in -DNA control in p97i indicates contamination with cytoplasm in this particular sample. See also Figure 4A for alternative western blot. CMG components (Cdc45 and Psf2) unloading is inhibited with p97i and ubiquitylated forms of Mcm7 accumulate on chromatin when p97 is not active.

C



Supplementary Figure 3

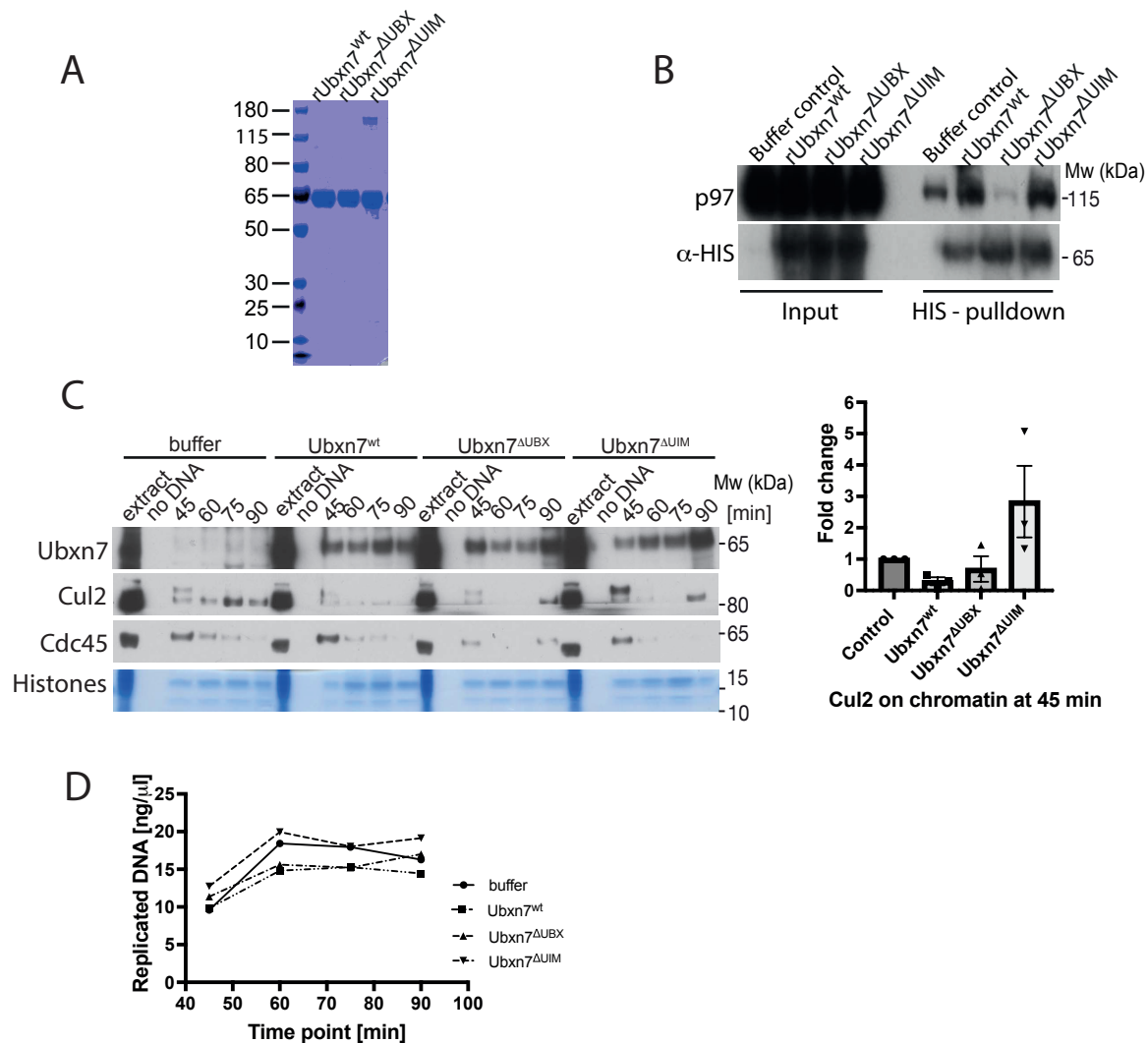
(A) Immunodepletion of Ubxn7 or Faf1 does not co-deplete each other. Faf1 and Ubxn7 were immunodepleted independently as described in materials and methods. The level of remaining proteins in the egg extract was analysed through western blotting of a series of dilutions of egg extract and samples of IgG-, Ubxn7- and Faf1-depleted extracts. PCNA serves as an example of protein that is not affected by either immunodepletion. **(B)** Immunodepletion of Ubxn7 does not immunodeplete any other bands. Whole gel of Ubxn7 immunodepletion. **(C)** Immunodepletion of Ubxn7 delays replisome disassembly. An alternative example of experiment in Figure 2C. **(D)** Immunodepletion of Ubxn7 does not lead to checkpoint activation and Chk1 phosphorylation. Nuclei were isolated at indicated timepoints during replication reaction in IgG- or Ubxn7-depleted extracts. Nuclei samples were analysed by western blotting with indicated antibodies. As a positive control a sample of each extract was treated with polymerase inhibitor aphidicolin (inhibitor of Family B of polymerases which stops nascent DNA synthesis, leads to uncoupling of helicase and polymerase and induces checkpoint activation) or aphidicolin and caffeine (inhibitor of both ATR and ATM kinases which start S-phase checkpoint response).



Supplementary Figure 4

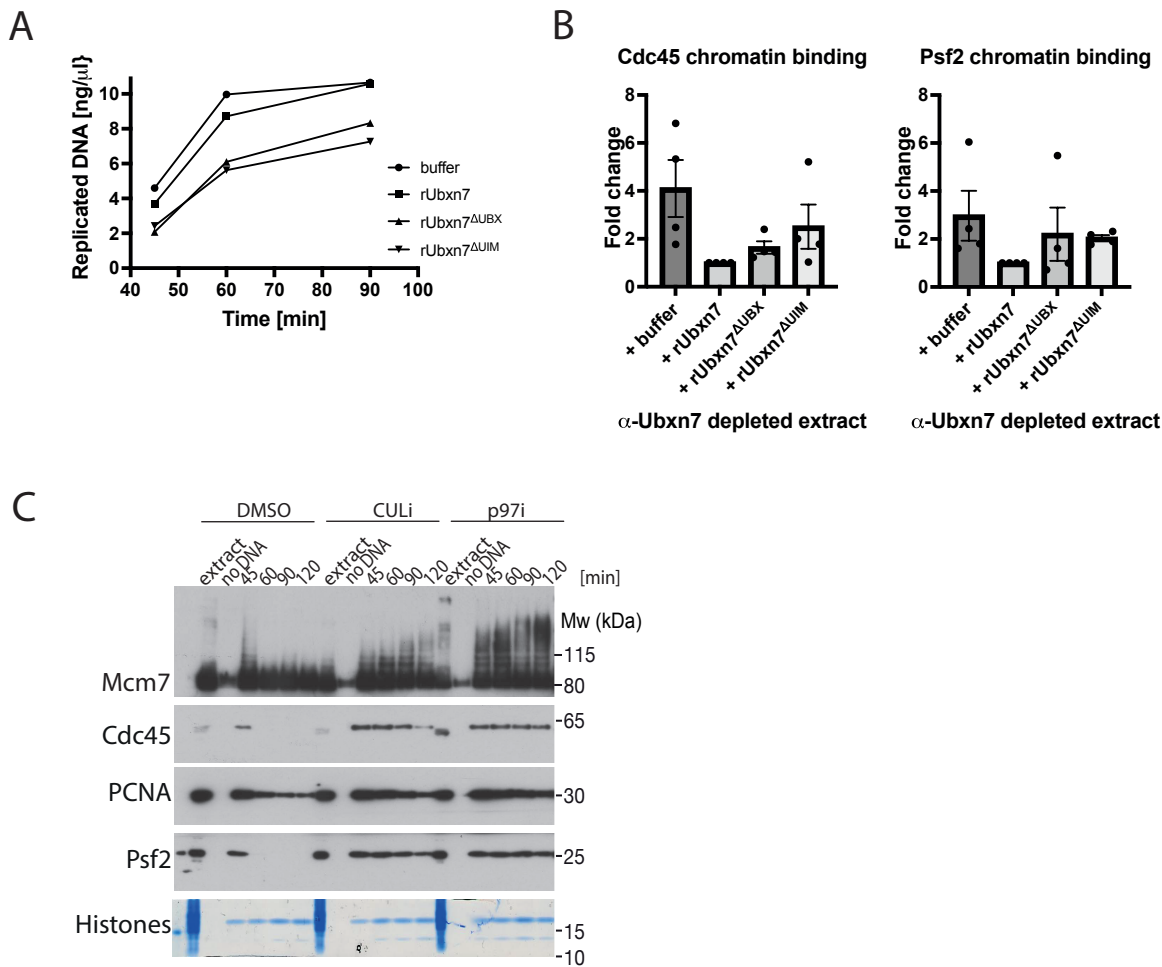
(A) Addition of p97i to egg extract does not affect extract's ability to synthesise DNA. Interphase egg extract was supplemented with DMSO or p97i and the incorporation of $\alpha^{32}\text{P}$ -dATP into newly synthesised DNA was measured at indicated times. Mean of $n=2$ for p97i with SEM. p97 and Ubxn7 accumulate on chromatin upon p97i treatment. An alternative experiment presented to the one in Figure 4A. The level of p97 and Ubxn7 bound to chromatin at 45, 60 or 75 min was quantified in DMSO and p97i treated extract. 45 min timepoint represents time when replisomes are present on chromatin in control and treatment sample, while at 60/75 min replisomes are mostly unloaded in control sample. Fold increase in p97i over control is presented as a mean value with individual value points ($n=4$ for p97 and $n=3$ for Ubxn7).

(B) Addition of CULi to egg extract does not affect extract's ability to synthesise DNA. Interphase egg extract was supplemented with DMSO or CULi and the incorporation of $\alpha^{32}\text{P}$ -dATP into newly synthesised DNA was measured at indicated times. Mean of $n=4$ with SEM. p97 and Ubxn7 decreased on chromatin upon CULi treatment - quantification of an experiment in Figure 4B as above ($n=4$). **(C)** Addition of 6His-UbiNOK to egg extract does not affect extract's ability to synthesise DNA. Analysed as above. Quantification of p97 and Ubxn7 accumulation on chromatin upon 6HIS-UbiNOK treatment as in Figure 4C ($n=3$).



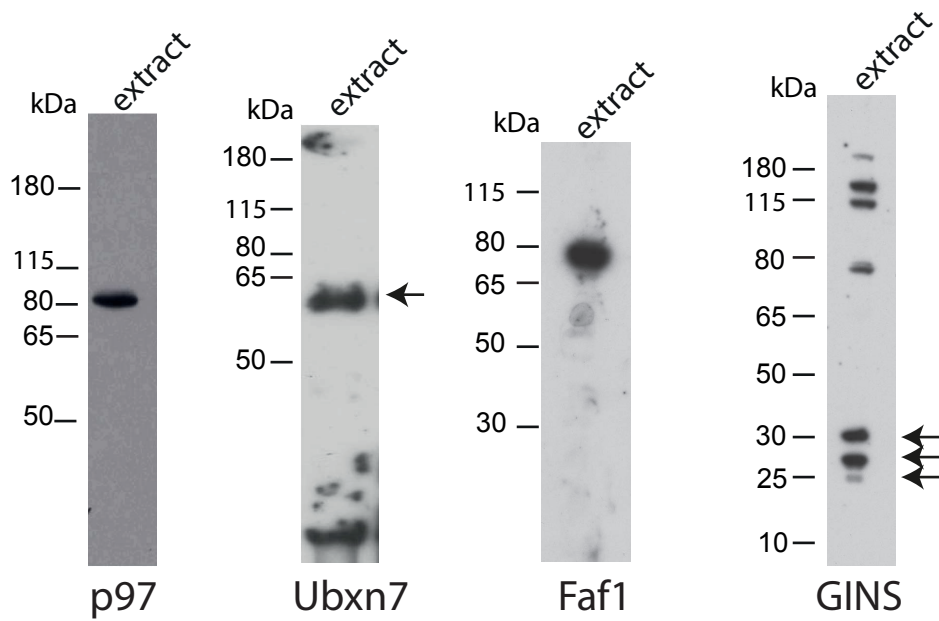
Supplementary Figure 5.

(A) Recombinant 6xHIS-Ubxn7, 6xHIS-Ubxn7^{ΔUBX} or 6xHIS-Ubxn7^{ΔUIM} were purified and equal quantity run on a PAGE gel and stained with coomassie. **(B)** Ubxn7^{ΔUBX} cannot interact with p97. Interphase egg extract was supplemented with recombinant 6xHIS-Ubxn7, 6xHIS-Ubxn7^{ΔUBX} or 6xHIS-Ubxn7^{ΔUIM} and the recombinant proteins were pulled out from replicating egg extract in the middle of S-phase. The ability of recombinant proteins to interact with p97 was analysed by western blotting. **(C)** Interphase egg extract was supplemented with Ubxn7 or mutants as in (A) and chromatin samples isolated at indicated timepoints during replication reaction. Chromatin samples were analysed by western blotting with indicated antibodies (left). The level of Cul2 bound to chromatin at 45 min of replication reaction was quantified (n=3). Fold change over buffer control is presented. Individual points, mean and SEM. **(D)** Addition of high concentration of rUbxn7 or its mutants to the egg extract does not inhibit egg extract ability to replicate DNA. LFB1/50 buffer or 6HIS-Ubxn7, 6HIS-Ubxn7^{ΔUBX} or 6HIS-Ubxn7^{ΔUIM} at 0.3 mg/ml final concentration. Extract ability to incorporate α-³²PdATP into nascent DNA was quantified.



Supplementary Figure 6.

(A) Addition of recombinant 6xHIS-Ubxn7, 6xHIS-Ubxn7 Δ UBX or 6xHIS-Ubxn7 Δ UIM to rescue Ubxn7-depleted extract does not inhibit extracts ability to synthesise DNA. Ubxn7 depleted extract was supplemented with 6xHIS-Ubxn7, 6xHIS-Ubxn7 Δ UBX or 6xHIS-Ubxn7 Δ UIM and extract ability to incorporate α - 32 PdATP into nascent DNA quantified. **(B)** UBX and UIM domains are needed for Ubxn7 activity. Quantification of experiment in Figure 5A. The chromatin bound Cdc45 and Psf2 at 75 min of replication reaction in Ubxn7-depleted extract supplemented with recombinant 6xHIS-Ubxn7, 6xHIS-Ubxn7 Δ UBX or 6xHIS-Ubxn7 Δ UIM were quantified, n=4. Individual points, mean and SEM are presented. **(C)** Mcm7 accumulates on chromatin modified with short ubiquitin chains upon cullin inhibition. Interphase egg extract was supplemented with DMSO, CULi (MLN4924) or p97i (NMS873) and chromatin was isolated during replication reaction at indicated time points after sperm DNA addition. Chromatin samples analysed as in Figure 1A.



Supplementary Figure 7


All of the antibodies raised for this study. For all of the antibodies, a 0.5 μ l sample of egg extract was resolved on PAGE and immunoblotted using the new affinity purified antibody.

TRAIP resolves DNA replication-transcription conflicts during the S-phase of unperturbed cells

Received: 4 April 2022

Accepted: 8 August 2023

Published online: 21 August 2023

 Check for updates

Shaun Scaramuzza^{1,4}, Rebecca M. Jones^{1,6}, Martina Muste Sadurni^{1,6}, Alicja Reynolds-Winczura¹, Divyasree Poovathumkadavil¹, Abigail Farrell¹, Toyooki Natsume^{1,2,3,5}, Patricia Rojas¹, Cyntia Fernandez Cuesta¹, Masato T. Kanemaki^{1,2,3}, Marco Saponaro¹ & Agnieszka Gambus¹ ✉

Cell division is the basis for the propagation of life and requires accurate duplication of all genetic information. DNA damage created during replication (replication stress) is a major cause of cancer, premature aging and a spectrum of other human disorders. Over the years, TRAIP E3 ubiquitin ligase has been shown to play a role in various cellular processes that govern genome integrity and faultless segregation. TRAIP is essential for cell viability, and mutations in TRAIP ubiquitin ligase activity lead to primordial dwarfism in patients. Here, we have determined the mechanism of inhibition of cell proliferation in TRAIP-depleted cells. We have taken advantage of the auxin induced degron system to rapidly degrade TRAIP within cells and to dissect the importance of various functions of TRAIP in different stages of the cell cycle. We conclude that upon rapid TRAIP degradation, specifically in S-phase, cells cease to proliferate, arrest in G2 stage of the cell cycle and undergo senescence. Our findings reveal that TRAIP works in S-phase to prevent DNA damage at transcription start sites, caused by replication-transcription conflicts.

Cell proliferation is the basis for the propagation of life and requires accurate duplication of all genetic information before correct cell division. However, these processes encounter impediments that threaten their faultless execution and lead to genomic instability. Moreover, problems encountered during DNA replication (replication stress) often result in under-replicated DNA that needs to be resolved during mitosis. Cells have developed a number of means to respond to these challenges, such as replication-coupled DNA repair pathways and S-phase checkpoint responses that protect the stability of replication forks, inhibit the initiation of replication in new areas of the genome, and block cell cycle progression to allow for DNA damage resolution¹. Insufficiencies in these S-phase responses and persistence

of unreplicated DNA past S-phase, induce rescue mechanisms during mitosis, such as mitotic DNA synthesis (MiDAS) and anaphase-bridge resolution. Failure of all these pathways results in DNA breakage, chromosome missegregation, and chromosomal rearrangements. Genome-wide, such unreplicated regions correlate with common fragile sites (CFS), responsible for recurrent re-arrangements often found in human disease^{2,3}.

TRAIP (TRAF-interacting protein, also known as TRIP or RNF206) E3 ubiquitin ligase has recently been shown to play a role in a number of the above processes. TRAIP is essential for cell proliferation at an early stage of development in the mouse embryo⁴ and CRISPR/Cas9-mediated deletion of TRAIP in a number of human cell

¹Institute of Cancer and Genomic Sciences, Birmingham Centre for Genome Biology, University of Birmingham, Birmingham, UK. ²Department of Chromosome Science, National Institute of Genetics, Research Organization of Information and Systems, Mishima, Shizuoka, Japan. ³Department of Genetics, The Graduate University for Advanced Studies (SOKENDAI), Mishima, Shizuoka, Japan. ⁴Present address: Cancer Research UK – Manchester Institute, Manchester Cancer Research Centre, Manchester, UK. ⁵Present address: Research Center for Genome & Medical Sciences, Tokyo Metropolitan Institute of Medical Science, Tokyo, Japan. ⁶These authors contributed equally: Rebecca M. Jones, Martina Muste Sadurni. ✉e-mail: a.gambus@bham.ac.uk

lines is lethal⁵. Moreover, homozygous mutations of the TRAIP ubiquitin ligase domain in humans lead to microcephalic primordial dwarfism⁶.

At the cellular level, TRAIP has been shown to be essential for the appropriate repair of DNA damage caused by mitomycin C (MMC) and other inter-strand crosslinks (ICLs) generating drugs: camptothecin (CPT), UV, and hydroxyurea (HU)^{6–9}. TRAIP has also been reported to regulate mitotic progression; cells with downregulated TRAIP go through mitosis faster and with more chromosome segregation errors^{10,11}. TRAIP usually accumulates in nucleoli in cells and re-localises to sites of DNA damage and replication stress^{6–8,12}. This co-localisation with PCNA upon DNA damage is mediated by a PCNA-interacting protein (PIP)-box motif located at the C-terminus of TRAIP^{7,8}. However, TRAIP was also shown to interact with unchallenged replication forks in *Xenopus* egg extract¹³ and, in human cells, TRAIP has been shown to interact with nascent DNA during unperturbed S-phase through Nascent Chromatin Capture (NCC) and iPOND^{7,14,15}.

At the molecular level, TRAIP has been shown to orchestrate the response to ICLs in *Xenopus laevis* egg extract through the ubiquitylation of the eukaryotic replicative helicase (CMG complex, from CDC45/MCM2-7/GINS) as two replication forks converge at the ICL¹³. In such a situation, short ubiquitin chains synthesised by TRAIP on CMGs promote the recruitment of NEIL3 glycosylase and unhooking of the ICL, whilst longer ubiquitin chains are required for CMG unloading by p97 segregase, allowing access for endonucleases and Fanconi anaemia pathway proteins that perform ICL repair^{13,16,17}. Using the same model system, TRAIP has also been shown to act when the replisome encounters DNA-protein crosslinks (DPCs), which impair replication forks progression. In such a situation, however, TRAIP ubiquitylates not the CMG helicase within the blocked replisome, but the protein barrier itself¹⁸. Moreover, in human cells, TRAIP was also shown to interact with RNF20-RNF40 ubiquitin ligase at double-strand breaks and affect ionizing-radiation induced monoubiquitylation of histone H2B^{19,20}, as well as the localisation of BRCA1 interacting partner RAP80 to DNA double-strand breaks¹⁹.

On the other hand, in mitosis, in *Xenopus laevis* egg extract, *C. elegans* embryos, and mouse embryonic stem cells, we and others have shown that TRAIP ubiquitylates any replicative helicases left on chromatin from replication in S-phase, leading to their unloading by the p97 segregase^{21–24}. Such replisomes retained on chromatin until mitosis likely protect the DNA they are bound to, preventing access and subsequent DNA processing by nucleases. As a result, TRAIP-driven replisome disassembly in mitosis can lead to fork breakage and complex DNA re-arrangements in *Xenopus* egg extract²³ and allows for MiDAS in human cells²². Finally, TRAIP depletion was reported to lead to decreased stability of kinetochore-microtubule attachments and diminished spindle assembly checkpoint function through lowered MAD2 levels at centromeres^{10,25}.

With so many varied functions of TRAIP reported, the question arises: which one of its functions is most crucial for cell viability, proliferation, and prevention of microcephalic dwarfism? To answer this, we have generated auxin-inducible degrons of TRAIP in the colon carcinoma HCT116 cell lines and immortalised retinal pigment epithelial cells hTERT-RPE1, which facilitate the degradation of TRAIP within 30 min of auxin (IAA) addition to the cell media. With these, we could confirm that upon rapid TRAIP degradation, cells cease to proliferate, arrest in G2 stage of the cell cycle and undergo senescence. By further investigating the effect of TRAIP degradation on specific stages of the cell cycle we found that TRAIP plays an essential role in S-phase and that the lack of TRAIP results in the generation of DNA damage at sites of replication-transcription collisions. We propose a model whereby TRAIP acts at sites of collision and allows the conflicts to be resolved.

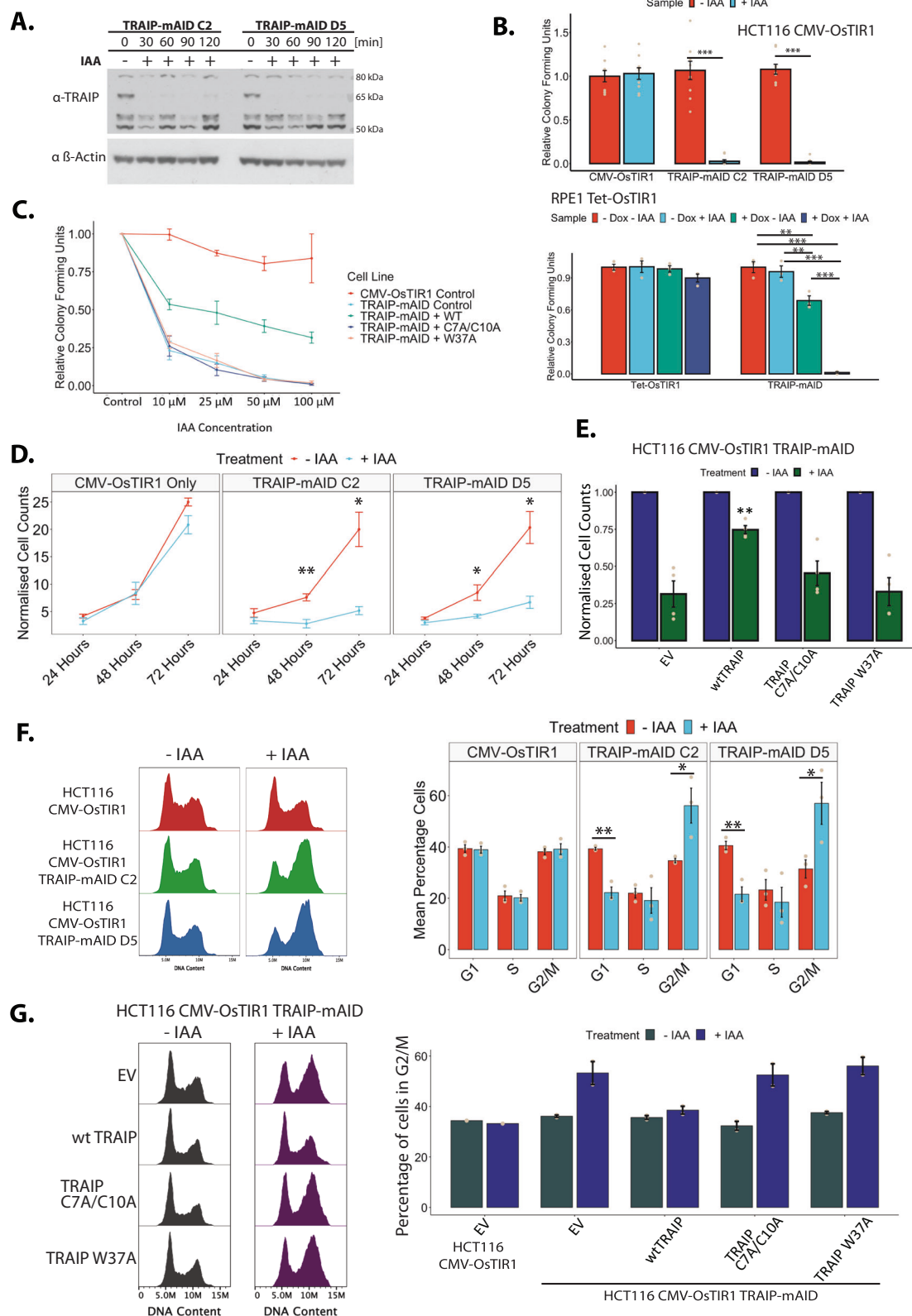
Results

To investigate the role of TRAIP during the unperturbed eukaryotic cell cycle, we established conditional auxin-inducible degron (AID) cell lines^{26,27}. As modifying the N-terminus of TRAIP was reported to impact TRAIP localisation in the cell⁸, endogenous TRAIP was tagged C-terminally in an HCT116 cell line expressing OsTIR1, an E3 ligase component recognising the degron, with either a mini-auxin-inducible degron (mAID) tag, or an mCLOVER-fused variant (mAC); henceforth referred to as TRAIP-mAID and TRAIP-mAC, respectively (Supplementary Fig. 1A, B). Two clones of each HCT116 TRAIP-mAID and TRAIP-mAC were generated and used throughout this work to ensure that the observed phenotypes are not CRISPR off-target effects. The hTERT-RPE1 cell line chosen for TRAIP modification expressed OsTIR1 from an inducible Tet promoter, requiring the addition of tetracycline or doxycycline to express it (Supplementary Fig. 1A). Bi-allelic tagging was verified by PCR amplification from the genomic *TRAIP* locus (Supplementary Fig. 1C, D). It was also confirmed at the protein level by the disappearance of the endogenous untagged TRAIP protein from the whole cell extracts prepared using degron cell lines (Supplementary Fig. 1E). Bi-allelic modification of *TRAIP* with degron tags did not affect cell proliferation and fitness (Supplementary Fig. 1F, G). Activation of the AID system, through the addition of Indole-3-acetic acid (auxin, IAA) to the cell growth media ensured rapid protein degradation in ~30 minutes (Fig. 1A).

TRAIP activity is essential for cell proliferation

We first set out to understand the global consequences of TRAIP depletion for cell viability, proliferation, and cell cycle progression. Colony assays were used to assess the respective impact of auxin treatment itself, and TRAIP degradation, on cell viability. Long-term auxin treatment (7–14 days) led to abrogation of colony growth in all the conditional TRAIP degron cell lines (Fig. 1B; Supplementary Fig. 2A). No reductions in the overall colony forming ability were found when auxin was added to control cell lines, indicating that the drug treatment itself was not cytotoxic. These data confirmed that TRAIP was an essential protein as previously described^{4,5}. Importantly, we could significantly rescue the cell growth in the auxin-treated HCT116 TRAIP-mAID degron cells by expression of exogenous full-length (wild-type, wt) TRAIP, but not an active site mutant C7A/C10A of TRAIP or TRAIP W37A⁶ (Fig. 1C). This indicates that TRAIP ubiquitin ligase activity is essential for cell viability in our system. TRAIP expression is highly regulated in the cell and overexpression of wtTRAIP was reported to be toxic⁷, which is a likely reason why the expression of wtTRAIP in our experiments does not fully rescue lethality of the TRAIP-mAID degradation.

To investigate the underlying reason for the observed growth inhibition, we next investigated the effects of shorter periods of protein degradation (24–72 Hrs) on cell proliferation and cell cycle progression. HCT116 cells lacking TRAIP exhibited clear defects to cell growth at all time points tested (Fig. 1D, Supplementary Fig. 2B), while RPE1 cells showed less dramatic defect (Supplementary Fig. 2C). Again, we could rescue the proliferation defect observed after 72 h of TRAIP-mAID degradation in HCT116 cells by expression of wtTRAIP, but not TRAIP C7A/C10A or TRAIP W37A (Fig. 1E). Furthermore, flow cytometric analysis revealed a reduction in the number of cells in G1 stage of the cell cycle, as well as the accumulation of TRAIP-depleted cells with G2/M DNA content (Fig. 1F, Supplementary Fig. 2D, E), which could be rescued in HCT116 cells by expression of wtTRAIP but not the ubiquitin ligase dead mutants (Fig. 1G). Altogether, these results show that our TRAIP degron cell lines exhibit phenotypes analogous to those observed previously upon downregulation of TRAIP by siRNA or in patients' cells with impaired ubiquitin ligase activity of TRAIP^{6–8} and thus provide a useful tool for the determination of the cell-cycle, stage-specific and essential function of TRAIP. Moreover, the essential function of TRAIP depends on its ubiquitin ligase activity.



TRAIP-depleted cells accumulate in G2 stage of the cell cycle

As the underlying mechanism of cell death in cells depleted of TRAIP has not been previously determined, we decided first to investigate the mechanism by which TRAIP-depleted cells stop proliferating. We first determined in which cell cycle stage cells lacking TRAIP were accumulating: G2 or mitosis. We focused on HCT116 cells, as they proliferate faster and at higher cell densities, facilitating cell cycle analysis

by flow cytometry and easier detection of cell cycle defects. Quantification of the total proportion of cells displaying phosphorylation of Histone H3 on S10 (marker of mitosis) by flow cytometry showed no differences to the numbers of mitotic cells following TRAIP degradation (24 h auxin treatment) (Supplementary Fig. 3A). The same was confirmed by mitotic indexing experiments (Supplementary Fig. 3B, no WEE1i). To specifically visualise the G2 population of cells, cells

Fig. 1 | Rapid auxin-induced degradation of TRAIP-mAID leads to G2 cell cycle arrest and inhibition of cell proliferation. **A** An asynchronous cell culture of HCT116 TRAIP-mAID cells was supplemented with auxin (IAA) and samples taken at indicated times. The level of TRAIP-mAID was assessed by western blotting with TRAIP antibody. Two independent clones of TRAIP-mAID are presented ($n = 3$). **B** Cells were grown in presence or absence of auxin (IAA) and in case of hTERT-RPE1 cells in presence or absence of Doxycycline. The resultant colonies were visualised. Quantification of three biological repeats; depicted as the mean normalised colonies formed \pm SEM. Pairwise hypothesis testing was conducted using Mann–Whitney U tests, with significance values indicated on the plot (HCT116 Cells: TRAIP-mAID C2: $p < 0.001$; TRAIP-mAID D5: $p < 0.001$; RPE1 Cells: significant differences were observed between TRAIP-mAID cell lines only. -Dox -IAA vs +Dox -IAA: $p = 0.004$; -Dox -IAA vs +Dox +IAA: $p = < 0.001$). **C** HCT116 TRAIP-mAID cells were transfected with retroviruses expressing WT, C7A/C10A or W37A mutants of TRAIP. Colony assay viability was assessed at different concentrations of auxin. Quantification of $n = 3$. Error bars depicted show the mean colony forming units \pm SEM. **D** TRAIP-mAID cells were grown in optional presence of auxin (IAA) and cell proliferation counted over the 72 h. Quantification of $n = 3$ for two independent TRAIP-mAID clones. Data is shown as the mean \pm SEM. Pairwise statistical

comparison were conducted at each timepoint using t -tests, with significance indicated on the plot (TRAIP-mAID C2: 48 h - $p = 0.00940$, 72 h - $p = 0.0363$; TRAIP-mAID D5: 48 h - $p = 0.04$, 72 h - $p = 0.0305$). **E** HCT116 TRAIP-mAID cells expressing different versions of TRAIP as in **C** were grown in presence of auxin for 72 h and counted. Data shown as the mean cell counts (normalised to control) \pm SEM. Statistical significance was conducted to compare each +IAA treatment between cell lines (Empty Vector +IAA vs WT TRAIP + IAA, $p = 0.0121$). **F** TRAIP-mAID cells (two independent clones) were grown for 24 h in optional presence of auxin (IAA) and analysed for their DNA content by FACS. Example FACS plots (left) and quantification of number of cells in different stages of the cell cycle (mean \pm SEM) over three independent experiments for two independent clones (right) are shown. Pairwise comparisons were carried out using t -tests, significance is indicated on the plot (TRAIP-mAID C2: G1 - $p = 0.0120$, G2/M - $p = 0.04$; TRAIP-mAID D5: G1 - $p = 0.00874$, G2/M - $p = 0.04$). **G** HCT116 TRAIP-mAID cells expressing different versions of TRAIP as in **C** were grown in presence of auxin for 24 h and analysed for their DNA content by flow cytometry. Example FACS plots (left) and quantification of number of cells in different stages of the cell cycle (mean \pm SEM) over two independent experiments (right). Source data are provided as a Source Data file.

were treated with auxin for 24 hours to degrade endogenous TRAIP and stained with three markers of G2/M progression: DAPI for condensed chromosomes, Mitosin (CENPF) for G2 and mitosis, and the S10 phosphorylation of Histone H3 for mitosis (Fig. 2A). A significant increase was found in the proportions of cells in G2 stage of the cell cycle following treatment with auxin and TRAIP degradation (Fig. 2A, no WEE1i), while no differences again were found when considering those cells in either early or late mitosis (Supplementary Fig. 3C). Finally, the G2 cell cycle accumulation was overcome through inhibition of the G2 checkpoint kinase WEE1 using MK-1775 inhibitor (Fig. 2A and Supplementary Fig. 3C, D). We conclude, therefore, that the loss of TRAIP results in a G2 cell cycle arrest dependent on WEE1.

G2-arrested TRAIP-depleted cells exit the cell cycle through senescence

Analyses of the HCT116 TRAIP-mAID cell line treated for 24 h with auxin also revealed an increase in the size of nuclei and overall cell size (Supplementary Fig. 4A, B). Intriguingly, increased cell size, reductions in cell proliferation, and cell cycle accumulation are all hallmarks of cell cycle exit via senescence²⁸. To explore this further, we used flow cytometry to detect the senescence marker β -galactosidase. Indeed, following as little as 24 h of auxin treatment, cells were positive for this marker of cell senescence (Fig. 2B). Subsequent comparison of the positive β -galactosidase cell population with total DNA content revealed the specific activation of senescence in the accumulating G2/M cells (Fig. 2C). In contrast, we have detected no increase in the proportion of apoptotic cells (Supplementary Fig. 4C, D) and we observed no increase in cells exhibiting mitotic catastrophe phenotypes (data not shown).

G2 arrest in TRAIP-depleted cells is a result of DNA damage checkpoint activation

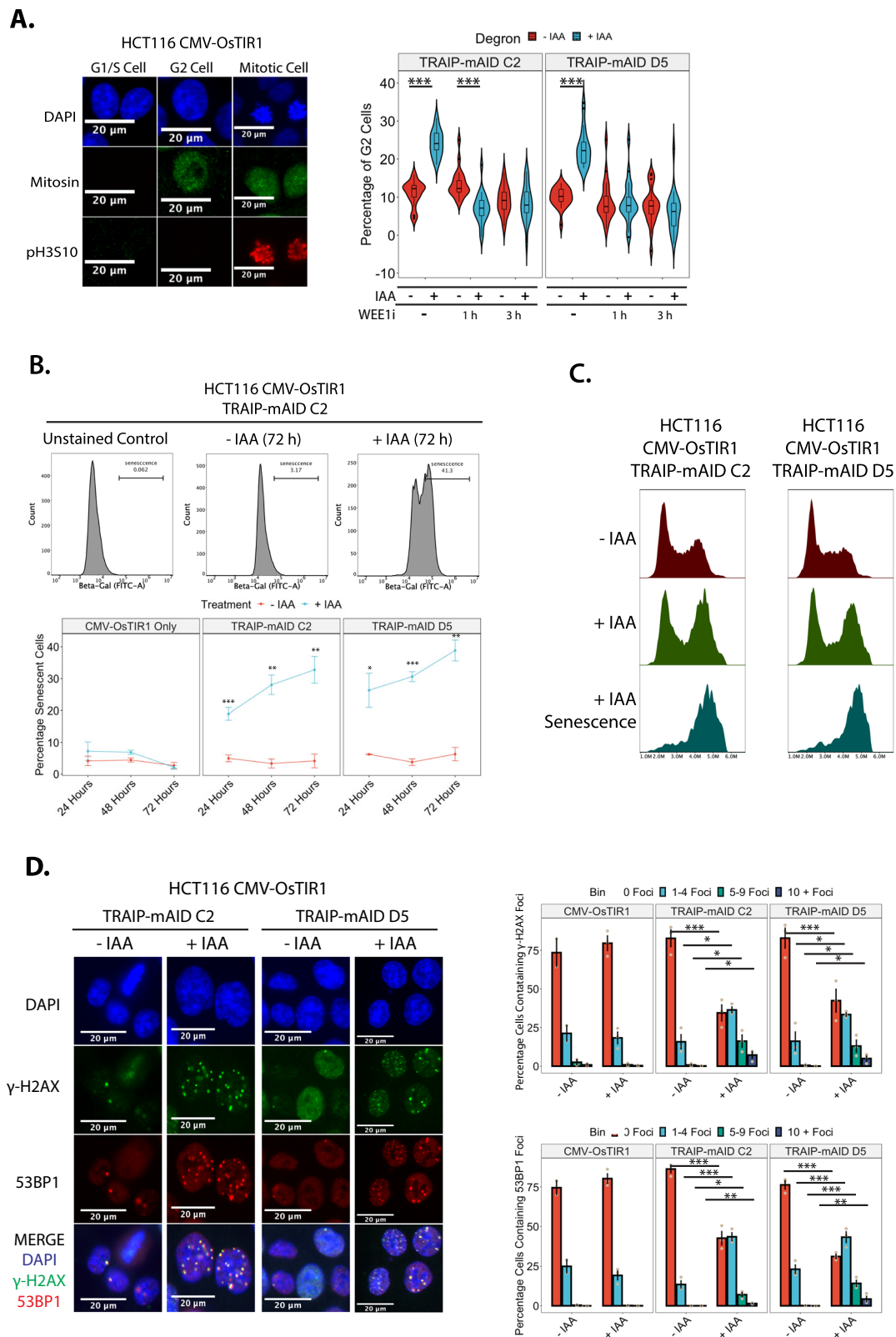
G2 cell cycle arrest is often a consequence of DNA damage checkpoint activation²⁹ and TRAIP was previously linked to numerous DNA damage repair pathways. To check whether DNA damage accumulation upon degradation of TRAIP may be indeed responsible for the observed G2 arrest, cells were treated with auxin for 24 hours and stained for the general DNA damage marker γ -H2AX (S139 phosphorylation on H2AX) as well as the double-stranded DNA break-specific marker 53BP1. This revealed a general, but subtle, accumulation of DNA damage foci in the two independent HCT116 TRAIP-mAID cell lines (Fig. 2D) and in the hTERT-RPE1 TRAIP-mAID cells (Supplementary Fig. 5A). All these indicate that TRAIP is important for the maintenance of genomic stability. Moreover, inhibition of ATR, but not ATM, was able to rescue the observed G2 cell cycle arrest

(Supplementary Fig. 5B) suggesting that the damage is likely created during S or G2 stages of the cell cycle. We conclude, therefore, that the loss of TRAIP results in the creation of DNA damage, checkpoint activation, and the accumulation of cells in G2 stage of the cell cycle. As a result of this, cells enter senescence and stop proliferating.

TRAIP is essential for completion of S-phase

To understand specifically when during the cell cycle TRAIP was essential, we combined the rapid nature of the AID system with established cell synchronisation techniques in HCT116 cells. Cells depleted of TRAIP accumulate in G2 stage of the cell cycle due to ATR checkpoint activation. TRAIP is known also to play a role in S-phase, we, therefore, started our investigations assessing whether TRAIP was essential during S-phase. Cells were arrested in G1 with lovastatin, and auxin added for the last hour of G1 arrest. First, we determined that there was no defect in cells entering S-phase (Supplementary Fig. 6A). Second, we assessed the relative impact of TRAIP depletion during S-phase on the cell cycle using the previously described G2 cell cycle arrest as a readout. When cells progressed through S-phase and into G2 lacking TRAIP, G2 cell cycle accumulation could be observed (Fig. 3A). Third, to verify whether TRAIP is required specifically during the G2 stage of the cell cycle, TRAIP was optionally degraded 15 hours post release from G1 arrest, when cells were in late S-phase. When auxin was added during late S-phase, no G2 cell cycle accumulation could be detected (Fig. 3B). These data indicated that TRAIP was essential specifically for mechanisms existing during S-phase.

Finally, TRAIP was previously reported to have many functions also during mitosis^{10,11,21–24}. To determine whether we could observe that TRAIP regulates mitotic progression in our cells, we arrested cells specifically in G2 stage of the cell cycle with RO-3306, degraded TRAIP, released cells to mitosis, and followed chromosomal condensation and segregation (Supplementary Fig. 6B). In this we could observe that, irrespectively of TRAIP degradation, cells condensed chromosomes at a similar rate (Supplementary Fig. 6C). On the other hand, we found fewer chromosome segregating cells at 60 min post release into mitosis when TRAIP was absent (Supplementary Fig. 6D). This suggests that TRAIP is indeed regulating the timing of mitotic progression independently of its S-phase role. Therefore, to determine whether any functions of TRAIP in mitosis could contribute to the increased DNA damage response seen in the next S-phase, TRAIP was degraded specifically before mitosis, and its effect on the next cell cycle arrest was explored. Cells were arrested in G2 and treated with auxin for 1 hour prior to release into mitosis. Approximately 2 hours following release, when cells were in G1 phase of the cell cycle, auxin was optionally washed off to allow protein re-expression before entry into the next



S-phase. Timepoints were taken 24 hours after release into mitosis. Using this experimental set-up, cell cycle accumulation in G2 was only seen when cells progressed through both mitosis and S-phase without TRAIP. No such accumulation was seen in those samples where TRAIP was allowed to re-express prior to S-phase entry (Fig. 3C). We, therefore, conclude that the essential function of TRAIP is executed during S-phase.

TRAIP depletion leads to generation of DNA damage at transcription start sites (TSS)

Given the essential requirement of TRAIP during S-phase progression, we explored whether auxin treatment had any effect on global DNA replication. Cells treated with and without auxin for 24 hours were pulsed with the thymidine analogues EdU and BrdU for 1 hour, and analogue incorporation was analysed using immunofluorescence and

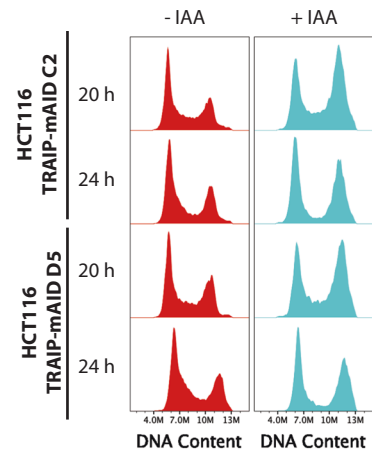
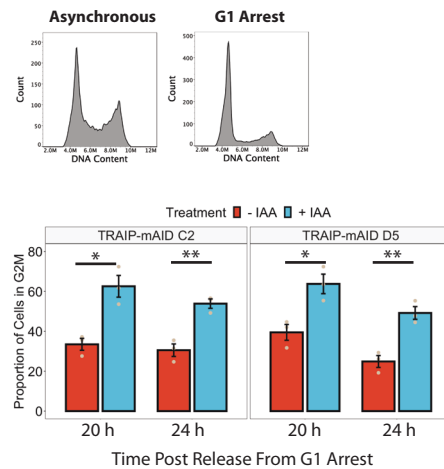
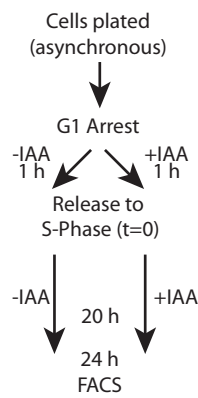
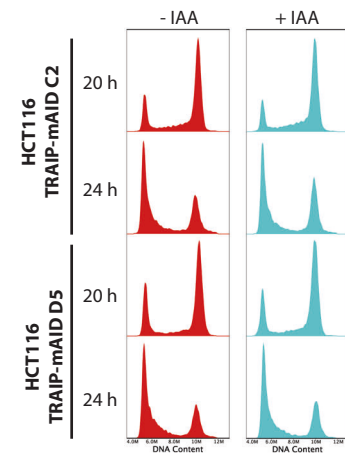
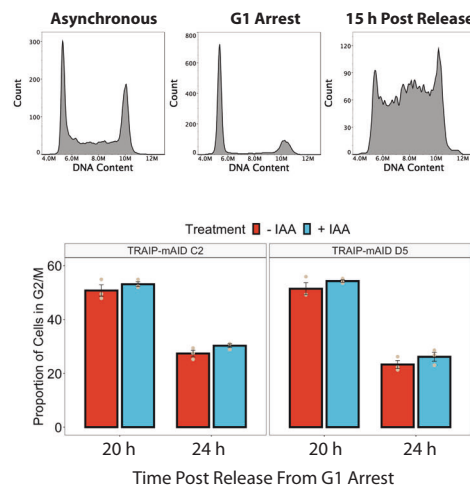
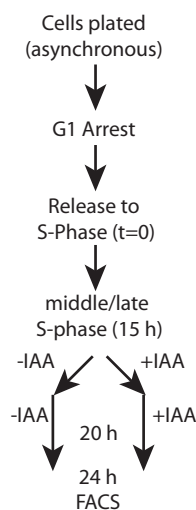
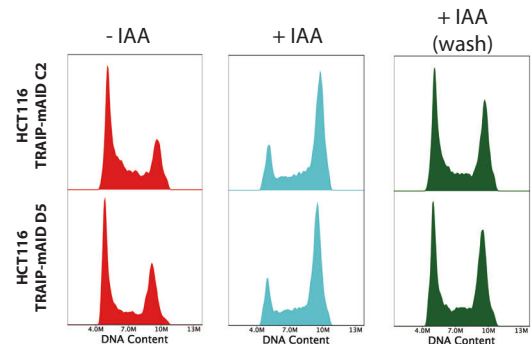
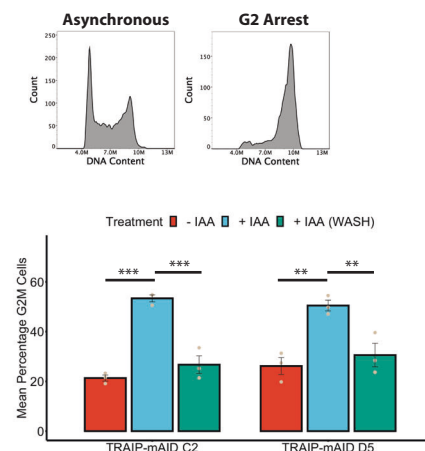
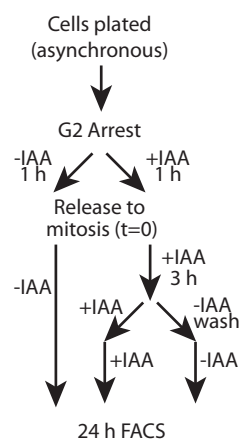
Fig. 2 | TRAIP degradation leads to DNA damage, G2 cell cycle arrest and cell senescence. **A** TRAIP-mAID cells (two independent clones) were grown for 24 h in optional presence of auxin (IAA), and optional addition of WEELi for indicated times, and analysed for accumulation of cells in G2 (Mitosis staining) or in mitosis (pH3S10 staining). Quantification of three independent experiments. Data depicted as violin plots, displaying boxplots highlighting the median and corresponding interquartile ranges. Statistical analysis was carried out using one-way ANOVA and subsequent post hoc testing, significance is indicated on the plots (ANOVA: $p < 0.0001$. Tukey's post hoc tests: all indicated comparisons on the plot $p < 0.0001$). **B** TRAIP-mAID cells were grown for 24–72 h in optional presence of auxin (IAA) and the level of senescent cells analysed by FACS measurement of senescence marker β -galactosidase. Example FACS plots (top) and quantification of 3 independent experiments in 2 independent clones (bottom). Quantified data is shown as the mean \pm SEM. Pairwise hypothesis testing was carried out using t-tests, with significance indicated on the plot (TRAIP-mAID C2: 24 h – $p = 0.00118$, 48 h –

$p = 0.00651$, 72 h – $p = 0.00926$; TRAIP-mAID D5: 24 h – $p = 0.03$, 48 h – $p = 0.00031$, 72 h – $p = 0.0022$). **C** TRAIP-mAID cells were grown for 72 h in optional presence of auxin (IAA). β -galactosidase staining was combined with DNA content analysis by FACS. β -galactosidase positive cells have G2/M DNA content. **D** TRAIP-mAID cells were grown in optional presence of auxin (IAA) for 24 h and stained with markers of DNA damage response (γ H2AX and 53BP1). Example of immuno-fluorescent visualisation of DNA damage (left) and quantification of percentage of cells containing increasing numbers of γ H2AX and 53BP1 foci over 3 independent experiments (right). Significance testing carried out using one-way ANOVA and subsequent Tukey's post hoc testing (TRAIP-mAID C2: ANOVA – $p < 0.001$; Tukey's post hoc test – 0 Foci: $p = < 0.001$; 1–4 Foci: $p < 0.001$; 5–9 Foci: $p = 0.0168$; 10 + Foci: $p = 0.0059$. TRAIP-mAID D5: ANOVA – $p < 0.001$; Tukey's post hoc test – 0 Foci: $p < 0.001$; 1–4 Foci: $p < 0.001$; 5–9 Foci: $p = 0.0046$. Source data are provided as a Source Data file.

FACS respectively (Supplementary Fig. 7A, B). A lower number of cells was detected incorporating EdU/BrdU upon TRAIP degradation, suggesting fewer cells in S-phase. However, the cells that were in S-phase and labelled with BrdU or EdU, showed the same level of analogue incorporation, suggesting a similar rate of replication progression independent of TRAIP degradation status (Supplementary Fig. 7A, B). Based on our previous observations, it is likely that the lower proportions of cells in S-phase are due to the G2 cell cycle arrest and overall fewer cycling cells. TRAIP has also been previously implicated in replisome disassembly in model organisms during mitosis and stressed conditions^{13,18,21–24}. We, therefore, wondered whether TRAIP was needed for global replisome disassembly during S-phase. The levels of chromatin-bound replicative helicase (MCM2-7) were assessed using flow cytometry following extraction of soluble proteins from permeabilised cells. No differences could be detected in either the loading or unloading of MCM2-7 during the otherwise unperturbed cell cycle (Supplementary Fig. 7C). Despite these results, the S-phase progression upon TRAIP degradation is not without problems. To investigate this further, cells progressing through S-phase with or without TRAIP were arrested in G2 with RO-3306 and pulsed with EdU to detect any late cell cycle DNA synthesis. When cells progressed through S-phase without TRAIP, our results suggest that they struggled to complete DNA synthesis on time as EdU incorporation could be detected in late G2/early mitosis (Supplementary Fig. 8A).

To gain insight into the mechanistic requirements for TRAIP during S-phase, we next used γ -H2AX ChIP-Seq to map genome-wide the location of the accumulating DNA damage. We first confirmed that the previously observed DNA damage accumulation was indeed specific to TRAIP's function during S-phase in both cell backgrounds (Supplementary Fig. 8B, C). HCT116 TRAIP-mAID cells were then prepared for sequencing at the 16-hour timepoint (late S-phase) as determined to display the maximal accumulation of DNA damage (Supplementary Fig. 8B). H2AX chromatin immuno-precipitation was used for sample normalisation, and we performed two independent repeats of this experiment. Reassuringly, the ChIP-Seq detected an overall increase to the γ -H2AX signal at a subset of genomic loci detected following auxin treatment in both repeats (example in Fig. 4A and Supplementary Fig. 9A). We first checked whether the position of γ -H2AX signal correlated with known DNA replication features: replication initiation sites and replication termination zones (both mapped in HCT116 cells by alternative techniques by³⁰ and³¹) and CFS³². However, no correlation could be found in either of the repeats (Fig. 4B and Supplementary Fig. 9B). Subsequently we performed a peak calling analysis to determine hotspots of DNA damage in the two repeats. We determined 1799 γ -H2AX signal peaks in the first experiment and 5984 in the second. 545 γ -H2AX signal peaks were common between both experiments (example of a hotspot common peak is presented in Fig. 4A). Interestingly, when we analysed the location of these 545 γ -H2AX hotspots, we found that they were largely associated with RNA Pol II transcripts. Indeed, we found that 95.77% of these peaks were

present on genes, and 88.24% present specifically around the TSS \pm 2 kb (Fig. 4C). We could also see a similar correlation with TSS for all γ -H2AX peaks called in both experiments, not only the common hotspots. Guided by this finding, we analysed the positions of all TRAIP degradation-induced γ -H2AX signals in both repeats in relation to all transcribed genes. Importantly, we found a general increase of γ -H2AX signal at TSS, even when the damage levels were not increased enough for stringent conserved peak calling analysis (Fig. 4D and Supplementary Fig. 9C). Hence, we focused on understanding what was special about the TSS of the genes exhibiting the hotspots of DNA damage upon TRAIP degradation. Firstly, we excluded an enrichment for genes involved in any particular cellular pathway through Go-term analysis (Supplementary Table 1). Next, we characterised replication dynamics across these sites using previously published replication data for HCT116³⁰, to determine the replication timing associated with these sites and we found that hotspot TSS sites are preferentially replicated in early S-phase (Supplementary Fig. 9D). We then identified the closest replication origin, as assigned by Koyanagi et al. to the γ -H2AX peak³¹, determining also whether the replication fork will reach the TSS in a codirectional or head-to-head orientation with the RNA Pol II. We found that γ -H2AX peaks are close to their nearest origin, on average only 29 kb away (Fig. 4E). In comparison, TSS of genes that do not show an increase in γ -H2AX levels following TRAIP depletion (top 450 genes from Supplementary Fig. 9C) are 41 kb away from their nearest origin (Fig. 4E). Moreover, γ -H2AX peaks occur preferentially around the TSS of the first transcribed gene encountered by the replication fork (75% of the total combining codirectional 1 and head-to-head 1), with the same frequency of replication fork and gene orientation being codirectional or head-to-head (Fig. 4F). In comparison, TSS of the genes with the lowest changes in γ -H2AX levels tend to occur less frequently on the first transcribed gene encountered by the replication fork (65% of the cases, Fig. 4F, chi-square test 0.034). We then overlaid this information with previously published datasets for precision run-on sequencing (PRO-Seq), tracking strand-specific nascent transcription activity³³, as well as RNA Pol II chromatin immuno-precipitation sequencing (ChIP-Seq)³⁴ in HCT116 cells. Interestingly, when we analysed the PRO-Seq signal at the hotspot TSS, we found that 98.25% of all the genes with a γ -H2AX hotspot presented clear levels of bi-directional transcription at their TSS, independently of the reciprocal orientation, either because of bi-directional promoters or TSS-associated antisense transcription. We measured therefore the extent of the antisense transcription by calculating the ratio between the levels of the antisense transcription and the sense transcription. To do this, we used the strand-specific PRO-Seq data, and determined for each gene the amount of antisense transcription occurring in the region -1000 bp \rightarrow TSS on the opposite strand of the gene. This was then divided by the amount of sense transcription TSS \rightarrow $+1000$ bp. We found that, compared to all the rest of the transcribed genes, those with a γ -H2AX hotspot peak presented higher levels of antisense transcription at their TSS (Fig. 4G). We also did the same analysis with

A.**B.****C.**

total RNA Pol II ChIP-Seq data³⁴ finding the same result (Fig. 4G, Supplementary Fig. 9E). In comparison, genes with the lowest changes of γ -H2AX levels at their TSS, present lower levels of antisense transcription both by PRO-Seq and ChIP-Seq of RNA Pol II (Fig. 4G). Altogether, our data indicate that TSS genomic regions are particularly challenging to replicate in the absence of TRAIP. Moreover, although γ -H2AX signal is generally increased at the majority of TSS, it is the TSS of the first transcribed gene with high levels of antisense to sense transcription

that DNA damage most often arises at and can be detected at population level.

Cells experience more DNA damage-generating encounters between replication and transcription upon TRAIP degradation

As we observed that DNA damage was preferentially located at TSS following TRAIP degradation, we hypothesised that the RNA polymerase accumulated at these sites could present a barrier for the

Fig. 3 | TRAIP is essential for S-phase progression during unperturbed cell cycle. **A** TRAIP-mAID cells were arrested in G1 stage of the cell cycle and TRAIP degraded before release of cells into S-phase. Cell-cycle progression was analysed by FACS at 20 and 24 h post release. The experimental set-up (left), example of cell cycle profiles at the time of synchronisation (middle, top), examples of FACS profiles at 20 and 24 h post release (right), and quantification of cells with G2/M DNA content (mean \pm SEM) over three independent experiments with two independent clones (middle, bottom). Pairwise hypothesis testing conducted using *t* tests, with significance indicated (TRAIP-mAID C2: 20 h G1 – *p* = 0.0288, 24 h G1 – *p* = 0.0171, 20 h G2/M – *p* = 0.00514, 24 h G2/M – *p* = 0.00514; TRAIP-mAID D5: 20 h G1 – *p* = 0.00825, 24 h G1 – *p* = 0.0196, 20 h G2/M – *p* = 0.0198, 24 h G2/M – *p* = 0.00517. **B** TRAIP-mAID cells were arrested in G1 stage of the cell cycle, released into S-phase, and auxin (IAA) added in middle/late S-phase. Cell-cycle progression

was analysed by FACS at 20 and 24 h post cell release into S-phase. All analyses presented as in **A**. **C** TRAIP-mAID cells were arrested in G2 stage of the cell cycle and TRAIP degraded before release of cells into mitosis. After release auxin (IAA) was optionally washed off 3 h after release, so that cells progressed through next S-phase with or without TRAIP. Cell-cycle progression was analysed by FACS at 24 h post release from G2 arrest. All analyses presented as in **A**. Any difference between treatment groups was determined using one-way ANOVA and post hoc testing, significance is summarised on the plot (one-way ANOVA: *p* < 0.0001; Tukey's post hoc testing, TRAIP-mAID C2: –IAA vs +IAA, *p* < 0.001; –IAA vs +IAA WASH, *p* = 0.800; +IAA vs +IAA WASH, *p* < 0.001. TRAIP-mAID D5: –IAA vs +IAA, *p* = 0.00107; –IAA vs +IAA WASH, *p* = 0.898; +IAA vs +IAA WASH, *p* = 0.00554). Source data are provided as a Source Data file.

passing replisome. To test this, we decided to inhibit the loading of the RNA Pol II at TSS using the TFIID inhibitor triptolide³⁴. Cells were arrested in G1 where TRAIP was degraded before being released into S-phase. Upon S-phase entry, cells were exposed to triptolide for 90 minutes, as it has been shown previously that short-term treatment with triptolide does not affect DNA replication progression³⁵ (Supplementary Fig. 10A). Strikingly, all of the DNA damage observed upon TRAIP degradation in HCT116 cells could be rescued by inhibiting RNA Pol II recruitment to the TSS by triptolide treatment (Fig. 5A). This rescue was also observed in hTERT-RPE1 cells (Fig. 5B). Importantly, we also tested whether the DNA damage specifically at TSS can be abolished by triptolide treatment. To do so, we selected four bi-directional TSS that were enriched in γ -H2AX signal upon TRAIP degradation (Fig. 4) and designed primers that could amplify them by PCR. We arrested cells in G1, released into S-phase, and treated them with triptolide as in the previous experiment. This time, however, we performed γ -H2AX ChIP followed by RT-PCR to monitor for levels of damage specifically at these genomic loci. Reassuringly, our selected TSS sites showed an increase of γ -H2AX signal after TRAIP degradation, which was rescued by triptolide treatment in three cases (Fig. 5C). In the case of the remaining TSS (Ph4B), the level of γ -H2AX induced after triptolide treatment alone was as high as after TRAIP degradation, so the combined treatment did not decrease the damage signal (Fig. 5C).

We then treated cells in a similar way with another transcription inhibitor DRB. DRB is a CDK9 inhibitor that leads to transcription inhibition through the accumulation of RNA Pol II at the TSS, inhibiting its progression through the gene body³⁶. We could observe that DRB treatment alone created an increased level of γ -H2AX and 53BP1 foci, analogous to that of TRAIP degradation. DRB treatment did not lower the proportion of cells displaying an increased number of γ -H2AX and 53BP1 foci upon TRAIP degradation, but the effect of DRB treatment was also not additive with TRAIP degradation (Supplementary Fig. 10B). Altogether, these data suggest that the mechanism by which TRAIP is essential during S-phase is dependent on the presence of RNA Pol II specifically at the TSS.

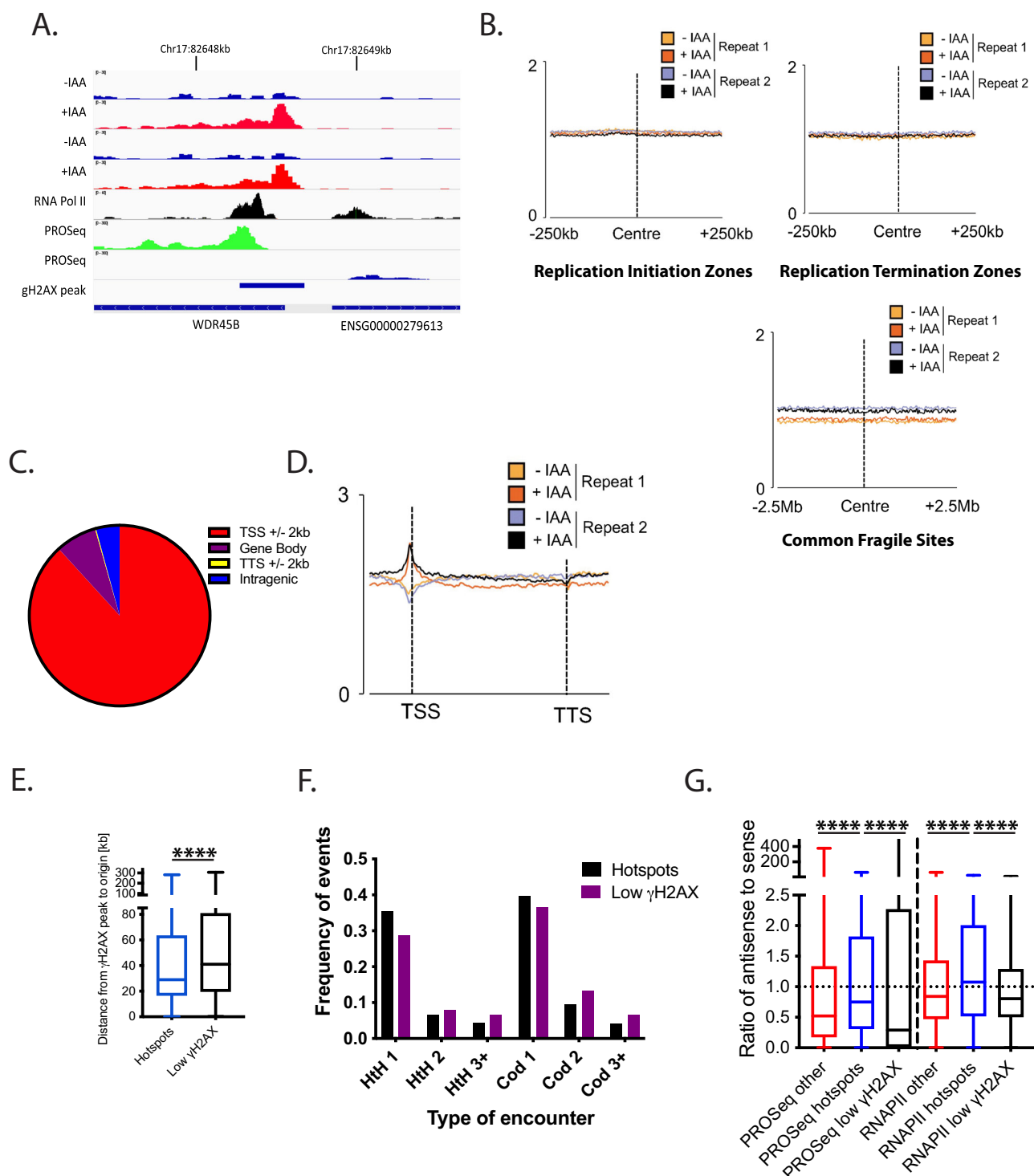
Conflicts or collisions between the replicative helicase and transcription machinery are known to be a major source of genomic instability in otherwise unperturbed cells; through both interactions between the protein complexes themselves, or the formation of DNA:RNA hybrids (R-loops)³⁷. Given the requirements of RNA Pol II bound DNA for the accumulation of DNA damage after auxin treatment, it is likely that TRAIP is required for either limiting the creation of conflicts between DNA replication and transcription or for the resolution of such encounters. We first tested therefore whether degradation of TRAIP increases levels of transcription in the cells by measuring the total level of RNA synthesis but observed no differences (Supplementary Fig. 11A). Next, we tested whether degradation of TRAIP-mAID increased the total level of RNA Pol II on chromatin, but this also was not the case (Supplementary Fig. 11B). To directly determine whether there is a higher level of replication-transcription conflicts in the absence of TRAIP, we used proximity ligation assays (PLA)

to explore any differences in the proximity of active transcription and nascent DNA. Cells were arrested in G1 where TRAIP was degraded before being released into S-phase. Approximately 12.5 hours following release when cells were in early S-phase (known to have high levels of both transcription and replication and when our γ -H2AX hotspots are replicated), the thymidine analogue EdU was added for 20 minutes. Cells were then harvested, and PLA assays were used to detect interactions between active transcription (phosphorylated RNA Pol II) and nascent replicated DNA (Fig. 5D). Intriguingly, we observed an increase in the amount of active RNA Pol II present in proximity to nascent DNA following TRAIP degradation, suggesting that TRAIP is indeed important for resolving replication-transcription encounters on chromatin and maintaining fork progression. To confirm this result, we also used the PLA assay to determine the proximity of RNA Pol II to components of the replisome: PCNA, and AND-1, with similar results: an absence of TRAIP during S-phase led to an increase in incidences of RNA Pol II and replisome proximity (Fig. 5E).

TRAIP depletion does not lead to DNA damage during S-phase in absence of transcription

To further explore the importance of TRAIP for the regulation of replication-transcription collisions we next turned to the *X. laevis* egg extract model system, which can support robust DNA replication activity in the absence of any transcription. During early embryogenesis in *Xenopus* embryos 12 cleavage cell cycles are achieved without transcription and only restricted protein translation. Most required factors for DNA replication and cell division are accumulated in the egg. The significant level of gene transcription is induced in the embryo only at the stage of midblastula transition. As *Xenopus* egg extract is derived from *Xenopus* eggs and the replicated DNA substrate is demembranated *Xenopus* sperm, the replication observed resembles embryonic replication during early cleavage divisions in the absence of transcription.

We raised antibodies against *X.l.* TRAIP (Supplementary Fig. 12A) and using this antibody we immunodepleted TRAIP from *Xenopus* egg extract to less than 10% of its original quantity (Fig. 6A). We could observe that although a lack of TRAIP in the extract did not affect its ability to synthesise DNA during S-phase, as previously reported²³, it did inhibit mitotic unloading of post-termination replisomes, which is a known function of TRAIP in this system (Supplementary Fig. 12B). This verified that our immunodepleted extract was indeed devoid of TRAIP's activity. Given our findings in the mammalian system, we next examined whether we could observe any signs of creation of DNA damage or checkpoint activation during S-phase without TRAIP in *Xenopus* egg extract system lacking transcriptional activity. We could detect no increase of γ -H2AX signal on chromatin upon TRAIP depletion, despite the DNA damage signalling cascade being functional in TRAIP-depleted extract, as treatment with restriction enzyme (EcoRI), which induces double-strand breaks, could activate a robust γ -H2AX signal on chromatin in both IgG- and TRAIP-depleted extracts (Fig. 6B). Similarly, we could observe no induction of phosphorylated Chk1 in



the nucleoplasm in the absence of TRAIP, while such a signal was readily induced by treatment of replicating extract with inhibitor of replicative polymerases (aphidicolin) and inhibited by ATM/ATR inhibitor (caffeine) (Fig. 6C). This further supports our hypothesis that TRAIP works in S-phase to protect genome stability by resolving conflicts between replication and transcription machineries; in the absence of transcription, such DNA damage does not occur.

TRAIP ubiquitylation substrates are likely unloaded by UBXD7-p97 complex

We next wanted to determine the mechanism by which TRAIP acts to resolve replication-transcription encounters. Previous research has

indicated that the formation of R-loops is often the underlying cause of replication-transcription conflicts³⁸ and R-loops accumulating at the TSS can stimulate TSS-associated transcription³⁹. We tested therefore whether we can observe the accumulation of R-loops in response to TRAIP-mAID degradation, as detected by S9.6 antibody, but did not see their accumulation (Supplementary Fig. 11C). Moreover, the DNA damage induced by TRAIP-mAID degradation could not be rescued by overexpression of RNaseH1, which can degrade RNA:DNA hybrids (Supplementary Fig. 11D). Altogether, the DNA damage created in absence of TRAIP due to replication-transcription collisions is likely not driven through resolution of R-loops on chromatin.

Fig. 4 | Absence of TRAIP during S-phase leads to generation of DNA damage at transcription start sites (TSS). **A** An example of TRAIP degradation induced γ H2AX peak over two independent repeats of γ H2AX ChIP-seq experiments. Transcription direction and position of accumulation of RNA Pol II³⁴ and of PRO-Seq³³ around the promoter are also presented. **B** γ H2AX ChIP signal from two independent experiments was compared with positions of replication initiation and termination zones as mapped by³⁰, or common fragile sites as mapped by³². Each graph is centred around the centre of initiation/termination/fragile site. **C** Graphical representation of the position of the called conserved γ H2AX peaks (damage hotspots), with 88.24% of γ H2AX peaks in proximity of TSS. **D** Average binned metagene profile for γ H2AX levels normalised to H2AX at transcribed genes in HCT116 cells, from TSS to transcription termination sites for the two repeat experiments. **E** Distance between the γ H2AX peaks at TSS at hotspots and the TSS of genes with the lowest fold change in γ H2AX levels and origins of replication identified in Koyanagi et al., 2021. The positions of TSS with called common γ H2AX

peaks are significantly closer to the origin of replication than the distance between TSS and origin of replication in genes that do not show increased γ H2AX signal upon TRAIP degradation. Box whiskers plots with line at the median; Mann–Whitney *t* test; *****p* value < 0.0001. **F** The proportion of 1st, 2nd, and further on (3+) transcribed genes encountered by replication forks emerging from the closest replication origin, presented for presented for “hotspots” = genes with reproducible γ H2AX peak in two experimental repeats; and “Low γ H2AX” = genes with no increase in γ H2AX levels. Chi-square *p* value < 0.05. **G** Quantification of the ratio between antisense- and sense transcription at TSS \pm 1 kb of hotspots, all other transcribed genes, and transcribed genes with low levels of γ H2AX increase following TRAIP depletion. PRO-Seq strand-specific signal³³ and RNA Pol II chromatin immuno-precipitation sequencing³⁴ was quantified –1000 bp to TSS for antisense transcription, and TSS to 1000 bp for the sense transcription. Box whiskers plots with line at the median; Mann–Whitney *t* test; *****p* value < 0.0001. Source data are provided as a Source Data file.

TRAIP was shown previously to be able to ubiquitylate for removal a DPC barrier in front of the replisome¹⁸, but also to ubiquitylate replisomes that converge at DNA inter-strand crosslink (ICL) leading to their removal from chromatin¹³. Moreover, RNA Pol II is known to be ubiquitylated by a number of ubiquitin ligases in order to remove it from chromatin (reviewed in ref. 40). It is possible therefore that TRAIP can ubiquitylate either RNA Pol II machinery, which is presenting to replication fork as a barrier, or the replisome itself. To investigate potential mechanism of TRAIP action we first explored any interactions between TRAIP and RNA Pol II in the cells, to see if TRAIP is present at the right place to fulfil this job. In order to do so, we took advantage of the Clover tag in TRAIP-mAC and looked for a proximity signal arising from TRAIP-mAC and RNA Pol II in the cells, using GFP antibody to detect TRAIP-mAC using the PLA technique. We could indeed detect such a proximity that was lost upon auxin addition and TRAIP-mAC degradation (Fig. 7A). As TRAIP was also reported to be enriched at replisomes in human cells^{7,14,15}, it has, therefore, the opportunity to act on either RNA Pol II or the replisome to resolve the conflict between these machineries and avoid DNA damage.

Both, ubiquitylated RNA Pol II⁴¹ and the replisome¹³ are removed from chromatin with assistance of p97 segregase. We aimed therefore to determine whether the TRAIP-driven ubiquitylation at transcription-replication collisions would be followed by p97 extraction of ubiquitylated complexes. However, we and others have shown that inhibition of p97 with small molecule inhibitors leads to the generation of far more DNA damage and inhibition of S-phase progression than in the case of TRAIP degradation^{42–44}. We decided therefore to look for a cofactor of p97 that may direct p97 to TRAIP-ubiquitylated substrates at replication-transcription encounters. We started with the two most likely candidates: SPRTN, which assists p97 with removal from chromatin of DPCs ubiquitylated by TRAIP^{18,45} and UBXD7, which was shown to facilitate replisome unloading during replication termination^{46,47} and is also a human homologue of the *S.cerevisiae* Ubx5 cofactor facilitating not only unloading of RNA Pol II from chromatin in budding yeast, but also assisting Wss1 protease and Cdc48 (*S.cerevisiae* p97) at DPCs^{41,48}. Interestingly, siRNA down-regulation of SPRTN did not lead to generation of DNA damage (γ -H2AX and 53BP1 foci) in otherwise unperturbed S-phase. Conversely, siUBXD7 did lead to an accumulation of DNA damage repair foci in S-phase to a similar level as after TRAIP-mAID degradation, and combining siUBXD7 and TRAIP degradation did not further increase the level of detected DNA damage response (γ -H2AX and 53BP1 foci), suggesting that these two factors are epistatic and act in the same pathway (Fig. 7D).

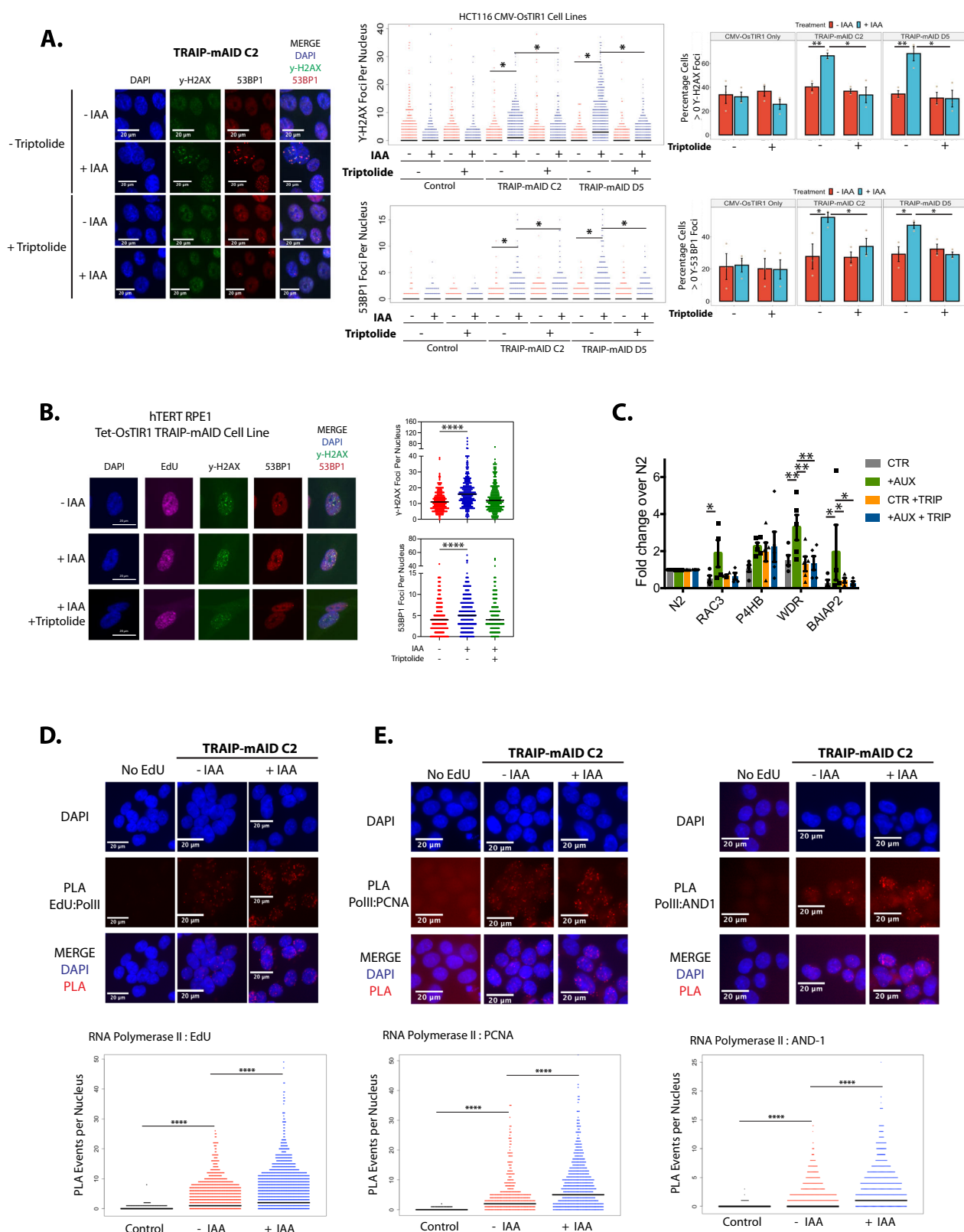
Discussion

Our work leads us to propose a model of TRAIP activity during S-phase. TSS with bi-directional transcription present a uniquely difficult problem for replication, as replication forks are likely to approach

transcription machinery in a head-to-head orientation on both sites of such TSS. These sites are more likely to result in replication-transcription collisions, which can be resolved by TRAIP ubiquitin ligase activity. TRAIP can ubiquitylate either RNA Pol II or the replisome in such situations, leading to unloading of the problematic machinery by the p97-UBXD7 complex and resolution of the conflicts without generation of DNA damage (Fig. 8).

Over the years, much evidence has accumulated indicating that TRAIP ubiquitin ligase plays wide-ranging roles in the maintenance of genomic integrity. TRAIP-depleted cells were shown previously to display a diverse spectrum of phenotypes: gross chromosomal rearrangements, problems with DNA damage response activation, micronuclei, and accumulation in G2 stage of the cell cycle^{6–8}. The functions of TRAIP were studied upon specific stimuli e.g., induction of double-strand breaks, induction of inter-strand crosslinks, stimulation of MiDAS, or inhibition of replicative polymerases etc.^{7,13,19,22}. However, the primary consequence of TRAIP depletion, the essential function of TRAIP for cell viability in unperturbed conditions, was not known.

Here, we have taken advantage of the degron system to rapidly degrade TRAIP within cells upon auxin addition, to dissect the importance of various functions of TRAIP in different stages of the cell cycle. TRAIP-deficient human cells have been shown to proliferate slowly even in the absence of exogenous DNA damage and the reduction of cellular proliferation during development is a likely cause of microcephalic dwarfism observed in patients with TRAIP mutations^{6,49}. Here, for the first time we have determined the mechanism of inhibition of cell proliferation in TRAIP-depleted cells. Firstly, we have shown that upon degradation of TRAIP, cells show signs of spontaneous DNA damage, leading to ATR checkpoint activation, G2 cell cycle arrest, and withdrawal from the cell cycle into senescence. Senescence is classically induced by telomere erosion in cells as the organism ages, due to activation of DDR. However, other stresses that engage DDR, such as exposure to oxidants, γ -irradiation, UVB light, or DNA-damaging chemotherapies can all induce senescence (reviewed in ref. 50). Many of these DDR stimuli can also induce apoptosis. It has been suggested that the level of stress can influence the choice between senescence and apoptosis, with senescence being induced by less severe damage^{50,51}. We can observe a low level of DNA damage foci induced by degradation of TRAIP, which is likely the reason for this cell fate choice. Senescence was also classically mechanistically defined as an irreversible cell cycle arrest in G1 phase (G0). However, many senescent cells in our body have 4 N DNA content⁵² and several studies showed that p21 also mediates permanent DNA damage-induced cell cycle arrest in G2, by inhibiting mitotic CDK complexes and pRb phosphorylation (reviewed in²⁸). Interestingly, this choice of a cease of proliferation by senescence may have additional consequences for TRAIP mutation-driven disease onset. Senescent cells are not eliminated but stably viable and can influence neighbouring cells through secreted soluble factors (senescence-



associated secretory phenotype, SASP). SASP attracts inflammatory cells to eliminate senescent cells but has been also associated with tissue and organ deterioration⁵⁰.

TRAIP has been shown over the years to have many functions in mitosis. TRAIP can unload rogue replisomes during mitosis^{20–22}, is important for execution of MIDAS^{21–23,53}, and regulates the spindle assembly checkpoint^{10,25}. However, the insults to genome stability

generated by cells progressing through mitosis without TRAIP are not responsible for the perturbed cell proliferation and G2 arrest. Instead, we conclude that the functions of TRAIP during S-phase are of utmost importance for cell viability. This is not to say that TRAIP does not have roles in mitosis. Indeed, we can observe delayed progression through mitosis when TRAIP was degraded specifically before onset of mitosis. It is also likely that a continuous lack of TRAIP from S-phase and

Fig. 5 | DNA damage induced in S-phase by TRAIP degradation depends on presence of transcription machinery. **A** HCT116 TRAIP-mAID cells were arrested in G1 stage of the cell cycle and TRAIP degraded before release of cells into S-phase. Upon S-phase entry cells were exposed to triptolide for 90 min. γ H2AX and 53BP1 foci induced were visualised by immunofluorescence and quantified. Example pictures (left) and quantification of three independent experiments is presented as quantification of number of γ H2AX and 53BP1 foci per nucleus (middle) or percentage of positive cells (>0 foci) in population (right) (mean \pm SEM). Differences between conditions was identified using t tests (γ H2AX: TRAIP-mAID C2 - Triptolide: $p = 0.00622$; TRAIP-mAID D5 - Triptolide: $p = 0.00798$; TRAIP-mAID C2 + IAA \pm Triptolide: $p = 0.0297$; TRAIP-mAID D5 + IAA \pm Triptolide: $p = 0.0318$). 53BP1: TRAIP-mAID C2 - Triptolide: $p = 0.0424$; TRAIP-mAID D5 - Triptolide: $p = 0.0474$; TRAIP-mAID C2 + IAA \pm Triptolide: $p = 0.0286$; TRAIP-mAID D5 + IAA \pm Triptolide: $p = 0.03709$). **B** TRAIP was degraded in hTERT-RPE1 TRAIP-mAID cells for 24 h. In the last 90 min, cells were optionally exposed to triptolide and in the last 20 min, cells pulsed with EdU. γ -H2AX, 53BP1 foci, and EdU incorporation were visualised by immunofluorescence and quantified. Example pictures (left) and quantification of 2–3 independent experiments is presented as number of γ -H2AX and 53BP1 foci

per EdU-positive nucleus. Mann–Whitney t test; **** p value < 0.0001 . **C** HCT116 TRAIP-mAID cells were treated as in **A** but instead of DNA damage foci analysis, γ H2AX ChIP was conducted followed by RT-PCR to detect indicated TSS. N2 is a amplifying a fragment from gene desert on chromosome 13. Mean of $n \geq 3$ with SEM. T -test per gene per condition: PH4B ctr vs IAA $p = 0.034$, WDR ctr vs IAA $p = 0.018$, WDR IAA vs IAA+Trip $p = 0.016$. **D** TRAIP-mAID cells were arrested in G1 stage of the cell cycle and TRAIP degraded before release of cells into S-phase. In early S-phase EdU was added for 20 min and proximity between incorporated EdU and RNA Pol II visualised by PLA. Example pictures (top) and quantification all PLA events per nucleus are presented (bottom). Mann–Whitney t test; **** p value < 0.0001 ($n = 3$). **E** PLA between PCNA and RNA Pol II (left) and AND-1 and RNA Pol II (right) after optional treatment with auxin. Experiments were carried out analogously to that detailed above; cells were arrested in G1 where TRAIP was degraded through IAA treatment, before being released into S-phase, and samples taken -12.5 hours post release. Example pictures (top) and quantification of all PLA events per nucleus are presented (bottom). Mann–Whitney t test; **** p value < 0.0001 ($n = 3$). Source data are provided as a Source Data file.

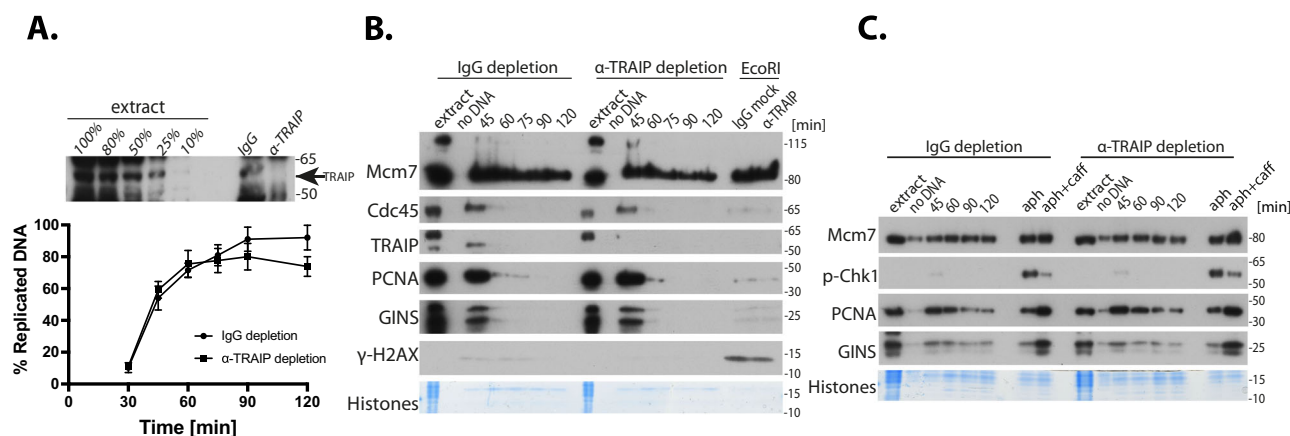


Fig. 6 | Depletion of TRAIP does not induce S-phase checkpoint activity in *Xenopus laevis* egg extract. **A** TRAIP was immunodepleted from *Xenopus laevis* egg extract to less than 10% as judged by immunoblotting of depleted extract (top). The ability of TRAIP-depleted extract to synthesise DNA was established by measuring α^{32} P-dATP incorporation into newly synthesised DNA and compared with replication of non-specific IgG-depleted extract. **B** DNA replication reaction was established in non-specific IgG- and TRAIP-depleted egg extracts and chromatin isolated at indicated timepoints during replication reaction. Chromatin samples were analysed by western blotting with indicated antibodies. A “no DNA” sample shows

chromatin specificity of the signal. Histones stained with Coomassie serve as a loading control. Samples of both extracts treated with restriction enzyme EcoRI to induce double-strand breaks (isolated at 60 min of reaction) serve as positive control for γ H2AX signal. **C** DNA replication was established as in **B** but instead of chromatin whole nuclei containing nucleoplasm were isolated to measure level of active phosphorylated Chk1. Samples of both extracts treated with the DNA Polymerase inhibitor aphidicolin serve as positive controls for Chk1 activation, while samples treated with aphidicolin and caffeine indicate ATM/ATR dependence of these signals. Source data are provided as a Source Data file.

through mitosis, exacerbates the problems experienced by cells depleted of TRAIP in S-phase. Some cells undergoing DNA damage-induced G2 senescence have been shown with time to be able to escape the G2/M checkpoint, progress through mitosis, and arrest in the subsequent G1 phase. This progression can also happen without chromosome segregation (mitotic bypass) leading to an accumulation of tetraploid G1 cells²⁸. In either case, the replicative problems generated during S-phase due to the absence of TRAIP, could present a substrate for TRAIP activity during mitosis and mitotic functions of TRAIP could reduce the overall genomic instability generated by TRAIP depletion. Unfortunately, we are unable to test this possibility due to the time required to resynthesise TRAIP, which is incompatible with S-phase without TRAIP and following mitosis with TRAIP.

TRAIP has been shown previously to be important for the cellular response to DNA replication stress upon different types of insults^{6–8}. It has also been suggested to be a master regulator of ICL repair during DNA replication, as its activity promotes two alternative pathways of ICL repair in *X. laevis* egg extract¹³. However, patients with TRAIP mutations display dwarfism rather than the classical Fanconi anaemia clinical outcome, which is characteristic for mutations within ICL

repair factors^{6,54}. Instead, our results indicate that without exogenous sources of replication stress, the major endogenous source of replication fork impediments that require TRAIP activity is in encountering transcription machinery. In the absence of TRAIP during S-phase in human cells, we observe increased levels of persisting DNA replication-transcription encounters. We can also detect enrichment of the DNA damage response at TSS sites, where replication forks likely collide with RNA Pol II. Importantly, this damage can be completely rescued by the temporary removal of RNA Pol II from chromatin. Moreover, in the *Xenopus* egg extract model system where efficient DNA replication can be established without the presence of concurrent transcription, TRAIP is not essential for the completion of S-phase, nor can we detect any signs of DNA damage or checkpoint activation.

In human cells, coexistence of DNA transcription and DNA replication is a well-established potential source of endogenous replication stress. It is often exacerbated by oncogenic deregulations stimulating transcription, whilst simultaneously promoting premature entry into S-phase, leading to a higher probability of interference between the two processes^{35,55}. The role of TRAIP in the resolution of such conflicts is consistent with the observation that TRAIP-deficient cells show fork

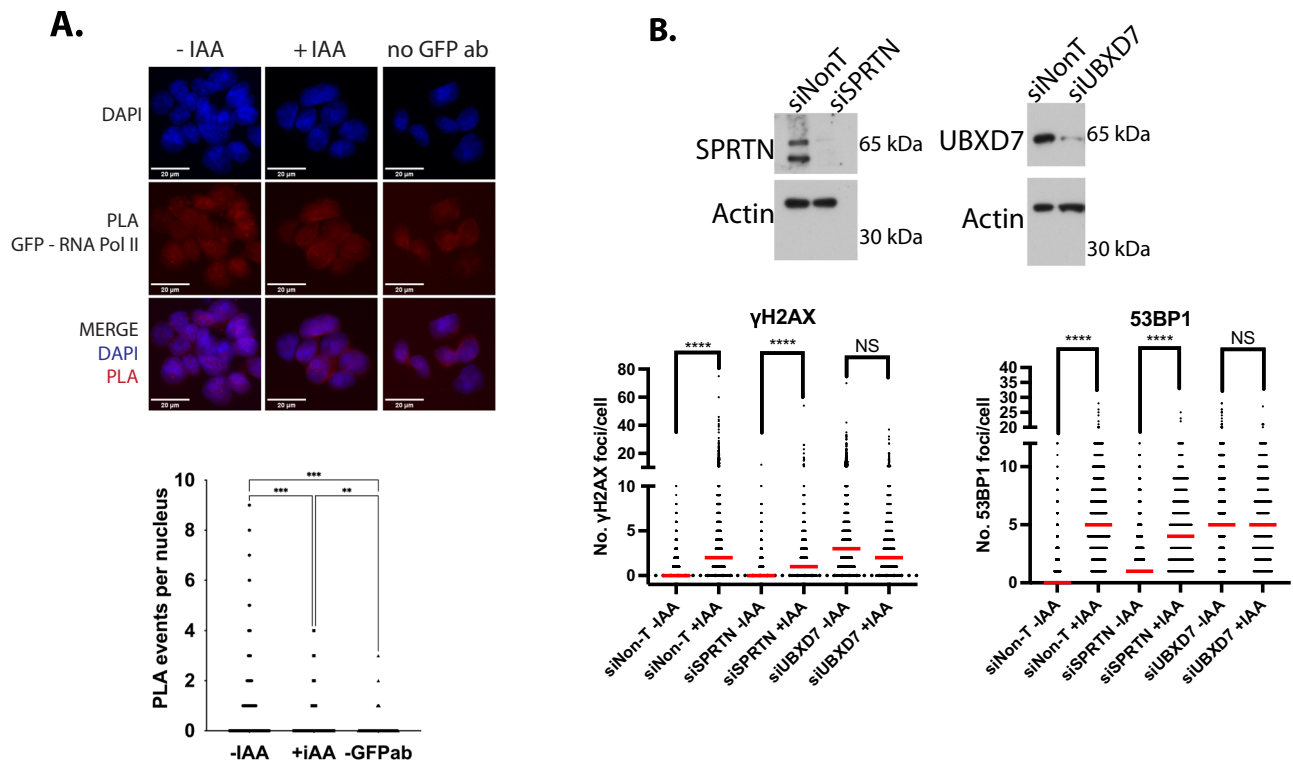


Fig. 7 | TRAIP facilitates resolution of replication transcription encounters. **A** PLA assay between TRAIP-mAC (GFP antibodies) and RNA Pol II. Example pictures (top) and quantification of all PLA events per nucleus are presented (bottom). **B** SPRTN or UBXD7 were downregulated with siRNA in HCT116 TRAIP-mAID cells

and the protein level verified by western blot (left). TRAIP-mAID was degraded for 24 h and γH2AX or 53BP1 foci were visualised and quantified in cells in S-phase (right) ($n = 3$). Mann-Whitney t test; **** p value < 0.0001 . Source data are provided as a Source Data file.

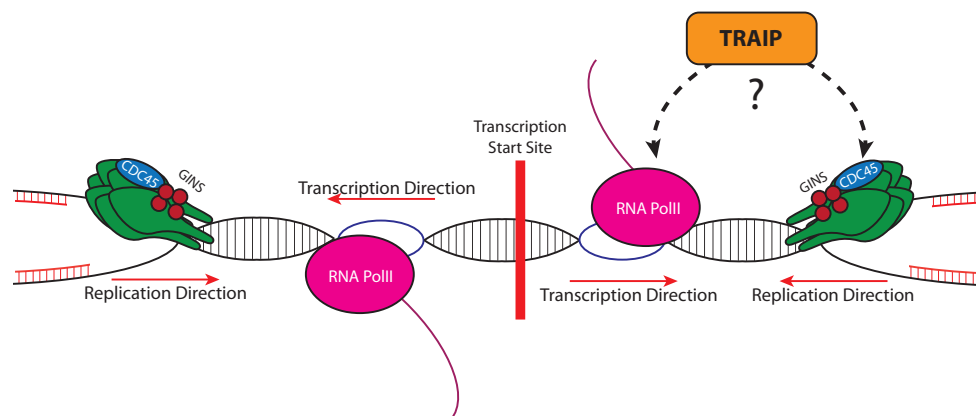


Fig. 8 | Model of TRAIP activity during S-phase. During unperturbed DNA replication the bi-directional transcription start sites (TSS) represent a difficult to replicate region, as replication forks approaching such TSS from either direction, encounter transcription machinery in a head-to-head orientation. Such collisions

can lead to genomic instability if not resolved. TRAIP facilitates resolution of these replication-transcription encounters through its ubiquitin ligase activity directed either towards the replisome or the transcription machinery.

asymmetry in the DNA fibre assays, suggesting site-specific stalling of one of the forks emanating from the same origin of replication⁷.

What is the mechanism by which TRAIP may promote resolution of replication-transcription collisions? Our analysis of the hotspots of DNA damage created in the absence of TRAIP suggests that the problems most often arise when the newly established replication fork encounters the first gene promoter where RNA Pol II has accumulated. Moreover, the hotspot sites represent particularly crowded sites, with high levels of transcription moving in both directions from the promoter. Despite the orientation of annotated gene transcription being equally often in head-to-head or codirectional with the direction of

progression of the replication fork, the equal levels of sense to antisense transcription at hotspot TSS suggest that the fork will ultimately encounter the transcription machinery in a head-to-head orientation. These bi-directional transcription units may therefore represent a particularly difficult impediment for replication fork progression. Indeed, sites with high levels of antisense transcription have already been identified as hotspots for transcription-replication interactions and for G2/M DNA synthesis^{38,56}. Previous research has also identified that TSS-associated transcription is stimulated by the presence of R-loops accumulating at the TSS³⁹ and the propensity to form R-loops is a feature of transcription-replication interaction hotspots³⁸.

However, when we assessed R-loop levels using the R-loop specific antibody S9.6 by immunofluorescence, we did not identify an increase in cells depleted of TRAIP, and overexpression of RNaseH1 did not rescue the DNA damage generated in S-phase without TRAIP. These results suggest that TRAIP depletion is not leading to a global increase in R-loop levels in cells, and their resolution is not important for TRAIP-driven mechanisms.

The transcription machinery encountered by the replication fork very much resembles a DNA-protein barrier and TRAIP has been shown previously to facilitate replisome bypass of DPC (protein covalently crosslinked to DNA by aldehydes or chemotherapeutics)¹⁸. In this situation, TRAIP stimulates the bypass of the DPC by the replication machinery and also ubiquitylates DPC to stimulate its degradation by SPRTN and the proteasome^{18,57}. It is therefore likely that TRAIP could act similarly when encountering tightly associated RNA Pol II. It is well established that removal of RNA Pol II from chromatin in response to DNA damage is driven by ubiquitylation of RNA Pol II and subsequent unfolding and unloading by p97 segregase⁴⁰. We have shown here that TRAIP and RNA Pol II can be found in close proximity in S-phase nuclei. However, more research is needed to establish RNA Pol II as TRAIP substrate. Alternatively, the replisomes themselves could be the substrate of TRAIP ubiquitylation activity. Whatever the substrate, our data suggest that p97 together with UBXD7 is likely to unload ubiquitylated complexes from chromatin following TRAIP ubiquitylation.

Finally, downregulation or immunodepletion of TRAIP in human cells and *Xenopus* egg extract system was reported previously to lead to chromosomal instability and re-arrangements, which are a hallmark of cancer development^{7,8,23}. Notably, however, TRAIP-deficient patients were not reported to characterise with cancer predisposition, similarly to other Seckel syndrome patients^{6,49}. It is possible therefore that the G2 arrest and senescence we observe upon degradation of TRAIP is not compatible with increased proliferation and tumour development. Inhibition of TRAIP could therefore be significantly detrimental to cancerous cells.

Methods

Plasmid construction

DONOR and CRISPR plasmids were constructed for the generation of conditional Auxin-Inducible Degron Cell lines as detailed in Natsume et al.²⁶. CRISPR-Cas9 was expressed using the pX330-U6-Chimeric_BB-CBh-hSpCas9 plasmid⁵⁸ (Addgene #42230) and targeted the C-terminus coding region containing the stop codon (5'-CTCACTGTTCTCAGACCAC-3'). Donor plasmids were generated following a published protocol²⁷. Briefly, we cloned homology arms upstream and downstream of the CRISPR target region to pBluescript^{26,27} (-500 bp each). After inverse PCR, a cassette containing mAID or mAID-Clover (mAC) with a selection marker was cloned to make a donor plasmid. Two donor plasmids were created: *TRAIP*-mAID and *TRAIP*-mAC, containing either Hygromycin (HCT116) or Neomycin (hTERT-RPE1) resistance for selection.

Generation of TRAIP conditional degron cell lines

HCT116 cell lines constitutively expressing the *Oryza sativa* auxin-sensitive F-box protein (OsTIR1)²⁶ were transfected with the previously described DONOR and CRISPR plasmids. Parental HCT116 cell lines were seeded to individual wells of a six-well plate at a final working concentration of 1×10^5 cells/ml. Transfection was conducted 2 days following plating using Fugene HD, OPTI-MEM, 200 ng/ μ l DONOR plasmid, and 200 ng/ μ l CRISPR plasmid. Parental hTERT-RPE1 cell lines were diluted to a working concentration of 1×10^6 cells/ml, washed with PBS, and re-suspended in Resuspension Buffer R (Neon Transfection System, ThermoFisher Scientific). The re-suspended cell reaction was supplemented with both DONOR and CRISPR plasmids (1500 ng total) and electroporated $3 \times$ at 1350 V for 20 ms, 2 pulses per reaction. The resulting electroporated cell suspension was transferred

to individual wells of a six-well plate and incubated for 2–3 days before being subject to the selection procedure below. Control reactions were transfected with DONOR plasmids only. Approximately 24 hours later for HCT116 cells or 72 hours later for hTERT-RPE1 cells, the transfected cultures were collected and diluted at different concentrations in 10 cm dishes. The selection was carried out 24 hours after dilution (100 μ g/ml Hygromycin or 1 mg/ml G418) and maintained continuously for 11–13 days. Once sufficient colonies were observed, 48 from each condition were isolated, grown in individual wells of a 96-well plate until confluent, and screened for bi-allelic gene insertion using genomic PCR. Adherent cells were washed twice with Dulbecco's PBS (-) (D-PBS (-)) and treated with DirectPCR Lysis Reagent (Viagen: 0.5 \times DirectPCR Lysis Reagent, 20 mg/ml proteinase K) overnight at 55 °C. Proteinase K activity was stopped through incubation of the 96-well plate at 85 °C for 90 minutes in humid conditions. Genomic PCR was carried out using GoTaq HotStart Green Master Mix (Promega), as per manufacturer's instruction (*TRAIP* F: AGATGTGGTGAGTGTGGCTTC; *TRAIP* R: GCTGCAGTGATCT-CATTCTTTCT; mAID: ATCTTTAGGACAAGCACTCTTCTCC). Bi-allelic gene insertion was first screened using the Microchip Electrophoresis System (Multi-NA; Shimadzu), and any subsequent bi-allelic tag status confirmed using DNA gel electrophoresis with 2% agarose gels. HCT116 cells were maintained in McCoy's 5 A medium supplemented with 10% Fetal Bovine Serum, 2 mM L-glutamine, 100 U/ml Penicillin, and 100 μ g/ml Streptomycin; hTERT-RPE1 cells were maintained in DMEM-F12 medium supplemented analogously to McCoy's 5 A medium using Tetracycline-free Fetal Bovine Serum. All cultures were grown at 37 °C with 5% CO₂.

Generation of RNase HI-GFP stable cell lines

HCT116 CMV-OsTIR1 TRAIP-mAID cell lines were further modified through viral transduction to introduce the Dox-inducible overexpression of GFP-tagged RNase HI. RNase HI-GFP plasmids were a kind gift from Dr Kienan Savage⁵⁹. Virus production was carried out using HEK293T cells, cultured in DMEM media supplemented as detailed for DMEM-F12. To produce virus, cells were harvested, re-suspended in IMDM media supplemented as detailed, and seeded at a working concentration of 3×10^5 cells/ml on 2×15 cm tissue culture dishes. Approximately 24 hours later, cells were transfected as detailed. A total of 25 μ g of RNase HI-GFP plasmid was combined with 16.25 μ g of packaging plasmid and 9 μ g of envelope plasmid. Plasmids were diluted appropriately in 0.1 \times TE buffer and distilled H₂O before being supplemented with 2.5 M CaCl₂. Finally, 2 \times HBS was added to a final concentration of 1 \times and the transfection mixture was added to the cells. Precisely 16 hours following transfection the media was changed to fresh supplemented IMDM. Approximately 24 hours later, the cell media was collected, filtered using a 0.22 μ m syringe filter, and centrifuged to remove cell debris (400 \times g, 5 minutes). The resulting virus suspension was aliquoted and stored at -80 °C until use. To transduce cells, HCT116 CMV-OsTIR1 TRAIP-mAID clones were seeded onto six-well plates at a working concentration of 2×10^5 cells/ml. The virus was added dropwise to the cells and incubated for 24 hours; when the media was replaced with pre-warmed supplemented McCoy's 5A. Approximately 24 hours later, cells were harvested and plated onto 10 cm dishes at a 1–200 dilution and treated with 10 μ g/ml Blasticidin. Cells were incubated with the appropriate antibiotic for 7–10 days, changing the media every 3 days. RNase HI expression was confirmed through GFP expression under a fluorescent microscope.

Generation of TRAIP rescue cell lines

HCT116 CMV-OsTIR1 TRAIP-mAID cell lines were modified to introduce constitutively expressed wild-type, C7A/C10A, or W37A mutant TRAIP through retrovirus transduction. Retrovirus plasmid constructs containing the *TRAIP* sequences were a kind gift from Prof. Andrew Jackson⁶. Virus production was carried out using HEK293T cells, grown

as detailed previously. Briefly, HEK293T cells were seeded onto 10 cm tissue culture plates and grown until approximately 40–50% confluent. The transfection plasmids were prepared as follows: 300 μ l OptiMEM reduced serum media, 6 μ g *TRAIP* construct, 3.8 μ g Clontech GAG/POL plasmid, 2.2 μ g Clontech VSVG plasmid. This mix was combined with 24 μ l PEI pre-prepared in 300 μ l OptiMEM and incubated at room temperature for 20 minutes. The transfection mix was added dropwise to the HEK293T cells and cells incubated overnight. Approximately 16 hours later the media was replaced with fresh, pre-warmed media and incubated for a further 24 hours. Following this, medium was collected and passed through a 0.22 μ m filter to remove cell debris. Virus was stored at -80°C until use. Parental cell lines were transduced as detailed previously, analogously to lentivirus.

Detecting TRAIP protein levels

Immunoblotting was used to detect both TRAIP band shifts corresponding to the inserted tag size, and protein degradation. Whole-cell extracts were generated by re-suspending harvested cell pellets in UTB extraction buffer (8 M Urea, 50 mM TRIS-HCl, 150 mM β -Mercaptoethanol) for 10 minutes on ice. The cell lysate was then sonicated (BioRuptor: 30 sec on, 30 sec off, 5 min cycles, medium power) and centrifuged at $14,000\times g$ for 20 minutes to separate soluble and insoluble fractions. The soluble fraction was collected and mixed with 4 \times SDS-PAGE Loading Buffer (NuPAGE) to a final concentration of 1 \times . Approximately 50 μ g of total protein content was run-on 4–12% gradient SDS-PAGE gels (Invitrogen) and transferred to Nitrocellulose membranes for 90 minutes at 80 V. Transferred membranes were blocked (5% Milk in TBST) for 1 hour before being incubated in primary antibody at 4°C overnight. Membranes were washed 3×10 minutes in TBST and incubated in secondary antibody for 2 hours at room temperature. The membranes were then washed 3×10 minutes in TBST before being developed using ECL detection spray (Advansta WesternBright). Antibodies used for immunoblotting were as follows: Anti-TRAIP antibodies were kindly provided by professor N. Mailand⁷ and used 1:300 in 5% Milk in TBST. Anti- β Actin loading controls used 1:5000 in 5% BSA in TBST (C4 anti-Actin HRP Santa Cruz).

Drug treatments

TRAIP degradation in HCT116 cells was induced through the addition of 500 μ M Indole-3 acetic acid (IAA) to cell media, subsequently diluted 1:5 in the existing growth media to provide a final working concentration of 100 μ M. Protein degradation in hTERT-RPE1 cell lines was carried out using a final working concentration of 25 μ M IAA, prepared analogously to that described for HCT116 cells. The respective working concentrations of other inhibitor treatments used are described: 10 μ M ATM inhibitor (Strattech KU-55933), 4 μ M ATR inhibitor (Strattech AZD6738), 5 μ M MK-1775 (Strattech), 100 nM Triptolide (Sigma-Aldrich T3652), 100 μ M DRB (Sigma-Aldrich D1916), 0.4 μ M Aphidicolin (A0781, Sigma).

Cell viability assays

For colony-forming assays, cells were diluted to a working concentration of 1000 cells/ml and plated to individual wells of a six-well plate at different seeding concentrations (100, 250, 500, 750, 1000 cells/well). For assays using hTERT-RPE1 cell lines, 500 cells were seeded onto 10 cm tissue culture dishes. HCT116 cell lines were treated with Auxin (IAA) 24 hours after plating whilst hTERT-RPE1 cells were first treated with 100 ng/ml Doxycycline 24 hours after plating, and IAA added the following day (48 hours after plating). Cell media containing Doxycycline was refreshed every 3–4 days. All cells were incubated until sufficient colony formation was observed (~ 10 – 14 days). At this point, the cell media was removed, and colonies stained using Methylene Blue staining (2% methylene blue in 50% ethanol) buffer for 5 minutes at room temperature. Colonies were rinsed with H_2O and dried overnight. For quantification, the percentage colony forming

efficiency was calculated by dividing the number of counted colonies by the original number of cells plated, allowing comparison between different seeding concentrations. To then allow comparison between different cell lines, the calculated percentage colony forming efficiency was normalised to a control cell line (Untreated HCT116 CMV-OsTIR1 only or hTERT-RPE1 Tet-OsTIR1 only; Efficiency in test clone/Efficiency in Control). For cell proliferation assays, cells were diluted to 1×10^4 cells/ml and plated into either 60-mm dishes for HCT116 cell lines or 10 cm dishes for hTERT-RPE1 degron cell lines. Cells were treated with IAA and Dox as appropriate as detailed above, and cells grown for a further 72 hours. At each timepoint (24, 48, 72 hrs post auxin treatment) cells were harvested and the total cell numbers counted using a COUNTESS cell counter. Cell counts were normalised to the seeding concentration. In addition, following cell counting, the remainder of the samples were prepared for Flow Cytometry as detailed.

Cell death assays

Cell senescence was detected using the Cell Meter Senescence Activity Assay (AAT Bioquest). Cells were plated for proliferation curves as described. At each timepoint, cells were harvested and washed with PBS. Cell pellets were re-suspended in Xite Green β -D-galactopyranoside solution for 45 minutes at 37°C . Stained cells were washed again in PBS, re-suspended in 500 μ l Assay Buffer, and analysed using a Flow Cytometer. Senescent cells were detected using the FITC 488 channel, with unstained controls utilised to distinguish between positive and negative cell populations. Apoptotic cells were detected using the Annexin V Apoptosis Detection Kit (Invitrogen). Cells were grown and harvested as detailed. The resulting pellet was re-suspended in 1 \times binding buffer supplemented with AF488 fluorochrome coated Annexin V. Samples were incubated for 15 minutes at room temperature and washed in Binding Buffer. Stained cells were then re-suspended in 200 μ l Binding buffer supplemented with 50 μ g/ml Propidium Iodide and 50 μ g/ml RNase A. Cells analysed using a flow cytometer, with apoptotic cells detected using the FITC 488 channel.

Cell synchronisation

For G1 cell synchronisation, asynchronous cells were treated with 20 μ M Lovastatin (Acros Organics) for 24 hours. To then release cells from the G1 arrest, cells were washed $3\times$ in pre-warmed growth media before fresh media supplemented with 2 mM Mevalonic Acid (Sigma-Aldrich) was added. Cells entered S-phase ~ 12 hours post release. To arrest cells in G2 stage of the cell cycle, asynchronous cells were treated with 9 μ M RO-3306 (Merck Life Sciences) for 16 hours. G2 release was achieved through washing the cells $3\times$ in pre-warmed media before fresh growth media was added. Released cells enter mitosis ~ 30 – 60 minutes post release. To sequentially arrest cells in G1 and G2, cells were treated as described for G1 cell cycle arrest. Approximately 8 hours after G1 release, 9 μ M RO-3306 was added, and the cells incubated for 16 hours to facilitate G2 arrest. Cells were released as detailed.

Immunofluorescence

Asynchronous cells were seeded onto pre-sterilised 20 mm glass cover slides placed into each well of a 6-well plate. Any respective drug treatments were carried out as described. To label S-phase cells, 10 μ M EdU treatments were included for 20 or 60 minutes prior to cell fixation. To fix cells, the growth media was removed, and the cells washed once in D-PBS (–). Washed cells were fixed using 4% Paraformaldehyde in PBS for 15 minutes at room temperature. Cells were then permeabilised in 0.5% TritonX-100 in PBS for 5 minutes at room temperature and washed twice. If required, EdU or EU Click-IT was carried out as per the manufacturer's protocol (Invitrogen) to detect S-phase cells prior to antibody staining or to measure transcription activity. Antibody staining was subsequently carried out: 100 μ l of primary antibody (in

washing buffer: 5% BSA 0.1% Tween-20 in PBS) was added dropwise to cover the glass cover slip and incubated for 2 hours at room temperature. Cells were then washed 3× in washing buffer and 2× in D-PBS (–). Secondary antibody solution was added analogous to primary antibody and incubated for 2 hours at room temperature in the dark. Antibodies used are described: Mouse anti-Ser139 γ -H2AX (Sigma-Aldrich JBW301; 1:1000), Rabbit anti-53BP1 (Novus Biologicals NB100-904; 1:1000), Rabbit anti-S9.6 (Francis Crick Institute; 1:200), Mouse anti-Mitotin (BD Biosciences 610768; 1:300), Rabbit anti-P-Histone H3S10 (Cell Signalling 9701; 1:1000), AF488 anti-mouse secondary (Invitrogen A32723; 1:1000), AF555 anti-rabbit secondary (Invitrogen A21428; 1:1000). Stained cells were washed as detailed before being mounted onto glass slides using DAPI mounting media (Fluoroshield). Slides were dried at room temperature before being imaged using a Leica DM600 Widefield Fluorescent microscope with Leica LASX V. 3.7.4.23463 software. All images were exported as raw grayscale TIFs, analysed using CellProfiler (v4.0.6) and ImageJ (v2.1.0).

siRNA depletion

HCT116 TRAIP-mAID CMV-OstIR1 cells were seeded at 1×10^5 cells/ml and 24 h later, transfected with 50 nM Non-targeting (Horizon Discovery, D-001810-10-05), UBXD7 (Horizon Discovery, L-023533-02-0005) or SPRTN/C1orf124 (Horizon Discovery, L-015442-02-0005) siRNA, using Dharmafect 1 transfection reagent and manufacturer's protocol. Cells were harvested or fixed 72 h later and analysed by western blotting or immunofluorescence. Depletion was confirmed through western blotting, using antibodies: Rabbit anti-UBXD7 (Thermo Fisher Scientific 15779771; 1:1000) and Rabbit anti-SPRTN (Novus Biologicals NBPI-84163; 1:1000).

Flow cytometry

Three types of flow cytometry experiment were carried out: un-extracted cells, BrdU detection, and extracted cells. For un-extracted cells, following the required experimental procedures (e.g., proliferation curves) cells were harvested and fixed in 70% ethanol in PBS for 16 hours at -20°C . Following fixation, cells were washed twice in washing buffer (5% BSA, 0.1% Tween-20, PBS) and antibody staining carried out if required. Briefly, washed cells were re-suspended in 100 μl primary antibody in washing buffer and incubated at room temperature for 1 hour, rocking to prevent cells from settling. The cells were washed twice in washing buffer and re-suspended in 100 μl secondary antibody in washing buffer for 1 hour at room temperature in the dark. Stained cells were washed 1× in washing buffer and 2× in D-PBS (–) before being re-suspended in either Hoechst Staining Buffer (5 $\mu\text{g}/\text{ml}$ Hoechst 33582, PBS) or Propidium Iodide Staining Buffer (50 $\mu\text{g}/\text{ml}$ Propidium Iodide, 50 $\mu\text{g}/\text{ml}$ RNase A, PBS). For BrdU detection, 10 μM of BrdU was added to the growth media 1 hour prior to harvesting. Cells were collected and fixed in ethanol as described. Fixed cells were washed once in PBS before being re-suspended in 1 ml 2 M HCL supplemented with 0.1 mg/ml Pepsin for 20 minutes. Cells were then washed, and antibody staining carried out as described. To explore the replisome binding pattern on chromatin, cells were extracted using CSK buffer (25 mM HEPES pH 7.4, 50 mM NaCl, 3 mM MgCl_2 , 300 mM Sucrose, 0.5% TritonX-100, 1× complete protease inhibitors) to remove soluble fractions. The protocol used to extract cells has been described elsewhere (Formet & Jackson, 2015). Antibodies used are as follows: Rabbit anti-P-Histone H3S10 (Cell Signalling 9701; 1:500); Mouse anti-MCM7 (Santa Cruz 9966; 1:500); Mouse anti-BrdU (BD Biosciences 347580, clone B44; 1:5); AF488 anti-mouse secondary (Invitrogen A32723; 1:1000); AF555 anti-rabbit secondary (Invitrogen A21428; 1:1000); AttoN647 anti-rabbit secondary (Sigma-Aldrich 40839; 1:500). Cells were analysed using a Beckman Cytoflex instrument with CytExpert v2.5 software. Data analysis was carried out using FlowJo (v10.7.1). For all analysis, doublets were first excluded by gating the populations of interest using FSC-A vs SSC-A followed by

FSC-A vs FSC-H. Second, gates required for quantification were applied based on control samples, and applied universally to all other samples within the experiment. For example, for cell cycle analysis untreated DNA distributions were empirically gated as G1 (2 N DNA content), G2/M (4 N DNA content), and S-phase (region between 2 N and 4 N). The set gates were then overlaid onto treatment samples to determine any consequential changes. An example of cell cycle stages gating is presented in Supplementary Fig. 2D.

ChIP-sequencing

For ChIP-sequencing, HCT116 TRAIP degron cells were diluted to 2×10^5 cells/ml and seeded onto 20 cm dishes (2× per condition). Plated cells were arrested in G1 as described, treated with auxin (IAA) to degrade TRAIP, and released into S-phase. 16 hours after release, cells were harvested and the resulting cell suspension supplemented with 1% Formaldehyde (Sigma-Aldrich) for 10 minutes at room temperature. Formaldehyde crosslinking was quenched using 125 mM Glycine (Sigma-Aldrich). Fixed cells were pelleted (400 g, 3 minutes, 4°C) and the pellet washed 2× with ice-cold PBS. Cell extraction was then carried out through sequential incubations in ChIP lysis buffer (5 mM HEPES pH 8.0, 85 mM KCL, 0.5% NP40) and ChIP nuclear lysis buffer (50 mM Tris-HCL pH 8.0, 10 mM EDTA pH 8.0, 1% SDS) for 15 and 30 minutes on ice, respectively. Cell lysates were divided into equal aliquots and sonicated (30 amplitude, 15 sec on, 25 sec off, 12 cycles). Sufficient sonication (resulting in 300–500 bp DNA fragments) was confirmed through DNA gel electrophoresis. Chromatin immunoprecipitation was carried out using Protein A Dynabeads conjugated to approximately 1 μg of rabbit anti-Ser139 γ -H2AX (Abcam 29893) or rabbit anti-H2AX (Merck Millipore 07627) antibodies, as detailed in Wang et al.⁵⁶. Immuno-precipitation was validated by quantitative PCR using primers targeting the actin housekeeping gene (Forward: CATGTACGTTGCTATCCAGGC, Reverse: CTCCTTAATGTCACGCACGAT). The PCR was performed using AppliedBiosystems QuantStudio5 with Thermo Fisher Connect software and analysed in Microsoft Excel.

Library preparation was carried out using NEBNext Ultra II DNA Library Preparation Kit for Illumina NEB, as per manufacturer's instruction. The prepared libraries were sequenced using single-end sequencing with a High-75 kit, using Illumina NexSeq instruments. γ -H2AX ChIP-Seq, precision run-on sequencing (PRO-Seq)³³ and RNA Pol II chromatin immuno-precipitation sequencing³⁴ in HCT116 cells were aligned to the hg38 genome using Bowtie 2 v.2.4.2 on the online platform Galaxy (<https://usegalaxy.org>⁶⁰). γ -H2AX ChIP-Seq peaks were called in the +IAA treated sample against the γ -H2AX ChIP-Seq in its –IAA control using MACS2 v.2.1.1 with parameters as detailed in⁵⁶. The bedtools intersect intervals function on the online platform Galaxy was used to identify the conserved γ -H2AX ChIP-Seq peaks in the two repeats. The distance between the γ -H2AX ChIP-Seq peak or the TSS with lowest γ -H2AX fold change +IAA/–IAA was calculated using the position of the origins of replication in HCT116 cells provided by Dr Daigaku³¹. The PRO-Seq dataset was used to determine the reciprocal direction between the oncoming replication fork and gene transcription (head-to-head or codirectional), as well as whether the TSS was the first, second, or third and above-transcribed gene encountered. Replication timing for the γ -H2AX ChIP-Seq peak was derived analysing replication timing in HCT116 cells from³⁰. The read coverage profiles were generated using the computational environment EaSeq, normalising the γ -H2AX ChIP-Seq file to the H2AX ChIP-Seq file with the function “average”⁶¹.

To identify the list of transcribed genes in HCT116 cells, the counts for each gene were computed by featureCounts on the online platform Galaxy using the annotation of the GENCODE genes (GRCh38.p10) on an ENCODE polyA RNA-Seq hg38 aligned file (ENCFF823JEV). Read per kilobase per million (RPKM) were calculated over each gene and genes that had an RPKM > 1 were considered as transcribed.

The levels of antisense to sense transcription were calculated using the PRO-Seq and RNA Pol II ChIP-Seq datasets using the function “quantify” in EaSeq, for the antisense –1000 bp to the TSS, and for the sense from the TSS to +1000 bp. For the PRO-Seq, as this was strand-specific antisense transcription levels were specifically measured on the strand opposite to the sense transcription. Heatmaps were generated with the function “HeatMap” of EaSeq around TSS ± 2500 bp. To identify the genes with the lowest increase in γ -H2AX ChIP-Seq levels following TRAIP depletion, the normalised levels of γ -H2AX ChIP-Seq signal to H2AX was calculated across the TSS ± 1000 bp of all transcribed genes in both the repeats and averaged for each gene. Then gene TSS were sorted by the fold change in γ -H2AX ChIP-Seq levels in the +IAA compared to the –IAA.

ChIP RT-PCR

For the RT-PCR PCR, primers were designed at a series of conserved γ H2AX peaks over transcribed genes. ChIPs were performed for γ H2AX and H2AX as described above, with γ H2AX levels normalised to H2AX levels. γ H2AX/H2AX at the target sites were then normalised to the γ H2AX/H2AX levels at a negative control region (N2), that is a region in a gene desert on chromosome 13. Cells were grown as above, with triptolide added for 90 minutes. Primers used: BAIAP2 For (CTTCGTCCTCCGTCCTGCTG) and BAIAP2 Rev (GAAGACC CCAAAGTCCCAG) amplifying 278 bp product; RAC3 For (TGTGATAC ATTCTGGCCCCG) and RAC3 Rev (GAACCCCGACGGACAG) amplifying a 179 bp product; P4HB For (CGGATTGGACACTCACACCA) and P4HB Rev (CAGAGTCCGTGCTACCGAAA) amplifying a 223 bp product; WDR45B For (CACCGTGGTCTGGTTGAAG) and WDR45B Rev (CATG AACCTCCTGCCGTGTA) amplifying a 71 bp product; N2 For (AGCT ATCTGTGCGAGCAGC) and N2 Rev (CATCCCCCTCTGTTAGTGAAGG) amplifying a 112 bp product.

Proximity ligation assays

PLA were carried out using the DuoLink PLA Kit. The provided manufacturer's instruction was optimised for use on cell suspensions. Parental cell lines were diluted to 2×10^5 cells/ml and seeded to 60-mm tissue culture dishes. Cells were arrested in G1, where auxin (IAA) was added, and released into S-phase. Approximately 12 hours following cell cycle release, 10 μ M EdU was added for 20 minutes to label nascent DNA. For PLA reactions using antibody recognition only, cells were harvested approximately 12.5 hours following cell cycle release to provide a similar timepoint to that when incorporating EdU treatment. Cells were then harvested and extracted using CSK buffer as described previously. Extracted, permeabilised cells were subjected to the Click-It reaction to conjugate biotin to incorporated EdU (Invitrogen, as per manufacturer's protocol). Cells were washed 2 \times in PLA washing buffer and re-suspended in 50 μ l of each primary antibody made up in washing buffer (elongating RNA Polymerase II (serine 5): Mouse anti-Rpb1 CTD (Cell Signalling 2629 S, 4H8; 1:250); Rabbit anti-biotin (Bethyl Laboratories A150-109A; 1:500); Rabbit anti-GFP (Chromotek PABG1; 1:250); Rabbit anti-AND1 (Novus Biological NBPI-89091; 1:250); Mouse anti-GFP (Roche 11814460001; 1:250)) overnight at 4 °C. Following primary antibody incubation, cells were washed 3 \times in PLA wash buffer A and incubated in 30 μ l secondary antibody solution (6 μ l ‘+’, 6 μ l ‘–’, 18 μ l 3% FBS in PBS) for 100 minutes at 37 °C. Cells were washed again 3 \times in washing buffer A and re-suspended in 30 μ l Ligation Buffer, incubated for 60 minutes at 37 °C. Any interacting PLA probes were then amplified using a rolling circle assay. Washed cell pellets were re-suspended in PLA Amplification buffer for 100 minutes at 37 °C. Finally, cells were washed 2 \times in washing buffer B, re-suspended in 0.01 \times washing buffer B diluted in distilled H₂O. Diluted cell suspensions were added to 20 mm cover slips and centrifuged to adhere cells to cover slips (400 g, 5 min). Slides were mounted using DuoLink PLA DAPI mounting media. Cells were analysed using a Leica DM600 widefield microscope and analysed using CellProfiler. For analysis,

nuclei regions of interest were first segmented using the DAPI signal. Only PLA signal residing within the nuclei were quantified.

Statistical analyses

All statistical analyses, except from ChIP-Sequencing data, was carried out using RStudio (v 1.0.153). The imported data was first subject to normality testing through qqplots to determine the appropriate statistical testing method. All plots were created using ggplot2 and the plug-in ggpubr⁶². Two biological repeats for each γ -H2AX and H2AX ChIP-Seq in –IAA and +IAA were analysed, with repeats assessed for correlation before being combined. Student *t* test and Mann–Whitney *U* test were calculated using the software Prism (GraphPad). All statistical analyses were two-sided unless otherwise stated in the figure legend. All measurements were taken from distinct samples and no repeated measurements were taken.

X. Laevis methods

All the work carried out with *X. Laevis* egg extract was approved by the University of Birmingham Ethics Committee and by UK home office project license no: P081C27D8.

Inhibitors and recombinant proteins

EcoRI (R6011, Promega) was purchased at stock 12 U/ μ l and added to the extract at 0.05 U/ μ l, Aphidicolin (A0781, Sigma) was dissolved in DMSO at 8 mM and added to the extract along with demembrated sperm nuclei at 40 μ M. Caffeine (C8960, Sigma) was dissolved in water at 100 mM and added to the extract along with demembrated sperm nuclei at 5 mM. MLN4924 (A01139, Active Biochem) was dissolved in DMSO at 20 mM and added to the extract 15 minutes after addition of sperm nuclei at 10 μ M.

Recombinant His-tagged *X. Laevis* CyclinA1 NΔ56 (pET23a-*X. laevis* cyclinA1 NΔ56), was expressed and purified as previously described²¹. CyclinA1 NΔ56 was used at a final concentration of 826 nM in the egg extract to drive the extract into mitosis.

Antibodies

Mouse anti-PCNA (Sigma P8825; 1:2000); Rabbit anti-TRAIP (Novus Biologicals NBPI-87125; 1:500); Rabbit anti-P-Chk1 (S345) (Cell Signalling 2341; 1:1000); Rabbit anti-Ser139 γ -H2AX (Trevigen 4418-APC-020; 1:1000).

Affinity-purified anti-Cdc45, anti-Psf2⁶³, anti-Mcm7²¹, and anti-GINS antibody⁶⁴ were previously described. Affinity-purified anti-TRAIP is described in Supplementary Fig. 12.

Recombinant *X. Laevis* SUMO-TRAIP was purified as previously described²¹ and was also used for raising antibodies in rabbits. The resulting antibody sera was purified in-house against the purified antigen. The specificity of this new antibody is presented in Supplementary Fig. 12A.

X. Laevis egg extract preparation

Metaphase II arrested egg extracts were prepared as previously described⁶⁵ from unfertilised female frog oocytes. In order to increase the amount of stage 6 (mature) oocytes, 10 frogs were primed with 150 units follicle stimulating hormone Foligon (Intervet) 2–7 days before eggs were required. Frogs were injected with 400–600 units of serum gonadotropin Chorulon (Intervet), and subsequently transferred to laying tanks containing 2.5 l of 1 \times MMR (0.1M NaCl, 2 mM KCl, 1 mM MgCl₂, 2 mM CaCl₂, 0.1 mM EDTA, 5 mM HEPES, pH to 7.8 with NaOH). Frogs were kept in the tanks laying eggs overnight at ≤ 23 °C. Eggs from different frogs were collected the next morning in a 1 l glass beaker.

Good quality eggs were rinsed with 1 \times MMR and de-jellied by rinsing them in cysteine solution (2.2% cysteine, 5 mM EGTA, pH to 7.6 with KOH). De-jellied eggs were rinsed again with 1 \times MMR, and then washed in UEB buffer (50 mM KCl, 50 mM HEPES, 5 mM MgCl₂, 5 mM EGTA, 2 mM DTT, pH to 7.6 with KOH) and white/swollen apoptotic

eggs floating on the top were removed. The de-jellied eggs were packed into 14 ml round bottom polypropylene tubes (187261; Greiner) with 1 ml UEB containing 10 µg/ml protease inhibitors: aprotinin, leupeptin, and pepstatin and 50 µg/ml Cytochalasin D (C8273-5MG, Sigma). The tubes were then spun to pack the eggs in a Beckman JS13 rotor at 800 × g for 1 minute, room temperature (RT). The white apoptotic swollen eggs that float to the top were removed followed by another centrifugation at high speed at 10,000 × g for 10 min at RT. This results in separating the eggs into a lipid layer at the top, brown cytoplasmic fraction in the middle, and an insoluble egg yolk pellet at the bottom. The cytoplasmic layer was collected using a 20 G needle and a 1 ml syringe via side puncture. Extract was supplemented with 10 µg/ml protease inhibitors, 10 µg/ml Cytochalasin D, and 15% of LFB1/50 (10% sucrose, 50 mM KCl, 40 mM HEPES pH 8, 20 mM K phosphate pH 8, 2 mM MgCl₂, 1 mM EGTA, 2 mM DTT, 1 µg/ml of each: aprotinin, leupeptin and pepstatin). The extract transferred to SW55 ultracentrifuge tubes (344058, Beckmann) which were then subjected to a final clarifying spin at 30,000 × g for 20 min at 4 °C. After the spinning, the yellow lipid plug from the top was removed, and the pale yellow cytoplasmic fraction collected. The collected extract was then supplemented with 1% v-v of glycerol, and frozen in liquid nitrogen in small beads and stored at −80 °C.

DNA synthesis assay

Interphase *X. laevis* egg extract was supplemented with 10 ng/µl of demembrated *Xenopus* sperm nuclei and incubated at 23 °C for indicated times. Synthesis of nascent DNA was then measured by quantification of radiolabelled α³²P-dATP (NEG512H250UC, Perkin Elmer) incorporation into newly synthesised DNA, as described before⁶⁵.

Chromatin isolation time-course

Interphase *X. laevis* egg extract was supplemented with 10 ng/µl of demembrated sperm DNA and subjected to indicated treatments. The reaction was incubated at 23 °C for indicated length of time when chromatin was isolated in ANIB100 buffer (50 mM HEPES pH 7.6, 100 mM KOAc, 10 mM MgOAc, 2.5 mM Mg-ATP, 0.5 mM spermidine, 0.3 mM spermine, 1 µg/ml of each aprotinin, leupeptin and pepstatin, 25 mM β-glycerophosphate, 0.2 µM microcystin-LR and 10 mM 2-chloroacetamide (Merck) as described previously⁶⁵. To study mitosis, the interphase extract was supplemented with MLN4924 and allowed replication to complete. Once completed extract was treated with CyclinA1 NΔ56.

During the chromatin isolation procedure, a sample without addition of sperm DNA (no DNA) is processed in an analogous way, usually at the end of the time course, to serve as a chromatin specificity control. The bottom of the PAGE gel on which the chromatin samples were resolved was cut off and stained with Colloidal Coomassie (SimplyBlue, Life Technologies) to stain histones which provide loading controls and indications of sample contamination with egg extract (cytoplasm).

Nuclei isolation for Chk1 phosphorylation

The nuclei isolation was performed as previously described⁶⁶.

Immunodepletion

TRAIP immunodepletions were performed using Dynabeads Protein A (10002D, Life Technologies) coupled to *Xenopus* TRAIP antibodies raised in rabbits and affinity purified or non-specific rabbit IgG (I5006, Sigma). The TRAIP antibodies were coupled at 600 µg per 1 ml of beads. Effective immunodepletion required 2 rounds of 1 h incubation of egg extract with antibody-coupled beads at 50% beads ratio (e.g., 2 rounds of 100 µl of egg extract incubated with 50 µl of coupled beads).

Reporting summary

Further information on research design is available in the Nature Portfolio Reporting Summary linked to this article.

Data availability

The sequencing data discussed in this publication have been deposited in NCBI's Gene Expression Omnibus and are accessible through GEO Series accession number [GSE201158](https://www.ncbi.nlm.nih.gov/geo/query/acc.cgi?acc=GSE201158). Source data are provided in this paper.

References

- Labib, K. & De Piccoli, G. Surviving chromosome replication: the many roles of the S-phase checkpoint pathway. *Philos. Trans. R. Soc. Lond. B Biol. Sci.* **366**, 3554–3561 (2011).
- Chan, K. L., Palmai-Pallag, T., Ying, S. & Hickson, I. D. Replication stress induces sister-chromatid bridging at fragile site loci in mitosis. *Nat. Cell Biol.* **11**, 753–760 (2009).
- Macheret, M. et al. High-resolution mapping of mitotic DNA synthesis regions and common fragile sites in the human genome through direct sequencing. *Cell Res.* **30**, 997–1008 (2020).
- Park, E. S. et al. Early embryonic lethality caused by targeted disruption of the TRAF-interacting protein (TRIP) gene. *Biochem. Biophys. Res. Commun.* **363**, 971–977 (2007).
- Hart, T. et al. High-resolution CRISPR screens reveal fitness genes and genotype-specific cancer liabilities. *Cell* **163**, 1515–1526 (2015).
- Harley, M. E. et al. TRAIP promotes DNA damage response during genome replication and is mutated in primordial dwarfism. *Nat. Genet.* **48**, 36–43 (2016).
- Hoffmann, S. et al. TRAIP is a PCNA-binding ubiquitin ligase that protects genome stability after replication stress. *J. Cell Biol.* **212**, 63–75 (2016).
- Feng, W. et al. TRAIP regulates replication fork recovery and progression via PCNA. *Cell Discov.* **2**, 16016 (2016).
- Wallace, H. A. et al. TRIP/NOPO E3 ubiquitin ligase promotes ubiquitination of DNA polymerase ε. *Development* **141**, 1332–1341 (2014).
- Chapard, C. et al. TRAIP is a regulator of the spindle assembly checkpoint. *J. Cell Sci.* **127**, 5149–5156 (2014).
- Park, I. S., Jo, K. S., Won, H. S. & Kim, H. Dimerization of TRAF-interacting protein (TRAIP) regulates the mitotic progression. *Biochem. Biophys. Res. Commun.* **463**, 864–869 (2015).
- Chen, Y. et al. Nucleolar residence of the seckel syndrome protein TRAIP is coupled to ribosomal DNA transcription. *Nucleic Acids Res.* **46**, 10119–10131 (2018).
- Wu, R. A. et al. TRAIP is a master regulator of DNA interstrand crosslink repair. *Nature* **567**, 267–272 (2019).
- Chapard, C., Hohl, D. & Huber, M. The TRAF-interacting protein (TRAIP) is a novel E2F target with peak expression in mitosis. *Oncotarget* **6**, 20933–20945 (2015).
- Wessel, S. R., Mohni, K. N., Luzwick, J. W., Dungrawala, H. & Cortez, D. Functional analysis of the replication fork proteome identifies BET proteins as PCNA regulators. *Cell Rep.* **28**, 3497–3509 e3494 (2019).
- Fullbright, G., Rycenga, H. B., Gruber, J. D. & Long, D. T. p97 promotes a conserved mechanism of helicase unloading during DNA cross-link repair. *Mol. Cell Biol.* **36**, 2983–2994 (2016).
- Long, D. T., Joukov, V., Budzowska, M. & Walter, J. C. BRCA1 promotes unloading of the CMG helicase from a stalled DNA replication fork. *Mol. Cell* **56**, 174–185 (2014).
- Larsen, N. B. et al. Replication-coupled DNA-protein crosslink repair by SPRTN and the proteasome in xenopus egg extracts. *Mol. Cell* **73**, 574–588.e577 (2019).
- Soo Lee, N. et al. TRAIP/RNF206 is required for recruitment of RAP80 to sites of DNA damage. *Nat. Commun.* **7**, 10463 (2016).

20. Boudny, M. & Trbusek, M. ATR-CHK1 pathway as a therapeutic target for acute and chronic leukemias. *Cancer Treat. Rev.* **88**, 102026 (2020).
21. Priego Moreno, S., Jones, R. M., Poovathumkadavil, D., Scaramuzza, S. & Gambus, A. Mitotic replisome disassembly depends on TRAP1 ubiquitin ligase activity. *Life Sci. Alliance* **2**, e201900390 (2019).
22. Sonnevile, R. et al. TRAP1 drives replisome disassembly and mitotic DNA repair synthesis at sites of incomplete DNA replication. *Elife* **8**, e48686 (2019).
23. Deng, L. et al. Mitotic CDK promotes replisome disassembly, fork breakage, and complex DNA rearrangements. *Mol. Cell* **73**, 915–929.e916 (2019).
24. Villa, F. et al. CUL2(LRR1), TRAP1 and p97 control CMG helicase disassembly in the mammalian cell cycle. *EMBO Rep.* **22**, e52164 (2021).
25. Yuan, Y. F., Ren, Y. X., Yuan, P., Yan, L. Y. & Qiao, J. TRAP1 is involved in chromosome alignment and SAC regulation in mouse oocyte meiosis. *Sci. Rep.* **6**, 29735 (2016).
26. Natsume, T., Kiyomitsu, T., Saga, Y. & Kanemaki, M. T. Rapid protein depletion in human cells by auxin-inducible degron tagging with short homology donors. *Cell Rep.* **15**, 210–218 (2016).
27. Yesbolatova, A., Natsume, T., Hayashi, K. I. & Kanemaki, M. T. Generation of conditional auxin-inducible degron (AID) cells and tight control of degron-fused proteins using the degradation inhibitor auxinole. *Methods* **164–165**, 73–80 (2019).
28. Gire, V. & Dulic, V. Senescence from G2 arrest, revisited. *Cell Cycle* **14**, 297–304 (2015).
29. Saldivar, J. C. et al. An intrinsic S/G2 checkpoint enforced by ATR. *Science* **361**, 806–810 (2018).
30. Zhao, P. A., Sasaki, T. & Gilbert, D. M. High-resolution Repli-Seq defines the temporal choreography of initiation, elongation and termination of replication in mammalian cells. *Genome Biol.* **21**, 76 (2020).
31. Koyanagi, E. et al. Global landscape of replicative DNA polymerase usage in the human genome. *bioRxiv*, <https://doi.org/10.1101/2021.11.14.468503> (2021).
32. Fungtammasan, A., Walsh, E., Chiaromonte, F., Eckert, K. A. & Makova, K. D. A genome-wide analysis of common fragile sites: what features determine chromosomal instability in the human genome? *Genome Res.* **22**, 993–1005 (2012).
33. Andrysik, Z., Bender, H., Galbraith, M. D. & Espinosa, J. M. Multi-omics analysis reveals contextual tumor suppressive and oncogenic gene modules within the acute hypoxic response. *Nat. Commun.* **12**, 1375 (2021).
34. Erickson, B., Sheridan, R. M., Cortazar, M. & Bentley, D. L. Dynamic turnover of paused Pol II complexes at human promoters. *Genes Dev.* **32**, 1215–1225 (2018).
35. Kotsantis, P. et al. Increased global transcription activity as a mechanism of replication stress in cancer. *Nat. Commun.* **7**, 13087 (2016).
36. Saponaro, M. et al. RECQL5 controls transcript elongation and suppresses genome instability associated with transcription stress. *Cell* **157**, 1037–1049 (2014).
37. Skourti-Stathaki, K. & Proudfoot, N. J. A double-edged sword: R loops as threats to genome integrity and powerful regulators of gene expression. *Genes Dev.* **28**, 1384–1396 (2014).
38. St Germain, C. P. et al. Genomic patterns of transcription-replication interactions in mouse primary B cells. *Nucleic Acids Res.* **50**, 2051–2073 (2022).
39. Tan-Wong, S. M., Dhir, S. & Proudfoot, N. J. R-loops promote anti-sense transcription across the mammalian genome. *Mol. Cell* **76**, 600–616.e606 (2019).
40. Noe Gonzalez, M., Blears, D. & Svejstrup, J. Q. Causes and consequences of RNA polymerase II stalling during transcript elongation. *Nat. Rev. Mol. Cell Biol.* **22**, 3–21 (2021).
41. Verma, R., Oania, R., Fang, R., Smith, G. T. & Deshaies, R. J. Cdc48/p97 mediates UV-dependent turnover of RNA Pol II. *Mol. Cell* **41**, 82–92 (2011).
42. Vaz, B., Halder, S. & Ramadan, K. Role of p97/VCP (Cdc48) in genome stability. *Front. Genet.* **4**, 60 (2013).
43. Franz, A. et al. Chromatin-associated degradation is defined by UBXN-3/FAF1 to safeguard DNA replication fork progression. *Nat. Commun.* **7**, 10612 (2016).
44. Jones, R. M. et al. Characterising replisome disassembly in human cells. *bioRxiv*, <https://doi.org/10.1101/2022.07.12.499744> (2022).
45. Ruggiano, A. et al. The protease SPRTN and SUMOylation coordinate DNA-protein crosslink repair to prevent genome instability. *Cell Rep.* **37**, 110080 (2021).
46. Tarcan, Z., Poovathumkadavil, D., Skagia, A. & Gambus, A. The p97 segregase cofactor Ubxn7 facilitates replisome disassembly during S-phase. *J. Biol. Chem.* **298**, 102234 (2022).
47. Kochenova, O. V., Mukkavalli, S., Raman, M. & Walter, J. C. Cooperative assembly of p97 complexes involved in replication termination. *Nat. Commun.* **13**, 6591 (2022).
48. Noireterre, A., Bagdiul, I., Serbyn, N. & Stutz, F. Ubx5-Cdc48 assists the protease Wss1 at DNA-protein crosslink sites in yeast. *bioRxiv*, <https://doi.org/10.1101/2022.05.30.493988> (2022).
49. Klingseisen, A. & Jackson, A. P. Mechanisms and pathways of growth failure in primordial dwarfism. *Genes Dev.* **25**, 2011–2024 (2011).
50. Childs, B. G., Baker, D. J., Kirkland, J. L., Campisi, J. & van Deursen, J. M. Senescence and apoptosis: dueling or complementary cell fates? *EMBO Rep.* **15**, 1139–1153 (2014).
51. Vousden, K. H. & Lane, D. P. p53 in health and disease. *Nat. Rev. Mol. Cell Biol.* **8**, 275–283 (2007).
52. Mao, Z., Ke, Z., Gorbunova, V. & Seluanov, A. Replicatively senescent cells are arrested in G1 and G2 phases. *Aging* **4**, 431–435 (2012).
53. Glover, T. W., Wilson, T. E. & Arlt, M. F. Fragile sites in cancer: more than meets the eye. *Nat. Rev. Cancer* **17**, 489–501 (2017).
54. Taylor, A. M. R. et al. Chromosome instability syndromes. *Nat. Rev. Dis. Prim.* **5**, 64 (2019).
55. Macheret, M. & Halazonetis, T. D. Intragenic origins due to short G1 phases underlie oncogene-induced DNA replication stress. *Nature* **555**, 112–116 (2018).
56. Wang, J. et al. Persistence of RNA transcription during DNA replication delays duplication of transcription start sites until G2/M. *Cell Rep.* **34**, 108759 (2021).
57. Duxin, J. P., Dewar, J. M., Yardimci, H. & Walter, J. C. Repair of a DNA-protein crosslink by replication-coupled proteolysis. *Cell* **159**, 346–357 (2014).
58. Cong, L. et al. Multiplex genome engineering using CRISPR/Cas systems. *Science* **339**, 819–823 (2013).
59. Lappin, K. M. et al. Cancer-associated SF3B1 mutations confer a BRCA-like cellular phenotype and synthetic lethality to PARP inhibitors. *Cancer Res.* **82**, 819–830 (2022).
60. Afgan, E. et al. The Galaxy platform for accessible, reproducible and collaborative biomedical analyses: 2018 update. *Nucleic Acids Res.* **46**, W537–W544 (2018).
61. Lerdrup, M., Johansen, J. V., Agrawal-Singh, S. & Hansen, K. An interactive environment for agile analysis and visualization of ChIP-seq data. *Nat. Struct. Mol. Biol.* **23**, 349–357 (2016).
62. Wickham, H. & Sievert, C. ggplot2: elegant graphics for data analysis. 2nd edn (Springer, 2016).
63. Gambus, A., Khoudoli, G. A., Jones, R. C. & Blow, J. J. MCM2-7 form double hexamers at licensed origins in *Xenopus* egg extract. *J. Biol. Chem.* **286**, 11855–11864 (2011).
64. Tarcan, Z., Poovathumkadavil, D., Skagia, A. & Gambus, A. The p97 cofactor Ubxn7 facilitates replisome disassembly during S-phase. *bioRxiv* <https://doi.org/10.1101/2021.12.16.472925> (2021).

65. Gillespie, P. J., Gambus, A. & Blow, J. J. Preparation and use of *Xenopus* egg extracts to study DNA replication and chromatin associated proteins. *Methods* **57**, 203–213 (2012).
66. Moreno, S. P., Bailey, R., Campion, N., Herron, S. & Gambus, A. Polyubiquitylation drives replisome disassembly at the termination of DNA replication. *Science* **346**, 477–481 (2014).

Acknowledgements

This work was supported by the BBSRC-funded MIBTP studentship, JSPS Summer programme, and BBSRC funded MIBTP Career Development Fellowship for S.S. Wellcome Trust Investigator Award (215510/Z/19/Z) funded R.J. and A.G., while BBSRC BB/T001860/1 funded A.R.-W. The University of Birmingham, BBSRC (BB/S016155/1) and Cancer Research UK (C17422/A25154) to M.S.

Author contributions

S.S., R.J., M.M.S., D.P., A.F., A.R.-W., and C.F.C. acquired and analysed the data within the manuscript. P.R. and M.S. analysed the ChIP-seq data. T.N. and M.T.K. assisted with the generation of TRAIP-mAID and TRAIP-mAC HCT116 and RPE cell lines. M.S. and A.G. designed the study and wrote the manuscript.

Competing interests

The authors declare no competing interests.

Additional information

Supplementary information The online version contains supplementary material available at <https://doi.org/10.1038/s41467-023-40695-y>.

Correspondence and requests for materials should be addressed to Agnieszka Gambus.

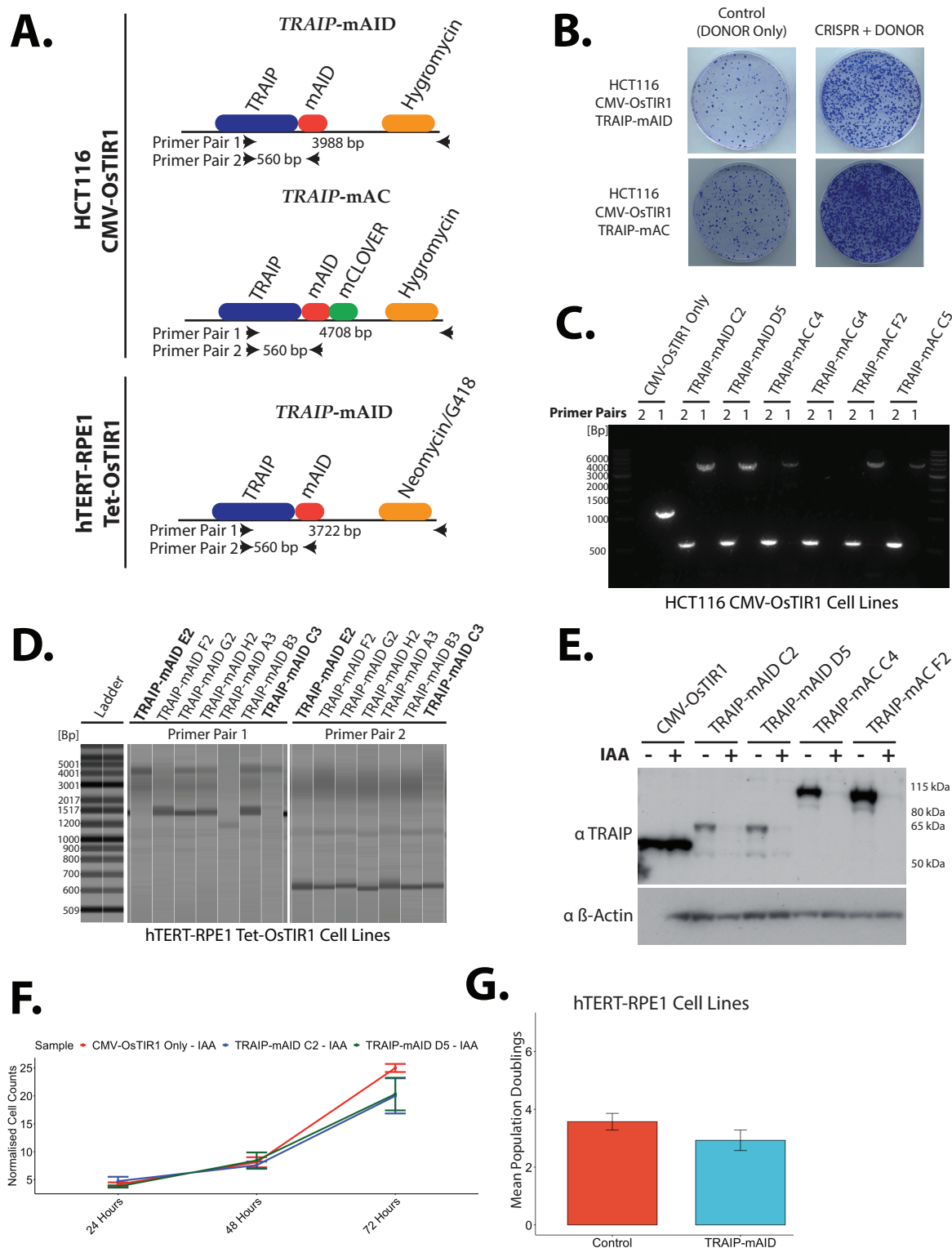
Peer review information *Nature Communications* thanks George-Lucian Moldovan and the other, anonymous, reviewer(s) for their contribution to the peer review of this work. A peer review file is available.

Reprints and permissions information is available at <http://www.nature.com/reprints>

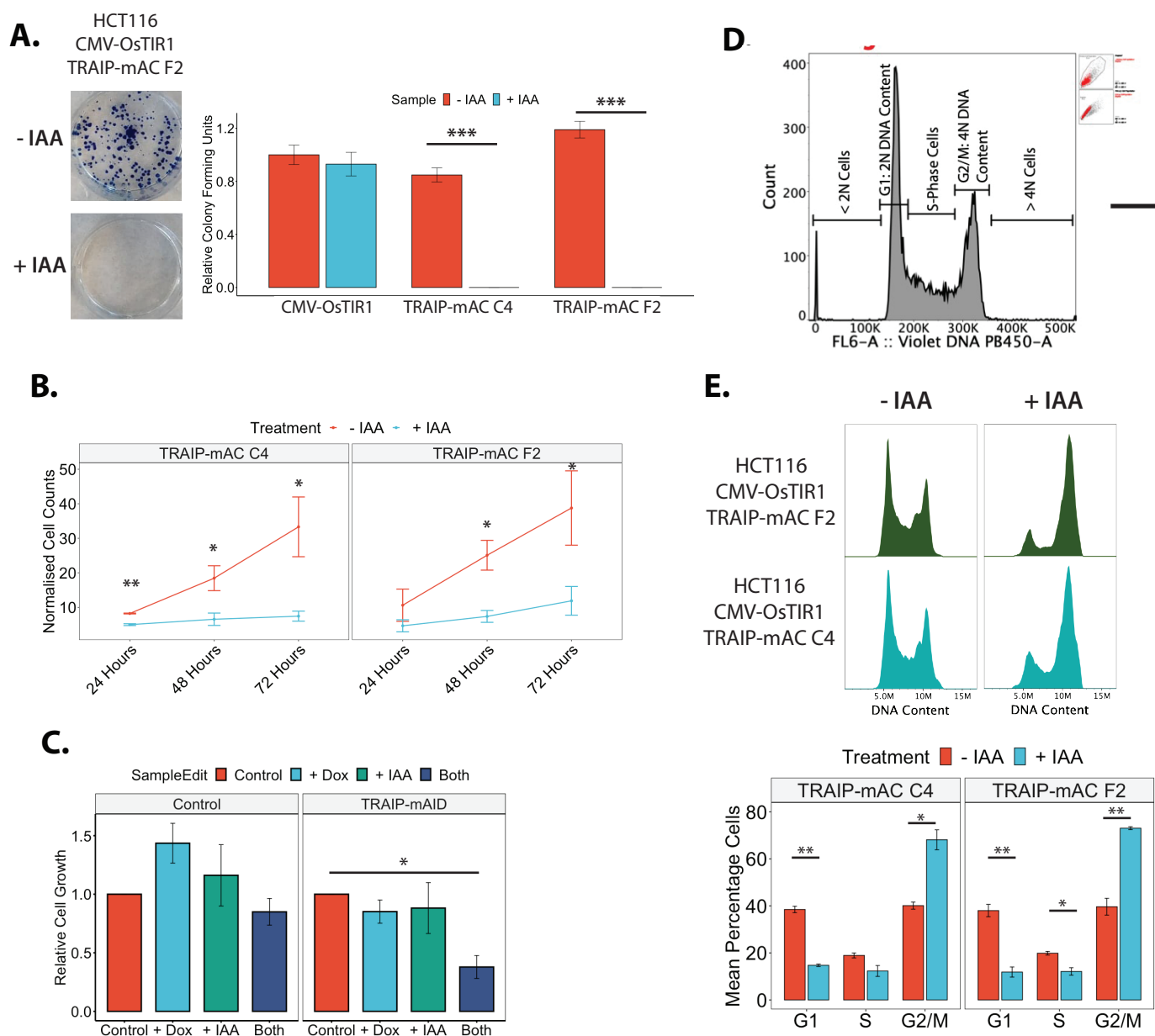
Publisher's note Springer Nature remains neutral with regard to jurisdictional claims in published maps and institutional affiliations.

Open Access This article is licensed under a Creative Commons Attribution 4.0 International License, which permits use, sharing, adaptation, distribution and reproduction in any medium or format, as long as you give appropriate credit to the original author(s) and the source, provide a link to the Creative Commons licence, and indicate if changes were made. The images or other third party material in this article are included in the article's Creative Commons licence, unless indicated otherwise in a credit line to the material. If material is not included in the article's Creative Commons licence and your intended use is not permitted by statutory regulation or exceeds the permitted use, you will need to obtain permission directly from the copyright holder. To view a copy of this licence, visit <http://creativecommons.org/licenses/by/4.0/>.

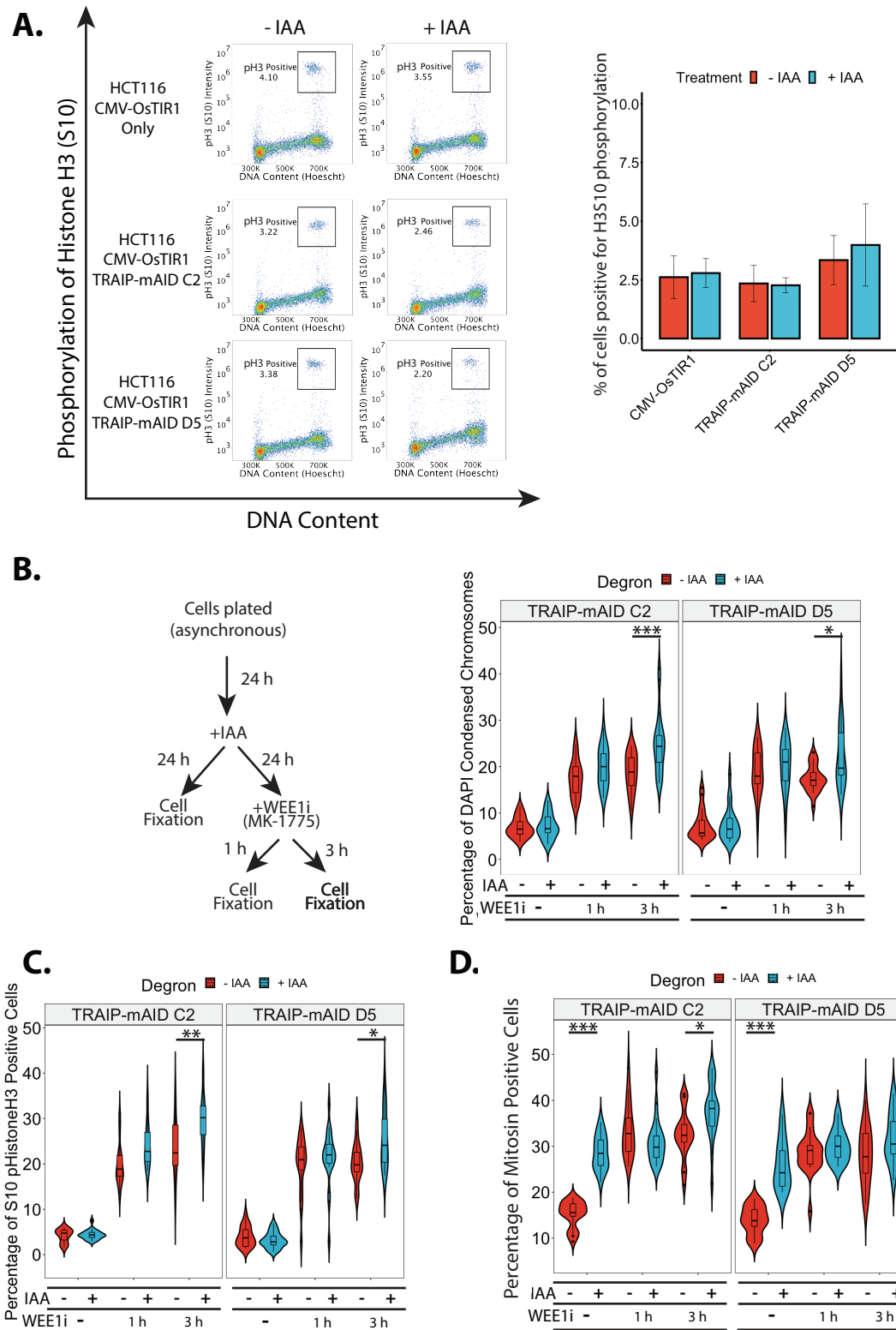
© The Author(s) 2023



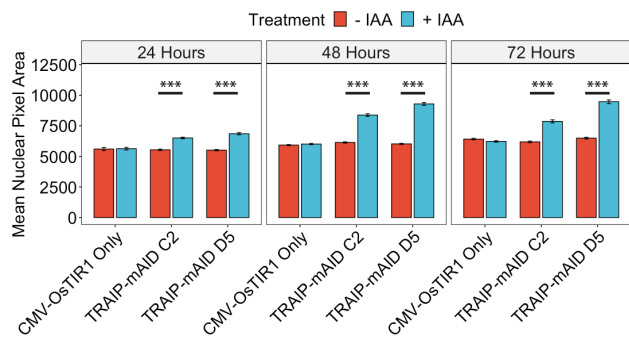
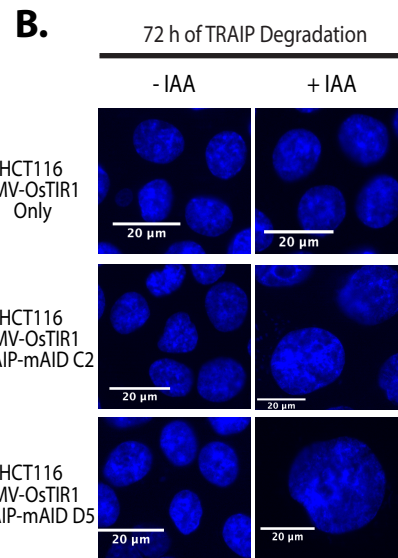
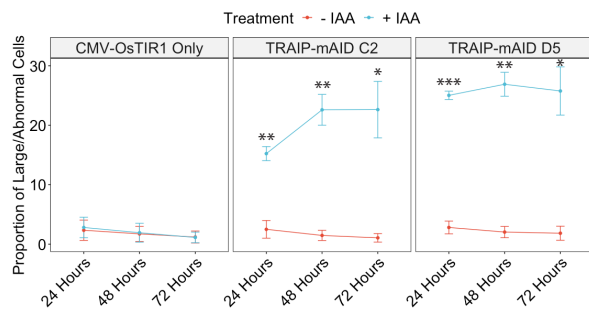
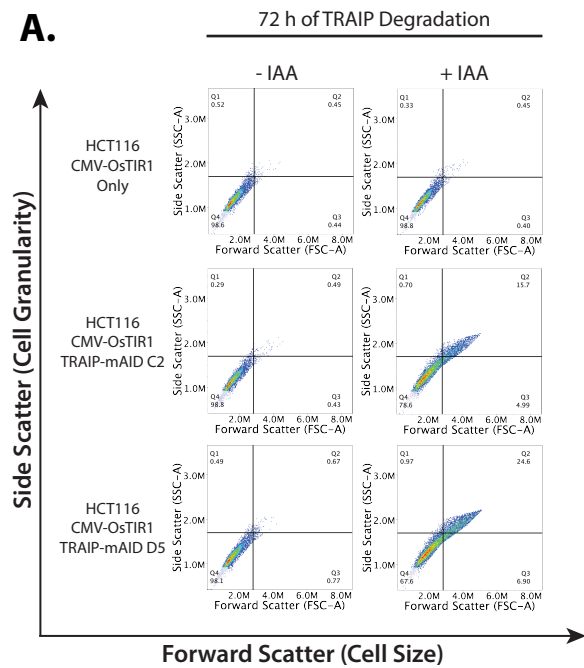
Supplementary Figure 1. Creation and validation of TRAIP degrons in HCT116 and RPE1 cells. (A) Design of TRAIP tagged with auxin inducible degron (mAID) or mClover tagged degron (mAC). Primer pairs used for verification of correct genomic incorporation is presented below the diagrams. **(B)** Examples of cell colonies obtained after guide RNAs transfection stained with crystal violet. **(C)** Validation of biallelic tagging of TRAIP in different HCT116 clones using primer pairs indicated in (A) (n=2) **(D)** Validation of biallelic tagging of TRAIP in different RPE1 clones using primer pairs indicated in (A). **(E)** Validation of biallelic tagging and tagged TRAIP degradation in HCT116 cells by western blotting with TRAIP antibodies (n=3) **(F)** Growth curves of control (CMV-OsTIR1) and two clones of HCT116 TRAIP-mAID cells (n = 3). Hypothesis testing was carried out using one-way ANOVA for each individual timepoint (24 h: Df=2, F=0.892, p=0.458. 48 h: Df=2, F=0.18, p=0.839. 72 h: Df=2, F=1.236, p=0.355). **(G)** Mean number of population doublings over 72 h growth in hTERT-RPE1 TRAIP-mAID cells or hTERT-RPE1 Tet-OsTIR1 parental cell lines. n = 2. Source data are provided as a Source Data file.



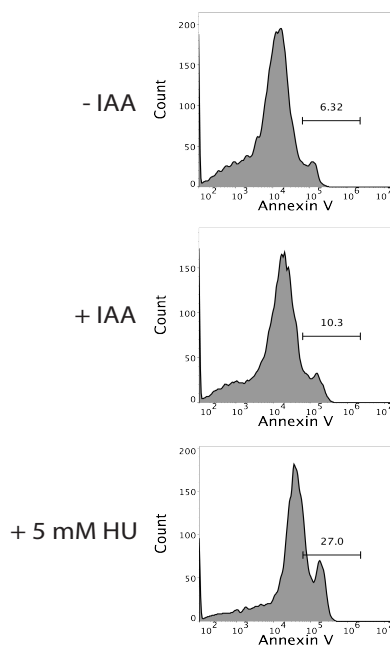
Supplementary Figure 2. Phenotypes of inhibited proliferation and cell cycle arrest upon TRAIP degradation are reproduced in HCT116 TRAIP-mAC and RPE1 cell lines. (A) Example of colony assay after auxin treatment. Cells were fixed and stained with methylene blue (left). Quantification of colony forming assay in two independent TRAIP-mAC clones n=3 (right). Statistical analyses was carried out using T-tests. Significant differences were identified between TRAIP-mAC C4 ($p=0.000161$) and TRAIP-mAID F2 ($p=0.000159$). **(B)** Growth curves of TRAIP-mAC cells upon 24, 48 and 72 h of auxin treatment. Cells were counted at every timepoint and normalised to the seeding densities n=3. Statistical significance was calculated using T-tests for TRAIP-mAC C4 (24 hours: $p=0.002158$; 48 hours: $p=0.03$; 72 hours: $p=0.04613$) and TRAIP-mAC F2 (48 hours: $p=0.0399$; 72 hours: $p=0.03326$). **(C)** hTERT-RPE1 control (Tet-osTIR1) and TRAIP-mAID cells were optionally treated for 72 h with doxycycline and/or auxin as indicated. Statistical analyses - T-tests $p = 0.02392$. Significant differences were detected in hTERT-RPE1 TRAIP-mAID untreated control vs Both treatments only. **(D)** Example of FACS gating strategy used for cell cycle analysis. Total DNA content, with gates applied to identify potential apoptotic cells (< 2N DNA content), G1 cells (2N DNA Content), G2/M Cells (4N DNA content), S-phase, and any cells with re-replication (> 4N DNA content). The small boxes to the top right depict the gating strategy used for isolating primary cell populations and removing doublets **(E)** TRAIPmAC clones arrest at G2/M stage of the cell cycle. Examples of FACS cell cycle profiles of two TRAIP-mAC clones upon 24 h of optional auxin treatment (above). Quantification of cell cycle stages in TRAIP-mAC clones after 24 h auxin treatment n=3 (below). Statistical analysis (t-tests) - G1: TRAIP-mAID C4 ($p=0.00122$), and TRAIP-mAID F2 ($p=0.00175$); G2/M - TRAIP-mAC C4 ($p=0.0153$), TRAIP-mAC F2 ($p=0.00978$). Source data are provided as a Source Data file.



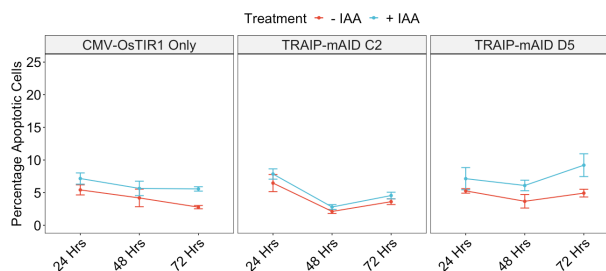
Supplementary Figure 3. TRAIP depleted cells accumulate in G2 stage of the cell cycle. (A) HCT116 degron cell lines were treated with auxin for 24 h and stained for S10 phosphorylation on histone H3 (pH3). Example FACS plots with pH3 staining against DNA content. Mitotic cells are selected in the black box (left). Quantification of the percentage of cells in mitosis (pH3 positive) upon 24 h of TRAIP degradation n=3 (right). Statistical analysis revealed no differences in the data. **(B)** Schematic of the experiment (left) and quantification of the percentage of cells found to be in mitosis after 24 h of auxin treatment by quantification of cells with condensed chromosomes after DAPI staining and fluorescent microscopy (mitotic index) (right). Significance (ANOVA and pairwise testing) is summarised on the plot: TRAIP-mAID C2 ($p < 0.001$) and TRAIP-mAID D5 ($p = 0.0162$). **(C)** Quantification of H3S10 phosphorylation by fluorescent microscopy in TRAIP degron cell upon 24 h of auxin treatment and optional treatment with WEE1 inhibitor MK-1775. Significance (ANOVA and pairwise testing) is summarised on the plot: TRAIP-mAID C2: $p = 0.00260$; TRAIP-mAID D5: $p = 0.0170$. **(D)** Quantification of mitosis positive cells upon treatment as in (C). Significance (ANOVA and pairwise comparison) is summarised on the plot: TRAIP-mAID C2 Untreated ($p < 0.001$), TRAIP-mAID C2 + Wee1i 3 hours ($p = 0.0294$), and TRAIP-mAID D5 untreated ($p < 0.001$). Source data are provided as a Source Data file.



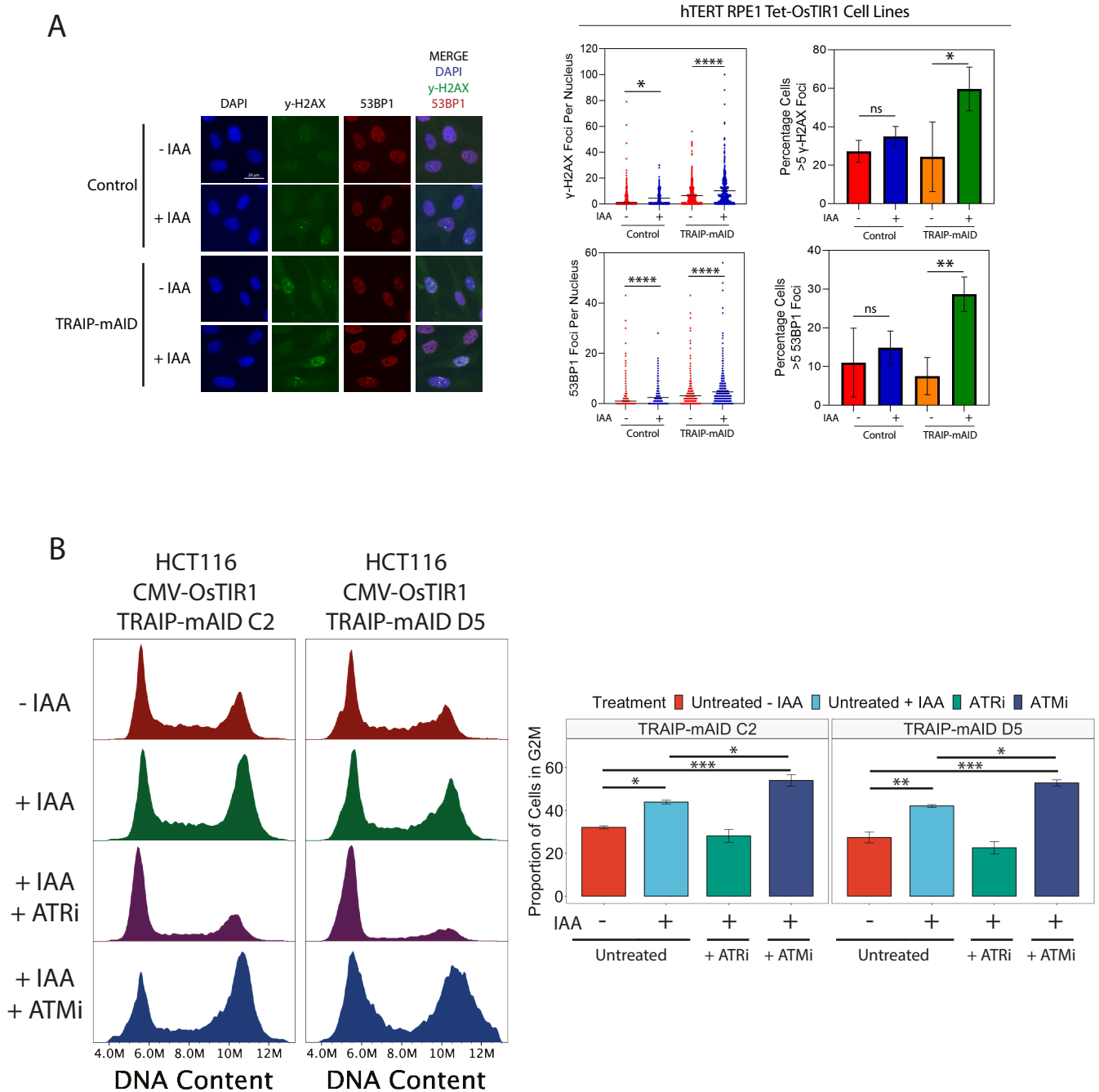
C. HCT116 CMV-OsTIR1 TRAIP-mAID C2
24 h of IAA treatment



D.



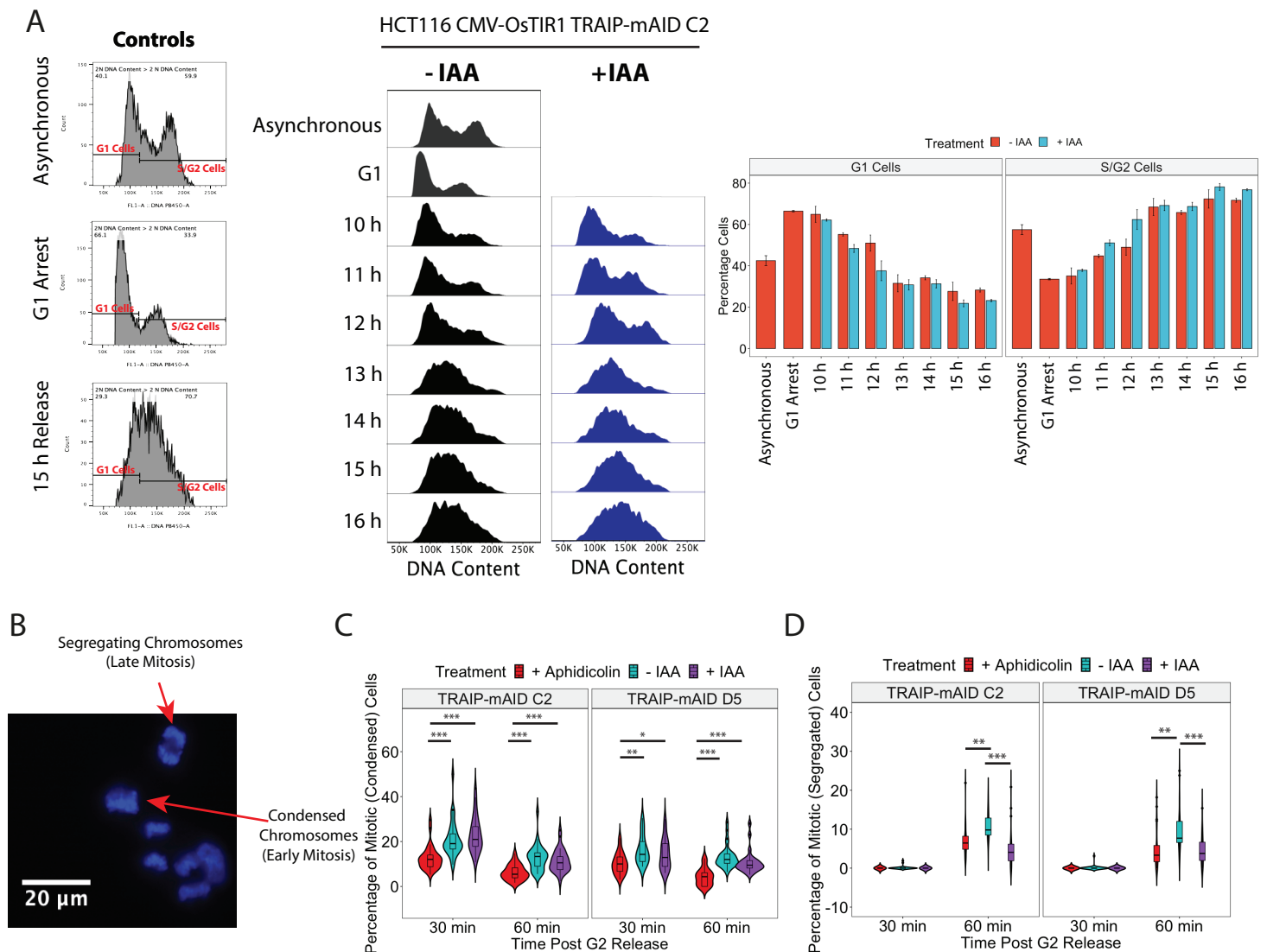
Supplementary Figure 4. Analysis of consequences of TRAIP depletion. (A) The size of TRAIP degron cells was analysed by flow cytometry after auxin addition. The example FACS plots after 72 h of IAA treatment (top) and quantification over 24, 46 and 72h TRAIP degradation n=3 (bottom) is presented. (B) The size of nuclei was analysed by DAPI staining and fluorescence microscopy. Example pictures after 72 h of IAA treatment (top) and quantification over 24, 46 and 72h TRAIP degradation n=3 (bottom) is presented. (C) Annexin V staining assay validation. TRAIP-mAID cell lines were treated optionally with auxin for 24 h or HU for 24 h. Annexin V positive cells were detected by FACS. Example FACS profiles presented. (D) Quantification of percentage of TRAIP degron cells positive for Annexin V after 24, 48 or 72 h of auxin treatment. Source data are provided as a Source Data file.



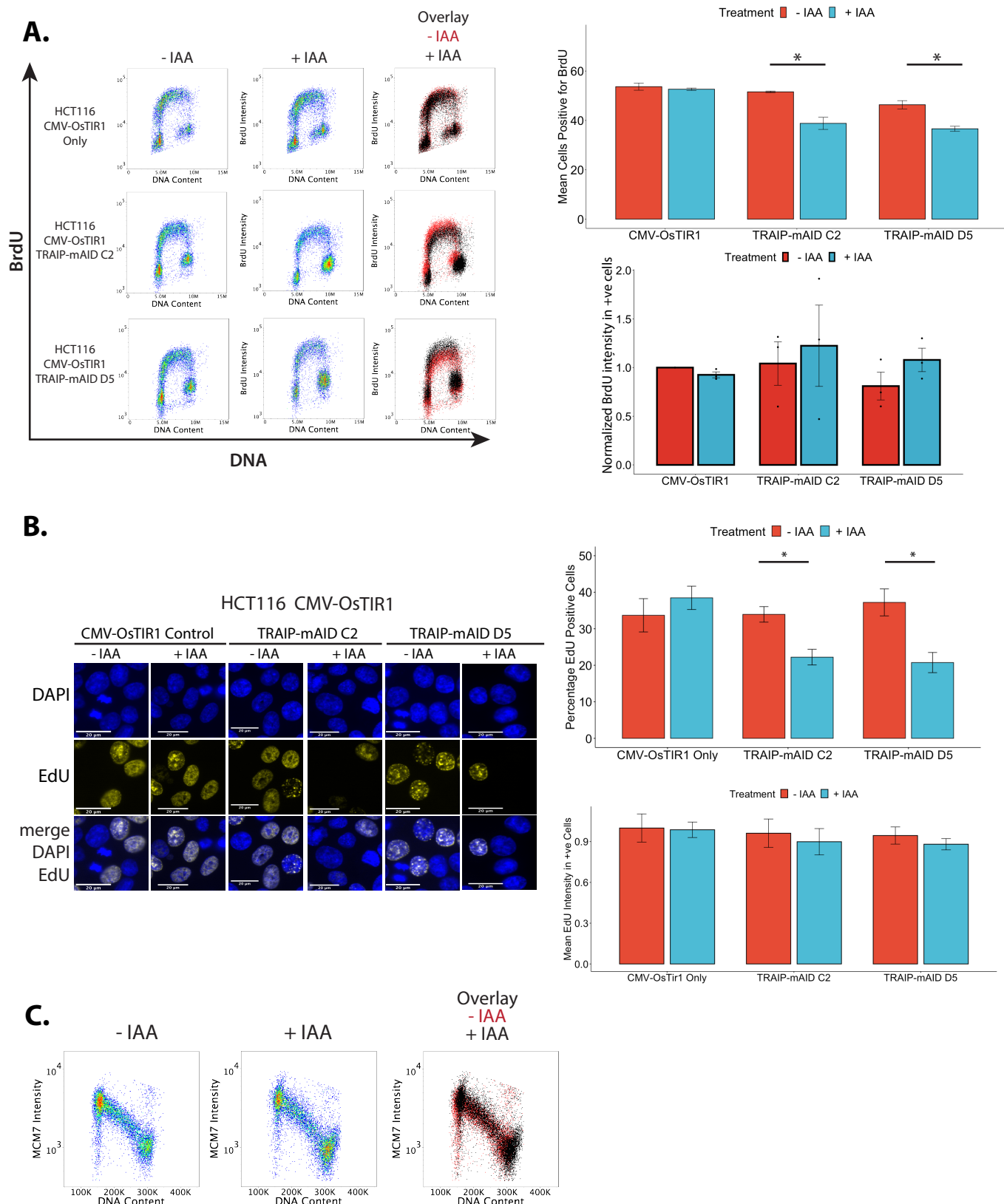
Supplementary Figure 5. (A) Accumulation of DNA damage in RPE1 TRAIP-mAID cells upon auxin treatment. Example photos (left), total number of foci detected per nucleus over $n=3$ (middle). Mann-Whitney test performed. γ -H2AX foci/nucleus control -IAA vs +IAA; $p=0.0154$, TRAIP-mAID -IAA vs +IAA; $p<0.0001$. 53BP1 foci/nucleus control -IAA vs +IAA; <0.0001 , TRAIP-mAID -IAA vs +IAA; <0.0001 . T.test performed for cells with >5 γ -H2AX foci TRAIP-mAID -IAA vs +IAA; $p=0.018$. >5 γ -H2AX foci TRAIP-mAID -IAA vs +IAA; $p=0.006$.

(B) G2 arrest in TRAIP depleted cells is dependent on functioning ATR checkpoint pathway. TRAIP degran clones were treated for 24 h with auxin and optionally with ATRi or ATMi. Cell cycle profile of cells was analysed by FACS. Example of FACS plots (left) and quantification of cells in G2/M stage of the cell cycle $n=3$ (right).

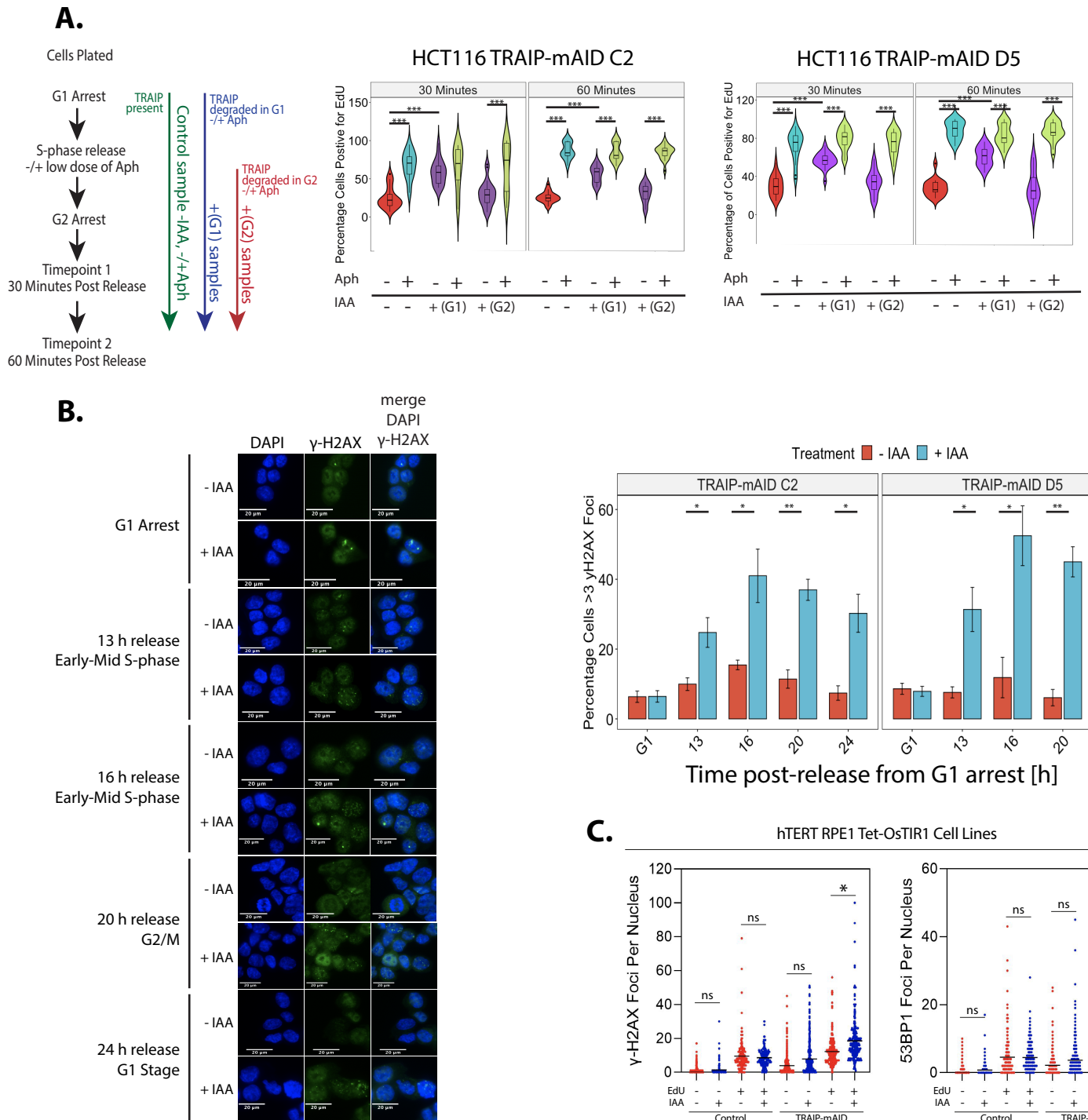
Source data are provided as a Source Data file.



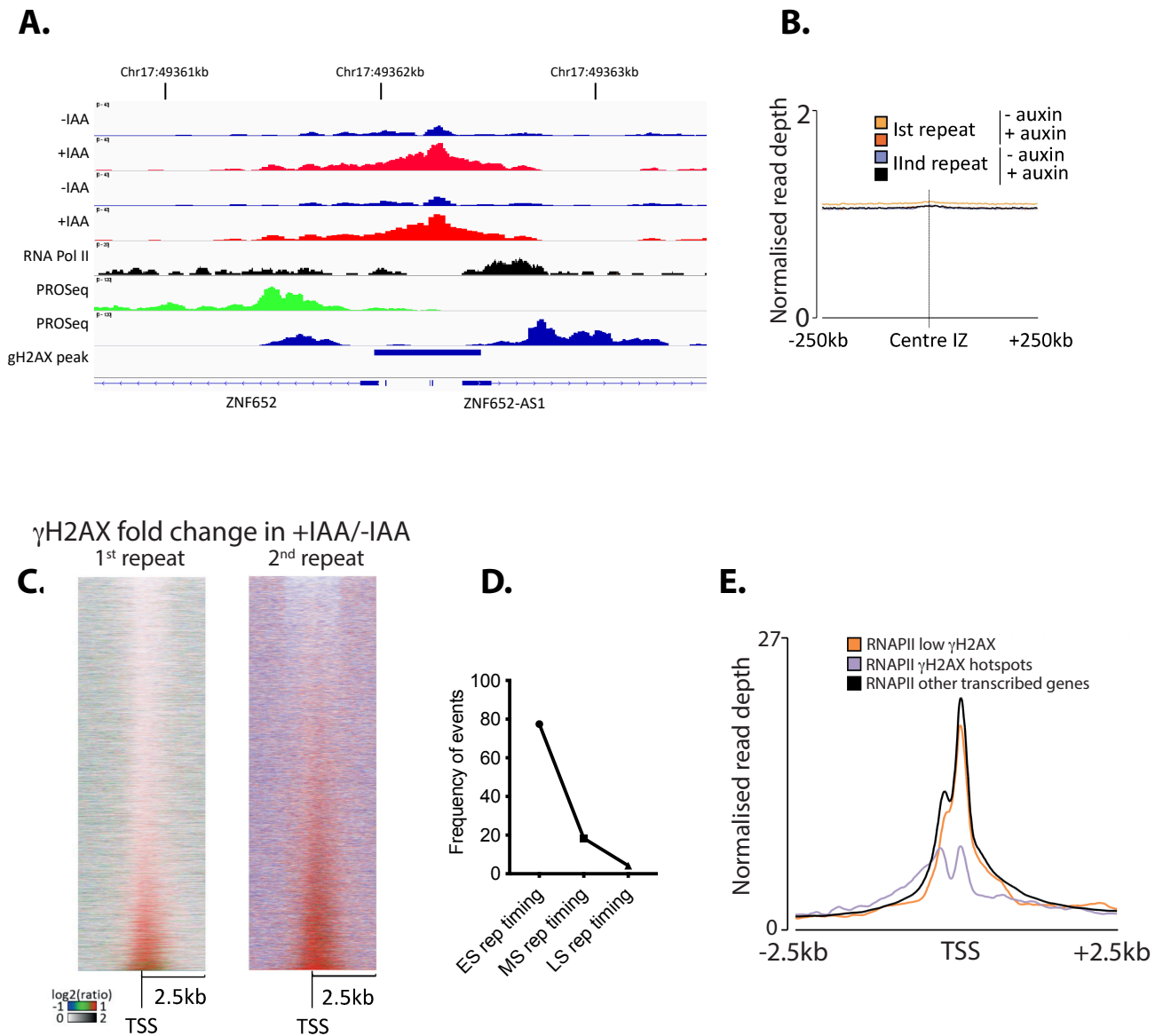
Supplementary Figure 6. TRAIP regulates mitotic progression. (A) TRAIP degradation at the end of G1 does not affect progression into S-phase. HCT116 degron cells were arrested in G1 with lovastatin, TRAIP degraded and cells released from G1 arrest. Cell cycle progression at indicated times was assessed by DNA content and flow cytometry. Left: Control arrest samples and example quantification gates indicating those cells in G1 or in S/G2. Middle: Example cell cycle profiles +/- IAA throughout the arrest. No visual differences could be observed between treatments. Right: Quantification of G1 or S/G2 cells by the gates depicted in controls. Statistical significant testing was carried out using T-tests, but no differences could be found. $n = 2$. **(B-D)** TRAIP regulates mitotic progression. HCT116 degron cells were arrested in G2 with RO-3306. TRAIP was degraded, cells released into mitosis and progression through mitosis observed at 30 and 60 min post release. As a control cells were treated with aphidicolin during RO-3306 treatment to slow down progression through the cell cycle. **(B)** example of detection of cells with condensed and segregating chromosomes. **(C)** Quantification of percentage of cells with condensed chromosomes $n = 3$. Shown are aphidicolin controls (red), - IAA (blue), and + IAA (purple); depicted as violin plots showing the median, interquartile range, and overall data distribution. Statistical significance were determined using one-way ANOVA and pairwise post-hoc testing. Significance is indicated on the plot. Increased proportions of cells were shown in -IAA/+IAA samples compared to controls at all timepoints ($p < 0.001$ for all comparisons shown). Conversely, no differences were observed between -IAA and + IAA samples. **(D)** Quantification of percentage cells with segregating chromosomes. Data depicted as in (C). Statistical analysis testing was carried out using one-way ANOVA and pairwise post-hoc testing. No differences were detected at 30 minutes post release. For 60 minute timepoints, significance is indicated on the plot: TRAIP-mAID C2 60 mins + aphidicolin control vs - IAA: $p = 0.00117$, - IAA vs + IAA: $p < 0.001$; TRAIP-mAID D5 60 mins + aphidicolin control vs - IAA: $p = 0.00209$; - IAA vs + IAA: $p < 0.001$. Source data are provided as a Source Data file.



Supplementary Figure 7. TRAIP degradation does not affect global DNA replication. (A) Cells optionally treated with IAA for 24 h were pulsed with BrdU for 1 h and BrdU incorporation into DNA analysed by FACS. Example FACS plots are presented (left) and quantification of number of cells incorporating BrdU and the level of BrdU incorporation normalised to control in replicating cells over $n=3$ (right), mean and SEM. Statistical analysis was carried out using t. tests, and any significant differences discovered is summarised on the plot (TRAIP-mAID C2: $p = 0.0331$; TRAIP-mAID D5: $p = 0.0126$). **(B)** Cells optionally treated with IAA for 24 h were pulsed with EdU for 1 h and EdU incorporation into DNA detected by immunofluorescence. Example microscopy images are presented (left) and quantification of number of cells incorporating EdU and level of EdU signal in replicating cells over $n=3$ (right). Statistical analyses was carried out on the data using t. tests and significant differences are summarised on the plots (TRAIP-mAID C2: $p = 0.0178$; TRAIP-mAID D5: $p = 0.0264$). **(C)** Cells were optionally treated with IAA for 24 h, nuclei extracted and the level of chromatin bound MCM7 analysed by FACS. Source data are provided as a Source Data file.

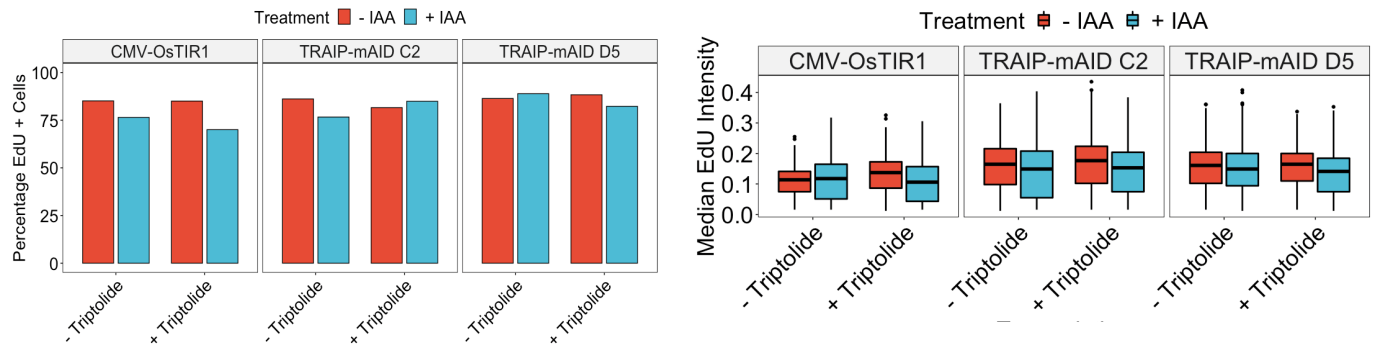


Supplementary Figure 8. DNA replication defect and DNA damage observed in cells after TRAIP depletion. (A) TRAIP Degradation Prolongs DNA Replication into G2/M. HCT116 degron cells were synchronised and treated as depicted in the schamatic (left). Quantification of the total proportion of cells positive for EdU incorporation for experiments using TRAIP-mAID C2 and TRAIP-mAID D5 (n = 3). Any differences between groups were determined using one-way ANOVA testing and post-hoc pairwise comparisons, indicated on the plots ($p > 0.001$ for all comparisons shown). **(B)** TRAIP was degraded just before S-phase as in (A). At indicated time points the DNA damage foci (γ H2AX and 53BP1 foci) were analysed by immunofluorescence. Example images are presented (left) and quantification of percentage of cells with over 3 γ H2AX foci over n=3 experiments (right). Significant differences (t.tests) are summarised on the graph for TRAIP-mAID C2 (13 Hrs post release: $p = 0.028$; 16 Hrs post release: $p = 0.037$; 20 Hrs post release, $p = 0.0016$; 24 Hrs post release, $p = 0.019$) and TRAIP-mAID D5 (13 Hrs post release: $p = 0.028$; 16 Hrs post release, $p = 0.010$; 20 Hrs post release, $p = 0.0019$; 24 Hrs post release, $p = 0.032$). **(C)** Accumulation of DNA damage in RPE1 TRAIP-mAID cells upon auxin treatment in EdU-negative vs EdU-positive cells. Students T-tests performed: γ -H2AX TRAIP-mAID -IAA vs +IAA (EdU pos); $p=0.045$. 53BP1 TRAIP-mAID -IAA vs +IAA (EdU pos); $p=0.002$. Source data are provided as a Source Data file.



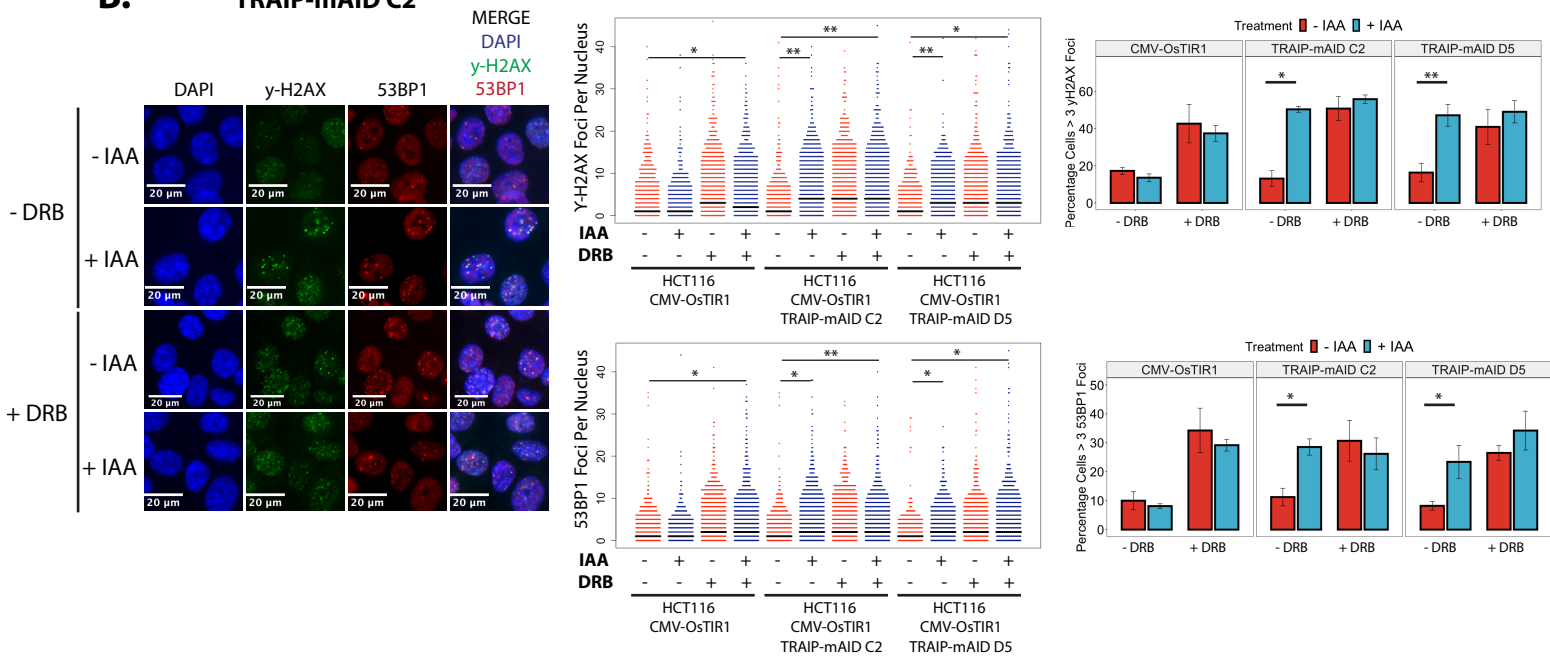
Supplementary Figure 9. The increase of γ H2AX upon TRAIP degradation does not correlate with replication features but with transcription start sites. (A) An example of mapped γ H2AX peak. Similar to the example in Figure 4A. **(B)** Correlation of γ H2AX signal with replication initiation and termination zones as determined by Daigaku et al. 2022. **(C)** Heatmaps of γ H2AX signal centered on transcription start sites (TSS). TSS sorted by γ H2AX fold change in +IAA/-IAA. Two independent repeats are presented. **(D)** Replication timing of hotspots. **(E)** Metagene profile of RNA Pol II ChIP-Seq from Erickson et al. at the TSS +/- 2.5 kb for genes with a gH2AX hotspot following TRAIP degradation, genes with low enrichment levels of gH2AX, and all the other transcribed genes, showing clear differences in the profile and distribution of RNA Pol II at the TSS region. Source data are provided as a Source Data file.

A.



B.

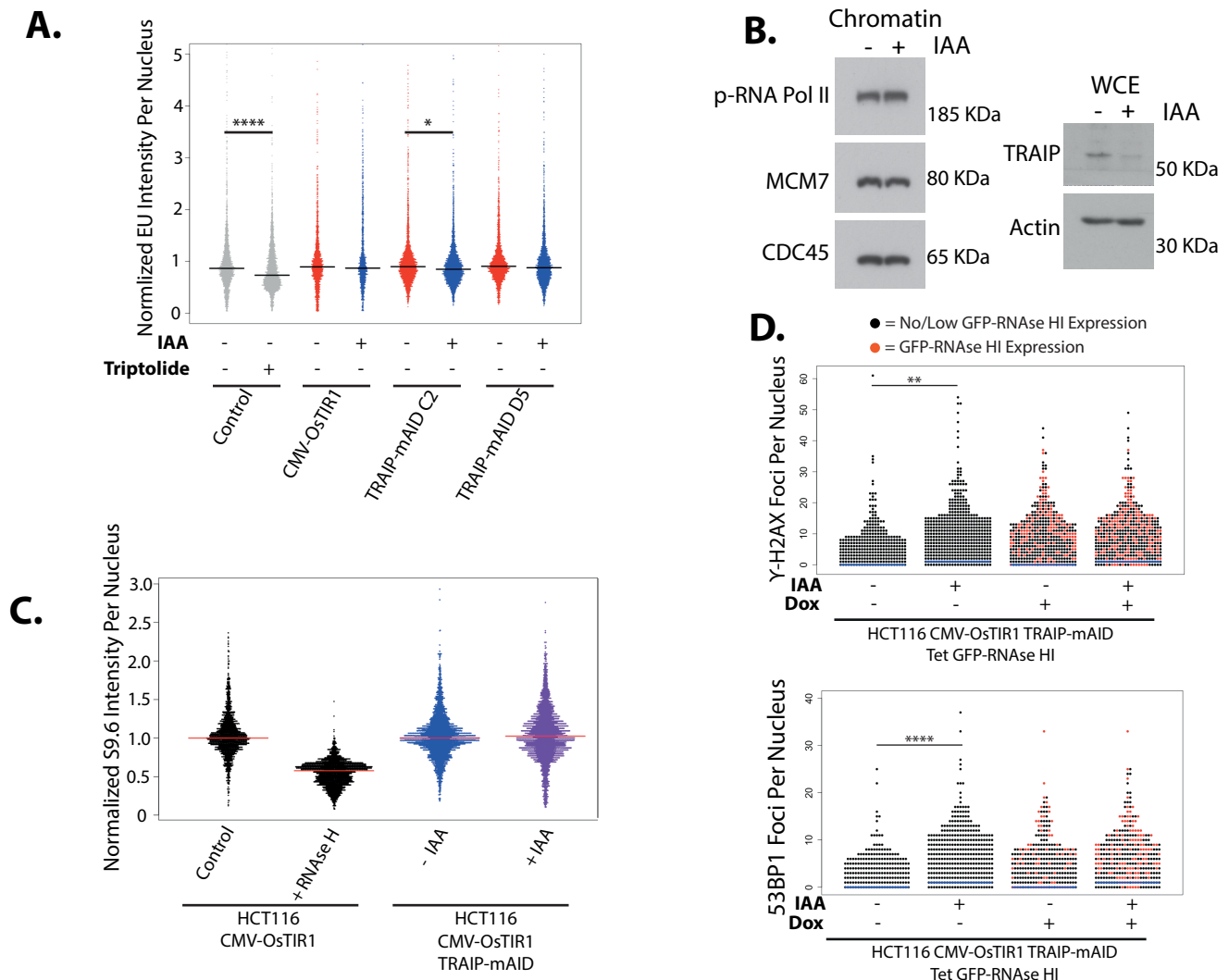
TRAIP-mAID C2



Supplementary Figure 10. (A) Short Triptolide treatment in S-phase does not inhibit DNA replication.

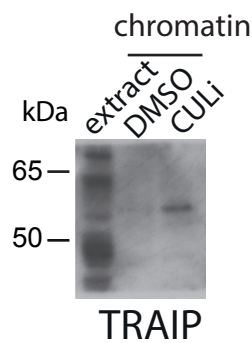
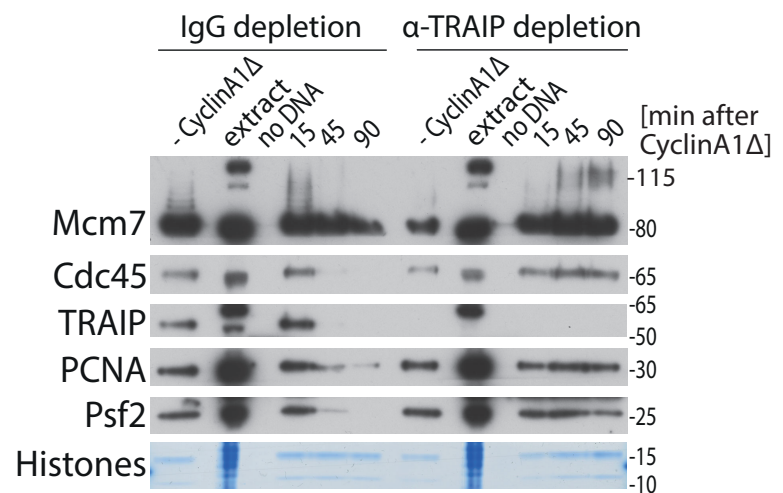
Cells were synchronised in G1 with optional degradation of TRAIP for last 1 h of arrest and released into mitosis. Cells were then treated for 90 min with Triptolide, 3 h after release from G1 arrest. Cells were pulsed for 1 h with EdU and its incorporation was analysed using fluorescent microscopy. Shown are the overall percentage of cells positive for EdU (left), as well as median EdU intensity per cell (right).

(B) DRB treatment during S-phase is epistatic with TRAIP degradation. Cells were synchronised in G1, where TRAIP was degraded prior to entry to S-phase. Upon S-phase entry DRB was added for 90 minutes and cells fixed, then stained for DNA damage markers. Left: Example microscopy images. Middle: Total foci counts per nucleus. Ttest for pairwise comparisons. γ H2AX: all ** < 0.009, * < 0.036; 53BP1: ** p = 0.00965, all * < 0.048. Right: Quantification of the proportion of nuclei containing > 3 DNA damage foci. Source data are provided as a Source Data file.



Supplementary Figure 11. Effects of TRAIP-mAID degradation on transcription. (A) Degradation of TRAIP-mAID does not increase global transcription levels. HCT116 TRAIP-mAID cells were arrested in G1, where TRAIP was degraded as described previously. Upon entry to S-phase (12 h post release), triptolide was optionally added to the control sample for 90 minutes. In all samples EU was added for 60 minutes 13.5 h following release from G1 arrest to label newly synthesised RNA. Incorporated EU was visualised using immunofluorescence following a copper-catalysed Click-IT reaction following manufacturers protocols. The median EU intensity per nucleus was quantified and normalised to the control (- IAA - Triptolide), shown as beeswarm plots. Statistical testing was conducted using pairwise t.tests: Control vs Triptolide treatment: $p < 0.0001$; TRAIP-mAID C2 - IAA vs + IAA: $p = 0.0102$. $N = 3$.

(B) No global increase of RNA Pol II on chromatin in absence of TRAIP. HCT116 TRAIP-mAID cells were arrested in G1, TRAIP optionally degraded and cells released into S-phase. In the middle of S-phase (12 h after G1 release) WCE and chromatin fractions were prepared and analysed by western blotting with indicated antibodies ($n=3$). **(C) No changes in R-loops level was detected upon TRAIP depletion.** The S9.6 RNA:DNA hybrid antibody was used to detect any major changes to R-loop levels in the HCT116 degon cells. S-phase cells with and without TRAIP were stained for the S9.6 antibody and the respective fluorescence measured using Cell Profiler. Quantification of S9.6 intensity. **(D) Overexpression of RNaseH1 does not rescue DNA damage repair signals (γ H2AX and 53BP1 foci) after TRAIP degradation.** HCT116 TRAIP-mAID cells were transduced with lentivirus to facilitate the Tet-inducible expression of GFP-RNase HI. Asynchronous cells were treated optionally with DOX or IAA as indicated and fixed for DNA damage foci. Shown are the quantified number of foci per cell. Black circles are cells with no detectable GFP; cells with low or no GFP-RNase HI expression. Red circles depict cells with detectable GFP; cells with GFP-RNase HI expressed. Medians are shown by blue bar. Statistical analysis was carried out using t.tests. with significance shown on the plot (γ H2AX - IAA vs + IAA: $p = 0.001709$; 3BP1 - IAA vs + IAA: $p = 0.0009167$. Source data are provided as a Source Data file.

A.**B.**

Supplementary Figure 12. TRAIP depleted *Xenopus* egg extract is unable to unload replisomes in mitosis. **(A)** Characterisation of X./ TRAIP antibody raised for this study. The level of TRAIP in the egg extract is low and all of our TRAIP antibodies recognise other bands in full egg extract. We have therefore also resolved samples of chromatin with accumulated replisomes (cullin inhibitor MLN4924 treatment for 90 min, CULi) to confirm that the band between 65 and 50 kD is indeed behaving as expected from TRAIP (n=3) **(B)** TRAIP depleted extract cannot unload replisomes in mitosis. Non-specific IgG or α-TRAIP depleted egg extract was used to replicate DNA to completion in presence of neddylation inhibitor MLN4924, which inhibits activity of Cullin type ubiquitin ligases and blocks S-phase pathway of replisome disassembly. Once replication was completed, extracts were supplemented with Cyclin A1Δ to stimulate progression into mitosis. Chromatin was isolated at indicated timepoints and replisome presence on chromatin was monitored by western blotting with indicated antibodies. In mock depleted extract CMGs (as visualised by Cdc45, Psf2) are removed from chromatin, while in α-TRAIP depleted egg extract they are retained on chromatin due to lack of TRAIP (n=4). Source data are provided as a Source Data file.

Supplementary Table 1. Summary of the significant GOTerms identified from the genes isolated using γ -H2AX ChIP sequencing

Analysis Type	Gene Ontology Term	Count (# Genes)	Frequency (%)	Corrected P- Value (Benjamini)
Biological Process (GOTerm BP)	positive regulation of transcription from RNA polymerase II promoter	55	10.5	0.0014
Biological Process (GOTerm BP)	negative regulation of transcription from RNA polymerase II promoter	42	8	0.0077
Biological Process (GOTerm BP)	ephrin receptor signaling pathway	12	2.3	0.013
Biological Process (GOTerm BP)	vascular endothelial growth factor receptor signaling pathway	11	2.1	0.013
Biological Process (GOTerm BP)	transcription from RNA polymerase II promoter	31	5.9	0.034
Biological Process (GOTerm BP)	transcription, DNA-templated	81	15.4	0.045
Biological Process (GOTerm BP)	regulation of actin cytoskeleton organization	8	1.5	0.071
Biological Process (GOTerm BP)	covalent chromatin modification	12	2.3	0.071
Biological Process (GOTerm BP)	protein phosphorylation	27	5.1	0.08
Molecular Function (GOTerm MF)	protein binding	289	55	0.0026
Cellular Component (GOTerm CC)	nucleus	206	39.2	0.000000016
Cellular Component (GOTerm CC)	nucleoplasm	114	21.7	0.000047
Cellular Component (GOTerm CC)	cytoplasm	175	33.3	0.0041
Cellular Component (GOTerm CC)	cytosol	117	22.3	0.017
Biological Process (GOTerm BP)	positive regulation of transcription from RNA polymerase II promoter	55	10.5	0.0014

Bibliography

Agrotis, A., Lamoliatte, F., Williams, T.D., et al. (2023) Multiple phosphorylation of the Cdc48/p97 cofactor protein Shp1/p47 occurs upon cell stress in budding yeast. *Life Science Alliance*, 6 (4). doi:10.26508/lisa.202201642.

Akutsu, M., Dikic, I. and Bremm, A. (2016) Ubiquitin chain diversity at a glance. *Journal of cell science*, 129 (5). doi:10.1242/jcs.183954.

Alabert, C. and Groth, A. (2012) Chromatin replication and epigenome maintenance. *Nature reviews. Molecular cell biology*, 13 (3). doi:10.1038/nrm3288.

Alexandru, G., Graumann, J., Smith, G., et al. (2008) UBXD7 binds multiple ubiquitin ligases and implicates p97 in HIF1alpha turnover. *Cell*, 134 (5). doi:10.1016/j.cell.2008.06.048.

Allison, D. and Wang, G. (2019) R-loops: formation, function, and relevance to cell stress. *Cell stress*, 3 (2). doi:10.15698/cst2019.02.175.

Almeida, S., Ryser, S., Obarzanek-Fojt, M., et al. (2011) The TRAF-Interacting Protein (TRIP) Is a Regulator of Keratinocyte Proliferation. *Journal of Investigative Dermatology*, 131 (2): 349–357. doi:10.1038/jid.2010.329.

Almouzni, G. and Méchali, M. (1988) Assembly of spaced chromatin promoted by DNA synthesis in extracts from *Xenopus* eggs. *The EMBO journal*, 7 (3). doi:10.1002/j.1460-2075.1988.tb02861.x.

Ardito, F., Giuliani, M., Perrone, D., et al. (2017) The crucial role of protein phosphorylation in cell signaling and its use as targeted therapy (Review). *International journal of molecular medicine*, 40 (2). doi:10.3892/ijmm.2017.3036.

Attali, I., Botchan, M.R. and Berger, J.M. (2021) Structural Mechanisms for Replicating DNA in Eukaryotes. *Annual Review of Biochemistry*, 90: 77–106. doi:10.1146/annurev-biochem-090120-125407.

Bando, M., Katou, Y., Komata, M., et al. (2009) Csm3, Tof1, and Mrc1 form a heterotrimeric mediator complex that associates with DNA replication forks. *The Journal of biological chemistry*, 284 (49). doi:10.1074/jbc.M109.065730.

Barnieh, F., Loadman, P. and Falconer, R. (2021) Progress towards a clinically-successful ATR inhibitor for cancer therapy. *Current research in pharmacology and drug discovery*, 2. doi:10.1016/j.crphar.2021.100017.

Bartek, J. and Lukas, J. (2001) Pathways governing G1/S transition and their response to DNA damage. *FEBS Letters*, 490 (3): 117–122. doi:10.1016/S0014-5793(01)02114-7.

Bella, J., Hindle, K.L., McEwan, P.A., et al. (2008) The leucine-rich repeat structure. *Cellular and Molecular Life Sciences*, 65 (15): 2307–2333. doi:10.1007/s00018-008-8019-0.

Bellush, J. and Whitehouse, I. (2017) DNA replication through a chromatin environment. *Philosophical transactions of the Royal Society of London. Series B, Biological sciences*, 372 (1731). doi:10.1098/rstb.2016.0287.

Berti, M., Chaudhuri, A.R., Thangavel, S., et al. (2013) Human RECQ1 promotes restart of replication forks reversed by DNA topoisomerase I inhibition. *Nature structural & molecular biology*, 20 (3). doi:10.1038/nsmb.2501.

Berti, M., Cortez, D. and Lopes, M. (2020) The plasticity of DNA replication forks in response to clinically relevant genotoxic stress. *Nature reviews. Molecular cell biology*, 21 (10). doi:10.1038/s41580-020-0257-5.

Berti, M. and Vindigni, A. (2016) Replication stress: getting back on track. *Nature Structural & Molecular Biology*, 23 (2): 103–109. doi:10.1038/nsmb.3163.

Besse, A., Campos, A.D., Webster, W.K., et al. (2007) TRAF-interacting protein (TRIP) is a RING-dependent ubiquitin ligase. *Biochemical and Biophysical Research Communications*, 359 (3): 660–664. doi:10.1016/j.bbrc.2007.05.149.

Bhargava, R., Onyango, D.O. and Stark, J.M. (2016) Regulation of Single-Strand Annealing and its Role in Genome Maintenance. *Trends in Genetics*, 32 (9): 566–575. doi:10.1016/j.tig.2016.06.007.

Bhowmick, R. and Hickson, I.D. (2017) The “enemies within”: regions of the genome that are inherently difficult to replicate. *F1000Research*, 6 (666): 666. doi:10.12688/f1000research.11024.1.

Bicknell, L.S., Bongers, E.M.H.F., Leitch, A., et al. (2011) Mutations in the Pre-Replication Complex cause Meier-Gorlin syndrome. *Nature genetics*, 43 (4): 356–359. doi:10.1038/ng.775.

Blow, J. and Dutta, A. (2005) Preventing re-replication of chromosomal DNA. *Nature reviews. Molecular cell biology*, 6 (6). doi:10.1038/nrm1663.

Blow, J.J. and Laskey, R.A. (2016) *Xenopus* cell-free extracts and their contribution to the study of DNA replication and other complex biological processes. *The International Journal of Developmental Biology*, 60 (7-8-9): 201–207. doi:10.1387/ijdb.160142jb.

Boehm, E., Gildenberg, M. and Washington, M. (2016) The Many Roles of PCNA in Eukaryotic DNA Replication. *The Enzymes*, 39. doi:10.1016/bs.enz.2016.03.003.

Bremm, A., Moniz, S., Mader, J., et al. (2014) Cezanne (OTUD7B) regulates HIF-1 α homeostasis in a proteasome-independent manner. *EMBO reports*, 15 (12): 1268–1277. doi:10.15252/embr.201438850.

Burger, J., Merlet, J., Tavernier, N., et al. (2013) CRL2LRR-1 E3-Ligase Regulates Proliferation and Progression through Meiosis in the *Caenorhabditis elegans* Germline. *PLoS Genetics*, 9 (3). doi:10.1371/journal.pgen.1003375.

Burgers, P. and Kunkel, T. (2017) Eukaryotic DNA Replication Fork. *Annual review of biochemistry*, 86. doi:10.1146/annurev-biochem-061516-044709.

Butt, T., Edavettal, S., Hall, J., et al. (2005) SUMO fusion technology for difficult-to-express proteins. *Protein expression and purification*, 43 (1). doi:10.1016/j.pep.2005.03.016.

Cai, W. and Yang, H. (2016) The structure and regulation of Cullin 2 based E3 ubiquitin ligases and their biological functions. *Cell division*, 11. doi:10.1186/s13008-016-0020-7.

Cardote, T.A.F., Gadd, M.S. and Ciulli, A. (2017) Crystal Structure of the Cul2-Rbx1-EloBC-VHL Ubiquitin Ligase Complex. *Structure*, 25 (6): 901-911.e3. doi:10.1016/j.str.2017.04.009.

- Chapard, C., Hohl, D. and Huber, M. (2015) The TRAF-interacting protein (TRAIP) is a novel E2F target with peak expression in mitosis. *Oncotarget*, 6 (25). doi:10.18632/oncotarget.3055.
- Chapard, C., Meraldi, P., Gleich, T., et al. (2014) TRAIP is a regulator of the spindle assembly checkpoint. *Journal of cell science*, 127 (Pt 24). doi:10.1242/jcs.152579.
- Chowdhury, P., Ge, L., K, L., et al. (2014) Targeting TopBP1 at a convergent point of multiple oncogenic pathways for cancer therapy. *Nature communications*, 5. doi:10.1038/ncomms6476.
- Cortez, D. (2015) Preventing replication fork collapse to maintain genome integrity. *DNA repair*, 32. doi:10.1016/j.dnarep.2015.04.026.
- Costa, A. and Diffley, J. (2022) The Initiation of Eukaryotic DNA Replication. *Annual review of biochemistry*, 91. doi:10.1146/annurev-biochem-072321-110228.
- Costa, A., Ilves, I., Tamberg, N., et al. (2011) The structural basis for MCM2-7 helicase activation by GINS and Cdc45. *Nature structural & molecular biology*, 18 (4). doi:10.1038/nsmb.2004.
- Coster, G., Frigola, J., Beuron, F., et al. (2014) Origin Licensing Requires ATP Binding and Hydrolysis by the MCM Replicative Helicase. *Molecular Cell*, 55 (5): 666. doi:10.1016/j.molcel.2014.06.034.
- Cotton, T.R. and Lechtenberg, B.C. (2020) Chain reactions: molecular mechanisms of RBR ubiquitin ligases. *Biochemical Society Transactions*, 48 (4): 1737. doi:10.1042/BST20200237.
- Courtemanche, N. and Barrick, D. (2008) The leucine-rich repeat domain of Internalin B folds along a polarized N-terminal pathway. *Structure (London, England: 1993)*, 16 (5): 705. doi:10.1016/j.str.2008.02.015.
- Courtot, L., Hoffmann, J.-S. and Bergoglio, V. (2018) The Protective Role of Dormant Origins in Response to Replicative Stress. *International Journal of Molecular Sciences*, 19 (11). doi:10.3390/ijms19113569.
- Coverley, D., Pelizon, C., Trewick, S., et al. (2000) Chromatin-bound Cdc6 persists in S and G2 phases in human cells, while soluble Cdc6 is destroyed in a cyclin A-cdk2 dependent process. *Journal of cell science*, 113 (Pt 11). doi:10.1242/jcs.113.11.1929.
- Dang, Y. and Guan, J. (2020) Nanoparticle-based drug delivery systems for cancer therapy. *Smart Materials in Medicine*, 1: 10–19. doi:10.1016/j.smim.2020.04.001.
- Dao, T.P., Majumdar, A. and Barrick, D. (2014) Capping motifs stabilize the leucine-rich repeat protein PP32 and rigidify adjacent repeats: Roles of Caps in the Folding of the LRR Protein PP32. *Protein Science*, 23 (6): 801–811. doi:10.1002/pro.2462.
- Deegan, T., Mukherjee, P., Fujisawa, R., et al. (2020) CMG helicase disassembly is controlled by replication fork DNA, replisome components and a ubiquitin threshold. *eLife*, 9. doi:10.7554/eLife.60371.
- Deng, L., Wu, R., Sonnevile, R., et al. (2019) Mitotic CDK Promotes Replisome Disassembly, Fork Breakage, and Complex DNA Rearrangements. *Molecular cell*, 73 (5). doi:10.1016/j.molcel.2018.12.021.
- Dewar, J., Budzowska, M. and Walter, J. (2015) The mechanism of DNA replication termination in vertebrates. *Nature*, 525 (7569). doi:10.1038/nature14887.

- Dewar, J., Low, E., Mann, M., et al. (2017a) CRL2Lrr1 promotes unloading of the vertebrate replisome from chromatin during replication termination. *Genes & development*, 31 (3). doi:10.1101/gad.291799.116.
- Dewar, J. and Walter, J. (2017) Mechanisms of DNA replication termination. *Nature reviews. Molecular cell biology*, 18 (8). doi:10.1038/nrm.2017.42.
- Dewar, J.M., Low, E., Mann, M., et al. (2017b) CRL2Lrr1 promotes unloading of the vertebrate replisome from chromatin during replication termination. *Genes & Development*, 31 (3): 275–290. doi:10.1101/gad.291799.116.
- Dikic, I., Wakatsuki, S. and Walters, K.J. (2009) Ubiquitin binding domains — from structures to functions. *Nature reviews. Molecular cell biology*, 10 (10): 659–671. doi:10.1038/nrm2767.
- Duan, S. and Pagano, M. (2021) Ubiquitin ligases in cancer: Functions and clinical potentials. *Cell chemical biology*, 28 (7). doi:10.1016/j.chembiol.2021.04.008.
- Fan, Y., Köberlin, M.S., Ratnayeke, N., et al. (2021) LRR1-mediated replisome disassembly promotes DNA replication by recycling replisome components. *The Journal of Cell Biology*, 220 (8). doi:10.1083/jcb.202009147.
- Feng, W., Guo, Y., Huang, J., et al. (2016) TRAIP regulates replication fork recovery and progression via PCNA. *Cell Discovery*, 2 (1): 1–14. doi:10.1038/celldisc.2016.16.
- Follonier, C., Oehler, J., Herrador, R., et al. (2013) Friedreich's ataxia-associated GAA repeats induce replication-fork reversal and unusual molecular junctions. *Nature structural & molecular biology*, 20 (4). doi:10.1038/nsmb.2520.
- Fragkos, M., Ganier, O., Coulombe, P., et al. (2015) DNA replication origin activation in space and time. *Nature Reviews Molecular Cell Biology*, 16 (6): 360–374. doi:10.1038/nrm4002.
- Fu, Y., Yardimci, H., Long, D., et al. (2011) Selective bypass of a lagging strand roadblock by the eukaryotic replicative DNA helicase. *Cell*, 146 (6). doi:10.1016/j.cell.2011.07.045.
- Fujisawa, R., Polo Rivera, C. and Labib, K. (2022) Multiple UBX proteins reduce the ubiquitin threshold of the mammalian p97-UFD1-NPL4 unfoldase. *eLife*, 11. doi:10.7554/eLife.76763.
- Fukushima, H., Ogura, K., Wan, L., et al. (2013) SCF-mediated Cdh1 degradation defines a negative feedback system that coordinates cell-cycle progression. *Cell reports*, 4 (4). doi:10.1016/j.celrep.2013.07.031.
- Galderisi, U., Jori, F.P. and Giordano, A. (2003) Cell cycle regulation and neural differentiation. *Oncogene*, 22 (33): 5208–5219. doi:10.1038/sj.onc.1206558.
- Gallina, I., Hendriks, I.A., Hoffmann, S., et al. (2021) The ubiquitin ligase RFWD3 is required for translesion DNA synthesis. *Molecular Cell*, 81 (3): 442–458.e9. doi:10.1016/j.molcel.2020.11.029.
- Gambus, A., Jones, R.C., Sanchez-Diaz, A., et al. (2006) GINS maintains association of Cdc45 with MCM in replisome progression complexes at eukaryotic DNA replication forks. *Nature Cell Biology*, 8 (4): 358–366. doi:10.1038/ncb1382.
- Gambus, A., Khoudoli, G., Jones, R., et al. (2011) MCM2-7 form double hexamers at licensed origins in *Xenopus* egg extract. *The Journal of biological chemistry*, 286 (13). doi:10.1074/jbc.M110.199521.

- Garcia-Barcena, C., Osinalde, N., Ramirez, J., et al. (2020) How to Inactivate Human Ubiquitin E3 Ligases by Mutation. *Frontiers in Cell and Developmental Biology*, 8. doi:10.3389/fcell.2020.00039.
- Gatti, M., Pinato, S., Maiolica, A., et al. (2015) RNF168 Promotes Noncanonical K27 Ubiquitination to Signal DNA Damage. *Cell Reports*, 10 (2): 226–238. doi:10.1016/j.celrep.2014.12.021.
- Gavet, O. and Pines, J. (2010) Progressive activation of CyclinB1-Cdk1 coordinates entry to mitosis. *Developmental cell*, 18 (4). doi:10.1016/j.devcel.2010.02.013.
- Ge, X.Q., Jackson, D.A. and Blow, J.J. (2007) Dormant origins licensed by excess Mcm2–7 are required for human cells to survive replicative stress. *Genes & Development*, 21 (24): 3331–3341. doi:10.1101/gad.457807.
- Georgescu, R., Yuan, Z., Bai, L., et al. (2017) Structure of eukaryotic CMG helicase at a replication fork and implications to replisome architecture and origin initiation. *Proceedings of the National Academy of Sciences of the United States of America*, 114 (5): E697–E706. doi:10.1073/pnas.1620500114.
- Gillespie, P.J., Gambus, A. and Blow, J.J. (2012) Preparation and use of *Xenopus* egg extracts to study DNA replication and chromatin associated proteins. *Methods*, 57 (2): 203–213. doi:10.1016/j.ymeth.2012.03.029.
- Glover, T. (2006) Common fragile sites. *Cancer letters*, 232 (1). doi:10.1016/j.canlet.2005.08.032.
- Glover, T., Wilson, T. and Arlt, M. (2017) Fragile sites in cancer: more than meets the eye. *Nature reviews. Cancer*, 17 (8). doi:10.1038/nrc.2017.52.
- Goldstein, G., Scheid, M., Hammerling, U., et al. (1975) Isolation of a polypeptide that has lymphocyte-differentiating properties and is probably represented universally in living cells. *Proceedings of the National Academy of Sciences of the United States of America*, 72 (1): 11. doi:10.1073/pnas.72.1.11.
- Goswami, P., Abid Ali, F., Douglas, M.E., et al. (2018) Structure of DNA-CMG-Pol epsilon elucidates the roles of the non-catalytic polymerase modules in the eukaryotic replisome. *Nature Communications*, 9 (1): 1–13. doi:10.1038/s41467-018-07417-1.
- Guo, Z., Zeng, Y., Chen, Y., et al. (2020) TRAP promotes malignant behaviors and correlates with poor prognosis in liver cancer. *Biomedicine & Pharmacotherapy = Biomedecine & Pharmacotherapie*, 124: 109857–109857. doi:10.1016/j.biopha.2020.109857.
- Haglund, K., Di Fiore, P. and Dikic, I. (2003) Distinct monoubiquitin signals in receptor endocytosis. *Trends in biochemical sciences*, 28 (11). doi:10.1016/j.tibs.2003.09.005.
- Han, Y., Yun, M., Choi, M., et al. (2019) TRAP regulates Histone H2B monoubiquitination in DNA damage response pathways. *Oncology reports*, 41 (6). doi:10.3892/or.2019.7092.
- Hänzelmann, P. and Schindelin, H. (2017) The Interplay of Cofactor Interactions and Post-translational Modifications in the Regulation of the AAA+ ATPase p97. *Frontiers in Molecular Biosciences*, 4: 21. doi:10.3389/fmolb.2017.00021.
- Harley, M.E., Murina, O., Leitch, A., et al. (2016) TRAP promotes DNA damage response during genome replication and is mutated in primordial dwarfism. *Nature genetics*, 48 (1): 36. doi:10.1038/ng.3451.

- Harper, S. and Speicher, D.W. (2011) Purification of proteins fused to glutathione S-transferase. *Methods in Molecular Biology (Clifton, N.J.)*, 681: 259–280. doi:10.1007/978-1-60761-913-0_14.
- Hart, T., Chandrashekhar, M., Aregger, M., et al. (2015) High-Resolution CRISPR Screens Reveal Fitness Genes and Genotype-Specific Cancer Liabilities. *Cell*, 163 (6). doi:10.1016/j.cell.2015.11.015.
- Hashimoto, Y., Sadano, K., Miyata, N., et al. (2023) Novel role of DONSON in CMG helicase assembly during vertebrate DNA replication initiation. *The EMBO Journal*, 42 (17): e114131. doi:10.15252/embj.2023114131.
- Hashimoto, Y. and Tanaka, H. (2018) Mitotic entry drives replisome disassembly at stalled replication forks. *Biochemical and biophysical research communications*, 506 (1). doi:10.1016/j.bbrc.2018.10.064.
- Hatakeyama, S., Matsumoto, M., Yada, M., et al. (2004) Interaction of U-box-type ubiquitin-protein ligases (E3s) with molecular chaperones. *Genes to Cells*, 9 (6): 533–548. doi:10.1111/j.1356-9597.2004.00742.x.
- Havens, C.G. and Walter, J.C. (2011) Mechanism of CRL4Cdt2, a PCNA-dependent E3 ubiquitin ligase. *Genes & Development*, 25 (15): 1568–1582. doi:10.1101/gad.2068611.
- Hawkins, M., Retkute, R., Müller, C.A., et al. (2013) High-Resolution Replication Profiles Define the Stochastic Nature of Genome Replication Initiation and Termination. *Cell Reports*, 5 (4): 1132. doi:10.1016/j.celrep.2013.10.014.
- Heller, R.C., Kang, S., Lam, W.M., et al. (2011) Eukaryotic origin-dependent DNA replication in vitro reveals sequential action of DDK and S-CDK kinases. *Cell*, 146 (1): 80–91. doi:10.1016/j.cell.2011.06.012.
- Hernández-Carralero, E., Cabrera, E., Vega, I.A., et al. (2018) Control of DNA Replication Initiation by Ubiquitin. *Cells*, 7 (10). doi:10.3390/cells7100146.
- Hicke, L. and Dunn, R. (2003) *Regulation of Membrane Protein Transport by Ubiquitin and Ubiquitin-Binding Proteins*. doi:10.1146/annurev.cellbio.19.110701.154617.
- Hicke, L., Schubert, H.L. and Hill, C.P. (2005) Ubiquitin-binding domains. *Nature Reviews. Molecular Cell Biology*, 6 (8): 610–621. doi:10.1038/nrm1701.
- Hindle, A., Bose, C., Lee, J., et al. (2022) Rlip Depletion Alters Oncogene Transcription at Multiple Distinct Regulatory Levels. *Cancers*, 14 (3): 527. doi:10.3390/cancers14030527.
- Hoegel, C., Pfander, B., Moldovan, G., et al. (2002) RAD6-dependent DNA repair is linked to modification of PCNA by ubiquitin and SUMO. *Nature*, 419 (6903). doi:10.1038/nature00991.
- Hoffmann, S., Smedegaard, S., Nakamura, K., et al. (2016) TRAIP is a PCNA-binding ubiquitin ligase that protects genome stability after replication stress. *Journal of Cell Biology*, 212 (1): 63–75. doi:10.1083/jcb.201506071.
- Hong, M., Li, T., Xue, W., et al. (2022) Genetic engineering of baculovirus-insect cell system to improve protein production. *Frontiers in Bioengineering and Biotechnology*, 10: 994743. doi:10.3389/fbioe.2022.994743.

Hoogenboom, W.S., Klein Douwel, D. and Knipscheer, P. (2017) Xenopus egg extract: A powerful tool to study genome maintenance mechanisms. *Developmental Biology*, 428 (2): 300–309. doi:10.1016/j.ydbio.2017.03.033.

Hormaechea-Agulla, D., Kim, Y., Song, M.S., et al. (2018) New Insights into the Role of E2s in the Pathogenesis of Diseases: Lessons Learned from UBE2O. *Molecules and Cells*, 41 (3): 168. doi:10.14348/molcells.2018.0008.

Huang, D.T., Hunt, H.W., Zhuang, M., et al. (2007) Basis for a ubiquitin-like protein thioester switch toggling E1–E2 affinity. *Nature*, 445 (7126): 394–398. doi:10.1038/nature05490.

Humphreys, L., Smith, P., Chen, Z., et al. (2021) The role of E3 ubiquitin ligases in the development and progression of glioblastoma. *Cell death and differentiation*, 28 (2). doi:10.1038/s41418-020-00696-6.

Hurley, J.H., Lee, S. and Prag, G. (2006) Ubiquitin-binding domains. *The Biochemical Journal*, 399 (3): 361–372. doi:10.1042/BJ20061138.

Ibarra, A., Schwob, E. and Méndez, J. (2008) Excess MCM proteins protect human cells from replicative stress by licensing backup origins of replication. *Proceedings of the National Academy of Sciences of the United States of America*, 105 (26): 8956–8961. doi:10.1073/pnas.0803978105.

Irie, T. and Sawa, M. (2023) CDC7 kinase inhibitors: a survey of recent patent literature (2017–2022). *Expert Opinion on Therapeutic Patents*. Available at: <https://www.tandfonline.com/doi/abs/10.1080/13543776.2023.2262138> (Accessed: 1 December 2023).

Jang, S.-M., Redon, C.E., Thakur, B.L., et al. (2020) Regulation of cell cycle drivers by Cullin-RING ubiquitin ligases. *Experimental & Molecular Medicine*, 52 (10): 1637–1651. doi:10.1038/s12276-020-00508-4.

Jasencakova, Z. and Groth, A. (2010) Restoring chromatin after replication: how new and old histone marks come together. *Seminars in cell & developmental biology*, 21 (2). doi:10.1016/j.semcd.2009.09.018.

Jenkyn-Bedford, M., Jones, M.L., Baris, Y., et al. (2021) A conserved mechanism for regulating replisome disassembly in eukaryotes. *Nature*, 600 (7890): 743–747. doi:10.1038/s41586-021-04145-3.

Jenness, C., Wynne, D.J. and Funabiki, H. (2018) Protein Immunodepletion and Complementation in *Xenopus laevis* Egg Extracts. *Cold Spring Harbor protocols*, 2018 (9). doi:10.1101/pdb.prot097113.

Jones, R.M., Ruiz, J.H., Scaramuzza, S., et al. (2022) *Characterising replisome disassembly in human cells*.

Kang, S., Kang, M., Ryu, E., et al. (2018) Eukaryotic DNA replication: Orchestrated action of multi-subunit protein complexes. *Mutation research*, 809. doi:10.1016/j.mrfmmm.2017.04.002.

Kavalchuk, M., Jomaa, A., Müller, A.U., et al. (2022) Structural basis of prokaryotic ubiquitin-like protein engagement and translocation by the mycobacterial Mpa-proteasome complex. *Nature Communications*, 13 (1): 1–13. doi:10.1038/s41467-021-27787-3.

Kelsall, I.R. (2022) Non-lysine ubiquitylation: Doing things differently. *Frontiers in Molecular Biosciences*, 9: 1008175. doi:10.3389/fmolb.2022.1008175.

- Keszhelyi, A., Minchell, N.E. and Baxter, J. (2016) The Causes and Consequences of Topological Stress during DNA Replication. *Genes*, 7 (12). doi:10.3390/genes7120134.
- Kingsley, G., Skagia, A., Passaretti, P., et al. (2023) DONSON facilitates Cdc45 and GINS chromatin association and is essential for DNA replication initiation. *Nucleic Acids Research*, 51 (18): 9748–9763. doi:10.1093/nar/gkad694.
- Kitagawa, K., Kotake, Y. and Kitagawa, M. (2009) Ubiquitin-mediated control of oncogene and tumor suppressor gene products. *Cancer science*, 100 (8). doi:10.1111/j.1349-7006.2009.01196.x.
- Knipscheer, P., Räschle, M., Schärer, O.D., et al. (2012) “Replication-Coupled DNA Interstrand Cross-Link Repair in *Xenopus* Egg Extracts.” In Bjergbæk, L. (ed.) *DNA Repair Protocols*. Methods in Molecular Biology. Totowa, NJ: Humana Press. pp. 221–243. doi:10.1007/978-1-61779-998-3_16.
- Kobe, B. and Kajava, A. (2001) The leucine-rich repeat as a protein recognition motif. *Current opinion in structural biology*, 11 (6). doi:10.1016/s0959-440x(01)00266-4.
- Kochenova, O.V., Mukkavalli, S., Raman, M., et al. (2022) Cooperative assembly of p97 complexes involved in replication termination. *Nature Communications*, 13 (1): 1–17. doi:10.1038/s41467-022-34210-y.
- Komander, D. and Rape, M. (2012) The ubiquitin code. *Annual review of biochemistry*, 81. doi:10.1146/annurev-biochem-060310-170328.
- Kumagai, A., Shevchenko, A. and Dunphy, W. (2011) Direct regulation of Treslin by cyclin-dependent kinase is essential for the onset of DNA replication. *The Journal of cell biology*, 193 (6). doi:10.1083/jcb.201102003.
- Larsen, N.B., Gao, A.O., Sparks, J.L., et al. (2019) Replication-Coupled DNA-Protein Crosslink Repair by SPRTN and the Proteasome in *Xenopus* Egg Extracts. *Molecular Cell*, 73 (3): 574. doi:10.1016/j.molcel.2018.11.024.
- Laskey, R.A. and Madine, M.A. (2003) A rotary pumping model for helicase function of MCM proteins at a distance from replication forks. *EMBO reports*. doi:10.1038/sj.embor.embor706.
- Lau, A.W., Inuzuka, H., Fukushima, H., et al. (2013) Regulation of APC^{Cdh1} E3 ligase activity by the Fbw7/cyclin E signaling axis contributes to the tumor suppressor function of Fbw7. *Cell Research*, 23 (7): 947. doi:10.1038/cr.2013.67.
- Lee, I. and Schindelin, H. (2008) Structural insights into E1-catalyzed ubiquitin activation and transfer to conjugating enzymes. *Cell*, 134 (2). doi:10.1016/j.cell.2008.05.046.
- Lee, S.Y., Lee, S.Y. and Choi, Y. (1997) TRAF-interacting Protein (TRIP): A Novel Component of the Tumor Necrosis Factor Receptor (TNFR)- and CD30-TRAF Signaling Complexes That Inhibits TRAF2-mediated NF- κ B Activation. *Journal of Experimental Medicine*, 185 (7): 1275–1286. doi:10.1084/jem.185.7.1275.
- Levitt, M. (1981) Effect of proline residues on protein folding. *Journal of Molecular Biology*, 145 (1): 251–263. doi:10.1016/0022-2836(81)90342-9.
- Li, S. and Wu, X. (2020) Common fragile sites: protection and repair. *Cell & Bioscience*, 10 (1): 1–9. doi:10.1186/s13578-020-00392-5.

- Lim, Y., Tamayo-Orrego, L., Schmid, E., et al. (2023) In silico protein interaction screening uncovers DONSON's role in replication initiation. *Science*. doi:10.1126/science.adi3448.
- Lin, C.-Y., Wu, M.-Y., Gay, S., et al. (2014) H2B Mono-ubiquitylation Facilitates Fork Stalling and Recovery during Replication Stress by Coordinating Rad53 Activation and Chromatin Assembly. *PLOS Genetics*, 10 (10): e1004667. doi:10.1371/journal.pgen.1004667.
- Liu, Y., Mukherjee, R., Bonn, F., et al. (2021) Serine-ubiquitination regulates Golgi morphology and the secretory pathway upon Legionella infection. *Cell Death & Differentiation*, 28 (10): 2957–2969. doi:10.1038/s41418-021-00830-y.
- Liu, Y., Nielsen, C.F., Yao, Q., et al. (2014) The origins and processing of ultra fine anaphase DNA bridges. *Current Opinion in Genetics & Development*, 26: 1–5. doi:10.1016/j.gde.2014.03.003.
- Liu, Z., Oughtred, R. and Wing, S. (2005) Characterization of E3Histone, a novel testis ubiquitin protein ligase which ubiquitinates histones. *Molecular and cellular biology*, 25 (7). doi:10.1128/MCB.25.7.2819-2831.2005.
- Löoke, M., Maloney, M. and Bell, S. (2017) Mcm10 regulates DNA replication elongation by stimulating the CMG replicative helicase. *Genes & development*, 31 (3). doi:10.1101/gad.291336.116.
- Low, E., Chistol, G., Zaher, M.S., et al. (2020) The DNA replication fork suppresses CMG unloading from chromatin before termination. *Genes & Development*, 34 (21–22): 1534–1545. doi:10.1101/gad.339739.120.
- Łukasik, P., Załuski, M. and Gutowska, I. (2021) Cyclin-Dependent Kinases (CDK) and Their Role in Diseases Development–Review. *International Journal of Molecular Sciences*, 22 (6). doi:10.3390/ijms22062935.
- MacNeill, S. (2010) Structure and function of the GINS complex, a key component of the eukaryotic replisome. *The Biochemical journal*, 425 (3). doi:10.1042/BJ20091531.
- Maculins, T., Nkosi, P.J., Nishikawa, H., et al. (2015) Tethering of SCFDia2 to the Replisome Promotes Efficient Ubiquitylation and Disassembly of the CMG Helicase. *Current Biology*, 25 (17): 2254–2259. doi:10.1016/j.cub.2015.07.012.
- Magdalou, I., Lopez, B.S., Pasero, P., et al. (2014) The causes of replication stress and their consequences on genome stability and cell fate. *Seminars in Cell & Developmental Biology*, 30: 154–164. doi:10.1016/j.semcdb.2014.04.035.
- Mailand, N. and Diffley, J. (2005) CDKs promote DNA replication origin licensing in human cells by protecting Cdc6 from APC/C-dependent proteolysis. *Cell*, 122 (6). doi:10.1016/j.cell.2005.08.013.
- Mailand, N., Gibbs-Seymour, I. and Bekker-Jensen, S. (2013) Regulation of PCNA-protein interactions for genome stability. *Nature reviews. Molecular cell biology*, 14 (5). doi:10.1038/nrm3562.
- Malumbres, M. (2014) Cyclin-dependent kinases. *Genome Biology*, 15 (6): 1–10. doi:10.1186/gb4184.
- Malumbres, M. and Barbacid, M. (2001) To cycle or not to cycle: a critical decision in cancer. *Nature reviews. Cancer*, 1 (3). doi:10.1038/35106065.

- Mannervik, B. and Danielson, U.H. (1988) Glutathione transferases--structure and catalytic activity. *CRC critical reviews in biochemistry*, 23 (3): 283–337. doi:10.3109/10409238809088226.
- Maric, M., Maculins, T., De Piccoli, G., et al. (2014) Cdc48 and a ubiquitin ligase drive disassembly of the CMG helicase at the end of DNA replication. *Science (New York, N.Y.)*, 346 (6208). doi:10.1126/science.1253596.
- Maric, M., Mukherjee, P., Tatham, M.H., et al. (2017) Ufd1-Npl4 Recruit Cdc48 for Disassembly of Ubiquitylated CMG Helicase at the End of Chromosome Replication. *Cell Reports*, 18 (13): 3033–3042. doi:10.1016/j.celrep.2017.03.020.
- Matsumoto, M.L., Wickliffe, K.E., Dong, K.C., et al. (2010) K11-Linked Polyubiquitination in Cell Cycle Control Revealed by a K11 Linkage-Specific Antibody. *Molecular Cell*, 39 (3): 477–484. doi:10.1016/j.molcel.2010.07.001.
- Matsushima, N., Tachi, N., Kuroki, Y., et al. (2005) Structural analysis of leucine-rich-repeat variants in proteins associated with human diseases. *Cellular and Molecular Life Sciences*, 62 (23): 2771–2791. doi:10.1007/s00018-005-5187-z.
- Mazouzi, A., Velimezi, G. and Loizou, J.I. (2014) DNA replication stress: Causes, resolution and disease. *Experimental Cell Research*, 329 (1): 85–93. doi:10.1016/j.yexcr.2014.09.030.
- McGarry, T.J. and Kirschner, M.W. (1998) Geminin, an Inhibitor of DNA Replication, Is Degraded during Mitosis. *Cell*, 93 (6): 1043–1053. doi:10.1016/S0092-8674(00)81209-X.
- Merlet, J., Burger, J., Tavernier, N., et al. (2010) The CRL2LRR-1 ubiquitin ligase regulates cell cycle progression during *C. elegans* development. *Development (Cambridge, England)*, 137 (22): 3857. doi:10.1242/dev.054866.
- Merlet, J. and Pintard, L. (2013) Role of the CRL2(LRR-1) E3 ubiquitin-ligase in the development of the germline in *C. elegans*. *Worm*, 2 (3). doi:10.4161/worm.25716.
- Metzger, M.B., Hristova, V.A. and Weissman, A.M. (2012) HECT and RING finger families of E3 ubiquitin ligases at a glance. *Journal of Cell Science*, 125 (3): 531–537. doi:10.1242/jcs.091777.
- Meyer, H., Bug, M. and Bremer, S. (2012) Emerging functions of the VCP/p97 AAA-ATPase in the ubiquitin system. *Nature cell biology*, 14 (2). doi:10.1038/ncb2407.
- Minshull, J., Blow, J. and Hunt, T. (1989) Translation of cyclin mRNA is necessary for extracts of activated xenopus eggs to enter mitosis. *Cell*, 56 (6). doi:10.1016/0092-8674(89)90628-4.
- Mitxitorena, I., Somma, D., Mitchell, J.P., et al. (2020) The deubiquitinase USP7 uses a distinct ubiquitin-like domain to deubiquitinate NF- κ B subunits. *Journal of Biological Chemistry*, 295 (33): 11754–11763. doi:10.1074/jbc.RA120.014113.
- Montagnoli, A., Moll, J. and Colotta, F. (2010) Targeting cell division cycle 7 kinase: a new approach for cancer therapy. *Clinical cancer research : an official journal of the American Association for Cancer Research*, 16 (18). doi:10.1158/1078-0432.CCR-10-0185.
- Montagnoli, A., Valsasina, B., Croci, V., et al. (2008) A Cdc7 kinase inhibitor restricts initiation of DNA replication and has antitumor activity. *Nature chemical biology*, 4 (6). doi:10.1038/nchembio.90.

Moreno, S., Bailey, R., Campion, N., et al. (2014) Polyubiquitylation drives replisome disassembly at the termination of DNA replication. *Science (New York, N.Y.)*, 346 (6208). doi:10.1126/science.1253585.

Moreno, S. and Gambus, A. (2015) Regulation of Unperturbed DNA Replication by Ubiquitylation. *Genes*, 6 (3). doi:10.3390/genes6030451.

Moreno, S. and Gambus, A. (2020) Mechanisms of eukaryotic replisome disassembly. *Biochemical Society transactions*, 48 (3). doi:10.1042/BST20190363.

Moreno, S.P., Jones, R.M., Poovathumkadavil, D., et al. (2019a) Mitotic replisome disassembly depends on TRAIP ubiquitin ligase activity. *Life Science Alliance*, 2 (2). doi:10.26508/lsa.201900390.

Moreno, S.P., Jones, R.M., Poovathumkadavil, D., et al. (2019b) Mitotic replisome disassembly depends on TRAIP ubiquitin ligase activity. *Life Science Alliance*, 2 (2). doi:10.26508/lsa.201900390.

Morris, J.R. and Solomon, E. (2004) BRCA1 : BARD1 induces the formation of conjugated ubiquitin structures, dependent on K6 of ubiquitin, in cells during DNA replication and repair. *Human Molecular Genetics*, 13 (8): 807–817. doi:10.1093/hmg/ddh095.

Muramatsu, S., Hirai, K., Tak, Y.-S., et al. (2010) CDK-dependent complex formation between replication proteins Dpb11, Sld2, Pol (epsilon), and GINS in budding yeast. *Genes & Development*, 24 (6): 602–612. doi:10.1101/gad.1883410.

Neelsen, K. and Lopes, M. (2015) Replication fork reversal in eukaryotes: from dead end to dynamic response. *Nature reviews. Molecular cell biology*, 16 (4). doi:10.1038/nrm3935.

Nethanel, T., Reisfeld, S., Dinter-Gottlieb, G., et al. (1988) An Okazaki piece of simian virus 40 may be synthesized by ligation of shorter precursor chains. *Journal of Virology*, 62 (8): 2867–2873. doi:10.1128/JVI.62.8.2867-2873.1988.

Nielsen, C.F., Huttner, D., Bizard, A.H., et al. (2015) PICH promotes sister chromatid disjunction and co-operates with topoisomerase II in mitosis. *Nature Communications*, 6 (1): 1–15. doi:10.1038/ncomms9962.

Nishikawa, H., Ooka, S., Sato, K., et al. (2004) Mass Spectrometric and Mutational Analyses Reveal Lys-6-linked Polyubiquitin Chains Catalyzed by BRCA1-BARD1 Ubiquitin Ligase*. *Journal of Biological Chemistry*, 279 (6): 3916–3924. doi:10.1074/jbc.M308540200.

Nishitani, H., Sugimoto, N., Roukos, V., et al. (2006) Two E3 ubiquitin ligases, SCF-Skp2 and DDB1-Cul4, target human Cdt1 for proteolysis. *The EMBO journal*, 25 (5). doi:10.1038/sj.emboj.7601002.

O'Connor, H.F. and Huibregtse, J.M. (2017) Enzyme-Substrate Relationships in the Ubiquitin System: Approaches for Identifying Substrates of Ubiquitin Ligases. *Cellular and molecular life sciences : CMLS*, 74 (18): 3363. doi:10.1007/s00018-017-2529-6.

Ohi, M.D., Kooi, C.W.V., Rosenberg, J.A., et al. (2003) Structural insights into the U-box, a domain associated with multi-ubiquitination. *Nature structural biology*, 10 (4): 250. doi:10.1038/nsb906.

Ordureau, A., Sarraf, S.A., Duda, D.M., et al. (2014) Quantitative Proteomics Reveal a Feedforward Mechanism for Mitochondrial PARKIN Translocation and Ubiquitin Chain Synthesis. *Molecular Cell*, 56 (3): 360–375. doi:10.1016/j.molcel.2014.09.007.

- Otten, E.G., Werner, E., Crespillo-Casado, A., et al. (2021) Ubiquitylation of lipopolysaccharide by RNF213 during bacterial infection. *Nature*, 594 (7861): 111–116. doi:10.1038/s41586-021-03566-4.
- Park, E.-S., Choi, S., Kim, J.-M., et al. (2007) Early embryonic lethality caused by targeted disruption of the TRAF-interacting protein (TRIP) gene. *Biochemical and Biophysical Research Communications*, 363 (4): 971–977. doi:10.1016/j.bbrc.2007.09.103.
- Park, E.-S., Choi, S., Shin, B., et al. (2015) Tumor Necrosis Factor (TNF) Receptor-associated Factor (TRAF)-interacting Protein (TRIP) Negatively Regulates the TRAF2 Ubiquitin-dependent Pathway by Suppressing the TRAF2-Sphingosine 1-Phosphate (S1P) Interaction. *The Journal of Biological Chemistry*, 290 (15): 9660. doi:10.1074/jbc.M114.609685.
- Petryk, N., Kahli, M., d'Aubenton-Carafa, Y., et al. (2016) Replication landscape of the human genome. *Nature Communications*, 7 (1): 1–13. doi:10.1038/ncomms10208.
- Pickart, C. and Eddins, M. (2004) Ubiquitin: structures, functions, mechanisms. *Biochimica et biophysica acta*, 1695 (1–3). doi:10.1016/j.bbamcr.2004.09.019.
- Pickart, C. and Fushman, D. (2004) Polyubiquitin chains: polymeric protein signals. *Current opinion in chemical biology*, 8 (6). doi:10.1016/j.cbpa.2004.09.009.
- Powis, G., Meuillet, E.J., Indarte, M., et al. (2023) Pleckstrin Homology [PH] domain, structure, mechanism, and contribution to human disease. *Biomedicine & Pharmacotherapy*, 165: 115024. doi:10.1016/j.biopha.2023.115024.
- Promonet, A., Padioleau, I., Liu, Y., et al. (2020) Topoisomerase 1 prevents replication stress at R-loop-enriched transcription termination sites. *Nature Communications*, 11 (1): 1–12. doi:10.1038/s41467-020-17858-2.
- Qi, J. and Ronai, Z. (2015) Dysregulation of ubiquitin ligases in cancer. *Drug resistance updates : reviews and commentaries in antimicrobial and anticancer chemotherapy*, 23. doi:10.1016/j.drug.2015.09.001.
- Qian, H., Zhang, Y., Wu, B., et al. (2020) Structure and Function of HECT E3 Ubiquitin Ligases and their Role in Oxidative Stress. *Journal of Translational Internal Medicine*, 8 (2): 71. doi:10.2478/jtim-2020-0012.
- Quan, Y., Xia, Y., Liu, L., et al. (2015) Cell cycle regulated interaction between Mcm10 and double hexameric Mcm2-7 is required for helicase splitting and activation during S phase. *Cell reports*, 13 (11): 2576–2586. doi:10.1016/j.celrep.2015.11.018.
- Ramazi, S. and Zahiri, J. (2021) Post-translational modifications in proteins: resources, tools and prediction methods. *Database: The Journal of Biological Databases and Curation*, 2021. doi:10.1093/database/baab012.
- Robinson, P. and Ardley, H. (2004) Ubiquitin-protein ligases--novel therapeutic targets? *Current protein & peptide science*, 5 (3). doi:10.2174/1389203043379800.
- Sakamaki, J., Ode, K.L., Kurikawa, Y., et al. (2022) Ubiquitination of phosphatidylethanolamine in organellar membranes. *Molecular Cell*, 82 (19): 3677-3692.e11. doi:10.1016/j.molcel.2022.08.008.

Saldivar, J., Cortez, D. and Cimprich, K. (2017) The essential kinase ATR: ensuring faithful duplication of a challenging genome. *Nature reviews. Molecular cell biology*, 18 (10). doi:10.1038/nrm.2017.67.

Sampson, C., Wang, Q., Otkur, W., et al. (2023) The roles of E3 ubiquitin ligases in cancer progression and targeted therapy. *Clinical and Translational Medicine*, 13 (3). doi:10.1002/ctm2.1204.

Satyanarayana, A. and Kaldis, P. (2009) A dual role of Cdk2 in DNA damage response. *Cell division*, 4. doi:10.1186/1747-1028-4-9.

Saxena, S. and Zou, L. (2022) Hallmarks of DNA replication stress. *Molecular cell*, 82 (12). doi:10.1016/j.molcel.2022.05.004.

Scaramuzza, S., Jones, R.M., Sadurni, M.M., et al. (2023) TRAIP resolves DNA replication-transcription conflicts during the S-phase of unperturbed cells. *Nature Communications*, 14 (1): 1–20. doi:10.1038/s41467-023-40695-y.

Schafer, K. (1998) The cell cycle: a review. *Veterinary pathology*, 35 (6). doi:10.1177/030098589803500601.

Schreiber, A., Stengel, F., Zhang, Z., et al. (2011) Structural basis for the subunit assembly of the anaphase-promoting complex. *Nature*, 470 (7333). doi:10.1038/nature09756.

Schulman, B.A. and Harper, J.W. (2009) Ubiquitin-like protein activation by E1 enzymes: the apex for downstream signalling pathways. *Nature reviews. Molecular cell biology*, 10 (5): 319. doi:10.1038/nrm2673.

Scott, D., Rhee, D., Duda, D., et al. (2016) Two Distinct Types of E3 Ligases Work in Unison to Regulate Substrate Ubiquitylation. *Cell*, 166 (5). doi:10.1016/j.cell.2016.07.027.

Seul Park, I., Jo, K.-S., Won, H.-S., et al. (2015) Dimerization of TRAF-interacting protein (TRAIP) regulates the mitotic progression. *Biochemical and Biophysical Research Communications*, 463 (4): 864–869. doi:10.1016/j.bbrc.2015.06.026.

Sharma, B. and Taganna, J. (2020) Genome-wide analysis of the U-box E3 ubiquitin ligase enzyme gene family in tomato. *Scientific reports*, 10 (1). doi:10.1038/s41598-020-66553-1.

Sheaff, R.J. and Kuchta, R.D. (1993) Mechanism of calf thymus DNA primase: slow initiation, rapid polymerization, and intelligent termination. *Biochemistry*, 32 (12): 3027–3037. doi:10.1021/bi00063a014.

Simon, A.C., Zhou, J.C., Perera, R.L., et al. (2014) A Ctf4 trimer couples the CMG helicase to DNA polymerase α in the eukaryotic replisome. *Nature*, 510 (7504): 293–297. doi:10.1038/nature13234.

Sloper-Mould, K.E., Jemc, J.C., Pickart, C.M., et al. (2001) Distinct Functional Surface Regions on Ubiquitin. *Journal of Biological Chemistry*, 276 (32): 30483–30489. doi:10.1074/jbc.M103248200.

Sluimer, J. and Distel, B. (2018) Regulating the human HECT E3 ligases. *Cellular and molecular life sciences : CMLS*, 75 (17). doi:10.1007/s00018-018-2848-2.

Sonneville, R., Bhowmick, R., Hoffmann, S., et al. (2019a) TRAIP drives replisome disassembly and mitotic DNA repair synthesis at sites of incomplete DNA replication. doi:10.7554/eLife.48686.

- Sonneville, R., Bhowmick, R., Hoffmann, S., et al. (2019b) *TRAIP drives replisome disassembly and mitotic DNA repair synthesis at sites of incomplete DNA replication*. doi:10.7554/eLife.48686.
- Sonneville, R., Moreno, S., Knebel, A., et al. (2017) CUL-2LRR-1 and UBXN-3 drive replisome disassembly during DNA replication termination and mitosis. *Nature cell biology*, 19 (5). doi:10.1038/ncb3500.
- Soo Lee, N., Jin Chung, H., Kim, H.-J., et al. (2016) TRAIP/RNF206 is required for recruitment of RAP80 to sites of DNA damage. *Nature Communications*, 7 (1): 1–13. doi:10.1038/ncomms10463.
- Soucy, T., Smith, P., Milhollen, M., et al. (2009) An inhibitor of NEDD8-activating enzyme as a new approach to treat cancer. *Nature*, 458 (7239). doi:10.1038/nature07884.
- Sparks, J. and Walter, J.C. (2019) Extracts for Analysis of DNA Replication in a Nucleus-Free System. *Cold Spring Harbor Protocols*, 2019 (3): pdb.prot097154. doi:10.1101/pdb.prot097154.
- Speroni, J., Federico, M., Mansilla, S., et al. (2012) Kinase-independent function of checkpoint kinase 1 (Chk1) in the replication of damaged DNA. *Proceedings of the National Academy of Sciences of the United States of America*, 109 (19). doi:10.1073/pnas.1116345109.
- Spratt, D.E., Walden, H. and Shaw, G.S. (2014) RBR E3 ubiquitin ligases: new structures, new insights, new questions. *Biochemical Journal*, 458 (Pt 3): 421. doi:10.1042/BJ20140006.
- Starostina, N., Simpliciano, J., McGuirk, M., et al. (2010) CRL2(LRR-1) targets a CDK inhibitor for cell cycle control in *C. elegans* and actin-based motility regulation in human cells. *Developmental cell*, 19 (5). doi:10.1016/j.devcel.2010.10.013.
- Strausfeld, U., Howell, M., Descombes, P., et al. (1996) Both cyclin A and cyclin E have S-phase promoting (SPF) activity in *Xenopus* egg extracts. *Journal of cell science*, 109 (Pt 6). doi:10.1242/jcs.109.6.1555.
- Sun, L. and Chen, Z.J. (2004) The novel functions of ubiquitination in signaling. *Current opinion in cell biology*, 16 (2). doi:10.1016/j.ceb.2004.02.005.
- Sun, Y., Saha, L.K., Saha, S., et al. (2020) Debulking of topoisomerase DNA-protein crosslinks (TOP-DPC) by the proteasome, non-proteasomal and non-proteolytic pathways. *DNA repair*, 94: 102926. doi:10.1016/j.dnarep.2020.102926.
- Swatek, K.N. and Komander, D. (2016) Ubiquitin modifications. *Cell Research*, 26 (4): 399–422. doi:10.1038/cr2016.39.
- Tanaka, S., Nakato, R., Katou, Y., et al. (2011) Origin association of Sld3, Sld7, and Cdc45 proteins is a key step for determination of origin-firing timing. *Current biology: CB*, 21 (24): 2055–2063. doi:10.1016/j.cub.2011.11.038.
- Tarcan, Z., Poovathumkadavil, D., Skagia, A., et al. (2022) The p97 segregase cofactor Ubxn7 facilitates replisome disassembly during S-phase. *The Journal of biological chemistry*, 298 (8). doi:10.1016/j.jbc.2022.102234.
- Toma-Fukai, S. and Shimizu, T. (2021) Structural Diversity of Ubiquitin E3 Ligase. *Molecules (Basel, Switzerland)*, 26 (21). doi:10.3390/molecules26216682.
- Trujillo, K.M. and Osley, M.A. (2012) A Role for H2B Ubiquitylation in DNA Replication. *Molecular cell*, 48 (5): 734. doi:10.1016/j.molcel.2012.09.019.

- Trujillo, M. (2018) News from the PUB: plant U-box type E3 ubiquitin ligases. *Journal of Experimental Botany*, 69 (3): 371–384. doi:10.1093/jxb/erx411.
- Uhlen, M., Zhang, C., S, L., et al. (2017) A pathology atlas of the human cancer transcriptome. *Science (New York, N.Y.)*, 357 (6352). doi:10.1126/science.aan2507.
- Ulrich, H.D. and Walden, H. (2010) Ubiquitin signalling in DNA replication and repair. *Nature Reviews. Molecular Cell Biology*, 11 (7): 479–489. doi:10.1038/nrm2921.
- Umbreit, N., Zhang, C., Lynch, L., et al. (2020) Mechanisms generating cancer genome complexity from a single cell division error. *Science (New York, N.Y.)*, 368 (6488). doi:10.1126/science.aba0712.
- Vaughan, R.M., Kupai, A. and Rothbart, S.B. (2021) Chromatin regulation through ubiquitin and ubiquitin-like histone modifications. *Trends in biochemical sciences*, 46 (4): 258. doi:10.1016/j.tibs.2020.11.005.
- Villa, F., Fujisawa, R., Ainsworth, J., et al. (2021) CUL2LRR1, TRAIP and p97 control CMG helicase disassembly in the mammalian cell cycle. *EMBO Reports*, 22 (3): e52164. doi:10.15252/embr.202052164.
- Volpi, I., Gillespie, P., Chadha, G., et al. (2021) The role of DDK and Treslin-MTBP in coordinating replication licensing and pre-initiation complex formation. *Open biology*, 11 (10). doi:10.1098/rsob.210121.
- Vrtis, K.B., Dewar, J.M., Chistol, G., et al. (2021) Single-strand DNA breaks cause replisome disassembly. *Molecular Cell*, 81 (6): 1309–1318.e6. doi:10.1016/j.molcel.2020.12.039.
- Walczak, H., Iwai, K. and Dikic, I. (2012) Generation and physiological roles of linear ubiquitin chains. *BMC Biology*, 10 (1): 1–6. doi:10.1186/1741-7007-10-23.
- Wang, A.Z., Langer, R. and Farokhzad, O.C. (2012) Nanoparticle delivery of cancer drugs. *Annual Review of Medicine*, 63: 185–198. doi:10.1146/annurev-med-040210-162544.
- Wang, C., Song, B., Dai, Y., et al. (2021) Genome-wide identification and functional analysis of U-box E3 ubiquitin ligases gene family related to drought stress response in Chinese white pear (*Pyrus bretschneideri*). *BMC Plant Biology*, 21 (1): 1–20. doi:10.1186/s12870-021-03024-3.
- Wang, J.D., Michelitsch, M.D. and Weissman, J.S. (1998) *GroEL-GroES-Mediated Protein Folding Requires an Intact Central Cavity on JSTOR*. Available at: <https://www.jstor.org/stable/46030> (Accessed: 19 September 2023).
- Wang, Q., Liu, X., Cui, Y., et al. (2014) The E3 Ubiquitin Ligase AMFR and INSIG1 Bridge the Activation of TBK1 Kinase by Modifying the Adaptor STING. *Immunity*, 41 (6): 919–933. doi:10.1016/j.immuni.2014.11.011.
- Wang, S., Xia, W., Qiu, M., et al. (2016) Atlas on substrate recognition subunits of CRL2 E3 ligases. *Oncotarget*, 7 (29): 46707–46716. doi:10.18632/oncotarget.8732.
- Wang, Y., Argiles-Castillo, D., Kane, E., et al. (2020) HECT E3 ubiquitin ligases - emerging insights into their biological roles and disease relevance. *Journal of cell science*, 133 (7). doi:10.1242/jcs.228072.

- Wäsch, R. and Engelbert, D. (2005) Anaphase-promoting complex-dependent proteolysis of cell cycle regulators and genomic instability of cancer cells. *Oncogene*, 24 (1). doi:10.1038/sj.onc.1208017.
- Weber, J., Polo, S. and Maspero, E. (2019) HECT E3 Ligases: A Tale With Multiple Facets. *Frontiers in Physiology*, 10. doi:10.3389/fphys.2019.00370.
- Wohlschlegel, J., Dwyer, B., Dhar, S., et al. (2000) Inhibition of eukaryotic DNA replication by geminin binding to Cdt1. *Science (New York, N.Y.)*, 290 (5500). doi:10.1126/science.290.5500.2309.
- Wu, R.A., Pellman, D.S. and Walter, J.C. (2021) The ubiquitin ligase TRAIP: double-edged sword at the replisome. *Trends in cell biology*, 31 (2): 75. doi:10.1016/j.tcb.2020.11.007.
- Wu, R.A., Semlow, D.R., Kamimae-Lanning, A.N., et al. (2019) TRAIP is a master regulator of DNA interstrand cross-link repair. *Nature*, 567 (7747): 267. doi:10.1038/s41586-019-1002-0.
- Wyatt, D.W., Feng, W., Conlin, M.P., et al. (2016) Essential Roles for Polymerase θ -Mediated End Joining in the Repair of Chromosome Breaks. *Molecular Cell*, 63 (4): 662–673. doi:10.1016/j.molcel.2016.06.020.
- Xia, Y. (2021) The Fate of Two Unstoppable Trains After Arriving Destination: Replisome Disassembly During DNA Replication Termination. *Frontiers in Cell and Developmental Biology*, 9: 658003. doi:10.3389/fcell.2021.658003.
- Xia, Y., Sonnevile, R., Jenkyn-Bedford, M., et al. (2023) DNSN-1 recruits GINS for CMG helicase assembly during DNA replication initiation in *Caenorhabditis elegans*. *Science (New York, N.Y.)*, 381 (6664). doi:10.1126/science.adi4932.
- Yang, Q., Zhao, J., Chen, D., et al. (2021) E3 ubiquitin ligases: styles, structures and functions. *Molecular Biomedicine*, 2. doi:10.1186/s43556-021-00043-2.
- Yao, N.Y. and O'Donnell, M. (2012) The RFC Clamp Loader: Structure and Function. *Sub-cellular biochemistry*, 62: 259. doi:10.1007/978-94-007-4572-8_14.
- Yardimci, H., Loveland, A., Habuchi, S., et al. (2010) Uncoupling of sister replisomes during eukaryotic DNA replication. *Molecular cell*, 40 (5). doi:10.1016/j.molcel.2010.11.027.
- Ye, Y. and Rape, M. (2009) Building ubiquitin chains: E2 enzymes at work. *Nature reviews. Molecular cell biology*, 10 (11): 755. doi:10.1038/nrm2780.
- Yeeles, J., Deegan, T., Janska, A., et al. (2015) Regulated eukaryotic DNA replication origin firing with purified proteins. *Nature*, 519 (7544). doi:10.1038/nature14285.
- Yeeles, J., Janska, A., Early, A., et al. (2017) How the Eukaryotic Replisome Achieves Rapid and Efficient DNA Replication. *Molecular cell*, 65 (1). doi:10.1016/j.molcel.2016.11.017.
- Yuan, W.-C., Lee, Y.-R., Lin, S.-Y., et al. (2014) K33-Linked Polyubiquitination of Coronin 7 by Cul3-KLHL20 Ubiquitin E3 Ligase Regulates Protein Trafficking. *Molecular Cell*, 54 (4): 586–600. doi:10.1016/j.molcel.2014.03.035.
- Yuan, Y., Ren, Y., Yuan, P., et al. (2016) TRAIP is involved in chromosome alignment and SAC regulation in mouse oocyte meiosis. *Scientific reports*, 6. doi:10.1038/srep29735.

- Zegerman, P. and Diffley, J.F.X. (2007) Phosphorylation of Sld2 and Sld3 by cyclin-dependent kinases promotes DNA replication in budding yeast. *Nature*, 445 (7125): 281–285. doi:10.1038/nature05432.
- Zellweger, R., Dalcher, D., Mutreja, K., et al. (2015) Rad51-mediated replication fork reversal is a global response to genotoxic treatments in human cells. *The Journal of cell biology*, 208 (5). doi:10.1083/jcb.201406099.
- Zeman, M. and Cimprich, K. (2014) Causes and consequences of replication stress. *Nature cell biology*, 16 (1). doi:10.1038/ncb2897.
- Zhang, W., Xu, C., Bian, C., et al. (2011) Crystal structure of the Cys2His2-type zinc finger domain of human DPF2. *Biochemical and biophysical research communications*, 413 (1). doi:10.1016/j.bbrc.2011.08.043.
- Zheng, L. and Shen, B. (2011) Okazaki fragment maturation: nucleases take centre stage. *Journal of molecular cell biology*, 3 (1). doi:10.1093/jmcb/mjq048.
- Zheng, N. and Shabek, N. (2017) *Ubiquitin Ligases: Structure, Function, and Regulation*. doi:10.1146/annurev-biochem-060815-014922.
- Zheng, Y., Jia, H., Wang, P., et al. (2023) Silencing TRAIIP suppresses cell proliferation and migration/invasion of triple negative breast cancer via RB-E2F signaling and EMT. *Cancer Gene Therapy*, 30 (1): 74–84. doi:10.1038/s41417-022-00517-7.
- Zhou, H., Zaher, M.S., Walter, J.C., et al. (2021) Structure of CRL2Lrr1, the E3 ubiquitin ligase that promotes DNA replication termination in vertebrates. *Nucleic Acids Research*, 49 (22): 13194–13206. doi:10.1093/nar/gkab1174.
- Zhou, J.C., Janska, A., Goswami, P., et al. (2017) CMG–Pol epsilon dynamics suggests a mechanism for the establishment of leading-strand synthesis in the eukaryotic replisome. *Proceedings of the National Academy of Sciences*, 114 (16): 4141–4146. doi:10.1073/pnas.1700530114.
- Zhou, Q. and Geahlen, R.L. (2009) The protein-tyrosine kinase Syk interacts with TRAF-interacting protein TRIP in breast epithelial cells. *Oncogene*, 28 (10): 1348–1356. doi:10.1038/onc.2008.493.
- Zimmerman, E.S., Schulman, B.A. and Zheng, N. (2010) Structural assembly of cullin-RING ubiquitin ligase complexes. *Current opinion in structural biology*, 20 (6): 714. doi:10.1016/j.sbi.2010.08.010.

